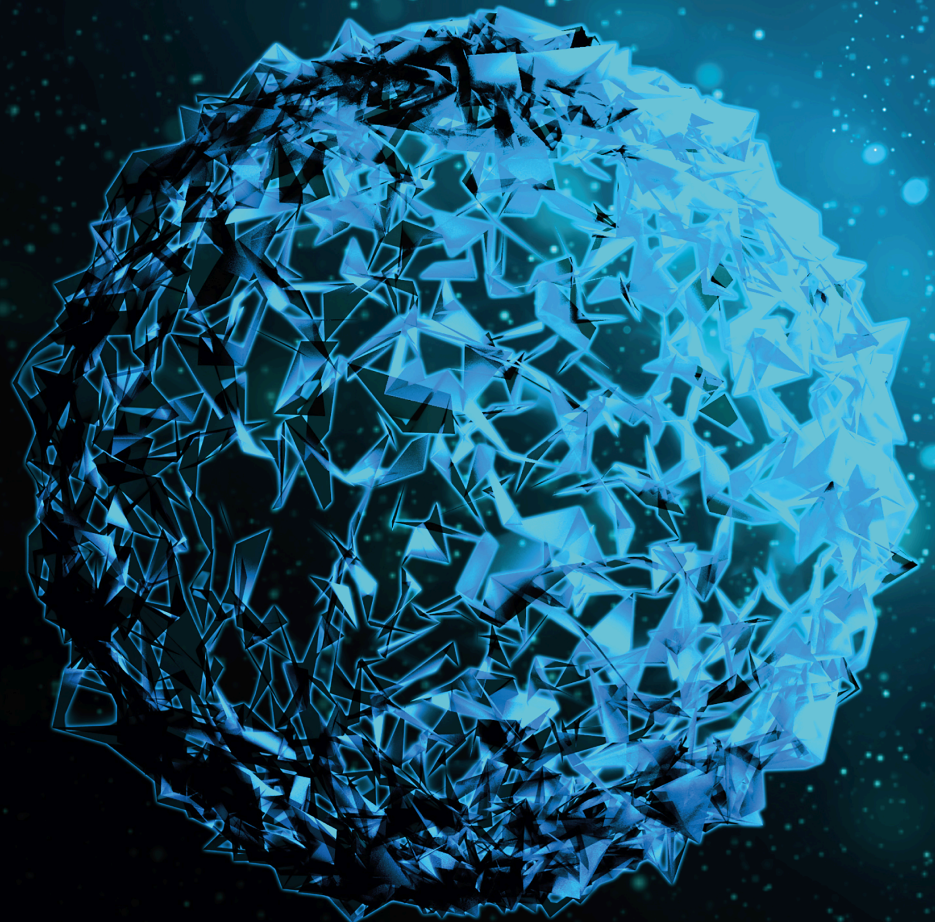


Adaptive Evolution of Autoimmune Proteins in Animals 2022

Lead Guest Editor: Hafiz Ishfaq Ahmad

Guest Editors: Du Xiaoyong, Gulnaz Afzal, and Abdelmotaleb Ahmed Elokil





**Adaptive Evolution of Autoimmune Proteins in
Animals 2022**

BioMed Research International

Adaptive Evolution of Autoimmune Proteins in Animals 2022

Lead Guest Editor: Hafiz Ishfaq Ahmad

Guest Editors: Du Xiaoyong, Gulnaz Afzal, and
Abdelmotalieb Ahmed Elokil



Copyright © 2024 Hindawi Limited. All rights reserved.

This is a special issue published in "BioMed Research International." All articles are open access articles distributed under the Creative Commons Attribution License, which permits unrestricted use, distribution, and reproduction in any medium, provided the original work is properly cited.

Section Editors

Penny A. Asbell, USA
David Bernardo , Spain
Gerald Brandacher, USA
Kim Bridle , Australia
Laura Chronopoulou , Italy
Gerald A. Colvin , USA
Aaron S. Dumont, USA
Pierfrancesco Franco , Italy
Raj P. Kandpal , USA
Fabrizio Montecucco , Italy
Mangesh S. Pednekar , India
Letterio S. Politi , USA
Jinsong Ren , China
William B. Rodgers, USA
Harry W. Schroeder , USA
Andrea Scribante , Italy
Germán Vicente-Rodríguez , Spain
Momiao Xiong , USA
Hui Zhang , China

Academic Editors

Immunology

Contents

Retracted: ZOMEK via the p-Akt/Nrf2 Pathway Restored PTZ-Induced Oxidative Stress-Mediated Memory Dysfunction in Mouse Model

BioMed Research International

Retraction (1 page), Article ID 9893738, Volume 2024 (2024)

Retracted: Empirical Method for Thyroid Disease Classification Using a Machine Learning Approach

BioMed Research International

Retraction (1 page), Article ID 9876036, Volume 2024 (2024)

Retracted: Assessment of Acupoint Therapy of Traditional Chinese Medicine on Cough Variant Asthma: A Meta-analysis

BioMed Research International

Retraction (1 page), Article ID 9856747, Volume 2024 (2024)

Retracted: Study on Various Luteal Characteristics Using Doppler Ultrasonography for Early Pregnancy Diagnosis in Nili-Ravi Buffaloes

BioMed Research International

Retraction (1 page), Article ID 9854013, Volume 2024 (2024)

Retracted: CRISPR-Cas System: An Adaptive Immune System's Association with Antibiotic Resistance in *Salmonella enterica* Serovar Enteritidis

BioMed Research International

Retraction (1 page), Article ID 9849515, Volume 2024 (2024)

Retracted: Deleterious Effects of Amoxicillin on Immune System and Haematobiochemical Parameters of a Rabbit

BioMed Research International

Retraction (1 page), Article ID 9835625, Volume 2024 (2024)

Retracted: Acetochlor Affects Bighead Carp (*Aristichthys Nobilis*) by Producing Oxidative Stress, Lowering Tissue Proteins, and Inducing Genotoxicity

BioMed Research International

Retraction (1 page), Article ID 9832123, Volume 2024 (2024)

Retracted: Growth Response in *Oryctolagus cuniculus* to Selenium Toxicity Exposure Ameliorated with Vitamin E

BioMed Research International

Retraction (1 page), Article ID 9828413, Volume 2024 (2024)

Retracted: A Novel Protein Elicitor (PELL1) Extracted from *Lecanicillium lecanii* Induced Resistance against *Bemisia tabaci* (Hemiptera: Aleyrodidae) in *Gossypium hirsutum* L

BioMed Research International

Retraction (1 page), Article ID 9820506, Volume 2024 (2024)

Retracted: Investigation on Immune-Related Protein (Heat Shock Proteins and Metallothionein) Gene Expression Changes and Liver Histopathology in Cadmium-Stressed Fish

BioMed Research International

Retraction (1 page), Article ID 9815615, Volume 2024 (2024)

Retracted: Biologically Synthesized Peptides Show Remarkable Inhibition Activity against Angiotensin-Converting Enzyme: A Promising Approach for Peptide Development against Autoimmune Diseases

BioMed Research International

Retraction (1 page), Article ID 9810576, Volume 2024 (2024)

Retracted: Correlation Analysis of Cytochrome P450 SNPs in Hepatitis B-Caused Cirrhosis Patients

BioMed Research International

Retraction (1 page), Article ID 9807928, Volume 2024 (2024)

Retracted: Therapeutical Significance of Serpina3n Subsequent Cerebral Ischemia via Cytotoxic Granzyme B Inactivation

BioMed Research International

Retraction (1 page), Article ID 9804638, Volume 2024 (2024)

Retracted: Exploration of ACE-Inhibiting Peptides Encrypted in *Artemisia annua* Using *In Silico* Approach

BioMed Research International

Retraction (1 page), Article ID 9804234, Volume 2024 (2024)

Retracted: Diversity of Rotavirus Strains among Children with Acute Diarrhea in Karachi, Pakistan

BioMed Research International

Retraction (1 page), Article ID 9796247, Volume 2024 (2024)

Retracted: Biologically Synthesized Copper Nanoparticles Show Considerable Degradation of Reactive Red 81 Dye: An Eco-Friendly Sustainable Approach

BioMed Research International

Retraction (1 page), Article ID 9785373, Volume 2024 (2024)

Retracted: Training a Feedforward Neural Network Using Hybrid Gravitational Search Algorithm with Dynamic Multiswarm Particle Swarm Optimization

BioMed Research International

Retraction (1 page), Article ID 9783980, Volume 2024 (2024)


Retracted: Divergent Analyses of Genetic Relatedness and Evidence-Based Assessment of Therapeutics of *Staphylococcus aureus* from Semi-intensive Dairy Systems

BioMed Research International

Retraction (1 page), Article ID 9763963, Volume 2024 (2024)




Contents

[Retracted] ZOMEc via the p-Akt/Nrf2 Pathway Restored PTZ-Induced Oxidative Stress-Mediated Memory Dysfunction in Mouse Model

Rifat Jahan , Mohammad Yousaf , Hamayun Khan , Nousheen Bibi, Musarrat Ijaz, Touseef Rehan, and Shahid Ali Shah









Research Article (14 pages), Article ID 8902262, Volume 2022 (2022)

[Retracted] A Novel Protein Elicitor (PELL1) Extracted from *Lecanicillium lecanii* Induced Resistance against *Bemisia tabaci* (Hemiptera: Aleyrodidae) in *Gossypium hirsutum* L

Abdul Basit, Muhammad Yaseen, Maham Babar, Yong Wang, Yusuf Ali Abdulle, Dewen Qiu, Yunzhu Li , Muhammad Amjad Bashir , Muhammad Sarmad Shahzad, Hasnain Farooq , Reem A. Alajmi, David N. Mangi, Ambreen Sehar, and Humaira Parveen







Research Article (8 pages), Article ID 3097521, Volume 2022 (2022)

[Retracted] Study on Various Luteal Characteristics Using Doppler Ultrasonography for Early Pregnancy Diagnosis in Nili-Ravi Buffaloes

Umair Riaz, Mubbashar Hassan , Muhammad I. Khan , Umer Farooq , Farah Ali , Khalid Mehmood , Aftab Shaukat , Mushtaq H. Lashari , and Liguang Yang 



Research Article (6 pages), Article ID 3896068, Volume 2022 (2022)

[Retracted] Investigation on Immune-Related Protein (Heat Shock Proteins and Metallothionein) Gene Expression Changes and Liver Histopathology in Cadmium-Stressed Fish

Ghazala Jabeen , Sarwat Ishaq , Mateen Arshad , Shafaq Fatima , Zakia Kanwal , and Farah Ali 




Research Article (11 pages), Article ID 2075791, Volume 2022 (2022)

[Retracted] Assessment of Acupoint Therapy of Traditional Chinese Medicine on Cough Variant Asthma: A Meta-analysis

Hengjia Tu  and Qingling Zhang 

Research Article (13 pages), Article ID 4168308, Volume 2022 (2022)

[Retracted] Biologically Synthesized Copper Nanoparticles Show Considerable Degradation of Reactive Red 81 Dye: An Eco-Friendly Sustainable Approach

Muhammad Asim Rafique, Adil Jamal , Zainab Ali, Shumaila Kiran , Sarosh Iqbal, Sofia Nosheen, Zulqarnain Ansar, and Md Belal Hossain 





Research Article (9 pages), Article ID 7537955, Volume 2022 (2022)

[Retracted] Correlation Analysis of Cytochrome P450 SNPs in Hepatitis B-Caused Cirrhosis Patients

Qing-Ya Li , Xiaona Yang , and Zhi-Zhong Guo 

















Research Article (8 pages), Article ID 9891184, Volume 2022 (2022)

[Retracted] Biologically Synthesized Peptides Show Remarkable Inhibition Activity against Angiotensin-Converting Enzyme: A Promising Approach for Peptide Development against Autoimmune Diseases

Nosheen Mujtaba, Nazish Jahan, Adil Jamal , Shazia Abrar, Shumaila Kiran , Atizaz Rasool, Md Belal Hossain , Fayez Saeed Bahwerth , Ibtesam Nomani, and Khalid Javed Iqbal




Research Article (12 pages), Article ID 2396192, Volume 2022 (2022)

[Retracted] Divergent Analyses of Genetic Relatedness and Evidence-Based Assessment of Therapeutics of *Staphylococcus aureus* from Semi-intensive Dairy Systems

Sidra Aziz , Nahla Muhammad Saeed , Hiewa Othman Dyary , Muhammad Muddassir Ali , Rao Zahid Abbas , Aziz ur Rehman , Sammina Mahmood , Laiba Shafique , Zaeem Sarwar , Fakhara Khanum , Tean Zaheer , Khurram Ashfaq , Mughees Aizaz Alvi , Muhammad Shafeeq , Arslan Saleem , and Amjad Islam Aqib 

Research Article (13 pages), Article ID 5313654, Volume 2022 (2022)

[Retracted] Empirical Method for Thyroid Disease Classification Using a Machine Learning Approach

Tahir Alyas , Muhammad Hamid , Khalid Alissa, Tauqeer Faiz, Nadia Tabassum , and Aqeel Ahmad

Research Article (10 pages), Article ID 9809932, Volume 2022 (2022)

[Retracted] Training a Feedforward Neural Network Using Hybrid Gravitational Search Algorithm with Dynamic Multiswarm Particle Swarm Optimization

Arfan Ali Nagra, Tahir Alyas , Muhammad Hamid , Nadia Tabassum , and Aqeel Ahmad

Research Article (10 pages), Article ID 2636515, Volume 2022 (2022)

[Retracted] Therapeutical Significance of Serpina3n Subsequent Cerebral Ischemia via Cytotoxic Granzyme B Inactivation

Mehwish Saba Aslam , Mobeena Saba Aslam , Komal Saba Aslam, Asia Iqbal, and Liudi Yuan 

Research Article (13 pages), Article ID 1557010, Volume 2022 (2022)

[Retracted] Acetochlor Affects Bighead Carp (*Aristichthys Nobilis*) by Producing Oxidative Stress, Lowering Tissue Proteins, and Inducing Genotoxicity

Yasir Mahmood , Riaz Hussain , Abdul Ghaffar , Farah Ali , Sadia Nawaz , Khalid Mehmood , and Ahrar Khan 



Research Article (12 pages), Article ID 9140060, Volume 2022 (2022)

[Retracted] Exploration of ACE-Inhibiting Peptides Encrypted in *Artemisia annua* Using *In Silico* Approach

Muhammad Naveed Shahid , Maryam Zawar , Adil Jamal , Bahaeldeen Babiker Mohamed , Sana Khalid , and Fayez Saeed Bahwerth 


Research Article (10 pages), Article ID 5367125, Volume 2022 (2022)

[Retracted] Growth Response in *Oryctolagus cuniculus* to Selenium Toxicity Exposure Ameliorated with Vitamin E

Rukhshanda Rehman , Nuzhat Sial, Amina Ismail, Shabir Hussain , Sobia Abid, Maryium Javed, Khansa Nadeem, and Muhammad Ayoub

Research Article (9 pages), Article ID 8216685, Volume 2022 (2022)


[Retracted] Diversity of Rotavirus Strains among Children with Acute Diarrhea in Karachi, Pakistan

Nain Tarra Bukhari, Gulnaz Parveen , Pir Asmat Ali, Amtul Sami, Yasmeen Lashari, Naila Mukhtar, Raisa Bano, Nargis Haider, Atiya Hussain Khowaja, and Shahana Urooj Kazmi

Research Article (6 pages), Article ID 5231910, Volume 2022 (2022)

Contents

[Retracted] CRISPR-Cas System: An Adaptive Immune System's Association with Antibiotic Resistance in *Salmonella enterica* Serovar Enteritidis

Muhammad Zulqarnain Haider, Muhammad Abu Bakr Shabbir , Tahir Yaqub, Adeel Sattar, Muhammad Kashif Maan, Sammina Mahmood, Tahir Mehmood, and Hassaan Bin Aslam
Research Article (7 pages), Article ID 9080396, Volume 2022 (2022)

[Retracted] Deleterious Effects of Amoxicillin on Immune System and Haematobiochemical Parameters of a Rabbit

Khalid Hussain, Mushtaq Hussain Lashari , Umer Farooq , and Tahir Mehmood
Research Article (8 pages), Article ID 8691261, Volume 2022 (2022)

Retraction

Retracted: ZOMEK via the p-Akt/Nrf2 Pathway Restored PTZ-Induced Oxidative Stress-Mediated Memory Dysfunction in Mouse Model

BioMed Research International

Received 12 March 2024; Accepted 12 March 2024; Published 20 March 2024

Copyright © 2024 BioMed Research International. This is an open access article distributed under the Creative Commons Attribution License, which permits unrestricted use, distribution, and reproduction in any medium, provided the original work is properly cited.

This article has been retracted by Hindawi following an investigation undertaken by the publisher [1]. This investigation has uncovered evidence of one or more of the following indicators of systematic manipulation of the publication process:

- (1) Discrepancies in scope
- (2) Discrepancies in the description of the research reported
- (3) Discrepancies between the availability of data and the research described
- (4) Inappropriate citations
- (5) Incoherent, meaningless and/or irrelevant content included in the article
- (6) Manipulated or compromised peer review

The presence of these indicators undermines our confidence in the integrity of the article's content and we cannot, therefore, vouch for its reliability. Please note that this notice is intended solely to alert readers that the content of this article is unreliable. We have not investigated whether authors were aware of or involved in the systematic manipulation of the publication process.

Wiley and Hindawi regrets that the usual quality checks did not identify these issues before publication and have since put additional measures in place to safeguard research integrity.

We wish to credit our own Research Integrity and Research Publishing teams and anonymous and named external researchers and research integrity experts for contributing to this investigation.

The corresponding author, as the representative of all authors, has been given the opportunity to register their agreement or disagreement to this retraction. We have kept a record of any response received.

References

- [1] R. Jahan, M. Yousof, H. Khan et al., "ZOMEK via the p-Akt/Nrf2 Pathway Restored PTZ-Induced Oxidative Stress-Mediated Memory Dysfunction in Mouse Model," *BioMed Research International*, vol. 2022, Article ID 8902262, 14 pages, 2022.

Retraction

Retracted: Empirical Method for Thyroid Disease Classification Using a Machine Learning Approach

BioMed Research International

Received 12 March 2024; Accepted 12 March 2024; Published 20 March 2024

Copyright © 2024 BioMed Research International. This is an open access article distributed under the Creative Commons Attribution License, which permits unrestricted use, distribution, and reproduction in any medium, provided the original work is properly cited.

This article has been retracted by Hindawi following an investigation undertaken by the publisher [1]. This investigation has uncovered evidence of one or more of the following indicators of systematic manipulation of the publication process:

- (1) Discrepancies in scope
- (2) Discrepancies in the description of the research reported
- (3) Discrepancies between the availability of data and the research described
- (4) Inappropriate citations
- (5) Incoherent, meaningless and/or irrelevant content included in the article
- (6) Manipulated or compromised peer review

The presence of these indicators undermines our confidence in the integrity of the article's content and we cannot, therefore, vouch for its reliability. Please note that this notice is intended solely to alert readers that the content of this article is unreliable. We have not investigated whether authors were aware of or involved in the systematic manipulation of the publication process.

Wiley and Hindawi regrets that the usual quality checks did not identify these issues before publication and have since put additional measures in place to safeguard research integrity.

We wish to credit our own Research Integrity and Research Publishing teams and anonymous and named external researchers and research integrity experts for contributing to this investigation.

The corresponding author, as the representative of all authors, has been given the opportunity to register their agreement or disagreement to this retraction. We have kept a record of any response received.

References

- [1] T. Alyas, M. Hamid, K. Alissa, T. Faiz, N. Tabassum, and A. Ahmad, "Empirical Method for Thyroid Disease Classification Using a Machine Learning Approach," *BioMed Research International*, vol. 2022, Article ID 9809932, 10 pages, 2022.

Retraction

Retracted: Assessment of Acupoint Therapy of Traditional Chinese Medicine on Cough Variant Asthma: A Meta-analysis

BioMed Research International

Received 12 March 2024; Accepted 12 March 2024; Published 20 March 2024

Copyright © 2024 BioMed Research International. This is an open access article distributed under the Creative Commons Attribution License, which permits unrestricted use, distribution, and reproduction in any medium, provided the original work is properly cited.

This article has been retracted by Hindawi following an investigation undertaken by the publisher [1]. This investigation has uncovered evidence of one or more of the following indicators of systematic manipulation of the publication process:

- (1) Discrepancies in scope
- (2) Discrepancies in the description of the research reported
- (3) Discrepancies between the availability of data and the research described
- (4) Inappropriate citations
- (5) Incoherent, meaningless and/or irrelevant content included in the article
- (6) Manipulated or compromised peer review

The presence of these indicators undermines our confidence in the integrity of the article's content and we cannot, therefore, vouch for its reliability. Please note that this notice is intended solely to alert readers that the content of this article is unreliable. We have not investigated whether authors were aware of or involved in the systematic manipulation of the publication process.

Wiley and Hindawi regrets that the usual quality checks did not identify these issues before publication and have since put additional measures in place to safeguard research integrity.

We wish to credit our own Research Integrity and Research Publishing teams and anonymous and named external researchers and research integrity experts for contributing to this investigation.

The corresponding author, as the representative of all authors, has been given the opportunity to register their agreement or disagreement to this retraction. We have kept a record of any response received.

References

- [1] H. Tu and Q. Zhang, "Assessment of Acupoint Therapy of Traditional Chinese Medicine on Cough Variant Asthma: A Meta-analysis," *BioMed Research International*, vol. 2022, Article ID 4168308, 13 pages, 2022.

Retraction

Retracted: Study on Various Luteal Characteristics Using Doppler Ultrasonography for Early Pregnancy Diagnosis in Nili-Ravi Buffaloes

BioMed Research International

Received 12 March 2024; Accepted 12 March 2024; Published 20 March 2024

Copyright © 2024 BioMed Research International. This is an open access article distributed under the Creative Commons Attribution License, which permits unrestricted use, distribution, and reproduction in any medium, provided the original work is properly cited.

This article has been retracted by Hindawi following an investigation undertaken by the publisher [1]. This investigation has uncovered evidence of one or more of the following indicators of systematic manipulation of the publication process:

- (1) Discrepancies in scope
- (2) Discrepancies in the description of the research reported
- (3) Discrepancies between the availability of data and the research described
- (4) Inappropriate citations
- (5) Incoherent, meaningless and/or irrelevant content included in the article
- (6) Manipulated or compromised peer review

The presence of these indicators undermines our confidence in the integrity of the article's content and we cannot, therefore, vouch for its reliability. Please note that this notice is intended solely to alert readers that the content of this article is unreliable. We have not investigated whether authors were aware of or involved in the systematic manipulation of the publication process.

Wiley and Hindawi regrets that the usual quality checks did not identify these issues before publication and have since put additional measures in place to safeguard research integrity.

We wish to credit our own Research Integrity and Research Publishing teams and anonymous and named

external researchers and research integrity experts for contributing to this investigation.

The corresponding author, as the representative of all authors, has been given the opportunity to register their agreement or disagreement to this retraction. We have kept a record of any response received.

References

- [1] U. Riaz, M. Hassan, M. I. Khan et al., "Study on Various Luteal Characteristics Using Doppler Ultrasonography for Early Pregnancy Diagnosis in Nili-Ravi Buffaloes," *BioMed Research International*, vol. 2022, Article ID 3896068, 6 pages, 2022.

Retraction

Retracted: CRISPR-Cas System: An Adaptive Immune System's Association with Antibiotic Resistance in Salmonella enterica Serovar Enteritidis

BioMed Research International

Received 12 March 2024; Accepted 12 March 2024; Published 20 March 2024

Copyright © 2024 BioMed Research International. This is an open access article distributed under the Creative Commons Attribution License, which permits unrestricted use, distribution, and reproduction in any medium, provided the original work is properly cited.

This article has been retracted by Hindawi following an investigation undertaken by the publisher [1]. This investigation has uncovered evidence of one or more of the following indicators of systematic manipulation of the publication process:

- (1) Discrepancies in scope
- (2) Discrepancies in the description of the research reported
- (3) Discrepancies between the availability of data and the research described
- (4) Inappropriate citations
- (5) Incoherent, meaningless and/or irrelevant content included in the article
- (6) Manipulated or compromised peer review

The presence of these indicators undermines our confidence in the integrity of the article's content and we cannot, therefore, vouch for its reliability. Please note that this notice is intended solely to alert readers that the content of this article is unreliable. We have not investigated whether authors were aware of or involved in the systematic manipulation of the publication process.

Wiley and Hindawi regrets that the usual quality checks did not identify these issues before publication and have since put additional measures in place to safeguard research integrity.

We wish to credit our own Research Integrity and Research Publishing teams and anonymous and named external researchers and research integrity experts for contributing to this investigation.

The corresponding author, as the representative of all authors, has been given the opportunity to register their agreement or disagreement to this retraction. We have kept a record of any response received.

References

- [1] M. Z. Haider, M. A. B. Shabbir, T. Yaqub et al., "CRISPR-Cas System: An Adaptive Immune System's Association with Antibiotic Resistance in Salmonella enterica Serovar Enteritidis," *BioMed Research International*, vol. 2022, Article ID 9080396, 7 pages, 2022.

Retraction

Retracted: Deleterious Effects of Amoxicillin on Immune System and Haematobiochemical Parameters of a Rabbit

BioMed Research International

Received 12 March 2024; Accepted 12 March 2024; Published 20 March 2024

Copyright © 2024 BioMed Research International. This is an open access article distributed under the Creative Commons Attribution License, which permits unrestricted use, distribution, and reproduction in any medium, provided the original work is properly cited.

This article has been retracted by Hindawi following an investigation undertaken by the publisher [1]. This investigation has uncovered evidence of one or more of the following indicators of systematic manipulation of the publication process:

- (1) Discrepancies in scope
- (2) Discrepancies in the description of the research reported
- (3) Discrepancies between the availability of data and the research described
- (4) Inappropriate citations
- (5) Incoherent, meaningless and/or irrelevant content included in the article
- (6) Manipulated or compromised peer review

The presence of these indicators undermines our confidence in the integrity of the article's content and we cannot, therefore, vouch for its reliability. Please note that this notice is intended solely to alert readers that the content of this article is unreliable. We have not investigated whether authors were aware of or involved in the systematic manipulation of the publication process.

Wiley and Hindawi regrets that the usual quality checks did not identify these issues before publication and have since put additional measures in place to safeguard research integrity.

We wish to credit our own Research Integrity and Research Publishing teams and anonymous and named external researchers and research integrity experts for contributing to this investigation.

The corresponding author, as the representative of all authors, has been given the opportunity to register their agreement or disagreement to this retraction. We have kept a record of any response received.

References

- [1] K. Hussain, M. H. Lashari, U. Farooq, and T. Mehmood, "Deleterious Effects of Amoxicillin on Immune System and Haematobiochemical Parameters of a Rabbit," *BioMed Research International*, vol. 2022, Article ID 8691261, 8 pages, 2022.

Retraction

Retracted: Acetochlor Affects Bighead Carp (*Aristichthys Nobilis*) by Producing Oxidative Stress, Lowering Tissue Proteins, and Inducing Genotoxicity

BioMed Research International

Received 12 March 2024; Accepted 12 March 2024; Published 20 March 2024

Copyright © 2024 BioMed Research International. This is an open access article distributed under the Creative Commons Attribution License, which permits unrestricted use, distribution, and reproduction in any medium, provided the original work is properly cited.

This article has been retracted by Hindawi following an investigation undertaken by the publisher [1]. This investigation has uncovered evidence of one or more of the following indicators of systematic manipulation of the publication process:

- (1) Discrepancies in scope
- (2) Discrepancies in the description of the research reported
- (3) Discrepancies between the availability of data and the research described
- (4) Inappropriate citations
- (5) Incoherent, meaningless and/or irrelevant content included in the article
- (6) Manipulated or compromised peer review

The presence of these indicators undermines our confidence in the integrity of the article's content and we cannot, therefore, vouch for its reliability. Please note that this notice is intended solely to alert readers that the content of this article is unreliable. We have not investigated whether authors were aware of or involved in the systematic manipulation of the publication process.

Wiley and Hindawi regrets that the usual quality checks did not identify these issues before publication and have since put additional measures in place to safeguard research integrity.

We wish to credit our own Research Integrity and Research Publishing teams and anonymous and named external researchers and research integrity experts for contributing to this investigation.

The corresponding author, as the representative of all authors, has been given the opportunity to register their agreement or disagreement to this retraction. We have kept a record of any response received.

References

- [1] Y. Mahmood, R. Hussain, A. Ghaffar et al., "Acetochlor Affects Bighead Carp (*Aristichthys Nobilis*) by Producing Oxidative Stress, Lowering Tissue Proteins, and Inducing Genotoxicity," *BioMed Research International*, vol. 2022, Article ID 9140060, 12 pages, 2022.

Retraction

Retracted: Growth Response in *Oryctolagus cuniculus* to Selenium Toxicity Exposure Ameliorated with Vitamin E

BioMed Research International

Received 12 March 2024; Accepted 12 March 2024; Published 20 March 2024

Copyright © 2024 BioMed Research International. This is an open access article distributed under the Creative Commons Attribution License, which permits unrestricted use, distribution, and reproduction in any medium, provided the original work is properly cited.

This article has been retracted by Hindawi following an investigation undertaken by the publisher [1]. This investigation has uncovered evidence of one or more of the following indicators of systematic manipulation of the publication process:

- (1) Discrepancies in scope
- (2) Discrepancies in the description of the research reported
- (3) Discrepancies between the availability of data and the research described
- (4) Inappropriate citations
- (5) Incoherent, meaningless and/or irrelevant content included in the article
- (6) Manipulated or compromised peer review

The presence of these indicators undermines our confidence in the integrity of the article's content and we cannot, therefore, vouch for its reliability. Please note that this notice is intended solely to alert readers that the content of this article is unreliable. We have not investigated whether authors were aware of or involved in the systematic manipulation of the publication process.

Wiley and Hindawi regrets that the usual quality checks did not identify these issues before publication and have since put additional measures in place to safeguard research integrity.

We wish to credit our own Research Integrity and Research Publishing teams and anonymous and named external researchers and research integrity experts for contributing to this investigation.

The corresponding author, as the representative of all authors, has been given the opportunity to register their agreement or disagreement to this retraction. We have kept a record of any response received.

References

- [1] R. Rehman, N. Sial, A. Ismail et al., "Growth Response in *Oryctolagus cuniculus* to Selenium Toxicity Exposure Ameliorated with Vitamin E," *BioMed Research International*, vol. 2022, Article ID 8216685, 9 pages, 2022.

Retraction

Retracted: A Novel Protein Elicitor (PELL1) Extracted from *Lecanicillium lecanii* Induced Resistance against *Bemisia tabaci* (Hemiptera: Aleyrodidae) in *Gossypium hirsutum* L

BioMed Research International

Received 12 March 2024; Accepted 12 March 2024; Published 20 March 2024

Copyright © 2024 BioMed Research International. This is an open access article distributed under the Creative Commons Attribution License, which permits unrestricted use, distribution, and reproduction in any medium, provided the original work is properly cited.

This article has been retracted by Hindawi following an investigation undertaken by the publisher [1]. This investigation has uncovered evidence of one or more of the following indicators of systematic manipulation of the publication process:

- (1) Discrepancies in scope
- (2) Discrepancies in the description of the research reported
- (3) Discrepancies between the availability of data and the research described
- (4) Inappropriate citations
- (5) Incoherent, meaningless and/or irrelevant content included in the article
- (6) Manipulated or compromised peer review

The presence of these indicators undermines our confidence in the integrity of the article's content and we cannot, therefore, vouch for its reliability. Please note that this notice is intended solely to alert readers that the content of this article is unreliable. We have not investigated whether authors were aware of or involved in the systematic manipulation of the publication process.

Wiley and Hindawi regrets that the usual quality checks did not identify these issues before publication and have since put additional measures in place to safeguard research integrity.

We wish to credit our own Research Integrity and Research Publishing teams and anonymous and named

external researchers and research integrity experts for contributing to this investigation.

The corresponding author, as the representative of all authors, has been given the opportunity to register their agreement or disagreement to this retraction. We have kept a record of any response received.

References

- [1] A. Basit, M. Yaseen, M. Babar et al., "A Novel Protein Elicitor (PELL1) Extracted from *Lecanicillium lecanii* Induced Resistance against *Bemisia tabaci* (Hemiptera: Aleyrodidae) in *Gossypium hirsutum* L," *BioMed Research International*, vol. 2022, Article ID 3097521, 8 pages, 2022.

Retraction

Retracted: Investigation on Immune-Related Protein (Heat Shock Proteins and Metallothionein) Gene Expression Changes and Liver Histopathology in Cadmium-Stressed Fish

BioMed Research International

Received 12 March 2024; Accepted 12 March 2024; Published 20 March 2024

Copyright © 2024 BioMed Research International. This is an open access article distributed under the Creative Commons Attribution License, which permits unrestricted use, distribution, and reproduction in any medium, provided the original work is properly cited.

This article has been retracted by Hindawi following an investigation undertaken by the publisher [1]. This investigation has uncovered evidence of one or more of the following indicators of systematic manipulation of the publication process:

- (1) Discrepancies in scope
- (2) Discrepancies in the description of the research reported
- (3) Discrepancies between the availability of data and the research described
- (4) Inappropriate citations
- (5) Incoherent, meaningless and/or irrelevant content included in the article
- (6) Manipulated or compromised peer review

The presence of these indicators undermines our confidence in the integrity of the article's content and we cannot, therefore, vouch for its reliability. Please note that this notice is intended solely to alert readers that the content of this article is unreliable. We have not investigated whether authors were aware of or involved in the systematic manipulation of the publication process.

Wiley and Hindawi regrets that the usual quality checks did not identify these issues before publication and have since put additional measures in place to safeguard research integrity.

We wish to credit our own Research Integrity and Research Publishing teams and anonymous and named

external researchers and research integrity experts for contributing to this investigation.

The corresponding author, as the representative of all authors, has been given the opportunity to register their agreement or disagreement to this retraction. We have kept a record of any response received.

References

- [1] G. Jabeen, S. Ishaq, M. Arshad, S. Fatima, Z. Kanwal, and F. Ali, "Investigation on Immune-Related Protein (Heat Shock Proteins and Metallothionein) Gene Expression Changes and Liver Histopathology in Cadmium-Stressed Fish," *BioMed Research International*, vol. 2022, Article ID 2075791, 11 pages, 2022.

Retraction

Retracted: Biologically Synthesized Peptides Show Remarkable Inhibition Activity against Angiotensin-Converting Enzyme: A Promising Approach for Peptide Development against Autoimmune Diseases

BioMed Research International

Received 12 March 2024; Accepted 12 March 2024; Published 20 March 2024

Copyright © 2024 BioMed Research International. This is an open access article distributed under the Creative Commons Attribution License, which permits unrestricted use, distribution, and reproduction in any medium, provided the original work is properly cited.

This article has been retracted by Hindawi following an investigation undertaken by the publisher [1]. This investigation has uncovered evidence of one or more of the following indicators of systematic manipulation of the publication process:

- (1) Discrepancies in scope
- (2) Discrepancies in the description of the research reported
- (3) Discrepancies between the availability of data and the research described
- (4) Inappropriate citations
- (5) Incoherent, meaningless and/or irrelevant content included in the article
- (6) Manipulated or compromised peer review

The presence of these indicators undermines our confidence in the integrity of the article's content and we cannot, therefore, vouch for its reliability. Please note that this notice is intended solely to alert readers that the content of this article is unreliable. We have not investigated whether authors were aware of or involved in the systematic manipulation of the publication process.

Wiley and Hindawi regrets that the usual quality checks did not identify these issues before publication and have since put additional measures in place to safeguard research integrity.

We wish to credit our own Research Integrity and Research Publishing teams and anonymous and named external researchers and research integrity experts for contributing to this investigation.

The corresponding author, as the representative of all authors, has been given the opportunity to register their agreement or disagreement to this retraction. We have kept a record of any response received.

References

- [1] N. Mujtaba, N. Jahan, A. Jamal et al., "Biologically Synthesized Peptides Show Remarkable Inhibition Activity against Angiotensin-Converting Enzyme: A Promising Approach for Peptide Development against Autoimmune Diseases," *BioMed Research International*, vol. 2022, Article ID 2396192, 12 pages, 2022.

Retraction

Retracted: Correlation Analysis of Cytochrome P450 SNPs in Hepatitis B-Caused Cirrhosis Patients

BioMed Research International

Received 12 March 2024; Accepted 12 March 2024; Published 20 March 2024

Copyright © 2024 BioMed Research International. This is an open access article distributed under the Creative Commons Attribution License, which permits unrestricted use, distribution, and reproduction in any medium, provided the original work is properly cited.

This article has been retracted by Hindawi following an investigation undertaken by the publisher [1]. This investigation has uncovered evidence of one or more of the following indicators of systematic manipulation of the publication process:

- (1) Discrepancies in scope
- (2) Discrepancies in the description of the research reported
- (3) Discrepancies between the availability of data and the research described
- (4) Inappropriate citations
- (5) Incoherent, meaningless and/or irrelevant content included in the article
- (6) Manipulated or compromised peer review

The presence of these indicators undermines our confidence in the integrity of the article's content and we cannot, therefore, vouch for its reliability. Please note that this notice is intended solely to alert readers that the content of this article is unreliable. We have not investigated whether authors were aware of or involved in the systematic manipulation of the publication process.

Wiley and Hindawi regrets that the usual quality checks did not identify these issues before publication and have since put additional measures in place to safeguard research integrity.

We wish to credit our own Research Integrity and Research Publishing teams and anonymous and named external researchers and research integrity experts for contributing to this investigation.

The corresponding author, as the representative of all authors, has been given the opportunity to register their agreement or disagreement to this retraction. We have kept a record of any response received.

References

- [1] Q.-Y. Li, X. Yang, and Z.-Z. Guo, "Correlation Analysis of Cytochrome P450 SNPs in Hepatitis B-Caused Cirrhosis Patients," *BioMed Research International*, vol. 2022, Article ID 9891184, 8 pages, 2022.

Retraction

Retracted: Therapeutic Significance of Serpina3n Subsequent Cerebral Ischemia via Cytotoxic Granzyme B Inactivation

BioMed Research International

Received 12 March 2024; Accepted 12 March 2024; Published 20 March 2024

Copyright © 2024 BioMed Research International. This is an open access article distributed under the Creative Commons Attribution License, which permits unrestricted use, distribution, and reproduction in any medium, provided the original work is properly cited.

This article has been retracted by Hindawi following an investigation undertaken by the publisher [1]. This investigation has uncovered evidence of one or more of the following indicators of systematic manipulation of the publication process:

- (1) Discrepancies in scope
- (2) Discrepancies in the description of the research reported
- (3) Discrepancies between the availability of data and the research described
- (4) Inappropriate citations
- (5) Incoherent, meaningless and/or irrelevant content included in the article
- (6) Manipulated or compromised peer review

The presence of these indicators undermines our confidence in the integrity of the article's content and we cannot, therefore, vouch for its reliability. Please note that this notice is intended solely to alert readers that the content of this article is unreliable. We have not investigated whether authors were aware of or involved in the systematic manipulation of the publication process.

Wiley and Hindawi regrets that the usual quality checks did not identify these issues before publication and have since put additional measures in place to safeguard research integrity.

We wish to credit our own Research Integrity and Research Publishing teams and anonymous and named external researchers and research integrity experts for contributing to this investigation.

The corresponding author, as the representative of all authors, has been given the opportunity to register their agreement or disagreement to this retraction. We have kept a record of any response received.

References

- [1] M. S. Aslam, M. S. Aslam, K. S. Aslam, A. Iqbal, and L. Yuan, "Therapeutic Significance of Serpina3n Subsequent Cerebral Ischemia via Cytotoxic Granzyme B Inactivation," *BioMed Research International*, vol. 2022, Article ID 1557010, 13 pages, 2022.

Retraction

Retracted: Exploration of ACE-Inhibiting Peptides Encrypted in *Artemisia annua* Using *In Silico* Approach

BioMed Research International

Received 12 March 2024; Accepted 12 March 2024; Published 20 March 2024

Copyright © 2024 BioMed Research International. This is an open access article distributed under the Creative Commons Attribution License, which permits unrestricted use, distribution, and reproduction in any medium, provided the original work is properly cited.

This article has been retracted by Hindawi following an investigation undertaken by the publisher [1]. This investigation has uncovered evidence of one or more of the following indicators of systematic manipulation of the publication process:

- (1) Discrepancies in scope
- (2) Discrepancies in the description of the research reported
- (3) Discrepancies between the availability of data and the research described
- (4) Inappropriate citations
- (5) Incoherent, meaningless and/or irrelevant content included in the article
- (6) Manipulated or compromised peer review

The presence of these indicators undermines our confidence in the integrity of the article's content and we cannot, therefore, vouch for its reliability. Please note that this notice is intended solely to alert readers that the content of this article is unreliable. We have not investigated whether authors were aware of or involved in the systematic manipulation of the publication process.

Wiley and Hindawi regrets that the usual quality checks did not identify these issues before publication and have since put additional measures in place to safeguard research integrity.

We wish to credit our own Research Integrity and Research Publishing teams and anonymous and named external researchers and research integrity experts for contributing to this investigation.

The corresponding author, as the representative of all authors, has been given the opportunity to register their agreement or disagreement to this retraction. We have kept a record of any response received.

References

- [1] M. N. Shahid, M. Zawar, A. Jamal, B. B. Mohamed, S. Khalid, and F. S. Bahwerth, "Exploration of ACE-Inhibiting Peptides Encrypted in *Artemisia annua* Using *In Silico* Approach," *BioMed Research International*, vol. 2022, Article ID 5367125, 10 pages, 2022.

Retraction

Retracted: Diversity of Rotavirus Strains among Children with Acute Diarrhea in Karachi, Pakistan

BioMed Research International

Received 12 March 2024; Accepted 12 March 2024; Published 20 March 2024

Copyright © 2024 BioMed Research International. This is an open access article distributed under the Creative Commons Attribution License, which permits unrestricted use, distribution, and reproduction in any medium, provided the original work is properly cited.

This article has been retracted by Hindawi following an investigation undertaken by the publisher [1]. This investigation has uncovered evidence of one or more of the following indicators of systematic manipulation of the publication process:

- (1) Discrepancies in scope
- (2) Discrepancies in the description of the research reported
- (3) Discrepancies between the availability of data and the research described
- (4) Inappropriate citations
- (5) Incoherent, meaningless and/or irrelevant content included in the article
- (6) Manipulated or compromised peer review

The presence of these indicators undermines our confidence in the integrity of the article's content and we cannot, therefore, vouch for its reliability. Please note that this notice is intended solely to alert readers that the content of this article is unreliable. We have not investigated whether authors were aware of or involved in the systematic manipulation of the publication process.

Wiley and Hindawi regrets that the usual quality checks did not identify these issues before publication and have since put additional measures in place to safeguard research integrity.

We wish to credit our own Research Integrity and Research Publishing teams and anonymous and named external researchers and research integrity experts for contributing to this investigation.

The corresponding author, as the representative of all authors, has been given the opportunity to register their agreement or disagreement to this retraction. We have kept a record of any response received.

References

- [1] N. T. Bukhari, G. Parveen, P. A. Ali et al., "Diversity of Rotavirus Strains among Children with Acute Diarrhea in Karachi, Pakistan," *BioMed Research International*, vol. 2022, Article ID 5231910, 6 pages, 2022.

Retraction

Retracted: Biologically Synthesized Copper Nanoparticles Show Considerable Degradation of Reactive Red 81 Dye: An Eco-Friendly Sustainable Approach

BioMed Research International

Received 12 March 2024; Accepted 12 March 2024; Published 20 March 2024

Copyright © 2024 BioMed Research International. This is an open access article distributed under the Creative Commons Attribution License, which permits unrestricted use, distribution, and reproduction in any medium, provided the original work is properly cited.

This article has been retracted by Hindawi following an investigation undertaken by the publisher [1]. This investigation has uncovered evidence of one or more of the following indicators of systematic manipulation of the publication process:

- (1) Discrepancies in scope
- (2) Discrepancies in the description of the research reported
- (3) Discrepancies between the availability of data and the research described
- (4) Inappropriate citations
- (5) Incoherent, meaningless and/or irrelevant content included in the article
- (6) Manipulated or compromised peer review

The presence of these indicators undermines our confidence in the integrity of the article's content and we cannot, therefore, vouch for its reliability. Please note that this notice is intended solely to alert readers that the content of this article is unreliable. We have not investigated whether authors were aware of or involved in the systematic manipulation of the publication process.

Wiley and Hindawi regrets that the usual quality checks did not identify these issues before publication and have since put additional measures in place to safeguard research integrity.

We wish to credit our own Research Integrity and Research Publishing teams and anonymous and named external researchers and research integrity experts for contributing to this investigation.

The corresponding author, as the representative of all authors, has been given the opportunity to register their agreement or disagreement to this retraction. We have kept a record of any response received.

References

- [1] M. A. Rafique, A. Jamal, Z. Ali et al., "Biologically Synthesized Copper Nanoparticles Show Considerable Degradation of Reactive Red 81 Dye: An Eco-Friendly Sustainable Approach," *BioMed Research International*, vol. 2022, Article ID 7537955, 9 pages, 2022.

Retraction

Retracted: Training a Feedforward Neural Network Using Hybrid Gravitational Search Algorithm with Dynamic Multiswarm Particle Swarm Optimization

BioMed Research International

Received 12 March 2024; Accepted 12 March 2024; Published 20 March 2024

Copyright © 2024 BioMed Research International. This is an open access article distributed under the Creative Commons Attribution License, which permits unrestricted use, distribution, and reproduction in any medium, provided the original work is properly cited.

This article has been retracted by Hindawi following an investigation undertaken by the publisher [1]. This investigation has uncovered evidence of one or more of the following indicators of systematic manipulation of the publication process:

- (1) Discrepancies in scope
- (2) Discrepancies in the description of the research reported
- (3) Discrepancies between the availability of data and the research described
- (4) Inappropriate citations
- (5) Incoherent, meaningless and/or irrelevant content included in the article
- (6) Manipulated or compromised peer review

The presence of these indicators undermines our confidence in the integrity of the article's content and we cannot, therefore, vouch for its reliability. Please note that this notice is intended solely to alert readers that the content of this article is unreliable. We have not investigated whether authors were aware of or involved in the systematic manipulation of the publication process.

Wiley and Hindawi regrets that the usual quality checks did not identify these issues before publication and have since put additional measures in place to safeguard research integrity.

We wish to credit our own Research Integrity and Research Publishing teams and anonymous and named external researchers and research integrity experts for contributing to this investigation.

The corresponding author, as the representative of all authors, has been given the opportunity to register their agreement or disagreement to this retraction. We have kept a record of any response received.

References

- [1] A. A. Nagra, T. Alyas, M. Hamid, N. Tabassum, and A. Ahmad, "Training a Feedforward Neural Network Using Hybrid Gravitational Search Algorithm with Dynamic Multiswarm Particle Swarm Optimization," *BioMed Research International*, vol. 2022, Article ID 2636515, 10 pages, 2022.

Retraction

Retracted: Divergent Analyses of Genetic Relatedness and Evidence-Based Assessment of Therapeutics of *Staphylococcus aureus* from Semi-intensive Dairy Systems

BioMed Research International

Received 12 March 2024; Accepted 12 March 2024; Published 20 March 2024

Copyright © 2024 BioMed Research International. This is an open access article distributed under the Creative Commons Attribution License, which permits unrestricted use, distribution, and reproduction in any medium, provided the original work is properly cited.

This article has been retracted by Hindawi following an investigation undertaken by the publisher [1]. This investigation has uncovered evidence of one or more of the following indicators of systematic manipulation of the publication process:

- (1) Discrepancies in scope
- (2) Discrepancies in the description of the research reported
- (3) Discrepancies between the availability of data and the research described
- (4) Inappropriate citations
- (5) Incoherent, meaningless and/or irrelevant content included in the article
- (6) Manipulated or compromised peer review

The presence of these indicators undermines our confidence in the integrity of the article's content and we cannot, therefore, vouch for its reliability. Please note that this notice is intended solely to alert readers that the content of this article is unreliable. We have not investigated whether authors were aware of or involved in the systematic manipulation of the publication process.

Wiley and Hindawi regrets that the usual quality checks did not identify these issues before publication and have since put additional measures in place to safeguard research integrity.

We wish to credit our own Research Integrity and Research Publishing teams and anonymous and named external researchers and research integrity experts for contributing to this investigation.

The corresponding author, as the representative of all authors, has been given the opportunity to register their agreement or disagreement to this retraction. We have kept a record of any response received.

References

- [1] S. Aziz, N. M. Saeed, H. O. Dyary et al., "Divergent Analyses of Genetic Relatedness and Evidence-Based Assessment of Therapeutics of *Staphylococcus aureus* from Semi-intensive Dairy Systems," *BioMed Research International*, vol. 2022, Article ID 5313654, 13 pages, 2022.

Retraction

Retracted: ZOMEK via the p-Akt/Nrf2 Pathway Restored PTZ-Induced Oxidative Stress-Mediated Memory Dysfunction in Mouse Model

BioMed Research International

Received 12 March 2024; Accepted 12 March 2024; Published 20 March 2024

Copyright © 2024 BioMed Research International. This is an open access article distributed under the Creative Commons Attribution License, which permits unrestricted use, distribution, and reproduction in any medium, provided the original work is properly cited.

This article has been retracted by Hindawi following an investigation undertaken by the publisher [1]. This investigation has uncovered evidence of one or more of the following indicators of systematic manipulation of the publication process:

- (1) Discrepancies in scope
- (2) Discrepancies in the description of the research reported
- (3) Discrepancies between the availability of data and the research described
- (4) Inappropriate citations
- (5) Incoherent, meaningless and/or irrelevant content included in the article
- (6) Manipulated or compromised peer review

The presence of these indicators undermines our confidence in the integrity of the article's content and we cannot, therefore, vouch for its reliability. Please note that this notice is intended solely to alert readers that the content of this article is unreliable. We have not investigated whether authors were aware of or involved in the systematic manipulation of the publication process.

Wiley and Hindawi regrets that the usual quality checks did not identify these issues before publication and have since put additional measures in place to safeguard research integrity.

We wish to credit our own Research Integrity and Research Publishing teams and anonymous and named external researchers and research integrity experts for contributing to this investigation.

The corresponding author, as the representative of all authors, has been given the opportunity to register their agreement or disagreement to this retraction. We have kept a record of any response received.

References

- [1] R. Jahan, M. Yousof, H. Khan et al., "ZOMEK via the p-Akt/Nrf2 Pathway Restored PTZ-Induced Oxidative Stress-Mediated Memory Dysfunction in Mouse Model," *BioMed Research International*, vol. 2022, Article ID 8902262, 14 pages, 2022.

Research Article

ZOMEK via the p-Akt/Nrf2 Pathway Restored PTZ-Induced Oxidative Stress-Mediated Memory Dysfunction in Mouse Model

Rifat Jahan ^{1,2}, Mohammad Yousaf ¹, Hamayun Khan ¹, Nousheen Bibi,³
Musarrat Ijaz,⁴ Touseef Rehan,⁵ and Shahid Ali Shah⁶

¹Department of Chemistry Islamia College University, Peshawar 25120, Pakistan

²Department of Biochemistry, Shaheed Benazir Bhutto Women University, Peshawar, Pakistan

³Department of Bioinformatics, Shaheed Benazir Bhutto Women University, Peshawar, Pakistan

⁴Department of Statistics, Shaheed Benazir Bhutto Women University, Peshawar, Pakistan

⁵Department of Food and Nutrition, Shaheed Benazir Bhutto Women University, Peshawar, Pakistan

⁶Neuro Molecular Medicine Research Center Peshawar, Pakistan

Correspondence should be addressed to Rifat Jahan; rifatchem@sbbwu.edu.pk
and Mohammad Yousaf; yousaf672010@hotmail.com

Received 20 May 2022; Accepted 12 August 2022; Published 19 September 2022

Academic Editor: Gulnaz Afzal

Copyright © 2022 Rifat Jahan et al. This is an open access article distributed under the Creative Commons Attribution License, which permits unrestricted use, distribution, and reproduction in any medium, provided the original work is properly cited.

A new mechanistic approach to overcome the neurodegenerative disorders caused by oxidative stress in Alzheimer's disease (AD) is highly stressed in this article. Thus, a newly formulated drug (zinc *ortho*-methyl carbonodithioate (ZOMEK)) was investigated for five weeks on seven-week-old BALB/c male mice. ZOMEK 30 mg/kg was postadministered intraperitoneally during the third week of pentylenetetrazole (PTZ) injection. The brain homogenates of the mice were evaluated for their antioxidant potential for ZOMEK. The results including catalase (CAT), glutathione S transferase (GST), and lipid peroxidation (LPO) demonstrated that ZOMEK significantly reverted the oxidative stress stimulated by PTZ in the mouse brain. ZOMEK upregulated p-Akt/Nrf-2 pathways (also supported by molecular docking methods) to revoke PTZ-induced apoptotic protein markers. ZOMEK reversed PTZ-induced neuronal synapse deficits, improved oxidative stress-aided memory impairment, and inhibited the amyloidogenic pathway in mouse brains. The results suggested the potential of ZOMEK as a new, safe, and neurotherapeutic agent to cure neurodegenerative disorders by decreasing AD-like neuropathology in the animal PTZ model.

1. Introduction

Alzheimer's disease (AD) in the brain has been accounted to possess a huge amount of oxidative stress and burden accompanied by the accumulation of both amyloid-beta ($A\beta$ as plaques) and hyperphosphorylated protein [1]. As per reported literature, several metals such as zinc, iron, and copper have a key role in amyloid accumulation and neurodegeneration [2]. Smart studies have reported that both copper and zinc can bind firmly with the N-terminal metal-binding domain of $A\beta$ and its precursor proteins [3, 4]. Moreover, a huge amount of zinc is involved both in memory and cognitive sites of the brain especially the hippocampus being severely damaged during observing AD fea-

tures [5, 6]. At physiological conditions, there is a balance between the reactive oxygen species (ROS) and antioxidants, but it could be damaged by severity of ROS which makes antioxidant defense less efficient; thus, neurodegeneration occurs and results in cell death [7]. These oxidative and anti-oxidative mechanisms are balanced by certain molecules, such as nuclear factor erythroid 2-related factor-2 (Nrf-2) and heme oxygenase-1 (HO-1) in normal conditions. Briefly, when Nrf-2 is exposed to oxidative stress, it is transported to the nucleus where it initiates antioxidant mechanisms [8]. This translocation of Nrf-2 results in the transcription of several antioxidant proteins like heme oxygenase-1 (HO-1), glutathione (GSH), and catalase to spread the oxidative stress and protect the cell from

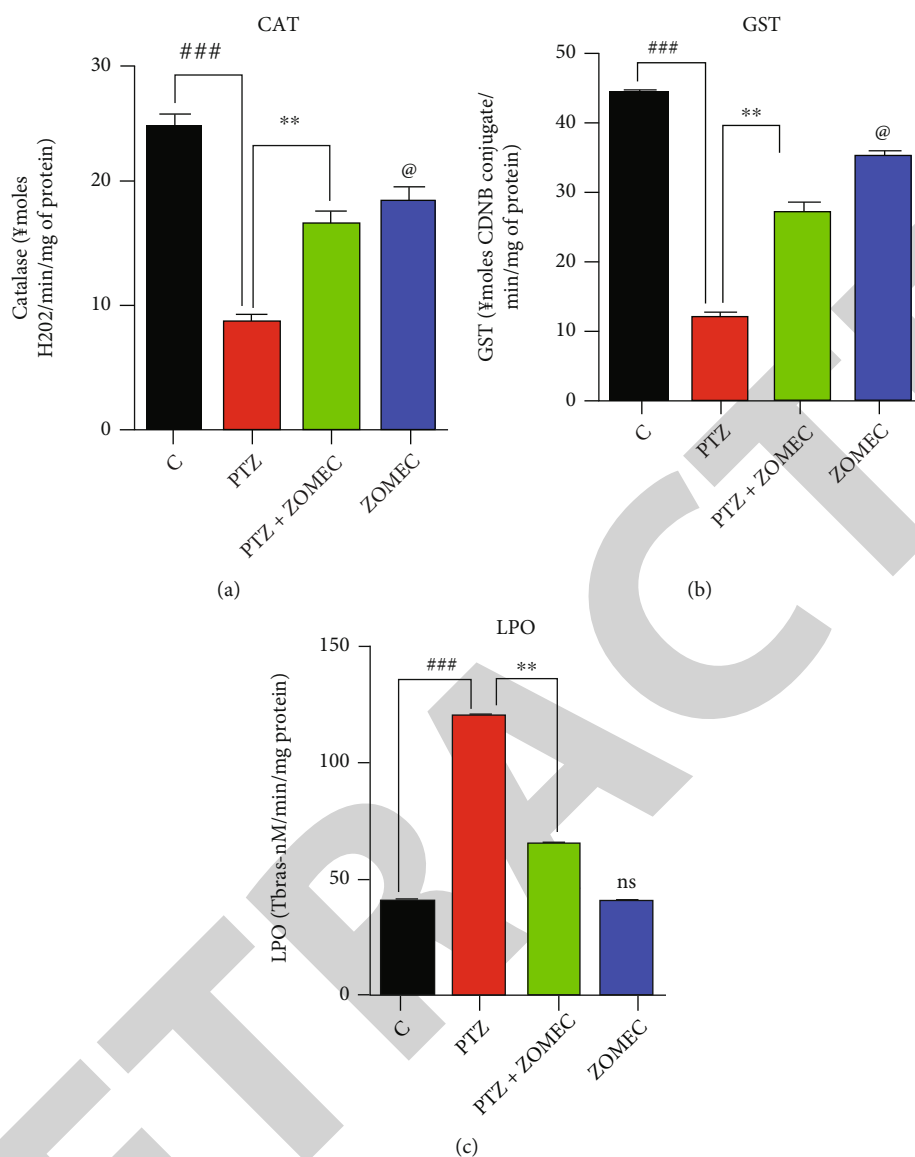


FIGURE 1: ZOME reduced PTZ-induced oxidative stress. Shown are the different antioxidant enzyme assays including (a) CAT, (b) GST, and (c) LPO. Significance: ### $p \leq 0.001$, ** $p \leq 0.01$, @ $p \leq 0.05$, and ns = no significance.

apoptosis and inflammation [9, 10]. Further, phosphorylated Akt is regarded as a signal of cell growth and antiapoptosis, while its reduced levels increase the apoptosis by enhancing proapoptotic BAX and BAX/Bcl-2 ratios [11]. A proapoptotic BAX protein that damages the mitochondrial outer membrane and releases cytochrome C activates caspases and finally damages PARP-1 production [12–14]. An antiapoptotic Bcl-2 protein is associated with the outer membrane of mitochondria and can reduce the release of cytochrome C [15]. So the elevated oxidative stress induces cellular abnormalities, impairs the DNA, and leads to dysfunction of mitochondrial energy production, all of which may help in the progression of aging processes and neurodegenerative disease [16]. There are several reported agents like organotin complexes, biomaterials, prodrugs, and biocompatible drug carriers to treat and reduce the oxidative stress overcoming the neurodegenerative disorder [17–24].

Several compounds are used as seizure-inducing drugs, i.e., kainic acid, pilocarpine, and pentylenetetrazole (PTZ) [25], where PTZ drug is the most commonly used models for screening anticonvulsants and anticonvulsants. PTZ is a GABA-A antagonist that is noncompetitive [26]. PTZ kindling is reported to cause a change in the level of neurotransmitters (GABA, glutamate, DA, NE, 5-HT, and their metabolites) in the mouse's brains, in addition to decreasing the oxidative stress, neuroinflammation, and neurodegeneration [27, 28]. Nerve cell death is an energy-dependent molecular cascade process that is highly ordered and involves new gene transcription. An increase in oxidative stress is involved in abnormal nerve function. On the other hand, cell apoptosis occurs in AD. Caspases and BCL2 proteins are two major families that lead to nerve cell death in neurodegenerative diseases [29]. Donepezil (Aricept) is a drug that is used for the treatment of all the stages of AD.

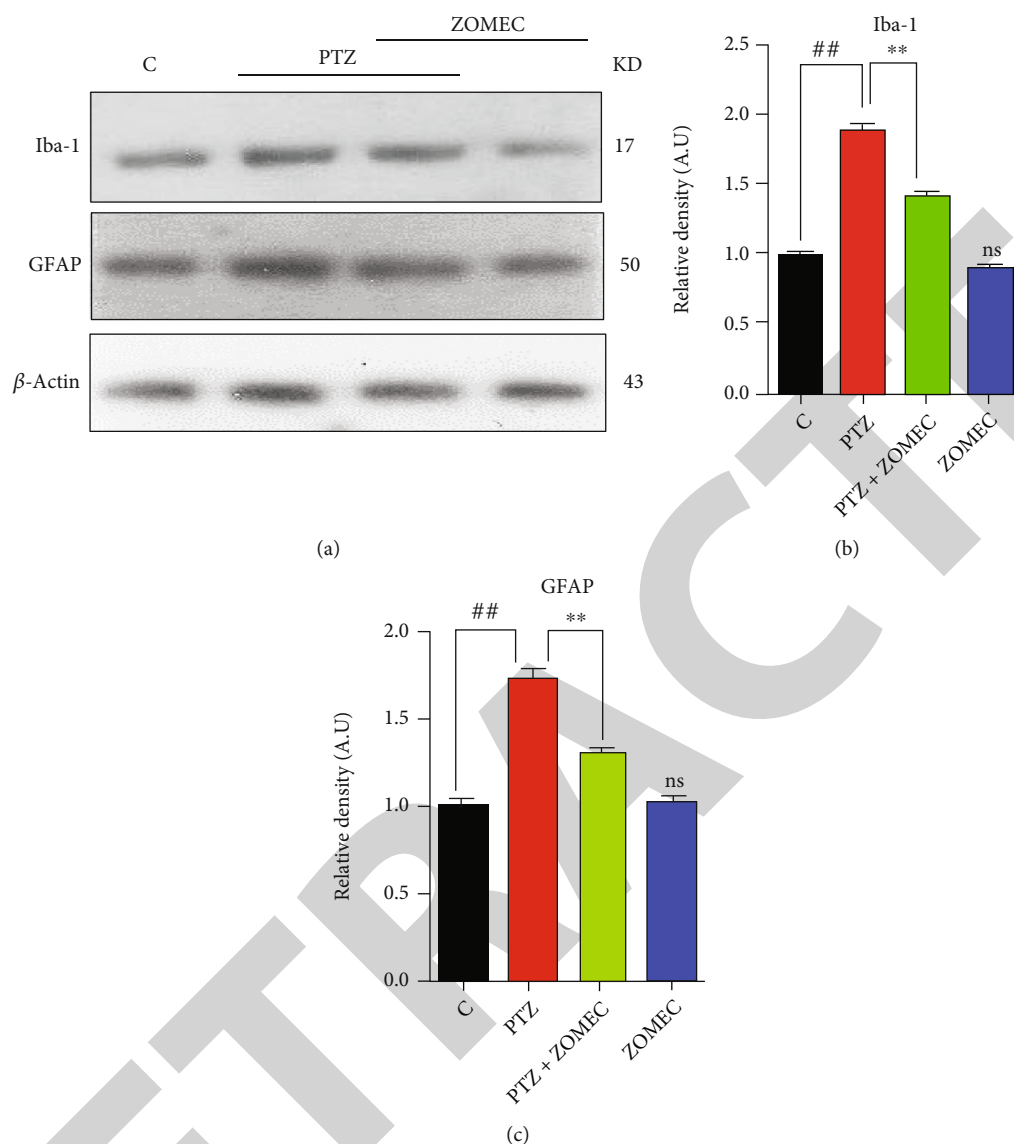


FIGURE 2: Activated glial cells (PTZ-induced) were deactivation by our test drug ZOMECE. (a) Shown are the immunoblots of glial cells, Iba-1 and GFAP (both microglia and astrocytes). (b) Histogram of microglia. (c) Histogram of astrocytes. Significance: ## $p \leq 0.01$, ** $p \leq 0.01$, and ns = no significance.

Galantamine (Razadyne) and rivastigmine (Exelon) are approved for the treatment of AD patients (mild to moderate). Besides these, memantine extended release and donepezil (Namzaric), memantine (Namenda), azeliragon, pioglitazone, troriluzole, zagotenemab, intepirdine, lumateperone, suvorexant, and aripiprazole are used to treat AD patients [30].

Previous reports recommend that AD affects the endogenous defense system of the body by decreasing the antioxidant concentration. When the antioxidant system of an organism fails to overcome oxidative stress, cellular damage occurs and oxidants accumulate principally in the mitochondria [31]. It is well known through various studies that the oxygen radicals are removed from the body and the cells are rescued by antioxidants such as superoxide dismutase (SOD). Researchers have emphasized and found good results after developing safe and

effective antioxidants that could help to prevent neurodegenerative diseases. Considering such neurodegenerative diseases, the therapeutic potential of ZOMECE as a neuroprotective and antioxidant agent was evaluated by using PTZ-induced oxidative stress in BALB/c mice.

The current study is aimed at investigating the new therapeutic agent; ZOMECE was evaluated in reducing PTZ-induced ROS-mediated neuronal synapse deficits, memory and cognition, and $A\beta$ in the brain of mice.

2. Materials and Methods

2.1. Preparation of ZOMECE. ZOMECE was prepared as per the reported procedure mentioned in Figure SI (supplementary materials) [32].

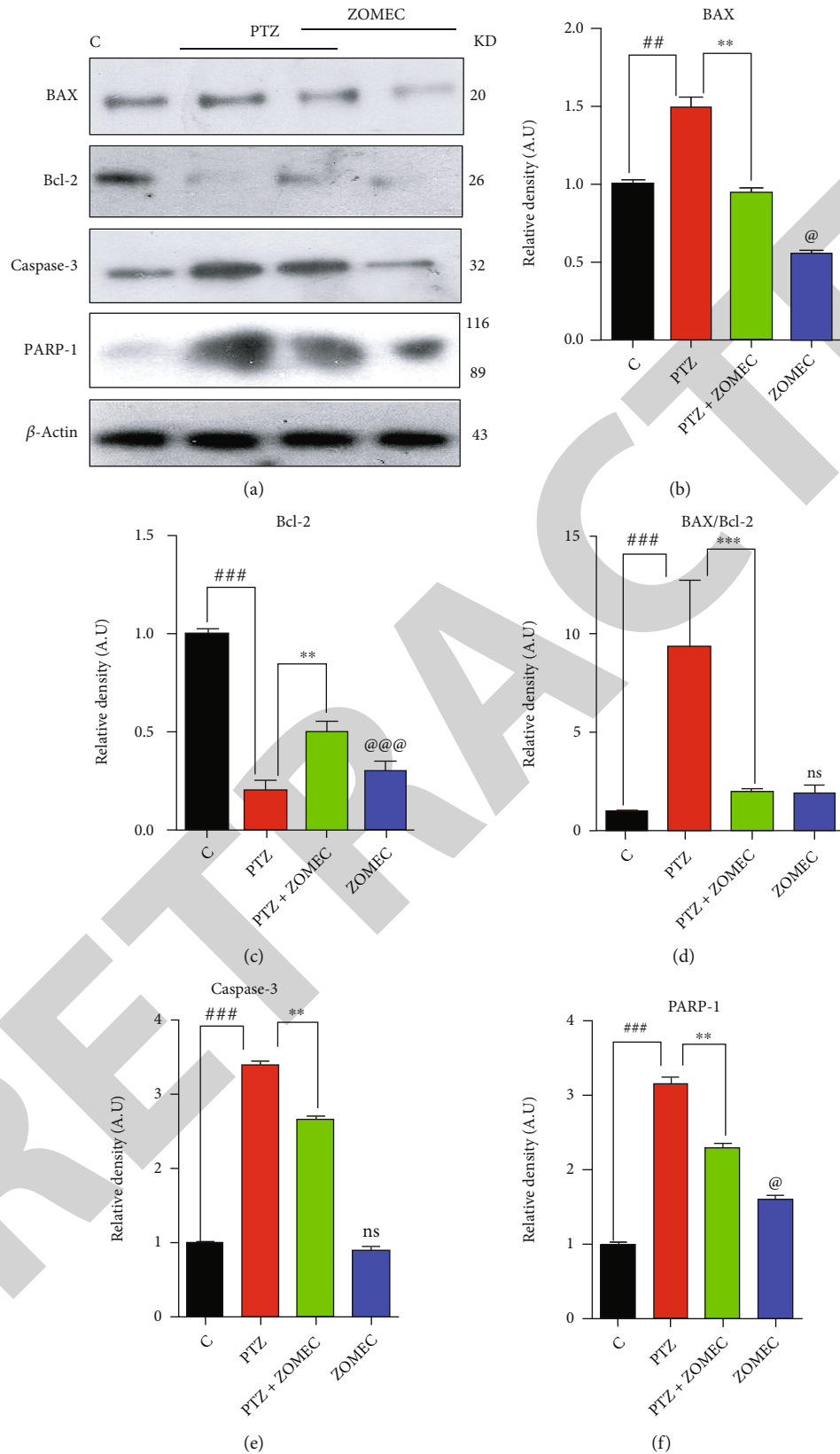


FIGURE 3: ZOMEK reduced PTZ-induced neuroapoptosis in adult mice. Shown are the different apoptotic protein markers including (a) immunoblot of BAX, Bcl2, BAX/Bcl2, caspase-3, and PARP-1, while histograms of all the markers are shown as (b) BAX, (c) Bcl2, (d) BAX/Bcl2, (e) caspase-3, and (f) PARP-1. Significance: ### $p \leq 0.001$, ## $p \leq 0.01$, *** $p \leq 0.001$, ** $p \leq 0.01$, @ $p \leq 0.05$, @@@ $p \leq 0.001$, and ns = no significance.

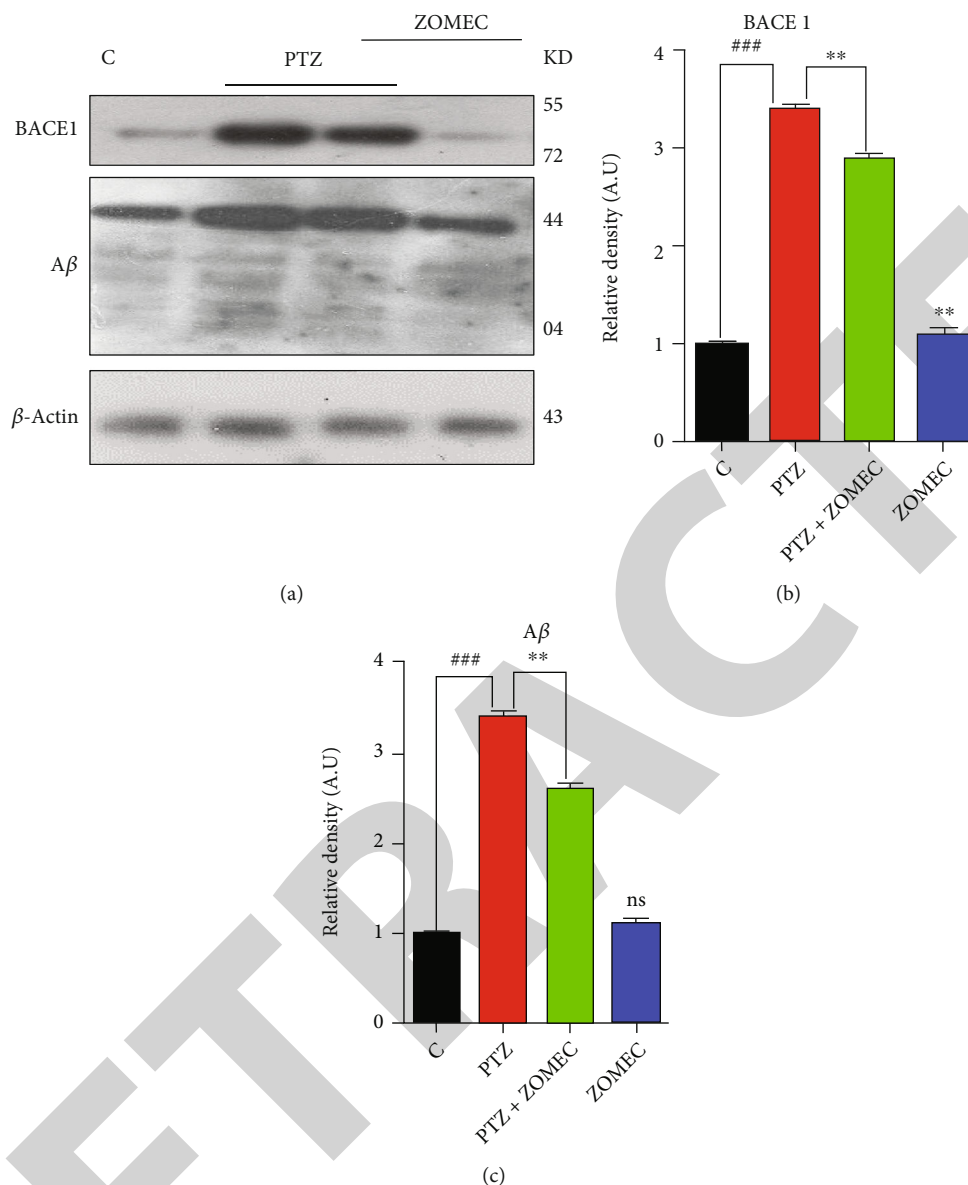


FIGURE 4: ZOMEK significantly downregulated Aβ accumulation and BACE1 production in mouse brains. Shown are the western blot results of Aβ and BACE1. (a) Immunoblot of Aβ and BACE1. (b) Histogram of Aβ. (c) BACE1. These representative bar graphs show the relative density of proteins in the selected groups. Significance: ### $p \leq 0.001$, ** $p \leq 0.01$, and ns = no significance.

2.2. Animals and Drug Treatment. The solutions were prepared in a saline solution of 0.9% while ZOMEK (administered after the third week on daily basis) was dissolved in DMSO and diluted with saline water (0.9% NaCl). Each mouse group was intraperitoneally (I.P.) injected. The control group was injected with normal saline only. The experimental procedures were performed with all the measures established by the Ethics Committee of the NMMRC (Neuro Molecular Medicine Research Center reference no. 22/2020) according to the guidelines of NIH (International Institute of Health, USA). Seven-week-old BALB/c male mice were selected for the experiments. The treatment groups included a control group (saline), PTZ group (35 mg/kg BW), PTZ +ZOMEK group (35 mg/kg BW and 30 mg/kg BW, respec-

tively), and ZOMEK group (30 mg/kg BW). PTZ was administered on alternative days for five weeks intraperitoneally.

2.3. Behavioral Tests

2.3.1. Morris Water Maze (MWM). MWM test was performed to evaluate the long-term memory and spatial learning of the mice [33].

2.3.2. Y-Maze (YM). The YM test was performed to study the mouse's exploratory behavior [33].

2.4. Collection of Brain Tissue. After five weeks of PTZ and ZOMEK treatment, the animals ($n = 5$ /group) were sacrificed (chloroform was used to anesthetize mice). The brains

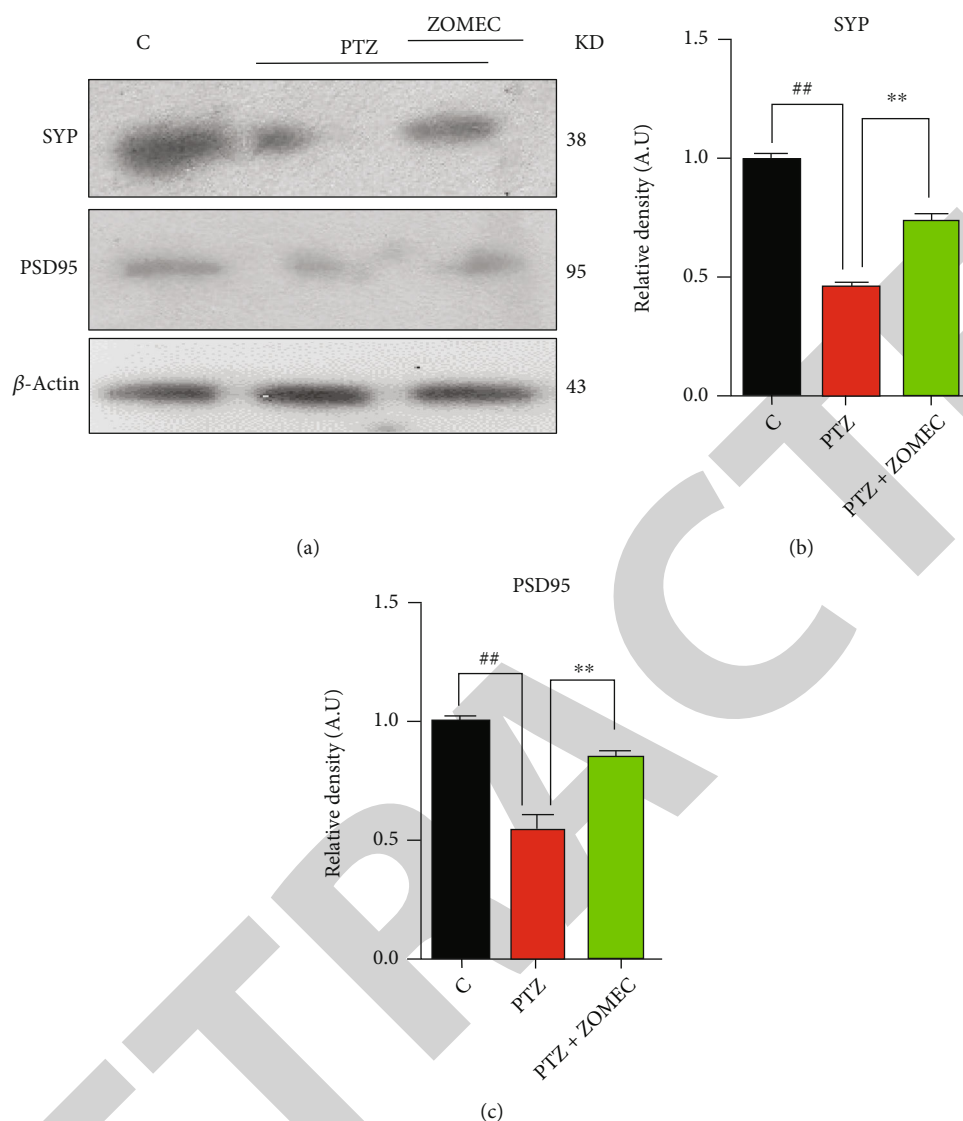


FIGURE 5: ZOMEK increased SYP and PSD95 activities in the brain ($n = 5$ animals/group). (a) Immunoblot of SYP and PSD95. (b) The histogram shows a significant increase of SYP levels in the PTZ+ZOMEK group. (c) Significant increase of PSD95 activity with the administration of ZOMEK. Significance: ## $p \leq 0.01$ and ** $p \leq 0.01$.

were dissected, and the required cortical brain parts were carefully removed and placed in a Petri dish containing phosphate buffer saline (PBS) and RNA lysis buffer in a 1:1 solution for about sixty seconds and then frozen in dry ice.

2.5. Antioxidant Activity of ZOMEK

2.5.1. Glutathione S Transferase (GST) Level. GST activity was measured using 1-chloro-2,4-dinitrobenzene (CDNB). Each well was filled with a mixture of 1mM CDNB (10 μ L), 5mM reduced glutathione (10 μ L), buffer solution (270 μ L), and the sample (10 μ L). The absorbance was noted at 340 nm [34]. The kit used was GST catalog no. AB3282 (Sigma-Aldrich).

2.5.2. Catalase Activity. Sigma-Aldrich kit (Cat. C0979) was used to determine catalase activity. To 50 mM sodium phosphate buffer (340 μ L) at pH 7.0, the brain tissue supernatant

(100 μ L) was added. The mixture was incubated for five minutes with 2 M H_2O_2 (150 μ L). Absorbance was noted at 240 nm for three minutes [35].

2.5.3. Determining Concentration of Lipid Peroxidation. In the current study, LPO assay kit catalog no. MAK085 was used. Malondialdehyde level of the mouse brain was found by boiling a mixture of the brain tissue supernatant (100 μ L), 8.1% of SDS solution (100 μ L), 20% of acetic acid (375 μ L), and 0.25% of thiobarbituric acid (1 mL of TBA) for 1 h. After boiling, 200 μ L of the mixture was pipetted into a ninety-six-well plate, and absorbance was noted at 532 nm. MDA levels were extrapolated from the MDA standard curve of plotted concentrations [34].

2.6. Western Blot Analysis. The brain tissues were homogenized in 0.01 M PBS containing a protease inhibitor cocktail. After centrifugation, the protein samples were subjected to

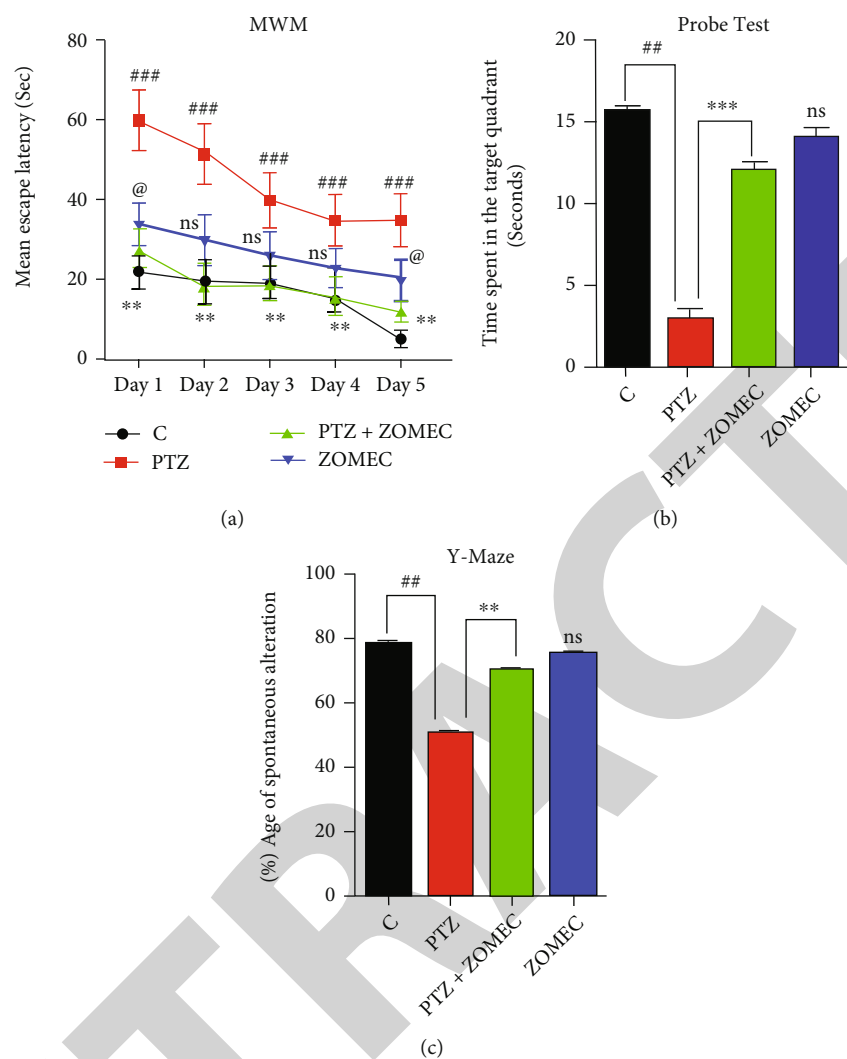


FIGURE 6: ZOMEK successfully reversed PTZ-induced memory dysfunction in mice ($n = 5$ animals/group). (a) Given are the results for mean escape latency of the MWM for all four experimental groups for five days. (b) Probe test: performed during MWM on day sixth when the submerged stand was absent. (c) The percent spontaneous alteration of selected mouse groups in Y-maze. Significance: ## $p \leq 0.01$, *** $p \leq 0.001$, ** $p \leq 0.01$, @ $p \leq 0.05$, and ns = no significance.

quantification and were run through SDS-PAGE on 15% gels under reducing conditions and then shifted onto a polyvinylidene fluoride membrane (PVDF). The broad range protein marker 10-250 KD (Precision Plus Protein Standards, Kaleidoscope, Bio-Rad) was run to find out the molecular weights of the proteins. 5 μ L of the primary antibody was taken in 7 mL of Tris buffer saline tween (TBST) solution. Primary antibodies ionized calcium-binding adaptor molecule 1 (Iba-1; sc-32725), glial fibrillary acidic protein (GFAP; sc-33673), nuclear factor-erythroid factor 2-related factor 2 (Nrf-2; sc-365949), heme oxygenase (HO-1; sc-136960), phosphorylated protein kinase B (p-Akt; sc-514032), BCL2-associated X protein (BAX; sc-7480), B cell lymphoma 2 (Bcl2; sc-7382), caspase-3 (CASP3; sc-7272), poly (ADP-ribose) polymerase 1 (PARP-1; sc-8007), and beta-actin (β -actin; sc-47778) of manufacturer Santa Cruz USA were applied on PVDF membrane, respectively, by

keeping them overnight on an orbital shaker at 4°C. 4 μ L of secondary antibody in 20 mL of TBST solution (Blotting Grade Affinity Purified Goat Anti-Mouse IgG (H+L) Horseradish Peroxidase Conjugate, cat. #170-6516, Bio-Rad Laboratories, USA) was used for the detection of the target proteins. The secondary antibody was applied to the membrane and placed on a shaker for three to four hours at room temperature so that it can attach to the primary antibody. The bands of the western blot were visualized using electrochemiluminescence (ECL), a detection reagent (Amersham Pharmacia Biotech, Uppsala, Sweden) [36, 37].

2.7. Ligand and Receptor 3D Structures. 3D structure of ZOMEK was generated from ChemDraw (<http://www.cambridgesoft.com>) followed by the geometry optimization. The structure of the p-Akt was taken from the protein data bank (PDB) (<https://www.rcsb.org/>). The three-dimensional

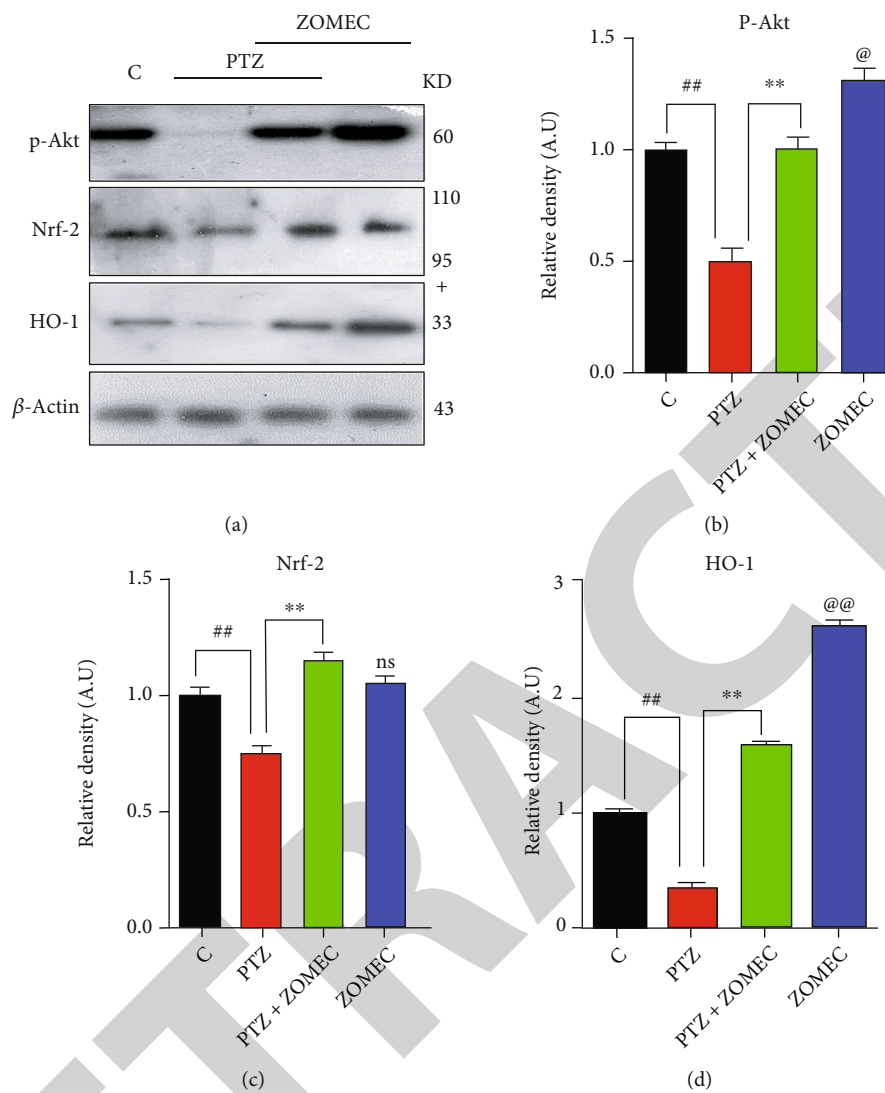


FIGURE 7: Continued.

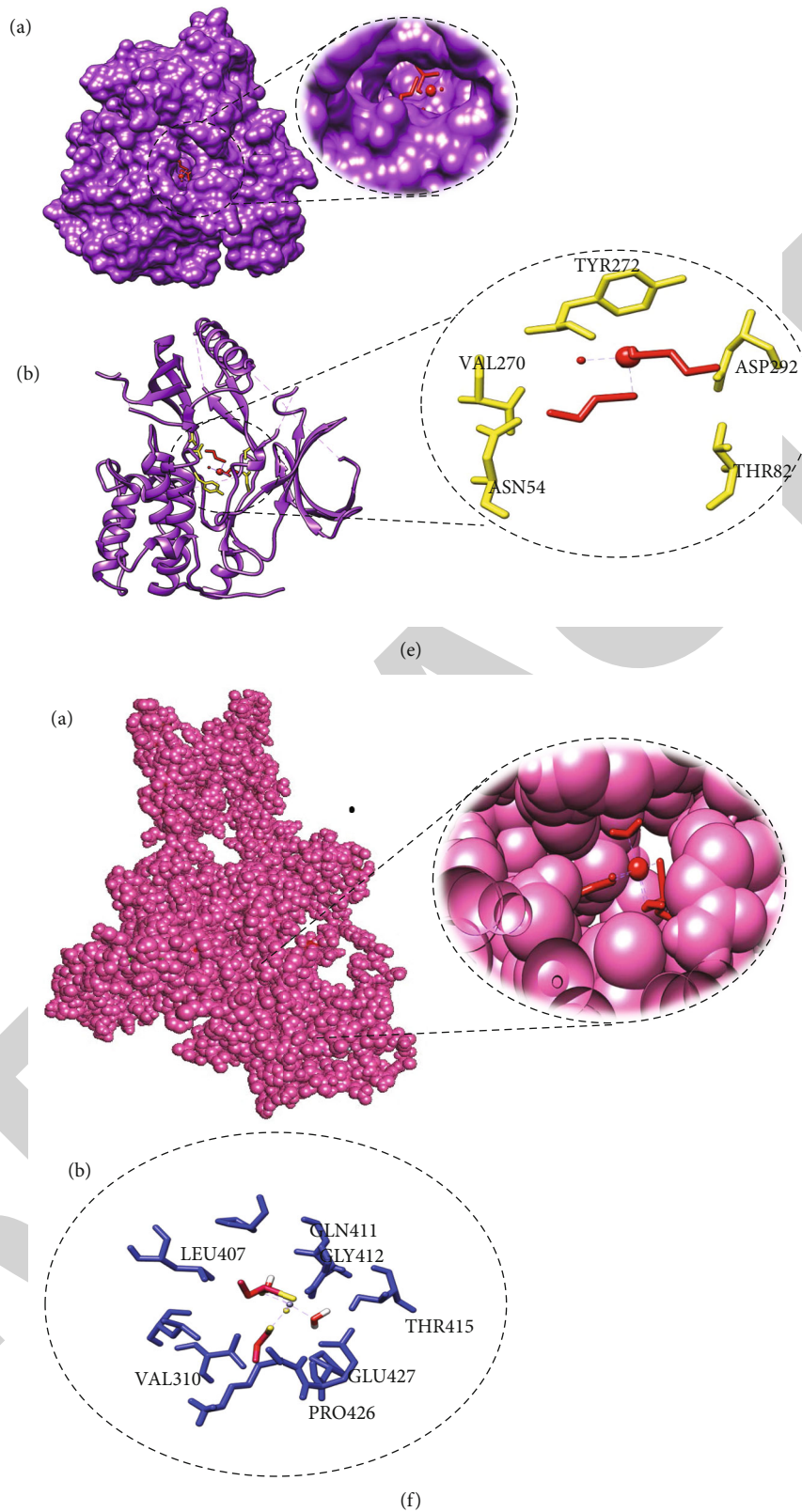


FIGURE 7: ZOMEAC activated the p-Akt/Nrf-2 signaling pathway to decrease neurodegeneration and memory impairment. (a) Immunoblot results for p-Akt and Nrf-2 protein markers. (b) p-Akt histogram. (c) Nrf-2 histogram. (d) HO-1 histogram. (e) Binding mode and interaction of ZOMEAC with p-Akt. (e) A: hydrophobic representation of p-Akt protein with bound ZOMEAC shown in zoom view. B: p-Akt protein in ribbon representation with binding residues shown in yellow sticks and ZOMEAC in red sticks. (f) Binding mode and interaction of ZOMEAC with Nrf2. (f) A: hydrophobic representation of Nrf2 protein with bound ZOMEAC shown in zoom view. B: Nrf2 protein in ribbon representation with binding residues shown in blue sticks and ZOMEAC in red sticks. Significance: ### $p \leq 0.001$, *** $p \leq 0.001$, ** $p \leq 0.01$, @ $p \leq 0.05$, @@ $p \leq 0.01$, and ns = no significance.

TABLE 1: ZOMEc (30 mg/kg) activated the p-Akt/Nrf2 pathway by decreasing memory dysfunction.

| Receptors | Global energy | Attractive VdW | Hydrogen bonding | Hydrophobic interaction |
|-----------|---------------|----------------|---|--|
| p-Akt | -33.50 | -13.30 | ^a VAL270, ^b TYR272, and ^c ASP292 | ^d ASN54 and ^e THR82 |
| Nrf2 | -26.42 | -8.59 | ^f GLU427, ^g GLN411, and ^h LEU407 | ^a VAL319, ⁱ GLY412, ^e THR415, and ^j PRO426 |

^aValine, ^btyrosine, ^caspartic acid, ^dasparagine, ^ethreonine, ^fglutamate, ^gglutamine, ^hleucine, ⁱglycine, and ^jproline.

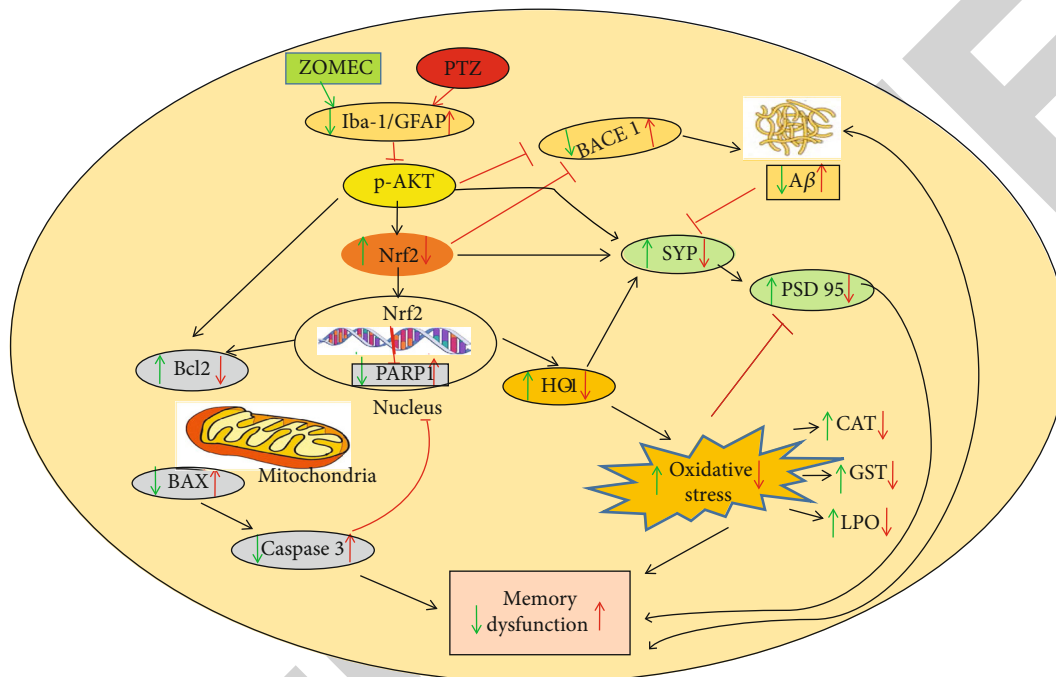


FIGURE 8: The schematic representation of the proposed pathway followed by ZOMEc.

structure of Nrf2 protein was constructed through the homology modeling approach (<http://www.rcsb.org>) using the I-TASSER server [38].

2.8. Molecular Docking. The molecular docking of ZOMEc with Nrf-2 and p-Akt was done by using PatchDock. PatchDock is an algorithm for molecular docking. The input is two molecules of any type: proteins, DNA, peptides, and drugs. The output is a list of potential complexes sorted by the shape complementarity criteria.

2.9. Statistical Analysis. Computer support ImageJ version 1.51 by NIH, USA, and Prism 5 by GraphPad Software were used for quantification of bands and preparation of their histograms. The analysis of the data was completed with the help of analysis of variance (ANOVA) followed by Tukey's test. The density values of the data are presented as the mean ± SEM of five mice per group and are representative of three independent experiments. *p* values less than 0.05 were considered to be statistically significant; **p* < 0.05, ***p* < 0.01, and ****p* < 0.001 indicate comparison between the PTZ and ZOMEc+PTZ groups; #*p* < 0.05, ##*p* < 0.01, and ###*p* < 0.001 indicate comparison between the control and PTZ groups; @*p* < 0.05, @@*p* < 0.01, and @@@*p* < 0.001 indi-

cate comparison between the control and ZOMEc groups; and ns indicates no significance among the groups.

3. Results

3.1. ZOMEc Ameliorated Oxidative Stress Markers Induced by PTZ in the Mouse Brain. Previous studies indicated that both CAT and GST are the major antioxidant agents [39]. For this reason, the brain tissue homogenates of mice were analyzed with different antioxidant assays including CAT, GST, and LPO. The results indicated that PTZ significantly inhibited CAT (9 μmol/min/mg of protein) which was increased to 17 μmol/min/mg of protein by the group attenuated with PTZ+ZOMEc in comparison to the control one (25 μmol/min/mg of protein). GST was significantly reduced in PTZ-attenuated mice (12 μmol/min/mg of protein) as compared to the control (44 μmol/minute/mg of protein), while ZOMEc increased the GST levels in the PTZ +ZOMEc group (27 μmol/min/mg of protein) compared with the PTZ group. As far as LPO is concerned, its activity was increased in the diseased mice (120 μmol/min/mg of protein) as compared to the control one (40 μmol/min/mg of protein). In the PTZ+ZOMEc group, the LPO was 65 μmol/min/mg of protein. The group of healthy mice receiving ZOMEc showed no significant difference in LPO

(42 $\mu\text{mol}/\text{min}/\text{mg}$ of protein) compared to the control group (40 $\mu\text{mol}/\text{min}/\text{mg}$ of protein). However, a statistical difference was seen in CAT (19 $\mu\text{mol}/\text{min}/\text{mg}$ of protein) and GST (34 $\mu\text{mol}/\text{min}/\text{mg}$ of protein) as compared with the control group (25 $\mu\text{mol}/\text{min}/\text{mg}$ of protein and 44 $\mu\text{mol}/\text{min}/\text{mg}$ of protein, respectively) (Figures 1(a)–1(c)).

3.2. ZOMEc Inhibited PTZ-Activated Glial Cell Activation in the Mouse Brain. PTZ can activate the glial cells in adult male mouse brains [40]. The current study similarly found that the male mice that were attenuated with PTZ significantly increased the protein expression of microglia (Iba) and astrocytes (GFAP) compared with the control group, while the PTZ+ZOMEc inhibited the expression of both the proteins to a significant level compared with the PTZ group as shown in Figures 2(a)–2(c). The ZOMEc group when compared to the control group showed no significance in the protein expression of Iba-1 and GFAP.

3.3. ZOMEc Attenuated Mouse-Reversed PTZ-Induced Neuroapoptosis/Neurodegeneration. The previous reports confirmed that neuronal cell death due to PTZ is apoptotic death [31]. To confirm this statement, the brain homogenates of the selected groups were used through western blot analysis. The results showed that PTZ activated the apoptotic cascade and enhanced the expression of caspase-3, BAX, and PARP-1 proteins. It considerably downregulated Bcl2 protein and increased BAX/Bcl2 ratio in the homogenates of mouse brains compared with the control group. Interestingly, the test compound ZOMEc treatment in the PTZ+ZOMEc group not only reduced the proteins caspase-3, BAX, and PARP-1 but also decreased BAX/Bcl2 ratio compared with the PTZ group. The ZOMEc group significantly reduced BAX and Bcl2 and increased PARP-1 compared with the control group. However, no significant difference was noticed in BAX/Bcl2 and caspase-3 when compared with the control group as depicted in Figures 3(a)–3(f).

3.4. ZOMEc Abrogated PTZ-Induced Amyloidogenic A β Pathways in Mice. A β and BACE1 have been shown to increase in neurodegenerative diseases [28]. The level of BACE1 and A β proteins was investigated through western blot analysis. The results indicated that PTZ induction significantly upregulated the A β and BACE1 protein activity in the mouse brain compared with the control group. The PTZ+ZOMEc-induced mouse group significantly lowered the BACE1 and A β (amyloidogenic pathway) expression compared with the PTZ group. In the ZOMEc group, no significant difference was seen in BACE1 and A β compared with the control mice as shown in Figures 4(a)–4(c).

3.5. ZOMEc Treatment Improved Pre- and Postsynapse Protein Production in PTZ-Induced Mice. The synaptic abnormalities that arise in the hippocampus are associated with cognitive impairment. Presynaptic, i.e., synaptophysin (SYP), and postsynaptic, i.e., postsynaptic density protein (PSD-95), proteins play an important role in these synaptic abnormalities [41]. In the current study, the comparative expression of SYP and PSD-95 in the brain homogenate of the selected mouse groups was analyzed through the western

blot. The expression of both the proteins significantly increased in the brain of PTZ+ZOMEc group mice, while PTZ-induced mice were noted with a decreased protein concentration of SYP and PSD95 as shown in Figures 5(a)–5(c).

3.6. ZOMEc Rectified PTZ-Induced Memory Dysfunction in Mice. The effect of ZOMEc on long-term memory and spatial learning in AD (PTZ-induced) mice was estimated through MWM. To find the submerged target, the mean latency decreased gradually in selected groups. On the first day of the behavior test, the immersed target was found in sixty seconds by the PTZ-administered mouse group while the mice with the compound ZOMEc (30 mg/kg) along with PTZ (35 mg/kg) found it in twenty-eight seconds. ZOMEc-treated mice found the platform in thirty-nine seconds and the control group in twenty-three seconds. On the subsequent days, the PTZ-attenuated group finished the task of the immersed target. But the mean escape latency (seconds) was found greater for the PTZ-administered group compared to the other experimental mouse groups as shown in Figure 6(a).

Further probe test was performed (when the target stand was absent), and the data was recorded on day six. Data collected showed that the PTZ group mice spent time more in the respective quadrant in comparison to the control group. ZOMEc+PTZ group mice spent twelve seconds during the probe test, while no significance was seen in the ZOMEc group compared with the control group (Figure 6(b)). The Y-maze resulted in a significant increase in percent spontaneous alteration in the PTZ+ZOMEc AD mice compared with the control group. On the other hand, the PTZ group resulted in reduced percent spontaneous alteration, while no significance was observed in the ZOMEc group when compared with the control group (Figure 6(c)).

3.7. ZOMEc Stimulated p-Akt/Nrf-2 Signaling Pathways. Nrf-2 and HO-1 are said to be the protection systems in the body that are antioxidative. Their level decreases due to an increase in oxidative stress [42]. Being an antioxidant, the protein (Nrf2 and HO-1) expression was checked through western blot analysis. Results indicated that PTZ decreased both the proteins to a greater extent in PTZ-induced AD mice compared to the control group. The PTZ+ZOMEc group showed an increase in protein expression significantly as compared with PTZ, while the ZOMEc group showed no significance in the case of Nrf-2 and increased the level of HO-1 as compared with the control group. Further, western blot analysis resulted in a decreased level of p-Akt in AD mouse brains compared to control, while the PTZ+ZOMEc group showed an increase in p-AKT expression compared with the PTZ group. A significant rise was seen in the ZOMEc group compared with the control as shown in Figures 7(a)–7(d).

3.8. Bioinformatics Analysis. To find the role of the compound ZOMEc in AD mice, its binding was visualized with p-Akt through molecular docking. Through docking analysis, the binding of ZOMEc with the p-Akt active site was found with a binding free energy of -13.30 (Table 1).

VAL270, TYR272, and ASP292 made conventional hydrogen bonds with ZOMEAC apart from several hydrophobic interactions by ASN54 and THR82 amino acids (Figure 7(e), Table 1). The computational analysis further supported the wet laboratory western blot experiments, in which ZOMEAC stimulated the p-Akt protein. The experimental results found through western blot recommended that ZOMEAC stimulated the Nrf2 signaling pathway (present in the cytoplasm with keap1). The molecular docking analysis of ZOMEAC and Nrf2 was carried out to evaluate whether ZOMEAC binds to Nrf2 and makes possible its movement towards the nucleus. Docking analysis revealed that ZOMEAC binds with the Nrf2 active site with the binding free energy of -8.59 (Table 1). GLU427, GLN411, and LEU407 make conventional hydrogen bonds with ZOMEAC apart from several hydrophobic interactions with VAL319, GLY412, THR415, and PRO426 amino acids (Figure 7(f), Table 1).

The table shows global energy, attractive VdW, hydrogen bonding, and hydrophobic interaction of ZOMEAC with p-Akt and Nrf2. The results showed that p-Akt and Nrf2 have strong interaction with ZOMEAC, which increases their efficacy and helps in curing PTZ-induced neurodegeneration. The computational analysis supported our western blot experiments in which ZOMEAC stimulated the Nrf2 protein. Nrf2 translocates into the nucleus to bind to antioxidant-responsive elements in genes encoding antioxidant enzyme heme oxygenase-1 (HO-1). The increased expression of this enzyme plays a key role in mediating cellular detoxification, antioxidation, and anti-inflammatory effects.

4. Discussion

The therapeutic potential of ZOMEAC as a neuroprotective and antioxidative agent was evaluated by using PTZ-induced oxidative stress in BALB/c mice. It has been proven through the results that ZOMEAC treatment upregulated CAT and GST and downregulated LPO as shown in Figures 1(a)–1(c). Thus, ZOMEAC considerably decreased oxidative stress in adult mouse brains, consistent with the previous study [43]. Some heavy metals, such as cadmium and nickel, have been reported with toxic levels causing damage to the brain and other organs of the body [22, 24]. When these metals exceed a certain level within the body, their first targeted organelle is mitochondria. Their toxic effect includes oxidative damage to the cells, stunted growth, overexpression of genes, abnormal biochemical and physiological changes, altered behavior, and inadequate metabolism [17].

The study confirms that ZOMEAC treatment of mice results in increased SYP and PSD95 protein expressions. In consecutive five days of behavior test, the mean escape latencies of the adult mice were lowered in finding the immersed target. The mice in the control group exhibited a decrease in mean escape latency. It can be figured out in Figure 6(a) that the mouse group treated with PTZ resulted in longer escape latencies compared with the control group. The results specified that spatial learning dysfunction and memory impairment take place in PTZ-attenuated male albino mice. The PTZ+ZOMEAC group appreciably decreased the escape laten-

cies to the target compared with the PTZ-administered mouse group. The current study revealed that ZOMEAC significantly increased Nrf-2/Ho-1 protein expression in mouse groups. These results were also supported by the docking results shown in Figure 7.

The proposed schematic diagram shows the mechanism of action of ZOMEAC as shown in Figure 8. The test compound ZOMEAC showed an increased survival pathway of the cell by increasing the expression of p-Akt/Nrf2 proteins. A large increase in Iba-1 GFAP, p-Akt, Nrf2, and BAX/Bcl-2 proteins was noted.

The diagram shows how PTZ induces its toxic effect by inhibiting p-Akt/Nrf-2 signaling pathways. The effect of ZOMEAC on the expression of proteins is shown with a green arrow while the protein results found after PTZ administration are shown with a red arrow.

5. Conclusion

ZOMEAC as a therapeutic agent was applied in an animal model to treat neurodisorder caused by oxidative stress. The results verified a decrease in $A\beta$ production, neuroinflammation, and oxidative stress by applying ZOMEAC. The expression of protein markers BAX/Bcl2, caspase-3, and PARP-1 was found through western blot. Interestingly, ZOMEAC reversed PTZ-induced neuronal synapse deficits, improved oxidative stress-aided memory impairment, and inhibited the amyloidogenic pathway in mouse brains. Thus, ZOMEAC might be one of the first-choice drug candidates to treat AD and associated diseases next-generation neurotherapeutics.

Data Availability

Data will be provided on request.

Ethical Approval

On behalf of all coauthors, it is stated that this study was performed with all the measures established by the Ethics Committee of the NMMRC (Neuro Molecular Medicine Research Center) according to the guidelines of NIH (International Institute of Health, USA).

Consent

All the authors agreed to the publication of the current study. The treatments of mice were subject to ethical consideration.

Conflicts of Interest

The authors declare no competing interests.

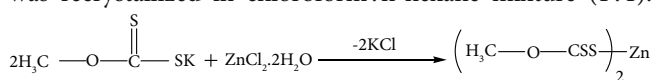
Authors' Contributions

All authors contributed to the study's conception and design. Analysis and testing of the study were performed by Rifat Jahan, Mohammad Yousaf, Hamayun Khan, Musarrat Ijaz, Nousheen Bibi, Touseef Rehan, and Shahid

Ali Shah. Further, the manuscript was suggested for publication by all the authors after technical proofreading.

Supplementary Materials

Preparation of ZOMEC. Solution of zinc chloride dehydrate (1 mmol) in 10 mL methanol was added to a solution of potassium O-alkyl carbonodithioate (1 mmol) in methanol (30 mL) in a two-necked round bottom flask (100 mL) with continuous stirring at room temperature for 4 h. The solvent was evaporated slowly at room temperature; the solid product obtained was filtered off and dried in air. The product was recrystallized in chloroform:n-hexane mixture (1:1).



The synthesized compound was confirmed experimentally by nuclear magnetic spectroscopy $^1\text{H-NMR}$ spectrum of the test drug. (*Supplementary Materials*)

References

- [1] Y. Christen, "Oxidative stress and Alzheimer disease," *American Journal of Clinical Nutrition*, vol. 71, no. 2, pp. 621S–629S, 2000.
- [2] H. Kozlowski, A. Janicka-Klos, J. Brasun, E. Gaggelli, D. Valensin, and G. Valensin, "Copper, iron, and zinc ions homeostasis and their role in neurodegenerative disorders (metal uptake, transport, distribution and regulation)," *Coordination Chemistry Reviews*, vol. 253, no. 21–22, pp. 2665–2685, 2009.
- [3] K. J. Barnham, W. J. McKinstry, G. Multhaup et al., "Structure of the Alzheimer's disease amyloid precursor protein copper binding domain," *Journal of Biological Chemistry*, vol. 278, no. 19, pp. 17401–17407, 2003.
- [4] T. Miura, K. Suzuki, N. Kohata, and H. Takeuchi, "Metal binding modes of Alzheimer's amyloid β -peptide in insoluble aggregates and soluble complexes," *Biochemistry*, vol. 39, no. 23, pp. 7024–7031, 2000.
- [5] X. Huang, R. D. Moir, R. E. Tanzi, A. I. Bush, and J. T. Rogers, "Redox-active metals, oxidative stress, and Alzheimer's disease pathology," *Annals of the New York Academy of Sciences*, vol. 1012, no. 1, pp. 153–163, 2004.
- [6] M. P. Cuajungco and K. Y. Fagét, "Zinc takes the center stage: its paradoxical role in Alzheimer's disease," *Brain Research Reviews*, vol. 41, no. 1, pp. 44–56, 2003.
- [7] F. A. Hoerberichts and E. J. Woltering, "Multiple mediators of plant programmed cell death: interplay of conserved cell death mechanisms and plant-specific regulators," *BioEssays*, vol. 25, no. 1, pp. 47–57, 2003.
- [8] A. Khan, M. Ikram, T. Muhammad, J. Park, and M. O. Kim, "Caffeine modulates cadmium-induced oxidative stress, neuroinflammation, and cognitive impairments by regulating Nrf-2/HO-1 in vivo and in vitro," *Journal of Clinical Medicine*, vol. 8, no. 5, p. 680, 2019.
- [9] M. Hu, Y. Liu, L. He, X. Yuan, W. Peng, and C. Wu, "Antiepileptic effects of protein-rich extract from *Bombyx batryticatus* on mice and its protective effects against H_2O_2 -induced oxidative damage in PC12 cells via regulating PI3K/Akt signaling pathways," *Oxidative Medicine Cellular Longevity*, vol. 2019, pp. 1–13, 2019.
- [10] C. C. T. Aguiar, A. B. Almeida, P. V. P. Araújo et al., "Oxidative stress and epilepsy: literature review," *Oxidative medicine and cellular longevity*, vol. 2012, 2012.
- [11] M. B. Farhadi and M. Fereidoni, "Neuroprotective effect of menaquinone-4 (MK-4) on transient global cerebral ischemia/reperfusion injury in rat," *PLoS One*, vol. 15, no. 3, article e0229769, 2020.
- [12] W. C. Dunty Jr., S. Y. Chen, R. M. Zucker, D. B. Dehart, and K. K. Sulik, "Selective vulnerability of embryonic cell populations to ethanol-induced apoptosis: implications for alcohol-related birth defects and neurodevelopmental disorder," *Alcoholism: Clinical and Experiment Research*, vol. 25, no. 10, pp. 1523–1535, 2001.
- [13] M. J. Roy, A. Vom, P. E. Czabotar, and G. Lessene, "Cell death and the mitochondria: therapeutic targeting of the BCL-2 family-driven pathway," *British Journal of Pharmacology*, vol. 171, no. 8, pp. 1973–1987, 2014.
- [14] J. Martínez-Fábregas, I. Díaz-Moreno, K. González-Arzola et al., "Structural and functional analysis of novel human cytochrome *c* targets in apoptosis," *Molecular and Cellular Proteomics*, vol. 13, no. 6, pp. 1439–1456, 2014.
- [15] C. Wang, M. Liu, Y. Pan, B. Bai, and J. Chen, "Global gene expression profile of cerebral ischemia-reperfusion injury in rat MCAO model," *Oncotarget*, vol. 8, no. 43, pp. 74607–74622, 2017.
- [16] R. H. Haas, "Mitochondrial dysfunction in aging and diseases of aging," *Biology*, vol. 8, no. 2, p. 48, 2019.
- [17] Q. Sun, Y. Li, L. Shi et al., "Heavy metals induced mitochondrial dysfunction in animals: molecular mechanism of toxicity," *Toxicology*, vol. 469, article 153136, 2022.
- [18] M. L. Namratha, M. Lakshman, M. Jeevanalatha, and B. A. Kumar, "Testicular Toxicity induced by glyphosate (GLP) and ameliorative effect of Vitamin C in wistar rats," *Continental Veterinary Journal*, vol. 1, pp. 32–36, 2020.
- [19] Y. Liu, J. Yi, and Y. Li, "Residue of thiram in food, suppresses immune system stress signals and disturbs sphingolipid metabolism in chickens," *Veterinary Immunology and Immunopathology*, vol. 1, no. 247, article 110415, 2022.
- [20] S. Naseem, A. Ghaffar, R. Hussain, and A. Khan, "Inquisition of toxic effects of pyriproxyfen on physical, hemato-biochemical and histopathological parameters in Labeorohita fish," *Pakistan Veterinary Journal*, 2022.
- [21] J. Q. Wang, R. Hussain, A. Ghaffar et al., "Clinicohematological, mutagenic, and oxidative stress induced by pendimethalin in freshwater fish bighead carp (*Hypophthalmichthys nobilis*)," *Oxidative Medicine and Cellular Longevity*, vol. 2022, 2022.
- [22] M. S. Khan, S. A. Buzdar, R. Hussain et al., "Hematobiochemical, oxidative stress, and histopathological mediated toxicity induced by nickel ferrite (NiFe_2O_4) nanoparticles in rabbits," *Oxidative Medicine and Cellular Longevity*, vol. 2022, 14 pages, 2022.
- [23] G. Afzal, H. I. Ahmad, R. Hussain et al., "Bisphenol A induces histopathological, hematobiochemical alterations, oxidative stress, and genotoxicity in common carp (*Cyprinus carpio L.*)," *Oxidative Medicine and Cellular Longevity*, vol. 2022, 14 pages, 2022.
- [24] G. Jabeen, F. Manzoor, M. Arshad, and B. I. Barbol, "Effect of cadmium exposure on hematological, nuclear and morphological alterations in erythrocyte of fresh water fish (Labeorohita)," *Continental Veterinary Journal*, vol. 1, no. 1, pp. 20–24, 2021.

Retraction

Retracted: A Novel Protein Elicitor (PELL1) Extracted from *Lecanicillium lecanii* Induced Resistance against *Bemisia tabaci* (Hemiptera: Aleyrodidae) in *Gossypium hirsutum* L

BioMed Research International

Received 12 March 2024; Accepted 12 March 2024; Published 20 March 2024

Copyright © 2024 BioMed Research International. This is an open access article distributed under the Creative Commons Attribution License, which permits unrestricted use, distribution, and reproduction in any medium, provided the original work is properly cited.

This article has been retracted by Hindawi following an investigation undertaken by the publisher [1]. This investigation has uncovered evidence of one or more of the following indicators of systematic manipulation of the publication process:

- (1) Discrepancies in scope
- (2) Discrepancies in the description of the research reported
- (3) Discrepancies between the availability of data and the research described
- (4) Inappropriate citations
- (5) Incoherent, meaningless and/or irrelevant content included in the article
- (6) Manipulated or compromised peer review

The presence of these indicators undermines our confidence in the integrity of the article's content and we cannot, therefore, vouch for its reliability. Please note that this notice is intended solely to alert readers that the content of this article is unreliable. We have not investigated whether authors were aware of or involved in the systematic manipulation of the publication process.

Wiley and Hindawi regrets that the usual quality checks did not identify these issues before publication and have since put additional measures in place to safeguard research integrity.

We wish to credit our own Research Integrity and Research Publishing teams and anonymous and named

external researchers and research integrity experts for contributing to this investigation.




The corresponding author, as the representative of all authors, has been given the opportunity to register their agreement or disagreement to this retraction. We have kept a record of any response received.

References

- [1] A. Basit, M. Yaseen, M. Babar et al., "A Novel Protein Elicitor (PELL1) Extracted from *Lecanicillium lecanii* Induced Resistance against *Bemisia tabaci* (Hemiptera: Aleyrodidae) in *Gossypium hirsutum* L," *BioMed Research International*, vol. 2022, Article ID 3097521, 8 pages, 2022.

Research Article

A Novel Protein Elicitor (PELL1) Extracted from *Lecanicillium lecanii* Induced Resistance against *Bemisia tabaci* (Hemiptera: Aleyrodidae) in *Gossypium hirsutum* L

Abdul Basit,^{1,2} Muhammad Yaseen,³ Maham Babar,⁴ Yong Wang,¹ Yusuf Ali Abdulle,² Dewen Qiu,² Yunzhu Li ,¹ Muhammad Amjad Bashir ,⁵ Muhammad Sarmad Shahzad,⁵ Hasnain Farooq ,^{6,7} Reem A. Alajmi,⁸ David N. Mangi,⁹ Ambreen Sehar,¹⁰ and Humaira Parveen¹¹

¹Department of Plant Pathology, Agriculture College, Guizhou University, Guiyang 550025, China

²State Key Laboratory of Plant Diseases and Insect Pests, Institute of Plant Protection, Chinese Academy of Agricultural Science, Beijing, China

³DHQ Hospital, Mandi Bahauddin Punjab, Pakistan

⁴WMO Nishtar Hospital, Multan Punjab, Pakistan

⁵Department of Plant Protection Faculty of Agricultural Sciences, Ghazi University, Dera Ghazi Khan Punjab, Pakistan

⁶Department of Environmental Sciences, University of California, Riverside, CA, USA

⁷Department of Forestry, Faculty of Agricultural Sciences, Ghazi University, Dera Ghazi Khan, Pakistan

⁸Zoology Department, College of Science, King Saud University, Riyadh, Saudi Arabia

⁹College of Agriculture University of Nairobi, Nairobi, Kenya

¹⁰DHQ Sheikhpura, Punjab, Pakistan

¹¹WMO Health Department, Punjab, Pakistan

Correspondence should be addressed to Yunzhu Li; gunzhuli@guzhu.edu.ca and Hasnain Farooq; hfarooq@gudgk.edu.pk

Received 8 May 2022; Accepted 18 July 2022; Published 23 August 2022

Academic Editor: Abdelmoteleb Elokil

Copyright © 2022 Abdul Basit et al. This is an open access article distributed under the Creative Commons Attribution License, which permits unrestricted use, distribution, and reproduction in any medium, provided the original work is properly cited.

Protein elicitors play a key role in signaling or displaying plant defense mechanism and emerging as vital tools for biocontrol of insects. This study was aimed at the characterization of the novel protein elicitor isolated from entomopathogenic fungi *Lecanicillium lecanii* (V3) strain and its activity against whitefly, *Bemisia tabaci*, in cotton (*Gossypium hirsutum* L.). The sequence of purified elicitor protein showed 100% similarity with hypothetical protein LEL_00878 (*Cordyceps confragosa* RCEF 1005) (GenBank accession no. OAA81333.1). This novel protein elicitor has 253 amino acid residues and 762 bp with a molecular mass of 29 kDa. Their combatant protein was expressed in *Escherichia coli* using pET-28a (+) plasmid. Bioassay was revealed to quantify the impact of numerous concentrations of protein (i.e., 58.32, 41.22, and 35.41 $\mu\text{g/ml}$) on the fecundity rate of *B. tabaci* on cotton plants. Bioassay results exhibited a significant effect ($P \leq 0.001$) of all the concentrations of protein on the fecundity rate of *B. tabaci*. In addition, the gene expression analysis found a significant upregulation of the major genes associated with salicylic acid (SA) and jasmonic acid (JA) defense pathways in elicitor protein-treated plants. Our results showed that the potential application of novel protein elicitor derived from *Lecanicillium lecanii* will be used as future biointensive controlling approaches against whitefly, *Bemisia tabaci*.

1. Introduction

The application of fungal elicitors has been described as among the most successful methods for increasing the production of secondary metabolites in plant cell culture [1, 2] and also reported that it is the best effective method for the improvement of hairy roots [3, 4]. Fungal elicitors involve metabolites and degradation products [5]. The elicitor molecules include lipids, glycoproteins, and proteins causing resistance against pathogens and herbivores in plants [6–8]. Fungal-derived proteins can induce hypersensitivity responses (HR) and trigger secondary metabolite accumulation. For instance, PebC1 protein elicitor isolated from *Botrytis cinerea* enhances disease resistance in *Arabidopsis thaliana*, causes disease resistance and drought tolerance, and improves plant growth in tomato plants [9]. A fungal elicitor protein (SsCut) extracted from *Sclerotinia sclerotiorum* causes numerous defense responses in the crop. A novel protein elicitor (PevD1) causes resistance of Verticillium wilt in cotton plants [10].

Several microbes including entomopathogenic fungi (EPF) have shown effectiveness against a broad range of insect pest [11, 12]. Furthermore, EPF has the capability to produce endophytes within various parts of plants [13, 14]. EPF develop systemic resistance against biotic stresses in several plants including pathogens and phytoparasites, improve plant growth [15], enhance yield [16] improving plant nutrition [17], and increase plant root growth [18, 19]. Several EPF have been described in broth cultures to secrete various insecticidal, antifeedant, and bioactive toxic substances [20].

Salicylic acid and jasmonic acid are two important signaling pathways involving plant defense mechanisms [21, 22]. Accumulative defense signaling pathways are activated in response to a herbivorous attack, but the jasmonate reaction is mainly related to chewing herbivorous [23], and salicylate responses are linked with phloem-sucking insect pests such as aphids and whiteflies [24, 25]. Our study is aimed at the purification and characterizations of the novel protein elicitor extracted from entomopathogenic fungi *Lecanicillium lecanii* (V3) strain and its potential bioactivity against whitefly, *B. tabaci*, in cotton. This result will help to provide a potential a new approach for *B. tabaci* control.

2. Materials and Methods

2.1. Insect Rearing. Adults of whitefly (*Bemisia tabaci*) were collected from Langfang Research Station, Institute of Plant Protection (IPP), Chinese Academy of Agricultural Sciences (CAAS), Beijing, China. Whitefly adults were reared in a controlled greenhouse at $26 \pm 2^\circ\text{C}$ 65% RH on cotton plants for the proper growth.

2.2. Fungus Growth. *Lecanicillium lecanii* (V3) strain was obtained from the Key Laboratory of Biopesticides Engineering, Department of Biopesticides and Biocontrol (IPP) (CAAS), and kept on PDA (potatoes dextrose agar) in a Petri plate for 15 days at 25°C . Conidia were harvested at 16 days. The petri dishes were flashed with 20 ml sterile

water and filtered by using sterile cheesecloth. Spore concentrations were determined under a microscope by using a hemocytometer.

2.3. Protein Isolation. V3 strain was grown in 1l of LB medium shaken at 150 rpm [26]. The cultured media was filtered through $0.45 \mu\text{M}$ of Whatman filter paper. The fungal filtrate was precipitated with 80% ammonium sulfate $(\text{NH}_4)_2\text{SO}_4$ overnight at 4°C , centrifuged at 12000 rpm, for 30 min at 4°C . The pellet was collected and resuspended in 30 ml with buffer A (50 mM Tris-HCl, pH = 8.0). Total protein was filtered through a $0.22 \mu\text{m}$ -membrane filter paper (Chen et al. 2012). Protein fragments were further purified using AKTA protein purification system, used an ion-exchange chromatography column, loading with buffer (A) (50 mM Tris-HCl, pH = 8.0), eluted with buffer (B) (50 mM Tris-HCl, 1 mM NaCl, pH = 8.0). The eluted peak was collected and centrifuged (3500 rpm for 30 min at 4°C) by using desalting column. The isolated protein was detected by SDS-PAGE. Protein concentrations were evaluated by Easy II Protein Quantitative Kit (BCA) method.

2.4. Amino Acid Sequencing. Liquid chromatography-mass spectrometry analysis of digested proteins in gel was performed to assess the protein sequence of amino acids. The protein was analyzed by ESI-MS/MS, and de novo quenching was evaluated. The purified protein was blast on the NCBI database, and the result showed 100% similarity with hypothetical protein LEL_00878 (*Cordyceps contraposed* RCEF 1005) (GenBank accession no. OAA81333.1). The sequence of this gene was used to design primers.

2.5. Gene Amplification. DNA was extracted by using the fungal DNA kit. According to the results from BLAST searches in the NCBI databases, a pair of primers was designed: F. primer (ATGGCAGGCGGCTCCTAC), R. primer (TCACAAACGAGCTGGTAAATGAAAC). The elicitor-encoding gene was amplified from *Verticillium lecanii*. The amplified gene was used for cloning.

2.6. Expression and Purification of Protein. The amplified gene was cloned into the pET-28a (+) plasmid using ligation-independent cloning (Aslanidis et al. 1990). BamHI and HindIII were used as restriction enzymes. The ligated plasmid was transformed into *E. coli* BL21 (DE3). Cells were grown at 37°C in the LB medium. The protein recombinant was induced with 0.2 mM IPTG at 17°C for 12 hours. Bacterial cells were centrifuged at 4°C , 10000 rpm for 10 minutes. The collected cells were resuspended with buffer A (50 mM Tris HCl, pH 8.0) and disrupted with an ultrasonic. Then, the cells were centrifuged at 13000 rpm for 25 minutes. Additional purification of the recombinant protein was executed by affinity chromatography with a His-Trap HP column, loading with buffer B (50 mM Tris-HCl, 200 mM NaCl, pH 8), eluted by buffer C (500 mM imidazole, 200 mM NaCl, 50 mM Tris-HCl, pH 8) directly, the eluted peak was desalted in desalting column HiTrap (GE Healthcare, Waukesha, WI, USA). The purified protein elicitor was detected by SDS-PAGE. Protein concentrations were evaluated as described previously [27].

TABLE 1: Primer pairs used to amplify genes involved in JA and SA pathways.

| Genes | F. primer | R. primer |
|------------------|-----------------------------|--------------------------|
| OPR3 | ATGTGACGCAACCTCGTTATC | CCGCCACTACACATGAAAGTT |
| b-1,3-Glucanase | AATGCGCTCTATGATCCG | GATGATTTATCAATAGCAGCG |
| Acidic chitinase | GCTCAGAATTCCCATGAAACTACAGGG | GGTTGGATCCTTTGCGACATTC |
| GhACT4 | TTGCAGACCGTATGAGCAAG | ATCCTCCGATCCAGACACTG |
| UBQ7 | GAATGTGGCGCCGGGACCTTC | ACTCAATCCCCACCAGCCTTCTGG |
| GhLOX | ACATGCCGAAGCCGCTGCTT | GGGCGTATTCGGGGCCCTTG |

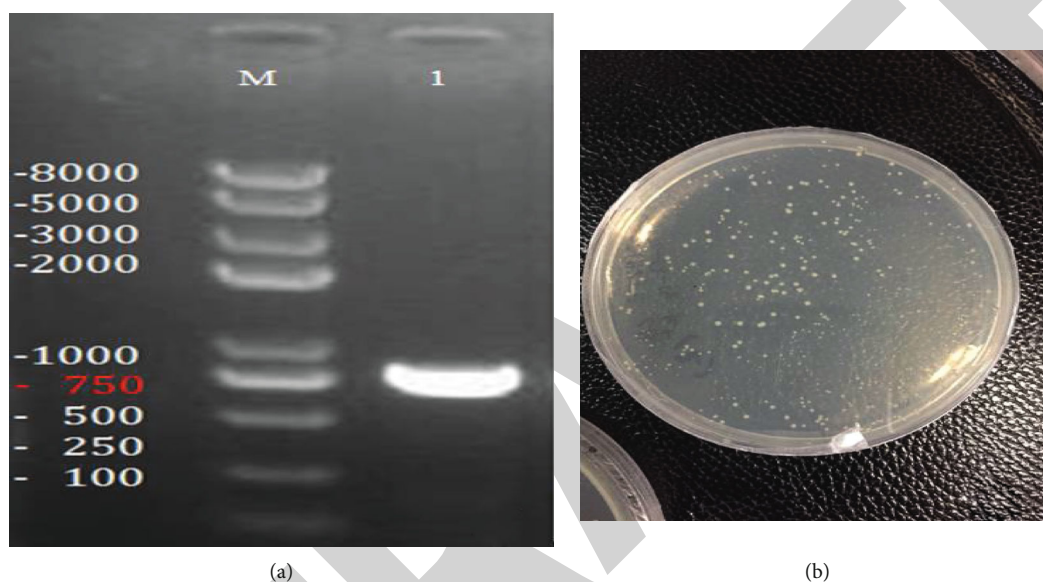


FIGURE 1: (a) Amplified gene of 762 bp on agarose gel. M: molecular weight marker; 1: size of the gene. (b) Positive clones were observed after target gene and pET-28a vector joined together by using T4 ligase enzyme.

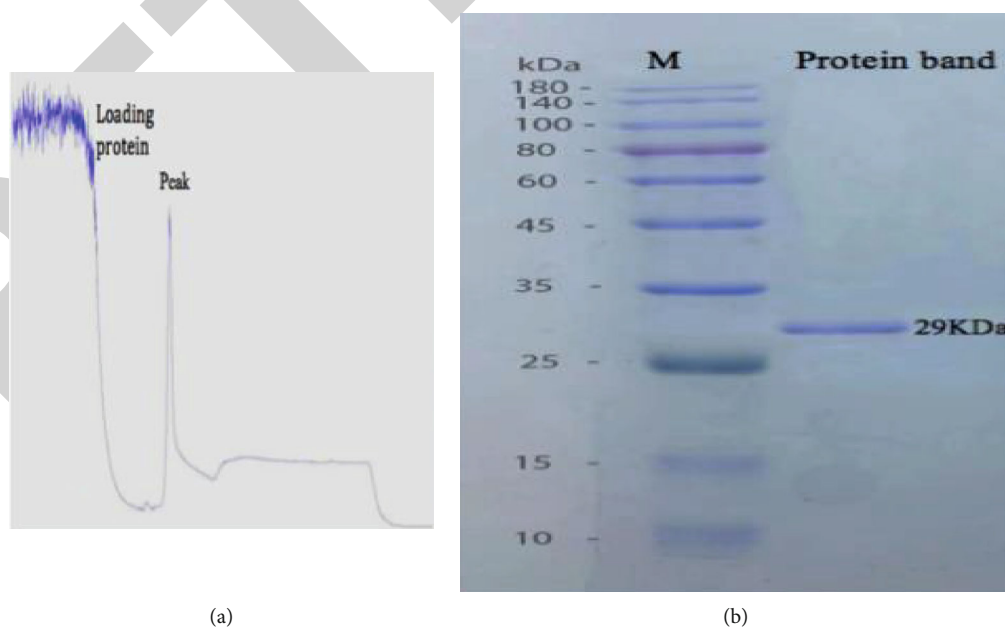


FIGURE 2: Purification of recombinant protein. (a) Total protein purified by the AKTA using a His-Trap HP column. (b) The purified protein on tricine (SDS-PAGE) displayed a single band with molecular mass of 29 kDa. M: protein molecular mass marker.

2.7. *Bioassay of Whitefly (B. tabaci)*. Laboratory bioassays were carried out on cotton plants to determine the bioactivity of a novel purified protein against *B. tabaci*. Three concentrations of purified protein (58.32, 41.22, and 35.41 $\mu\text{g ml}^{-1}$) were tested while buffer was used as control treatment. Until the cotton plants were covered thoroughly, they were treated with elicitor by using aerosol spray bottle @ 2-3 ml elicitor solution plant⁻¹. The plants were allowed to dry about 20 hours. In order to evaluate the fecundity of the white fly, 3-5 fresh nymph of white fly was released. The fecundity rate was determined by calculating the total no. of offspring that these new emerging nymph produced. The experiment was repeated three times independently with 10 replicates.

2.8. *PCR (RT-qPCR)*. Plant leaves were treated with 58.32 $\mu\text{g/ml}$ concentration of protein elicitor and *B. tabaci* allowed to feed at the same time on these treated and untreated plants. These leaves were extracted with total RNARNA ER301-01 kit (TransGen Biotech, Beijing, China) and cDNAAT341-01 kit (TransGen Biotech, Beijing, China) was synthesized. The relative expression of main genes related in cotton defense mechanism has been determined by RT-qPCR in *B. tabaci*-infested protein elicitor-treated and control plants. Jasmonic acid-associated genes used in this study were UBQ7, GhACT4, and GhLOX while salicylic acid-associated genes were OPR3, b-1,3-glucanase, and acidic chitinase. Primer pairs used to amplify these genes by RT-qPCR are given in Table 1. For each procedure, three experimental replicates were performed.

2.9. *Statistical Analysis*. The data regarding concentration of protein elicitors and time were subjected to analysis of variance (ANOVA) with factorial arrangement using Statistics 8.1 software (Tallahassee, FL, USA). Means were compared using the least significant difference (LSD) test at 5% level of probability. The expression levels of RT-qPCR were measured using the comparative CT method ($2^{-\Delta\Delta\text{CT}}$). Statistical data of protein elicitor-treated and untreated plants were compared with a probability level of 0.05 by using Student's *t*-test [28].

3. Results

3.1. *Purification, Cloning, and Characterization of a Novel Protein Elicitor*. Crude protein extracted from *Lecanicillium lecanii* (V3) strain was further purified using AKTA purification system. The isolated protein was detected by SDS-PAGE. The SDS-PAGE gel was cut, and the protein band was detected by liquid chromatography mass spectrometry analysis. Result was searched by NCBI-BLAST, and the best-matched protein was obtained (GenBank: OAA81333.1). This novel protein elicitor has 253 amino acid residues and 762 bp. To amplify the gene, primers were designed, and desired band of the gene (762 bp) was obtained from agarose gel (Figure 1(a)). The amplified gene ligated to plasmid pET-28a (+). Target Gene and pET-28a vector joined together by using T4 ligase enzyme. Cells were grown at 37°C in the LB plates overnight. On the next day,

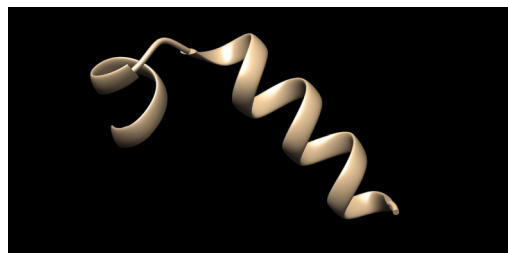


FIGURE 3: The 3D structure of purified protein extracted from *Lecanicillium lecanii*.

positive clone was observed on the plates (Figure 1(b)). The ligated plasmid was transformed into *E. coli*. Recombinant elicitor protein was purified by affinity chromatography (Figure 2(a)). The purified protein recombinant was characterized by a single band at 29 kDa on SDS-PAGE (Figures 2(b) and 3).

3.2. *Effect of Purified Protein Elicitor on the Fecundity of B. tabaci*. A significant result was observed on *B. tabaci* fecundity with the interaction of different purified protein concentrations (i.e., 58.32, 41.22, and 35.41 $\mu\text{g/ml}$). *B. tabaci* adults fed on purified protein (treated plants) produced fewer offspring than those fed control plants (untreated plants). The lowest fecundity rate was observed for the highest protein concentration (58.32 $\mu\text{g/ml}$), and the highest fecundity rate was recorded for the lowest protein concentration (35.41 $\mu\text{g/ml}$) (Figure 4).

3.3. *Expression Levels of SA- and JA-Linked Genes in response to Purified Protein Elicitor*. To evaluate the putative role of novel protein elicitor isolated from *L. lecanii* in induced resistance in cotton against *B. tabaci*, the expression levels of SA- and JA-associated genes were analyzed. The RT-qPCR analyses showed the genes linked with the JA (i.e., GhACT4, GhLOX, and UBQ7) were moderately upregulated at each time interval (12, 24, 48, and 60 h postexposure to *B. tabaci*) (Figure 5), while salicylic acid-associated genes (OPR3, b-1,3-gluconate, and acidic chitinase) were significantly upregulated (Figure 6).

4. Discussion

In recent years, protein elicitor-induced plant resistance has drawn a significant interest for substitute, novel, and eco-friendly plant defense approaches (Mishra et al. 2012). Pathogenic fungi and bacteria, either biotrophic or necrotrophic, constitute an essential source of elicitors such as MAMPs or PAMPs [29]. This study was aimed at an in vitro evaluation of protein elicitor, purified from entomopathogenic fungi, *Lecanicillium lecanii* (V3), to determine its potential role against *B. tabaci*. The isolates from *L. lecanii* showed promising results against *B. tabaci*. A significant effect of purified novel protein elicitor was recorded on the fecundity rate of *B. tabaci*. It was observed that the developmental capability of *B. tabaci* was slowly reduced after the application of the protein-treated plants as compared to untreated plants. Our results are in line with previous findings [28]

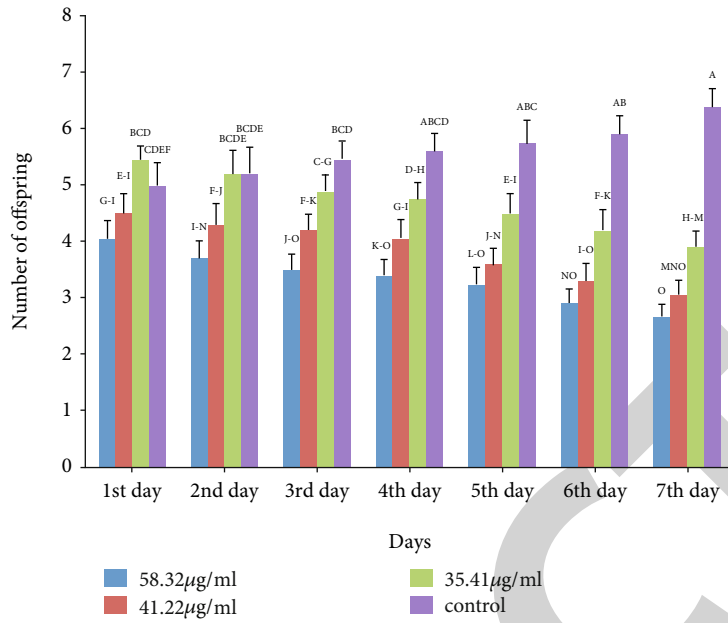


FIGURE 4: Average fecundity of *B. tabaci* after the treatments with different concentrations of protein. Letters on each bar showed the differences among concentrations (one-way ANOVA; LSD at $\alpha = 0.05$).

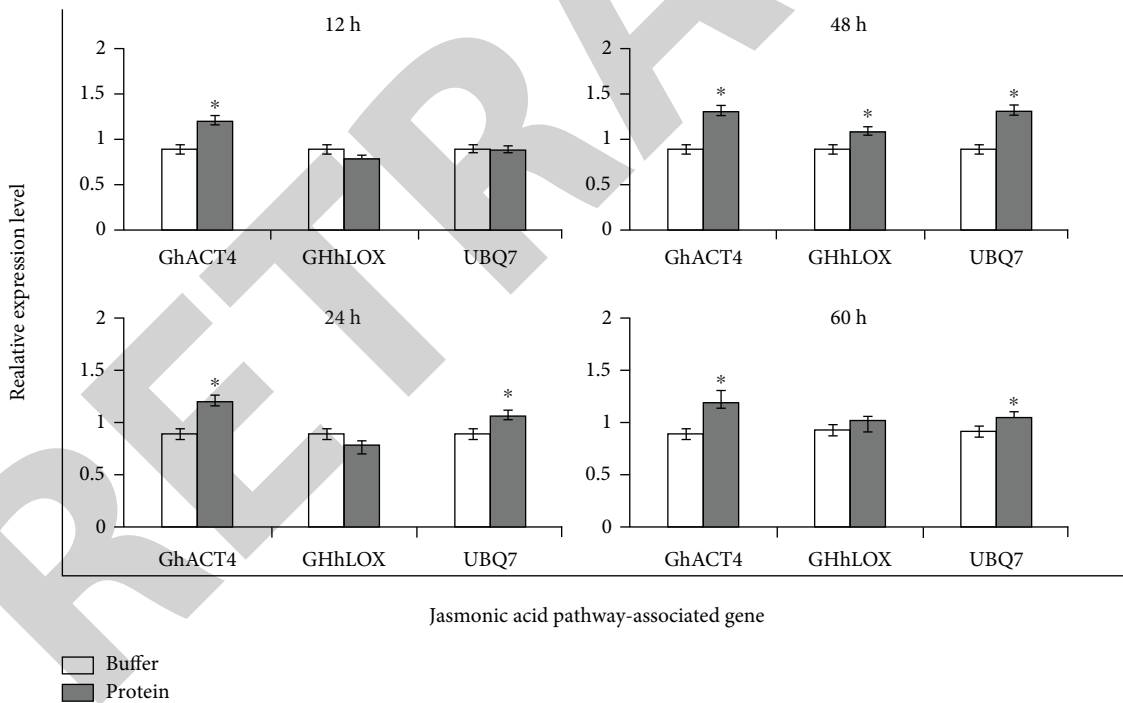


FIGURE 5: Relative expression of JA pathway plant defense observed after applying protein elicitor and *B. tabaci* infestation at various time intervals. The asterisk on bar indicated a significant difference from buffer control by Student's *t*-test ($P < 0.05$) for each gene.

demonstrating that the PeBC1 elicitor caused significantly low mean lifetime fecundity of *M. persicae*. These findings are also like those of [30] who showed a significantly decreased fecundity of *M. persicae* in tomato by the application of protein elicitor PeBL1. In agreement with earlier studies, this result indicates that the treatment of plants

with protein elicitor derived from entomopathogenic fungi has the potential to decrease population growth rates and performance of herbivorous insects. However, elicitors such as JA and MJ may induce the synthesis of different proteinase inhibitors in plants, as showed in tomato plants [31].

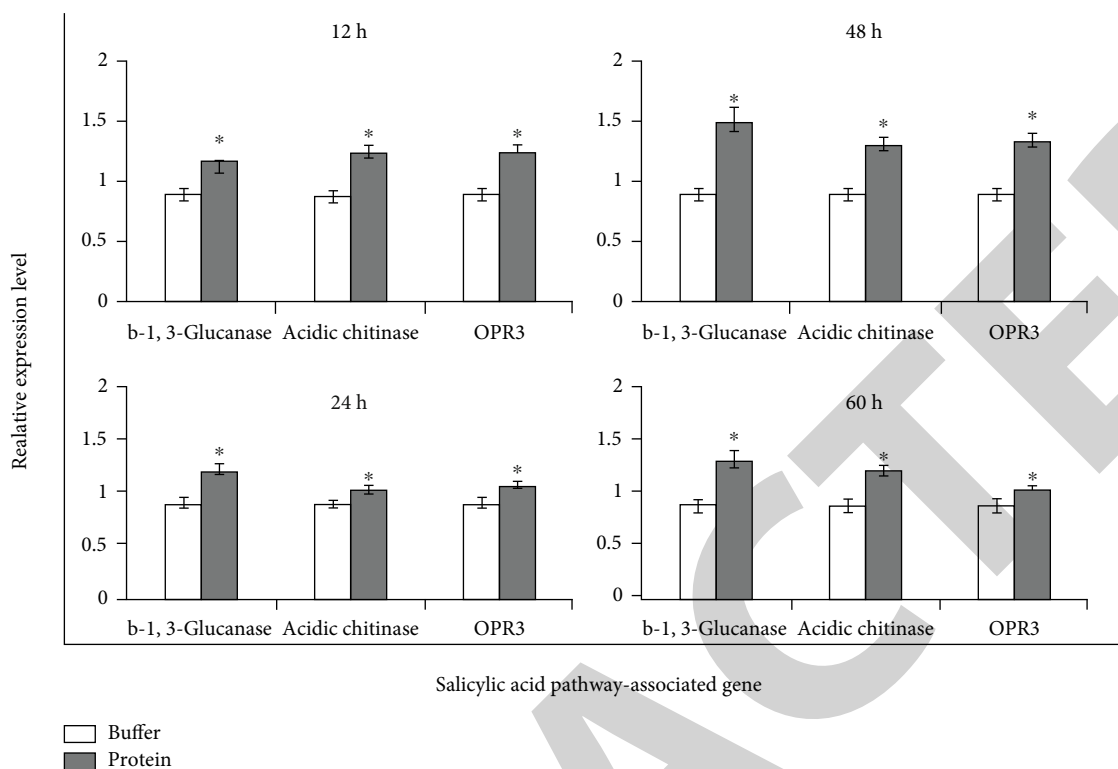


FIGURE 6: Relative expression of SA pathway plant defense observed after applying protein elicitor and *B. tabaci* infestation at various time intervals. The asterisk on bar indicated a significant difference from buffer control by Student's *t*-test ($P < 0.05$) for each gene.

SA, JA, and ethylene (ET) pathways play an important role in insect resistance response in plants. Plant defense pathways contribute to the signaling transduction and promote a more efficient plant defense response to insects [32]. Our findings revealed that SA-linked genes were strongly upregulated, and JA-linked genes were moderately upregulated by the application of *L. lecanii* purified protein. Our results are in line with a previous work by [33–36] which demonstrated that, in different concentrations of protein elicitor PeBb1 extracted from *B. bassiana*, the fecundity rate of *M. persicae* decreased and there was significant upregulation of the expression levels of ET and JA pathway-related genes in *Brassica rapa* ssp. Moreover, these findings corroborate that phloem-feeding herbivores, such as whitefly, activate SA defense pathway-related genes more strongly than those of the JA pathway [37–41].

5. Conclusion

In this study, we reported the purification, cloning, and characterization of a novel elicitor protein isolated from entomopathogenic fungi *Lecanicillium lecanii* (V3) strain as putative pest management tool against whitefly (*B. tabaci*). The effects with recombinant purified novel protein indicated a significant decrease in *B. tabaci* fecundity rate and a significant upregulation of the expression levels of SA and JA pathway-associated genes in the protein-treated cotton plants. These findings suggested that such proteins isolated from entomopathogenic fungi could be used as novel biocontrol pest tools against whitefly (*Bemisia tabaci*).

Data Availability

All data is available within the manuscript.

Conflicts of Interest

The authors declare that they have no conflict of interest.

Acknowledgments

The authors thank the Researchers Supporting Project Number RSP-2021/99, King Saud University, Riyadh, Saudi Arabia.

References

- [1] J. G. Ali and A. A. Agrawal, "Specialist versus generalist insect herbivores and plant defense," *Trends in Plant Science*, vol. 17, no. 5, pp. 293–302, 2012.
- [2] V. Coppola, M. Coppola, M. Rocco et al., "Transcriptomic and proteomic analysis of a compatible tomato-aphid interaction reveals a predominant salicylic acid-dependent plant response," *BMC Genomics*, vol. 14, no. 1, p. 515, 2013.
- [3] B. Bu, D. Qiu, and H. Zeng, "A fungal protein elicitor PevD1 induces *Verticillium* wilt resistance in cotton," *Plant Cell Reports*, vol. 33, pp. 461–470, 2013.
- [4] C. Diezel, C. C. von Dahl, E. Gaquerel, and I. T. Baldwin, "Different lepidopteran elicitors account for cross-talk in herbivory-induced phytohormone signaling," *Plant Physiology*, vol. 150, no. 3, pp. 1576–1586, 2009.

- [5] A. J. Boughton, K. Hoover, and G. W. Felton, "Impact of chemical elicitor applications on greenhouse tomato plants and population growth of the green peach aphid, *Myzus persicae*," *Entomologia Experimentalis et Applicata*, vol. 120, no. 3, pp. 175–188, 2006.
- [6] P. N. Dodds and J. P. Rathjen, "Plant immunity: towards an integrated view of plant-pathogen interactions," *Nature Reviews. Genetics*, vol. 11, no. 8, pp. 539–548, 2010.
- [7] H. D. Burges, *Formulation of Microbial Biopesticides: Beneficial Microorganisms, Nematodes and Seed Treatments*, Springer, Berlin/Heidelberg, Germany, 2012.
- [8] M. A. Bashir, S. Saeed, A. Sajjad et al., "Nesting behavior and biology of blue banded bee, *Amigella mucorea* (Hymenoptera: Apidae) in the sandy desert ecosystem," *Fresenius Environmental Bulletin*, vol. 29, pp. 114–120, 2020.
- [9] M. Batool, M. A. Bashir, M. A. Qayyoom et al., "Effect of k application on the growth and fe/zn use efficiency of salt-tolerant and sensitive maize genotypes in response to salinity," *Fresenius Environmental Bulletin*, vol. 29, pp. 3778–3789, 2020.
- [10] M. A. Bashir, M. S. Nisar, M. Batool et al., "Insecticidal effect of botanical material for the management of pulse beetle, (*Callosobruchus chinensis*): a step toward eco-friendly control," *Fresenius Environmental Bulletin*, vol. 29, pp. 5180–5188, 2020.
- [11] M. S. Nisar, M. A. Bashir, H. Naz, and S. Ahmed, "Comparative effect of termiticides and plant extracts on mortality and tunnel formation of *Odontotermes sobesus*," *Pure Appl. Biol.*, vol. 9, no. 3, pp. 1903–1910, 2020.
- [12] M. A. Bashir, S. Atta, M. S. Nisar et al., "Managing insects pest complex of cotton through foliar spray of insecticides," *Fresenius*, vol. 2020, pp. 5585–5777, 2020.
- [13] S. Chandra and R. Chandra, "Engineering secondary metabolite production in hairy roots," *Phytochemistry Reviews*, vol. 10, no. 3, pp. 371–395, 2011.
- [14] J. T. Kabaluk and J. D. Ericsson, "Metarhizium anisopliae Seed treatment increases yield of field corn when applied for wireworm control," *Agronomy Journal*, vol. 99, no. 5, pp. 1377–1381, 2007.
- [15] J. S. Thaler, A. A. Agrawal, and R. Halitschke, "Salicylate-mediated interactions between pathogens and herbivores," *Ecology*, vol. 91, no. 4, pp. 1075–1082, 2010.
- [16] X. Liao, T. R. O'Brien, W. Fang, and R. J. S. Leger, "The plant beneficial effects of *Metarhizium* species correlate with their association with roots," *Applied Microbiology and Biotechnology*, vol. 98, no. 16, pp. 7089–7096, 2014.
- [17] J. S. Thaler, P. T. Humphrey, and N. K. Whiteman, "Evolution of jasmonate and salicylate signal crosstalk," *Trends in Plant Science*, vol. 17, no. 5, pp. 260–270, 2012.
- [18] F. Liu, H. Liu, Q. Jia et al., "The internal glycine-rich motif and cysteine suppress several effects of the HpaGXoocprotein in plants," *Phytopathology*, vol. 96, no. 10, pp. 1052–1059, 2006.
- [19] F. E. Vega, N. Y. Meyling, J. Luangsa-ard, and M. Blackwell, "Fungal entomopathogens," in *Insect Pathology*, F. Vega and H. E. Kaya, Eds., pp. 171–220, Academic Press, San Diego, CA, USA, 2nd ed. edition, 2012.
- [20] A. K. Mishra, K. Sharma, and R. S. Misra, "Elicitor recognition, signal transduction and induced resistance in plants," *Journal of Plant Interactions*, vol. 7, no. 2, pp. 95–120, 2012.
- [21] Y. Wang, C. C. Dai, J. L. Cao, and D. S. Xu, "Comparison of the effects of fungal endophyte *Gilmaniella* sp. and its elicitor on *Atractylodes lancea* plantlets," *Journal of Microbiology and Biotechnology*, vol. 28, no. 2, pp. 575–584, 2012.
- [22] P. J. Moran, Y. Cheng, J. L. Cassell, and G. A. Thompson, "Gene expression profiling of *Arabidopsis thaliana* in compatible plant-aphid interactions," *Archives of Insect Biochemistry and Physiology*, vol. 51, no. 4, pp. 182–203, 2002.
- [23] J. Wu and I. T. Baldwin, "Herbivory-induced signalling in plants: perception and action," *Plant, Cell & Environment*, vol. 32, no. 9, pp. 1161–1174, 2009.
- [24] T. Nazir, A. Hanan, A. Basit et al., "Putative role of a yet uncharacterized protein elicitor PeBb1 derived from *Beauveria bassiana* ARSEF 2860 strain against *Myzus persicae* (Homoptera: Aphididae) in *Brassica rapa* ssp. *pekinensis*," *Pathogens*, vol. 9, p. 2, 2020.
- [25] H. Zhang, Q. Wu, S. Cao et al., "A novel protein elicitor (SsCut) from *Sclerotinia sclerotiorum* induces multiple defense responses in plants," *Plant Molecular Biology*, vol. 86, no. 4–5, pp. 495–511, 2014.
- [26] A. Ortiz-Urquiza, A. Vergara-Ortiz, C. Santiago-Álvarez, and E. Quesada-Moraga, "Insecticidal and sublethal reproductive effects of *Metarhizium anisopliae* culture supernatant protein extract on the Mediterranean fruit fly," *Journal of Applied Entomology*, vol. 134, pp. 581–591, 2010.
- [27] P. Zhang, F. Wang, and C. Zhu, "Influence of fungal elicitor and macroporous resin on shikonin accumulation in hairy roots of *Arnebiaeuchroma* (Royle) Johnst.," *Sheng Wu Gong Cheng Xue Bao*, vol. 29, pp. 214–223, 2013.
- [28] D. M. Metwally, R. A. Alajmi, M. D. Al-Shammari et al., "Identification of aphid species isolated from tomato crops using phylogenetic approaches in Riyadh and Hafar al-Batin, Saudi Arabia," *Fresenius Environmental Bulletin*, vol. 30, pp. 9367–9370, 2021.
- [29] K. A. Khan, M. A. Bashir, R. Mahmood et al., "Foraging behavior of western honey bee (*Apis mellifera*) in different time intervals on *Brassica campestris*," *Fresenius Environmental Bulletin*, vol. 30, pp. 2707–2712, 2021.
- [30] M. Batool, M. A. Qayyoom, A. Khalofah et al., "Comparative effect of soil and foliar applied FeSO₄ and ZnSO₄ for maize growth under saline conditions," *Fresenius Environmental Bulletin*, vol. 30, pp. 3508–3516, 2021.
- [31] L. Ruiu, "Microbial biopesticides in agroecosystems," *Agronomy*, vol. 8, no. 11, p. 235, 2018.
- [32] A. R. Sánchez-Rodríguez, S. Raya-Díaz, Á. M. Zamarreño, J. M. García-Mina, M. C. del Campillo, and E. Quesada-Moraga, "An endophytic *Beauveria bassiana* strain increases spike production in bread and durum wheat plants and effectively controls cotton leafworm (*Spodoptera littoralis*) larvae," *Biological Control*, vol. 116, pp. 90–102, 2018.
- [33] R. K. Sasan and M. J. Bidochka, "The insect-pathogenic fungus *Metarhizium robertsii* (Clavicipitaceae) is also an endophyte that stimulates plant root development," *American Journal of Botany*, vol. 99, no. 1, pp. 101–107, 2012.
- [34] C. Takeuchi, K. Nagatani, and Y. Sato, "Chitosan and a fungal elicitor inhibit tracheary element differentiation and promote accumulation of stress lignin-like substance in *Zinnia elegans* xylogenic culture," *Journal of Plant Research*, vol. 126, no. 6, pp. 811–821, 2013.
- [35] E. Algar, F. J. Gutierrez-Manero, and A. Bonilla, "Pseudomonas fluorescens N21.4 metabolites enhance secondary metabolism isoflavones in soybean (*Glycine max*) calli cultures," *Journal of Agricultural and Food Chemistry*, vol. 60, no. 44, pp. 11080–11087, 2012.

Retraction

Retracted: Study on Various Luteal Characteristics Using Doppler Ultrasonography for Early Pregnancy Diagnosis in Nili-Ravi Buffaloes

BioMed Research International

Received 12 March 2024; Accepted 12 March 2024; Published 20 March 2024

Copyright © 2024 BioMed Research International. This is an open access article distributed under the Creative Commons Attribution License, which permits unrestricted use, distribution, and reproduction in any medium, provided the original work is properly cited.

This article has been retracted by Hindawi following an investigation undertaken by the publisher [1]. This investigation has uncovered evidence of one or more of the following indicators of systematic manipulation of the publication process:

- (1) Discrepancies in scope
- (2) Discrepancies in the description of the research reported
- (3) Discrepancies between the availability of data and the research described
- (4) Inappropriate citations
- (5) Incoherent, meaningless and/or irrelevant content included in the article
- (6) Manipulated or compromised peer review

The presence of these indicators undermines our confidence in the integrity of the article's content and we cannot, therefore, vouch for its reliability. Please note that this notice is intended solely to alert readers that the content of this article is unreliable. We have not investigated whether authors were aware of or involved in the systematic manipulation of the publication process.

Wiley and Hindawi regrets that the usual quality checks did not identify these issues before publication and have since put additional measures in place to safeguard research integrity.

We wish to credit our own Research Integrity and Research Publishing teams and anonymous and named

external researchers and research integrity experts for contributing to this investigation.

The corresponding author, as the representative of all authors, has been given the opportunity to register their agreement or disagreement to this retraction. We have kept a record of any response received.

References

- [1] U. Riaz, M. Hassan, M. I. Khan et al., "Study on Various Luteal Characteristics Using Doppler Ultrasonography for Early Pregnancy Diagnosis in Nili-Ravi Buffaloes," *BioMed Research International*, vol. 2022, Article ID 3896068, 6 pages, 2022.

Research Article

Study on Various Luteal Characteristics Using Doppler Ultrasonography for Early Pregnancy Diagnosis in Nili-Ravi Buffaloes

Umair Riaz,^{1,2} Mubbashar Hassan ,³ Muhammad I. Khan ,⁴ Umer Farooq ,⁵ Farah Ali ,² Khalid Mehmood ,⁶ Aftab Shaikat ,¹ Mushtaq H. Lashari ,⁷ and Ligu Yang ¹

¹National Center for International Research on Animal Genetics, Breeding and Reproduction (NCIRAGBR), Huazhong Agricultural University, Wuhan, China

²Department of Theriogenology, Faculty of Veterinary and Animal Sciences, The Islamia University of Bahawalpur, Punjab, Pakistan

³Department of Clinical Sciences, University of Veterinary and Animal Science, Jhang Campus, Punjab, Pakistan

⁴Department of Theriogenology, Faculty of Veterinary and Animal Sciences, University of Veterinary and Animal Sciences, Lahore, Punjab, Pakistan

⁵Department of Physiology, Faculty of Veterinary and Animal Sciences, The Islamia University of Bahawalpur, Punjab, Pakistan

⁶Department of Clinical Medicine and Surgery, Faculty of Veterinary and Animal Sciences, The Islamia University of Bahawalpur, Punjab, Pakistan

⁷Department of Zoology, The Islamia University of Bahawalpur, Punjab, Pakistan

Correspondence should be addressed to Ligu Yang; ylg@mail.hzau.edu.cn

Received 20 March 2022; Accepted 11 June 2022; Published 8 August 2022

Academic Editor: Fu-Ming Tsai

Copyright © 2022 Umair Riaz et al. This is an open access article distributed under the Creative Commons Attribution License, which permits unrestricted use, distribution, and reproduction in any medium, provided the original work is properly cited.

The objective of current study was to assess the trend in various luteal characteristics *viz* luteal size (LS), plasma progesterone (P⁴) concentration, and luteal blood flow (LBF) using color Doppler imaging (CDI) and power Doppler imaging (PDI) modes in pregnant and nonpregnant Nili-Ravi buffaloes. Lactating, cyclic, and healthy Nili-Ravi buffaloes ($n = 09$) without any reproductive abnormality were selected in present study. Buffaloes were synchronized using Ov-Synch, and fixed-time artificial insemination was performed (day = 0). Pregnancy was diagnosed on 30-day post-AI using B-mode ultrasonography based on presence or absence of embryonic heartbeat. Ovaries of all animals were scanned from day 5 till 21 post-AI using both B-mode and Doppler ultrasonography to measure LS and LBF. After each ovarian ultrasound examination, blood samples were collected via jugular venipuncture to determine plasma P⁴ concentration. According to results, LBF using CDI and PDI was significantly higher ($P \leq 0.05$) in pregnant buffaloes on days 13 and 15 post-AI, respectively. The mean LS and plasma P⁴ concentration did not differ ($P \geq 0.05$) between pregnant and nonpregnant animals until day 15 post-AI. However, a significant difference ($P \leq 0.05$) was noticed for both on day 17 and onwards. It is concluded that LBF is a more sensitive luteal character as compared to LS and P⁴ for earlier pregnancy diagnosis in Nili-Ravi buffaloes when ascertained through CDI.

1. Introduction

Despite having a significant share in world's milk supply (97,417,135 tons/annum) [1], buffalo dairy production is affected by its reproductive attributes such as delayed puberty, seasonal breeding pattern, less pronounced estrus,

variable time of ovulation, high embryonic mortality, and increased calving interval [2, 3]. Milk yield per day is reduced significantly with the increase in calving interval resulting in economic losses [4]. In order to achieve economic viability and sustained milk production, a calving interval of ≤ 400 days should be attained [5]. Early detection

of nonpregnant animals and their reinsemination of is a key to achieve the goal of one calf per year [6].

The most reliable mean of pregnancy diagnosis in buffaloes is transrectal B-mode ultrasonography conducted around 24 to 30 days post-breeding [7, 8]. Similarly, other chemical based methods have also been reported to detect pregnancy in buffaloes and rely on quantification of progesterone (P^4) in milk and blood at around day 24 post-AI [9]. Pregnancy associated glycoproteins (PAGs) have also been reported for pregnancy diagnosis in buffalo with acceptable accuracy around day 25 postbreeding [10]. Apart from difficulty in conducting chemical-based methods under the field conditions, these methods require repeated sampling and are useful only after maternal recognition of pregnancy that takes place at around day 17 postbreeding [11].

Corpus luteum (CL) has a highest blood supply per tissue volume compared to all other organs, and angiogenesis increases with the growth of CL. In comparison to B-mode, color Doppler ultrasonography is a reliable method to monitor the information related to blood flow of an organ or tissue [12]. Color Doppler ultrasonography has widened the scale of diagnostic imaging from structural to functional aspect in bovine [13]. Modern color Doppler ultrasound scanners are equipped with two techniques *viz* color Doppler imaging (CDI) and power Doppler imaging (PDI) to analyze the blood flow where the latter is considered more sensitive and freer of aliasing artifacts. Hence, PDI is considered advantageous for measuring luteal blood flow (LBF) in cows [14], however, no such information is yet available in Nili-Ravi buffaloes.

Color Doppler ultrasonography has emerged as useful technique to quantify LBF for early identification of nonpregnant animals and for their subsequent reinseminations. Several studies in *Bos taurus* [15], *Bos indicus* [16], and in Mediterranean and Egyptian buffaloes have suggested that LBF is as an indicator of early pregnancy diagnosis [17, 18]; however, these studies on buffaloes lack in depth analysis of LBF and involve postbreeding monitoring of CL for a short or limited time-period with few observations. Moreover, comparative information on luteal dynamics of pregnant and nonpregnant Nili-Ravi buffaloes is not available to date. The objective of current study was to assess the trend in various luteal characteristics *viz* luteal size (LS), plasma progesterone (P^4) concentration, and luteal blood flow (LBF) using color Doppler imaging (CDI) and power Doppler imaging (PDI) modes in pregnant and nonpregnant Nili-Ravi buffaloes.

2. Materials and Methods

2.1. Compliance with Ethical Standards. Current study was performed in accordance with regulations provided by Animal Ethics Board of Huazhong Agricultural University; Grant no. (HZAUMO_2015-12), Wuhan, China. The experimental design was carried out according to good veterinary practices under farm conditions. Besides this, all possible care of animals was taken to ensure maximum welfare.

2.2. Animal Care and Management. Present study was carried out during the breeding season (September to December 2020) at Buffalo Research Institute, Pattoki, District Kasur, Punjab, Pakistan. Clinically healthy Nili-Ravi buffaloes ($n = 09$) of mixed-parity, with a mean (\pm SE) body weight of 432.5 ± 23.4 kg, lactating, and having mean (\pm SE) postpartum days of 163.2 ± 16.2 were selected. All buffaloes were having a regular estrous cycle and had no palpable abnormality in their reproductive tract. Mean body condition score (BCS) of buffaloes was 3.5 ± 0.4 on a 1–5 point scale (5-point scale: 1 = emaciated and 5 = obese) [19]. The buffaloes were kept under semicovered housing with free access to water, offered 30–40 kg of green fodder, 1–2 kg of concentrate comprising of 15% crude protein, and 65% total digestible nutrients per buffalo on daily basis.

2.3. Estrus Synchronization Protocol. All buffaloes were synchronized using Ov-Synch protocol in which 1st GnRH injection (Icirelin $50 \mu\text{g}/2 \text{ cc}$, I/M. Dalmarelin™ Fatro Co., Italy) was administered to buffaloes at a random day of estrous cycle followed by $\text{PGF}_2\alpha$ injection (cloprostenol $150 \mu\text{g}/2 \text{ cc}$, I/M. Dalmazin™ Fatro Co. Italy) at an interval of 7 days. A second injection of GnRH was administered 48 h after $\text{PGF}_2\alpha$, and fixed-time artificial insemination (AI) was performed after 16 h of the last GnRH injection and considered as day 0 in this study [20].

2.4. Ovarian B-Mode and Doppler Sonography for Luteal Dynamics. All buffaloes were subjected to ovarian ultrasound with B-mode and color Doppler mode scanning (My Lab™ 30 VET Gold, Esaote, Genoa, Italy) on alternated days from day 5 to 21 post-AI by a same operator to measure the LS and blood flow pattern. Initially, a linear array transducer (7.5 MHz) was used to scan LS using B-mode ultrasound; later, LBF was measured in the same cross-sectional image of CL by activating Doppler mode ultrasound. Each cross section was examined with both color (CDI) and power (PDI) modes of Doppler ultrasound (see Figure 1). For each animal, three separate observations were recorded using B-mode, CDI, and PDI. All images were stored in bitmap-format in ultrasound machine and transferred to universal storage drive. Thus, each buffalo was scanned 9 times, resulting in a total of 81 measurements. Buffaloes were retrospectively classified as pregnant (presence of embryonic heartbeat, $n = 4$) or nonpregnant (absence of embryo, $n = 5$) on day 30 after AI with B-mode ultrasound.

2.5. Image Analysis and Quantification. The stored images were examined using offline software “Image J” (National Health Institute, Bethesda, MD, USA). Diameter of CL was determined using B-mode images, as explained previously [21]. To measure the cross-sectional area, CL was cropped using “Image J” for pixel analysis. Similarly, using the same software, the area of color pixels within the CL was quantified, which was considered as a semiquantitative parameter of LBF. In each examination, mean values of three images were taken to minimize the chance of error.

2.6. Blood Samples and Progesterone Assay. After each ovarian ultrasound examination, blood samples were collected

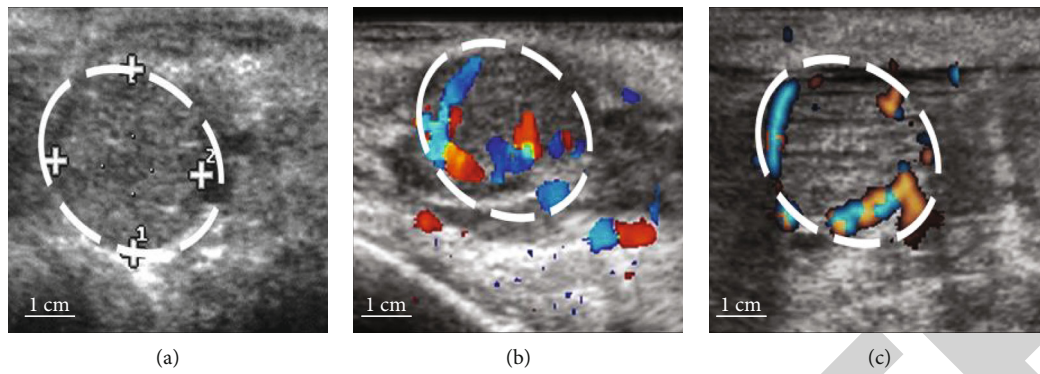


FIGURE 1: Representative ultrasound images of corpus luteum (CL) in Nili-Ravi buffaloes on day 5 postinsemination. (a) B-mode ultrasound image of CL taken by 7.5 MHz transrectal transducer. (b) Color Doppler image depicting luteal blood flow of day 5 postinsemination CL. (c) Power Doppler image depicting luteal blood flow of Day 5 post-insemination CL. The white dotted circles indicate the area of interest (AOI) used to calculate the cross-sectional area of the CL. Within the AOI, the coloured pixels were quantified using image J software (National Institute of Health, Bethesda, MD, USA) to assess the luteal blood flow.

via jugular venipuncture in vacutainer tubes containing heparin (Vacutainer® Systems Europe, Becton Dickinson, Meylan Cedex, France). Centrifugation of blood samples was performed at 4100 g for 10 mins, and the plasma was stored at -80°C until further analysis. Plasma concentrations of P^4 were measured by using a commercially available double antibody radioimmunoassay kit (Immunotech, Prague, Czech Republic) with a ^{125}I -labelled tracer. The interassay and intraassay coefficients of variation for P^4 assay were 6.2% and 3.5%, respectively, with a minimum detection limit of 0.3 ng/ml.

2.7. Statistical Analysis. Normal distribution of the data was verified using Kolmogorov-Smirnov and Shapiro-Wilk tests. Data is presented as mean (\pm SE). The difference between different days and between pregnant and nonpregnant groups for LS, P^4 and LBF was ascertained through analysis of variance (ANOVA) of repeated measure followed by least significant difference (LSD) as a post hoc test. Probability level of $P \leq 0.05$ was considered significant. Relationship between and among various studied attributes was deduced using Pearson’s correlation coefficient, and accordingly, the regression equations were derived through regression analyses. All data were analyzed using Statistical Package for Social Sciences (SPSS for Windows Version12, SPSS Inc., Chicago, IL, USA).

3. Results

Changes in LS, LBF (CDI, PDI), and P^4 during day 5 to 21 postinsemination in nonpregnant Nili-Ravi buffaloes are presented in Table 1. The mean (\pm SE) LS increased nonsignificantly ($P \geq 0.05$) till day 9 post-AI and began to increase significantly ($P \leq 0.05$) from day 11 till 17 post-AI in nonpregnant buffaloes. Afterward, CL size was found to be decreased ($P \leq 0.05$) on day 19 post-AI. The mean (\pm SE) plasma P^4 concentration and LBF (both with CDI and PDI) increased significantly ($P \leq 0.05$) from day 9 and 11, respectively, till day 17 post-AI, after which a decrease

TABLE 1: Comparison of luteal size (LS), plasma progesterone (P^4) concentration, and luteal blood flow (LBF) monitored with color and power Doppler imaging (CDI and PDI) in nonpregnant Nili-Ravi buffaloes ($n = 5$) from day 5 to 21 post-AI.

| Days | LS (cm ²) | P^4 (ng/ml) | LBF | |
|------|-----------------------------|----------------------------|-----------------------------|-----------------------------|
| | | | CDI (cm ²) | PDI (cm ²) |
| 5 | 1.4 \pm 0.1 ^a | 1.8 \pm 0.3 ^a | 0.4 \pm 0.07 ^a | 0.4 \pm 0.06 ^a |
| 7 | 1.6 \pm 0.1 ^a | 2.8 \pm 0.4 ^a | 0.6 \pm 0.08 ^a | 0.6 \pm 0.06 ^a |
| 9 | 1.9 \pm 0.07 ^a | 3.5 \pm 0.4 ^b | 0.6 \pm 0.05 ^a | 0.7 \pm 0.4 ^a |
| 11 | 2.1 \pm 0.09 ^b | 4.4 \pm 0.6 ^b | 0.8 \pm 0.08 ^b | 0.9 \pm 0.1 ^b |
| 13 | 2.5 \pm 0.1 ^b | 5.3 \pm 0.6 ^b | 1.0 \pm 0.1 ^b | 1.0 \pm 0.1 ^b |
| 15 | 2.4 \pm 0.1 ^b | 4.8 \pm 0.6 ^b | 0.9 \pm 0.1 ^b | 0.9 \pm 0.1 ^b |
| 17 | 1.9 \pm 0.1 ^b | 4.0 \pm 0.6 ^b | 0.8 \pm 0.1 ^b | 0.8 \pm 0.09 ^b |
| 19 | 1.6 \pm 0.2 ^a | 2.7 \pm 0.6 ^a | 0.5 \pm 0.05 ^a | 0.5 \pm 0.02 ^a |
| 21 | 1.2 \pm 0.2 ^a | 1.0 \pm 0.4 ^a | 0.2 \pm 0.01 ^a | 0.3 \pm 0.03 ^a |

Values are expressed as mean \pm standard error. ^{a,b} in rows indicate differences ($P < 0.05$) between CL parameters for a given day post-AI.

TABLE 2: Comparison of luteal size (LS), plasma progesterone (P^4) concentration, and luteal blood flow (LBF) monitored with color and power Doppler imaging (CDI and PDI) in pregnant Nili-Ravi buffaloes ($n = 4$) from day 5 to 21 post-AI.

| Days | LS (cm ²) | P^4 (ng/ml) | LBF | |
|------|----------------------------|----------------------------|-----------------------------|-----------------------------|
| | | | CDI (cm ²) | PDI (cm ²) |
| 5 | 1.3 \pm 0.2 ^a | 1.6 \pm 0.2 ^a | 0.5 \pm 0.05 ^a | 0.5 \pm 0.07 ^a |
| 7 | 1.8 \pm 0.1 ^b | 2.3 \pm 0.3 ^a | 0.7 \pm 0.03 ^b | 0.8 \pm 0.1 ^a |
| 9 | 2.1 \pm 0.1 ^b | 4.1 \pm 0.6 ^b | 0.8 \pm 0.1 ^b | 0.9 \pm 0.08 ^b |
| 11 | 2.6 \pm 0.2 ^b | 4.6 \pm 0.4 ^b | 1.1 \pm 0.1 ^b | 1.1 \pm 0.1 ^b |
| 13 | 2.7 \pm 0.1 ^b | 5.7 \pm 0.7 ^b | 1.1 \pm 0.06 ^b | 1.4 \pm 0.1 ^b |
| 15 | 2.7 \pm 0.1 ^b | 6.1 \pm 0.7 ^b | 1.5 \pm 0.06 ^b | 1.5 \pm 0.1 ^b |
| 17 | 2.8 \pm 0.1 ^b | 6.2 \pm 0.5 ^b | 1.6 \pm 0.01 ^b | 1.7 \pm 0.1 ^b |
| 19 | 2.9 \pm 0.1 ^b | 6.4 \pm 0.7 ^b | 1.8 \pm 0.06 ^b | 1.9 \pm 0.1 ^b |
| 21 | 3.2 \pm 0.1 ^b | 6.9 \pm 0.5 ^b | 2.1 \pm 0.06 ^b | 2.0 \pm 0.1 ^b |

Values are expressed as mean \pm standard error. ^{a,b} in rows indicate differences ($P < 0.05$) between CL parameters for a given day post-AI.

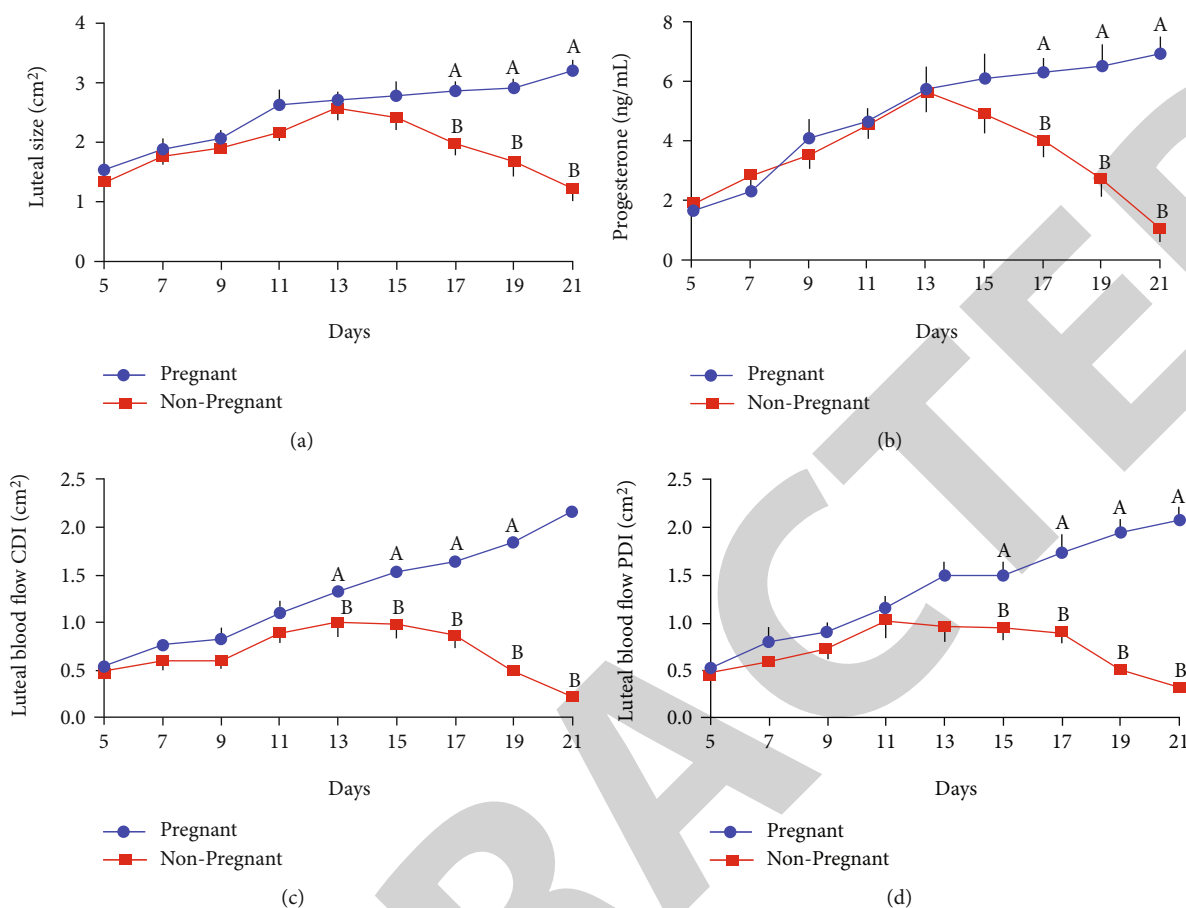


FIGURE 2: Comparison of various CL parameters between pregnant and nonpregnant Nili-Ravi buffaloes after artificial insemination (day 0) from days 5 to 21. (a) Luteal size. (b) Plasma progesterone concentration. (c) Luteal blood flow measured with Color Doppler Imaging (CDI). (D) Luteal blood flow measured with power Doppler imaging (PDI). Different letters (a, b) indicate significant ($P \leq 0.05$) differences between the groups.

($P \leq 0.05$) in P^4 concentration and LBF was observed on day 19 post-AI in nonpregnant Nili-Ravi buffaloes.

Changes in LS, LBF (CDI, PDI), and P^4 during day 5 to 21 postinsemination in pregnant Nili-Ravi buffaloes are presented in Table 2. The mean (\pm SE) LS increased significantly ($P \leq 0.05$) on day 7 to 21 post-AI. The mean CDI increased significantly ($P \leq 0.05$) from day 7 post-AI, while significant increase in mean PDI and plasma P^4 concentrations was observed from day 9 to 21 post-AI in pregnant buffaloes.

A comparison between LS, LBF (CDI, PDI), and P^4 between pregnant and nonpregnant Nili-Ravi buffaloes is presented in Figure 2. The mean (\pm SEM) LS and plasma P^4 concentration did not differ between pregnant and nonpregnant animals until day 15 post-AI. However, a significant difference was noticed on day 17 ($P \leq 0.05$) onwards (see Figures 2(a) and 2(b)). The mean LBF with CDI and PDI significantly differed ($P \leq 0.05$) at day 13 and 15 post-AI between pregnant and nonpregnant buffaloes, respectively (see Figures 2(c) and 2(d)).

Correlation coefficients between LS, CDI, PDI, and P^4 in pregnant and nonpregnant Nili-Ravi buffaloes are presented below (see Table 3). All CL attributes were positively correlated to each other, and highest values were found for

CDI \times PDI in nonpregnant buffaloes ($r = 0.7030$, adjusted $R^2 = 0.48$, $P \leq 0.01$) and for CDI \times PDI and CDI \times P^4 in pregnant buffaloes ($r = 0.98$, adjusted $R^2 = 0.97$, $P \leq 0.01$).

4. Discussion

The current study reports the relative changes between LS, plasma P^4 concentration, and LBF measured with two methods (CDI and PDI) in pregnant and nonpregnant Nili-Ravi buffaloes over the period of CL development and regression after insemination. Previously, fewer studies with different timeframes of CL measurements have been reported in Italian and Egyptian buffaloes [18, 22]. However, assessment of CL attributes using Doppler imaging during its growth and regression phases has not yet been reported for pregnant and nonpregnant Nili-Ravi buffaloes.

The key finding of the present study is that LBF, either measured with CDI or PDI, is a better indicator of luteal function and early pregnancy as compared to LS or plasma P^4 concentration between pregnant or nonpregnant Nili-Ravi buffaloes. The reason is that LBF begins to differ relatively earlier with CDI on day 13 and with PDI on day 15 post-AI, whereas the LS and plasma P^4 concentration

TABLE 3: Correlations coefficients among various CL parameters (LS, P⁴, PDI, and CDI) in pregnant and nonpregnant Nili-Ravi buffaloes.

| CL parameters | <i>r</i> value | Adjusted <i>R</i> ² | Regression equation |
|-----------------------------|----------------|--------------------------------|---------------------|
| Nonpregnant (<i>n</i> = 5) | | | |
| LS × CDI | 0.545** | 0.28 | $Y = 0.8x + 1.2$ |
| LS × PDI | 0.610** | 0.35 | $Y = 1.08x + 1.1$ |
| LS × P ⁴ | 0.554** | 0.29 | $Y = 1.7x + 1.2$ |
| CDI × PDI | 0.703** | 0.48 | $Y = 0.7x + 0.1$ |
| CDI × P ⁴ | 0.567** | 0.30 | $Y = 0.1x + 0.3$ |
| PDI × P ⁴ | 0.390** | 0.13 | $Y = 0.06x + 0.4$ |
| Pregnant (<i>n</i> = 4) | | | |
| LS × CDI | 0.804** | 0.63 | $Y = 0.9x + 1.2$ |
| LS × PDI | 0.735** | 0.52 | $Y = 0.8x + 1.4$ |
| LS × P ⁴ | 0.755** | 0.55 | $Y = 0.2x + 1.4$ |
| CDI × PDI | 0.988** | 0.97 | $Y = 0.9x - 0.2$ |
| CDI × P ⁴ | 0.988** | 0.97 | $Y = 0.9x - 0.2$ |
| PDI × P ⁴ | 0.961** | 0.91 | $Y = 0.2x - 0.1$ |

**Correlation is significant at $P \leq 0.01$. LS: luteal size; PDI: power Doppler imaging; CDI: color Doppler imaging; P⁴: progesterone.

showed divergence on day 17 post-AI between pregnant and nonpregnant Nili-Ravi buffaloes. This is in accordance with earlier report for Egyptian buffaloes and dairy cows in which a significantly higher LBF after AI was observed on day 14 and 15, respectively, and was associated with pregnancy [18, 23]. Studies on *Bos taurus* and *Bos indicus* have also reported similar changes in LBF of pregnant animals as compared to nonpregnant ones [15, 16]. Higher level of LBF in pregnant animals could be attributed to increased vascularity of luteal tissue owing to elevated demand of P⁴ concentration for embryonic support during the pregnancy [24].

In the current study, all functional traits of CL were observed to maintain an increasing trend in pregnant Nili-Ravi buffaloes during the critical period of maternal recognition of pregnancy which takes place around day 15-18 after AI [25]. On the other hand, buffaloes that failed to maintain pregnancy exhibited a decline in CL attributes around day 17 post-AI. This is in accordance with previous studies conducted in beef heifers and dairy cows emphasizing that newly flourishing embryo releases interferon tau (IFNT) before its attachment to uterine wall which in turns blocks the release of PGF2 α from uterine endometrium to prevent luteolysis [11, 26, 27]. During the critical time of maternal recognition of pregnancy, an increased LBF facilitates the relay of embryonic message to prevent luteolysis. This maintains the luteal function of P⁴ production at the time of maternal recognition of pregnancy through the utero-ovarian circulation [11].

In the present study, significant increase in LS took place quite earlier (day 7 post-AI) in pregnant buffaloes as compared to that of nonpregnant ones whereas LS remained consistent till day 11 post-AI. Earlier reports in Mediterranean buffaloes have also concluded that CL dimensions in

pregnant buffaloes increased between day 5 to 10 post-AI, and it can be used to predict the early established pregnancy compared to absolute size of CL [17, 22]. It has been reported that CLs which exhibit early development have greater expression of endothelial growth factor resulting in an increased angiogenesis and increased LBF [22].

Results of the current study indicate that the LBF either measured with CDI or PDI turns out to be a good indicator of luteal function as compared to LS and plasma P⁴ concentration. This could be due to steady growth in luteal vasculature of pregnant buffaloes which has been reported to increase up to 25% between day 6 and 12 postovulation in bovine ovary [28]. In the current study, LBF values with CDI and PDI did not differ significantly on any specific day of observation. Similar observation about PDI have been reported, and it has been suggested that PDI is more sensitive for LBF measurements. This variation could be due to limited number of sample size in the present study [14].

In the current study, functional traits of CL exhibited strong correlation among each other. The obvious reason of strong interrelationship among the attributes studied is that all these parameters are dependent on the functionality of one glandular organ which is CL. These findings are in agreement with previous studies in dairy cows and heifers reporting high correlation among CL attributes [15, 16, 27].

5. Conclusions

It is concluded that color Doppler ultrasonography of CL postbreeding can be utilized to predict early pregnancy in Nili-Ravi buffaloes. Among functional traits of CL, the LBF tends to be more sensitive and diverges earlier than LS and plasma P⁴ concentration between pregnant and nonpregnant Nili-Ravi buffaloes. These findings could be implied to rebreed buffaloes that fail to become pregnant without wasting successive estrus. In this way, these findings would be helpful in reducing calving interval and increase reproductive efficiency for an economically sustainable buffalo farming.

Data Availability

The numerical data used to support the findings of this study are available from the corresponding author upon request.

Conflicts of Interest

The authors declare no conflicts of interest regarding the publication of this paper.

Acknowledgments

The authors acknowledge the contribution of Muhammad Shahzad in conducting radioimmunoassay at Nuclear Institute for Agriculture and Biology (NIAB), Faisalabad, Punjab, Pakistan. The authors also acknowledge Dr. Muhammad Binyameen and Dr. Muhammad Waseem for their support in conduct of experimentation at the Buffalo Research

Retraction

Retracted: Investigation on Immune-Related Protein (Heat Shock Proteins and Metallothionein) Gene Expression Changes and Liver Histopathology in Cadmium-Stressed Fish

BioMed Research International

Received 12 March 2024; Accepted 12 March 2024; Published 20 March 2024

Copyright © 2024 BioMed Research International. This is an open access article distributed under the Creative Commons Attribution License, which permits unrestricted use, distribution, and reproduction in any medium, provided the original work is properly cited.

This article has been retracted by Hindawi following an investigation undertaken by the publisher [1]. This investigation has uncovered evidence of one or more of the following indicators of systematic manipulation of the publication process:

- (1) Discrepancies in scope
- (2) Discrepancies in the description of the research reported
- (3) Discrepancies between the availability of data and the research described
- (4) Inappropriate citations
- (5) Incoherent, meaningless and/or irrelevant content included in the article
- (6) Manipulated or compromised peer review

The presence of these indicators undermines our confidence in the integrity of the article's content and we cannot, therefore, vouch for its reliability. Please note that this notice is intended solely to alert readers that the content of this article is unreliable. We have not investigated whether authors were aware of or involved in the systematic manipulation of the publication process.

Wiley and Hindawi regrets that the usual quality checks did not identify these issues before publication and have since put additional measures in place to safeguard research integrity.

We wish to credit our own Research Integrity and Research Publishing teams and anonymous and named

external researchers and research integrity experts for contributing to this investigation.

The corresponding author, as the representative of all authors, has been given the opportunity to register their agreement or disagreement to this retraction. We have kept a record of any response received.

References

- [1] G. Jabeen, S. Ishaq, M. Arshad, S. Fatima, Z. Kanwal, and F. Ali, "Investigation on Immune-Related Protein (Heat Shock Proteins and Metallothionein) Gene Expression Changes and Liver Histopathology in Cadmium-Stressed Fish," *BioMed Research International*, vol. 2022, Article ID 2075791, 11 pages, 2022.

Research Article

Investigation on Immune-Related Protein (Heat Shock Proteins and Metallothionein) Gene Expression Changes and Liver Histopathology in Cadmium-Stressed Fish

Ghazala Jabeen ¹, Sarwat Ishaq ¹, Mateen Arshad ¹, Shafaq Fatima ¹,
Zakia Kanwal ¹ and Farah Ali ²

¹Department of Zoology, Lahore College for Women University, Lahore, Pakistan

²Department of Theriogenology, Faculty of Veterinary and Animal Sciences, Islamia University Bahawalpur, Pakistan

Correspondence should be addressed to Ghazala Jabeen; drghazala.jabeen@gmail.com

Received 9 May 2022; Accepted 18 July 2022; Published 3 August 2022

Academic Editor: Abdelmotaleb Elokil

Copyright © 2022 Ghazala Jabeen et al. This is an open access article distributed under the Creative Commons Attribution License, which permits unrestricted use, distribution, and reproduction in any medium, provided the original work is properly cited.

Heat shock proteins (HSP) are highly conserved in their structure and released in case of stress. Increased metallothionein (MT) synthesis is associated with increased capacity for binding heavy metals. Healthy juveniles of grass carp were exposed to sublethal dose (1.495 mg L^{-1}) of cadmium for 28 days. Simultaneously, a control group was also run to compare difference of total RNA expression levels in cadmium-treated and control groups. The cadmium levels in the tissues of treated fish recorded were $1.78 \pm 0.10 \text{ mg L}^{-1}$, $1.60 \pm 0.04 \text{ mg L}^{-1}$, and $2.00 \pm 0.05 \text{ mg L}^{-1}$, respectively. Several histological alterations including edema, hemorrhage, dilated sinusoids, hypertrophy, hyperplasia, congestion of central vein, and nuclear alterations were observed in cadmium-exposed fish. Stress gene (metallothionein and heat shock proteins) mRNA transcription levels were studied by mRNA extraction and cDNA preparation by using PCR. The expression level of heat shock protein gene was higher as compared to metallothionein and beta-2-microglobulin gene after cadmium exposure. This study reports various stress-related immune-responsive changes of immune proteins, heat shock proteins, metallothionein, and histopathological changes in fish due to cadmium toxicity that make the fish immunocompromised which may be considered as the biomarkers of cadmium toxicity in other experimental species.

1. Introduction

Heat shock proteins (HSP) are involved in signaling network to reprogram gene transcription, folding and unfolding of proteins, changes in mRNA translation, and degradation of misfolded proteins to ensure protein quality control [1]. Heat shock proteins act as the first line of protection for cells exposed to stressful conditions. They maintain the cell integrity and functionality of the cell signaling pathways critical for regular cell function and cell survival. Because these proteins are induced in the presence of stressors like hot and cold temperature shock, heavy metal toxicity, free radicals, oxidants, toxins, and viruses [2]. HSP70 is an inducible protein and considered major protein of HSP family. HSP per-

formed housekeeping functions and are molecular chaperones in cell.

Metallothioneins are cytosolic protein that conserved in cysteinyl residues. These residues are arranged in two thiol-rich sites with basic amino acids (lysine and arginine) and help to attach, transport, and store heavy metals through thiolate bonding [3]. Expression changes of metallothioneins gene are used as biomarker in fish for detecting water pollution due to heavy metals [4]. Metallothioneins are low molecular weight proteins produced in the presence of divalent ions of cadmium and attach with it for lower the toxicity. But when cadmium is present in high concentration and overcome on detoxification system of metallothionein, then cadmium toxicity effect will be increased [5, 6].

Cadmium is a nonessential element for organisms and considered most toxic heavy metal. Big industries' wastewater has high concentration of cadmium that mixes with river water [7]. Structural and functional changes occur in fish organs due to cadmium accumulation. Cadmium higher concentration was recorded in fish liver and kidney [8]. Heavy metals cadmium, mercury, copper, and zinc induce metallothionein. These are small proteins containing ~7 kDa weight. Cadmium accumulates in liver tissues and causes structural and functional alteration in liver tissues like congestion, blood vessel damages, hepatocyte degeneration, pancreatic cell necrosis, and change in the fats of peripancreatic hepatocytes [9]. Biomarkers are used for indication of histopathological changes and water pollutants. Histological biomarkers are related with the stress biomarkers. Metabolic activation initiated in the presence of many pollutants that induce cellular changes. Several xenobiotics mechanism of action produced specific enzymes that induce metabolic changes, cellular intoxication, cellular death, and cellular necrosis [10]. HSP70 has been sequenced in tilapia [11], rainbow trout [12] and zebrafish [13]. The expression of HSP70 is increased in the presence of proteotoxic environmental stressors.

Cadmium is a hazardous, toxic, and inessential metal that poses a serious health risk for aquatic biota and humans. The potential causes of cadmium toxicity are agricultural and industrial sources leading to the contamination of food and water [14]. The environmental cadmium exposure may be a risk factor due to the toxic impact on the liver and kidneys. These organs are more vulnerable to cadmium's toxicity due to their synthesis ability to produce Cd-inducible proteins, metallothionein proteins that protect the cells [15]. Cadmium exposure causes disorders in metabolic functions, reproduction, growth, developmental anomalies, and immunity suppression due to the accumulation of cadmium in the vital body organs [16–18]. Aquatic ecosystem contamination has proved to be a great threat to natural communities and ecosystem. Cadmium exposure instigates the histopathological changes in vital tissues of animals due to bioaccumulation of metal in the cells [19]. The liver is considered as the dynamic multifunctional organ involved in the metabolism and detoxification of the toxic metals due to the presence of immune-related cells like lymphocytes, neutrophils, kupffer cells, and macrophages [17, 18, 20]. Therefore, the objectives of the current study were to investigate the impact of cadmium on fish health, changes in tissue structure and mRNA expression levels of the immune-related proteins like metallothionein (MT), heat shock proteins (HSP), and beta-2-microglobulin (B2M) genes in control and cadmium-treated liver tissues by using PCR.

2. Materials and Methods

2.1. Experimental Design. A total of 100 freshwater fish (*Ctenopharyngodon idella*) weighing about 6.20 ± 2.38 g and measuring 9.60 ± 1.84 cm in length were collected in plastic bags supplemented with appropriate oxygen from a public fish seed hatchery. After acclimatization, fish were

divided into two groups, control group (normal tap water with continuous aeration) and treatment group subjected to sublethal concentration ($1/10 LC_{50}$, 1.495 mg L^{-1}) of cadmium based on predetermined value of LC_{50} calculated previously [21]. The experiment was conducted by employing a semistatic system. At the end of exposure periods, liver tissue was removed and stored at -40°C for analysis.

2.2. Chemical Analysis of Fish for Cadmium Accumulation. Cadmium concentrations were measured directly in digested filtrates by Zeeman Atomic Absorption Spectrometry (Z-500) by following method #3500-Cd B of A.P.H.A. (2005) by process of wet digestion. 0.5 g of samples of fish organs, i.e., liver, heart, and skin, were in 100 mL beakers and digested in V/V 3:1 composition of concentrated nitric acid and hydrochloric acid. The filtrates were analyzed for cadmium concentration on Zeeman Atomic Absorption Spectrometry (Z-500).

2.3. Qualitative and Quantitative Histological Assessment. Liver tissues of *C. idella* after cadmium exposure were randomly sampled for histopathological studies. The qualitative and quantitative assessment was carried out by analyzing the frequency, prevalence percentages, and histological alteration indices calculated by assessing histological alterations and comparison between the degrees of damage of the alterations in the same organ [22]. The identified individual alterations were given an importance factor according to the [23] that represented the intensity of the alterations to harm fish health. The score value and importance factor for each alteration were multiplied to find out the histological alteration index (HAI) values to calculate the degree of tissue damage by liver indices.

2.4. Total RNA Extraction and Preparation of cDNA. Liver tissue of 50 mg of grass carp *C. idella* was used for preparation of cDNA and extraction of total RNA for analysis of genes (metallothionein, heat shock proteins, and housekeeping gene B2M) expressions. Total RNA was extracted using a standard TRIzol procedure (Invitrogen) according to manufacturer's instructions. The DNA extraction kit was used for synthesis of cDNA according to the manufacturer's instructions. The purity of total RNA extracted and synthesized during the present study was checked and examined by agarose gel electrophoresis in which samples were run on 3% agarose gel to avoid disruption of bands. There was no or negligible degradation of total RNA during preparations and purification of samples. The samples were analyzed and amplified by using PCR technique by following the method of [24]. PCR was performed by the synthesis of primers for magnifications of heat shock proteins (HSP70), metallothionein (MT) genes, and housekeeping gene B2M (Table 1) calculated on the basis of specifically designed genomic DNA and sequence information of MT and HSP of *C. idella*. Housekeeping gene B2M was used as an internal control to normalize mRNA expressions in the PCR.

2.5. Statistical Analysis. All the data were presented as mean \pm S.D. The histological alterations were observed by using microscope and photographed through an OPTIKA

TABLE 1: List of primers used for the heat shock proteins (HSP70), metallothionein (MT), and beta-2-microglobulins (BM2), melting temperature (Tm).

| Gene | Forward and reverse sequence | Tm | GC content (%) | 3' complementarity | Product |
|------|------------------------------------|-------|----------------|--------------------|---------|
| HSP | Primer F: CTGCTGGATGTGGCTCCTCTGTC | 64.96 | 60.8764.96 | 1.00 | 107 |
| | Primer R: AAGGTCTGGGCTCTGTTTGGTGGG | 64.51 | 56.52 | 0.00 | |
| MT | Primer F: ATGGATCCTTGCGATTGCG | 58.68 | 52.63 | 2.00 | 182 |
| | Primer R: CATTGACAGCAGCTGGAGCC | 61.65 | 60.00 | 4.00 | |
| B2M | Primer F: GGCTGGCAGTTTCACCTCAC | 61.52 | 61.52 | 0.00 | 150 |
| | Primer R: CCACCCTTTGTCTGGCTTTG | 59.32 | 55.00 | 0.00 | |

microscope. SPSS Ver. 21 statistical software was used for analysis and descriptive statistics to represent biometric data, HAI values, C.F. of control and treated groups to calculate the percentage prevalence for the number of fish that demonstrated with the same histological alterations.

3. Results

3.1. Fish Meat Quality Indicators and Specimen Data. The mean value of body mass (w), length (L), and condition factor of control fish were 10.00 ± 0.90 g, 9.20 ± 0.24 cm, and 1.30 ± 0.34 g cm⁻³, respectively, for the control fish whereas the condition factor of exposed fish depicted significantly lower value of 0.80 ± 0.34 g cm⁻³ as compared to control fish. The body length and body weight of exposed fish were 10.20 ± 0.69 cm and 9.20 ± 0.25 g, respectively. The condition factor of control fish was higher (1.30 ± 0.034 g cm⁻³) as compared to the exposed fish which showed better quality and taste of fish while lower mean value of condition factor of exposed fish (0.80 ± 0.34 g cm⁻³) indicated deteriorated meat quality and condition due to toxicity of cadmium presented in Figure 1.

3.2. Bioaccumulation of Cadmium in Fish Tissues. Control and exposed fish were compared for cadmium accumulation in different organs. Figure 2 shows the metal accumulation levels in the liver, heart, and skin during chronic cadmium exposure. The accumulation values of cadmium in control carp fish were considerably low, but metal-exposed fish showed maximum value of accumulation. The mean value of cadmium in the liver of exposed fish, grass carp, was significantly high (1.78 ± 1.04 μ g g⁻¹). The heart of the Cd-exposed fish accumulated cadmium with the mean value of 1.60 ± 0.05 μ g g⁻¹ whereas the skin of the fish accumulated higher cadmium concentration (2.00 ± 0.04 μ g g⁻¹).

3.3. Histological Assessment of Fish (*C. idella*). Control fish liver represented particular parenchymatous appearance. The size and shape of the liver were normal for the unexposed fish (Figure 3(a)) whereas the exposed fish showed mild to severe lesions in the tissue structure, i.e., hypertrophy, vacuolar degeneration, hepatic necrosis, and dilated sinusoids (Figures 3(c)–3(e)).

Table 2 demonstrates the highest prevalence percentage of 90% observed for dilated sinusoids while the lowest prevalence percentage of 67% was recorded for partial degenera-

tion of hepatic mass. In case of cadmium-exposed fish, the value of prevalence percentage was the highest (93%) for hemorrhage and 63% was the lowest value for proliferation of hepatic cells (Table 2). The prevalence percentage for dilated sinusoids was 60% and 90% for chronic exposure groups, respectively. Table 3 shows comparison of semi-quantitative scoring of histological changes in the liver of 28-day exposed fish and control (unexposed fish) and pronounced abrasions were hepatic necrosis, hyperplasia, hemorrhage, hepatic infiltration, dilated sinusoids, pyknotic nuclei, edema, fat cell accumulation, and hypertrophy.

The analysis of histological alteration indices (HAI values) depicted that mean HAI value for the liver of 28-day-treated fish was 78. Mean HAI value for focal area of necrosis and vacuolar degeneration was the highest as compared to other individual alterations, and it was reported as 9 whereas proliferation of hepatocytes showed mean HAI value of 2 under the same exposure conditions (Table 4).

The organ index (I_{org}) of the liver tissue was calculated and described in Figure 4. The overall assessment of lesions found in liver tissue based on score and importance factor was 48. The comparison of reaction indices of various reaction patterns in liver tissues showed the highest reaction index for reaction pattern of regressive change was 32 while the lower organ index for reaction pattern of progressive change was observed as 8.

3.4. Changes in mRNA Expression Levels of Immune-Related Metallothionein and HSP70 under Sublethal Cadmium Exposure. The results of transcriptional levels of both genes were compared with housekeeping gene B2M transcriptional levels used as an internal control in liver samples of *C. idella* exposed to sublethal (1.495 mg L⁻¹) concentration of cadmium. A fragment of housekeeping gene BM2 with a molecular weight of 46440.17 Da was cloned and amplified using primers specially designed for cloning and amplification. The product of 150 bp of housekeeping gene was utilized as an internal control for the analysis of relative expression of metallothionein (MT) and heat shock proteins (HSP70) during cadmium exposure. Housekeeping gene during the present investigation served as mediator for the evaluation mRNA expressions, processes of nucleic acid extraction and depiction PCR quality and quality of liver samples obtained from exposed fish. All the samples of liver showed higher value of relative abundance of mRNA expressions for metallothionein gene ($p < 0.05$) as shown in Figure 5. The

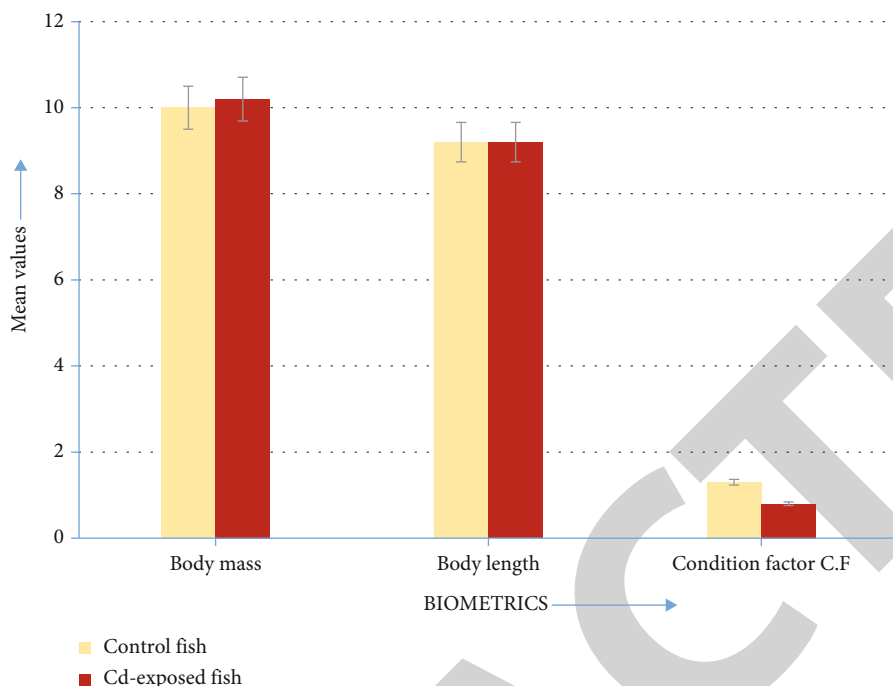


FIGURE 1: Mean values of body mass, body length, and condition factor of control and treated fish for visual health assessment.

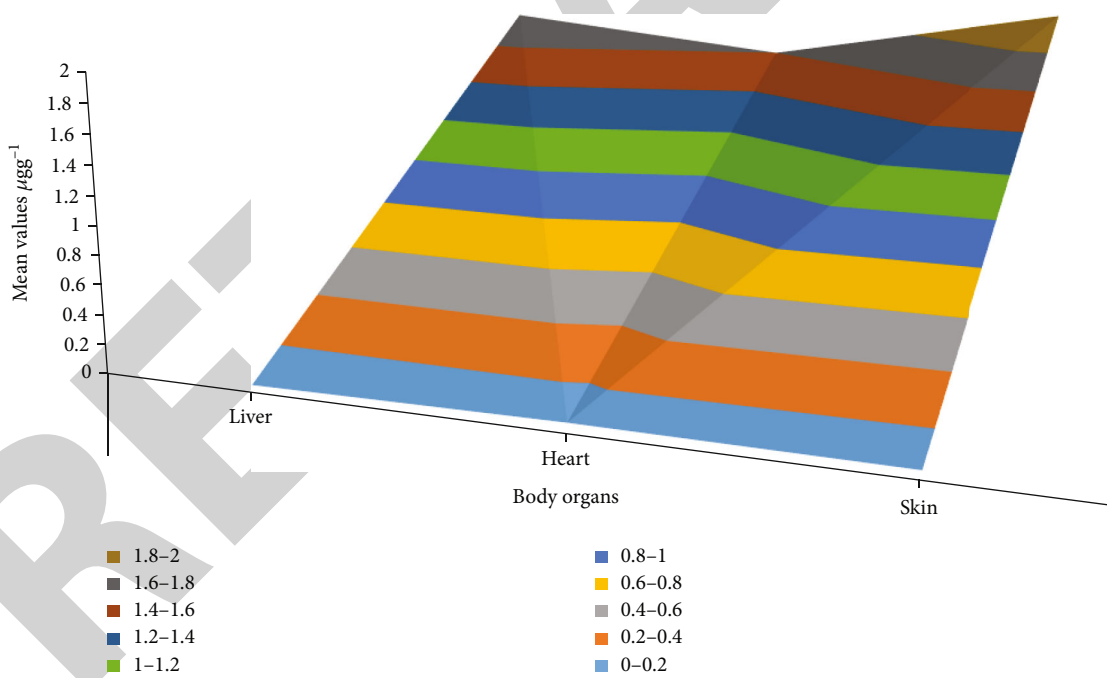


FIGURE 2: Bioaccumulation of cadmium in the liver, skin, and heart of fish after cadmium exposure.

molecular weight of metallothionein analyzed from the expressed transcriptional levels in the samples was 55892.06 Da. The metallothionein expression was compared and analyzed with a ladder consisting of 50 bp with lower and upper base pair sequences of 30 bp and 50 bp, respectively.

In the present investigation, expression analysis of HSP70 (a product of 107 base pairs) isolated from the liver

samples exposed to sublethal cadmium concentrations revealed a molecular weight of 32805.14 Da. The fragments of cDNA in lanes 1 and 5 showed the ladder and housekeeping gene sequences, respectively. The sequences of HSP70 were expressed in lane 2-4 are amplified by using HSP70 reversed and forward sequences and revealed to be about 107 base pairs (bp) examined on the 3% agarose gel. The interrelation of transcriptional levels and cadmium retention

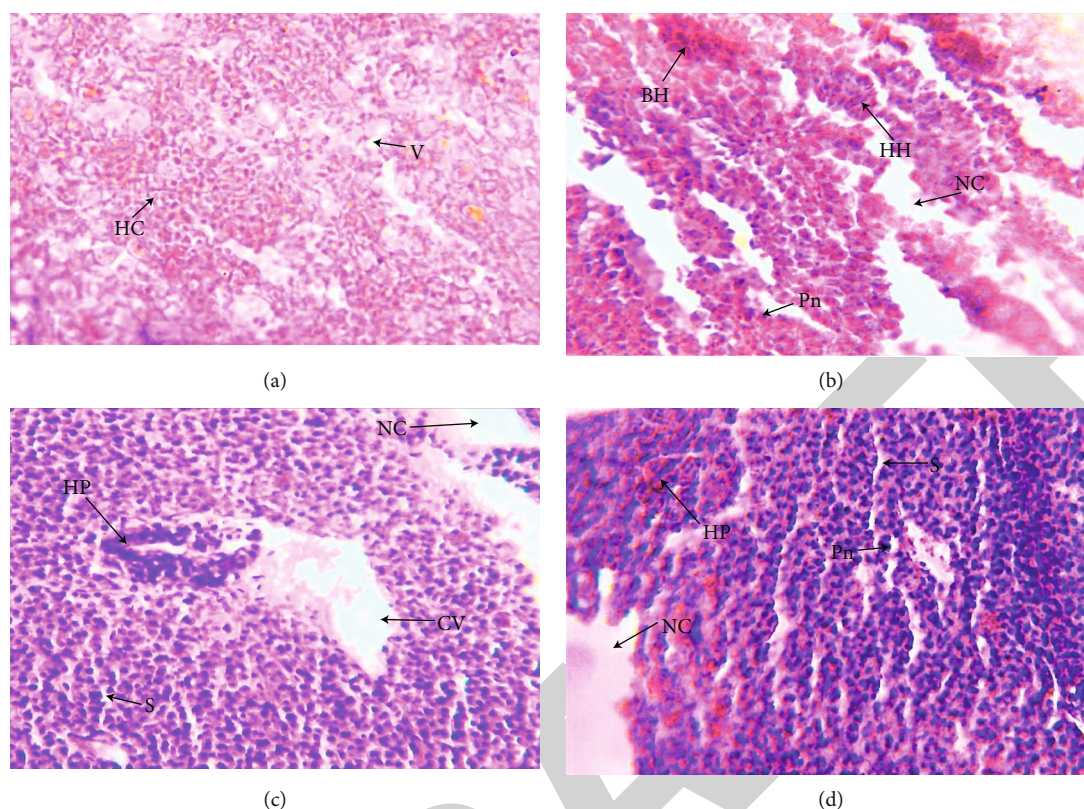


FIGURE 3: Photomicrograph of liver of fish: (a) control fish; (b–d) under cadmium exposure showing V: vessels; S: sinusoids; HC: hepatic cells; BH: blood damage; NC: necrosis; HH: hypertrophy; HV: hepatic vacuoles; Hae: hemorrhage (4 μm thick; H&E staining; 10x).

TABLE 2: Frequency and prevalence percentage of histological alteration of *Ctenopharyngodon idella* exposed under acute and chronic toxicity of cadmium.

| Organ | Histological alterations | Frequency (n = 30) | Prevalence (%) |
|----------------------|--------------------------------------|--------------------|----------------|
| Liver | Nuclear alteration | 22 | 73 |
| | Hepatic necrosis | 26 | 87 |
| | Hyperplasia | 25 | 83 |
| | Hemorrhage | 28 | 93 |
| | Hepatic infiltration | 23 | 77 |
| | Dilated sinusoids | 27 | 90 |
| | Congestion of central vein | 20 | 67 |
| | Pyknotic nuclei | 22 | 73 |
| | Proliferation of hepatic cells | 19 | 63 |
| | Edema | 23 | 77 |
| | Pigmented cell rupture | 21 | 70 |
| | Fat cell accumulation | 24 | 80 |
| | Hypertrophy | 25 | 83 |
| | Alarm cells | 19 | 63 |
| | Partial degeneration of hepatic mass | 20 | 67 |
| Vacuole degeneration | 25 | 83 | |

in the liver of exposed grass carp attained the maximum (3.5 fold, $p < 0.05$) in the Cd-treated fish samples as compared to the control. The comparison of transcriptional levels of HSP70 and MT revealed that mRNA expressions of metallo-

thionein gene were statistically significantly higher compared to the heat shock proteins. The analysis levels of expression of both genes (metallothionein and heat shock proteins 70) in the livers of treated fish exhibited higher

expressions than housekeeping gene B2M. The expression levels of all the genes analyzed during the present investigation followed the order of magnitude as HSP > MT > B2M.

4. Discussion

Heat shock proteins have demonstrated the capacity of inducing the long-lasting protective immune responses and HSPs have been considered as proinflammatory damage-associated molecular response especially HSP60 and HSP70 [25, 26]. In the present investigation, the adaptive immune response of freshwater fish *C. idella* was studied by investigating the differential expression levels changes of HSP and MT genes exposed to cadmium toxicity.

The most important environmental problems are heavy metal pollution that leads to adaptive evolution of immune proteins in animals. The heavy metal toxicity induces changes in the expression levels of HSP and MT gene. The heavy metals released from industrial, man-made activities, domestic processes, and anthropogenic have adversely contaminated the aquatic systems. Heavy metal pollution has disturbing effects on the ecological balance of the environment. The most toxic heavy metal is cadmium and toxic for aquatic life as an environmental pollutant. After the maximum level of metals in the polluted aquatic system fish start collection of metals directly from the environment [27, 28]. The cadmium contamination of aquatic ecosystems has increased cadmium deposits in tissues of aquatic organisms in all food chains [29, 30].

The treated exposed to sublethal dose of cadmium exhibited a range of abnormal behavior consisting of restlessness, irregular movement patterns, slow feeding, lack of balance, erratic swimming, air gulping, excessive secretion of mucus, rolling movement, and swimming in the backward direction. Similar behavioral changes were also observed by [31], while control fish established normal physiology with no distinct behavioral changes. There was no physical change like fin rot, dropsy, itching, no tumors, and lesions in control fish. The behavioral changes seen are symptomatic of internal disturbances of the body functions such as inhibition of enzymes, impairment of neural transmission, and disturbances in metabolic pathways stated by Altindag [32]. The abnormal behavioral manifestations revealed by the fingerlings on contact to lead are similar to that reported for other toxicants like cadmium and chromium explained by [33].

During present studies, cadmium concentration demonstrated the deteriorated condition of fish, bioaccumulation of metal in heart, skin, and liver tissues, and histological alterations in the liver of fish exposed to Cd-contaminated medium. The mean value of condition factor of control fish as compared to exposed fish highlights poor condition and deteriorated meat quality of the fish due to cadmium exposure. The mean condition factor of fish for the control and exposed group was 0.7 ± 0.2 , 0.8 ± 0.2 , and $0.8 \pm 0.2 \text{ g cm}^{-3}$, respectively, recorded by [34]. The results of present investigation are also in accordance with McHugh [35]. Nonsignificant effects of Cd on rainbow trout, fathead minnow, and channel catfish are reported by [36]. Under metallic toxicity, rainbow trout showed reduced growth and lower FCE

TABLE 3: Histological alterations in the liver of *Ctenopharyngodon idella* determined by using semiquantitative scoring method.

| Histological alterations | Control | Cd-exposed group |
|--------------------------------------|---------|------------------|
| Nuclear alterations | - | ++ |
| Hepatic necrosis | - | +++ |
| Hyperplasia | - | +++ |
| Hemorrhage | - | +++ |
| Hepatic infiltration | - | +++ |
| Dilated sinusoids | - | +++ |
| Cognition of central vein | - | ++ |
| Pyknotic nuclei | - | +++ |
| Proliferation of hepatocytes | - | ++ |
| Edema | - | +++ |
| Pigmented cell rupture | - | ++ |
| Fat cell accumulation | - | +++ |
| Hypertrophy | - | +++ |
| Alarm cell | - | ++ |
| Partial degeneration of hepatic mass | - | ++ |
| Vacuole degeneration | - | +++ |

Results of histological assessment evaluated as mild and minor abrasions $\leq 25\%$ represented by +; medium abrasions $\leq 50\%$ represented by ++; pronounced abrasions $\leq 75\%$ represented by +++; severe abrasions $\geq 75\%$ represented by ++++, and no histological alteration $\leq 0\%$ represented by -.

was due to slow rate of feeding; similarly, studies on the effect of chronic sublethal zinc exposure demonstrated growth inhibition in *Cirrhinus mrigala* [37].

Cadmium is a common heavy metal of natural waters and is highly toxic to the aquatic organisms even at very low concentration that can result into significantly lower condition factor indices in the exposed fish as observed during present investigation [38]. Effects of metallic toxicity on feed intake, growth, FCE, and condition factor of tilapia with decreased in meat quality interpreting it unhealthy for human consumption were reported by [39]. [40] also reported significantly decreased body condition factor and growth parameters of fish exposed to different concentrations of cadmium ($p < 0.05$) as compared to the control due to increase in stress as a result of cadmium exposure.

In the present investigation, the mean cadmium level in the liver of exposed fish (0.37 ± 0.027) was expressively higher compared to control fish. Perera et al. [41] reported higher concentration of cadmium in exposed fish liver when compared with control fish. The accumulation of metal in the liver of control and exposed fish was 12.4 and 82.1 mg/kg, respectively, and maximum metal accumulation in exposed fish as compared to control fish revealed negative impact of metals on tissues described by [42].

In the present investigation, the skin of the control fish revealed significantly lower mean cadmium concentration whereas the exposed fish accumulated cadmium with the mean value of $14.46 \pm 41.65 \text{ mg L}^{-1}$. The difference between the control and exposed fish for the accumulation of cadmium in the liver, heart, and skin remained significantly higher which showed negative impact of cadmium on fish

TABLE 4: HAI index assessment of the liver of exposed *Ctenopharyngodon idella* by using importance factor and score value of cadmium chronic toxicity.

| Histological abrasions | Importance factor (w) | Score value (a) | Index (I) | HAI ($a \times W$) |
|--------------------------------------|---------------------------|---------------------|---------------|----------------------|
| Hemorrhage | $W_{IC1} = 1$ | $a_{IC1} = 3$ | I_{IC} | 3 |
| Edema | $W_{IC2} = 2$ | $a_{IC2} = 3$ | | 6 |
| Hepatic necrosis | $W_{IR1} = 3$ | $a_{IR1} = 3$ | I_{IR} | 9 |
| Partial degeneration of hepatic mass | $W_{IR2} = 1$ | $a_{IR2} = 2$ | | 2 |
| Congestion of central vein | $W_{IR3} = 2$ | $a_{IR3} = 2$ | | 4 |
| Vacuole degeneration | $W_{IR4} = 3$ | $a_{IR4} = 3$ | | 9 |
| Alarm cells | $W_{IR5} = 1$ | $a_{IR5} = 2$ | | 2 |
| Focal area of necrosis | $W_{IR16} = 3$ | $a_{IR16} = 3$ | | 9 |
| Dilated sinusoids | $W_{IP1} = 3$ | $a_{IP1} = 3$ | I_{IP} | 9 |
| Pigmented cell ruptured | $W_{II1} = 2$ | $a_{II1} = 2$ | | 4 |
| Fat cell accumulation | $W_{II2} = 1$ | $a_{II2} = 3$ | | 3 |
| Hyperplasia | $W_{LP4} = 2$ | $a_{LP4} = 3$ | I_{LP} | 6 |
| Hypertrophy | $W_{LP5} = 1$ | $a_{LP5} = 3$ | | 3 |
| Hepatic infiltration | $W_{II3} = 1$ | $a_{II3} = 3$ | | 3 |
| Nuclear alteration | $W_{LR16} = 2$ | $a_{LR16} = 2$ | I_{LR} | 4 |
| Proliferation of hepatocytes | $W_{LI3} = 1$ | $a_{LI3} = 2$ | I_{LI} | 2 |
| Mean value of I_{liver} | | | | 78 |

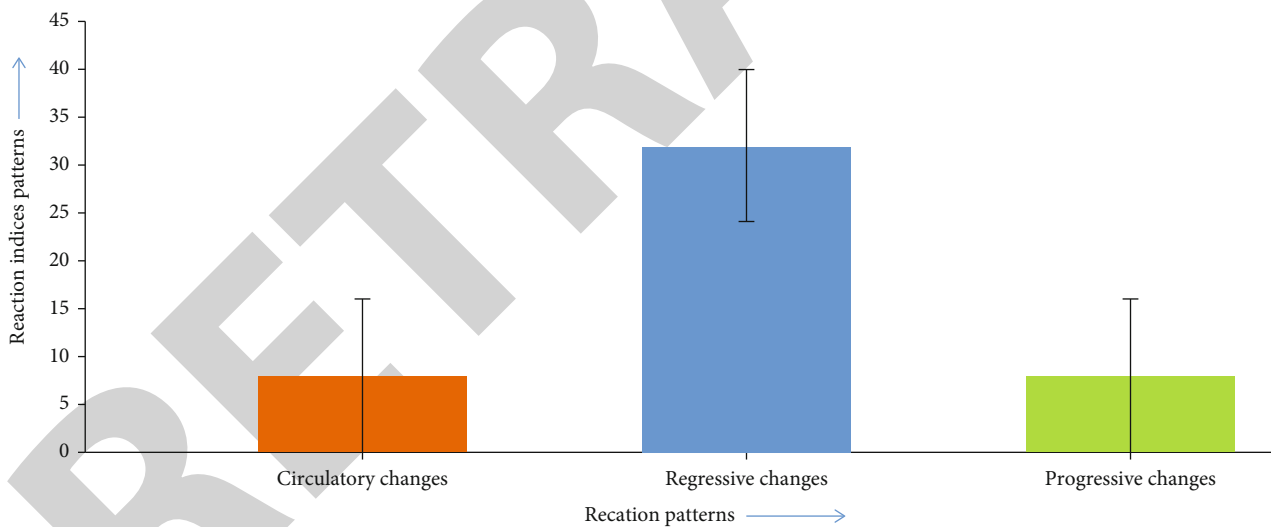


FIGURE 4: Calculation of reaction indices in the liver of fish exposed to sublethal cadmium levels.

body organs. The analysis of cadmium level in the tissues under the chronic exposure condition followed the order skin > liver > heart. Abdel-Warith et al. [43] reported that the higher accumulation of heavy metal in the liver may alter the level of various biochemical parameters and may also cause severe liver damage. Similar results were demonstrated by [44]. Malik et al. [45] reported that the concentration of heavy metals in liver of *L. rohita* and *C. straitus* was found to be higher than the other organs because the liver acted as an important organ for storage and detoxification.

The liver is a vital organ which is mostly affected by water pollutants because of its role in detoxification and bio-transformation processes. After acute and chronic cadmium exposure, the histological alteration in the liver of *Ctenopharyngodon idella* was hemorrhage, edema, hypertrophy, hyperplasia, and hepatic cell necrosis. Ptashynski et al. [46] and Fanta et al. [47] described these alterations in fish liver by pollutants. *Clarias gariepinus* was exposed with lead and determined the degeneration of hepatocytes and focal area necrosis in the liver of fish by [48].

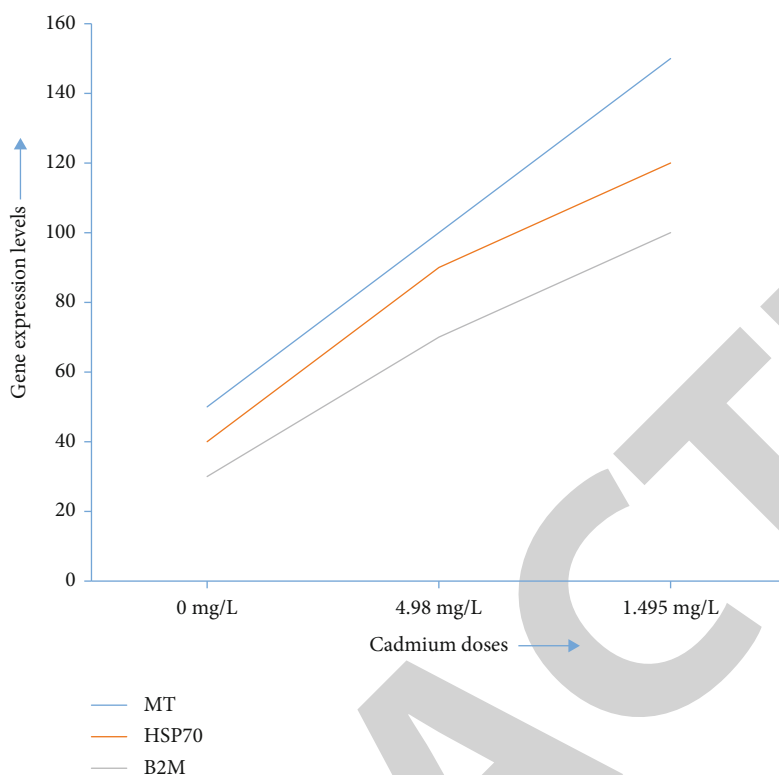


FIGURE 5: Comparison of mRNA expression of metallothionein, heat shock proteins (HSP70), and beta-2-microglobulin (B2M) due to cadmium dose kinetics under sublethal exposure conditions.

In the current investigation, the liver of exposed fish showed histopathological alteration such as hypertrophy, hyperplasia, necrosis, dilated sinusoids, inflammation, hemorrhages, pigmented cell rupture, focal area of necrosis, partial degeneration of hepatic mass, pyknotic nuclei, and congestion of central vein. The results are in accordance with [49] who described the similar histological alterations in the liver of fish, *Channa punctatus*, due to toxicant exposure. Progressive changes in the liver of exposed fish were hypertrophy, hyperplasia (enlargement of tissue by greater number of cells without change in volume of cells), and dilated sinusoids reported by the present study. In the present study, histological changes of desired organ investigated and pathological alterations determined during acute and chronic exposure of cadmium were explained into five major reaction patterns for assessment of histopathological alteration in exposed fish. According to the Wang et al. [17], Wang et al. [18], cadmium exposure caused histopathological changes in the liver and induced negative impact on immunity, stress defense mechanism, and metal transport system in grass carp (*Ctenopharyngodon idella*).

In the current study, the samples showed significantly increased expression of metallothionein gene due to cadmium accumulation and detoxification role performed by the liver. The analysis of relative abundance and transcriptional concentrations of metallothionein showed heightened levels in cadmium treated liver specimens as compared to the mRNA expression in the housekeeping genes as an inter-

nal control. The quantity of metallothionein gene expression in the liver varied significantly, and an initial 1.5-fold increase was observed due to toxic cadmium exposure and later it was magnified up to 3.5-fold showing direct dependence on the exposure duration and rate of cadmium accumulation in the liver of grass carp. [50] reported upregulated metallothionein expression levels in Cd-exposed fish due to accumulation of cadmium in the liver tissue suggestive of the cadmium toxicity effect on the regulation of gene transcription. The results are also in accordance with the study of [19, 21] who reported the effect of different absorption of cadmium was observed on tissue MT mRNA transcript level and showed that MT mRNA expression was definite and dose dependent on tissues of *Channa punctata*.

Different species of fish were used for observing the behavior of HSP70 in stress and unstressed cell. The heat shock cognate protein (HSC70) performed the different functions like formation of complex receptor, activin growth factor activation, and activation of morphogenetic protein of bone. Under stressed and normal condition, HSP70/HSC70 moved toward lysosomes which speed up protein degradation and catabolism [51].

In the present investigation, the analysis of HSP70 (a product of 107 base pairs) isolated from the liver samples revealed a molecular weight of 32805.14 Da. All the amplification products were similar to the corresponding genomic sequence of heat shock proteins. HSP levels have been

reported to be associated with the environmental stress conditions mainly involved in the cellular defense pathways and detoxification mechanisms [16, 52–54]. Cadmium exposure induced the upregulation of HSP70 and MT expressions in aquatic organisms in several studies reported by Yu et al. [55]; Sung et al. [56]; Chung et al. [57]; Maulvault et al. [58].

The amount of relative abundance of mRNA showed significant increase as a result of 28-day exposure period. The expression of MT and HSP70 genes in Cd-stressed fish depicted clearly that fish exhibited stress-dependent pattern of mRNA expressions following the sublethal cadmium exposure. The same increasing trend was observed for all genes in all the examined fishes. The present study revealed higher upregulation of expression of HSP70 due to stressed culture conditions and higher rate of accumulation in fish organs causing impairments in gene regulation mechanisms. [28] also investigated the immune responses and changes in the expression of immune-related genes in the liver tissue of fish after sublethal cadmium exposure of 28 days. They confirmed the upregulation of HSP60, HSP70, and HSP90 indicative of cadmium-induced cellular stress. Very little information is available regarding the immunotoxicity of heavy metals in the metal-exposed fish at the gene level. Therefore, we evaluated the immunotoxicity of cadmium and changes in the expression levels of immune-related genes and reported the quantity of relative expression of metallothionein (MT) and heat shock proteins increased with an increase in rate of cadmium accumulation under laboratory conditions. The same results were reported by Safari et al. [59] when juveniles of Persian sturgeon were used for determining mRNA-HSP70 expression in the liver and gills after 14-day exposure of sublethal doses of CdCl₂ (0.05, 0.1, and 0.2). HSP70 was cloned from liver cell of fish having 72-nucleotide fragment. The expression level of mRNA-HSP70 was increased ($p \leq 0.05$) in the tissues of the liver and gills of exposed fish when compared with control. [60] also reported the immunotoxicological effect of metals and [61, 62] revealed an increase in the HSP70 due to the overexpression of HSP70. In conclusion, it is confirmed from the present study that tissue stress resulting from the inflammation and toxicity exposure causes upregulated levels of intracellular HSPs and MT genes and may act as functional biomarker of evaluating the impact of toxicants on the immune responses of animals specifically HSP70 as a key regulator. So, the gene expression changes of immune-related proteins (HSP70 and MT) in exposed fish liver after chronic toxicity can be used a diagnostic tool of stress conditions and effect on the immune proteins.

Data Availability

The data used to support the findings of this study are included within the article.

Conflicts of Interest

The authors declare that they have no conflicts of interest.

References

- [1] L. A. R. Boopathy, S. Jacob-Tomas, C. Alecki, and M. Vera, "Mechanisms tailoring the expression of heat shock proteins to proteostasis challenges," *The Journal of Biological Chemistry*, vol. 298, no. 5, article 101796, 2022.
- [2] M. Ponomarenko, I. Stepanenko, and N. Kolchanov, *Heat shock proteins in Brenner's Encyclopedia of Genetics*, Academic Press, Elsevier Inc, UK, 2nd edition, 2013.
- [3] T. Eckschlager, V. Adam, J. Hrabeta, K. Figova, and R. Kizek, "Metallothioneins and cancer," *Current Protein and Peptide Science*, vol. 10, no. 4, pp. 360–375, 2009.
- [4] J. Sturve, A. Berglund, L. Balk et al., "Effects of dredging in Göteborg Harbor, Sweden, assessed by biomarkers in eelpout (*Zoarces viviparus*)," *Environmental Toxicology and Chemistry*, vol. 24, no. 8, pp. 1951–1961, 2005.
- [5] H. Bradl, *Heavy Metals in the Environment: Origin, Interaction and Remediation*, Elsevier/Academic Press, London, 2005.
- [6] W. G. Landis and M. Yu, *Introduction to Environmental Toxicology: Impacts of Chemicals upon Ecological Systems*, CRC Press (Lewis Publishers), Boca Raton, FL, 2003.
- [7] A. S. Randi, J. M. Monserrat, E. M. Rodriguez, and L. A. Romano, "Histopathological effects of cadmium on the gills of the freshwater fish, *Macropsobrycon uruguayanae* Eigenmann 1915 (Pisces, Atherinidae)," *Journal of Fish Diseases*, vol. 19, pp. 311–322, 1996.
- [8] S. Thophon, M. Kruatrachue, E. S. Upatham, P. Pokethitiyook, S. Sahaphong, and S. Jaritkhuan, "Histopathological alterations of white seabass, *Lates calcarifer*, in acute and sub-chronic cadmium exposure," *Environmental Pollution*, vol. 121, no. 3, pp. 307–320, 2003.
- [9] A. J. Dangre, S. Manning, and M. Brouwer, "Effects of cadmium on hypoxia-induced expression of hemoglobin and erythropoietin in larval sheepshead minnow, *Cyprinodon variegatus*," *Aquatic Toxicology*, vol. 99, no. 2, pp. 168–175, 2010.
- [10] L. I. Velkova-Jordanoska and G. Kostoski, "Histopathological analysis of liver in fish in reservoir Trebenista," *Natura Croatica: Periodicum Musei Historiae Naturalis Croatici*, vol. 14, no. 2, pp. 147–153, 2005.
- [11] A. Molina, F. Biemar, F. Muller et al., "Cloning and expression analysis of an inducible HSP70 gene from tilapia fish," *FEBS Letters*, vol. 474, no. 1, pp. 5–10, 2000.
- [12] M. Zafarullah, J. Wisniewski, N. W. Shworak, S. Schieman, S. Misra, and L. Gedamu, "Molecular cloning and characterization of a constitutively expressed heat-shock-cognate hsc71 gene from rainbow trout," *European Journal of Biochemistry*, vol. 204, pp. 893–990, 1992.
- [13] R. T. Graser, D. Malnar-Dragojevic, and V. Vincek, "Cloning and characterization of a 70 kd heat shock cognate (hsc70) gene from the zebrafish (*Danio rerio*)," *Genetica*, vol. 98, no. 3, pp. 273–276, 1996.
- [14] G. Genchi, M. S. Sinicropi, G. Lauria, A. Carocci, and A. Catalano, "The effects of cadmium toxicity," *International Journal of Environmental Research and Public Health*, vol. 17, no. 11, p. 3782, 2020.
- [15] D. Lee, Y. J. Choi, and J. Kim, "Toxic effects of waterborne cadmium exposure on hematological parameters, oxidative stress, neurotoxicity, and heat shock protein 70 in juvenile olive flounder, *Paralichthys olivaceus*," *Fish & Shellfish Immunology*, vol. 122, pp. 476–483, 2022.

- [16] J. J. Kim, Y. S. Kim, and V. Kumar, "Heavy metal toxicity: an update of chelating therapeutic strategies," *Journal of Trace Elements in Medicine and Biology*, vol. 54, pp. 226–231, 2019.
- [17] X. Wang, P. Gao, D. Li et al., "Risk assessment for microbial community changes in farmland soil contaminated with heavy metals and metalloids," *Ecotoxicology and Environmental Safety*, vol. 185, article 109685, 2019.
- [18] N. Wang, C. Gao, P. Zhang et al., "Effect of *Bacillus cereus* against cadmium induced hematological disturbances and immunosuppression in *Carassius auratus gibelio*," *Fish & Shellfish Immunology*, vol. 89, pp. 141–148, 2019.
- [19] W. B. Liu, M. M. Wang, L. Y. Dai et al., "Enhanced immune response improves resistance to cadmium stress in triploid crucian carp," *Frontiers in Physiology*, vol. 12, article 666363, 2021.
- [20] Y. Yang, C. Andrew, C. Meie, W. Weiping, C. Chen, and C. Peng, "Assessing cadmium exposure risks of vegetables with plant uptake factor and soil property," *Environmental Pollution*, vol. 238, pp. 263–269, 2018.
- [21] M. Tiwari, N. S. Nagpure, D. N. Saksena, and W. S. Lakra, "Metallothionein mRNA expressions in freshwater teleost, *Channa punctata* (Bloch) under the influence of heavy metal, cadmium – a dose kinetic study," *International Aquatic Research*, vol. 3, pp. 21–29, 2011.
- [22] G. Jabeen, F. Manzoor, A. Javid, H. Azmat, M. Arshad, and S. Fatima, "Evaluation of fish health status and histopathology in gills and liver due to metal contaminated sediments exposure," *Bulletin of Environmental Contamination and Toxicology*, vol. 100, no. 4, pp. 492–501, 2018.
- [23] D. Bernet, H. Schmidt, W. Meier, P. Burkhardt-Holm, and T. Wahli, "Histopathology in fish: proposal for a protocol to assess aquatic pollution," *Journal of Fish Diseases*, vol. 22, pp. 25–34, 1999.
- [24] K. J. Livak and T. D. Schmittgen, "Analysis of relative gene expression data using real-time quantitative PCR and the 2- $\Delta\Delta$ CT method," *Methods*, vol. 25, pp. 402–408, 2001.
- [25] Z. Dai, J. Cheng, L. Bao et al., "Exposure to waterborne cadmium induce oxidative stress, autophagy and mitochondrial dysfunction in the liver of *Procypris merus*," *Ecotoxicology and Environmental Safety*, vol. 204, article 111051, 2020.
- [26] T. Zininga, L. Ramatsui, and A. Shonhai, "Heat shock proteins as immunomodulators," *Molecules*, vol. 23, no. 11, p. 2846, 2018.
- [27] J. A. Adakole and D. S. Abolude, "Studies on effluent characteristics of a metal finishing company, Zaria-Nigeria," *Research Journal of Environmental and Earth Sciences*, vol. 1, no. 2, pp. 54–57, 2009.
- [28] S. S. Giri, S. S. Sen, W. J. Jin, V. Sukumaran, and S. C. Park, "Immunotoxicological effects of cadmium on *Labeo rohita*, with emphasis on the expression of HSP genes," *Fish & Shellfish Immunology*, vol. 54, pp. 164–171, 2016.
- [29] N. Dirilgen, "Accumulation of heavy metals in freshwater organisms: assessment of toxic interaction," *Turkish Journal of Chemistry*, vol. 25, no. 2, pp. 173–179, 2001.
- [30] S. S. Vutukuru, "Acute effects of hexavalent chromium on survival, oxygen consumption, hematological parameters and some biochemical profiles of the Indian major carp, *Labeo rohita*," *International Journal of environmental Research and Public Health*, vol. 2, no. 3, pp. 456–462, 2005.
- [31] P. S. Navaraj and J. Yasmin, "Toxicological evaluation of tannery industry waste water on *Oreochromis mossambicus*," *African Journal of Environmental Science and Technology*, vol. 6, no. 9, pp. 331–336, 2012.
- [32] A. Altindag, "Alterations in the immunological parameters of Tench (*Tinca tinca* L.) after acute and chronic exposure to lethal and sub lethal treatments with mercury, cadmium and lead," *Turkish Journal of Veterinary and Animal Sciences*, vol. 29, pp. 1163–1168, 2005.
- [33] P. Tawari-Fufeyin, J. Igetei, and M. E. Okoidigun, "Changes in the catfish (*Clarias gariepinus*) exposed to acute cadmium and lead poisoning," *Bioscience Research Communications*, vol. 20, no. 5, pp. 271–276, 2008.
- [34] J. C. Van Dyk, M. J. Cochrane, and G. M. Wagenaar, "Liver histopathology of the sharptooth catfish *Clarias gariepinus* as a biomarker of aquatic pollution," *Chemosphere*, vol. 87, no. 4, pp. 301–311, 2012.
- [35] K. G. McHugh, *Comprehensive fish health assessment and parasitological investigation of alien and indigenous fishes from the Amatola region, South Africa [Ph.D. thesis]*, The North-West University, South Africa, 2015.
- [36] J. E. Russell, D. R. Mount, T. L. Highland et al., "Effects of copper, cadmium, lead, and arsenic in a live diet on juvenile fish growth," *Canadian Journal of Fisheries and Aquatic Sciences*, vol. 67, pp. 1816–1826, 2010.
- [37] M. Mohanty, S. Adhikari, P. Mohanty, and N. Sarangi, "Effect of waterborne zinc on survival, growth, and feed intake of Indian major carp, *Cirrhinus mrigala* (Hamilton)," *Water, Air, and Soil Pollution*, vol. 201, no. 1-4, pp. 3–7, 2009.
- [38] S. Yaqub and M. Javed, "Acute toxicity of water-borne and dietary cadmium and cobalt for fish," *International Journal of Agriculture and Biology*, vol. 14, pp. 276–280, 2012.
- [39] A. Ali, S. M. Al-Ogaily, N. A. Al-Asgah, and J. Gropp, "Effect of sublethal concentrations of copper on the growth performance of *Oreochromis niloticus*," *Journal of Applied Ichthyology*, vol. 19, no. 4, pp. 183–188, 2003.
- [40] M. S. Heydarnejad, M. Khosravian-Hemamai, and A. Nematollahi, "Effects of cadmium at sub-lethal concentration on growth and biochemical parameters in rainbow trout (*Oncorhynchus mykiss*)," *Irish Veterinary Journal*, vol. 66, no. 1, p. 11, 2013.
- [41] P. Perera, S. Kodithuwakku, T. Sundarabharathy, and U. Edirisinghe, "Bioaccumulation of cadmium in freshwater fish: an environmental perspective," *Insight Ecology*, vol. 4, pp. 1–12, 2015.
- [42] S. Subathra and R. Karuppasamy, "Bioaccumulation and depuration pattern of copper in different tissues of *Mystus vitatus* related to various size groups," *Archives of Environmental Contamination and Toxicology*, vol. 54, no. 2, pp. 236–244, 2008.
- [43] A. A. Abdel-warith, E. M. Younis, N. A. Al-Asgah, and O. M. Wahbi, "Effect of zinc toxicity on liver histology of Nile tilapia, *Oreochromis niloticus*," *Scientific Research and Essays*, vol. 6, no. 17, pp. 3760–3769, 2011.
- [44] A. W. Y. Chen, C. J. Lin, Y. R. Ju, J. W. Tsai, and C. M. Liao, "Assessing the effects of pulsed waterborne copper toxicity on life-stage tilapia populations," *Science of the Total Environment*, vol. 417-418, pp. 129–137, 2012.
- [45] N. Malik, A. K. Biswas, T. A. Qureshi, K. Borana, and R. Virha, "Bioaccumulation of heavy metals in fish tissues of a freshwater lake of Bhopal," *Environmental Monitoring and Assessment*, vol. 160, no. 1-4, pp. 267–276, 2010.
- [46] M. D. Ptashynski, R. M. Pedlar, R. E. Evans, C. L. Baron, and J. F. Klaverkamp, "Toxicology of dietary nickel in Lake whitefish (*Coregonus clupeaformis*)," *Aquatic Toxicology*, vol. 58, no. 3-4, pp. 229–247, 2002.

Retraction

Retracted: Assessment of Acupoint Therapy of Traditional Chinese Medicine on Cough Variant Asthma: A Meta-analysis

BioMed Research International

Received 12 March 2024; Accepted 12 March 2024; Published 20 March 2024

Copyright © 2024 BioMed Research International. This is an open access article distributed under the Creative Commons Attribution License, which permits unrestricted use, distribution, and reproduction in any medium, provided the original work is properly cited.

This article has been retracted by Hindawi following an investigation undertaken by the publisher [1]. This investigation has uncovered evidence of one or more of the following indicators of systematic manipulation of the publication process:

- (1) Discrepancies in scope
- (2) Discrepancies in the description of the research reported
- (3) Discrepancies between the availability of data and the research described
- (4) Inappropriate citations
- (5) Incoherent, meaningless and/or irrelevant content included in the article
- (6) Manipulated or compromised peer review

The presence of these indicators undermines our confidence in the integrity of the article's content and we cannot, therefore, vouch for its reliability. Please note that this notice is intended solely to alert readers that the content of this article is unreliable. We have not investigated whether authors were aware of or involved in the systematic manipulation of the publication process.

Wiley and Hindawi regrets that the usual quality checks did not identify these issues before publication and have since put additional measures in place to safeguard research integrity.

We wish to credit our own Research Integrity and Research Publishing teams and anonymous and named external researchers and research integrity experts for contributing to this investigation.

The corresponding author, as the representative of all authors, has been given the opportunity to register their agreement or disagreement to this retraction. We have kept a record of any response received.

References

- [1] H. Tu and Q. Zhang, "Assessment of Acupoint Therapy of Traditional Chinese Medicine on Cough Variant Asthma: A Meta-analysis," *BioMed Research International*, vol. 2022, Article ID 4168308, 13 pages, 2022.

Research Article

Assessment of Acupoint Therapy of Traditional Chinese Medicine on Cough Variant Asthma: A Meta-analysis

Hengjia Tu ¹ and Qingling Zhang ²

¹Nanshan School, Guangzhou Medical University, Guangzhou, 510000 Guangdong, China

²State Key Laboratory of Respiratory Disease, National Clinical Research Center for Respiratory Disease, Guangzhou Institute of Respiratory Health, The First Affiliated Hospital of Guangzhou Medical University, Guangzhou, 510000 Guangdong, China

Correspondence should be addressed to Hengjia Tu; 2019111129@stu.gzhmu.edu.cn

Received 31 March 2022; Revised 27 June 2022; Accepted 8 July 2022; Published 30 July 2022

Academic Editor: Gulnaz Afzal

Copyright © 2022 Hengjia Tu and Qingling Zhang. This is an open access article distributed under the Creative Commons Attribution License, which permits unrestricted use, distribution, and reproduction in any medium, provided the original work is properly cited.

Acupoint application has been used in China to treat various illnesses for ages. In cough variant asthma (CVA), the main clinical sign is episodic night cough. Acupoint application therapy of traditional Chinese medicine is an effective procedure to treat cough variant asthma. The current study is designed to systematically assess the effectiveness of acupoint application therapy in traditional medicine for patients with cough variant asthma. The comprehensive computer retrieval related to comparison between acupoint application and nonacupoint application therapy for cough variant asthma was carried out in various databases ($n=8$) from database establishment until July 4, 2021. Both English and Chinese articles about original investigations in humans were searched. Two independent authors extracted the data, and disagreements were resolved by discussion. ReviewManager 5.3 software provided by Cochrane did a meta-analysis of selected randomized controlled trials (RCTs). Quality of experimentation and risk bias were analyzed by the Cochrane Handbook tool. A total of thirteen randomized controlled clinical articles along with 1237 patients were included in the study. Findings of meta-analysis showed that compared with nonacupoint application treatment, the total effective rate of acupoint application treatment is more effective (RD = 0.13, 95% CI (0.09, 0.17), $Z = 6.70$, $P < 0.00001$). Besides, acupoint application can improve patients' lung function, the lung function index FVC (mean difference = 0.55, 95% confidence interval (0.42, 0.68), $Z = 8.40$, $P < 0.00001$), FEV1 (MD = 0.35, 95% CI (0.23, 0.47), $Z = 5.86$, $P < 0.00001$), FEV1/FVC (%) (MD = 12.68, 95% CI (4.32, 21.03), $Z = 2.97$, $P = 0.003$), FEV1 (%) (MD = 8.63, 95% CI (8.01, 9.25), $Z = 27.44$, $P < 0.00001$), and PEF (day) (MD = 0.62, 95% CI (0.52, 0.71), $Z = 12.40$, $P < 0.00001$) of patients treated by acupoint application therapy were increased. Moreover, acupoint application might lower the level of immunoglobulin E (MD = -54.58, 95% CI (-63.54, -45.61), $Z = 11.93$, $P < 0.00001$) and EOS (MD = -0.21, 95% CI (-0.35, -0.06), $Z = 2.77$, $P = 0.006$). The LCQ (Leicester cough questionnaire) total score of CVA patients was also increased (MD = 2.30, 95% CI (1.55, 3.06), $Z = 5.98$, $P < 0.00001$). Acupoint application therapy is effective in controlling symptoms of CVA. It also has a positive effect in improving lung function and life quality of patients. It can reduce the eosinophil levels and peripheral blood IgE levels of patients as well.

1. Introduction

Cough variant asthma (CVA) is a particular form with typical common cold symptoms and dry, nonproductive cough. Other manifestations, like dyspnea or gasping, are not generally observed; however, there could be episodic night cough which can be alleviated by a bronchodilator [1]. The symptoms of chronic cough in CVA might result in physiological disorders, psychological nervousness, and disruption

of the socialization process. Previous findings revealed that persistent cough is the main risk factor (32.6%) of CVA in five territories of the Chinese Republic [2].

In addition, the prevalence of cough variant asthma is still prominent due to air pollution [3], smoking, allergens, and other reasons.

Current treatments for CVA are generally the same as ordinary respiratory illness, along with bronchodilators, glucocorticoid drugs, antihistamines, and leukotriene receptor

antagonists [4]. Although these medications effectively control CVA symptoms and regulate inflammatory responses, the course of treatment is often long, and the patient's long-term compliance with medication is unwarranted. At the same time, some drugs will also cause osteoporosis [5], induce tissue degeneration, and other adverse reactions.

Acupoint application (AP) is a traditional Chinese medicine (TCM) method with a long history. The main steps of this treatment are grinding the herbs into powder and turning them into herbal patches, directly sticking to acupoints or affected areas to treat chronic cough. Studies have shown that acupoint application can affect the level of immunoglobulin and eosinophils in patients with CVA, regulate the proportion of lymphocytes, and influence the proportion of some cytokines, such as TGF, TNF, and IF, to control the symptoms of CVA and achieve long-term relief [6–8].

Recently, there have been many studies demonstrating AP's positive results for curing CVA [9]. However, those studies are limited to a few parameters and have a small sample size. Similarly, few researchers have conducted a systematic literature review of acupoint application in children [10]. Still, those studies have limited findings and mainly focus on only children. We, therefore, systemically searched and analyzed the consequences of stimulating acupoints for the cure of cough variant asthma through the available literature from several databases. Randomized controlled trials have been conducted comparing AP-based treatment with non-AP-based treatments. Results have been assessed based on quality and probability of biasness after consulting the Cochrane Handbook [11].

2. Methodology

2.1. Search Strategy. We systematically searched the literature for the formation of every database to July 4, 2021. Databases include PubMed (<https://pubmed.ncbi.nlm.nih.gov/>), EMBASE (<https://www.embase.com/landing?status=grey>), Web of Science (<https://mjl.clarivate.com/search-results>), the Cochrane Library (<https://www.cochranelibrary.com/>), Chinese Journal Full-Text Database (CNKI) (<http://kns55.en.eastview.com/kns55/brief/result.aspx?dbPrefix=CJFD>), Database of Chinese Sci-Tech Periodicals (VIP) (<http://www.nlc.cn/newen/periodicals/>), "Wanfang" Database (<http://www.wanfangdata.com/>), and China Biology Medicine Disc (CBM) (<http://allie.dbcls.jp/pair/CBM;Chinese+BioMedical+Disc.html>). The following keywords were used: "stimulating acupoints," "acupoint sticking," "traditional Chinese medicine," "TCM," "acupoint," "CVA," "cough variant asthma," "cough type asthma," "cough-variant asthma," "randomized controlled trial," "random," "control and trial," and "RCT."

The search methodology for PubMed is mentioned below:

The following terms were applied: Medicine, Chinese Traditional [MeSH Terms] OR Traditional Chinese Medicine [MeSH Terms] OR Chinese Traditional Medicine [-MeSH Terms] OR acupuncture [Abstract] OR moxibustion [Abstract] OR "auricular points plaster therapy" [Abstract] OR "acupoint sticking" [Abstract] AND

"Cough Type Asthma" [Abstract] OR "Cough variant asthma" [Abstract] OR "Cough-Type Asthma" [Abstract] OR "Cough-variant asthma" [Abstract].

#1 "auricular points plaster therapy" [Abstract/Title].

#2 "acupoint sticking" [Abstract/Title].

#3 Traditional Chinese Medicine [MeSH Terms].

#4 "#1 OR #2 OR #3".

#5 "Cough Type Asthma" [Abstract/Title].

#6 "Cough variant asthma" [Abstract/Title].

#7 "Cough-variant asthma" [Abstract/Title].

#8 "CVA" [Abstract/Title].

#9 "#5 OR #6 OR #7 OR #8".

#10 "Randomized controlled trial" [Abstract/Title].

#11 "Random" [Abstract/Title].

#12 "Control" [Abstract/Title].

#13 "Trial" [Abstract/Title].

#14 "#10 OR #11 OR #12 OR #13".

#15 "#4 AND #9 AND #14".

Moreover, to include all the possible information, incomplete and finished experiments on the Chinese Scientific Experiments Register (update to July 2021) and World Health Organization ICTRP (<http://www.who.int/ictcp/en/>) were also explored.

2.2. Study Selection

2.2.1. Inclusion Standard for Literature

- (1) Randomized controlled trials on acupoint application on ACV were applied
- (2) Languages were only Chinese and English
- (3) By using the proper standard of diagnosis, individuals were evaluated as patients with CVA
- (4) From the already published information, the interference criteria for the test sample was acupoint application/acupoint application with a combination of other treatment methods. However, in the control group, no acupoint application treatment was included; e.g., data from Western medicine or traditional Chinese medicine were included in the control group
- (5) In similar research, when the test set was an acupoint application connected with different treatment strategies, with inference criteria utilized by the control set, it is necessary that only AP interference is similar to the experimental dataset

2.2.2. Literature Exclusion Standard

- (1) Items considered for exclusion were meeting recordings, theoretical research, case studies, and brief information experience of experts. These were not included
- (2) Repeatedly published information was excluded from this study
- (3) Articles not using the proper standard of diagnosis of CVA were also not included

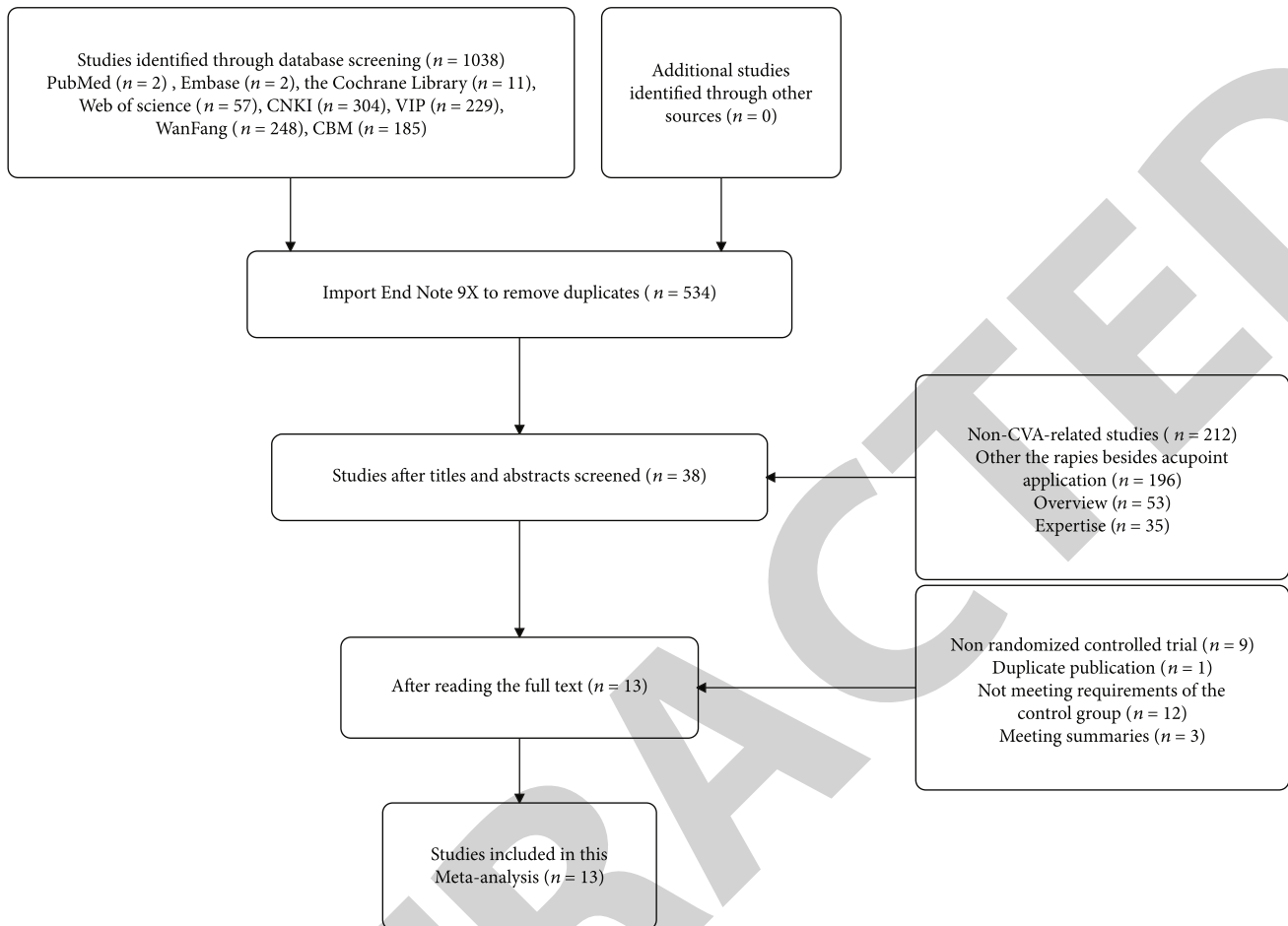


FIGURE 1: The process of literature search and study selection for the research.

- (4) Data about the trials on animals
- (5) Trials that were not properly controlled without clinical manifestation were not taken for this study
- (6) Incomplete literature data
- (7) Obvious errors such as self-contradiction and fabricating data were also excluded

2.3. Data Extraction and Management. From published articles, the study plan section was screened in the following manner: time of research, methodology, and blinding (including allocation concealment, blinding of research volunteers, health professionals, and assessment of results). These parameters were studied and included in the analysis.

From the studied sections, participants of those studied articles were also screened. The following features of the study participants, age limit, gender, disease identification, other signs, and treatment count, as well as control samples, key features of treatment and control groups, and total completed experiments as well as incomplete or withdrawn, were taken for further analysis.

In interventions, site for acupoint application, time of interference, and noninterference were focused.

From the results section of the literature, total effective rate, forced expiratory volume (FVC), forced expiratory volume in one second, FEV1/FVC (%), FEV1/prediction (FEV1/pre), peak expiratory flow (PEF), EOS count per milliliter in peripheral blood, IgE level per milliliter in the peripheral blood, and LCQ total score were taken for further study and analysis.

2.4. Quality Assessment. Evaluation of standard of research was done by ReviewManager 5.3 software risk bias assessment tool equipped from Cochrane Collaboration: (a) to generate the randomized data, (b) concealing the allocation, (c) blinding of research individuals, (d) blinding of the evaluation of results, (e) no proper information retrieved, (f) prediction of specific results, and (g) different partialities. Each group was regarded as “high risk of bias” and “low risk of bias”/“unclear risk of bias.”

2.5. Statistical Analysis. We used the Cochrane ReviewManager 5.3 software for meta-analysis and assessment of reviewed data. Dichotomous data were displayed as odds ratio/risk ratio having 95% confidence intervals that predict the chance of risk or relative risk. Continuous variable dataset assessment was done by MD odds ratio and 95%

TABLE 1: Characteristics of studies.

| Study | Number of patients Intervention group | Control group | Age | Gender (male/ female) | Interventions | Control group | Intervention duration (day) | Outcome assessment | Length of follow-up | Region |
|--------------------|--|---------------|---------------|--------------------------|--|---------------|-----------------------------|--------------------|---------------------|------------------|
| Yu Tong 2017 | 41 | 40 | 5.94 ± 1.28 | 45/36 | Acupoint application +normal treatment | (1) | 30 | 1, 2 | 6 months | Zhejiang, China |
| Xue Ming 2018 | 45 | 45 | 6.54 ± 2.1 | 46/44 | Acupoint application +normal treatment | (2) | 30 | 1, 5 | Not mentioned | Shanxi, China |
| Ma Ying 2018 | 66 | 66 | 4.77 ± 1.31 | 65/67 | Acupoint application +normal treatment | (1) | 365 | 2, 4 | 1 year | Henan, China |
| Wang Long 2017 | 25 | 25 | 40.41 ± 6.39 | 20/30 | Acupoint application +normal treatment | (2) | 28 | 1 | Not mentioned | Liaoning, China |
| Gao Xiyue 2017 | 31 | 31 | 8.95 ± 2.13 | 34/28 | Acupoint application +normal treatment | (1) | 30 | 6 | 3 months | Sichuan, Chian |
| Ye Jianlin 2017 | 90 | 90 | 6.35 ± 2.27 | 96/84 | Acupoint application +normal treatment | (2) | 28 | 1, 2 | Not mentioned | Guangdong, China |
| Li Limei 2019 | 30 | 30 | 5.62 ± 1.33 | 33/27 | Acupoint application +normal treatment | (1) | 90 | 1 | Not mentioned | Guangdong, China |
| Li Qiaoxiang 2017 | 60 | 60 | 7.28 ± 4.75 | 58/62 | Acupoint application +normal treatment | (1) | 45 | 1, 2, 3, 4 | Not mentioned | Hunan, China |
| Tang Jianwen 2015 | 48 | 48 | 64.05 ± 8.70 | 54/42 | Acupoint application +normal treatment | (3), (4) | 30 | 1, 2 | Not mentioned | Jiangsu, China |
| Zhao Qi 2018 | 42 | 42 | 6.13 ± 2.09 | 52/32 | Acupoint application +normal treatment | (8) | 28 | 1, 2, 3, 4 | Not mentioned | Sichuan, Chian |
| Zhang Xiaoyan 2014 | 50 | 46 | 4.65 ± 1.60 | 55/41 | Acupoint application +normal treatment | (5), (6) | 30 | 1 + 4 | Not mentioned | Hebei, China |
| Gou Li 2020 | 45 | 45 | 8.80 ± 0.80 | 44/46 | Acupoint application +normal treatment | (1), (7) | 28 | 1, 6 | Not mentioned | Henan, China |
| Sui Aifeng 2015 | 48 | 48 | 65.31 ± 10.49 | 47/49 | Acupoint application +normal treatment | (3), (4) | 1095 | 1, 2 | Not mentioned | Liaoning, China |

Notes: (1) montelukast, (2) aminophylline, (3) salmeterol, (4) fluticasone propionate, (5) ketotifen, (6) procaterol, (7) budesonide, (8) salbutamol. 1: total effective rate; 2: lung functions (FVC, FEV1, FEV1/FVC, PEF, and PEF); 3: the peripheral blood eosinophil (EOS) count; 4: peripheral blood IgE content; 5: asthma control test (ACT) score; 6: Leicester cough questionnaire (LCQ).

confidence intervals (CIs). Key point of evaluation is the research volunteers.

Assessment of the experiments was done for clinical heterogeneity (demographic features, features of ailments, and therapies), diversity in methodology (planning, execution, and risk of bias), and statistical diversity. The chi-square test was applied with a *P* value: if *P* value was less than 0.10, this showed statistically significant results. *I*² statistic was applied as guided by the Cochrane Handbook for Systematic Reviews of Interventions. Iff-square (*I*²) was used as a statistical method to assess data heterogeneity, the value of *I*² < 40% was indicative of less heterogeneity, whereas more than 75% indicated significant heterogeneity in experimentation. The funnel plot visually analyzed the “risk of reporting” bias.

Sensitivity analysis was done as described below: assessment of outcomes of two statistical models, i.e., random-effect model (REM) and fixed model, were applied and compared. If *I*² > 50%, the random-effect model (REM) was applied for assessment.

3. Results

3.1. Literature Survey. A total of 534 records were analyzed after excluding the duplicated data. This data was further meta-analyzed, and all the information related to the search for knowledge and protocol selection for research is presented in Figure 1.

3.2. Key Features of the Research. Out of the screened articles, thirteen articles were disclosed in 2014-2020 from nine provinces in China about AP in CVA. A total of 1237 volunteers participated in these researches, aged of 4-65 years. In previously published articles, the test groups consisted of patients who had undergone AP along with different treatments. In the control group, no AP was applied, and only Western or traditional Chinese medicines were used for the treatment of CVA.

The acupoint application test and control samples had 621 and 616 cases, respectively. Key features of all elected research are mentioned in Table 1.

3.3. Risk of Bias. Assessment of “risk of bias” is presented in Figure 2. Seven types of research were examined with minimum risk of bias in the assembly of randomly generated sequences, and other studies showed no precise results. Out of screened articles, six were found to carry a low risk of bias in allocation concealment, and others had an uncertain risk of bias in it. All other findings of articles were categorized based on higher risk. The selected researches showed a low risk of bias related to the incomplete dataset, SOR, and other biases.

3.4. Analysis of Total Effective Rate of Acupoint Application Therapy for Cough Variant Asthma. The sum of eleven types of research [9, 12–21] included 1043 participants who described total effective rates (Table 2). Heterogeneity among datasets was $\chi^2 = 11.37$, *P* = 0.33, and *I*² = 12%, and the fixed-effect model was applied for evaluation (Figure 3). Total effective rate of CVA treatment in the

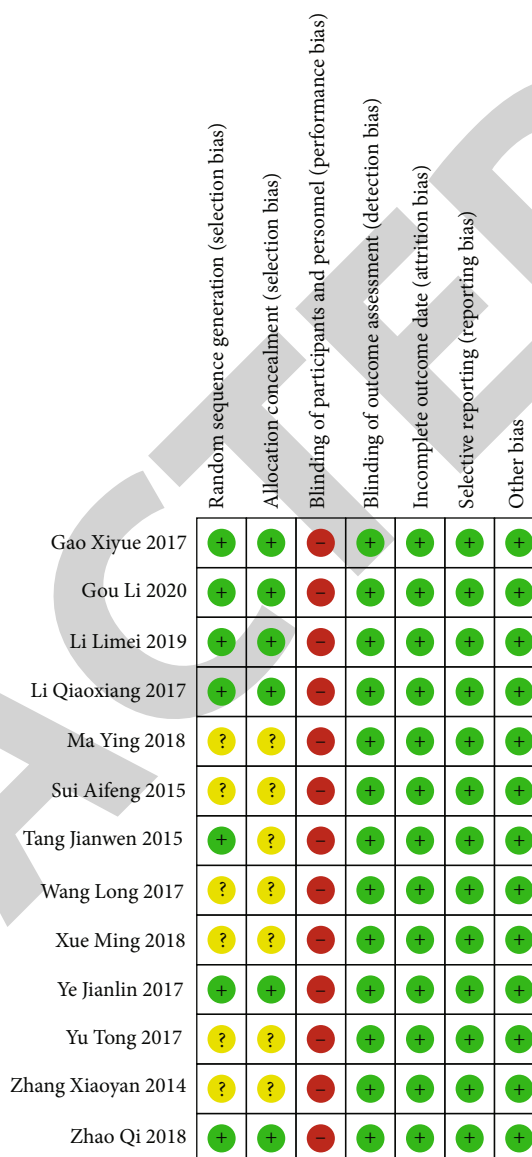


FIGURE 2: Assessment of the risk of bias of different research articles.

experimental group was more effective than that in the control group (RD = 0.13, 95% confidence interval (0.09, 0.17), *Z* = 6.70, *P* < 0.00001). The funnel plot revealed a uniform plot on both sides (left and right) and stacked on the upper side, showing a certain risk of bias, as shown in Figure 4.

3.5. Analysis of Lung Function Index in Acupoint Application Treatment of CVA

3.5.1. Analysis of Lung Function Index FVC in Acupoint Application Therapy of Cough Variant Asthma. Three articles [14, 16, 18] reported lung function index FVC (Table 3). We used a randomized-effect analysis that analyzed the cumulative impact of the amount of research, indicating that acupoint application treatment was more effective to the experimental set to improve lung function index FVC (MD = 0.55, 95% CI (0.42, 0.68), *Z* = 8.40, *P* < 0.00001) (Figure 5)

TABLE 2: Evaluation of total effective rate by chi-square and fixed effect model.

| Study or subgroup | Experimental | | Control | | Weight | Risk Difference M-H, fixed, 95% CI |
|--------------------|--------------|-------|---------|-------|--------|---------------------------------------|
| | Events | Total | Events | Total | | |
| Gou Li 2020 | 45 | 45 | 43 | 45 | 8.6% | 0.04 [-0.03, 0.12] |
| Li Limei 2019 | 29 | 30 | 21 | 30 | 5.8% | 0.27 [0.09, 0.44] |
| Li Qiaoxiang 2017 | 58 | 60 | 52 | 60 | 11.5% | 0.10 [0.00, 0.20] |
| Sui Aifeng 2015 | 45 | 48 | 37 | 48 | 9.2% | 0.17 [0.03, 0.30] |
| Tang Jianwen 2015 | 45 | 48 | 37 | 48 | 9.2% | 0.17 [0.03, 0.30] |
| Wang Long 2017 | 22 | 25 | 18 | 25 | 4.8% | 0.16 [-0.06, 0.38] |
| Xue Ming 2018 | 41 | 45 | 39 | 45 | 8.6% | 0.04 [-0.09, 0.17] |
| Ye Jianlin 2017 | 85 | 90 | 75 | 90 | 17.3% | 0.11 [0.02, 0.20] |
| Yu Tong 2017 | 38 | 41 | 30 | 40 | 7.8% | 0.18 [0.02, 0.33] |
| Zhang Xiaoyan 2014 | 47 | 50 | 37 | 46 | 9.2% | 0.14 [0.00, 0.27] |
| Zhao Qi 2018 | 40 | 42 | 33 | 42 | 8.1% | 0.17 [0.03, 0.31] |
| Total (95% CI) | | 524 | | 519 | 100% | 0.13 [0.09, 0.17] |
| Total events | 495 | | 422 | | | |

Heterogeneity: $\chi^2 = 11.37$; $df = 10$ ($P = 0.33$); $I^2 = 12\%$. Test for overall effect: $Z = 6.70$ ($P < 0.00001$).

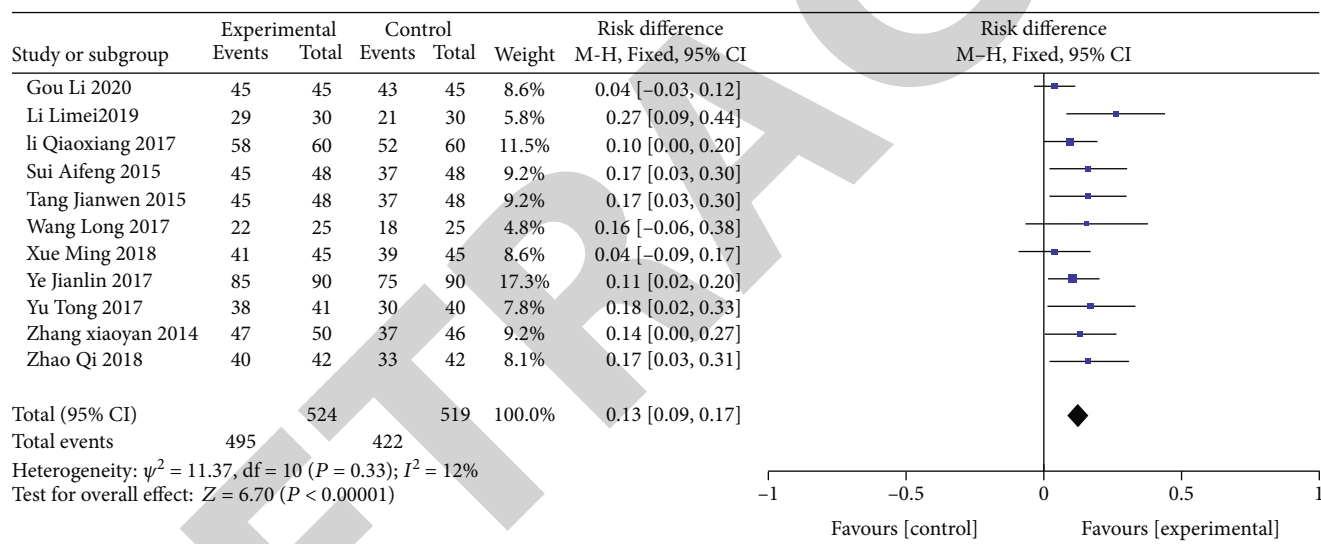


FIGURE 3: Analysis of the total effective rate for acupoint application therapy for CVA.

3.5.2. *Assessment of Pulmonary Function Index FEV1 in Acupoint Application Therapy of Cough Variant Asthma.* Five articles [12, 14, 16, 18, 22] described cough variant asthma pulmonary function measure FEV1 with acupoint application therapy (Table 4), in the case of 597 cases. The random-effect analysis model was applied for analysis (mean difference = 0.35, 95% confidence interval (0.23, 0.47), $Z = 5.86$, $P < 0.00001$). These findings suggested that AP has more ability to improve the pulmonary function index FEV1 compared to the control group (Figure 6). A test evaluated heterogeneity in research ($P = 0.003$, $I^2 = 76\%$), and a subgroup analysis was performed. In the subgroup of patients younger than 7, the subgroup evaluation of four researchers reported a statistically small difference (mean difference = 0.30, 95% confidence interval (0.22, 0.37), $Z = 8.00$, $P < 0.00001$). In the subgroup of patients older than 7, the subgroup analysis

showed a statistically significant difference (MD = 0.57, 95% CI (0.41, 0.73), $Z = 6.93$, $P < 0.00001$).

3.5.3. *Assessment of Pulmonary Function Index FEV1/FVC (%) in Acupoint Application Therapy of Cough Variant Asthma.* Three types of research [14, 16, 22] with 432 patients evaluated CVA pulmonary function indicator FEV1/FVC (%) of acupoint application therapy (Table 5). The random-effect analysis model was applied for analysis (MD = 12.68, 95% CI (4.32, 21.03), $Z = 2.97$, $P = 0.003$). This suggests that acupoint application improves pulmonary function index FEV1/FVC (%) better than the control group. Heterogeneity among researchers ($P < 0.00001$, $I^2 = 98\%$) and subgroup analysis were performed. For the subgroup of patients whose intervention period is less than 30 days, subgroup evaluation in the 180 patients resulted in a

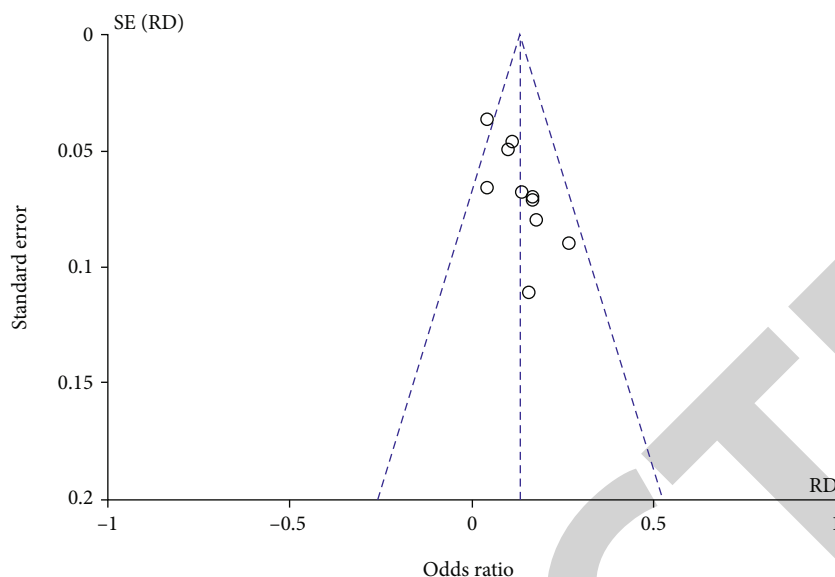


FIGURE 4: The funnel plot of the analysis of the total effective rate to show the risk of bias.

TABLE 3: FVC index of control and experimental groups to analyze the cumulative effect of research.

| Study or subgroup | Mean | Experimental SD | Total | Mean | Control SD | Total | Weight | Mean difference IV, random, 95% CI |
|-------------------|------|-----------------|-------|------|------------|-------|--------|------------------------------------|
| Li Qiaoxiang 2017 | 4.04 | 0.49 | 60 | 3.45 | 0.57 | 60 | 27.0% | 0.59 [0.40, 0.78] |
| Ye Jianlin 2017 | 3.83 | 0.54 | 90 | 3.4 | 0.47 | 90 | 35.3% | 0.43 [0.28, 0.58] |
| Zhao Qi 2018 | 3.2 | 0.31 | 42 | 2.57 | 0.33 | 42 | 37.8% | 0.63 [0.49, 0.77] |
| Total (95% CI) | | | 192 | | | 192 | 100% | 0.55 [0.42, 0.68] |

Heterogeneity: $\tau^2 = 0.01$; $\chi^2 = 4.01$; $df = 2$ ($P = 0.13$); $I^2 = 50\%$. Test for overall effect: $Z = 8.40$ ($P < 0.00001$).

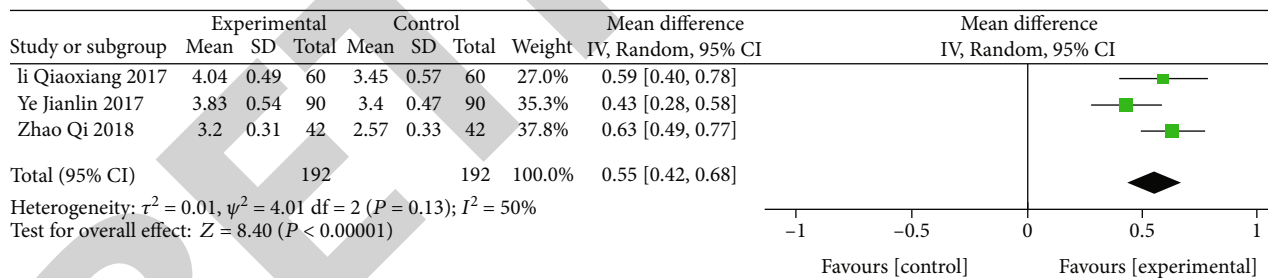


FIGURE 5: Analysis of lung function index FVC, which shows the effectiveness of acupoint application treatment in the experimental group.

statistically significant difference (MD = 5.05, 95% CI (3.30, 6.80), $Z = 5.65$, $P < 0.00001$). Statistically significant results were found in those patients ($n = 120$) whose intervention period was more than 30 days and less than 6 months (MD = 14.66, 95% CI (12.27, 17.05), $Z = 12.00$, $P < 0.00001$), whereas 120 patients were found with statistically significant results whose intervention period was more than 6 months (MD = 18.45, 95% CI (15.81, 21.09), $Z = 13.72$, $P < 0.00001$) (Figure 7).

3.5.4. Analysis of the Pulmonary Function Index FEV1 (%) in Acupoint Application Therapy of Cough Variant Asthma. The fixed-effect model showed that AP treatment was more effective for the experimental group for improving lung

function index FEV1 (%) (MD = 8.63, 95% CI (8.01, 9.25), $Z = 27.44$, $P < 0.00001$). The difference between the three subgroups was significantly small ($I^2 = 0\%$) (Table 6, Figure 8).

3.5.5. Analysis of the Pulmonary Function Index PEF (day) for Acupoint Application Therapy of Cough Variant Asthma. Three screened reports [16, 18, 22] reported lung function index PEF (day) (Table 7) of 336 patients. A fixed-effect model was applied for analysis of the cumulative impact of the amount of experiment (mean difference = 0.62, 95% analysis of confidence interval (0.52, 0.71), $Z = 12.40$, $P < 0.00001$) which demonstrated that AP treatment is more

TABLE 4: Analysis of the lung function index FEV1 which shows statistically significant differences among subgroups.

| Study or subgroup | Mean | Experimental | | Mean | Control | | Weight | Mean difference IV, random, 95% CI |
|--|------|--------------|-------|------|---------|-------|--------|---------------------------------------|
| | | SD | Total | | SD | Total | | |
| 1.3.1 age ≤ 7 | | | | | | | | |
| Ma Ying 2018 | 1.39 | 0.11 | 66 | 1.12 | 0.12 | 66 | 29.0% | 0.27 [0.23, 0.31] |
| Ye Jianlin 2017 | 2.6 | 0.43 | 90 | 2.2 | 0.36 | 90 | 23.2% | 0.40 [0.28, 0.52] |
| Yu Tong 2017 | 1.77 | 0.43 | 41 | 1.54 | 0.47 | 40 | 16.3% | 0.23 [0.03, 0.43] |
| Zhao Qi 2018 | 3.32 | 0.62 | 42 | 3.05 | 0.58 | 42 | 12.3% | 0.27 [0.01, 0.53] |
| Subtotal total (95% CI) | | | 239 | | | 238 | 80.8% | 0.30 [0.22, 0.37] |
| Heterogeneity: tau ² = 0.00; chi ² = 4.62; df = 3 (P = 0.20); I ² = 35% | | | | | | | | |
| Test for overall effect: Z = 8.00 (P < 0.00001) | | | | | | | | |
| 1.3.2 age > 7 | | | | | | | | |
| Li Qiaoxiang 2017 | 3.22 | 0.43 | 60 | 2.65 | 0.47 | 60 | 19.2% | 0.57 [0.41, 0.73] |
| Subtotal Total (95% CI) | | | 60 | | | 60 | 19.2% | 0.57 [0.41, 0.73] |
| Heterogeneity: not applicable | | | | | | | | |
| Test for overall effect: Z = 6.93 (P < 0.00001) | | | | | | | | |
| Total (95% CI) | | | 299 | | | 298 | 100% | 0.35 [0.23, 0.47] |

Heterogeneity: tau² = 0.01; chi² = 16.35; df = 4 (P = 0.003); I² = 76%. Test for overall effect: Z = 5.86 (P < 0.00001). Test for subgroup difference: chi² = 9.09; df = 1 (P = 0.003); I² = 89.0%.

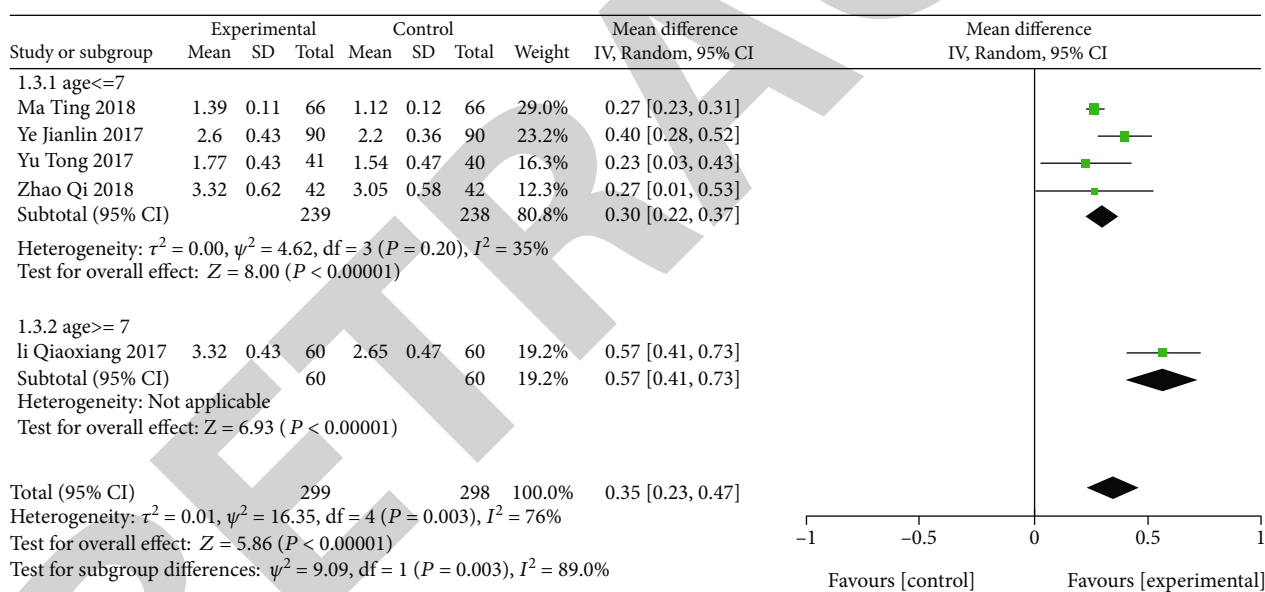


FIGURE 6: Analysis of the lung function index FEV1 through random-effect analysis model.

effective in improving the pulmonary function index PEF compared to the control group (Figure 9).

3.6. Analysis of the Laboratory Indices in Acupoint Application Treatment of CVA

3.6.1. Analysis of the Peripheral Blood IgE Level in Acupoint Application Treatment of CVA. Few studies [13, 16, 18, 19, 22] reported the peripheral blood IgE level as a measure of cough variant asthma for the acupoint application therapy (Table 8). This was observed in almost 522 cases. The fixed-effect analysis model was applied to analyze two groups of samples (MD = -54.58, 95% CI (-63.54, -45.61), Z = 11.93,

P < 0.00001), which reported that acupoint application treatment could better decrease the peripheral blood IgE level of CVA patients as compared to control samples (Figure 10).

3.6.2. Analysis of the Peripheral Blood Eosinophilic Granulocyte (EOS) Count in Acupoint Application Treatment of CVA. Two studies [16, 18] reported peripheral blood EOS count (*10⁹/L), the cough variant asthma measure for acupoint application therapy (Table 9), with the sum of 204 cases. Heterogeneity analysis evaluated significant homogeneity in research (I² = 66%). The random-effect analysis algorithm was applied to analyze two groups of samples (MD = -0.21, 95% CI (-0.35,

TABLE 5: Evaluation of effectiveness of acupoint application treatment on lung function of various groups of the research participants.

| Study or subgroup | Mean | Experimental SD | Total | Mean | Control SD | Total | Weight | Mean difference IV, random, 95% CI |
|---|-------|-----------------|-------|-------|------------|-------|--------|------------------------------------|
| 1.4.1 intervention period ≤ 30 days | | | | | | | | |
| Ye Jianlin 2017 | 62.76 | 6.41 | 90 | 57.71 | 5.54 | 90 | 33.7% | 5.05 [3.30, 6.80] |
| Subtotal total (95% CI) | | | 90 | | | 90 | 33.7% | 5.05 [3.30, 6.80] |
| Heterogeneity: not applicable Test for overall effect: $Z = 5.65$ ($P < 0.00001$) | | | | | | | | |
| 1.4.2 intervention period > 30 days and intervention period ≤ 6 months | | | | | | | | |
| Li Qiaoxiang 2017 | 76.99 | 7.24 | 60 | 62.33 | 6.09 | 60 | 33.3% | 14.66 [12.27, 17.05] |
| Subtotal total (95% CI) | | | 60 | | | 60 | 33.3% | 14.66 [12.27, 17.05] |
| Heterogeneity: not applicable Test for overall effect: $Z = 12.00$ ($P < 0.00001$) | | | | | | | | |
| 1.4.3 intervention period > 6 months | | | | | | | | |
| Ma Ying 2018 | 80.78 | 8.11 | 66 | 62.33 | 7.32 | 66 | 33.1% | 18.45 [15.81, 21.09] |
| Subtotal total (95% CI) | | | 66 | | | 66 | 33.1% | 18.45 [15.81, 21.09] |
| Heterogeneity: not applicable Test for overall effect: $Z = 13.72$ ($P < 0.00001$) | | | | | | | | |
| Total (95% CI) | | | 216 | | | 216 | 100% | 12.68 [4.32, 21.03] |

Heterogeneity: $\tau^2 = 53.16$; $\chi^2 = 83.74$; $df = 2$ ($P < 0.00001$); $I^2 = 98\%$. Test for overall effect: $Z = 2.97$ ($P = 0.003$). Test for subgroup difference: $\chi^2 = 83.74$; $df = 2$ ($P < 0.00001$); $I^2 = 97.6\%$.

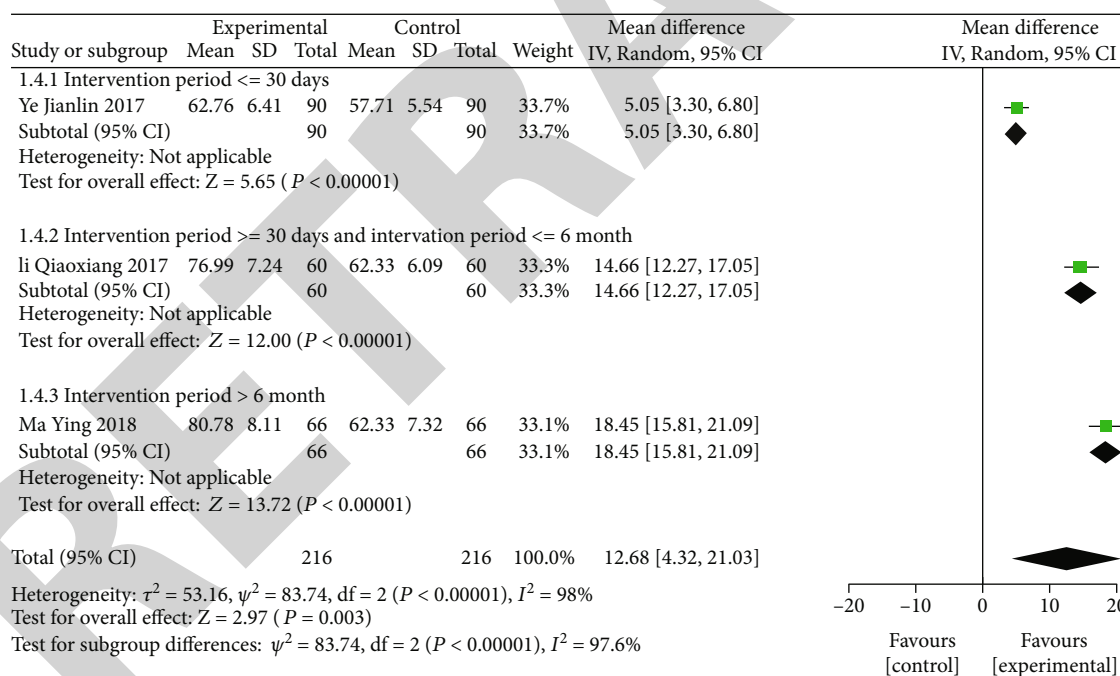


FIGURE 7: Analysis of the lung function index FEV1_FVC (%), which shows the improvement in lung function due to AP.

TABLE 6: Evaluation of effectiveness of AP therapy through pulmonary function index % through fixed-effect model.

| Study or subgroup | Mean | Experimental SD | Total | Mean | Control SD | Total | Weight | Mean difference IV, fixed, 95% CI |
|-------------------|-------|-----------------|-------|-------|------------|-------|--------|-----------------------------------|
| Sui Aifeng 2015 | 79.28 | 2.1 | 48 | 70.65 | 2.25 | 48 | 50.1% | 8.63 [7.76, 9.50] |
| Tang Jianwen 2015 | 79.29 | 2.1 | 48 | 70.66 | 2.26 | 48 | 49.9% | 8.63 [7.76, 9.50] |
| Total (95% CI) | | | 96 | | | 96 | 100% | 8.63 [8.01, 9.25] |

Heterogeneity: $\chi^2 = 0.00$; $df = 1$ ($P = 1.00$); $I^2 = 0\%$. Test for overall effect: $Z = 27.44$ ($P < 0.00001$).

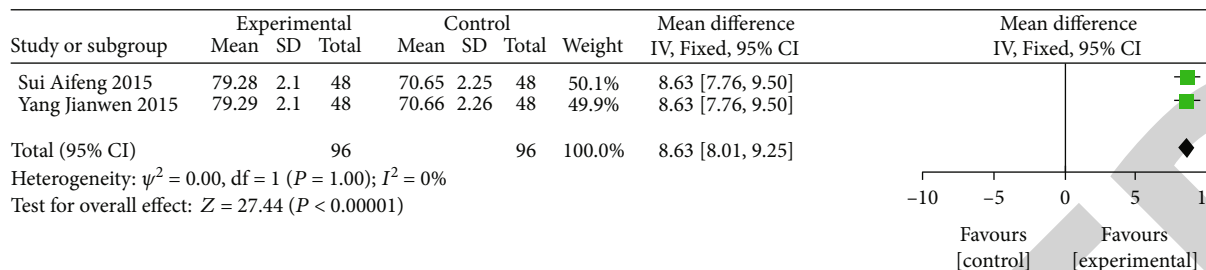


FIGURE 8: Analysis of the lung function index FEV1 (%) by fixed-effect model.

TABLE 7: Analysis of pulmonary function index (day) of three screened reports through fixed-effect model.

| Study or subgroup | Mean | Experimental | | Mean | Control | | Weight | Mean difference IV, fixed, 95% CI |
|-------------------|------|--------------|-------|------|---------|-------|--------|--------------------------------------|
| | | SD | Total | | SD | Total | | |
| Li Qiaoxiang 2017 | 3.42 | 0.87 | 60 | 2.91 | 0.44 | 60 | 15.6% | 0.51 [0.26, 0.76] |
| Ma Ying 2018 | 3.32 | 0.31 | 66 | 2.67 | 0.33 | 66 | 79.6% | 0.65 [0.54, 0.76] |
| Zhao Qi 2018 | 6.36 | 1.03 | 42 | 5.95 | 1.04 | 42 | 4.8% | 0.41 [-0.03, 0.85] |
| Total (95% CI) | 168 | | | 168 | | | 100% | 0.62 [0.52, 0.71] |

Heterogeneity: $\chi^2 = 1.91$; $df = 2$ ($P = 0.38$); $I^2 = 0\%$. Test for overall effect: $Z = 12.40$ ($P < 0.00001$).

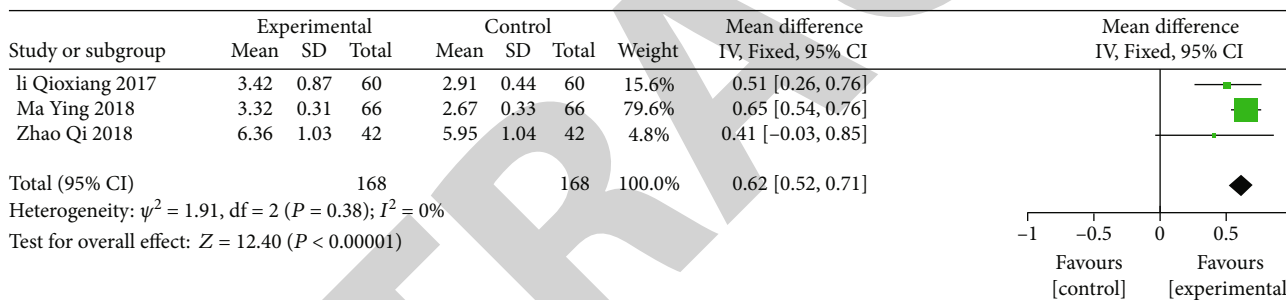


FIGURE 9: Analysis of the lung function index PEF to evaluate the cumulative effect of the AP treatment.

TABLE 8: Level of IgE in peripheral blood as a measure of CVA.

| Study or subgroup | Mean | Experimental | | Mean | Control | | Weight | Mean difference IV, fixed, 95% CI |
|--------------------|--------|--------------|-------|--------|---------|-------|--------|--------------------------------------|
| | | SD | Total | | SD | Total | | |
| Li Qiaoxiang 2017 | 119.33 | 79.63 | 60 | 167.94 | 89.23 | 60 | 8.8% | -48.61 [-78.87, -18.35] |
| Ma Ying 2018 | 131.2 | 26.4 | 66 | 189.3 | 31.7 | 66 | 81.2% | -58.10 [-68.05, -48.15] |
| Xue Ming 2018 | 124.24 | 112.45 | 45 | 171.58 | 112.99 | 45 | 3.7% | -47.34 [-93.92, -0.76] |
| Zhang Xiaoyan 2014 | 136.61 | 115.56 | 50 | 158.94 | 127.27 | 46 | 3.4% | -22.33 [-71.10, 26.44] |
| Zhao Qi 2018 | 134.61 | 117.61 | 42 | 156.49 | 124.88 | 42 | 3.0% | -21.88 [-73.76, 30.00] |
| Total (95% CI) | 263 | | | 259 | | | 100% | -54.58 [-63.54, -45.61] |

Heterogeneity: $\chi^2 = 3.93$; $df = 4$ ($P = 0.42$); $I^2 = 0\%$. Test for overall effect: $Z = 11.93$ ($P < 0.00001$).

-0.06), $Z = 2.77$, $P = 0.006$, indicating that acupoint application treatment could better decrease the peripheral blood EOS count of CVA patients as compared to control samples (Figure 11).

3.7. Analysis of the LCQ Score in Acupoint Application Treatment of CVA. Two studies [20, 23] reported LCQ scores, having a total of 152 cases. Heterogeneity analysis reported a small homogeneity in the research ($I^2 = 0\%$) (Table 10). The fixed-effect analysis model was applied to

analyze the 2 groups of samples (MD = 2.30, 95% CI (1.55, 3.06), $Z = 5.98$, $P < 0.00001$), evaluating acupoint application treatment which might lead to better increase of the LCQ score of CVA patients compared with the control group (Figure 12).

4. Discussion

It is widely believed that CVA is regarded as a particular form of respiratory illness with a histopathological process,

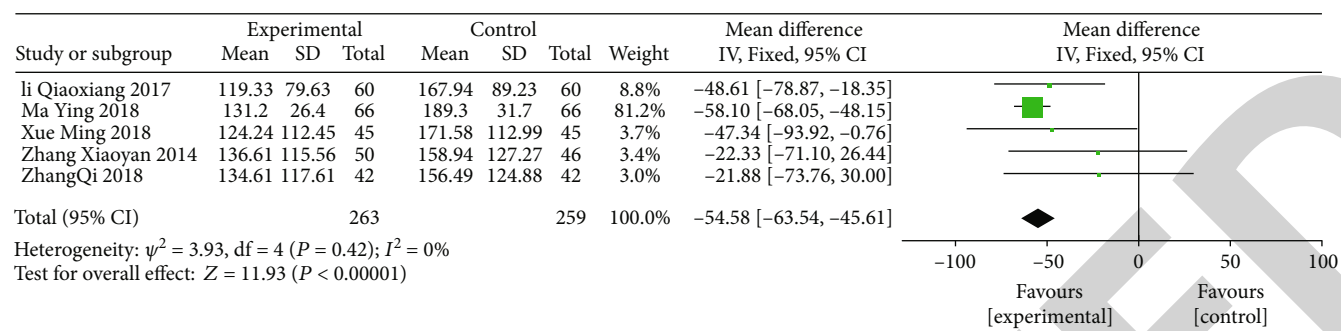


FIGURE 10: Analysis of the peripheral blood IgE level in patients suffering from CVA treated with acupoint application therapy.

TABLE 9: Decrease in peripheral blood EOS count of experimental samples as compared to control samples.

| Study or subgroup | Mean | Experimental | | Mean | Control | | Weight | Mean difference IV, random, 95% CI |
|-------------------|------|--------------|-------|------|---------|-------|--------|---------------------------------------|
| | | SD | Total | | SD | Total | | |
| Li Qiaoxiang 2017 | 1.09 | 0.33 | 60 | 1.23 | 0.21 | 60 | 55.4% | -0.14 [-0.24, -0.04] |
| Zhao Qi 2018 | 0.64 | 0.24 | 42 | 0.93 | 0.39 | 42 | 44.6% | -0.29 [-0.43, -0.15] |
| Total (95% CI) | | | 102 | | | 102 | 100% | -0.21 [-0.35, -0.06] |

Heterogeneity: $\tau^2 = 0.01$; $\chi^2 = 2.98$; $df = 1$ ($P = 0.08$); $I^2 = 66\%$. Test for overall effect: $Z = 2.77$ ($P = 0.006$).

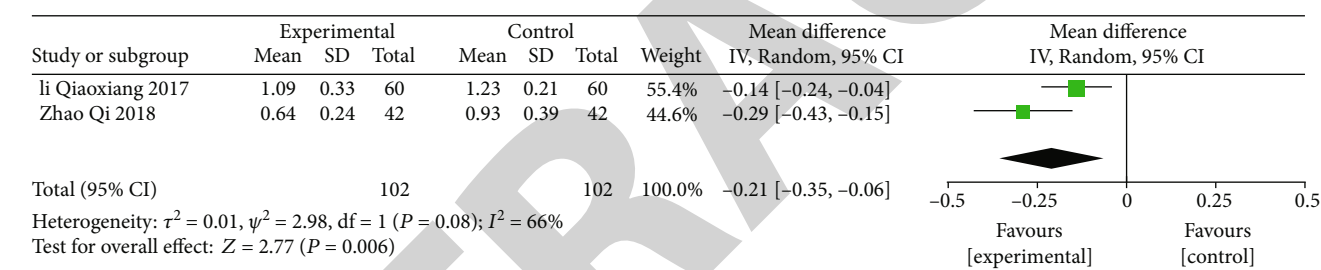


FIGURE 11: Heterogeneity analysis of the EOS count to evaluate the homogeneity of research.

TABLE 10: Fixed-effect model analysis which shows increase in LCQ score.

| Study or subgroup | Mean | Experimental | | Mean | Control | | Weight | Mean difference IV, fixed, 95% CI |
|-------------------|-------|--------------|-------|-------|---------|-------|--------|--------------------------------------|
| | | SD | Total | | SD | Total | | |
| Gao Xiyue 2017 | 15.7 | 2.18 | 30 | 13.25 | 2.83 | 32 | 36.3% | 2.45 [1.20, 3.70] |
| Gou Li 2020 | 18.06 | 2.53 | 45 | 15.84 | 2.02 | 45 | 63.7% | 2.22 [1.27, 3.17] |
| Total (95% CI) | | | 75 | | | 77 | 100% | 2.30 [1.55, 3.06] |

Heterogeneity: $\chi^2 = 0.08$; $df = 1$ ($P = 0.77$); $I^2 = 0\%$. Test for overall effect: $Z = 5.98$ ($P < 0.00001$).

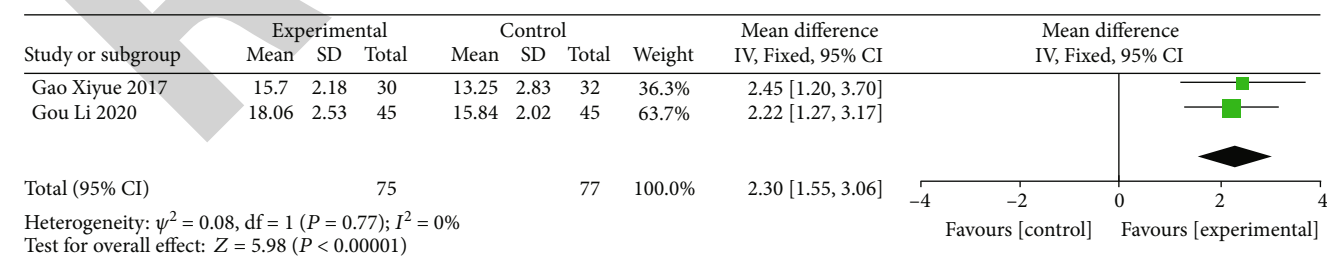


FIGURE 12: Heterogeneity analysis of the LCQ score of acupoint application.

just like common asthma. These include hyperresponsiveness (BHR), eosinophilic airway inflammation, and airway remodeling [24]. Various inflammatory cells, including

eosinophils, neutrophils, and mastocytes, interact with cytokines and inflammatory mediators to form a complex immune network and form chronic nonspecific

inflammation in this disorder, indirectly showing characteristic BHR, cough receptor hypersensitivity, inflammatory cell infiltration, and cells having genes expressed for inflammation [25]. This histopathological process leads to chronic cough, which is common in clinical practice. CVA may also be transformed into typical asthma.

Asthma can be treated by inhaled glucocorticoids and leukotriene modulator drugs, etc. These drugs are categorized into a control group and need to be taken for a long period for the therapy to be effective, whereas other drugs include palliative drugs which include short-acting $13\beta_2$ receptor agonists, inhaled anticholinergic drugs, and short-acting theophylline. These drugs are very effective in alleviating symptoms, reducing airway inflammation, and improving quality of life. However, adverse reactions of these drugs have also been observed. Glucocorticoids may cause hoarseness of voice and oral candida infection. The use of β receptor agonists may lead to sympathetic nerve excitation and accelerated heart rate, resulting in palpitations, chest pain, and other symptoms. So, it is advised to use these drugs only in emergencies and for the shorter period of time. Acupoint application is a nice alternative to these drugs [26].

Acupoint sticking therapy has a long history in traditional Chinese medicine. The main steps of this treatment are as follows. First, a variety of herbs were ground into a powder. Second, adhesive materials such as ginger water were prepared. Next, mix the powder with the adhesive to make a pulp salve that may look like “caking agent” and put it on certain acupuncture points of the body. For treating cough variant asthma, we often choose the “TianTu” (RN22), “DaZhu” (DU14), “FeiShu” (BL13), and “ShanZhong” (RN17) acupoints. Acupoint application allows drugs to be absorbed directly through the skin into capillaries without the need for liver metabolism, which preserves the biological activity of some drugs [7, 8].

Acupoint application has an advantage over other treatment therapies in treating asthma as acupoint stimulation promotes flow of blood to dispel pathogenic factors. This can stimulate the body’s immunity and reduce allergic states [27]. But still, no fully revealed mechanism of acupoint application has been observed in the treatment of cough variant asthma. IgE forms a complex immune interaction with various inflammatory factors like IL-4, IgA, IgE, and IgG to alleviate the symptoms of cough variant asthma [28]. So, it is suggested that the acupoint procedure can treat the CVA via regulating the inflammatory mediators [29].

Findings of this meta-analysis revealed that the rate of effectiveness, lung function index (FVC, FEV1, FEV1/FVC (%), PEF (day)) of the CVA sample showed more significant values as compared to the control group, whereas IgE and peripheral blood EOS count showed lower values when compared with control samples. This suggested that AP for cure of CVA has better efficacy than the other drug treatments.

The main advantage of this study is that we conducted a meta-analysis of 13 RCTs involving 1237 participants. Compared to previous systematic reviews of acupoint application for CVA [30], this study included a larger sample size and included age groups including infants, children, and the

elderly. In addition, differences in clinical response rate, lung function, LCQ scores, and some biochemical blood indicators were investigated.

However, this study still has some limitations. The foremost limitation is that, although the treatment of CVA by acupoint application is frequently used, random clinical controlled studies are usually single-center studies with a small sample size. There are problems such as having no recognized standard for efficacy evaluation and clinical heterogeneity. These problems suggest the need for high-quality clinical research methods in treating CVA by acupoint application, including correct randomization, double-blind, and allocation concealment methods, as well as large-scale multicenter studies. Second, since the acupoint application requires the application operating on the patient, and the herbs have a special smell, it is impossible to blind the patients during the operation in all employed research. Therefore, based on risk-of-bias assessment software provided by the Cochrane Organization, the “blinding of participants and personnel” in whole reports was evaluated as “high risk.” Third, the language of retrieval in the present research was in Chinese and English, and the literature was only from 8 databases. Besides, all the reports used in the meta-analysis were in Chinese, and all the experiments were conducted in China, limiting the present results’ specifications because of sample features. Fourth, due to the complexity of acupoint application, this study mainly focused on the treating method of acupoint application but did not explore the influence of different acupoint selections and the type of herbal medicine on treating effectiveness.

5. Conclusion

The current study concluded that acupoint application is better for the CVA treatment than the control group, which was treated with other traditional medicines. Moreover, it was observed that AP improved respiration and chronic airway inflammation by reducing eosinophil levels and peripheral blood IgE levels.

Data Availability

The data are available from the corresponding author upon reasonable request.

Conflicts of Interest

The authors declare that there are no conflicts of interest regarding the publication of this paper.

References

- [1] Asthmatic Group, RBOCMA, “Guidelines for the diagnosis and treatment of cough (2015),” *Chinese Journal of Tuberculosis and Respiratory Diseases*, vol. 39, no. 5, pp. 323–354, 2016.
- [2] K. Lai, J. Pan, R. Chen, B. Liu, W. Luo, and N. Zhong, “Epidemiology of cough in relation to China,” *Cough*, vol. 9, no. 1, p. 18, 2013.
- [3] H. Matsumoto, R. P. Tabuena, A. Niimi et al., “Cough triggers and their pathophysiology in patients with prolonged or

Retraction

Retracted: Biologically Synthesized Copper Nanoparticles Show Considerable Degradation of Reactive Red 81 Dye: An Eco-Friendly Sustainable Approach

BioMed Research International

Received 12 March 2024; Accepted 12 March 2024; Published 20 March 2024

Copyright © 2024 BioMed Research International. This is an open access article distributed under the Creative Commons Attribution License, which permits unrestricted use, distribution, and reproduction in any medium, provided the original work is properly cited.

This article has been retracted by Hindawi following an investigation undertaken by the publisher [1]. This investigation has uncovered evidence of one or more of the following indicators of systematic manipulation of the publication process:

- (1) Discrepancies in scope
- (2) Discrepancies in the description of the research reported
- (3) Discrepancies between the availability of data and the research described
- (4) Inappropriate citations
- (5) Incoherent, meaningless and/or irrelevant content included in the article
- (6) Manipulated or compromised peer review

The presence of these indicators undermines our confidence in the integrity of the article's content and we cannot, therefore, vouch for its reliability. Please note that this notice is intended solely to alert readers that the content of this article is unreliable. We have not investigated whether authors were aware of or involved in the systematic manipulation of the publication process.

Wiley and Hindawi regrets that the usual quality checks did not identify these issues before publication and have since put additional measures in place to safeguard research integrity.

We wish to credit our own Research Integrity and Research Publishing teams and anonymous and named external researchers and research integrity experts for contributing to this investigation.

The corresponding author, as the representative of all authors, has been given the opportunity to register their agreement or disagreement to this retraction. We have kept a record of any response received.

References

- [1] M. A. Rafique, A. Jamal, Z. Ali et al., "Biologically Synthesized Copper Nanoparticles Show Considerable Degradation of Reactive Red 81 Dye: An Eco-Friendly Sustainable Approach," *BioMed Research International*, vol. 2022, Article ID 7537955, 9 pages, 2022.

Research Article

Biologically Synthesized Copper Nanoparticles Show Considerable Degradation of Reactive Red 81 Dye: An Eco-Friendly Sustainable Approach

Muhammad Asim Rafique,¹ Adil Jamal ,² Zainab Ali,³ Shumaila Kiran ,⁴ Sarosh Iqbal,⁴ Sofia Nosheen,⁵ Zulqarnain Ansar,⁴ and Md Belal Hossain ⁶

¹School of Economics and Management, Yanshan University, Qinhuangdao, Hebei Province, China

²Sciences and Research, College of Nursing, Umm Al Qura University, Makkah-715, Saudi Arabia

³Government Health Department Sialkot, Sialkot, Pakistan

⁴Department of Applied Chemistry, Government College University, Faisalabad-38000, Pakistan

⁵Department of Environmental Science, Lahore College for Women University, Lahore, Pakistan

⁶Department of Plant Pathology, Faculty of Agriculture, Sher-e-Bangla Agricultural University, Sher-e-Bangla Nagar, Dhaka 1207, Bangladesh

Correspondence should be addressed to Shumaila Kiran; shumaila.asimch@gmail.com and Md Belal Hossain; dr.mbhossain@sau.edu.bd

Received 10 April 2022; Accepted 4 July 2022; Published 16 July 2022

Academic Editor: Abdelmotaleb Elokil

Copyright © 2022 Muhammad Asim Rafique et al. This is an open access article distributed under the Creative Commons Attribution License, which permits unrestricted use, distribution, and reproduction in any medium, provided the original work is properly cited.

Diospyros kaki leaf extract was used in this study as a favorable basis for the synthesis of copper nanoparticles (Cu NPs). X-ray diffraction (XRD) and UV-visible spectroscopy approaches were used to characterize the biologically synthesized copper nanoparticles. The XRD analysis showed that copper nanoparticles were face-centered cubic structure. Various experimental levels like conc. of dye, concentration of Cu NPs, pH, reaction time, and temperature were optimized to decolorize reactive red 81 dye using the synthesized Cu NPs. Reactive red 81 dye was decolorized maximum using Cu NPs of 0.005 mg/L. Additionally, reactive red 81 dye was decolorized at its maximum at pH = 6, temperature = 50°C. Our study reported that chemical oxidation demand (COD) and total organic carbon (TOC) deduction efficacies were 74.56% and 73.24%. Further degradation study of reactive red 81 dye was also carried out. Cu NPs have the ability and promising potential to decolorize and degrade reactive red 81 dye found in wastewater.

1. Introduction

Water is one of the most abundant natural resources on the planet, but just 1% of it is usable by humans [1, 2]. In the water supply system, continuing pollution of freshwater resources is a critical concern [3]. The textile sector makes a substantial contribution to the global economy and employs a huge number of people [4, 5]. Textile and garment sectors emit toxic waste high in organic compounds, especially colors, which are the principal outputs to the production process [6]. To discharge of dye-containing effluents, they have to go through a thorough preprocessing

procedure that safeguards the human health and the environment [7–9]. Chemical, environmental, and toxicological aspects influence the numerous therapy options available. Adsorption [10], electrochemical [11], photodegradation [12], and bioremediation are some of the methods exploited in these investigations [13]. Wastewater treatment and drinkable water can assist to address these problems [14], but current treatment methods are unable to completely remove new contaminants and meet high water quality standards [15]. Moreover, current treatment technologies have serious flaws, such as a higher energy demand, poor pollutant removal, and harmful sludge development [14].

Biological wastewater treatment is widely utilized, although it is slow and can occasionally result in microbe toxicity as a result of toxic chemicals [16, 17].

Nanomaterials can be made in a variety of ways [18]. For the detoxification of industrial wastes, various effective, sustainable, and cost-effective nanomaterials with various features have been developed [19, 20]. Copper nanoparticles (Cu NPs) have been found to be effective in the breakdown of organic contaminants. Metallic nanoparticles were found to enhance dye degradation via reductive [21] or oxidative [22] mechanisms. Furthermore, the C-N link between the amine group and the core benzene ring of the molecule might break, resulting in primary amines as waste [22]. Hydroxyl radicals are produced in these environments, and they act in a Fenton-like reaction on the oxidative destruction of organic contaminants. Physical and chemical methods for producing nanoparticles are costly, require complex processes, and result in pollution as well as low productivity [23].

Scientists are working on developing biologically produced nanoparticles derived from plant extracts [24–28]. Plant-assisted nanoparticles can also be used to cure a range of diseases [29]. Persimmon, or *Diospyros kaki*, is a tropical, deciduous, pulpy/fibrous fruit from the Ebenaceae group. It is commonly cultivated in warm regions of the globe, mainly China, Korea, and other Asian countries. *D. kaki* exhibits a number of medicinal effects, such as powerful radical sequestration and antigen lethality in the seed [30], anti-inflammatory action in the leaves [31], anticarcinogenic, antihypertensive [32], and antidiabetic properties [33]. The goal of the current study was to develop low-cost, environmentally friendly methods for degrading reactive red 81 dye. *D. kaki* leaf extract was used to make stable Cu NPs in the first stage. Following the optimization of experimental variables, the second stage involved using these stable Cu NPs for decolorization of reactive red 81 dye.

2. Materials and Methods

2.1. Experimental Plan. All of analytical-grade chemicals and reagents applied in this research were acquired on the local market. The copper nanoparticles (Cu NPs) were synthesized utilizing *Diospyros kaki* leaf extract and were characterized using physical methods. After which they were employed to decolorize and degrade direct red dye.

2.2. Preparation of Extract and Cu NPs. Leaves of *D. kaki* were collected from the native marketplace and were washed thrice using distilled water to eradicate adhered dust particles. The washed samples were dried in shade. Dried mass of these samples was grinded to fine powder. Fine powder of green leaf extract (10 g) was mixed in 500 mL distilled water and heated to 70°C for 20 minutes. Then, solution was later filtered with funnel and Whatman filter paper. Filtered extracts were cooled at room temperature and labeled and kept at 10°C [34]. Copper sulphate (0.1 M) was mixed with 30 mL of leaf extract of *D. Kaki* and further diluted to 400 mL with distilled water. Solution was agitated at 90°C for 3 hrs. The change in color with the passage of time indi-

cated that copper salt was being reduced to copper nanoparticles. The blend was centrifuged for 20-25 minutes, and the residue (Cu nanoparticles) was dried for 12 hours at 145-150°C.

2.3. Characterization of Copper Nanoparticles (UV-Vis Spectroscopy and XRD). The qualitative biosynthesis of Cu NPs was investigated using UV-visible spectroscopy. An ultraviolet-visible (UV-Vis) spectrophotometer was used to validate Cu nanoparticle production. The peak absorbance of synthesized Cu NPs was measured in the spectrum region of 300-800 nm wavelengths. Shimadzu-Scientific Instruments (SSI), Kyoto, Japan, used the XRD 6000 series to obtain X-ray diffraction peaks utilizing a nickel filter and Cu-K α target. The spectra were gathered in two ranges: 25-55 and 0-150 for strength indices. The average crystallite size of Cu NPs can also be measured utilizing the following equation of Debye-Scherrer:

$$D = k\lambda/\beta \cos \theta.$$

D = average crystallite size (nm).

k = Scherrer constant with a value from 0.9 to 1.

λ = X – ray wavelength.

β = full width of half maximum.

θ = Bragg diffraction angle (degrees).

2.4. Experimental Procedure. 100 mL of reactive red 81 dye solution (0.01%) was taken, its pH was attuned to 6.1 mg of copper nanoparticles that were added into it, and the reaction mixture was kept at 45°C for ninety minutes. The reaction's progress was checked by taking little volume of reaction mixture after every 15 minutes and measuring its maximum absorbance (λ_{max}) using a spectrophotometer [35]. Reactive red 81 dye level was changed from 0.01-0.05%, and copper nanoparticle dosage was altered from 0.001-0.01 g/L. pH level was adjusted from 4-8 and temperature from 40-70°C. All factors were elevated by the similar procedure by varying only one factor at a time.

2.5. Chemical Analysis. All experiments regarding decolorization were done in triplicate UV-visible spectroscopy was used to assess absorbance at 450 nm being measured. The following formula was used to calculate the efficacy of decolorization (%) for all parameters.

$$\text{Decolorization}(\%) = \frac{(I - F)}{I} \times 100, \quad (1)$$

while I is the absorption at zero time, and F is the last absorption of the degraded color.

2.6. Mineralization Analysis and Degradation Study. Dye solution was evaluated using TOC and COD measurements. Vials were used to determine COD. These were filled with 3.6 mL of catalyst solution (silver sulphate in conc. H₂SO₄), a digesting solution of 1.5 mL (K₂CR₂O₇ in acidified HgSO₄), and 2.5 mL of reactive red 81 dye solution. In deionized water, a blank sample with all materials was also prepared instead of a reactive red 81 dye sample. The vials were placed at 150°C for 120 minutes. The vials were then cooled at room temperature, and the absorbance was

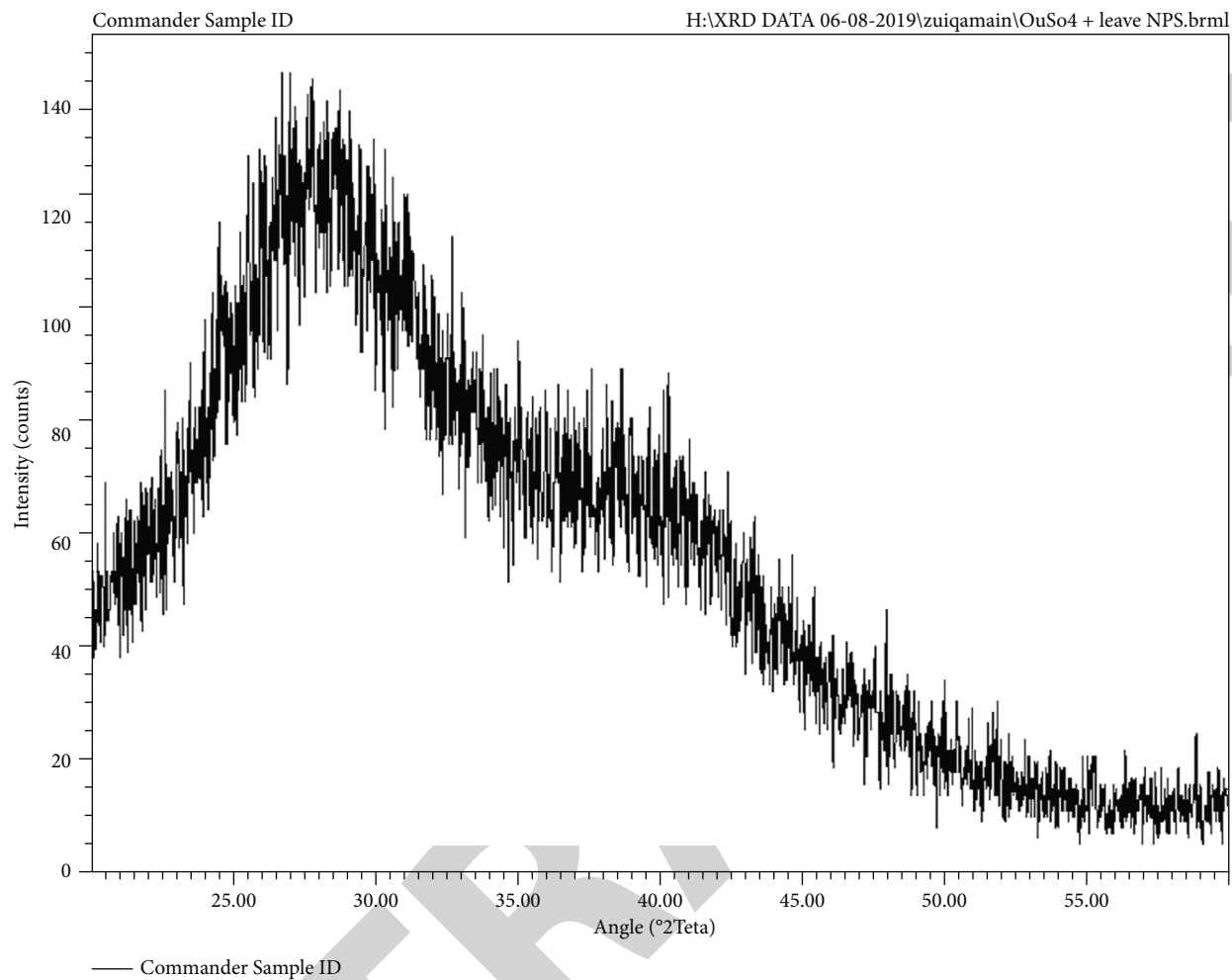


FIGURE 1: Characterization of copper nanoparticles by XRD.

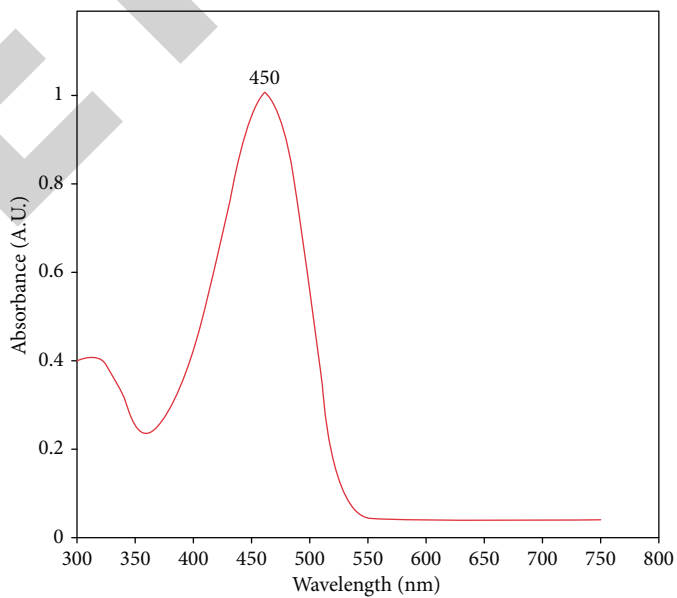


FIGURE 2: UV-vis spectroscopy result (λ_{max}) of direct red 81 dye.

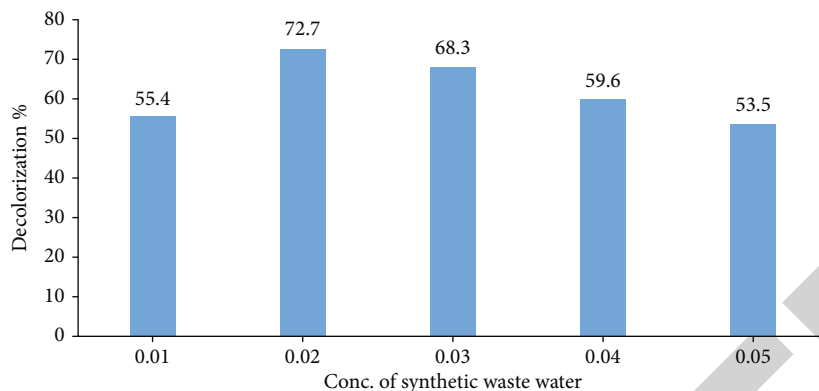


FIGURE 3: Decolorization of synthetic direct red 81 dye solution using Cu nanoparticles as a catalyst.

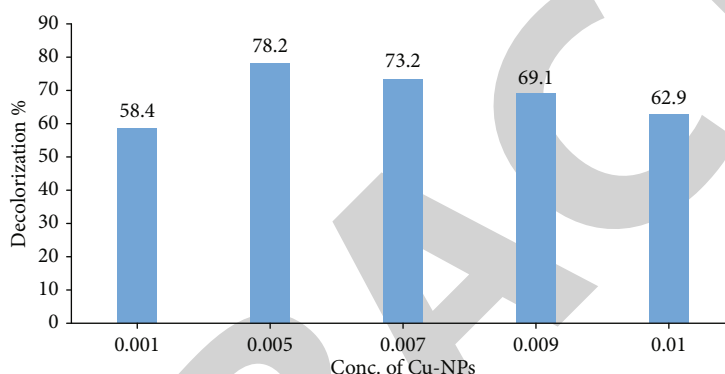


FIGURE 4: Decolorization of synthetic direct red 81 dye solution copper nanoparticle as catalyst.

recorded at 600 nm. A vial was filled with 1.6 mL concentrated H_2SO_4 , 1 mL $K_2CR_2O_7$ (2 N), and 4 mL reactive red 81 dye sample to determine the TOC value. The same sample was made with all ingredients except the dye solution, which functioned as a blank. The digestion vials were kept at $110^\circ C$ for 90 minutes. The vials were then cooled at room temperature, and the absorbance at 590 nm was recorded [36]. For a precise measurement of the sample, the absorbance of the blank sample was subtracted from the absorbance of the sample.

COD and TOC values were estimated using the formula given below:

$$\frac{TOC}{COD} = SF \times A. \quad (2)$$

When SF stands for standard factor, A stands for absorbance, and standard factor can be determined as follows:

$$\text{Standard factor} = \frac{\text{Conc. of standard}}{\text{absorbance}}. \quad (3)$$

The disintegration of reactive red 81 dye was measured in various phases involving the cracking of various connections and development of different moieties.

2.7. *Statistical Analysis.* All the parameters in experiments were performed in triplicates. Averages of triplicates were calculated. Results were computed using standard error and standard deviation mean.

3. Results and Discussions

3.1. *Characterization of Copper Nanoparticles and Scanning of λ_{max} .* XRD was used to characterize the copper nanoparticles. Figure 1 shows the XRD patterns for Cu NPs produced with *D. kaki* leaves extract. The graph shows powerful and strong peaks, indicating a crystalline face-centered cube (FCC) phase of produced Cu NPs. The strength of a solution can be determined by determining absorbed quantity. A UV-visible spectrophotometer was used to determine the wavelength of maximum absorption (λ_{max}). The maximum wavelength was reported to be 450 nm (Figure 2).

3.2. *Role of Experimental Conditions for Decolorization of Reactive Red 81 Dye Solution.* Decolorization of reactive red 81 dye was involved the optimization of parameters like concentration of dye solution, concentration of Cu NPs, pH, and temperature.

3.2.1. *Effect of Concentration of Dye and Catalyst (Cu NPs) for Decolorization of Reactive Red 81 Dye Solution.* Various

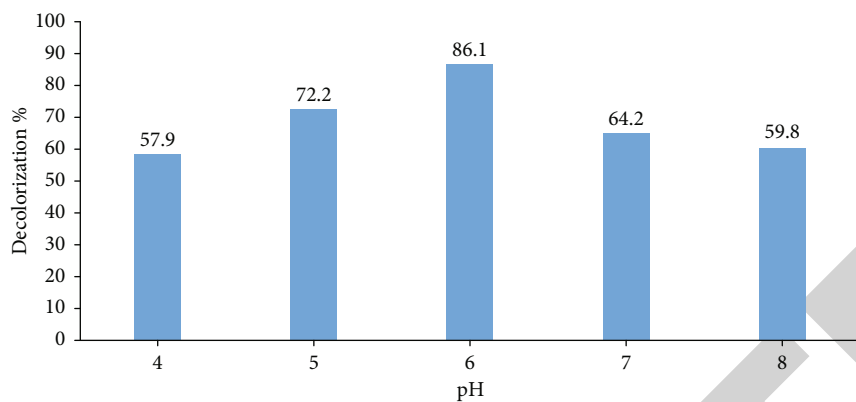


FIGURE 5: Decolorization of synthetic direct red 81 dye solution at different pH using Cu nanoparticles as a catalyst.

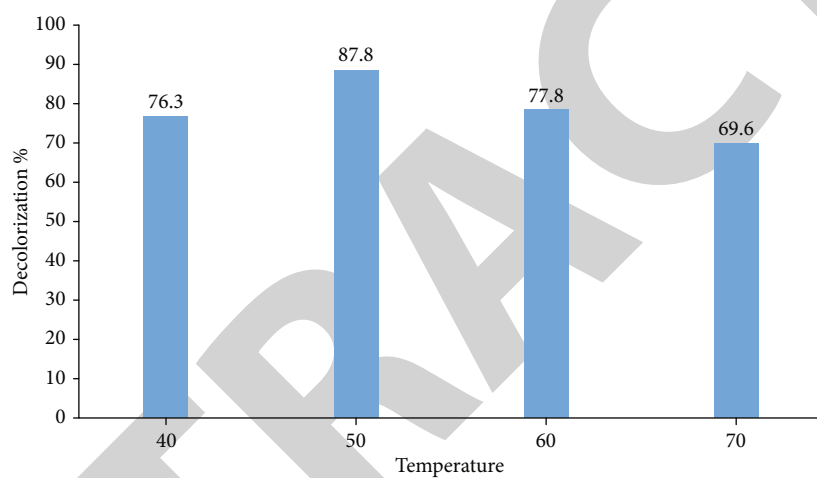


FIGURE 6: Decolorization of synthetic direct red 81 dye solution at different temperature using Cu nanoparticles as a catalyst.

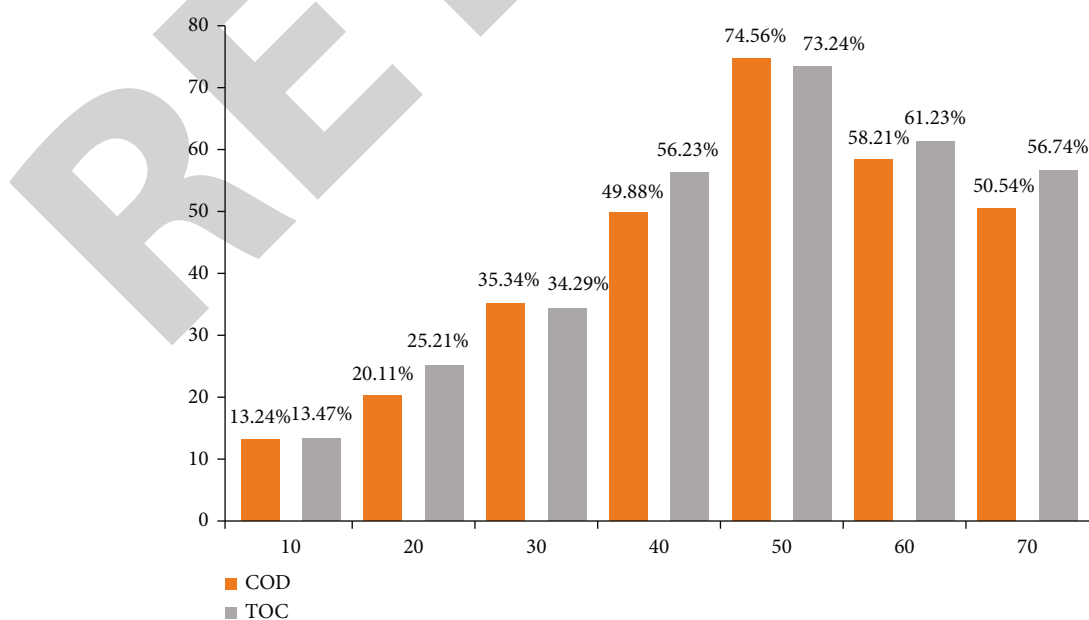


FIGURE 7: Effect of catalytic treatment interaction time on wastewater quality parameters.

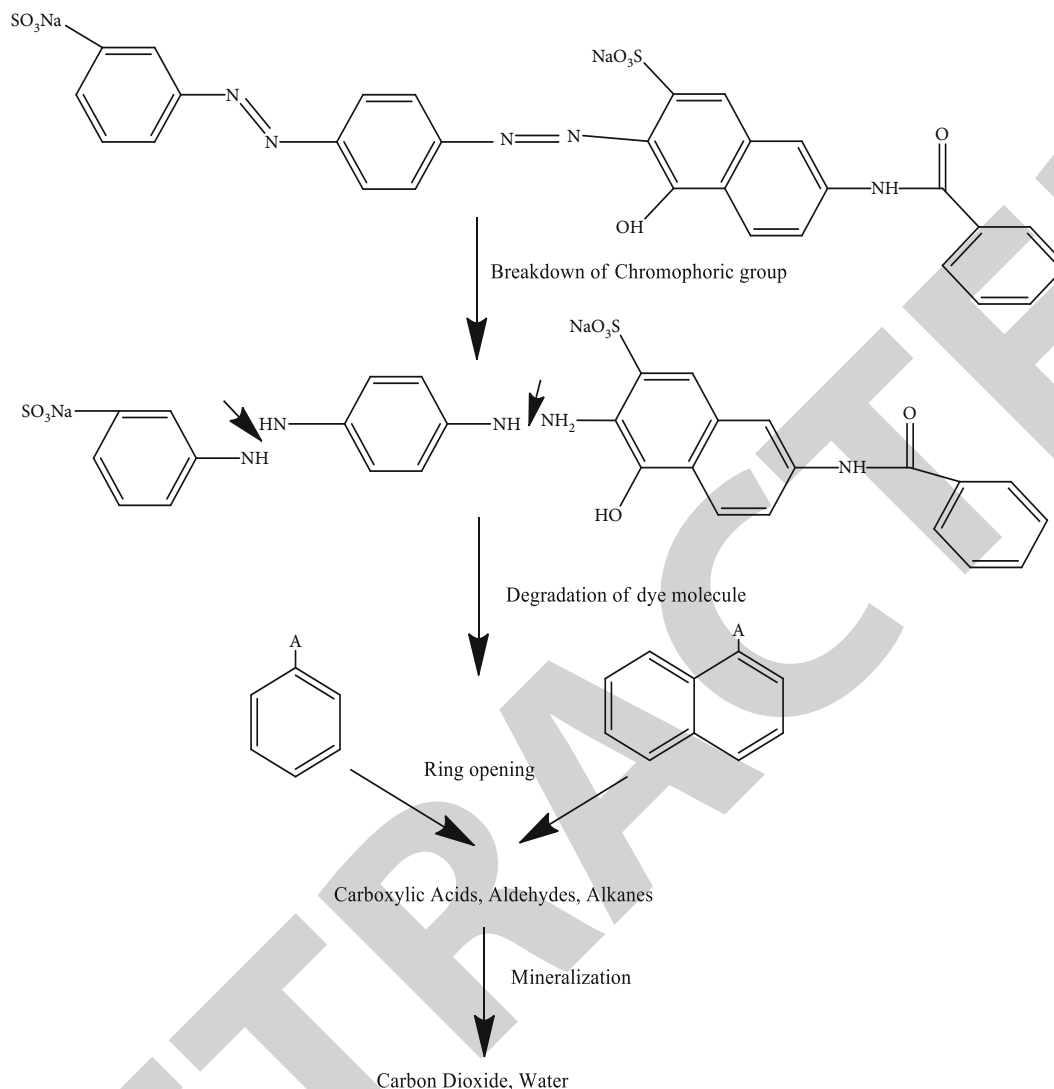


FIGURE 8: Proposed degradation pathway of direct red 81 dye.

amounts of reactive red 81 dye (0.01-0.05%) have been used in the ongoing study. Optimum decolorization (72.7%) of reactive red 81 dye was obtained at a dosage of 0.02%. Dye removal was reduced as the amount of reactive red 81 dye was increased (Figure 3). A greater number of dye molecules may self-associate, giving the medium a turbid appearance. Moreover, larger substrate concentrations may cause the catalyst to be inhibited, reducing the rate of the reaction [37–39]. Removal of dye was inhibited only when amount of reactive red 81 dye was high due to turbulence in the sample medium and the substrate acting as a blocker. The catalyst's efficiency is reduced when the amount of red 81 dye is at greatest [40–42].

In the current investigation, a variety of catalysts were being used. The % age of dye decolorized improved from 58.4 to 78.2% when catalyst level was raised from 0.001 to 0.005 g/L (Figures 3 and 4). As a consequence, it was found that the best acceptable catalyst dose for reactive red 81 dye decolorization is 0.005 g/L Cu NPs (Figure 4). The rate of dye decolorization increases as the catalyst concentration is increased. The dosage of Cu nanoparticles applied affects

dye decolorization significantly [43]. The explanation for this is that as the concentration is raised, the number of active sites rises [44]. There will be no further development in rate of the reaction when the energetic sites of catalytic agents are entirely saturated with dye particles [45]. Increasing catalyst levels might cause turbulence in the solution due to a decrease in reaction rate [46].

3.2.2. Effect of pH and Temperature for Decolorization of Reactive Red 81 Dye Solution. The dye solution's pH is important since it affects the dye's decolorization time and can modify the type of the charge density on the adsorbent's surface. In this work, we did a sequence of catalytic assays with pH levels from 4-8, whereas the other parameters stayed persistent. As the pH climbed from 4 to 6, the decolorization of the dye under study increased from 57.9% to 86.1% (Figures 3 and 5). Rises in pH up to 8 caused a reduction in dye clearance over time (Figure 5). Increases in pH up to 8 resulted in a gradual decrease in dye removal (Figure 5). Fewer dye molecules are deposited on the catalytic surface because dye molecules are protonated at quite

lower pH. At pH 6, attraction interactions between negative and positive charged catalytic surfaces interfaces were detected, indicating the highest interacting forces amongst dye nanoparticles at this pH [47, 48]. It is worth noting that the pH of the aquatic component has a significant impact on the adsorbent's charge [40]. In addition, catalysts have a pH value that is ideal for maximum catalytic potential [49]. Catalyst alteration can occur at pH levels greater than the optimum [50].

Experimental studies with an optimum dosage of Cu NPs (0.005 g/L) at temperatures ranging from 40-70°C have been performed out to evaluate the influence of temperature on the decolorization of reactive red 81 dye. As the temperature is increased from 40-50°C, the efficiency of dye decolorization rises from 76.3% to 87.8%, demonstrating that the catalytic action of Cu NPs is sensitive to temperature (Figures 3 and 6). The decolorization of the dye was reduced by up to 69.6% by raising the temperature to 70°C. As a consequence, 50°C was shown to be the best temperature for best dye removal of reactive red 81 dye by Cu nanoparticles (Figure 6). One theory is that catalysts have a large number of active regions for stimulating activities. Only at a certain temperature do catalysts achieve significant catalytic effect [40]. Temperatures that exceed the optimal value might cause permanent changes in the three-dimensional form of catalytic agents, resulting in declining the catalytic activity decline [51]. Our findings show that high temperature causes a decrease in dye decolorization (Figures 3 and 6). Temperature increases may cause a shift in the three-dimensional form of catalyst agents, reducing their dye adhesion ability [52].

3.2.3. Mineralization Study. For the management of reactive red 81 dye utilizing Cu NPs as a catalyst, the mineralized efficiency was evaluated utilizing quality control metrics like COD and TOC. The COD and TOC of reactive red 81 dye solution were measured. % decrease in COD and TOC was calculated throughout a series of contact times from ten to seventy minutes. When the contact duration is amplified from 10-50 minutes, the %decrease of these metrics rises (Figure 7). COD and TOC levels decreased as the duration of contact was lengthened to 70 minutes (Figure 7). The products of a reaction might function as inhibitor, slowing down the speed of the process [53]. As indicated by higher COD and TOC removal values, Cu NPs not only decomposed but also mineralized our dye molecule and the other generated reaction intermediates formed at various stages of catalytic reaction [40, 54].

3.2.4. Dye Degradation Study. Copper nanoparticles were employed to degrade direct red 81 dye which broke down the chromophore group firstly (Figure 8). The direct red dye's ring structure was later deteriorated. Intermediate products (carboxylic acids, aldehydes, and alkane) were generated once the dye molecule was degraded. During the mineralization, the basic substances such as carbon dioxide and water molecules were produced [24, 54].

4. Conclusion

Agro-waste stuff might be an excellent source of nanoparticles. Cu NPs were made physiologically using an aqueous extract of *Diospyros kaki* leaves. UV-visible and XRD analyses were used to characterize Cu NPs. Cu NPs were utilized to decolorize reactive red 81 dye. The dye decolorized up to 87.8% at 0.02% dye concentration, pH 6, and 0.005 g/L copper nanoparticle concentration at 50°C. COD and TOC levels were found to be 74.56% and 73.24%, correspondingly. The dye breakdown process produced the most basic components. Plant extracts could be employed in future investigations to produce additional metal oxide nanoparticles in a more environmentally friendly manner. So, it can be concluded that Cu NPs can potentially be employed to remove other notorious dyes present in industrial wastewater to eliminate their toxic effects, hence, saving the aquatic and terrestrial lives.

Abbreviations

| | |
|---|---------------------------|
| Cu NPs: | Copper nanoparticles |
| XRD: | X-ray diffraction |
| COD: | Chemical oxidation demand |
| TOC: | Total organic carbon |
| K ₂ CR ₂ O ₇ : | Potassium dichromate |
| HgSO ₄ : | Mercuric sulphate |
| H ₂ SO ₄ : | Sulphuric acid. |

Data Availability

All the data relevant to this study are mentioned in the manuscript. There is no any supplementary data.

Conflicts of Interest

The authors declare no conflicts of interest.

Authors' Contributions

SK and Md BH executed the idea, planned, organized, and supervised the study. ZA performed the experiments. AJ and MAR wrote the early and final draft of manuscript. SI and SN did the statistical analysis and results interpretation. All the authors finally read and approved the manuscript.

Acknowledgments

Thai research work was done in Department of Applied Chemistry, Government College University, Faisalabad, Pakistan, for providing the necessary chemicals and equipment to complete the experimental work magnificently. All authors are thankful to the Department of Applied Chemistry, Government College University, Faisalabad, Pakistan, for providing lab facilities being run by Dr. Shumaila Kiran, to carry out current study smoothly and successfully.

References

- [1] D. Grey, D. Garrick, D. Blackmore, J. Kelman, M. Muller, and C. Sadoff, "Water security in one blue planet: twenty-first century policy challenges for science," *Philosophical Transactions of the Royal Society A: Mathematical, Physical and Engineering Sciences*, vol. 371, no. 2002, p. 20120406, 2013.
- [2] A. S. Adeleye, J. R. Conway, K. Garner, Y. Huang, Y. Su, and A. A. Keller, "Engineered nanomaterials for water treatment and remediation: costs, benefits, and applicability," *Chemical Engineering Journal*, vol. 286, pp. 640–662, 2016.
- [3] S. Kiran, A. Ghaffar, S. Iqbal et al., "Characterization and valorization of sludge from textile wastewater plant for positive environmental applications," *Handbook of Biomass Valorization for Industrial Applications*, vol. 20, pp. 465–489, 2022.
- [4] M. Shahadat, A. Jha, S. U. Islam et al., "Recent advances in chitosan-polyaniline based nanocomposites for environmental applications: a review," *Polymer*, vol. 254, p. 124975, 2022.
- [5] A. Haque, S. Kiran, S. Nosheen et al., "Degradation of reactive blue 19 dye using copper nanoparticles synthesized from *Labeo rohita* fish scales: a greener approach," *Polish Journal of Environmental Studies*, vol. 29, no. 1, pp. 609–616, 2020.
- [6] M. Shahid and F. Mohammad, "Perspectives for natural product based agents derived from industrial plants in textile applications - a review," *Journal of Cleaner Production*, vol. 57, pp. 2–18, 2013.
- [7] C. C. Guaratini and M. V. Zanoni, "Corantes têxteis," *Química Nova*, vol. 23, no. 1, pp. 71–78, 2000.
- [8] L. E. Sendelbach, "A review of the toxicity and carcinogenicity of anthraquinone derivatives," *Toxicology*, vol. 57, no. 3, pp. 227–240, 1989.
- [9] F. A. Esteve-Turrillas and M. de la Guardia, "Environmental impact of recover cotton in textile industry," *Resources, Conservation and Recycling*, vol. 116, pp. 107–115, 2017.
- [10] H. Karaer and I. Kaya, "Synthesis, characterization of magnetic chitosan/active charcoal composite and using at the adsorption of methylene blue and reactive blue4," *Microporous and Mesoporous Materials*, vol. 232, pp. 26–38, 2016.
- [11] N. R. Neti and R. Misra, "Efficient degradation of reactive blue 4 in carbon bed electrochemical reactor," *Chemical Engineering Journal*, vol. 184, pp. 23–32, 2012.
- [12] J. M. Monteagudo, A. Durán, I. San Martín, and S. García, "Ultrasound-assisted homogeneous photocatalytic degradation of reactive blue 4 in aqueous solution," *Applied Catalysis B: Environmental*, vol. 152–153, pp. 59–67, 2014.
- [13] J. Axelsson, U. Nilsson, E. Terrazas, T. Alvarez Aliaga, and U. Welander, "Decolorization of the textile dyes reactive red 2 and reactive blue 4 using *Bjerkandera* sp. Strain BOL 13 in a continuous rotating biological contactor reactor," *Enzyme and Microbial Technology*, vol. 39, no. 1, pp. 32–37, 2006.
- [14] N. Ferroudj, J. Nzimoto, A. Davidson et al., "Maghemite nanoparticles and maghemite/silica nanocomposite microspheres as magnetic Fenton catalysts for the removal of water pollutants," *Applied Catalysis B: Environmental*, vol. 136–137, pp. 9–18, 2013.
- [15] X. Qu, J. Brame, Q. Li, and P. J. Alvarez, "Nanotechnology for a safe and sustainable water supply: enabling integrated water treatment and reuse," *Accounts of Chemical Research*, vol. 46, no. 3, pp. 834–843, 2013.
- [16] G. Zelmanov and R. Semiat, "Phenol oxidation kinetics in water solution using iron(3)-oxide-based nano-catalysts," *Water Research*, vol. 42, no. 14, pp. 3848–3856, 2008.
- [17] S. Chaturvedi, P. N. Dave, and N. K. Shah, "Applications of nano-catalyst in new era," *Journal of Saudi Chemical Society*, vol. 16, no. 3, pp. 307–325, 2012.
- [18] S. U. Islam, L. J. Rather, and F. Mohammad, "Phytochemistry, biological activities and potential of annatto in natural colorant production for industrial applications - a review," *Journal of Advanced Research*, vol. 7, no. 3, pp. 499–514, 2016.
- [19] V. K. Gupta, I. Tyagi, H. Sadegh, R. Shahryari-Ghoshekan, A. S. H. Makhoulouf, and B. Maazinejad, "Nanoparticles as adsorbent; a positive approach for removal of noxious metal ions: a review," *Science Technology and Development*, vol. 34, no. 3, pp. 195–214, 2015.
- [20] J. Theron, J. A. Walker, and T. E. Cloete, "Nanotechnology and water treatment: applications and emerging opportunities," *Critical Reviews in Microbiology*, vol. 34, no. 1, pp. 43–69, 2008.
- [21] S. S. Raut, S. P. Kamble, and P. S. Kulkarni, "Efficacy of zero-valent copper (Cu^0) nanoparticles and reducing agents for dechlorination of mono chloroaromatics," *Chemosphere*, vol. 159, pp. 359–366, 2016.
- [22] S. Dutta, R. Saha, H. Kalita, and A. N. Bezbaruah, "Rapid reductive degradation of azo and anthraquinone dyes by nano-scale zero-valent iron," *Environmental Technology and Innovation*, vol. 5, pp. 176–187, 2016.
- [23] G. Dong, Z. Ai, and L. Zhang, "Total aerobic destruction of azo contaminants with nanoscale zero-valent copper at neutral pH: promotion effect of in-situ generated carbon center radicals," *Water Research*, vol. 66, pp. 22–30, 2014.
- [24] S. Kiran, M. A. Rafique, S. Iqbal, S. Nosheen, S. Nazm, and A. Rasheed, "Synthesis of nickel nanoparticles using *Citrullus colocynthis* stem extract for remediation of reactive yellow 160 dye," *Environmental Science and Pollution Research*, vol. 27, no. 26, pp. 32998–33007, 2020.
- [25] S. Kiran, M. A. Rafique, A. Ashraf et al., "Green synthesis of nickel nanoparticles using fruit peels of citrus paradise for remediation of Congo red dye," *Journal of the Mexican Chemical Society*, vol. 65, no. 4, pp. 507–515, 2021.
- [26] M. A. Rafique, S. Kiran, S. Javed et al., "Green synthesis of nickel oxide nanoparticles using *Allium cepa* peels for degradation of Congo red direct dye: an environmental remedial approach," *Water Science and Technology*, vol. 84, no. 10–11, pp. 2793–2804, 2021.
- [27] M. A. Rafique, A. Jamal, G. Afzal et al., "Photocatalytic mediated remediation of synthetic dyes effluent using zero-valent iron: a comparative study," *Desalination and Water Treatment*, vol. 237, pp. 284–291, 2021.
- [28] Y. O. Al-Ghamdi, M. Jabli, R. Soury, and S. A. Khan, "Synthesis of copper oxide nanoparticles using *Pergularia tomentosa* leaves and decolorization studies," *International Journal of Phytoremediation*, vol. 24, no. 2, pp. 118–130, 2022.
- [29] P. Kuppusamy, M. M. Yusoff, G. P. Maniam, and N. Govindan, "Biosynthesis of metallic nanoparticles using plant derivatives and their new avenues in pharmacological applications - an updated report," *Saudi Pharmaceutical Journal*, vol. 24, no. 4, pp. 473–484, 2016.
- [30] Z. Zreen, A. Hameed, S. Kiran, T. Farooq, and M. S. Zaroog, "A Comparative Study of *Diospyros malabarica* (Gaub) Extracts in Various Polarity-Dependent Solvents for Evaluation of

Retraction

Retracted: Correlation Analysis of Cytochrome P450 SNPs in Hepatitis B-Caused Cirrhosis Patients

BioMed Research International

Received 12 March 2024; Accepted 12 March 2024; Published 20 March 2024

Copyright © 2024 BioMed Research International. This is an open access article distributed under the Creative Commons Attribution License, which permits unrestricted use, distribution, and reproduction in any medium, provided the original work is properly cited.

This article has been retracted by Hindawi following an investigation undertaken by the publisher [1]. This investigation has uncovered evidence of one or more of the following indicators of systematic manipulation of the publication process:

- (1) Discrepancies in scope
- (2) Discrepancies in the description of the research reported
- (3) Discrepancies between the availability of data and the research described
- (4) Inappropriate citations
- (5) Incoherent, meaningless and/or irrelevant content included in the article
- (6) Manipulated or compromised peer review

The presence of these indicators undermines our confidence in the integrity of the article's content and we cannot, therefore, vouch for its reliability. Please note that this notice is intended solely to alert readers that the content of this article is unreliable. We have not investigated whether authors were aware of or involved in the systematic manipulation of the publication process.

Wiley and Hindawi regrets that the usual quality checks did not identify these issues before publication and have since put additional measures in place to safeguard research integrity.

We wish to credit our own Research Integrity and Research Publishing teams and anonymous and named external researchers and research integrity experts for contributing to this investigation.

The corresponding author, as the representative of all authors, has been given the opportunity to register their agreement or disagreement to this retraction. We have kept a record of any response received.

References

- [1] Q.-Y. Li, X. Yang, and Z.-Z. Guo, "Correlation Analysis of Cytochrome P450 SNPs in Hepatitis B-Caused Cirrhosis Patients," *BioMed Research International*, vol. 2022, Article ID 9891184, 8 pages, 2022.

Research Article

Correlation Analysis of Cytochrome P450 SNPs in Hepatitis B-Caused Cirrhosis Patients

Qing-Ya Li , Xiaona Yang , and Zhi-Zhong Guo 

Henan University of Chinese Medicine, Zhengzhou 450046, China

Correspondence should be addressed to Qing-Ya Li; lqy2021@hactcm.edu.cn, Xiaona Yang; yxn@hactcm.edu.cn, and Zhi-Zhong Guo; doughnut0525@163.com

Received 19 March 2022; Revised 31 March 2022; Accepted 8 June 2022; Published 5 July 2022

Academic Editor: Hafiz Ishfaq Ahmad

Copyright © 2022 Qing-Ya Li et al. This is an open access article distributed under the Creative Commons Attribution License, which permits unrestricted use, distribution, and reproduction in any medium, provided the original work is properly cited.

Aim. The aim of the present research was to find the correlation of single nucleotide polymorphisms (SNPs) of cytochrome P450 (CYP450) and hepatitis B-caused cirrhosis. **Methods.** Collection of specimens was done from 297 volunteers with confirmed hepatitis B-caused cirrhosis as well as 120 healthy volunteers in China. Individuals were categorized into three classes, i.e., A, B, and C, on the basis of the Child-Pugh-Turcotte (CPT) value of diseased people, while the Child-Pugh-Turcotte score was determined by rating the below mentioned 5 parameters, i.e., serum volume of bilirubin as well as albumin, prothrombin time, ascites, and encephalopathy. Twenty-four SNPs in the CYP450 superfamily including *CYP1A2*, *CYP2A6*, *CYP2C9*, *CYP2C19*, *CYP2D6*, *CYP2E1*, and *CY3A4* were detected using the SNaPshot assay. **Results.** *CYP1A2*-G2964A, *CYP1A2*-C733A, and *CYP1A2*-T5347C in all 24 SNP loci attained significance. AA genotype at *CYP1A2*-G2964A ($P = 0.048$) and CC genotype at *CYP1A2*-T5347C ($P = 0.049$) were significantly correlated with hepatitis B-caused cirrhosis. Moreover, an allele at *CYP1A2*-G2964A ($P = 0.032$) and C allele at *CYP1A2*-T5347C ($P = 0.016$) were associated with hepatitis B-caused cirrhosis. Furthermore, AC plus AA genotype at *CYP1A2*-C733A correlated with a TCM syndrome, “damp abundance due to spleen asthenia syndrome” ($P = 0.039$) in individuals suffering from hepatitis B-resulted cirrhosis. **Conclusion.** The findings of the current study suggested that AA genotype at *CYP1A2*-G2964A and CC genotype at *CYP1A2*-T5347C may be higher risk in the occurrence of hepatitis B-caused cirrhosis. Moreover, patients with AC plus AA genotype at *CYP1A2*-C733A may be susceptible to appear having “damp abundance due to spleen asthenia syndrome.”

1. Introduction

Hepatitis B virus is considered as a crucial disease in China, as well as regarded as an important reason for virus-based hepatocellular disorders, i.e., liver cirrhosis (LC) and hepatocellular carcinoma (HCC) [1, 2]. Throughout the world, chronic hepatitis B virus disease is a key health risk in subsequent developing of hepatocellular carcinoma [3]. 350 million hepatitis B virus-affected individuals are present having 15-25% chances of death due to these virus-based hepatocellular diseases [4]. In the development of Hepatitis B virus disease, hepatotropic deoxyribonucleic acid virus is involved in damaging the hepatic system. Due to which, a wide range of physical indications appeared, from no symptoms/carrier formed to persistent hepatitis B or hepatitis B-caused cirrhosis, which can also cause HCC [5, 6]. Five-

year survival rate has been observed in individuals suffering from persistent hepatitis B, persistent hepatitis B virus disease that can also lead to pulmonary cirrhosis, persistent HBV disease, and chronic hepatitis B.

Already done researches have reported the association among genetic vulnerability of gene and hepatic disease, i.e., aldehyde dehydrogenase 2 (ALDH2) and hepatocellular carcinoma [7], interleukin-2, IFN- γ , interleukin-10, and hepatitis B and C virus or their coinfection [8] and CYP2E1 gene as well as hepatocellular carcinoma [9]. But this type of association is not fully explored yet.

The cytochrome P450 (CYP450) is a vast superfamily (46000 known members [10]) of haem-based mono-oxygenases. Compounds of this pervasive superfamily perform a significant function in the metabolism and production of exogenous medicine at large scale [11]. However,

the correlation between CYP450 gene and hepatitis B-caused cirrhosis remains poorly understood.

Classification of this infection is significant in examination of this infection. In liver cirrhosis, different genetic makeup has been applied for the categorization, i.e., CPT categorization, compensation/decompensation stage, pulmonary activities, and TCM syndrome. TCM disease, also known as “ZHENG,” is regarded as key basics of the concept of theory of this syndrome. Each examination and treatment technique in TCM is established on the basis of differentiation of “ZHENG” [12]. This also evaluated the TCM identification of outline of signs of the ailment rather than a normal collection of signs of syndrome.

In the current research, we evaluated the relationship between CYP450 single nucleotide polymorphism and hepatitis B-caused cirrhosis and the relationship between these polymorphisms and the phenotype of hepatitis B-caused cirrhosis.

2. Materials and Methods

2.1. Patients and Healthy Controls. A total of 297 individuals having cirrhosis caused by hepatitis B and 120 healthy controls were included in the current research. These individuals belonged to Longhua, Shuguang, Yueyang, and Putuo Hospitals located in Shanghai, the First Allied Hospital of Henan University of Traditional Chinese Medicine, and Ruikang Hospital in Guangxi, China, and had been chosen on the basis of age (from 18 to 65 years), gender, and ethnicity (Table 1). The healthy control subjects were volunteers from the Medical Examination Center. All patients and controls were Chinese yellow race. Blood sampling was done in all individuals, by providing informed consent and ethical review board acceptance according to the principles of the Declaration of Helsinki. 3 ml blood sample was obtained from every participant and then stored at -80°C prior to nucleic acid extraction.

2.2. Classification of Child-Pugh, Phase, and TCM Syndrome. Individuals that participated in the study were categorized in classes A, B, and C on the basis of the Child-Pugh-Turcotte (CPT) value of patients; the Child-Pugh-Turcotte value was computed with the help of 5 frameworks, i.e., serum volume of bilirubin as well as albumin, prothrombin time, ascites, and encephalopathy [13, 14]. When signs of patient were identified, compensation as well as decompensation phase was regarded as 2 categories of LC.

According to “diagnosis, syndrome differentiation of TCM and evaluate the curative effect of liver cirrhosis” [15], six of TCM syndrome types in individuals suffering from hepatitis B-caused cirrhosis were defined and classified. They are “liver-qi stagnation syndrome,” “damp abundance due to spleen asthenia syndrome,” “damp-heat syndrome,” “liver-kidney yin deficiency syndrome,” “blood stasis syndrome,” and “yang deficiency of spleen and kidney syndrome.”

2.3. Selection of SNPs in CYP450 Genes. In this study, the International Haplotype Mapping (<http://www.hapmap.org>), NCBI database (<http://www.ncbi.nlm.nih.gov/snp>), and FastSNP (<http://fastsnp.ibms.sinica.edu.tw>) were used

TABLE 1: Clinical data of patients with hepatitis B-caused cirrhosis.

| | |
|--------------------------------------|---------------|
| <i>Gender</i> | |
| Male (%) | 218 (73.40) |
| Female (%) | 79 (26.60) |
| Mean age (y) | 49.15 ± 10.28 |
| <i>Child-Pugh-Turcotte score (%)</i> | |
| A | 218 (75.43) |
| B | 57 (19.72) |
| C | 14 (4.84) |
| <i>Phase (%)</i> | |
| Compensation phase | 151 (50.84) |
| Decompensation phase | 146 (49.16) |
| <i>Area</i> | |
| Shanghai | 180 (60.61) |
| Guangxi | 69 (23.23) |
| Henan | 48 (16.16) |

for single nucleotide polymorphism selection. Twenty-four SNP loci in 7 genes of the CYP450 superfamily were selected including 4 of the *CYP1A2* gene, 6 of the *CYP2A6* gene, 4 of the *CYP2C9* gene, 4 of the *CYP2C19* gene, 2 of the *CYP2D6* gene, 2 of the *CYP2E1* gene, and 2 of the *CYP3A4* gene (Table 2).

2.4. DNA Extraction. Blood specimens of every participant were taken in potassium EDTA (K_2EDTA) vials. Chromosomal DNA was from 1 ml peripheral blood from single specimen, with the help of TIANamp Blood DNA Kit (Tiangen Biotech, Beijing, China) chromosomal DNA from 1 ml peripheral blood of each specimen. Afterwards, DNA was kept at -80°C for further processing.

2.5. SNP Genotyping. By using ABI PRISM® SNaPshot™ Multiplex Kit (Applied Biosystems, USA) and ABI 3730 XL DNA Analyzer (Applied Biosystems, USA), genotyping of single nucleotide polymorphisms was done. All procedures were done as earlier [16–18]. Primer sequences (Table 2) were chosen to amplify the DNA. Firstly, multiplex PCR was performed. Samples processed by multiplex polymerase chain reaction were examined/analyzed using two percent agarose-TBE gels for qualitative analysis and to check the yield. Secondly, other polymerase chain reaction products were processed with 5 U and 2 U shrimp alkaline phosphatase (rSAP) as well as exonuclease I, respectively, in order to exclude extra deoxyribonucleotide triphosphates. Thirdly, SNaPshot was done with the help of ABI PRISM® SNaPshot™ Multiplex Kit. Experiment was done with volume of $10\ \mu\text{l}$ consisting of $5\ \mu\text{l}$ SNaPshot Multiplex Ready Reaction Mix, $3\ \mu\text{l}$ rSAP/exonuclease-treated multiplex polymerase chain reaction samples, and $1\ \mu\text{l}$ of probe mix (Table 3). Extension processes were done in a PCR machine consist of 45 rounds for 20 s denaturing at 96°C , 5 s annealing at 50°C , and then 30 s elongation at 60°C . $10\ \mu\text{l}$ samples were processed with rSAP (1 U/sample) for 60 min at 37°C and then 15 min inactivation at 75°C . $0.5\ \mu\text{l}$ extension product that was diluted was added to $8.6\ \mu\text{l}$ of HiDi™

TABLE 2: Gene position, polymorphism, and primer sequences of CYP450 SNPs.

| Gene position | RS number | Polymorphism | Primer sequence 5'-3' | Gene frequencies (%) |
|----------------|------------|--------------|---|----------------------|
| CYP1A2-C558A | | C/A | F: 5'-CAGAATGCCCTCAACACCTT-3' R: 5'-CACTGACACCACCACCTGAT-3' | Low |
| CYP1A2-C733A | rs762551 | C/A | F: 5'-CTACTCCAGCCCCAGAAGTG-3' R: 5'-CTGATGCGTGTCTGTGCTT-3' | 62.06 |
| CYP1A2-G2964A | rs2069514 | G/A | F: 5'-AACACAACGGGACTTCTTGG-3' R: 5'-GGCATGACAATTGCTTGAAT-3' | 41.77 |
| CYP1A2-5347T>C | rs2470890 | T/C | F: 5'-ATCTACGGGCTGACCATGAA-3' R: 5'-CTTGGCCTCCTAAAATGCTG-3' | 14.29 |
| CYP2A6-383G>A | rs4986891 | G/A | F: 5'-CCCACCCTACTCCCTCTCTC-3' R: 5'-GTCCCCTGCTCACCGCCA-3' | Low |
| CYP2A6-5065G>A | rs28399454 | A/G | F: 5'-TTCCTGCTCTGAGACCCCT-3' R: 5'-GAAACTTGGTGTCCCTTTTGACT-3' | Low |
| CYP2A6-6558T>C | rs5031016 | C/T | F: 5'-GAACTTCCGCCTCAAGTCCT-3' R: 5'-GTCTTGGCCCTGCCCTTT-3' | Low |
| CYP2A6-1436G>T | rs5031017 | G/T | F: 5'-GAACTTCCGCCTCAAGTCCT-3' R: 5'-GTCTTGGCCCTGCCCTTT-3' | Low |
| CYP2A6-6600G>T | rs28399468 | G/T | F: 5'-GAACTTCCGCCTCAAGTCCT-3' R: 5'-GTCTTGGCCCTGCCCTTT-3' | Low |
| CYP2A6-479T>A | rs1801272 | A/T | F: 5'-GAACTTCCGCCTCAAGTCCT-3' R: 5'-GTCTTGGCCCTGCCCTTT-3' | Low |
| CYP2C9-1003C>T | rs28371685 | C/T | F: 5'-GCCATTTTCTCCTTTTCCA-3' R: 5'-GATACTATGAATTTGGGGACTTCG-3' | Low |
| CYP2C9-A1075C | rs1057910 | A/C | F: 5'-GCCATTTTCTCCTTTTCCA-3' R: 5'-GATACTATGAATTTGGGGACTTCG-3' | 4.61 |
| CYP2C9-449G>A | rs7900194 | A/G | F: 5'-GGGAGGATGGAAAACAGAGA-3' R: 5'-TAAGGTCAGTGATATGGAGTAGGG-3' | Low |
| CYP2C9-3276T>C | | C/T | F: 5'-ATTTTGGCCTGAAACCCATA-3' R: 5'-GCACATGCACACCTACCAAA-3' | Low |
| CYP2C19-G681A | rs4244285 | A/G | F: 5'-CAACCAGAGCTTGGCATATTG-3' R: 5'-TAAAGTCCCAGGGTTGTTG-3' | 41.37 |
| CYP2C19-G636A | rs4986893 | A/G | F: 5'-AAATTGTTTCCAATCATTTAGCT-3' R: 5'-ACTTCAGGGCTTGGTCAATA-3' | 4.55 |
| CYP2C19-C1297T | rs56337013 | C/T | F: 5'-ACTCATCCCTCCTATGATTCACC-3' R: 5'-TGTCAAGGTCCTTTGGGTCA-3' | Low |
| CYP2C19-A991G | rs3758581 | A/G | F: 5'-ATGATGTTTGGATACCTTCATCAT-3' R: 5'-GAGGAATAAAAAGAACATGGAGTTG-3' | 5.10 |
| CYP2D6-C188T | rs1065852 | C/T | F: 5'-CCATTTGGTAGTGAGGCAGGT-3' R: 5'-CCTGGTCAAGCAGTATGGT-3' | 85.14 |
| CYP2D6-G4268C | rs1135840 | C/G | F: 5'-AGCTTCTCGGTGCCCACT-3' R: 5'-CTGAGGAGGATGATCCCAAC-3' | 40.90 |
| CYP2E1-G1168A | | A/G | F: 5'-ACTTCTAGCCACGGGTCTCC-3' R: 5'-GACTCACCCCTGTCCCTGT-3' | Low |
| CYP2E1-G10059A | rs55897648 | A/G | F: 5'-CCAGATGAAAGCCCACATTT-3' R: 5'-CTGCTCCTCAAGGGAAGGTA-3' | Low |
| CYP3A4-T878C | rs28371759 | C/T | F: 5'-TGAAACCACCCCAAGTGTAC-3' R: 5'-CCCTCCTTCTCCATGTACCA-3' | Low |

TABLE 2: Continued.

| Gene position | RS number | Polymorphism | Primer sequence 5' -3' | Gene frequencies (%) |
|----------------|------------|--------------|--|----------------------|
| CYP3A4-A13989G | rs55951658 | C/T | F: 5'-CAGTGGACTACCCCTTGGAA-3' R: 5'-GCATCTAGCATAGGGCCCAT-3' | Low |

TABLE 3: SNaPshot probes for CYP450 detection.

| Gene position | Probe sequence (5'→3') | Size (bp) | Probes of type |
|----------------|--|-----------|----------------|
| CYP1A2-C558A | TTTTTTTTTTTTTTTTTTCACCACCTGATTGTAAGGGTC | 37 | G/T |
| CYP1A2-C733A | TTTTTTTTTTTTTTTTTAGGGTGAGCTCTGTGGGC | 33 | A/C |
| CYP1A2-G2964A | CGCAACCTCCGCCTCTC | 17 | A/G |
| CYP1A2-5347T>C | TTTCAGAATGGTGGTGTCTTCTTCA | 25 | A/G |
| CYP2A6-383G>A | TGGCGATGGAGAAGCGC | 17 | C/T |
| CYP2A6-5065G>A | CGAGATCCAAAGATTGGAGAC | 22 | A/G |
| CYP2A6-6558T>C | TTTTTTTTCCTCCAGTCACCTAAGGACA | 28 | C/T |
| CYP2A6-1436G>T | TTTTTTTTTTTTTTTTTTGTCCCCAAACACGTGG | 36 | G/T |
| CYP2A6-6600G>T | TTTTTTTTTTTTTTTTTTTCAGGAAGCTCATGGTGTAGTTT | 40 | A/C |
| CYP2A6-479T>A | TTTTTTTTTTTTTTTTTTTTTTTTTTTTTCTTCTCATCGACGCC | 46 | A/T |
| CYP2C9-1003C>T | AACGTGTGATTGGCAGAAAC | 20 | C/T |
| CYP2C9-A1075C | TTTTTTTTTTTTTTTTTTTTTTGCACGAGGTCCAGAGATAC | 41 | A/C |
| CYP2C9-449G>A | CGTGTTCAGAGGAAGCCC | 19 | A/G |
| CYP2C9-3276T>C | AAGGAAGCCCTGATTGATCT | 20 | C/T |
| CYP2C19-G681A | CCCACTATCATTGATTATTTCCC | 23 | A/G |
| CYP2C19-G636A | TTTTTTTTTAAACTTGGCCTTACCTGGAT | 30 | C/T |
| CYP2C19-C1297T | TTTTTTTTTTTTTTTCCCTCTCCACACAAATCC | 34 | A/G |
| CYP2C19-A991G | TTTTTTTTTTTTTTTTTTTTTTGCTCCGGTTCTTGCCAA | 38 | C/T |
| CYP2D6-C188T | GCTGGGCTGCACGCTAC | 17 | C/T |
| CYP2D6-G4268C | TTTTTTTTTTTTTTTTTTTTTTGCTTTGCTTTCCTGGTGA | 40 | C/G |
| CYP2E1-G1168A | GTACGTGGGCTCGCAGC | 17 | A/G |
| CYP2E1-G10059A | TTGTTTCTCCTAGGGCACAGTC | 22 | A/G |
| CYP3A4-T878C | TTTTTTTTTTCCTTTCAGCTCTGTCCGATC | 30 | C/T |
| CYP3A4-A13989G | TTTTTTTTTTTTTTGTGGGATTTATGAAAAGTGCC | 34 | A/G |

formamide, 0.9 μ l Genescan-120 LIZ size. Denaturation was done at 95°C for 5 minutes prior to cooling for 4 min; after that, separation was done by ABI PRISM 3730 XL Genetic Analyzer. The GeneMapper 4.0 tool (Applied Biosystems, USA) was applied for evaluation.

2.6. Statistical Analysis. From the dataset, it was evaluated that occurrence of genetic makeup followed the Hardy-Weinberg equilibrium between calculated and already predicted genotype scores through SNaPshot analysis. Genotypic and allelic frequency between groups and comparison between genotypes and phenotypes in terms of correlation were done through the X^2 test. $P < 0.05$ was regarded statistically significant for all analysis.

3. Results

3.1. Features of Study Population. Frequencies of 24 CYP 450 gene loci were assessed in 297 individuals that suffered from

hepatitis B-caused cirrhosis and 120 nondiseased volunteers as controls in China. HWE analysis evaluated nonsignificant difference for distribution of analyzed genotypes when compared with predicted distribution ($P > 0.05$). Age range was 18-65 years (mean \pm SD, 49.15 \pm 10.28, Table 1) of the research participants. Furthermore, age and gender of gene polymorphisms were not significantly different in our study population ($P > 0.05$).

3.2. Genotype and Allele of CYP450 in Patients and Healthy Controls. The SNaPshot method showed that 9 in 24 SNP loci with detectable frequencies were available for statistical analysis in volunteers that suffered from HBV infection-caused cirrhosis and controls (Table 4).

CYP1A2-G2964A and CYP1A2-T5347C showed some evidence of relevance between cases with hepatitis B-caused cirrhosis and controls (Table 4). It was showed that the AA homozygous genotype ($P = 0.048$, 95% CI: 0.160-1.016, OR = 0.403) and AG heterozygous genotype

TABLE 4: Frequency of *CYP1A2*-G2964A, *CYP1A2*-C733A, and *CYP1A2*-T5347C genotypes between patients with hepatitis B-caused cirrhosis and healthy controls.

| Gene/genotype | Cases (%) (n = 297) | Control (%) (n = 120) | OR (95% CI) | P |
|-----------------------|------------------------|--------------------------|---------------------|-------|
| <i>CYP1A2</i> -G2964A | | | | |
| GG | 133 (45.08) | 66 (55.00) | 1.0 (reference) | |
| AG | 132 (44.75) | 48 (40.00) | 0.733 (0.471-1.141) | 0.168 |
| AA | 30 (10.17) | 6 (5.00) | 0.403 (0.160-1.016) | 0.048 |
| <i>CYP1A2</i> -C733A | | | | |
| CC | 29 (9.80) | 16 (13.33) | 1.0 (reference) | |
| AC | 149 (50.34) | 60 (50.00) | 0.730 (0.370-1.441) | 0.363 |
| AA | 118 (39.86) | 44 (36.67) | 0.676 (0.335-1.363) | 0.272 |
| <i>CYP1A2</i> -T5347C | | | | |
| TT | 6 (2.02) | 5 (4.39) | 1.0 (reference) | |
| CT | 49 (16.50) | 46 (40.35) | 1.127 (0.322-3.944) | 0.852 |
| CC | 242 (81.48) | 63 (55.26) | 0.312 (0.092-1.057) | 0.049 |

($P = 0.168$, 95% CI: 0.471-1.141, OR = 0.733) at *CYP1A2*-G2964A were significant differences compared to GG wild-type genotype, respectively. CT heterozygous genotype ($P = 0.852$, 95% CI: 0.322-3.944, OR = 1.127) and CC homozygous genotype ($P = 0.049$, 95% CI: 0.092-1.057, OR = 0.312) at *CYP1A2*-T5347C were compared to TT wild-type genotype, respectively. But there was no significant correlation among genotypes of *CYP1A2*-C733A and hepatitis B-caused cirrhosis and controls.

Moreover, the allele of *CYP1A2*-G2964A and *CYP1A2*-T5347C was analyzed in cases with hepatitis B-caused cirrhosis and controls. G allele at *CYP1A2*-G2964A has significant differences compared to that of A allele ($P = 0.032$, 95% CI: 1.031-2.032, OR = 1.447). T allele at *CYP1A2*-T5347C has significant differences compared to that of C allele ($P = 0.016$, 95% CI: 0.404-0.912, OR = 0.607). However, there was no significant correlation between A allele at *CYP1A2*-G2964A and C allele at *CYP1A2*-T5347C and hepatitis B-caused cirrhosis and controls, respectively (Table 5).

3.3. Correlation between the Genotypes of *CYP1A2* and Child-Pugh Classification and Compensation or Decompensation Phase in Hepatitis B-Caused Cirrhosis. Nonsignificant correlation among genotypes of *CYP1A2* and Child-Pugh classification for hepatitis B-caused cirrhosis was observed. This was evaluated; P values were 0.181 and 0.198 between genotypes of *CYP1A2*-G2964A and *CYP1A2*-C733A and Child-Pugh classification (classes A and B+C), respectively (Table 6). P value was 0.605 between genotypes of *CYP1A2*-T5347C and Child-Pugh classification (class A, B+C).

No statistically significant correlation was observed among the genetic makeup of *CYP1A2* and hepatitis B-caused cirrhosis phase. The P values were 0.496 and 0.290 between genotypes of *CYP1A2*-G2964A and *CYP1A2*-C733A and phase (compensation, decompensation phase), respectively. The P value was 0.291 between genotypes of *CYP1A2*-T5347C and phase (compensation, decompensation phase).

3.4. Correlation between the Genotypes of *CYP1A2* and TCM Syndromes in Hepatitis B-Caused Cirrhosis. The correlation between *CYP1A2*-G2964A, *CYP1A2*-C733A, and *CYP1A2*-T5347C and traditional Chinese medicine syndromes was analyzed in volunteers having hepatitis B-caused cirrhosis. It was showed that AC heterozygous and AA homozygous genotypes at *CYP1A2*-C733A were significant differences compared to CC wild-type genotype ($P = 0.039$) between the “damp abundance due to spleen asthenia syndrome” and other traditional Chinese medicine syndromes. But no significance was observed in the correlation among the genetic makeup of *CYP1A2*-G2964A, *CYP1A2*-T5347C, and TCM syndromes (Table 7).

4. Discussion

The CYP450 is a superfamily consisting of catalytic molecules which can speed up metabolism of xenobiotic chemicals or medicines, compounds present in the environment and endogenous compounds. The role of CYP450 enzymes in cancer was studied over the last decade [19], and the relationships between genetic polymorphism and many types of cancer are the major research, such as colorectal cancer [20, 21] and breast cancer [22, 23]. However, the correlation between CYP450 polymorphism and hepatitis B-caused cirrhosis is less studied.

Single nucleotide polymorphisms are mutations in one base pair of genomic DNA that can be stably inherited in most human populations and has no difference in the various tissues of human. Hence, we can obtain the polymorphism information from expediently acquired materials such as peripheral blood, saliva, and hair for clinical diagnosis. In this study, peripheral blood specimens were obtained from 297 individuals suffering from hepatitis B-caused cirrhosis as well as 120 healthy controls.

According to the literature and SNP-related database, 24 loci of 7 genes were screened. It showed that 15 loci of them are low frequencies. Finally, 3 SNP loci of *CYP1A2* gene (*CYP1A2*-G2964A, *CYP1A2*-C733A, and *CYP1A2*-T5347C)

TABLE 5: Frequency of *CYP1A2*-G2964A, *CYP1A2*-C733A, and *CYP1A2*-T5347C alleles between patients with hepatitis B-caused cirrhosis and healthy controls.

| Gene/allele | Cases (%) (n = 297) | Control (%) (n = 120) | OR (95% CI) | P |
|-----------------------|------------------------|--------------------------|---------------------|-------|
| <i>CYP1A2</i> -G2964A | | | | |
| A | 192 (32.54) | 60 (25.00) | 1.447 (1.031-2.032) | 0.032 |
| G | 398 (67.46) | 180 (75.00) | | |
| <i>CYP1A2</i> -C733A | | | | |
| A | 385 (65.03) | 148 (61.67) | 1.156 (0.848-1.577) | 0.359 |
| C | 207 (34.97) | 92 (38.33) | | |
| <i>CYP1A2</i> -T5347C | | | | |
| C | 514 (87.71) | 195 (81.25) | 0.607 (0.404-0.912) | 0.016 |
| T | 72 (12.29) | 45 (18.75) | | |

TABLE 6: Correlation between *CYP1A2* and Child-Pugh classification and phase in patients with hepatitis B-caused cirrhosis.

| Gene/genotype | Child classification | | | P | Phase | | P |
|-----------------------|--------------------------|-------------------------|-------------------------|--------|------------------------|--------------------------|--------------------|
| | Class A (%) (n = 218) | Class B (%) (n = 57) | Class C (%) (n = 14) | | Compensation (n = 151) | Decompensation (n = 146) | |
| <i>CYP1A2</i> -G2964A | | | | | | | |
| GG | 101 (46.76) | 21 (36.84) | 8 (57.14) | 0.181 | 71 (47.02) | 62 (42.47) | 0.496 |
| AG | 93 (43.06) | 31 (54.39) | 3 (21.43) | | 67 (44.37) | 65 (44.52) | |
| AA | 22 (10.19) | 5 (8.77) | 3 (21.43) | | 13 (8.61) | 17 (11.64) | |
| <i>CYP1A2</i> -C733A | | | | | | | |
| CC | 19 (8.76) | 6 (10.53) | 4 (28.57) | 0.198 | 11 (7.28) | 18 (12.33) | 0.290 |
| AC | 110 (50.69) | 30 (52.63) | 5 (35.71) | | 76 (50.33) | 73 (50.00) | |
| AA | 88 (40.55) | 21 (36.84) | 5 (35.71) | | 64 (42.38) | 54 (36.99) | |
| <i>CYP1A2</i> -T5347C | | | | | | | |
| TT | 4 (1.83) | 2 (3.51) | 0 (0) | 0.605* | 5 (3.31) | 1 (0.68) | 0.291 [▲] |
| CT | 37 (16.97) | 6 (10.53) | 3 (21.43) | | 26 (17.22) | 23 (15.75) | |
| CC | 177 (81.19) | 49 (85.96) | 11 (78.57) | | 120 (82.19) | 122 (83.56) | |

*Fisher's exact test between class A and class B+C. [▲]Fisher's exact test.

TABLE 7: Correlation between *CYP1A2*-G2964A, *CYP1A2*-C733A, and *CYP1A2*-T5347C and TCM syndromes in patients with hepatitis B-caused cirrhosis.

| TCM syndrome type | <i>CYP1A2</i> -G2964A | | P | <i>CYP1A2</i> -C733A | | P | <i>CYP1A2</i> -T5347C | | P |
|--|-----------------------|-------|-------|----------------------|-------|--------|-----------------------|-------|--------|
| | GG | AG+AA | | CC | AC+AA | | TT | CT+CC | |
| Liver-qi stagnation syndrome | 29 | 32 | 0.759 | 5 | 61 | 0.566 | 2 | 59 | 0.630* |
| Damp abundance due to spleen asthenia syndrome | 21 | 21 | 0.575 | 8 | 30 | 0.039 | 0 | 46 | |
| Damp-heat syndrome | 29 | 40 | 0.613 | 7 | 62 | 0.944 | 1 | 69 | 1.000* |
| Liver-kidney yin deficiency syndrome | 17 | 24 | 0.636 | 2 | 39 | 0.399* | 0 | 42 | |
| Blood stasis syndrome | 31 | 37 | 0.977 | 6 | 62 | 0.794 | 3 | 60 | 0.200* |
| Yang deficiency of spleen and kidney syndrome | 6 | 6 | 0.753 | 1 | 11 | 1.000* | 0 | 12 | |
| Total | 133 | 160 | | 29 | 265 | | 6 | 288 | |

*Fisher's exact test.

were used for analysis. It was illustrated that *CYP1A2*-G2964A and *CYP1A2*-T5347C are correlated to varying degrees of the risk levels of hepatitis B-caused cirrhosis. The result also showed that the *CYP1A2*-T5347C and *CYP1A2*-G2964A have

stronger correlation with this disease (Table 4). Both the homozygous mutants in these 2 loci (AA for *CYP1A2*-G2964A and CC for *CYP1A2*-T5347C) have significant difference between cases and controls (both $P < 0.05$), whereas their

heterozygous mutants (AG for *CYP1A2*-G2964A and CT for *CYP1A2*-T5347C) between cases and controls have no significant difference, indicating that the homozygous mutants may play a more important role than heterozygous mutants in these loci in the process of hepatitis B-caused cirrhosis.

Single nucleotide polymorphism constitutes almost 90% human DNA polymorphism [24]. Less rate of mutation as well as significant arbitrary nature of variations in the bp constitutes single nucleotide polymorphism alleles well stable [25] and most (>80%) of them are usual in the entire human populations; however, allele frequencies vary [26]. In this study, the allele A frequency of *CYP1A2*-G2964A and the allele C frequency of *CYP1A2*-T5347C are both significantly correlated with hepatitis B-caused cirrhosis (both $P < 0.05$), whereas allele A frequency of *CYP1A2*-C733A has no correlation with this disease (Table 5). These results supported the above finding that there is significant correlation between the *CYP1A2*-G2964A genotype and hepatitis B-caused cirrhosis.

CYP1A2 is considered as the main member of the P450 superfamily [27]; it contributes 13% of total CYP protein of the liver [28]. *CYP1A2* action might be applied for monitoring the changes in hepatic activities in clinical work [29]. Moreover, this also performs function of metabolism of various clinical medicines, environmental toxic materials, and endogenous substrates [30]. Previous studies showed that the abundance of the *CYP1A2* *1F variant was higher in Caucasians, after its comparison with Japanese subjects [31]. On the other hand, people of Egypt had more incidence of *CYP1A2* *1F variant (0.68) than people of Japan (0.61). We analyzed the genotype distribution and allele frequency of 120 healthy people in our study, the presence of *CYP1A2* G2964A allele showed similarity when compared with individuals of Japan (G: 0.75 vs. 0.77; A: 0.25 vs. 0.23) [32], and the incidence of *CYP1A2* C2964A allele was the same when comparison was done with Germans (C: 0.62 vs. 0.68; A: 0.38 vs. 0.32) [33]. The frequency of A allele was similar compared with Qidong and Changsha in China (0.25 vs. 0.25 vs. 0.22) [34].

The TCM syndrome type is a consequence of disease classification. According to TCM theory, the patients of the same disease can be classified into different syndrome types. There is significant correlation between *CYP1A2*-C733A mutation genotypes and the TCM syndrome “damp abundance due to spleen asthenia syndrome.” It can be perceived for the classification of traditional Chinese medicine syndrome type in hepatitis B-resulted cirrhosis and may be helpful in the clinical diagnosis of TCM.

5. Conclusion

The current study evaluated the relationship between CYP450 SNPs and hepatitis B-caused cirrhosis. The results suggested that there is a correlation between AA genotype at *CYP1A2*-G2964A and CC genotype at *CYP1A2*-T5347C and hepatitis B-caused cirrhosis. Moreover, there is a correlation between AC plus AA genotype at *CYP1A2*-C733A and the “damp abundance due to spleen asthenia syndrome” of TCM.

Data Availability

The data that support the findings of this study are available from the corresponding author upon reasonable request.

Conflicts of Interest

The authors declare that they have no conflicts of interest.

Authors' Contributions

Qing-Ya Li collected samples and clinical data and performed the research and drafted the manuscript; Xiaona Yang and Zhi-Zhong Guo revised the manuscript.

Acknowledgments

This paper is a phased research result of the project of “Henan Provincial Scientific Research Project of TCM (2013ZY02061).” We thank Longhua Hospital, Shuguang Hospital, Putuo Hospital, and Yueyang Hospital of Shanghai University of TCM, Ruikang Hospital and the First Affiliated Hospital of Guangxi University of TCM, and the First Affiliated Hospital of Henan University of TCM, respectively.

References

- [1] T. Vescovo, B. Pagni, M. Piacentini, G. M. Fimia, and M. Antonioli, “Regulation of autophagy in cells infected with oncogenic human viruses and its impact on cancer development,” *Frontiers in Cell and Developmental Biology*, vol. 8, p. 47, 2020.
- [2] H. Zhao, P. Zhu, T. Han et al., “Clinical characteristics analysis of 1180 patients with hepatocellular carcinoma secondary to hepatitis B, hepatitis C and alcoholic liver disease,” *Journal of Clinical Laboratory Analysis*, vol. 34, no. 2, article e23075, 2020.
- [3] W. Nong, L. Ma, B. Lan et al., “Comprehensive identification of bridge genes to explain the progression from chronic hepatitis B virus infection to hepatocellular carcinoma,” *Journal of Inflammation Research*, vol. 14, pp. 1613–1624, 2021.
- [4] M. Tanaka, F. Katayama, H. Kato et al., “Hepatitis B and C virus infection and hepatocellular carcinoma in China: a review of epidemiology and control measures,” *Journal of Epidemiology*, vol. 21, no. 6, pp. 401–416, 2011.
- [5] M. A. Odenwald and S. Paul, “Viral hepatitis: past, present, and future,” *World Journal of Gastroenterology*, vol. 28, no. 14, pp. 1405–1429, 2022.
- [6] T. Q. Reuter, G. Gomes, M. Chuffi et al., “Hepatitis B virus genotypes and subgenotypes and the natural history and epidemiology of hepatitis B,” *Annals of Hepatology*, vol. 27, 2022.
- [7] S. Yao, X. Yin, T. Chen et al., “ALDH2 is a prognostic biomarker and related with immune infiltrates in HCC,” *American Journal of Cancer Research*, vol. 11, no. 11, pp. 5319–5337, 2021.
- [8] N. V. Vlasenko, N. S. Churilova, Y. V. Panasyuk et al., “Single nucleotide polymorphisms of the interleukin-1 superfamily members: association with viral hepatitis B and C,” *Journal of Microbiology, Epidemiology and Immunobiology*, vol. 98, no. 2, pp. 198–212, 2021.

Retraction

Retracted: Biologically Synthesized Peptides Show Remarkable Inhibition Activity against Angiotensin-Converting Enzyme: A Promising Approach for Peptide Development against Autoimmune Diseases

BioMed Research International

Received 12 March 2024; Accepted 12 March 2024; Published 20 March 2024

Copyright © 2024 BioMed Research International. This is an open access article distributed under the Creative Commons Attribution License, which permits unrestricted use, distribution, and reproduction in any medium, provided the original work is properly cited.

This article has been retracted by Hindawi following an investigation undertaken by the publisher [1]. This investigation has uncovered evidence of one or more of the following indicators of systematic manipulation of the publication process:

- (1) Discrepancies in scope
- (2) Discrepancies in the description of the research reported
- (3) Discrepancies between the availability of data and the research described
- (4) Inappropriate citations
- (5) Incoherent, meaningless and/or irrelevant content included in the article
- (6) Manipulated or compromised peer review

The presence of these indicators undermines our confidence in the integrity of the article's content and we cannot, therefore, vouch for its reliability. Please note that this notice is intended solely to alert readers that the content of this article is unreliable. We have not investigated whether authors were aware of or involved in the systematic manipulation of the publication process.

Wiley and Hindawi regrets that the usual quality checks did not identify these issues before publication and have since put additional measures in place to safeguard research integrity.

We wish to credit our own Research Integrity and Research Publishing teams and anonymous and named external researchers and research integrity experts for contributing to this investigation.

The corresponding author, as the representative of all authors, has been given the opportunity to register their agreement or disagreement to this retraction. We have kept a record of any response received.

References

- [1] N. Mujtaba, N. Jahan, A. Jamal et al., "Biologically Synthesized Peptides Show Remarkable Inhibition Activity against Angiotensin-Converting Enzyme: A Promising Approach for Peptide Development against Autoimmune Diseases," *BioMed Research International*, vol. 2022, Article ID 2396192, 12 pages, 2022.

Research Article

Biologically Synthesized Peptides Show Remarkable Inhibition Activity against Angiotensin-Converting Enzyme: A Promising Approach for Peptide Development against Autoimmune Diseases

Nosheen Mujtaba,¹ Nazish Jahan,¹ Adil Jamal ,² Shazia Abrar,³ Shumaila Kiran ,³ Atizaz Rasool,³ Md Belal Hossain ,⁴ Fayez Saeed Bahwerth ,⁵ Ibtisam Nomani,² and Khalid Javed Iqbal⁶

¹Department of Chemistry, Faculty of Sciences, University of Agriculture, Faisalabad, Pakistan

²College of Nursing, Umm Al Qura University, Makkah-715, Saudi Arabia

³Department of Applied Chemistry, Government College University, Faisalabad, Pakistan

⁴Department of Plant Pathology, Faculty of Agriculture, Sher-e-Bangla Agricultural University, Sher-e-Bangla Nagar, Dhaka-1207, Bangladesh

⁵Central Laboratory and Blood Bank, King Faisal Hospital, Makkah-24235, Saudi Arabia

⁶Department of Zoology, The Islamia University of Bahawalpur, Bahawalpur, Pakistan

Correspondence should be addressed to Shumaila Kiran; shumaila.asimch@gmail.com and Md Belal Hossain; dr.mbhossain@sau.edu.bd

Received 12 March 2022; Revised 26 May 2022; Accepted 7 June 2022; Published 20 June 2022

Academic Editor: Nikhil Agrawal

Copyright © 2022 Nosheen Mujtaba et al. This is an open access article distributed under the Creative Commons Attribution License, which permits unrestricted use, distribution, and reproduction in any medium, provided the original work is properly cited.

Angiotensin-converting enzyme (ACE) regulates several biological functions besides its vital role in immune functions. ACE is elevated in immune cells in inflammatory diseases including atherosclerosis, granuloma, chronic kidney disease, and also autoimmune diseases, like multiple sclerosis, rheumatoid arthritis, and type I diabetes. No significant information prevails in the literature regarding the isolation, identification, and profiling of potential ACE inhibitory peptides. In the present study, indigenous crop varieties like seeds (peanut, corn, oat, sunflower, chickpea, parsley, cottonseed, papaya, sesame, and flaxseed) were used to evaluate their ACE inhibition activity. Variables including hydrolysis time, enzyme-to-substrate ratio (E/S), pH, and temperature were standardized to acquire the most suitable and optimum ACE inhibition activity. Seeds of cotton, chickpea, and peanuts displayed remarkably maximum ACE inhibition activity than other plants. The study disclosed that maximum ACE inhibitory activity (86%) was evaluated from cottonseed at pH 8.0, temperature of 45°C, hydrolysis time of 2 hrs, and enzyme to the substrate (E/S) ratio of 1:5 followed by peanuts (76%) and chickpea (55%). SDS-PAGE confirmed that vicilin protein is present in cottonseed and peanut seed while cruciferin and napin proteins are present in chickpeas. LC-MS/MS analysis disclosed potential novel peptides in hydrolyzed cottonseed that can be ascribed as potential ACE inhibitors which have never been reported and studied earlier. The current study further showed that cottonseed peptides due to their promising ACE inhibitory activity can be a valuable source in the field of ACE inhibitor development.

1. Introduction

Angiotensin-converting enzyme (ACE) is involved in inflammation and in the stimulation of T-cells by certain antigenic peptides. In autoimmune disorders, ACE levels are increased. Certain immune functions are suppressed and inflammatory

or autoimmune diseases are inhibited by ACE inhibitors [1]. Autoimmune disease treatments minimize symptoms while suppressing the immune system. Most autoimmune disorders are inflammatory, involving T-cell responses and cytokine production [2]. Hence, as a result, biologics-based targeted therapies are designed to target specific proteins and protein-

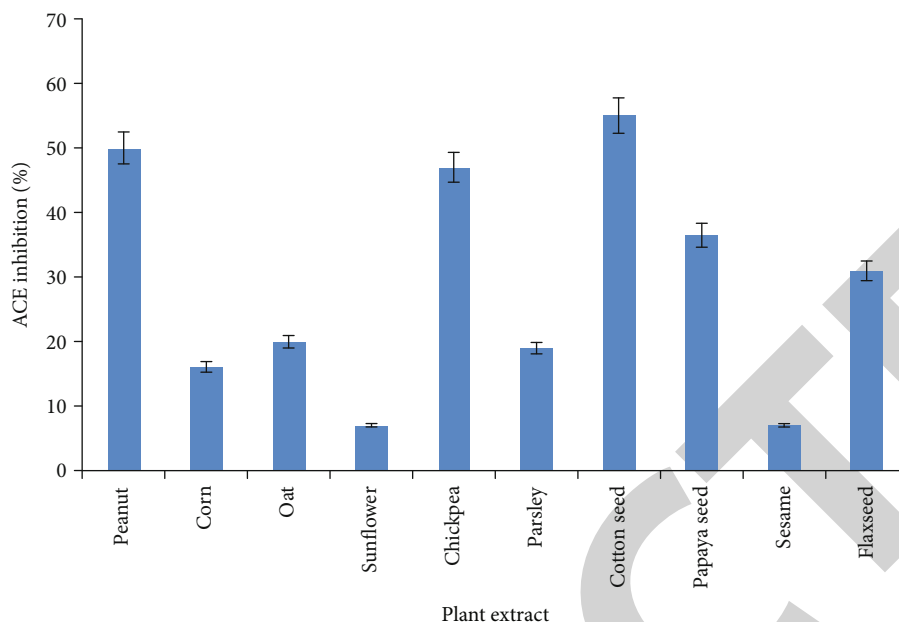


FIGURE 1: ACE inhibition activity of plant seed extracts.

protein interactions. Peptides and peptidomimetics are being developed with the goal of binding to these proteins and modulating the immune system. Several costimulatory substances that are involved in inflammation and the T-cell response have been identified as potential targets for the treatment of autoimmune diseases [3]. Additionally, with the rise in autoimmune diseases (type 1 diabetes, rheumatoid arthritis, lupus, psoriasis, celiac disease, etc.), the use of multifunctional immunomodulatory peptides and/or anti-inflammatory and antimicrobial peptides in vaccines has gained importance [4–6].

Peptides and peptidomimetics can act as immunomodulators by either blocking or stimulating the immune response to generate tolerance. The study of peptide synthesis and modified amino acid side chains has led to a new class of autoimmune therapeutic drugs [7]. Peptides combine the benefits of tiny molecules with proteins [8]. However, peptides have limited in vivo enzymatic stability, short half-life, and rapid renal elimination [9]. The design of peptides/peptidomimetics for immunomodulation in autoimmune diseases such as HIV infection, rheumatoid arthritis, multiple sclerosis, and systemic lupus is of prime importance.

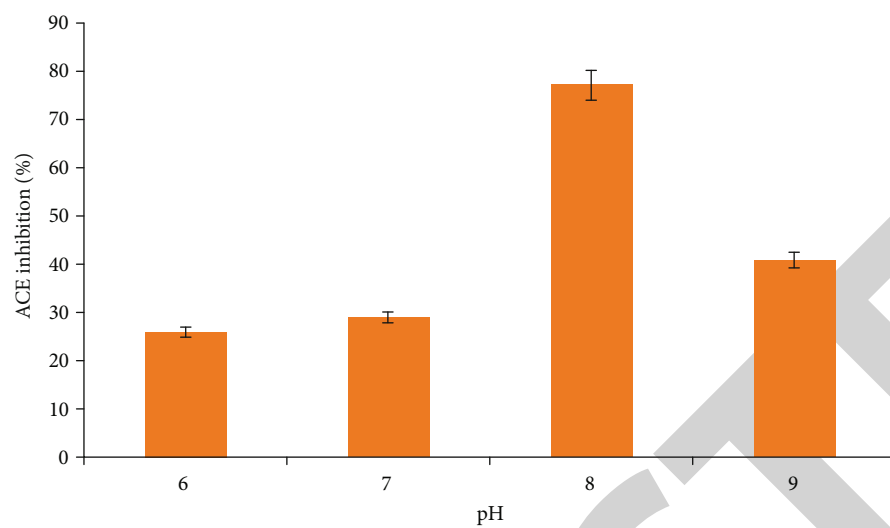
The discovery of plant primary metabolites such as proteins and peptides for disease management has ushered in a new era for the development of plant-based peptides as therapeutic candidates [10]. Bioactive peptides have been found in abundance in both animal and plant sources. Plants possess different ACE inhibitory peptides which can be obtained by enzymatic hydrolysis [11, 12]. The peanut, cottonseed, and chickpea are not only the most important crops broadly used as nutrient sources for animals and humans, but they also possess natural ACE inhibitory activity [13]. Plant peptides are still being investigated, and just a few bioactive peptides have been found in soy, wheat, and other plants [14]. Proteins have high-fat content in animals and can cause diseases such as hypertension and cardiac disease if consumed in large quantities. Plant proteins, on the other hand, have no associated fat and no side effects [15].

To the best of our knowledge and information available, no significant literature prevails regarding the screening and development of inhibitory peptides and their role in autoimmune diseases. Therefore, the aim of the present research was to evaluate the ACE inhibition potential of indigenous plants for the production of inhibitory peptides. Our study focused on the screening of plants for their ACE inhibition activity. This study also is aimed at development of potential ACE peptide inhibitors from plants and protein profiling using the liquid chromatography mass spectrometry (LC-MS/MS) approach. These identified potential ACE inhibitory peptides from plants can be used as a source in the development of antihypertensive drugs in the pharmaceutical field in the future to cure autoimmune diseases/disorders.

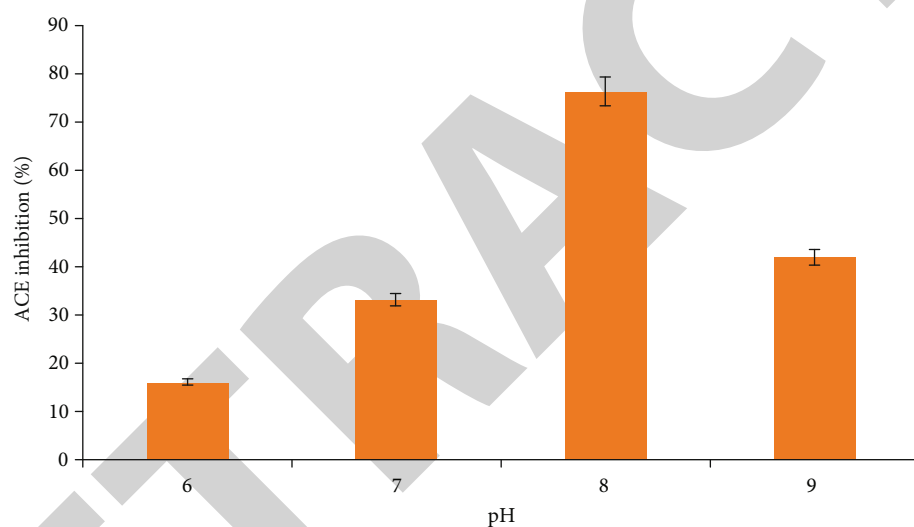
2. Material and Methods

2.1. Preparation of Crude Extracts. The seeds of local varieties used in this study were obtained from the Seed section of Ayyub Agriculture Research Institute (AARI), Faisalabad, Punjab, Pakistan. A fine powdered seed of each plant was mixed with distilled water thoroughly for 2 hrs until the mixture was homogenized. The extract was filtered through Whatman No. 1 filter paper, and the solvent was evaporated with a rotary evaporator. Extracts were stored at -20°C for further analysis.

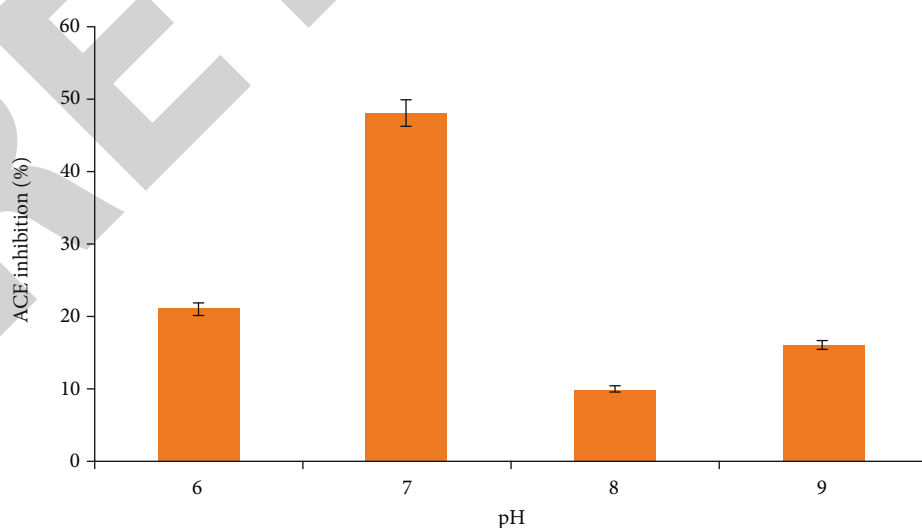
2.2. Extraction of Angiotensin-Converting Enzyme (ACE). ACE extracted from rabbit lung powder was used as reported earlier with minor modifications [16]. Freshly slaughtered healthy rabbit lungs were washed thoroughly with saline solution (0.8%) and pulverized later using phosphate-buffered saline (PBS). The pulverized tissue was centrifuged at 4000 g for 15 min. The supernatant was discarded, and the centrifuged sample was washed with acetone for 3–4 times followed by continuous stirring. Acetone was



(a)



(b)



(c)

FIGURE 2: (a) Optimization of pH for hydrolysis of cotton seed proteins. (b) Optimization of pH for hydrolysis of peanut proteins. (c) Optimization of pH for hydrolysis of chickpea proteins.

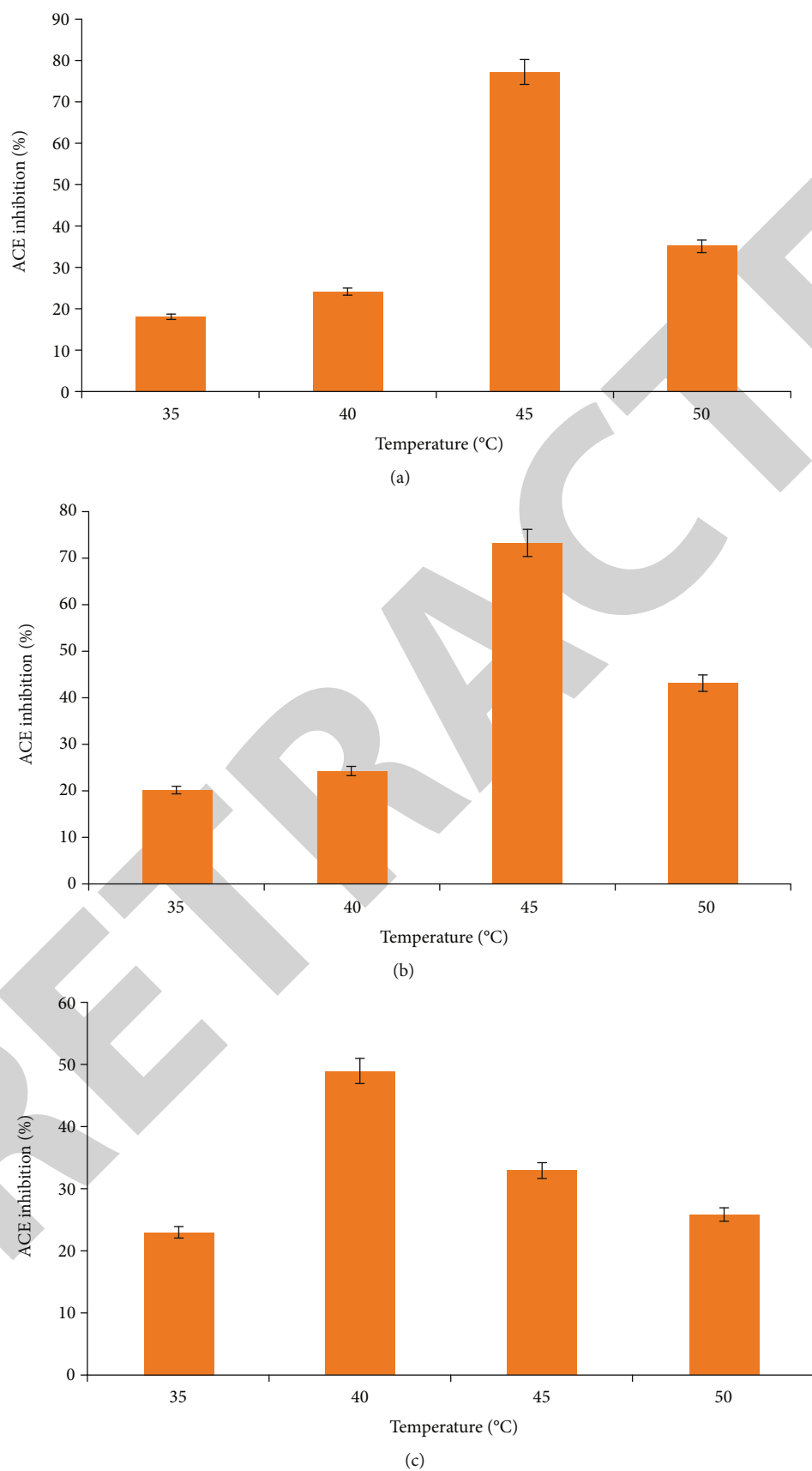
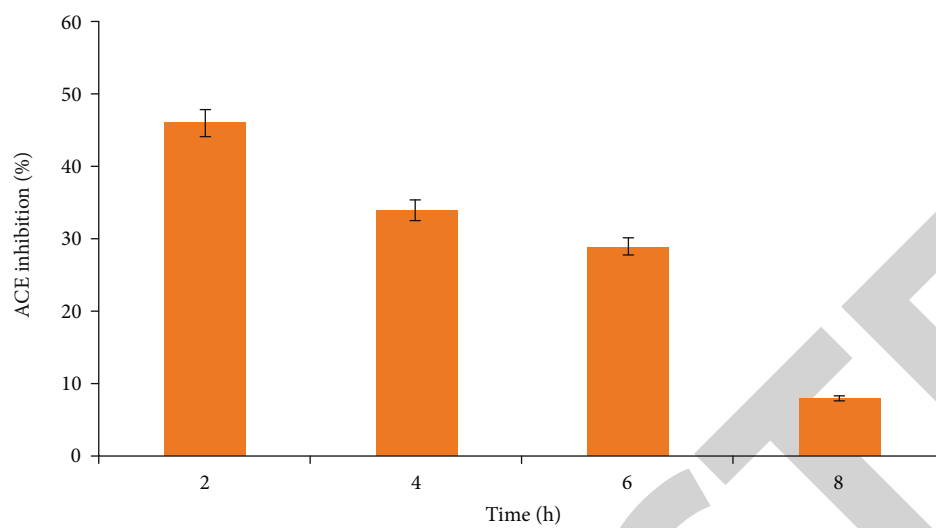
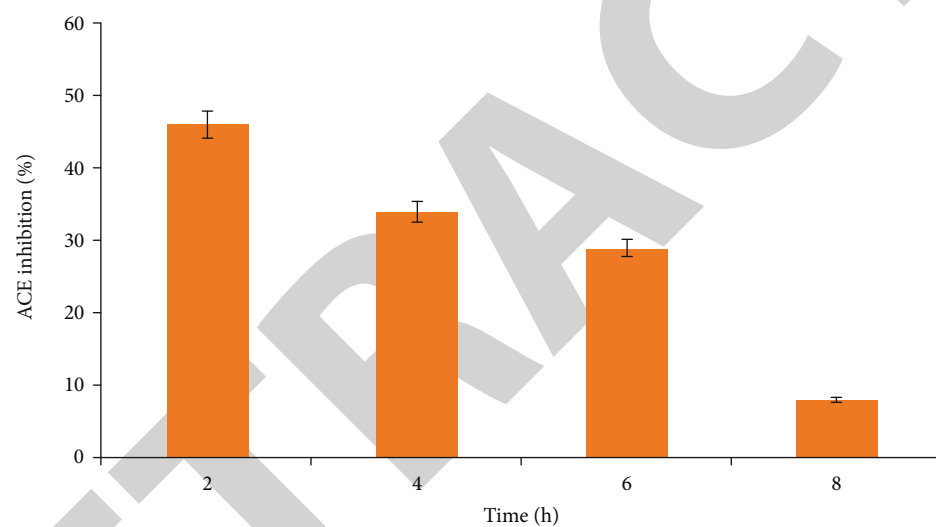


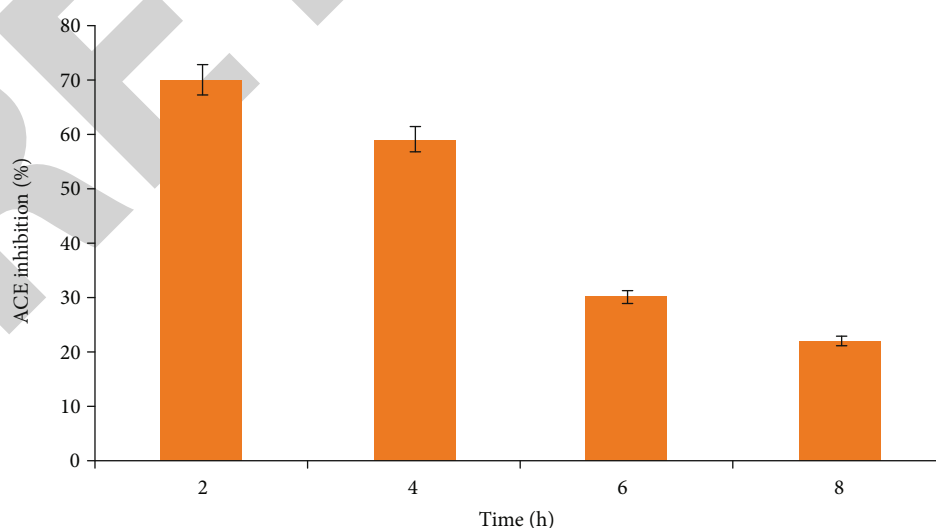
FIGURE 3: (a) Optimization of temperature for hydrolysis of cottonseed protein. (b) Optimization of temperature for hydrolysis of peanut protein. (c) Optimization of temperature for hydrolysis of chickpea protein.



(a)

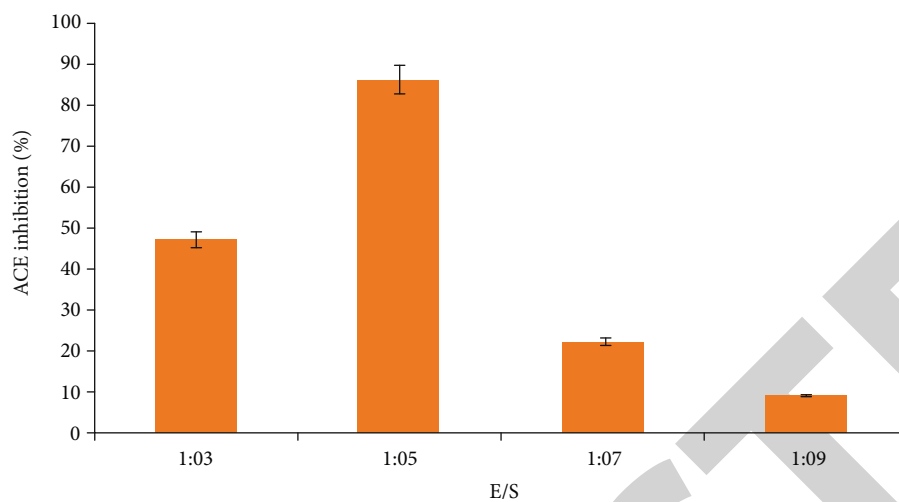


(b)

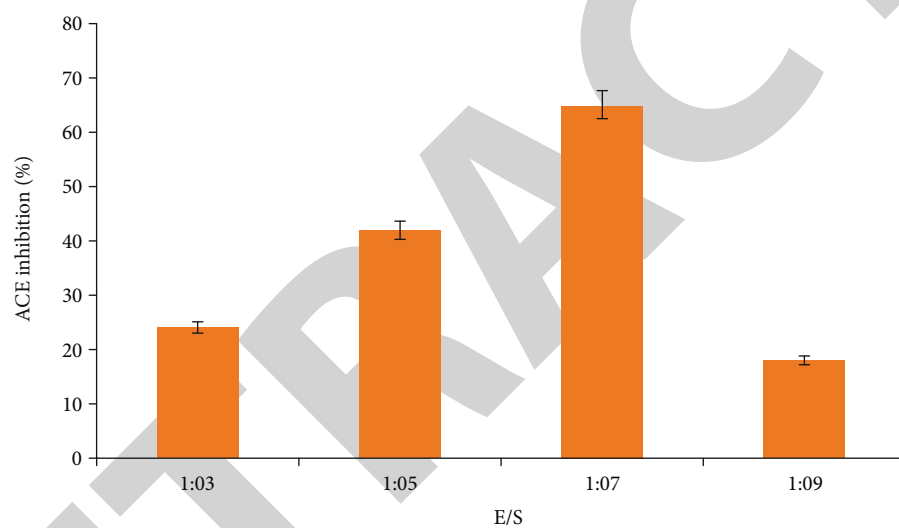


(c)

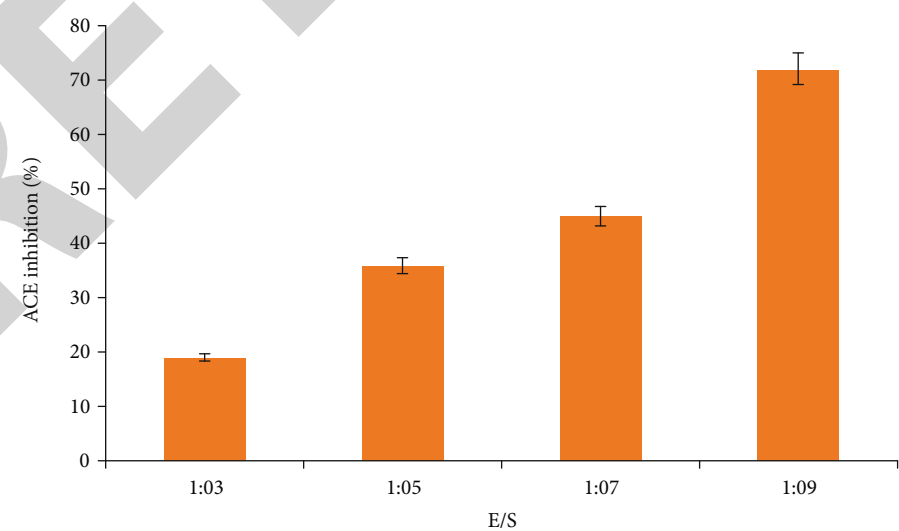
FIGURE 4: (a) Optimization of time for hydrolysis of chickpea protein. (b) Optimization of time for hydrolysis of peanut protein. (c) Optimization of time for hydrolysis of cottonseed protein.



(a)

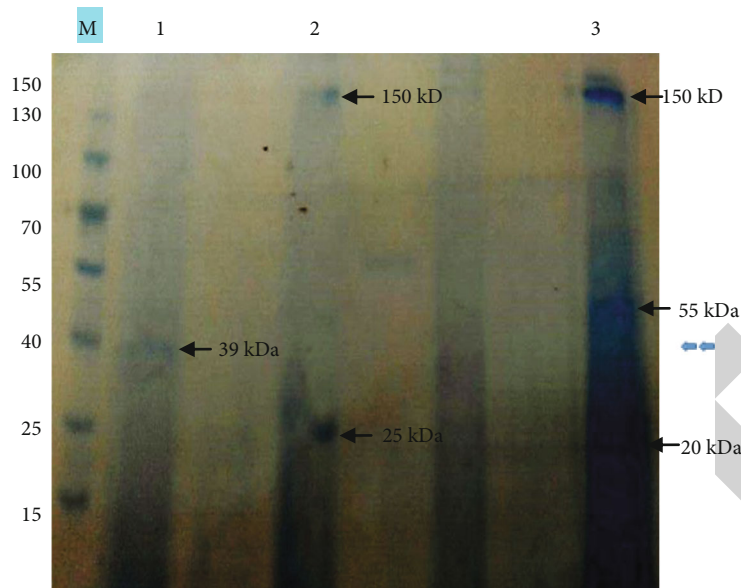


(b)



(c)

FIGURE 5: (a) Optimization of E/S for hydrolysis of cottonseed protein. (b) Optimization of E/S for hydrolysis of peanut protein. (c) Optimization of E/S for hydrolysis of chickpea protein.



M: Molecular marker(15-150kDa); Lane1: Cottonseed; Lane2: Chickpea; Lane3: Peanut

FIGURE 6: SDS-PAGE results for hydrolysis cottonseed, chickpea, and peanut proteins.

dissolved in phosphate buffer (pH 8.3). The sample was stirred for 10 hrs and centrifuged at 4000 g for 45 min at room temperature. Centrifuged samples were further proceeded for ACE extraction [17, 18]. The drug captopril was used as a positive control (1 mg/mL) [19, 20]. Captopril (25 mg) was ground to fine powder, and extract was prepared using 25 mL of deionized distilled water. The prepared extract was filtered using a Whatman filter paper.

2.3. Determination of ACE Inhibition Activity. The ACE inhibition activity of plants seeds was determined using the reported method [21]. To prepare 25 μ L of each sample solution, 60 μ L of Hippuryl-L-histidyl-L-leucine (5 mM) and 100 mM of sodium borate buffer (pH 8.3) having NaCl (300 mM) were mixed at 40°C for 15 minutes. The reaction was initiated by adding 10 μ L of ACE, and the mixture was further incubated later at 40°C for 35 min. The incubated reaction was terminated using HCl (1 M). 0.5 mL of ethyl acetate was added and centrifuged at 3000 rpm for 15 min at 4°C to extract hippuric acid (HA). Upper ethyl acetate layer (0.2 mL) was separated and was evaporated at room temperature. The resulted HA was dissolved in 1.0 mL deionized distilled water, and the optical density of this solution was calculated at 228 wavelength using a UV spectrophotometer. The ACE inhibition activity was determined by Zheng et al.'s method [22]. ACE inhibition (%) was calculated using the following formula:

$$\text{ACE inhibition (\%)} = 100 \times \frac{[(A - B) - (C - D)]}{(A - B)} \quad (1)$$

A is the absorbance of ACE, B is the absorbance of the reaction blank, C is the absorbance in the presence of ACE and inhibitor, and D is the absorbance of the sample blank.

All observations were carried out in triplicates, and results were expressed as the mean \pm SE.

2.4. Preparation of Protein Isolates and Sample Digestion.

The plants with higher ACE inhibition activity (>50% including peanut, chickpea and cottonseeds) were selected for protein extraction. Protein was isolated using the previously reported protocol [23]. Seeds of selected plants were ground to fine powder and defatted with *n*-hexane for 7 hours using the Soxhlet apparatus. Protein extracts (1:12 *w/v*) were prepared using NaOH (0.09 M) at room temperature. The extracts were centrifuged at 3000 rpm for 25 minutes. The higher film was standing apart, set to pH 5.5 using HCl (2 M), and centrifuged at 3000 rpm for 25 minutes. Samples were washed twice using pure water and quantified. Around 0.2 mL solution containing alcalase (0.05%) and inhibitor solution (protein) was incubated with potassium phosphate buffer (0.1 M) having pH 8.0 for 6 hours at 37°C. To stop the hydrolysis, samples were boiled for 6-7 min and centrifuged at room temp for 10-15 minutes [24].

2.5. Characterization of Peptides

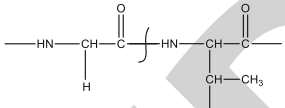
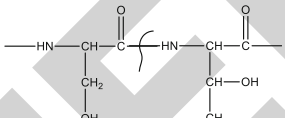
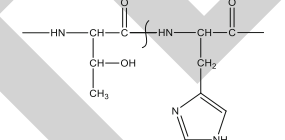
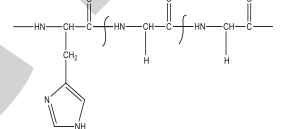
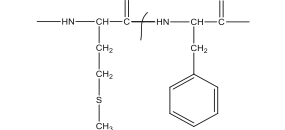
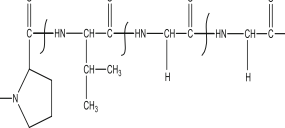
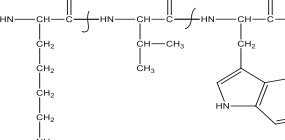
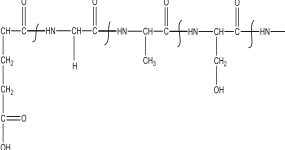
2.5.1. SDS-PAGE Analysis of ACE Inhibitory Peptides.

SDS-PAGE was used for the determination of the molecular mass of hydrolyzed proteins. Hydrolyzed proteins were dissolved in a buffer containing SDS and separated on a polyacrylamide gel matrix. After electrophoresis, the gel was carefully removed and placed in Coomassie blue staining solution for 1 hour [25]. The gel was destained for 60 minutes, and the bands were compared with a standard protein marker to determine the molecular mass of hydrolyzed proteins of cottonseeds, peanuts, and chickpeas.

2.5.2. LC-MS/MS Analysis of Peptides.

The hydrolyzed peptide fraction was introduced into a mass spectrometer (ISQ™ EM Single Quadrupole Mass Spectrometer, ISQEM-ESI-APCI, Thermo Fisher Scientific, Germany) using an electrospray

TABLE 1: Peptides identified in hydrolyzed protein profile of cottonseed in positive ionization mode.

| Peptide | Peptide structure |
|--|---|
| Valine-Glycine (Val-Gly) |  |
| Serine-Threonine (Ser-Thr) |  |
| Histidine-Threonine (His-Thr) |  |
| Glycine-Glycine-Histidine (Gly-His-His) |  |
| Phenylalanine-Methionine (Phe-Met) |  |
| Valine-Proline-Glycine-Glycine (Val-Pro-Gly-Gly) |  |
| Lysine-Valine-Tryptophan (Lys-Val-Trp) |  |
| Glutamic acid-Glycine-Alanine-Serine-Aspartic acid (Glu-Gly-Ala-Ser-Asp) |  |

ionization source. The spectra were obtained with a mass range of 50-2000 m/z in positive ionization mode. MS/MS was operated at 4.0 kV spray voltage, auxiliary gas 5 units/min, sheath gas 15 unit/min, 275°C capillary temperatures, and 100.50 V tube voltage. The fragmentation was carried out with collision-induced dissociation (CID) of 25-30 units/mass. The spectral data of ion peaks were obtained using Xcalibur Software (Thermo Fisher Scientific™).

2.6. *Statistical analysis.* All samples used in this study were measured as an average of triplicates. The data collected were analyzed by computing standard errors [26].

3. Results and Discussion

3.1. *ACE Inhibitory Activity of Plants.* Cottonseeds showed maximum ACE inhibitory activity (55%), followed by peanut (50%), chickpea (47%), papaya seeds (36.5%), and flaxseed (31%) (Figure 1). The variation in ACE interdict potential may be due to the different plant types and the nature of protein present in plants, or it may be ascribed as the presence of other metabolites in the extract which may interfere with the inhibition activity [27].

3.2. *Effect of pH, Temperature, Hydrolysis Time, and Enzyme to Substrate (E/S) Ratio on ACE Inhibition (%) Activity.*

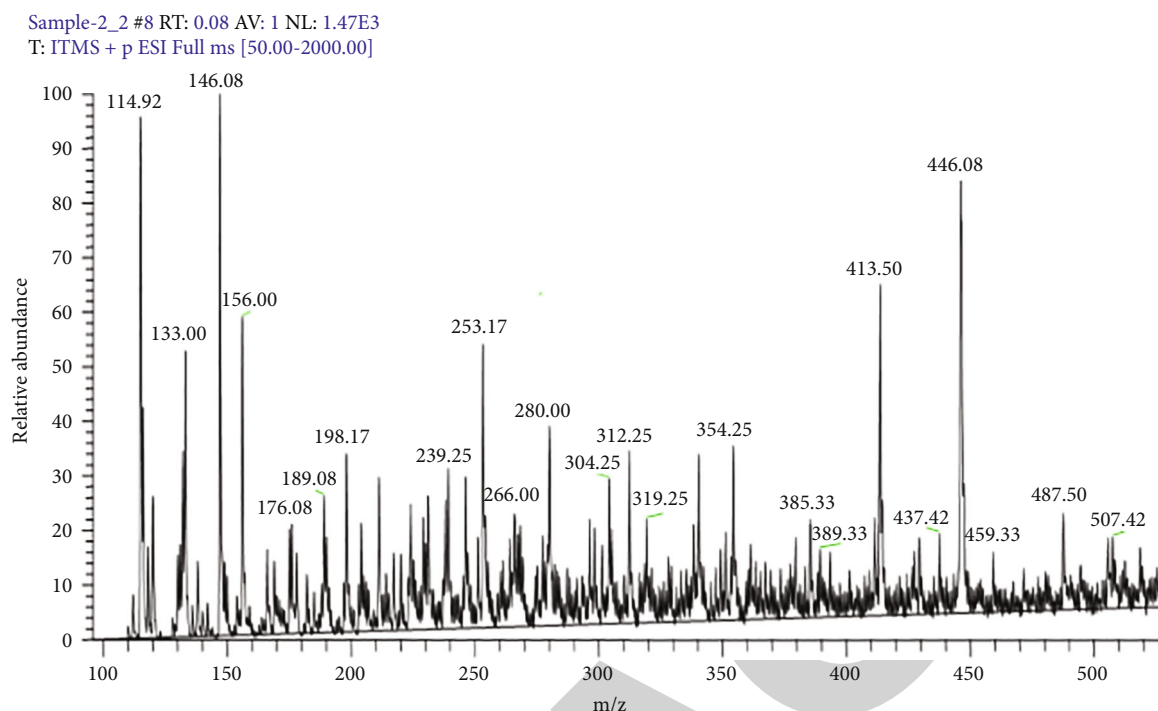


FIGURE 7: LC-MS/MS spectrum of hydrolyzed cottonseed protein.

Extremely high or low pH may completely result in the loss of activity of enzymes [28]. The effect of different pH (6-9) on ACE inhibition (%) of cottonseed, peanut, and chickpea was studied. Our study showed that change in pH significantly affected the ACE inhibition (%). By increasing pH, ACE inhibitory (%) action of cottonseed, peanut, and chickpea was augmented. An increase in pH from 6.0 to 8.0 resulted in the more ACE inhibitory activity of cotton seed (77%), peanut (76%), and chickpea (48%) proteins (Figure 2(a)). Cottonseed and peanut showed maximum ACE inhibition activity at pH 8.0 while chickpea at pH 7.0 (Figure 2(b)). Previous studies reported that optimum pH level is different for different plants and dependent upon reaction conditions [29].

Our studies demonstrate that a gradual increase in temperature resulted in increased ACE inhibition activity of cottonseed, peanut, and chickpea. The rise in temperature from 35 to 45°C resulted in increased ACE activity from 18% to 77.5% for cottonseed (Figure 2(a)) and 76.1% for peanut (Figure 2(b)). Chickpea protein showed increased ACE activity from 26% to 46% with increasing pH (Figure 2(c)). Our study disclosed that a rise in temperature led to 45°C increased ACE inhibition activity (10% to 70%) in cottonseed and peanut (Figures 3(a) and 3(b)), whereas increasing the temperature to 40°C decreased (48% to 33%) the ACE inhibitory activity in chickpea protein (Figure 3(c)). According to the enzymatic reaction dynamic principle, by increasing temperature, the reaction rate also increases, but here, this decrease in enzyme activity can be described as most of the enzyme denature as temperature increases to 40°C or even higher [30]. Previous studies proved that increase in temperature above the optimum temperature did not result in higher inhibition activity and also inhibits the hydrolysis reaction [31] which best supports our study results.

Our study results disclosed that cottonseed, peanut, and chickpea proteins showed maximum ACE inhibitory action when the hydrolysis reaction was performed for 2 hours (Figures 4(a)–4(c)). After 2 hrs hydrolysis time, chickpea, peanut, and cottonseed showed 46% (Figure 4(a)), 45% (Figure 4(b)), and 69% (Figure 4(c)) ACE inhibition activity, respectively. An increase in hydrolysis reaction time to 8 hrs resulted in gradually reduced ACE inhibition activity. Our study results are best supported by earlier findings [32]. An increase in time above 2 hrs did not cause any positive effect on protein yield and terminated the hydrolysis reaction [33].

The enzyme to substrate (E/S) ratio plays an important role in protein hydrolysis. It is clear from the experiments that if the concentration of enzymes is kept constant and the amount of substrate is increased then the rate of forwarding reaction enhances but only at a specific value because a further increase in E/S decreases the rate of reaction. Different E/S ratios were analyzed on cottonseed, peanut, and chickpea, i.e., from 1:3 to 1:9 under similar reaction conditions. We found that an increase in enzyme to substrate ratio resulted in increased ACE suppression activity. Cottonseed showed maximum ACE inhibitory activity (86%) at 1:5 (Figure 5(a)), peanut (68%) at 1:7 (Figure 5(b)), and chickpea (70%) at 1:9 E/S ratio (Figure 5(c)). Previous findings also reported that increased enzyme to substrate ratio resulted in increased turnover of protein hydrolysates [34, 35] which best supports our findings.

3.3. Polyacrylamide Gel Electrophoresis (SDS-PAGE). Our results demonstrated the molecular weight of cottonseed protein fraction of 39 kDa while chickpea protein showed 25 kDa and 150 kDa subunits, which indicate the presence of vicilin subunit of electrophoresed protein (Figure 6).

Our study findings revealed that the molecular weight of peanut protein fractions of 20kDa, 55kDa, and 150kDa (Figure 6) can be recognized as cruciferin and napin subunits of hydrolyzed protein [36]. Therefore, it is revealed from SDS-PAGE that hydrolysis with alcalase enzyme is important for the production of smaller subunits of protein that can be valuable candidates for antihypertensive treatment.

3.4. LC-MS/MS Analysis of Peptides. Liquid chromatography mass spectrometry (LC-MS/MS) is a powerful analytical technique, used for the identification of unknown compounds, and structure elucidation to find the chemical properties of different compounds/peptides. It is highly sensitive and selective for the analysis of compounds present in trace amounts [37, 38]. In the current study, LC-MS/MS is used for identification and structure elucidation of bioactive peptides to find the sequence of peptides present in a hydrolyzed fraction of cottonseed plant, i.e., Valine-Glycine (Val-Gly), Serine-Threonine (Ser-Thr), Histidine-Threonine (His-Thr), Glycine-Glycine-Histidine (Gly-His-His), Phenylalanine-Methionine (Phe-Met), Valine-Proline-Glycine-Glycine (Val-Pro-Gly-Gly), Lysine-Valine-Tryptophan (Lys-Val-Trp), and pentapeptide Glutamic acid-Glycine-Alanine-Serine-Aspartic acid (Glu-Gly-Ala-Ser-Asp) (Table 1). LC-MS/MS analysis of hydrolyzed fraction obtained from cotton seed showed peptides in positive ionization mode. The molecular peak at m/z 146 $[M+H]^+$ in the mass spectrum (Figure 7) was identified as valine-glycine dipeptide which showed other ions at m/z 56.75 due to $[M+H-Val]$ and m/z 73.83 due to removal of $[valine-NH=CH]$ in fragmentation pattern specific for Val-Gly dipeptide. The fragment ion spectra in our study were in agreement with the fragment ion peaks of Val-Gly peptide as reported earlier in plants [39, 40]. The peak at m/z 189 identified as Ser-Thr $[M+H]^+$ (Figure 7). Pattern visualized at m/z 101.92 is due to the removal of threonine $[M+H-Thr]$, at m/z 71.83 by dehydration $[Ser-H_2O]$, and at m/z 72.33 due to the elimination of $[Thr-NH=CH]$. Molecular ion peak at m/z 239 $[M+H]^+$ was detected as His-Thr dipeptide, at m/z 193.17 due to the removal of $[M+H-45]$, and m/z 157.75 due to the removal of $[M+H-81]$ (Figure 7).

The peak at m/z 253 $[M+H]^+$ corresponds to the His-Gly-Gly tri-peptide. The product peak at m/z 137.92 due to the $[M+H-Gly-Gly]$ and at m/z 109.83 due to $[His-NH=CH]$, and m/z 120 due to the removal of $[His-H_2O]$. A molecular ion peak at m/z 280 $[M+H]^+$ was identified as Phe-Met dipeptide (Figure 7) which produced a minor band at m/z 148.83 due to the phenylalanine amino acid, at m/z 166.92 due to the addition of water molecule $[Phe+H_2O]$, at m/z 133.92 due to the methionine amino acid, and at m/z 115.92 due to dehydration $[Met-H_2O]$ (Figure 7). The fragment ion profile in our study was similar to that reported previously [37]. The precursor ion at m/z 312 $[M+H]^+$ was detected as Val-Pro-Gly-Gly tetra-peptide. Spectra produced at m/z 255.83 and m/z 197.00 resulted due to the elimination of $[M+H-Gly-Gly]$, m/z 213.02 due to the $[M+H-Pro]$, and m/z 100.83 due to the Val peptide (Figure 7). A molecular ion peak at m/z 413 $[M+H]^+$ was due to Lys-Val-Trp tripep-

ptide (Figure 7), which produced peaks at m/z 314.18 due to $[M+H-Val]$, m/z 369.1 due to $[M+H-43]$, and m/z 338.6 due to $[M+H-73]$, and 226.00 is ascribed due to $[M+H-Trp]$. Pentapeptide Glu-Gly-Ala-Ser-Asp produced ion spectrum band at m/z 459 $[M+H]^+$, spectra at m/z 360.33 due to $[M+H-Val]$, m/z 441.16 due to dehydration $[M+H-H_2O]$, m/z 429.34 due to $[M+H-31]$, m/z 401.00 due to $[M+H-58]$, and m/z at 344.17 in the spectra can be attributed due to $[M+H-Asp]$ (Figure 7). Previous studies have reported that peptides having different amino acid sequences possess different ACE inhibition activities [41–44]. Further exploration of the multiple and different peptides of these cottonseed proteins may shed more light on the evolution, posttranslational modification, and isoform of cottonseed and other plant proteins with the potential of ACE inhibitory candidate peptides. The further in-depth study could also provide novel insight into the functional utilization of the relevant bioactive peptide fragments to determine whether they are the peptide precursors or the degraded product.

4. Conclusion and Future Outlook

According to the best of our information available, this was the first performed study regarding the protein profiling of cottonseed using LC-MS/MS technique, and the peptides obtained are explored for the first time. From the current findings, it is clear that cottonseed, peanut, and chickpea have the potential against hypertension. However, among all the studied plants, cottonseed contains important amino acids which are essential for antihypertensive activity. Hence, it can be concluded that antihypertensive proteins from cottonseed are valuable alternatives because of their cost-effectiveness and no side effect.

4.1. Study Limitations/Recommendations. There must be detailed studies on the specific structural unit of the peptides by MALDI-TOF analysis, which is very costly and time taking, followed by docking analysis and protein-protein interactions to analyze the best fit model of peptides in autoimmune disorders/diseases.

Data Availability

All the data relevant to this study are mentioned in the manuscript. There are no any supplementary data.

Conflicts of Interest

The authors declare no conflict of interest.

Authors' Contributions

NJ, SK, and BH executed the idea and planned, organized, and supervised the study. NM and AR performed the experiments. AJ and AR wrote the early and final draft of manuscript. SA, FSB, IN, and KJI are responsible for the statistical analysis and result interpretation. All the authors finally read and approved the manuscript.

Acknowledgments

All authors are thankful to the Department of Chemistry, University of Agriculture, Faisalabad, Pakistan, and Department of Applied Chemistry, Government College University, Faisalabad, Pakistan, for providing lab facilities to carry out current study smoothly and successfully.

References

- [1] C. S. Constantinescu, E. Ventura, B. Hilliard, and A. Rostami, "Effects of the angiotensin converting enzyme inhibitor captopril on experimental autoimmune encephalomyelitis," *Immunopharmacology and Immunotoxicology*, vol. 17, no. 3, pp. 471–491, 1995.
- [2] A. Webber, R. Hirose, and F. Vincenti, "Novel strategies in immunosuppression: issues in perspective," *Transplantation*, vol. 91, no. 10, pp. 1057–1064, 2011.
- [3] S. D. S. Jois, L. Jining, and L. M. Nagarajarao, "Targeting T-cell adhesion molecules for drug design," *Current Pharmaceutical Design*, vol. 12, no. 22, pp. 2797–2812, 2006.
- [4] B. Pahar, S. Madonna, A. Das, C. Albanesi, and G. Girolomoni, "Immunomodulatory role of the antimicrobial LL-37 peptide in autoimmune diseases and viral infections," *Vaccine*, vol. 8, no. 3, pp. 517–536, 2020.
- [5] M. Mahlapuu, C. Björn, and J. Ekblom, "Antimicrobial peptides as therapeutic agents: opportunities and challenges," *Critical Reviews in Biotechnology*, vol. 40, no. 7, pp. 978–992, 2020.
- [6] L. A. Barrero-Guevara, N. Bolaños, M. Parra, J. M. González, H. Groot, and C. Muñoz-Camargo, "New peptides with immunomodulatory activity in macrophages and antibacterial activity against multiresistant *Staphylococcus aureus*," *BioRxiv*, p. 838201, 2019.
- [7] A. S. Gokhale and S. Satyanarayanajois, "Peptides and peptidomimetics as immunomodulators," *Immunotherapy*, vol. 6, no. 6, pp. 755–774, 2014.
- [8] D. C. Wraith, "Therapeutic peptide vaccines for treatment of autoimmune diseases," *Immunology Letters*, vol. 122, no. 2, pp. 134–136, 2009.
- [9] J. H. Hamman, G. M. Enslin, and A. F. Kotzé, "Oral delivery of peptide drugs," *BioDrugs*, vol. 19, no. 3, pp. 165–177, 2005.
- [10] L. Otvos, "Peptide-based drug design: here and now," in *Peptide-based drug design*, L. Otvos, Ed., Humana Press, Totowa, 2008.
- [11] C. Borghi and A. F. G. Cicero, "Nutraceuticals with a clinically detectable blood pressure-lowering effect: a review of available randomized clinical trials and their meta-analyses," *British Journal of Clinical Pharmacology*, vol. 83, no. 1, pp. 163–171, 2017.
- [12] N. Mujtaba, N. Jahan, B. Sultana, and M. A. Zia, "Isolation and characterization of antihypertensive peptides from soy bean protein," *Journal of Pharmaceutical Sciences*, vol. 57, article e19061, 2021.
- [13] B.-H. Lee, Y.-S. Lai, and S.-C. Wu, "Antioxidation, angiotensin converting enzyme inhibition activity, nattokinase, and anti-hypertension of *Bacillus subtilis* (natto)-fermented pigeon pea," *Journal of Food and Drug Analysis*, vol. 23, no. 4, pp. 750–757, 2015.
- [14] R. Hartmann and H. Meisel, "Food-derived peptides with biological activity: from research to food applications," *Current Opinion in Biotechnology*, vol. 18, no. 2, pp. 163–169, 2007.
- [15] C. Martínez-Villaluenga and B. Hernández-Ledesma, "Peptides for health benefits 2019," *International Journal of Molecular Sciences*, vol. 21, no. 7, article 2543, 2020.
- [16] A. A. Mansurah, I. A. Aimola, R. O. Annette, and S. Abdullahi, "Isolation, partial purification and characterization of Angiotensin Converting Enzyme (ACE) from rabbit (*Oryctolagus cuniculus*) lungs," *American Journal of Drug Discovery and Development*, vol. 3, no. 3, pp. 120–129, 2013.
- [17] W. A. Wan Mohtar, A. A. Hamid, S. Abd-Aziz, S. K. S. Muhammad, and N. Saari, "Preparation of bioactive peptides with high angiotensin converting enzyme inhibitory activity from winged bean [*Psophocarpus tetragonolobus* (L.) DC.] seed," *Journal of Food Science and Technology*, vol. 51, no. 12, pp. 3658–3668, 2014.
- [18] S. K. Chaudhary, A. De, S. Bhadra, and P. K. Mukherjee, "Angiotensin-converting enzyme (ACE) inhibitory potential of standardized *Mucuna pruriens* seed extract," *Pharmaceutical Biology*, vol. 53, no. 11, pp. 1614–1620, 2015.
- [19] G. Donath-Nagy, S. Vancea, and S. Imre, "Comparative study of captopril derivatization reaction by LC-UV, LC-MS and CE-UV methods," *Croatica Chemica Acta*, vol. 84, no. 3, pp. 423–427, 2011.
- [20] L. B. Kuntze, R. C. Antonio, T. C. Izidoro-Toledo, C. A. Meschiari, J. E. Tanus-Santos, and R. F. Gerlach, "Captopril and Lisinopril only inhibit matrix metalloproteinase-2 (MMP-2) activity at millimolar concentrations," *Basic and Clinical Pharmacology and Toxicology*, vol. 114, no. 3, pp. 233–239, 2014.
- [21] G. H. Li, H. Liu, Y. H. Shi, and G. W. Le, "Direct spectrophotometric measurement of angiotensin I-converting enzyme inhibitory activity for screening bioactive peptides," *Journal of Pharmaceutical and Biomedical Analysis*, vol. 37, no. 2, pp. 219–224, 2005.
- [22] Y. Zheng, Y. Li, and G. Li, "ACE-inhibitory and antioxidant peptides from coconut cake albumin hydrolysates: purification, identification and synthesis," *RSC Advances*, vol. 9, no. 11, pp. 5925–5936, 2019.
- [23] S. Bernardi, M. P. Corso, I. J. Baraldi, E. Colla, and C. Canan, "Obtaining concentrated rice bran protein by alkaline extraction and stirring - optimization of conditions," *International Food Research Journal*, vol. 25, no. 3, pp. 1133–1139, 2018.
- [24] L. Paiva, E. Lima, A. I. Neto, and J. Baptista, "Angiotensin I-converting enzyme (ACE) inhibitory activity, antioxidant properties, phenolic content and amino acid profiles of *Fucus spiralis* L. protein hydrolysate fractions," *Marine Drugs*, vol. 15, no. 10, p. 311, 2017.
- [25] J. Sambrook and D. W. Russell, *Molecular cloning. A laboratory manual*, Cold Spring Harbor Laboratory Press, 2001.
- [26] R. G. Steel, *Principles and Procedures of Statistics a Biometrical Approach*, 1997, No. 519.5 S8.
- [27] T. B. Zou, T. P. He, H. B. Li, H. W. Tang, and E. Q. Xia, "The structure-activity relationship of the antioxidant peptides from natural proteins," *Molecules*, vol. 21, no. 1, p. 72, 2016.
- [28] W. F. Walkenhorst, J. W. Klein, P. Vo, and W. C. Wimley, "pH dependence of microbe sterilization by cationic antimicrobial peptides," *Antimicrobial Agents and Chemotherapy*, vol. 57, no. 7, pp. 3312–3320, 2013.

Retraction

Retracted: Divergent Analyses of Genetic Relatedness and Evidence-Based Assessment of Therapeutics of *Staphylococcus aureus* from Semi-intensive Dairy Systems

BioMed Research International

Received 12 March 2024; Accepted 12 March 2024; Published 20 March 2024

Copyright © 2024 BioMed Research International. This is an open access article distributed under the Creative Commons Attribution License, which permits unrestricted use, distribution, and reproduction in any medium, provided the original work is properly cited.

This article has been retracted by Hindawi following an investigation undertaken by the publisher [1]. This investigation has uncovered evidence of one or more of the following indicators of systematic manipulation of the publication process:

- (1) Discrepancies in scope
- (2) Discrepancies in the description of the research reported
- (3) Discrepancies between the availability of data and the research described
- (4) Inappropriate citations
- (5) Incoherent, meaningless and/or irrelevant content included in the article
- (6) Manipulated or compromised peer review

The presence of these indicators undermines our confidence in the integrity of the article's content and we cannot, therefore, vouch for its reliability. Please note that this notice is intended solely to alert readers that the content of this article is unreliable. We have not investigated whether authors were aware of or involved in the systematic manipulation of the publication process.

Wiley and Hindawi regrets that the usual quality checks did not identify these issues before publication and have since put additional measures in place to safeguard research integrity.

We wish to credit our own Research Integrity and Research Publishing teams and anonymous and named external researchers and research integrity experts for contributing to this investigation.

The corresponding author, as the representative of all authors, has been given the opportunity to register their agreement or disagreement to this retraction. We have kept a record of any response received.

References

- [1] S. Aziz, N. M. Saeed, H. O. Dyary et al., "Divergent Analyses of Genetic Relatedness and Evidence-Based Assessment of Therapeutics of *Staphylococcus aureus* from Semi-intensive Dairy Systems," *BioMed Research International*, vol. 2022, Article ID 5313654, 13 pages, 2022.

Research Article

Divergent Analyses of Genetic Relatedness and Evidence-Based Assessment of Therapeutics of *Staphylococcus aureus* from Semi-intensive Dairy Systems

Sidra Aziz ¹, Nahla Muhammad Saeed ², Hiewa Othman Dyary ²,
Muhammad Muddassir Ali ³, Rao Zahid Abbas ⁴, Aziz ur Rehman ⁵,
Sammina Mahmood ⁶, Laiba Shafique ⁷, Zaeem Sarwar ⁸, Fakhara Khanum ⁹,
Tean Zaheer ⁴, Khurram Ashfaq ¹⁰, Mughees Aizaz Alvi ¹⁰, Muhammad Shafeeq ¹⁰,
Arslan Saleem ¹¹ and Amjad Islam Aqib ¹²

¹Tehsil Headquarter Hospital, Mankera, Pakistan

²College of Veterinary Medicine, University of Sulaimani, Sulaymaniyah, Kurdistan Region, Iraq

³Institute of Biochemistry and Biotechnology, University of Veterinary and Animal Sciences, Lahore 54000, Pakistan

⁴Department of Parasitology, University of Agriculture, Faisalabad 38000, Pakistan

⁵Department of Pathobiology, University of Veterinary and Animal Sciences, Lahore Sub-Campus, Jhang 35200, Pakistan

⁶Department of Botany, Division of Science and Technology, University of Education, Lahore 54000, Pakistan

⁷State Key Laboratory for Conservation and Utilization of Subtropical Agro-Bioresources, Guangxi University, Nanning 530005, China

⁸Department of Theriogenology, Cholistan University of Veterinary and Animal Sciences, Bahawalpur 63100, Pakistan

⁹Department of Food Science and Technology, Government College Women University, Faisalabad 38000, Pakistan

¹⁰Department of Clinical Medicine and Surgery, University of Agriculture, Faisalabad 38000, Pakistan

¹¹Department of Aerospace and Geodesy, Technical University of Munich Arcisstr. 21, 80333 Munich, Germany

¹²Department of Medicine, Cholistan University of Veterinary and Animal Sciences, Bahawalpur 63100, Pakistan

Correspondence should be addressed to Nahla Muhammad Saeed; nahla.saeed@univsul.edu.iq,
Muhammad Muddassir Ali; muddassir.ali@uvas.edu.pk, and Amjad Islam Aqib; amjadislamaqib@cuvas.edu.pk

Received 12 March 2022; Accepted 27 May 2022; Published 20 June 2022

Academic Editor: Gulnaz Afzal

Copyright © 2022 Sidra Aziz et al. This is an open access article distributed under the Creative Commons Attribution License, which permits unrestricted use, distribution, and reproduction in any medium, provided the original work is properly cited.

Use of antibiotics without following standard guidelines is routine practice in developing countries which is giving rise to genetic divergence and increased drug resistance. The current study analyzed genetic divergence and drug resistance by *S. aureus* and therapeutic efficacy of novel antibiotic combinations. The study revealed that 42.30% (minimum 20%-maximum 70%) of milk samples are positive for *S. aureus*. Study also revealed seven SNPs in the *S. aureus nuc* gene (c.53A>G, c.61A>G, c.73T>C, c.93C>A, c.217C>T, c.280T>C, and c.331T>A). Local isolates Staph-2 and Staph-3 were closely related to *Bos taurus nuc* gene (bovine *S. aureus*), while Staph-1 was closely related to *Homo sapiens* (human *S. aureus*) indicating shifting of host. Change of two amino acids and staphylococcal nuclease conserved domain was observed in all local isolates of *S. aureus*. The isoelectric points predicted by protParam of Staph-1, Staph-2, and Staph-3 proteins were 9.30, 9.20, and 9.20, respectively. The antibiotic susceptibility profile of *S. aureus* presented highest resistance against penicillin (46.67%) and glycopeptide (43.33%). When a single antibiotic regimen was adopted in a field trial, the highest efficacy was reported in the case of oxytetracycline (80%) while lowest was presented by azithromycin. Among antibiotics' combined regimen, the highest efficacy (80%) was presented by gentamicin with oxytetracycline; cefotaxime with vancomycin; and ciprofloxacin with vancomycin. The current study concluded rising percentages of *S. aureus* from dairy milk, proofs of genetic host shifts, and altered responses of in on field therapeutics.

1. Introduction

Semi-intensive dairy systems represent 21% of milk production in Mexican dairy milk collection systems [1], while in other parts of the world, predominantly Asian countries, it is increasing day by day. Losses are attributed to the spread of different bacteria salient of which is *Staphylococcus aureus* (*S. aureus*). This bacterium is commensal and opportunistic that can colonize various animal species and humans [2]. The bacteria cause severe infections in humans and animals. The former infection involves skin and soft tissue infection (SSTI), which is clinically manifested as puffy infectious blood vessels, abscesses, papules, tuberculosis, and Staphylococcal scalded skin syndrome (SSSS). Isolated infections include toxic shock syndrome (TSS), pneumonia, or neonatal TSS-like human excitation [3]. Skin, mucous membrane, upper and lower respiratory tract, and urogenital tract are significant attacking sites in humans and animals [4, 5]. Pathogens may appear as fatal due to septic shock following intramammary infections in animals [6].

S. aureus is a widespread and infectious pathogen that exists in 30-40% of all cases of mastitis and 80% of sub-clinical bovine mastitis which may cost 35 USD yearly as losses worldwide [7, 8]. The capability of producing mastitis is governed by numerous virulence factors that are structural or secretory [9, 10]. The structural virulence factors belong to adhesions, protein A, and capsular polysaccharide, whereas in secretory proteases, hemolysins, coagulase, lipase, and hyaluronidase are included [11, 12]. Infection increases due to increased resistance to multiple antibiotics such as methicillin-resistant *S. aureus* (MRSA). Spread of this pathogen is restricted not only to bovine but also to other animals like goats [13]. Newer strains of *S. aureus*, i.e., vancomycin-resistant *S. aureus* (VRSA), are also rising in bovine milk [14] in addition to already reported MRSA. These strains are the most common cause of food poisoning and hospital infections [15–17] because of exoenzymes, exoproteins, and toxins [15, 18]. Ancestry analysis provided specificity within animals that is now changed to host shifts from one animal to another. Moreover, the pathogen is required to be considered for studying phenomena of protein folding and other molecular structures [16, 19].

S. aureus has the ability to yield extracellular thermostable nuclease, which is encoded by *nuc* gene. Among several other genes, this gene is found successful in distinguishing *S. aureus* in staphylococcal spp. This gene is thus considered a specific marker of *S. aureus* identification through PCR [16]. There are several researchers reporting *nuc* gene as a fast and reliable identification marker for *S. aureus*. Specificity and sensitivity of *nuc* gene to identify *S. aureus* have been reported as 89.6% and 93.3%, respectively [20]. Keeping in view the influencing semi-intensive dairy systems, this study aimed at (a) probing divergence of genetic relatedness of *S. aureus* within host and across host, (b) estimating the modified pattern of drug resistance profile against all classes of antibiotics, and (c) finding response of single and double antibiotic regimens against *S. aureus*-based clinical mastitis.

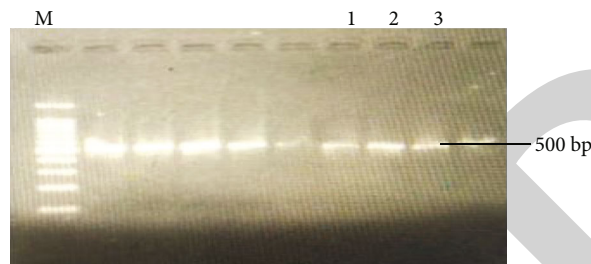


FIGURE 1: PCR amplicons of *nuc* gene (*S. aureus*). *M* = 1 kb DNA ladder (gene on 1 kb DNA ladder); Lane 1: Staph-1; Lane 2: Staph-2; Lane 3: Staph-3.

2. Results

2.1. Genetic Relatedness for Host Shift Analysis. Molecular identification of biochemically characterized *S. aureus* was targeted at 500 bp of *nuc* gene. The positive samples which were made part of this genetic relatedness are also pointed out along with other positive samples in Figure 1. Alignment of nucleic acid and protein sequences is given in Figures 2 and 3, respectively. Seven SNPs were identified in the *S. aureus nuc* gene at position c.53A>G (transition), c.61A>G (transition), c.73T>C (transition), c.93C>A (transversion), c.217C>T (transition), c.280T>C (transition), and c.331T>A (transversion) (Table 1). Nucleic acid alignment revealed that Staph-1, Staph-2, and Staph-3 were 97.37%, 98.02%, and 99.13% identical with a reference sequence, respectively. A phylogenetic tree of the *S. aureus nuc* gene was constructed. Five clades were observed in the phylogenetic tree when local *S. aureus* samples were compared with the *S. aureus nuc* gene of different species (different sources) from the NCBI database. Local *S. aureus nuc* (Staph-2 and Staph-3) gene sequences were closely related to the *S. aureus nuc* isolated from *Bos taurus*. These two local isolates (Staph-2 and Staph-3) clustered together only. Staph-1 (local isolate) gene sequence was closely related to *S. aureus nuc* isolated from *Homo sapiens* (vaginal and blood). This indicated that 33.33% of host shifts as one among three isolates were related to humans. Staph-1 clustered with *Homo sapiens* (blood, stool, sputum, contaminated platelets, wound, and swab), international space station surface, pork, food, and *Bos taurus* (Figure 2). The nucleic acid motif *p* value of the reference sequence was $4.66e - 191$. The *p* value of sample Staph-1 was $2.01e - 190$. Staph-2 and Staph-3 have the same *p* value ($1.64e - 191$). Sequences of motifs were discriminated by different colors represented in Figure 4. The protein motif *p* value of the reference sequence was found $4.31e - 160$ (Figure 5). The *p* value of sample Staph-1 was $1.77e - 159$. Staph-2 and Staph-3 have the same *p* value ($2.88e - 160$). Sequences of motifs were discriminated by different colors represented in Figure 3. Nucleotide motif construction involved an 1832 bp sequence, while amino acid motif construction involved a 608 bp sequence. Frequency of adenine and thiamine nucleotide in motifs was 0.328 while cytosine and guanine frequencies were 0.172. The only coding region was involved in the nucleotide structure (Figure 6). Asparagine was replaced by aspartic acid

| | | |
|-----------|--|-----|
| Staph-1 | TAGTTGTTTAGTGTTAACTTTAGTTGTAGTTTCAAGTCTAAGTAGCTCAGCAAAATGCATC | 60 |
| Reference | TAGTTGTTTAGTGTTAACTTTAGTTGTAGTTTCAAGTCTAAGTAGCTCAGCAAAATGCATC | 60 |
| Staph-2 | TAGTTGTTTAGTGTTAACTTTAGTTGTAGTTTCAAGTCTAAGTAGCTCAGCAGATGCATC | 60 |
| Staph-3 | TAGTTGTTTAGTGTTAACTTTAGTTGTAGTTTCAAGTCTAAGTAGCTCAGCAGATGCATC ***** | 60 |
| Staph-1 | GCAACAGATAACGGCGTAAATAGAAGTGGTTATGAAGATCCAACAGTATATAGTGCAAC | 120 |
| Reference | ACAAACAGATAATGGCGTAAATAGAAGTGGTTCTGAAGATCCAACAGTATATAGTGCAAC | 120 |
| Staph-2 | ACAAACAGATAACGGCGTAAATAGAAGTGGTTCTGAAGATCCAACAGTATATAGTGCAAC | 120 |
| Staph-3 | ACAAACAGATAACGGCGTAAATAGAAGTGGTTCTGAAGATCCAACAGTATATAGTGCAAC ***** | 120 |
| Staph-1 | TTCAACTAAAAAATTACATAAAGAACC TGCACATTAATTAAGCGATTGATGGTGATAC | 180 |
| Reference | TTCAACTAAAAAATTACATAAAGAACC TGCACATTAATTAAGCGATTGATGGTGATAC | 180 |
| Staph-2 | TTCAACTAAAAAATTACATAAAGAACC TGCACATTAATTAAGCGATTGATGGTGATAC | 180 |
| Staph-3 | TTCAACTAAAAAATTACATAAAGAACC TGCACATTAATTAAGCGATTGATGGTGATAC ***** | 180 |
| Staph-1 | GGTTAAATTAATGTACAAAGGTCAACCAATGACATTTAGACTATTATGTTGATA CACC | 240 |
| Reference | GGTTAAATTAATGTACAAAGGTCAACCAATGACATTCAGACTATTATGTTGATA CACC | 240 |
| Staph-2 | GGTTAAATTAATGTACAAAGGTCAACCAATGACATTTAGACTATTATGTTGATA CACC | 240 |
| Staph-3 | GGTTAAATTAATGTACAAAGGTCAACCAATGACATTTAGACTATTATGTTGATA CACC ***** | 240 |
| Staph-1 | TGAAACAAAGCATCCTAAAAAAGGTGTAGAGAAATATGGCCTGAAGCAAGTGCATTTAC | 300 |
| Reference | TGAAACAAAGCATCCTAAAAAAGGTGTAGAGAAATATGGTCTGAAGCAAGTGCATTTAC | 300 |
| Staph-2 | TGAAACAAAGCATCCTAAAAAAGGTGTAGAGAAATATGGTCTGAAGCAAGTGCATTTAC | 300 |
| Staph-3 | TGAAACAAAGCATCCTAAAAAAGGTGTAGAGAAATATGGTCTGAAGCAAGTGCATTTAC ***** | 300 |
| Staph-1 | GAAAAAATGGTAGAAAA TGCAAAGAAAA TGAAGTCGAGTTTGACAAAGGTCAAAGAAC | 360 |
| Reference | GAAAAAATGGTAGAAAA TGCAAAGAAAA TGAAGTCGAGTTTGACAAAGGTCAAAGAAC | 360 |
| Staph-2 | GAAAAAATGGTAGAAAA TGCAAAGAAAA TGAAGTCGAGTTTGACAAAGGTCAAAGAAC | 360 |
| Staph-3 | GAAAAAATGGTAGAAAA TGCAAAGAAAA TGAAGTCGAGTTTGACAAAGGTCAAAGAAC ***** | 360 |
| Staph-1 | TGATAAATA TGGACGTGGCTTAGCGTATATTTATGCTGATGGAAAAATGGTAAACGAAGC | 420 |
| Reference | TGATAAATA TGGACGTGGCTTAGCGTATATTTATGCTGATGGAAAAATGGTAAACGAAGC | 420 |
| Staph-2 | TGATAAATA TGGACGTGGCTTAGCGTATATTTATGCTGATGGAAAAATGGTAAACGAAGC | 420 |
| Staph-3 | TGATAAATA TGGACGTGGCTTAGCGTATATTTATGCTGATGGAAAAATGGTAAACGAAGC ***** | 420 |
| Staph-1 | TTTAGTTCGTCAAGGCTTGGCTAAAGTTGCTTATGTTT | 458 |
| Reference | TTTAGTTCGTCAAGGCTTGGCTAAAGTTGCTTATGTTT | 458 |
| Staph-2 | TTTAGTTCGTCAAGGCTTGGCTAAAGTTGCTTATGTTT | 458 |
| Staph-3 | TTTAGTTCGTCAAGGCTTGGCTAAAGTTGCTTATGTTT ***** | 458 |

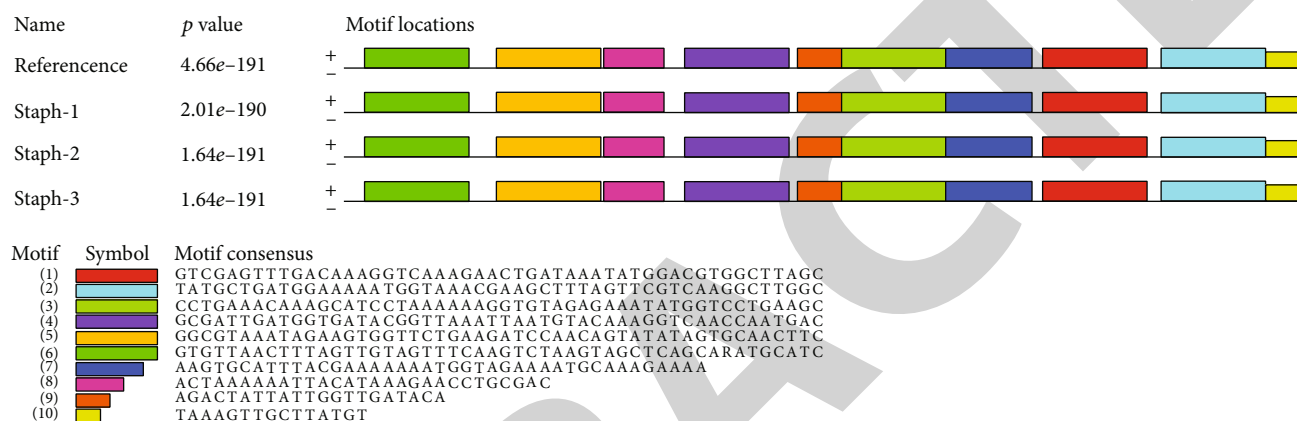
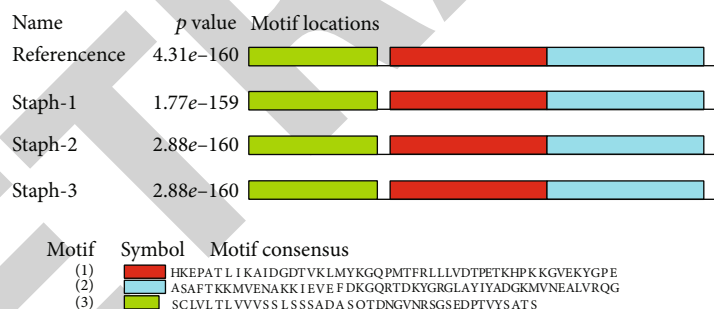
FIGURE 2: Alignment of *S. aureus* nuc gene (Staph-1, Staph-2, Staph-3, and reference).

| | | |
|-----------|---|-----|
| Staph-2 | SCLV LTLVVVSSLSS ADA SQT DNGVNR SGSEDP TVYSATST KKLHKEPATLIKAIDGDT | 60 |
| Staph-3 | SCLV LTLVVVSSLSS ADA SQT DNGVNR SGSEDP TVYSATST KKLHKEPATLIKAIDGDT | 60 |
| Reference | SCLV LTLVVVSSLSS ANA SQT DNGVNR SGSEDP TVYSATST KKLHKEPATLIKAIDGDT | 60 |
| Staph-1 | SCLV LTLVVVSSLSS ANA SQT DNGVNR SGYEDP TVYSATST KKLHKEPATLIKAIDGDT ***** | 60 |
| Staph-2 | VKLMYKGQPM TFRLLLVDT PETKHPKKGVEKYGPEASAF TKKMVENAKKI EEFDKGQRT | 120 |
| Staph-3 | VKLMYKGQPM TFRLLLVDT PETKHPKKGVEKYGPEASAF TKKMVENAKKI EEFDKGQRT | 120 |
| Reference | VKLMYKGQPM TFRLLLVDT PETKHPKKGVEKYGPEASAF TKKMVENAKKI EEFDKGQRT | 120 |
| Staph-1 | VKLMYKGQPM TFRLLLVDT PETKHPKKGVEKYGPEASAF TKKMVENAKKI EEFDKGQRT ***** | 120 |
| Staph-2 | DKYGRGLAY IYADGKMVNEALVRQGLAKVAYV | 152 |
| Staph-3 | DKYGRGLAY IYADGKMVNEALVRQGLAKVAYV | 152 |
| Reference | DKYGRGLAY IYADGKMVNEALVRQGLAKVAYV | 152 |
| Staph-1 | DKYGRGLAY IYADGKMVNEALVRQGLAKVAYV ***** | 152 |

FIGURE 3: Alignment of *S. aureus* nuc protein (Staph-1, Staph-2, Staph-3, and reference sequence).

TABLE 1: *S. aureus* nuc protein conserved domain structure (reference sequence, Staph-1, Staph-2, and Staph-3).

| Sample ID | Identified domain | Similarity score | Total nr sequences | Total architecture | Conserved domain structure |
|--|---|------------------|--------------------|--------------------|----------------------------|
| Reference protein, Staph-1, Staph-2, and Staph-3 | Chain A, <i>staphylococcal</i> nuclease | 1 | 5902 | 144 | |
| Staph-1 protein | Chain A, <i>staphylococcal</i> nuclease | 1 | 5902 | 144 | |
| Staph-2 protein | Chain A, <i>staphylococcal</i> nuclease | 1 | 5902 | 144 | |
| Staph-3 protein | Chain A, <i>staphylococcal</i> nuclease | 1 | 5902 | 144 | |

FIGURE 4: Nucleotide motifs of *S. aureus* nuc gene.FIGURE 5: nuc protein motifs of *S. aureus*.

(p.N18D), and serine was replaced by tyrosine (p.S31Y) (Table 2). The conserved domain of staphylococcal nuclease was observed in reference, Staph-1, Staph-2, and Staph-3 protein sequences. The gene structure (exonic region) of *S. aureus* nuc gene was found similar to the reference sequence (Figure 7). The protein structure of reference, Staph-1, Staph-2, and Staph-3 proteins resembles the staphylococcal nuclease protein (Figure 8). Protein-protein interaction was found in Staph-1, Staph-2, and Staph-3 proteins (Figure 9). Predicted functional partners of *S. aureus* nuc protein are given in Figure 10. STRING software predicted the association between genes based on observed patterns of simultaneous expression of genes (Figure 11).

2.2. Pattern of Prevalence and Drug Susceptibility Profile of *S. aureus*. The study found 42.33% (127/300) of milk samples

from commercial dairy farms positive for *S. aureus*. The range of *S. aureus* prevalence at the farm level varied from 20% (three farms in the study area) to 70% (only one farm observed). Four farms presented 30-37.04%, while one farm showed a 42.8% prevalence of *S. aureus* (Figure 12). Anti-biogram of *S. aureus* against 24 antibiotics from eight antibiotic groups showed varied responses. As an average effect of a class of antibiotics, penicillin and glycopeptides were found least effective in that 46.67 and 43.33% of *S. aureus* were resistant to these antibiotics (Table 3). On the other hand, fluoroquinolones, aminoglycosides, sulfonamides, macrolides, and tetracyclines were the most effective against *S. aureus* in the current study. Against cephalosporins, *S. aureus* were 36.67, 30%, and 33.33% resistant, intermediate, and sensitive, respectively. The pattern of susceptibility of isolate against individual antibiotics is

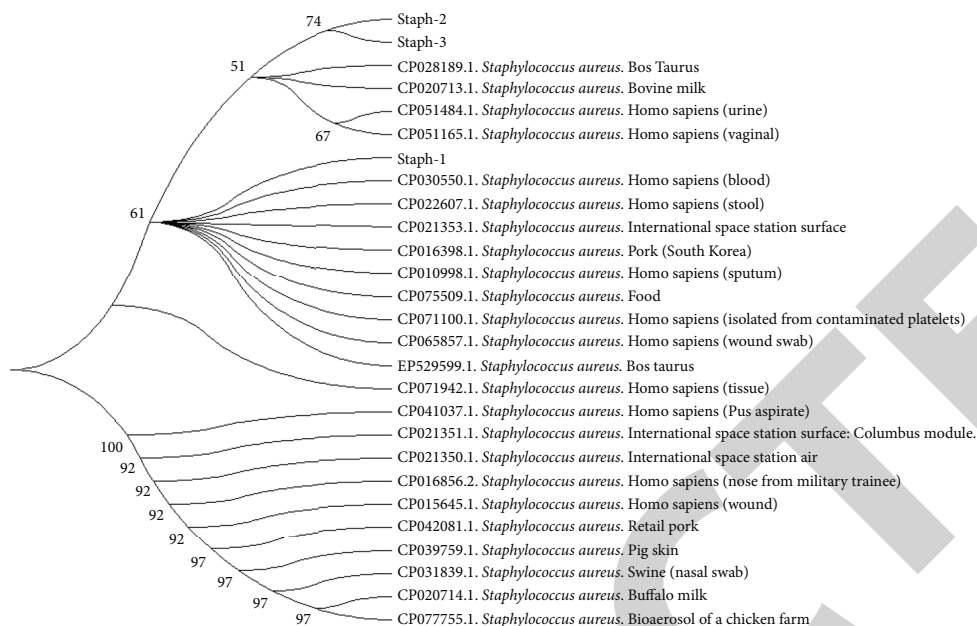


FIGURE 6: Phylogenetic tree of *S. aureus* nuc gene.

TABLE 2: *S. aureus* nuc protein physical and chemical properties (Staph-1, Staph-2, Staph-3, and reference sequence).

| Sample ID | Reference protein | Staph-1 protein | Staph-2 protein | Staph-3 protein |
|---------------------------------------|---|---|---|---|
| Number of amino acids | 152 | 152 | 152 | 152 |
| MW | 16561.02 | 16637.12 | 16562.01 | 16562.01 |
| pI | 9.32 | 9.30 | 9.2 | 9.2 |
| Number of negatively charged residues | 17 | 17 | 18 | 18 |
| Number of positively charged residues | 23 | 23 | 23 | 23 |
| Formula | C ₇₃₂ H ₁₁₉₄ N ₁₉₈ O ₂₂₇ S ₅ | C ₇₃₈ H ₁₁₉₈ N ₁₉₈ O ₂₂₇ S ₅ | C ₇₃₂ H ₁₁₉₃ N ₁₉₇ O ₂₂₈ S ₅ | C ₇₃₂ H ₁₁₉₃ N ₁₉₇ O ₂₂₈ S ₅ |
| Total number of atoms | 2356 | 2366 | 2355 | 2355 |
| II | 30.78 | 28.46 | 30.22 | 30.22 |
| Aliphatic index | 80.79 | 80.79 | 80.79 | 80.79 |
| GRAVY | -0.388 | -0.391 | -0.388 | -0.388 |

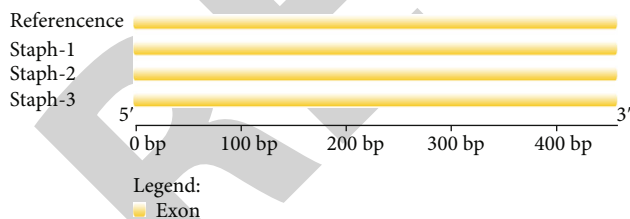


FIGURE 7: Gene structure (exonic region) of *S. aureus* nuc gene.

shown in Figures 13(a)–13(h). There were 40-50% isolates resistant to cefoxitin, cefotaxime, sulfathiazole, oxacillin, clarithromycin, and dalbavancin. The study also showed that 60% of isolates are resistant to ampicillin and vancomycin. The highest sensitivity was found against enoxacin (80%), followed by sulfamethoxazole/trimethoprim, amikacin (70%), gentamicin (60%), azithromycin (60%), and oxytetracycline (60%). About 40% of isolates expressed intermediate susceptibility against streptomycin, cefixime, sulfaphenazole, sulfadiazine, and clarithromycin.

2.3. *Field Trials.* The study noted that oxytetracycline showed the highest efficacy (80%) among single antibiotic regimens while azithromycin showed the least efficacy (20%). Cefotaxime, vancomycin, and ciprofloxacin showed 60% efficacy while 40% of cases supported gentamicin, sulfadimidine, and azithromycin (Table 4). Combination regimens showed an 80% success rate in favor of gentamicin with oxytetracycline, cefotaxime with vancomycin, and ciprofloxacin with vancomycin. Azithromycin in combination with sulfadimidine and azithromycin with gentamicin were the least effective drug regimens found in this trial.

3. Discussion

The clue of host shift of *S. aureus* in the current study (one of three *S. aureus* to be closely related to humans while distantly related to cows) was in line with findings of [21]. They reported clonal complexes (CCs), i.e., CC97 *S. aureus* isolate of cattle transmitted to humans while CC22 of humans found in cattle in Algeria. Human-associated strains of *S.*

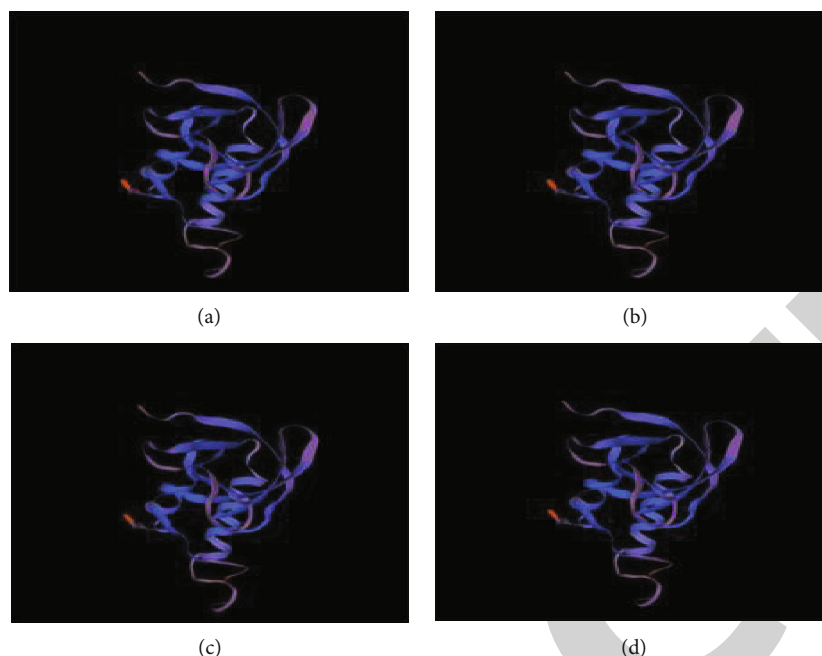


FIGURE 8: Protein structure (exonic region) of *S. aureus* nuc protein.

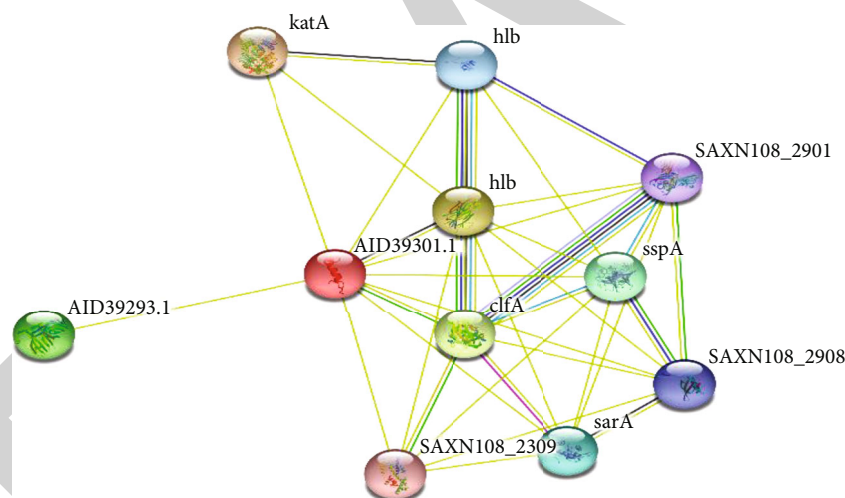


FIGURE 9: Protein-protein interaction of *S. aureus* nuc protein (Staph-1 protein, Staph-2 protein, and Staph-3 protein).

aureus, e.g., CC22 MRSA which was strictly responsible for hospital-acquired MRSA and community-acquired MRSA infections [22], were reported predominantly in Germany from dogs and cats [23]. *S. aureus* genes identified in humans' milk were found in *S. aureus* isolated from bovine milk [24]. SNP identification in this study was more than those identified by [25, 26]. They found 3 SNP clades, two belonging to bovine mastitis while one clade belonging to international human isolates. SNP-based analysis indicated the combination of clades existing in humans and animals. In close agreement with the findings of the current study, 5 SNP clusters were identified in bovine mastitis [26]. In another study, 15 SNPs were identified with resembling phenotype [27]. In another study, 12 genome SNPs were identified from bovine in UK. The livestock-associated *S. aureus*

strain (LA-MRSA), CC398, presented close phylogenetic relation to humans and turkeys. SNPs in the *nuc* gene lead to amino acid change revealed by in silico analysis. This change of amino acids might be associated with changes in the activity of the enzyme.

There is debate about the use of different genes to indicate differences and similarities with reported sequences. In our study, *nuc* gene was preferred for *S. aureus*. Sequence analysis and genotyping of the *S. aureus* *nuc* gene proved to be a suitable tool for detecting mastitis in dairy farm animals [27]. The results of [28] revealed that *nuc* genes are derived from thermophilic bacteria and picked up by common ancestor staphylococci. In a study, homology analysis revealed no significant similarities between two *nuc* genes (*nuc1* and *nuc2*) [28]. *nuc1* is specific to *S. aureus*. 79%












| Your input: | | Neighborhood Gene fusion Cooccurrence Coexpression Experiments Database [textmining [Homology]] Score |
|--|---|---|
|  AID39301.1 | Annotation not available (228 aa) | |
| Predicted functional partners: | | |
|  katA | Decomposes hydrogen peroxide into water and oxygen; serves to protect cells from the toxic effects of hydrogen perox... | ● 0.811 |
|  hly | Alpha-toxin binds to the membrane of eukaryotic cells resulting in the release of low-molecular weight molecules and I... | ● 0.722 |
|  clfA | Cell surface-associated protein implicated in virulence. Promotes bacterial attachment exclusively to the gamma-chain... | ● 0.718 |
|  AID39301.1 | Annotation not available | ● 0.578 |
|  sspA | Preferentially cleaves peptide bonds on the carboxyl-terminal side of aspartate and glutamate. Along with other extrac... | ● 0.576 |
|  sarA | Global regulator with both positive and negative effects that controls expressions of several virulence factors and biofil... | ● 0.572 |
|  hlb | Bacterial hemolysins are exotoxins that attack blood cell membranes and cause cell rupture. Beta-hemolysin is a phos... | ● 0.571 |
|  SAXN108_2908 | Extracellular zinc metalloprotease. | ● 0.510 |
|  SAXN108_2901 | Annotation not available | ● 0.503 |
|  SAXN108_2309 | Sigma factors are initiation factors that promote the attachment of RNA polymerase to specific initiation sites and are t... | ● 0.501 |

FIGURE 10: Predicted functional partners of *S. aureus* nuc protein (Staph-1 protein, Staph-2 protein, and Staph-3 protein).

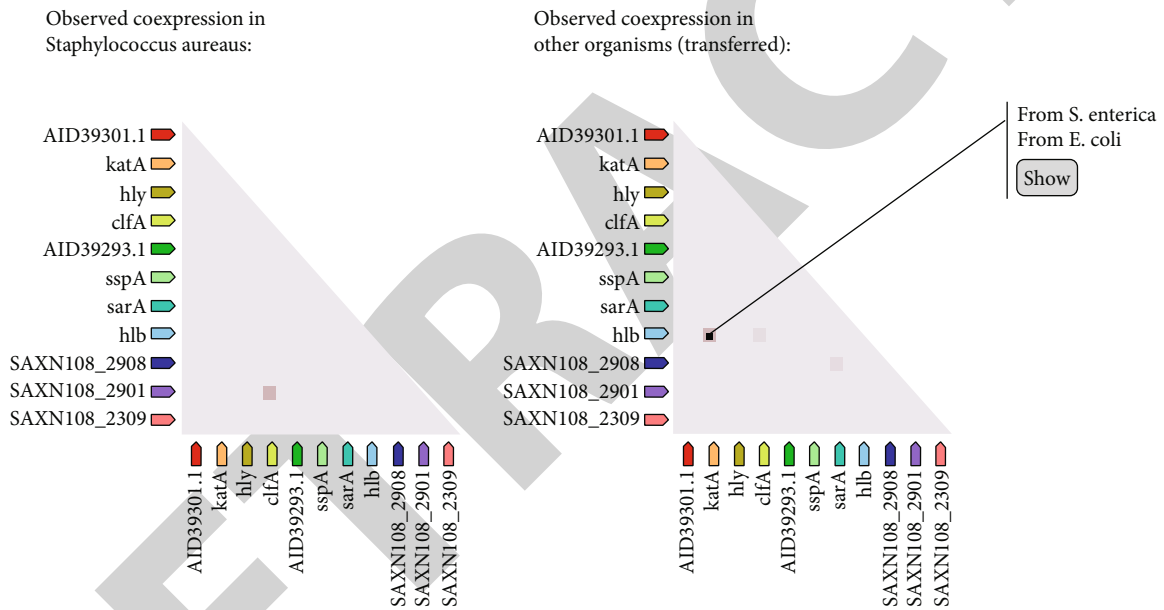


FIGURE 11: Coexpression of *S. aureus* nuc protein (Staph-1 protein, Staph-2 protein, and Staph-3 protein).

identity of *nuc2* gene was observed with *Staphylococcus epidermidis* gene. This identity suggested a close relationship of this gene with other species in the *Staphylococcus* genus. Phylogenetic trees of *nuc2* and *nuc1* genes were found in different clusters in another study [29]. *Staphylococci* were differentiated using the *nuc* gene similarly to 16S rRNA sequences used for taxonomy classification [20]. Homology comparison of the *nuc* gene revealed that this gene is present everywhere in the genus *Staphylococcus* except *Staphylococcus sciuri* [30]. More than 70% similarity with *nuc2* thermo-nuclease protein sequence from different species of *Staphylococcus* was observed in a study. Less than 60% similarity was observed with *S. aureus* *nuc1*. A higher-level homology of *Staphylococcus* was observed in the case of *S. epidermidis* (89.3%), *Staphylococcus hominis* (84.0%), and *Staphylococcus lugdunensis* (85.6%) [28]. Other scientists also used *nuc* gene to identify *S. aureus* [31]. Hamidi and

his colleagues assessed the ability of GENECUBE assays to detect *nuc* gene (identification of *S. aureus*) using a blood culture medium. They have found 100% specificity and sensitivity of GENECUBE assays in detecting *S. aureus* [32]. *S. aureus* presence in milk samples for confirmation of subclinical mastitis was examined by Hida et al. [33].

The higher prevalence of *S. aureus* contradicted with findings of another study conducted in the same country [34]. The reason for the discrepancy might be because they focused only on subclinical *S. aureus* and did not include clinical and normal milk samples. In another study, 39.03% of *S. aureus* were noted from subclinical mastitis. Another study reported a very high prevalence of *S. aureus* (61.60%) from subclinical mastitis cases [35]. Subclinical mastitis in the province of the study area revolves around 40-55%. In that context, the current study alarms to find new plans to combat this pathogen. The high rise in this

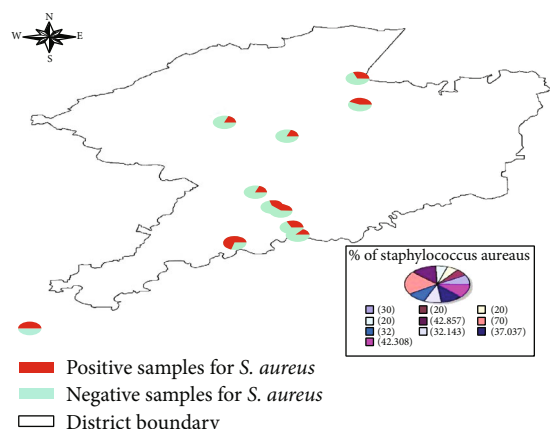


FIGURE 12: Distribution of *S. aureus* at different dairy farms; red color indicates positive cases. Percentage is also given in pie chart indicating the percentage of *S. aureus* at different farms which are indicated in different colors.

TABLE 3: Average percentages of antibiogram by different classes of antibiogram against *S. aureus*.

| Class of antibiotic | Resistant (%) | Intermediate (%) | Sensitive (%) |
|---------------------|---------------|------------------|---------------|
| Penicillins | 46.67 | 26.67 | 26.66 |
| Cephalosporins | 36.67 | 30 | 33.33 |
| Aminoglycosides | 20 | 26.67 | 53.33 |
| Sulfonamides | 20 | 33.33 | 46.67 |
| Macrolides | 33.33 | 16.67 | 50 |
| Tetracyclines | 23.33 | 30 | 46.67 |
| Fluoroquinolones | 10 | 10 | 80 |
| Glycopeptides | 43.33 | 26.67 | 30 |

pathogen is attributed to no or lack of preventive measures. The pathogen is contagious, while its transfer is reported between animal-animal, animal-human, and human-human. In a recent study, 72.91% of nasal samples produced *S. aureus*, while among these were 34.29% (24/70) pathogenic as identified by the *mecA* gene [36]. From animal sources (cat, dog, buffalo, calf, and buck), 28.7% of multiple drug-resistant *S. aureus* were noted [37]. These facts indicate the significant spread of this pathogen among dairy animals, pets, and humans.

There was 100% resistance of *S. aureus* (camel mastitis origin) against cefoxitin and oxacillin in a previous study [38]. *S. aureus* from bovine milk were found 100% sensitive to ciprofloxacin and trimethoprim/sulfamethoxazole, 90% against gentamicin and levofloxacin, 60% against tylosin, 50% against fusidic acid, and 40% against oxytetracycline [38, 39]. Another study on MRSA showed 80% sensitivity against ciprofloxacin. Resistance against antibiotics in this pathogen is attributed to extended beta-lactamase production encoded to be blaCTX-M55, ST-23 complex, ST-410, ST-167 genes, blaCTX-M15, blaCTX-M14, and ST-10. Such kind of response of antibiotics is not only confined to *S. aureus* of mastitis but also extended to *E. coli* from endometritis [40].

4. Materials and Methods

4.1. Milk Sample Collection. The study area consisted of developing commercial dairy systems with semi-intensive dairy systems in District Khanewal, Punjab, Pakistan. On a random basis, $n = 10$ dairy farms having not less than $n = 50$ animals in milking situation but with a commercial dairy system were approached with prior consent of the farmers. A total of $n = 300$ milk samples ($n = 30$ milk samples from each farm) were collected on a convenient sampling basis. The samples were aseptically collected in sterile tubes labeled with tags and shifted to the laboratory of central diagnostic, Cholistan University of Veterinary and Animal Sciences, Bahawalpur, Pakistan.

4.2. Isolation and Identification of *S. aureus*. Milk samples were centrifuged at 6000 rpm/15 minutes, and the supernatant was discarded. Sterile nutrient broth was added for further incubation at 37°C for 24 hours as prescribed in previous studies [36, 37]. The incubated samples were swabbed on mannitol salt agar, and growth obtained after 24 hours at 37°C was proceeded for biochemical analysis as per guidelines of Bergey's manual of determinative bacteriology. The pooled information was used to declare confirmation of bacteria.

4.3. Molecular Analysis. Isolates identified from biochemical tests were put to molecular analysis. For this purpose, randomly, 50% of *S. aureus* ($n = 64$) were selected. Primers of the nuc gene were designed using Primer 3 (<https://www.ncbi.nlm.nih.gov/tools/primer-blast/>) software (Nuc_forward 5' AAGGGCAATACGCAAAGAG3' and Nuc_reverse 5' AAACATAAGCAACTTTAGCCAAG3'). The reaction mixture contains PCR 2x master mix = 10 μ L (ThermoScientific Catalog # K0171), forward primer = 1 μ L (10 pmol/L), reverse primer = 1 μ L (10 pmol/L), DNA = 2 μ L (50 ng/L), deionized water = 6 μ L, and reaction volume was 20 μ L. Touchdown PCR (35 cycles) was used to amplify the nuc gene of *S. aureus*. Thermocycler profile includes initial denaturation 94°C (5 min), denaturation 94°C (45 sec), annealing 63°C-53°C (45 sec), extension 72°C (45 sec), and final extension 72°C (5 min). The dilutions of DNA (50 ng/ μ L) were made, and nuc gene was amplified. After amplification, these amplicons were purified using a purification kit (Gene JET PCR Purification Kit Catalog number: K0701) and sent for sequencing. *S. aureus* positive for nuc gene and presenting multidrug resistance were sent for sequence analysis. Isolates showing similar sequences were excluded while those ($n = 3$) presenting genetic variations and showing the highest drug resistance were discussed in this paper.

Single-nucleotide polymorphisms were observed in sequencing chromatograms using chromas software. BLAST (Basic Local Alignment Search Tool) was used to check the similarity of the *S. aureus* nuc gene with the reference sequence. Clustal omega was used for the alignment of nucleic acid and protein sequences. A phylogenetic tree was constructed using Mega X. Nucleic acid and protein motifs were constructed using MEME Suit (Multiple Expectation maximizations for Motif Elicitation) [41]. The gene

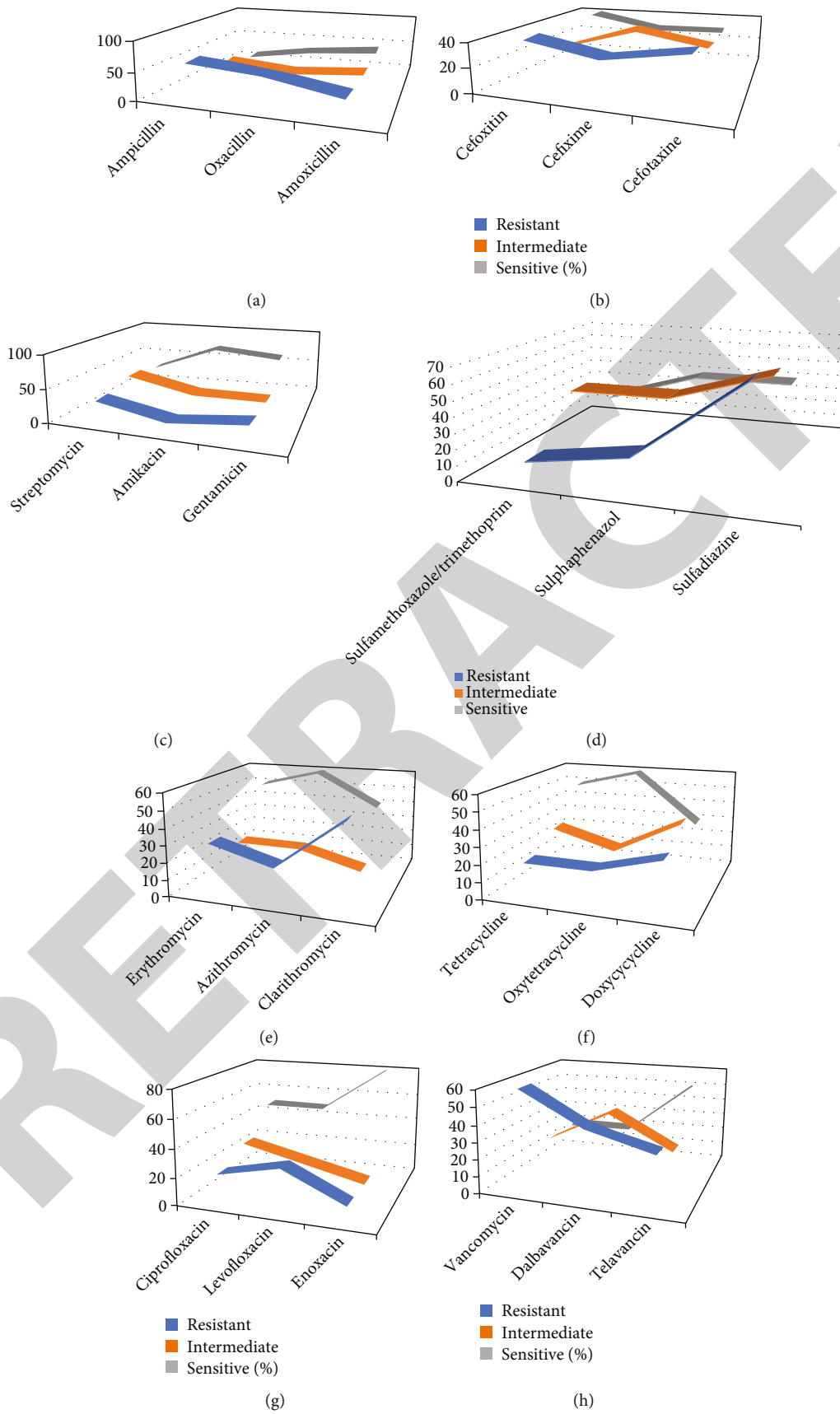


FIGURE 13: Comparison of percentage susceptibility (resistant, intermediate, and sensitive) isolates of *S. aureus* against individual antibiotics of different classes: (a) penicillin; (b) cephalosporins; (c) aminoglycosides; (d) sulfonamides; (e) macrolides; (f) tetracyclines.

TABLE 4: Percentage efficacy of different treatment groups against *S. aureus*-based clinical mastitis.

(a)

| Class of antibiotic | Antibiotic with dose rate | Bacteriostatic with bacteriostatic ($n = 5$) | | | |
|---------------------|-----------------------------------|--|---------------|--------------|-----------------|
| | | Alone | Sulfadimidine | Azithromycin | Oxytetracycline |
| Aminoglycoside | Gentamicin (G) (2.2-6 mg/kg BW) | 2/5 (40%) | 3/5 (60%) | 2/5 (40%) | 4/5 (80%) |
| Sulfonamide | Sulfadimidine (45 mg/kg BW) IM | 2/5 (40%) | — | 2/5 (40%) | 3/5 (60%) |
| Macrolide | Azithromycin (A) (6-10 mg/kg BW) | 1/5 (20%) | — | — | 3/5 (60%) |
| Tetracycline | Oxytetracycline (O) (17 mg/kg BW) | 4/5 (80%) | — | — | — |

(b)

| Class of antibiotic | Antibiotic with dose rate | Bactericidal with bactericidal ($n = 5$) | | |
|---------------------|--|--|---------------|------------|
| | | Alone | Ciprofloxacin | Vancomycin |
| Cephalosporin | Cefotaxime (Ce) (10 mg/kg BW) | 3/5 (60%) | 3/5 (60%) | 4/5 (80%) |
| Fluoroquinolones | Ciprofloxacin (Ci) (5-10 mg/kg body weight) (IV) | 3/5 (60%) | — | 4/5 (80%) |
| Glycopeptides | Vancomycin (V) (8-12 mg/kg BW) (IV) | 3/5 (60%) | — | — |

TABLE 5: Names of antibiotics along with their classes used in the study.

| Antibiotic group | Name of antibiotic | Antibiotic group | Name of antibiotic |
|--------------------|-------------------------------|----------------------|--------------------|
| (1) Penicillin | Ampicillin | (2) Macrolides | Erythromycin |
| | Oxacillin | | Azithromycin |
| | Amoxicillin | | Clarithromycin |
| (3) Cephalosporin | Cefoxitin | (4) Tetracyclines | Tetracycline |
| | Cefixime | | Oxytetracycline |
| | Cefotaxime | | Doxycycline |
| (5) Aminoglycoside | Streptomycin | (6) Fluoroquinolones | Ciprofloxacin |
| | Amikacin | | Levofloxacin |
| | Gentamicin | | Enoxacin |
| (7) Sulfonamide | Sulfamethoxazole/trimethoprim | (8) Glycopeptides | Vancomycin |
| | Sulfaphenazole | | Dalbavancin |
| | Sulfadiazine | | Telavancin |

structure of *S. aureus nuc* gene was determined by using a gene structure display server. Swiss model software predicted the 3D structure of thermonuclease. Protein-protein interactions were determined using STRING software (Search Tool for the Retrieval of Interacting Genes/Proteins). The physical and chemical properties of proteins were predicted by protParam *S. aureus* using guidelines given in the Clinical and Laboratory Standard Institute.

4.4. Susceptibility Profile. The genetically identified *S. aureus* was processed to respond to eight classes of antibiotics, each with three representative antibiotics (Table 5). The Clinical and Laboratory Standard Institute's [42] instructions were used to find the susceptibility (resistant, intermediate, and sensitive) profile of bacteria by both the disc diffusion method and the broth microdilution method. Where felt necessary, European Committee on Antimicrobial Susceptibility Testing was also consulted for analysis [43]. The need for the antibiotic profile of bacteria was deemed necessary because dairy systems lack proper veterinary sanitary control and technology for milk collection. These

directly affect the spread of pathogens along with their surge in resistance [44, 45].

4.5. Field Trial of Different Antibiotics against *S. aureus*. This trial consisted of the evaluation of different antibiotics against *S. aureus*-based clinical mastitis. The following criteria were used for this trial (Table 4, Figure 14).

4.5.1. Inclusion Criteria for Antibiotics

- (i) Field trial consisted of antibiotic groups based on their activity in *in vitro* trial
- (ii) Class of antibiotics representing more than 30% response against bacteria was included in field trial keeping in view their resistance. Penicillin was thus excluded with this criterion
- (iii) From each class, one antibiotic was selected based on its availability in the study area and its use as parenteral route to cover infection at ease

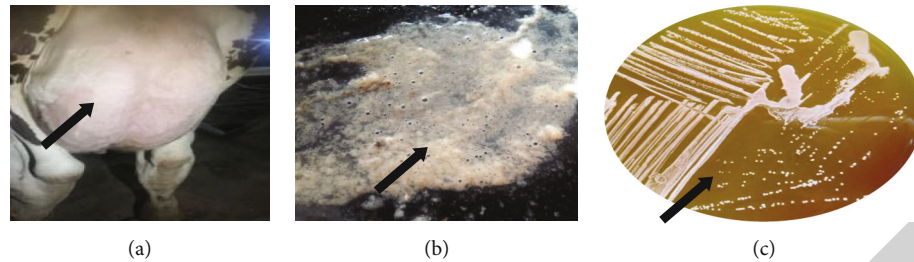


FIGURE 14: Clinical mastitis cases as an indication of inclusion criteria of animals for field trial of antibiotics: (a) udder inflammation, arrow is pointing out; (b) flakes in milk; (c) *S. aureus* growth on mannitol salt agar, arrow pointing out typical pinpoint colonies.

- (iv) All the antibiotics were used in a single regimen and next as a combination regimen
- (v) Combination was made on their apparent mode of action, i.e., bacteriostatic was used in combination with bacteriostatic while bactericidal in combination with bactericidal. The regimen consisted of nonsteroidal anti-inflammatory drug (NSAID) and antibiotics. Flunixin meglumine (Loxin, Selmore Pharmaceutical, Pakistan) was used at a dose rate of 2.2 mg/kg (single in a day)

4.5.2. Inclusion Criteria for Animals for Field Trials

- (i) Cattle suffering from clinical mastitis
- (ii) Cattle positive for *S. aureus*

Indicators of Success of Treatment. The success of treatment was measured based on the absence of clinical signs and clearance of *S. aureus* infection from milk. The latter was done based on bacteriological examination of milk samples as per standard protocols described in Bergey's manual of determinative bacteriology for the identification of bacteria. The presence of any or both indicators were considered a unsuccessful treatment.

4.6. Statistical Analysis. A nonparametric test was applied to calculate prevalence and antibiotic susceptibility using SPSS 22 version of statistical computer software. A phylogenetic tree was constructed using Mega X. Nucleic acid and protein motifs were created using MEME Suit (Multiple Expectation maximizations for Motif Elicitation).

Formulae:

$$\text{Prevalence of } S.aureus = \left(\frac{\text{number of } S.aureus \text{ isolated from milk}}{\text{number of milk samples tested}} \right) 100,$$

$$\begin{aligned} \% \text{ susceptibility of } S.aureus \text{ against antibiotics} \\ = \left(\frac{\text{number of } S.aureus \text{ susceptible against antibiotic}}{\text{number of } S.aureus \text{ tested}} \right) 100. \end{aligned} \quad (1)$$

NB: susceptible isolates were either resistant, intermediate, or sensitive which were decided based on their response to antibiotics against set standards.

5. Conclusions

Semi-intensive dairy systems were prevalent with antibiotic resistant *S. aureus*. SNPs and change of amino acids in *thermonuclease* protein in *S. aureus* reflected evidence of host shift. On the basis of group of antibiotics, penicillin and glycopeptides were the least effective while macrolides were found the highest efficacious group in an *in-vitro* trial. On an individual antibiotic basis, ampicillin and vancomycin were least effective while enoxacin and sulfamethoxazole/trimethoprim were most effective in an *in-vitro* trial. Response of a single antibiotic regimen, in field trial, supported oxytetracycline while a double antibiotic regimen supported gentamicin with oxytetracycline, cefotaxime with vancomycin, and ciprofloxacin with vancomycin. The study thus proposed adoption of evidence based therapeutics against bacterial pathogens keeping molecular study as an integral part of any treatment protocol.

Data Availability

No data were used.

Conflicts of Interest

The authors declare that they have no conflicts of interest.

Authors' Contributions

Data curation was performed by Sidra Aziz and Laiba Shafique; formal analysis was performed by Amjad Islam Aqib, Arslan Saleem, and Muhammad Shafeeq; funding acquisition was performed by Muhammad Mudassir Ali and Amjad Islam Aqib; Investigation was performed by Amjad Islam Aqib, Sammina Mahmood, and Arslan Saleem; resources were secured by Zaeem Sarwar and Khurram Ashfaq; software was secured by Muhammad Mudassir Ali and Arslan Saleem; supervision was performed by Amjad Islam Aqib; visualization was performed by Tean Zaheer and Rao Zahid Abbas; writing (original draft) was performed by Sidra Aziz, Amjad Islam Aqib, and Laiba Shafique; writing (review and editing) was performed by Hiewa Othman Dyary, Tean Zaheer, Fakhara Khanum, MugheesAizaz Alvi, and Nahla Muhammad Saeed. Sidra Aziz, Nahla Muhammad Saeed, and Amjad Islam Aqib share equal contribution.

References

- [1] E. J. Ramírez-Rivera, J. Rodríguez-Miranda, I. R. Huerta-Mora, A. Cárdenas-Cágal, and J. M. Juárez-Barrientos, "Tropical milk production systems and milk quality: a review," *Tropical Animal Health and Production*, vol. 51, no. 6, pp. 1295–1305, 2019.
- [2] C. Cuny, A. Friedrich, S. Kozytka et al., "Emergence of methicillin-resistant *Staphylococcus aureus* (MRSA) in different animal species," *International Journal of Medical Microbiology*, vol. 300, no. 2-3, pp. 109–117, 2010.
- [3] W. Morris, *The Collected Works of William Morris: With Introductions by His Daughter May Morris*, vol. 22, Cambridge University Press, 2012.
- [4] T. J. Johnson and L. K. Nolan, "Pathogenomics of the virulence plasmids of *Escherichia coli*," *Microbiology and Molecular Biology Reviews*, vol. 73, no. 4, pp. 750–774, 2009.
- [5] W. Vanderhaeghen, T. Cerpentier, C. Adriaensen, J. Vicca, K. Hermans, and P. Butaye, "Methicillin-resistant *Staphylococcus aureus* (MRSA) ST398 associated with clinical and subclinical mastitis in Belgian cows," *Veterinary Microbiology*, vol. 144, no. 1-2, pp. 166–171, 2010.
- [6] A. Cosandey, R. Boss, M. Luini et al., "*Staphylococcus aureus* genotype B and other genotypes isolated from cow milk in European countries," *Journal of Dairy Science*, vol. 99, no. 1, pp. 529–540, 2016.
- [7] A. A. Reshi, I. Husain, S. A. Bhat et al., "Bovine mastitis as an evolving disease and its impact on the dairy industry," *International Journal of Current Research and Review*, vol. 7, p. 48, 2015.
- [8] S. J. Wells, S. L. Ott, and A. H. Seitzinger, "Key health issues for dairy cattle—new and old," *Journal of Dairy Science*, vol. 81, no. 11, pp. 3029–3035, 1998.
- [9] Y. Guo, P. Qiu, H. Su et al., "Antimicrobial resistance and virulence genes distribution in *Trueperella pyogenes* isolated from dairy cows with clinical mastitis in Liaoning of China," *Pakistan Veterinary Journal*, vol. 41, no. 3, pp. 329–334, 2021.
- [10] E. E. Abdeen, W. S. Mousa, A. A. Abdel-Tawab, R. El-Faramawy, and U. H. Abo-Shama, "Phenotypic, genotypic and antibiogram among *Staphylococcus aureus* isolated from bovine subclinical mastitis," *Pakistan Veterinary Journal*, vol. 41, pp. 289–293, 2021.
- [11] H. Fagundes and C. A. F. Oliveira, "Infecções intramamárias causadas por *Staphylococcus aureus* e suas implicações em saúde pública," *Ciência rural*, vol. 34, no. 4, pp. 1315–1320, 2004.
- [12] Z. Iqbal, M. N. Seleem, H. I. Hussain, L. Huang, H. Hao, and Z. Yuan, "Comparative virulence studies and transcriptome analysis of *Staphylococcus aureus* strains isolated from animals," *Scientific Reports*, vol. 6, pp. 1–12, 2016.
- [13] M. Altaf, M. Ijaz, M. K. Iqbal et al., "Molecular characterization of methicillin resistant *Staphylococcus aureus* (MRSA) and associated risk factors with the occurrence of goat mastitis," *Pakistan Veterinary Journal*, vol. 40, no. 1, 2019.
- [14] M. U. Javed, M. Ijaz, Z. Fatima et al., "Frequency and antimicrobial susceptibility of methicillin and vancomycin-resistant *Staphylococcus aureus* from bovine milk," *Veterinary Journal*, vol. 41, no. 4, pp. 463–468, 2021.
- [15] S. Bronner, H. Monteil, and G. Prévost, "Regulation of virulence determinants in *Staphylococcus aureus*: complexity and applications," *FEMS Microbiology Reviews*, vol. 28, no. 2, pp. 183–200, 2004.
- [16] A. L. Cheung, A. S. Bayer, G. Zhang, H. Gresham, and Y. Q. Xiong, "Regulation of virulence determinants in vitro and in vivo in *Staphylococcus aureus*," *FEMS Immunology and Medical Microbiology*, vol. 40, no. 1, pp. 1–9, 2004.
- [17] A. A. Pragman and P. M. Schlievert, "Virulence regulation in *Staphylococcus aureus*: the need for in vivo analysis of virulence factor regulation," *FEMS Immunology and Medical Microbiology*, vol. 42, no. 2, pp. 147–154, 2004.
- [18] M. M. Dinges, P. M. Orwin, and P. M. Schlievert, "Exotoxins of *Staphylococcus aureus*," *Clinical Microbiology Reviews*, vol. 13, no. 1, p. 16, 2000.
- [19] J. Tang, R. Zhou, X. Shi, M. Kang, H. Wang, and H. Chen, "Two thermostable nucleases coexisted in *Staphylococcus aureus*: evidence from mutagenesis and in vitro expression," *FEMS Microbiology Letters*, vol. 284, no. 2, p. 176, 2008.
- [20] H. Fang and G. Hedin, "Rapid screening and identification of methicillin-resistant *Staphylococcus aureus* from clinical samples by selective-broth and real-time PCR assay," *Journal of Clinical Microbiology*, vol. 41, no. 7, p. 2894, 2003.
- [21] M. Akkou, C. Bouchiat, K. Antri et al., "New host shift from human to cows within *Staphylococcus aureus* involved in bovine mastitis and nasal carriage of animal's caretakers," *Veterinary Microbiology*, vol. 223, pp. 173–180, 2018.
- [22] G. M. Knight, E. L. Budd, L. Whitney et al., "Shift in dominant hospital-associated methicillin-resistant *Staphylococcus aureus* (HA-MRSA) clones over time," *Journal of Antimicrobial Chemotherapy*, vol. 67, no. 10, pp. 2514–2522, 2012.
- [23] S. Vincze, I. Stamm, P. A. Kopp et al., "Alarming proportions of methicillin-resistant *Staphylococcus aureus* (MRSA) in wound samples from companion animals, Germany 2010–2012," *PLoS One*, vol. 9, no. 1, p. e85656, 2014.
- [24] K. T. Franck, H. Gumpert, B. Olesen et al., "Staphylococcal aureus enterotoxin C and enterotoxin-like L associated with post-partum mastitis," *Frontiers in Microbiology*, vol. 8, p. doi:10.3389/fmicb.2017.00173, 2017.
- [25] M. O'Dea, R. J. Abraham, S. Sahibzada et al., "Antimicrobial resistance and genomic insights into bovine mastitis-associated *Staphylococcus aureus* in Australia," *Veterinary Microbiology*, vol. 250, p. 108850, 2020.
- [26] K. Fursova, A. Sorokin, S. Sokolov et al., "Virulence factors and phylogeny of *Staphylococcus aureus* associated with bovine mastitis in Russia based on genome sequences," *Science*, vol. 7, 2020.
- [27] R. Moretti, D. Soglia, S. Chessa et al., "Identification of SNPs associated with somatic cell score in candidate genes in Italian Holstein Friesian bulls," *Animals*, vol. 11, no. 2, p. 366, 2021.
- [28] A. O. Ali and H. Y. Mahmoud, "Sequencing and phylogenetic characterization of *S. aureus* thermonuclease gene," *Assiut Veterinary Medical Journal*, vol. 62, no. 148, pp. 6–12, 2016.
- [29] A. Y. C. Kwok and A. W. Chow, "Phylogenetic study of *Staphylococcus* and *Micrococcus* species based on partial Hsp 60 gene sequences," *International Journal of Systematic and Evolutionary Microbiology*, vol. 53, no. 1, pp. 87–92, 2003.
- [30] W.-T. Yang, C.-Y. Ke, W.-T. Wu, R.-P. Lee, and Y.-H. Tseng, "Effective treatment of bovine mastitis with intramammary infusion of *Angelica dahurica* and *Rheum officinale* extracts," *Evidence-based Complementary and Alternative Medicine*, vol. 2019, Article ID 7242705, 8 pages, 2019.
- [31] T. Sasaki, K. Kikuchi, Y. Tanaka, N. Takahashi, S. Kamata, and K. Hiramatsu, "Reclassification of phenotypically identified

Retraction

Retracted: Empirical Method for Thyroid Disease Classification Using a Machine Learning Approach

BioMed Research International

Received 12 March 2024; Accepted 12 March 2024; Published 20 March 2024

Copyright © 2024 BioMed Research International. This is an open access article distributed under the Creative Commons Attribution License, which permits unrestricted use, distribution, and reproduction in any medium, provided the original work is properly cited.

This article has been retracted by Hindawi following an investigation undertaken by the publisher [1]. This investigation has uncovered evidence of one or more of the following indicators of systematic manipulation of the publication process:

- (1) Discrepancies in scope
- (2) Discrepancies in the description of the research reported
- (3) Discrepancies between the availability of data and the research described
- (4) Inappropriate citations
- (5) Incoherent, meaningless and/or irrelevant content included in the article
- (6) Manipulated or compromised peer review

The presence of these indicators undermines our confidence in the integrity of the article's content and we cannot, therefore, vouch for its reliability. Please note that this notice is intended solely to alert readers that the content of this article is unreliable. We have not investigated whether authors were aware of or involved in the systematic manipulation of the publication process.

Wiley and Hindawi regrets that the usual quality checks did not identify these issues before publication and have since put additional measures in place to safeguard research integrity.

We wish to credit our own Research Integrity and Research Publishing teams and anonymous and named external researchers and research integrity experts for contributing to this investigation.

The corresponding author, as the representative of all authors, has been given the opportunity to register their agreement or disagreement to this retraction. We have kept a record of any response received.

References

- [1] T. Alyas, M. Hamid, K. Alissa, T. Faiz, N. Tabassum, and A. Ahmad, "Empirical Method for Thyroid Disease Classification Using a Machine Learning Approach," *BioMed Research International*, vol. 2022, Article ID 9809932, 10 pages, 2022.

Research Article

Empirical Method for Thyroid Disease Classification Using a Machine Learning Approach

Tahir Alyas ¹, Muhammad Hamid ², Khalid Alissa,³ Tauqeer Faiz,⁴ Nadia Tabassum ⁵, and Aqeel Ahmad⁶

¹Department of Computer Science, Lahore Garrison University, Lahore 54000, Pakistan

²Department of Statistics and Computer Science, University of Veterinary and Animal Sciences, Lahore 54000, Pakistan

³Saudi Aramco Cybersecurity Chair, Networks and Communications Department, College of Computer Science and Information Technology, Imam Abdulrahman Bin Faisal University, P.O. Box 1982, Dammam 31441, Saudi Arabia

⁴Department of Enterprise Computing, Skyline University College, Sharjah, UAE

⁵Department of Computer Science & Information Technology, Virtual University of Pakistan, Lahore 54000, Pakistan

⁶University of Chinese Academy of Sciences (UCAS), Beijing, China

Correspondence should be addressed to Muhammad Hamid; muhammad.hamid@uvas.edu.pk

Received 16 April 2022; Accepted 20 May 2022; Published 7 June 2022

Academic Editor: Gulnaz Afzal

Copyright © 2022 Tahir Alyas et al. This is an open access article distributed under the Creative Commons Attribution License, which permits unrestricted use, distribution, and reproduction in any medium, provided the original work is properly cited.

There are many thyroid diseases affecting people all over the world. Many diseases affect the thyroid gland, like hypothyroidism, hyperthyroidism, and thyroid cancer. Thyroid inefficiency can cause severe symptoms in patients. Effective classification and machine learning play a significant role in the timely detection of thyroid diseases. This timely classification will indeed affect the timely treatment of the patients. Automatic and precise thyroid nodule detection in ultrasound pictures is critical for reducing effort and radiologists' mistake rate. Medical images have evolved into one of the most valuable and consistent data sources for machine learning generation. In this paper, various machine learning algorithms like decision tree, random forest algorithm, KNN, and artificial neural networks on the dataset create a comparative analysis to better predict the disease based on parameters established from the dataset. Also, the dataset has been manipulated for accurate prediction for the classification. The classification was performed on both the sampled and unsampled datasets for better comparison of the dataset. After dataset manipulation, we obtained the highest accuracy for the random forest algorithm, equal to 94.8% accuracy and 91% specificity.

1. Introduction

Approximately about 4.6 percent of the population of ages 12 and greater suffers from hypothyroidism, and 1.2 percent of people in the USA have hyperthyroidism, equal to 1 out of 100 people. Machine learning is implemented in many fields today. But most significant improvements are made in the field of medicine. To detect thyroid disease, blood tests and medical imaging are performed (ultrasound). Awareness about thyroid disease is necessary as it will play a significant role in the early detection and curing of this problem. The thyroid is an organ in the human body. It produces the hormone required by the

human body. The hormones travel in the bloodstream, and it affects the metabolism and growth of humans. It is located below Adam's apple. Thyroid functionality is used for the interpretation and diagnosis of the disease. The thyroid gland produces hormones that control the growth and metabolism used for the body's energy purposes. The thyroid gland also contributes to development in children and adults. The thyroid gland also maintains body temperature. Minor issues with the gland can cause a problem all over the body. The functionality of the thyroid gland and the test results conducted after taking a blood sample are used to signify if the thyroid gland is working correctly. This hormone's secretion tells whether

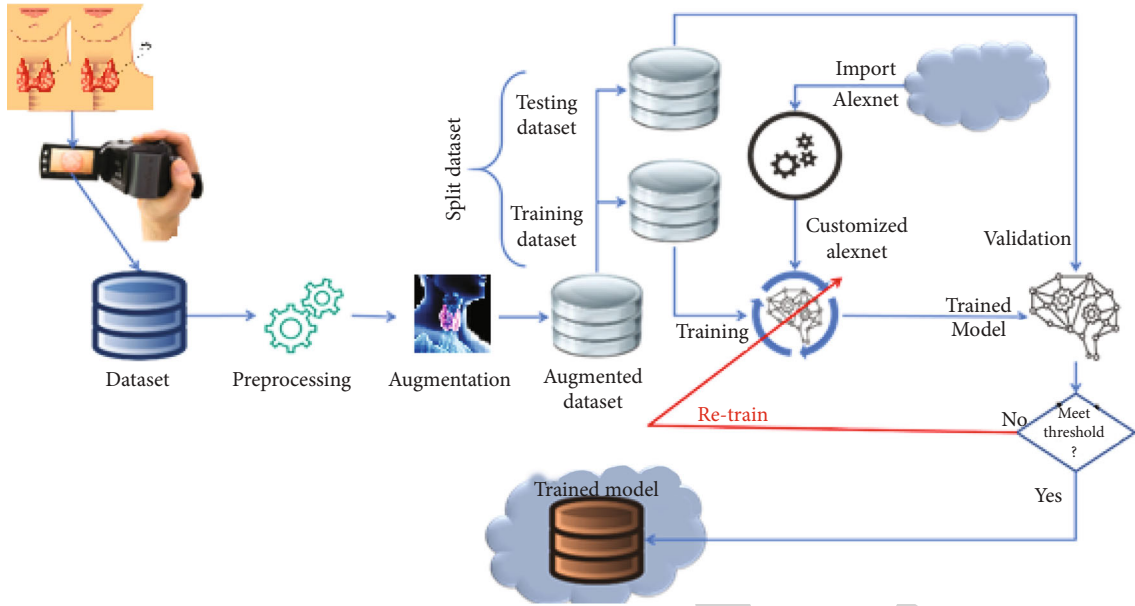


FIGURE 1: Proposed framework.

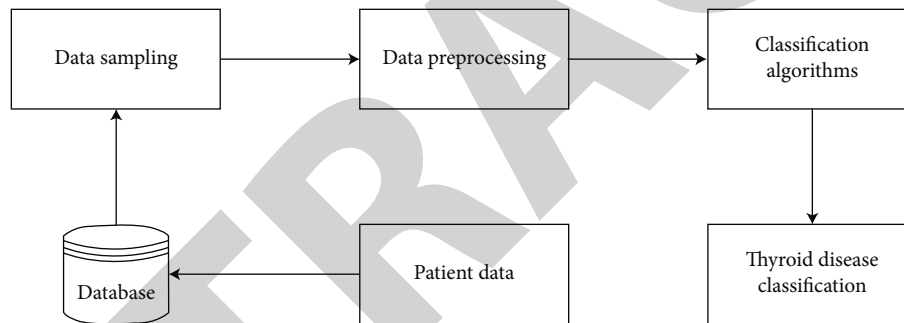


FIGURE 2: System diagram.

the thyroid is producing too much hormone or too little hormone for proper function. The condition in which little thyroid hormone is produced is called hypothyroidism. When the hormone is too much, it is referred to as hyperthyroidism. The thyroid gland produces two main hormones—triiodothyronine (T3) and thyroxine (T4).

Thyroid disorder is one of the most frequent illnesses among women. Thyroid illness can manifest itself as hypothyroidism. Female patients are more likely to develop hypothyroidism [1].

The conditions that thyroid disease causes are very similar to other diseases, so distinguishing is sometimes difficult. Another type of hormone produced is called calcitonin. An appropriate amount of iodine is essential for the gland to produce these hormones.

Because it produces hormones, the thyroid gland impacts the human body's metabolic processes. An increase in thyroid hormone production causes hyperthyroidism. The use of an online ensemble of decision trees to detect thyroid-related disorders is proposed in this research. This study is aimed at increasing thyroid illness diagnosis accuracy [2].

TABLE 1: Machine specification for simulations.

| Specifications | Value |
|----------------|--------------------------------|
| CPU | 1.5–2.7 GHZ |
| GPU | 920 m NVidia |
| RAM | 12 GB |
| Generation | 4 th |
| Internet | 8 Mbps upload, 8 Mbps download |

Thyroid dysfunction is a classification problem and can be solved using data mining techniques. The symptoms of thyroid disease include high cholesterol, high blood pressure, and an unusual pulse rate. Using data analysis for thyroid disease classification, we can make data-based decisions to diagnose this disease on time accurately.

In the recent decade, disorders of the human body's glands have developed alarmingly. The thyroid is one of these glands whose sickness has spread worldwide. The thyroid gland's primary job is to check metabolism and cell activity [3].

TABLE 2: Dataset description.

| | | | | | |
|---------------------------|-----------------------------|----------------------|------|---------------|------------|
| Dataset characteristics | Multivariate, domain theory | Number of instances | 7200 | Area | Life |
| Attribute characteristics | Categorical, real | Number of attributes | 25 | Date donated | 1987-01-01 |
| Associated tasks | Classification | Missing values? | N/A | Some web hits | 254314 |

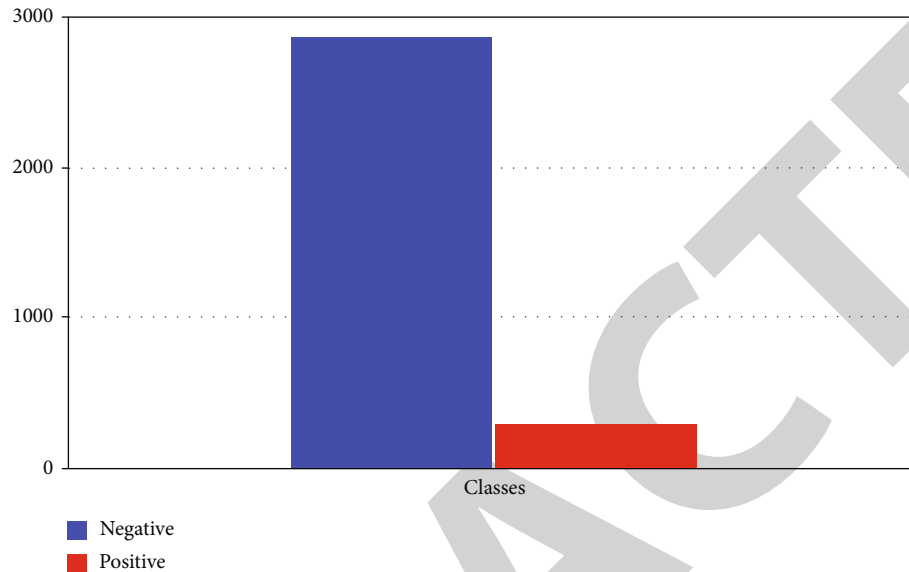


FIGURE 3: Dataset distribution.

Our model will help medical professionals to predict and use this classifier for further study and diagnosis. So the primary purpose of this research is to use a machine learning algorithm to diagnose thyroid dysfunction.

The crucial and difficult work in the healthcare profession is to detect health concerns and provide adequate treatment of disease at an early stage. There are certain disorders that can be recognized and treated early [4]. Based on the classification, Data mining is used in various healthcare services.

Based on the classification, machine learning is used in various medical services. The most important and difficult responsibility in the medical industry is to diagnose a patient’s health problems and give proper care and treatment for the disease early. As an example, consider thyroid illness. Thyroid diagnosis is traditionally done by a comprehensive examination and numerous blood testing [5].

Thyroids are helpful to the overall body. Its probable failure might result in thyroid hormone production that is either inadequate or excessive. As a result of one or more swellings growing inside the thyroid, it might become inflamed or enlarged. Some of these nodules may harbour cancerous tumors. Sodium levothyroxine, often known as LT4, is a synthetic thyroid hormone used to treat hypothyroidism [6].

2. Literature Review

Few studies have been performed on thyroid disease, and the authors have evaluated many of the studies to create a

Steps:

- 1: UCI repository dataset
- 2: Preprocessing
- 3: Missing value removal
- 4: Removal of imbalance of classes
- 5: Reducing data loss removal
- 6: Dataset manipulation
- 7: Imbalance removed
- 8: Classifier implementation

Output based on steps:

- Accuracy from the classifier.
- Precision.
- Best classifier for disease and prediction.

ALGORITHM 1: Thyroid disease classification algorithm.

proper background on the disease classification. Gou and Du proposed a system [7] that consists of a Generalized Discriminant Analysis and Wavelet Support Vector Machine (GDA_WSVM) approach for the analysis of thyroid illnesses which incorporates three phases. Yang et al.’s targets are diagnosing thyroid illnesses with a professional system [8]. These are feature extraction – feature reduction phase, classification phase, and test of GDA_WSVM for correct diagnosis of thyroid diseases phase.

In the proposed system, fuzzy regulations are incorporated via the fuzzy neuron technique.

Poudel et al. [9] proposed that information benefit primarily based on a synthetic immune popularity system (IG-AIRS) might help diagnose thyroid characteristics

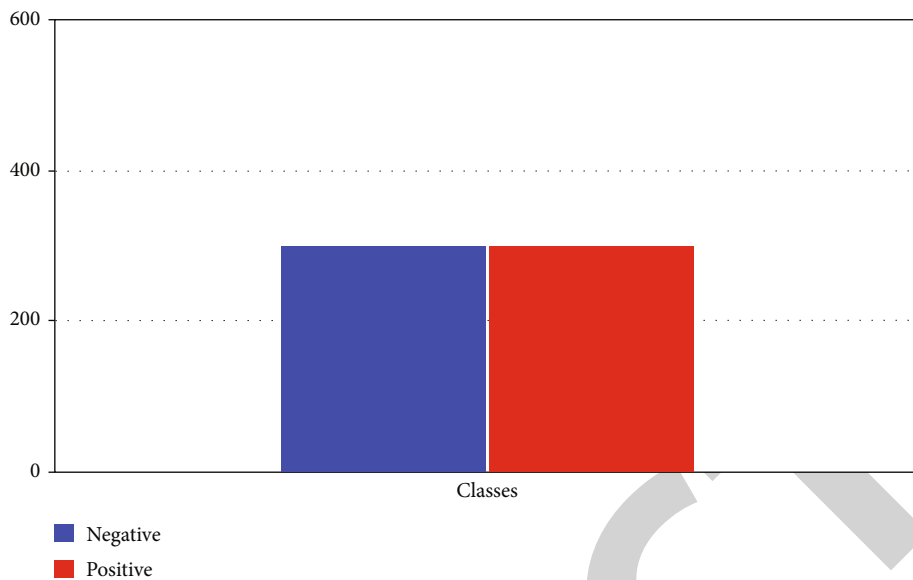


FIGURE 4: Downsampled dataset.

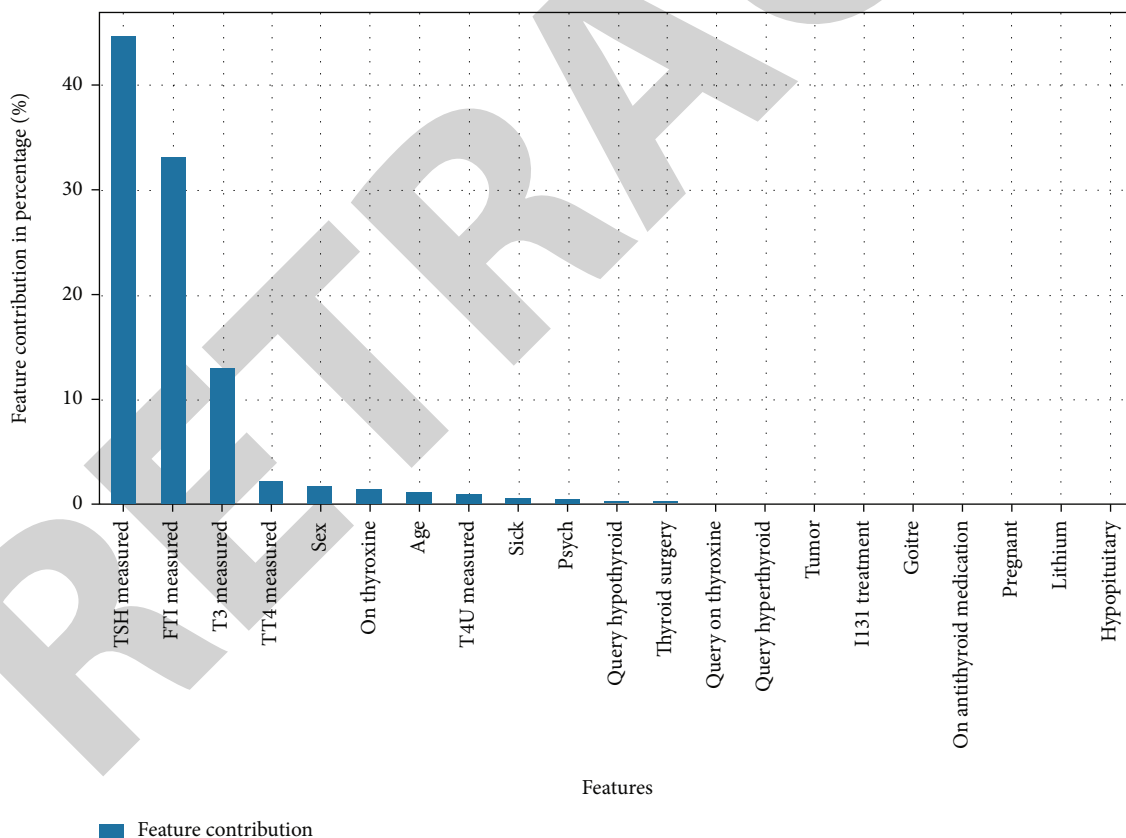


FIGURE 5: Features contributing to classification.

primarily based totally on laboratory tests and might open the manner to numerous unwell diagnoses aided by the use of the latest scientific exam data. Parkavi centred on ant primarily based clustering algorithms. The category used distinct dissimilarity metrics like Euclidean, cosine, and

Gower measures. The category used is distance primarily based category systems.

Prerana et al. used digital biosignal devices to determine thyroid dysfunction and used AI/ML to distinguish between benign and malignant thyroid disease [10]. In [11], the

authors used the local Fisher discriminant analysis (LFDA) and kernelized extreme learning machine method for thyroid disease diagnosis. Shankar et al. [12] evaluated the TUSP automated detection technique to predict thyroid disease by removing the long ultrasound imaging process. Aswathi and Antony [13] used unlabeled data to perform unsupervised learning to improve thyroid classification problems and optimize them. In [14], the CNN is evaluated to detect thyroid disease by using ultrasound images to improve the accuracy of the disease's prediction.

Banu [15] has targeted growing an AIS-based device gaining knowledge of a classifier for clinical analysis and investigating the functionality of the proposed classifier. The proposed classifier efficiently advanced the identity manner of thyroid gland disease.

The goal of Senashova and Samuels [16] is to create a professional gadget for thyroid prognosis. In [17], an expert system for thyroid disease diagnosis (ESTDD) is used. In this professional gadget, authors have used neuro-fuzzy regulations that can diagnose thyroid illnesses with 90.33% accuracy. In [18], Kang et al. used machine models to classify the dataset and improve the classification precision by 10% by dataset manipulation. The authors in [19] used the particle swarm optimization technique to enhance the feature selection process in disease detection. Han et al. used a Bethesda technique to detect thyroid nodules in patients in the Brazilian thyroid centre [20]. An LDA technique was presented in [21] that used the feature extraction method to increase the accuracy of the thyroid disease prediction model.

Automatic and precise thyroid nodule detection in ultrasound pictures is critical for reducing effort and radiologists' mistake rate. Even though deep learning has demonstrated high image classification performance, the intrinsic restrictions of medical pictures, such as a small dataset and time-consuming access to lesion labels, pose hurdles to this effort [22].

On pathological image classification benchmarks, deep learning approaches have shown promise. However, few studies on thyroid cancer autotclassification have been conducted due to the intricacy of pathological thyroid carcinoma pictures and labeled data's paucity [23].

3. Proposed Methodology

The proposed framework will take input in the form of dataset and then forward to the preprocessing module. In the preprocessing module, the normalization of images is performed in this module. After preprocessing the images, augmentation is performed. In augmentation, the dataset is divided into two parts: the training dataset and the testing dataset. After the augmentation process, import AlexNet and compare it with the customized AlexNet, and meet the criteria and store it in a trained model as shown in Figure 1. The missing values will be checked in the preprocessing steps. If we detect a missing value, the mean value will replace the value in that column. As the missing value had a data loss of about 91%, that parameter is removed from the dataset. We have adapted the dataset to be better

TABLE 3: Dataset attributes.

| Attribute | Value |
|--------------------|------------------------------|
| Age | Integer |
| On thyroxine | Male (M), female(F) |
| Query on thyroxine | False (f), true (t) |
| On antithyroid | False (f), true (t) |
| Sick | False (f), true (t) |
| Pregnant | False (f), true (t) |
| Thyroid surgery | False (f), true (t) |
| T131 treatment | False (f), true (t) |
| Query hypothyroid | False (f), true (t) |
| Query hyperthyroid | False (f), true (t) |
| Lithium | False (f), true (t) |
| Goiter | False (f), true (t) |
| Tumor | False (f), true (t) |
| Hypopituitary | False (f), true (t) |
| Psych | False (f), true (t) |
| TSH measured | False (f), true (t) |
| TSH | Real |
| T3 measured | False (f), true (t) |
| T3 | Real |
| TT4 measured | False (f), true (t) |
| TT4 | Real |
| T4U measured | False (f), true (t) |
| T4U | Real |
| FTI measured | False (f), true (t) |
| FTI | Real |
| TBG measured | False (f), true (t) |
| TBG | Real |
| Referral source | SVHC, other, SVI, STMW, SVHD |
| Class | Negative (1), positive (0) |

TABLE 4: Comparison of all classifiers.

| Classifier | Sensitivity | Specificity |
|-------------------|-------------|-------------|
| (1) KNN | 59% | 91% |
| (2) ANN | 94% | 81% |
| (3) Naïve Bayes | 93% | 78% |
| (4) Random forest | 94.8% | 91% |

processed with the chosen models. Initially, only two columns are removed. In the second step of the methodology, we performed dataset manipulation by undersampling the classes. Classes 0 and 1 are highly different in size: class 0 has 2870 samples, while class 1 only contains 293 values. The uneven class representation will cause the accuracy to be very high as machine learning algorithms are sensitive to skewed values. The results will contain many false-positive values, and accuracies will be high compared to the more balanced dataset as shown in Figure 2.

The last step was to divide the dataset into training and testing datasets. We have kept the traditional split which is

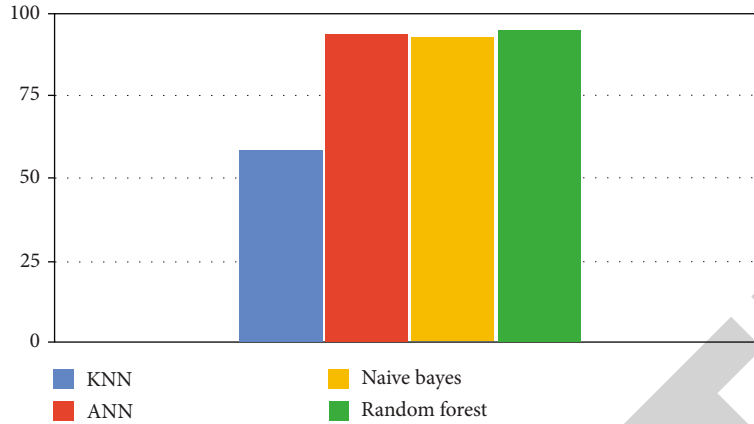


FIGURE 6: Classifiers' performance.

70 percent of the data used for the training and 30 percent of the dataset used for testing purposes. While keeping in mind the dataset distribution, we have to oversample the majority class (class 0) and undersample the minority class (class 1).

Extracting accurate information for medical purposes is an essential task, and it defiantly helps future medical decisions. Feature selection is made to reduce the dimensionality in the dataset. It removes the irrelevant and redundant entries in the dataset. Hence, it increases the accuracy and improves the results. The feature selection identifies the most relevant features for the classification in the classification problems. When raw data is extracted many times, there are missing values in the dataset. The primary demographics contain information regarding the diseased patient's age, gender, medication, patient condition, and hormone levels like TSH, T3, and TT4 and category. The classification will contain two classes. Class 0 is negative, and class 1 is positive. Normal means that the patient is not suffering from thyroid disease.

3.1. Preprocessing Steps

- (1) Data cleansing
- (2) Data processing
- (3) Data elimination
- (4) Data wrangling

Preprocessing is arranged to overcome the different processing issues involving noisy data, redundant information, and missing values. The high quality of data will produce high-quality results according to the measuring metrics. The cost of computations will also reduce.

4. Simulation Environment

The experiments will be performed on a machine Core i5, with 8 GB RAM 500 hard disks. The programming language used is Python 3. The backend is based on Anaconda and Jupyter Notebook. We are utilizing Jupyter Notebook as it will provide the benefits of running on the online servers as shown in Table 1.

The K -nearest neighbor is a simple supervised machine learning algorithm; it is mostly used for the classification and regression problem. The model classifies the data on the points which are most similar to it. It classifies basically on the similarity measure as shown in

$$d(x, y) = \sqrt{\sum_{i=1}^m (x_i - y_i)^2}. \quad (1)$$

Biological neural networks inspire ANN. It is a collection of nodes called neurons. It simulates the behaviour of biological systems. ANN can be used in both supervised and unsupervised training. A node receives the input from an external source in the form of a pattern interpreted, and output is created in equations (2) and (3).

$$z = f(b + x \cdot w) = f\left(b + \sum_{i=1}^n x_i w_i\right) \quad x \in d_{1 \times n}, w \in d_{n \times 1}, b \in d_{1 \times 1}, z \in d_{1 \times 1}. \quad (2)$$

Naïve Bayes is a very proficient and scalable algorithm. It is based on the Bayes theorem. Naïve Bayes is used in many data mining problems.

$$P(y|X) = \frac{P(X|y)P(y)}{P(X)}. \quad (3)$$

Random forest contains decision tree classifiers. Randomly sample a subset of the training set to train each tree, and then, a decision tree is built. Random forest resolves the issue of overfitting in the training set; that is why it is preferred over the decision tree.

$$RFf_i = \frac{\sum_j \text{norm } f_{ij}}{\sum_{j \in \text{all features}, k \in \text{all trees}} \text{norm } f_{jk}}. \quad (4)$$

The dataset is obtained from the UCI data thyroid disease repository. It includes 7200 multivariate types of records. Each record has 25 features. 18 are continuous data types, and 7 are discrete data types as shown in Table 2.

In addition to the upper description, the classes are subdivided as follows:

- (i) Class 0: negative—2870 samples
- (ii) Class 1: positive—293 samples

The dataset contains missing values represented in Figure 3, with a question mark. Remove those features to reduce the data loss. With this step, we will achieve better accuracy after the classification. From the above, we can evaluate that the dataset is imbalanced with more negative occurrence than positive. So, class 0 is the majority class. When the dataset is imbalanced, it requires sampling to equalize the dataset and make the class representation equal to get better accuracy.

The proposed thyroid classification algorithm (Algorithm 1) takes the input from the dataset and performs a number of steps to identify the best classifier for the thyroid disease dataset.

The dataset was downsampled as shown in Figure 4 to make the classes equal in both cases. As the machine learning models are sensitive to skewed data, we equalized the dataset; therefore, our results will be accurate rather than paradoxical.

In Figure 4, the dataset has been acquired through the UCI dataset thyroid disease repository, and focus on implementing it on machine learning algorithms. The dataset contains the attributes of age, gender, and some thyroid markers like TSH, T3, and T4U to categorize the disease.

After dataset analysis, we determined that only a minority of the cases in the dataset are positive for the disease. In Figure 5, TSH, FTI, and T3 measurements are adding all the value to classify the model; they add up to 90% towards the classification as these features contribute more to the dataset alone as shown in Table 3.

The performance is evaluated based on different statistical measures, and sensitivity, specificity, precision, and recall were utilized to measure the results of the machine learning algorithms [24, 25]. The true positive rate refers to the accurately classified positive classes in the machine learning model as shown in

$$\text{True Positive Rate} = \frac{\text{True Positive}}{\text{False Negative} + \text{True Positive}} \cdot \quad (5)$$

The data points correctly classified as negative and originally negative are considered true negative rates in

$$\text{True Negative Rate} = \frac{\text{True Negative}}{\text{True Negative} + \text{False Positive}} \cdot \quad (6)$$

Precision is a good indicator of the accuracy of a model. It measures how many times a positive class is encountered during the testing phase. The precision will explain the clas-

TABLE 5: KNN result at different K values.

| K | Train | Sensitivity | Specificity |
|-----|-------|-------------|-------------|
| 2 | 93.7% | 99.1% | 0.11 |
| 10 | 92.6% | 99.5% | 0.05 |
| 20 | 92% | 99.7% | 0.08 |
| 25 | 91.8% | 99.6% | 0.009 |

TABLE 6: KNN result with a sampled dataset.

| K | Sensitivity | Specificity |
|-----|-------------|-------------|
| 2 | 67% | 80% |
| 10 | 70% | 89% |
| 20 | 65% | 91% |
| 25 | 59% | 91% |

TABLE 7: ANN result with 1000 epochs.

| Epochs | Sensitivity | Specificity |
|--------|-------------|-------------|
| 1000 | 77.4% | 99% |

TABLE 8: Random forest result.

| Classifier | Sensitivity | Specificity |
|---------------|-------------|-------------|
| Random forest | 84.4% | 99.4% |

TABLE 9: Random forest result.

| Classifier | Sensitivity | Specificity |
|---------------|-------------|-------------|
| Random forest | 94.8% | 91.2% |

TABLE 10: Naive Bayes result.

| Classifier | Sensitivity | Specificity |
|-------------|-------------|-------------|
| Naive Bayes | 98% | 97% |

TABLE 11: Naive Bayes result.

| Classifier | Sensitivity | Specificity |
|-------------|-------------|-------------|
| Naive Bayes | 93% | 78% |

sifier's accuracy and display actual positive values in the results as shown in

$$\text{Precision} = \frac{\text{True Positives}}{\text{True Positives} + \text{False Positives}} \cdot \quad (7)$$

Recall calculates how many times the model labeled a positive value true positive as shown in

$$\text{Precision} = \frac{\text{True Positives}}{\text{True Positives} + \text{False Negatives}} \cdot \quad (8)$$

$F1$ score is a harmonic mean between precision and recall and cannot avoid the other measure of $F1$, which is a function of precision and recall. The greater the $F1$ score, the higher the model's performance in

$$F1 = 2 * \frac{1}{(1/\text{precision}) + (1/\text{recall})}. \quad (9)$$

A score is needed to balance between precision and recall.

5. Experimental Results and Analysis

After the implementation of the algorithm, we conducted a comparison of all the classifier results [13, 26]. We evaluated the results based on the true positive and true negative rates. True positive rates are the patients who do have the disease, and true negative rates are those who do not have the disease.

This proposed system is evaluated in the comparative results based on whether the person has the disease or not. Sensitivity and specificity are used to display the results. KNN [27, 28] is the least impressive model that can be used to classify the disease. It produced 59% and 91% specificity results. On the other hand, random forest produced the best results with 94.8% and 91% on the dataset. Naïve Bayes performed at 93% and 78%, and ANN produced 94% and 81%, respectively, as shown in Table 4.

In the neighbors' classifier, two tests are carried out with the said model. The first consists of training and validating using the unbalanced database and partitioning the data, taking 30% for validation and 70% for training; the results are shown in Figure 6.

KNN result at different K values is shown in Table 5 with a sensitivity value of 99.7% when $K = 20$.

In the next phase, we sampled the classes and reduced the dataset's size to implement the KNN classifier. We are only taking 300 values of each class 0 and 1 to reduce the paradoxical accuracy. The results are shown in Table 6 with KNN result of 91% with a dataset.

The accuracy is less, but it contains more true positives and more true negatives. Due to the missing values and skewness in the dataset, the results with the unsampled dataset were high, but they contained many false positives and false negatives. While performing the artificial neural network (ANN) [29, 30], we utilized a 40:60 ratio of the dataset for training and testing. Firstly, implementation is performed on the unsampled dataset. The model is trained for 1000 epochs as shown in Table 7.

Next, we implemented the artificial neural network on an undersampled dataset with equal class representation in both scenarios. Both the positive and negative values were set to 300 to improve the accuracy of the results.

For the third experimentation, we are using a random forest classifier. We are using 30/70 percent data split for the training. The number of estimators is 15, as shown in Table 8.

Next, we implemented the model on a downsampled dataset that contains equal values of both classes. The num-

bers of trees in the forest are 100, at which we drew our conclusion of the results as shown in Table 9.

In the last, we implemented the naïve Bayes algorithm on both the unsampled and sampled datasets. The results are discussed in Table 10.

The naïve Bayes algorithm is applied on a downsampled dataset of 300 values of each class. The conclusion is drawn after 20 k-fold cross-validations in Table 11.

6. Overall Result System

Compared to the overall results with four classifiers on the same dataset, KNN and random forest showed better results with 94.8% system accuracy.

7. Conclusion

This study signifies machine learning and data mining techniques to benefit the medical field and healthcare system. According to the regular protocol, this study will help the doctors use this as a supplementary system. We have evaluated the dataset based on precision and recall. Random forest was performed to be 94.8 percent accurate on average. Random forest is the most efficient in classification, and KNN is the least efficient.

On the other hand, ANN and naïve Bayes performed a level above the average of the KNN. With more training and a more extensive dataset, as expected, there will be better results from the artificial neural network. Our proposed method may also be helpful in creating a medical-related application or use it with neuro-fuzzy interference. The efficient and accurate diagnosis of thyroid disease will benefit the whole medical community. The healthcare system can be further enhanced, and better medical decisions can be taken.

Data Availability

Data can be available upon request.

Conflicts of Interest

The authors declare that they have no conflicts of interest to report regarding the present study.

Authors' Contributions

Tahir Alyas and Muhammad Hamid presented the idea of using machine learning in medical healthcare and identifying the problem statement. Khalid Alissa and Muhammad Hamid developed the theory and performed the machine learning computations using different algorithms. Muhammad Hamid and Nadia Tabassum collected the research materials and dataset for the manuscript. Nadia Tabassum and Tauqeer Faiz verified the analytical methods, programming coding, and results and refined the manuscript after reviewers' comments. Aqeel Ahmed performed data analysis and data normalization and supervised the findings of this research work. He also contributed to the design and implementation of the research. We acknowledged Abdul Salam

Mohammad for his valuable suggestion for improving the manuscript. All authors discussed the results and contributed to the final manuscript.

References

- [1] A. Shrivastava and P. Ambastha, "An ensemble approach for classification of thyroid disease with feature optimization," *International Education and Research Journal*, vol. 3, no. 5, pp. 1–4, 2019.
- [2] G. Chaubey, D. Bisen, S. Arjaria, and V. Yadav, "Thyroid disease prediction using machine learning approaches," *National Academy Science Letters*, vol. 3, pp. 128–133, 2021.
- [3] A. Dewangan, A. Shrivastava, and P. Kumar, "Classification of thyroid disease with feature selection technique," *International Journal of Engineering & Technology*, vol. 2, no. 3, pp. 128–133, 2016.
- [4] A. Begum and A. Parkavi, "Prediction of thyroid disease using data mining techniques," in *International Conference on Advanced Computing & Communication Systems (ICACCS)*, pp. 342–345, Coimbatore, India, 2019.
- [5] J. H. Moon and S. Steinhilber, "Digital medicine in thyroidology: a new era of managing thyroid disease," *Endocrinology and Metabolism*, vol. 34, no. 2, pp. 124–131, 2019.
- [6] C. Ma, J. Guan, W. Zhao, and C. Wang, "An efficient diagnosis system for Thyroid disease based on enhanced Kernelized Extreme Learning Machine Approach," in *International Conference on Cognitive Computing*, pp. 86–101, Cham, 2018.
- [7] M. Guo and D. Yongzhao, "Classification of thyroid ultrasound standard plane images using ResNet-18 networks," in *2019 IEEE 13th International Conference on Anti-counterfeiting, Security, and Identification (ASID)*, pp. 324–328, Xiamen, China, 2019.
- [8] W. Yang, J. Zhao, Y. Qiang et al., "DScGANs: integrate domain knowledge in training dual-path semi-supervised conditional generative adversarial networks and S3VM for ultrasonography thyroid nodules classification," in *International conference on medical image computing and computer-assisted intervention*, vol. 11767 of Lecture Notes in Computer Science, pp. 558–566, Springer, Cham, 2019.
- [9] P. Poudel, A. Illanes, M. Sadeghi, and M. Friebe, "Patch based texture classification of thyroid ultrasound images using convolutional neural network," in *2019 41st Annual International Conference of the IEEE Engineering in Medicine and Biology Society (EMBC)*, pp. 5828–5831, Berlin, Germany, 2019.
- [10] A. S. Prerana and K. Taneja, "Predictive data mining for diagnosis of thyroid disease using neural network," *International Journal of Research in Management, Science & Technology*, vol. 3, no. 2, pp. 75–80, 2015.
- [11] K. Chandel, S. Veenita Kunwar, T. C. Sabitha, and S. Mukherjee, "A comparative study on thyroid disease detection using K-nearest neighbor and naive Bayes classification techniques," *CSI Transactions on ICT*, vol. 4, no. 2-4, pp. 313–319, 2016.
- [12] K. Shankar, S. Lakshmanaprabu, D. Gupta, A. Maselena, and V. Albuquerque, "Optimal feature-based multi-kernel SVM approach for thyroid disease classification," *The Journal of Supercomputing*, vol. 28, no. 76, pp. 1128–1143, 2020.
- [13] A. Aswathi and A. Antony, "An intelligent system for thyroid disease classification and diagnosis," in *2018 Second International Conference on Inventive Communication and Computational Technologies (ICICCT)*, pp. 1261–1264, Coimbatore, India, 2018.
- [14] B. K. Reuters, M. C. O. C. Mamone, E. S. Ikejiri et al., "Bethesda classification and cytohistological correlation of thyroid nodules in a Brazilian thyroid disease center," *European Thyroid Journal*, vol. 7, no. 3, pp. 133–138, 2018.
- [15] R. Banu, "Classification model using random forest and SVM to predict thyroid disease," *International Journal Of Scientific & Technology Research*, vol. 9, no. 2, pp. 1680–1685, 2018.
- [16] O. Senashova and M. Samuels, "Diagnosis and management of nodular thyroid disease," *Vascular and Interventional Radiology*, vol. 25, no. 2, article 100816, 2022.
- [17] X. Zhang, V. C. Lee, J. Rong, J. C. Lee, and F. Liu, "Deep convolutional neural networks in thyroid disease detection: a multi-classification comparison by ultrasonography and computed tomography," *Computer Methods and Programs in Biomedicine*, vol. 220, article 106823, 2022.
- [18] M. Kang, T. S. Wang, T. W. Yen, K. Doffek, D. B. Evans, and S. Dream, "The clinical utility of preoperative thyroglobulin for surgical decision making in thyroid disease," *Journal of Surgical Research*, vol. 270, pp. 230–235, 2022.
- [19] L. L. Lunddorf, A. Ernst, N. Brix et al., "Maternal thyroid disease in pregnancy and timing of pubertal development in sons and daughters," *Fertility and Sterility*, 2022.
- [20] B. Han, M. Zhang, X. Gao, Z. Wang, F. You, and H. Li, "Automatic classification method of thyroid pathological images using multiple magnification factors," *Neurocomputing*, vol. 460, pp. 231–242, 2021.
- [21] W. Yang, Y. Dong, Q. Du et al., "Integrate domain knowledge in training multi-task cascade deep learning model for benign-malignant thyroid nodule classification on ultrasound images," *Engineering Applications of Artificial Intelligence*, vol. 98, article 104064, 2021.
- [22] L. Aversano, M. L. Bernardi, M. Cimitile et al., "Thyroid disease treatment prediction with machine learning approaches," *Procedia Computer Science*, vol. 192, pp. 1031–1040, 2021.
- [23] N. Tabassum, A. Rehman, M. Hamid, M. Saleem, S. Malik, and T. Alyas, "Intelligent nutrition diet recommender system for diabetic's patients," *Intelligent Automation & Soft Computing*, vol. 29, no. 3, pp. 319–335, 2021.
- [24] A. S. Alotaibi, N. Alabdian, A. M. Alotaibi, H. Aljaafary, and M. Alqahtani, "The utilization of spironolactone in heart failure patients at a tertiary Hospital in Saudi Arabia," *Cureus*, vol. 12, no. 8, pp. 1–7, 2020.
- [25] M. B. Qureshi, M. A. Alqahtani, and N. Min-Allah, "Grid resource allocation for real-time data-intensive tasks," *IEEE Access*, vol. 5, pp. 22724–22734, 2017.
- [26] A. R. Rao and B. S. Renuka, "A machine learning approach to predict thyroid disease at early stages of diagnosis," in *2020 IEEE International Conference for Innovation in Technology (INOCON)*, pp. 2020–2023, Bangluru, India, 2020.
- [27] M. A. Khan, W. U. H. Abidi, M. A. Al Ghamdi et al., "Forecast the influenza pandemic using machine learning," *Computers, Materials and Continua*, vol. 66, no. 1, pp. 331–340, 2020.
- [28] W. U. H. Abidi, M. S. Daoud, B. Ihnaini et al., "Real-time shell bidding fraud detection empowered with fused machine learning," *IEEE Access*, vol. 9, pp. 113612–113621, 2021.

Retraction

Retracted: Training a Feedforward Neural Network Using Hybrid Gravitational Search Algorithm with Dynamic Multiswarm Particle Swarm Optimization

BioMed Research International

Received 12 March 2024; Accepted 12 March 2024; Published 20 March 2024

Copyright © 2024 BioMed Research International. This is an open access article distributed under the Creative Commons Attribution License, which permits unrestricted use, distribution, and reproduction in any medium, provided the original work is properly cited.

This article has been retracted by Hindawi following an investigation undertaken by the publisher [1]. This investigation has uncovered evidence of one or more of the following indicators of systematic manipulation of the publication process:

- (1) Discrepancies in scope
- (2) Discrepancies in the description of the research reported
- (3) Discrepancies between the availability of data and the research described
- (4) Inappropriate citations
- (5) Incoherent, meaningless and/or irrelevant content included in the article
- (6) Manipulated or compromised peer review

The presence of these indicators undermines our confidence in the integrity of the article's content and we cannot, therefore, vouch for its reliability. Please note that this notice is intended solely to alert readers that the content of this article is unreliable. We have not investigated whether authors were aware of or involved in the systematic manipulation of the publication process.

Wiley and Hindawi regrets that the usual quality checks did not identify these issues before publication and have since put additional measures in place to safeguard research integrity.

We wish to credit our own Research Integrity and Research Publishing teams and anonymous and named external researchers and research integrity experts for contributing to this investigation.

The corresponding author, as the representative of all authors, has been given the opportunity to register their agreement or disagreement to this retraction. We have kept a record of any response received.

References

- [1] A. A. Nagra, T. Alyas, M. Hamid, N. Tabassum, and A. Ahmad, "Training a Feedforward Neural Network Using Hybrid Gravitational Search Algorithm with Dynamic Multiswarm Particle Swarm Optimization," *BioMed Research International*, vol. 2022, Article ID 2636515, 10 pages, 2022.

Research Article

Training a Feedforward Neural Network Using Hybrid Gravitational Search Algorithm with Dynamic Multiswarm Particle Swarm Optimization

Arfan Ali Nagra,¹ Tahir Alyas ¹, Muhammad Hamid ², Nadia Tabassum ³,
and Aqeel Ahmad⁴

¹Department of Computer Science, Lahore Garrison University, Lahore 54000, Pakistan

²Department of Statistics and Computer Science, University of Veterinary and Animal Sciences, Lahore 54000, Pakistan

³Department of Computer Science, Virtual University of Pakistan, Lahore 54000, Pakistan

⁴University of Chinese Academy of Sciences (UCAS), Beijing, China

Correspondence should be addressed to Muhammad Hamid; muhammad.hamid@uvas.edu.pk

Received 13 April 2022; Accepted 17 May 2022; Published 30 May 2022

Academic Editor: Gulnaz Afzal

Copyright © 2022 Arfan Ali Nagra et al. This is an open access article distributed under the Creative Commons Attribution License, which permits unrestricted use, distribution, and reproduction in any medium, provided the original work is properly cited.

One of the most well-known methods for solving real-world and complex optimization problems is the gravitational search algorithm (GSA). The gravitational search technique suffers from a sluggish convergence rate and weak local search capabilities while solving complicated optimization problems. A unique hybrid population-based strategy is designed to tackle the problem by combining dynamic multiswarm particle swarm optimization with gravitational search algorithm (GSADMSPSO). In this manuscript, GSADMSPSO is used as novel training techniques for Feedforward Neural Networks (FNNs) in order to test the algorithm's efficiency in decreasing the issues of local minima trapping and existing evolutionary learning methods' poor convergence rate. A novel method GSADMSPSO distributes the primary population of masses into smaller subswarms, according to the proposed algorithm, and also stabilizes them by offering a new neighborhood plan. At this time, each agent (particle) increases its position and velocity by using the suggested algorithm's global search capability. The fundamental concept is to combine GSA's ability with DMSPSO's to improve the performance of a given algorithm's exploration and exploitation. The suggested algorithm's performance on a range of well-known benchmark test functions, GSA, and its variations is compared. The results of the experiments suggest that the proposed method outperforms the other variants in terms of convergence speed and avoiding local minima; FNNs are being trained.

1. Introduction

In computational intelligence, neural networks (NNs) are one of the most advanced creations. Neurons in the human brain are often employed to solve categorization problems. The basic notions of NNs were first articulated in 1943 [1]. Feedforward [2], Kohonen self-organizing network [3], radial basis function (RBF) network [4], recurrent neural network [5], and spiking neural networks [6] are some of the NNs explored in this paper.

Data flows in one direction via the networks in FNN. In recurrent NNs, data is shared in two directions between the

neurons. Regardless of the variances amongst NNs, they all learn in the same way. The ability of a NN to learn from experience is referred to as learning. Similar to real neurons, artificial neural networks (ANN) [7, 8] have been constructed with strategies to familiarise themselves with a set of specified inputs. In this context, there are two types of learning: supervised [9] and unsupervised [10]. The NN is given feedback from an outside source in the first way. The NN familiarises itself with inputs without any external feedback in unsupervised learning. Feedforward Neural Networks with multilayer [11] have recently become popular. In practical applications, FNNs with several layers are the

most powerful neural networks. Multilayer FNNs have been shown to be fairly accurate for both continuous and discontinuous functions [12]. Many studies find that learning is an important aspect of any NN. For the standard [13] or enhanced [14], the leading applications have employed the Backpropagation (BP) algorithm as the training strategy for FNNs. Backpropagation (BP) is a gradient-based approach with drawbacks such as delayed convergence [15] and the ability to become trapped in local minima.

Various optimization approaches have already been applied simulated annealing, for example, which may be used to train FNNs (SA) [16], particle swarm optimization (PSO) algorithms [17], Magnetic Optimization Algorithm (MOA) [18], GG-GSA [19], and PSOGSA [20]. Genetic Algorithm (GA) [21], Differential Evolution (DE) [22], Ant Colony Optimization (ACO) [23], Artificial Bee Colony (ABC) [24], Hybrid Central Force Optimization and Particle Swarm Optimization (CFO-PSO) [25], Social Spider Optimization algorithm (SSO) [26], Chemical Reaction Optimization (CRO) [27], Charged System Search (CSS) [28], Invasive Weed Optimization (IWO) [29], and Teaching-Learning Based Optimization (TLBO) trainer [30] are some of the most popular evolutionary training algorithms. According to [31, 32], PSO and GSA are one of the best optimization techniques for eliminating both issues of slow convergence rate and trap in local optima. Recently, hybrid methods had been introduced to overcome the weakness of slow convergence [33, 34]. Most of the previous algorithms fail to reach the minimal selection; the hybrid gravitational search algorithm with social ski-driver- (GSA-SSD-) based model has been introduced to overcome the convergence problem [35].

To overcome these weaknesses, GSADMSPSO [36] is used as a Feedforward Neural Network (FNN) as a new approach to examine the algorithm's efficiency and reduce the difficulties of minima in the immediate vicinity trapping and slow steady convergence. Algorithms for evolutionary learning GSADMSPSO distribute the primary population of masses into smaller subswarms, according to the suggested algorithm, and also stabilize them by offering a fresh neighborhood plan [37]. At this time, each agent (particle) increases its position and velocity by using the suggested algorithm's global search capability. The fundamental concept is to combine GSA's ability with DMSPSO's to improve the performance of a given algorithm's exploration and exploitation [38]. The suggested method's performance is compared to that of GSA and its variants using well-known benchmark test functions [39, 40]. The experimental results show that in terms of avoiding local minima and accelerating convergence, the proposed approach beats existing FNN training variations. The following is the order of this paper's remaining sections: Section 1 introduces the basic concept of GSA. The dynamic multiswarm particle swarm optimization and gravitational search approach are discussed in Section 2; then, in Section 3, we go over the GSADMSPSO methodology in depth. The experiment's findings are provided in Section 4. Section 5 discusses contrast analysis. In the concluding section, the findings are given.

2. Related Work

2.1. Multilayer Perceptron with Feedforward Neural Network. The connections of FNNs between the neurons are unidirectional and one-way. In neural networks [2], neurons are in parallel layers. The first layer is the input layer, the second layer is the concealed layer, and the last layer is the output layer. Figure 1 shows an example of a FNN using MLP.

The output of a given data has been calculated in step by step procedure [18]: the average sum of weight in input is calculated in

$$s_j = \sum_{i=1}^n (W_{ij}X_i) - \theta_j, \quad j = 1, 2, \dots, h. \quad (1)$$

The hidden layer values are calculated in

$$s_j = \text{sigmoid}(s_j) = \frac{1}{1 + \exp(-s_j)}, \quad j = 1, 2, \dots, h. \quad (2)$$

The output MSE and accuracy have been calculated in

$$O_k = \sum_{j=1}^h (w_{jk}.s_j) - \theta', \quad k = 1, 2, \dots, m, \quad (3)$$

$$O_k = \text{sigmoid}(O_k) = \frac{1}{1 + \exp(-O_k)}, \quad j = 1, 2, \dots, m. \quad (4)$$

From input, the output of MLPs has been observed with the help of biases and weights in equations (1) to (4).

2.2. Gravitational Search Algorithm. The typical GSA is a newly projected search algorithm. GSA firstly initializes the positions of N agents randomly, shown as

$$X_i = (x_i^1, \dots, x_i^d, \dots, x_i^D) \quad (5)$$

for $i = 1, 2, \dots, N$, where D is the dimension index of the search space and x_i^d represents the i^{th} agent in the d^{th} dimension:

$$q_i(t) = \frac{\text{fit}_i - \text{worst}(t)}{\text{best}(t) - \text{worst}(t)}, \quad (6)$$

$$M_i(t) = \frac{q_i(t)}{\sum_{j=1}^N q_j(t)}, \quad (7)$$

where $\text{fit}_i(t)$ and $M_i(t)$ represent the fitness and $\text{best}(t)$ and $\text{worst}(t)$ are defined in the following equations:

$$\text{best}(t) = \min_{j \in \{1, \dots, N\}} \text{fit}_j(t), \quad (8)$$

$$\text{worst}(t) = \max_{j \in \{1, \dots, N\}} \text{fit}_j(t). \quad (9)$$

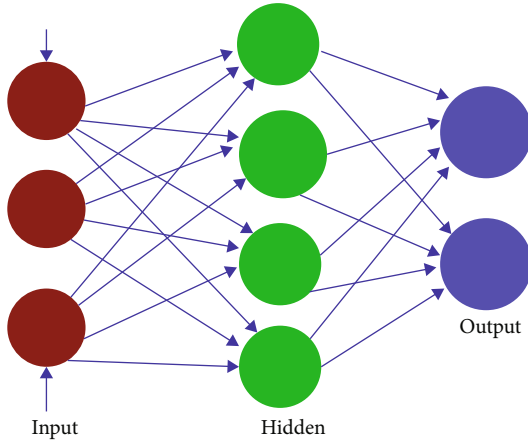


FIGURE 1: One hidden layer in a multilayer perceptron.

The force acting on i^{th} agent from j^{th} agent is as follows:

$$f_{ij}^d(t) = G(t) \frac{M_i(t) \times M_j(t)}{R_{i,j} + \epsilon} (x_j^d(t) - x_i^d(t)). \quad (10)$$

$G(t)$ is a function of the iteration time:

$$G(t) = G_0 e^{-\alpha t/T}, \quad (11)$$

where G_0 is the initial value, α is a shrinking parameter, and T represents the maximum number of iterations:

$$F_i^d(t) = \sum_{j \in K\text{best}, j \neq i} \text{rand}_j F_{ij}^d(t), \quad (12)$$

where $K\text{best}$ is the set of the first K agents with the biggest mass; the acceleration of the i^{th} agent is calculated as follows:

$$a_i^d(t) = \frac{F_i^d(t)}{M_i(t)}. \quad (13)$$

Further velocity is updated using the following equation:

$$v_i^d(t+1) = \text{rand}_i \times v_i^d(t) + a_i^d(t), \quad (14)$$

$$x_i^d(t+1) = x_i^d(t) + v_i^d(t+1). \quad (15)$$

By summing up the equations, acceleration can also be written as

$$a_i^d(t) = \sum_{j \in K\text{best}, j \neq i} \text{rand}_j \times M_j(t) \frac{G(t)}{R_{ij}(t) + \epsilon} (x_j^d(t) - x_i^d(t)). \quad (16)$$

2.3. The Hybrid GSABP Algorithm. In the optimization problems, there are a lot of local minima. The hybrid method final results reflect the aptitude of the algorithm in overcoming local minima and attaining a close global optimum [36]. The error of FNN is often large in the initial period of the training process. For solving real-world and complex optimization problems, one of the most well-known methods is the gravitational search algorithm (GSA). The gravitational search technique suffers from a slow convergence rate and weak local search capabilities while solving complicated optimization problems. The BP algorithm has a strong ability to search local optimum, but its ability to search global optimum is weak. The hybrid GSABP is proposed to combine the global search ability of GSA with the local search ability of BP. This combination takes advantage of both algorithms to optimize the weights and biases of the FNN.

3. The Proposed Hybrid Algorithm

The main concern to hybridize the algorithm is to maintain the constancy between exploration and exploitation. In the initial iterations, it is achieved step size of agents. In the final iterations, it is very difficult to avoid the global optima. Then, in the later iteration, the fitness focus is on small step size for exploitation. For better performance and to solve the problem of early convergence, a hybrid technique is adopted. In final iterations, we have a problem of slow exploitation and deterioration. Weights are used to assess fitness function in GSA. As a result, fit masses are seen as slow-moving, hefty items.

Then, at first iterations, particles ought to travel across the scope of the search. After that, they have found a good answer; they must wrinkle around it in order to obtain the most effective solution out of it. In GSA, the masses get heavier. Because masses swarm around a solution in the later stages of iterations, their weights are virtually identical. Their gravitational forces are about equal in intensity, and they fascinate each other. As a result, they are unable to travel rapidly to the best answer. A variety of issues have been faced by GSA. The algorithm that has been presented has the capacity to overcome the challenges that GSA has had to deal with. As a result, in this paper, GSADMSPSO proposes a neighborhood approach with dynamic multiswarm (DMS).

In the first iteration, the proposed technique promotes exploration, and in the final iteration, it prioritizes exploitation. The proposed approach initially works on masses of agents in the first phase. Because the agent's weight fitness is poor, it will not be able to achieve peak performance and to look into the search area. Agents that are light in weight can be used; heavy-weight agents, on the other hand, can be chosen to utilize their surroundings using neighborhood strategy. As a consequence, a dynamic multiswarm (DMS) is used, along with a novel neighborhood strategy, as illustrated in the equation below:

$$m_i(t) = \begin{cases} \frac{0.9 * \text{fit}_i}{\text{best}_i(t) - \text{worst}_i(t)} \text{ mod } (\text{fit}_i) = 0, & \text{then regroup the subswarm,} \end{cases} \quad (17)$$

where $fit_i(t)$ indicates the fitness value of the agent $_i$ and $worst_i(t)$ and $best_i(t)$ are defined as follows:

$$best(t) = \text{low}_{j \in \text{regroup of swarms}} fit_j(t), \quad (18)$$

$$worst(t) = \text{high}_{j \in \text{regroup of swarm}} fit_j(t). \quad (19)$$

The swarm is divided into several subswarms according to equation (17), and each agent's neighbors can attract it by smearing the gravitational pull on it. They use their own members to look for higher placements in the search area. The subswarms, on the other hand, are dynamic, and a regrouping schedule is frequently used to reorganize them, which is a periodic interchange of information. Through an arbitrary regrouping timetable, agents from various subswarms are rebuilt into a new configuration. As a result, DMS can choose the neighbors with the shortest distance. These neighbors called an agent is agent $_i$. As a result, each component impacts the agent's ability to attract another swarm agent. The DMS has defined the worst and best agent. In the last iteration, the global lookup capability of the DMS PSO algorithm was employed, and equations (20) and (21) are utilised to update the individual's location and velocity:

$$v_i^{t+1} = wv_i^t + c_1 r_1 a_i^d(t) + c_2 r_2 (gbest - x_i(t)), \quad (20)$$

$$x_i^{t+1} = x_i^t + v_i^{t+1}, \quad (21)$$

where $V_i(t)$ is the velocity at which agent $_i$, c_1 and c_2 are accelerating coefficients at iteration t . r_1 select a number between 0 and 1 at random which is r_2 . The first part is similar to GSA's, with a focus on mass research. The second element is in charge of enticing people to the best crowds thus far. Each mass's distance between you and the best mass is computed using $gbest - x_i(t)$ a random percentage of the ultimate force aimed towards the most advantageous mass.

Set the parameters of the algorithm; N is the total number of particles, including the total number of particles. In the suggested approach, the amount of times you have iterated is t , $G0$ is the gravitational constant, and a is the decreasing coefficient. Create populations at random. The particle's location vector is set as $X_i = (x_1, x_2, x_3, \dots, x_n)$; the velocity is initialized as $v_i = (v_{i1}, v_{i2}, v_{i3}, \dots, v_{in})^t$; the particles are divided into the global best value for numerical subswarms $gbest$ and the ideal value for each individual $pbest$. Eventually, using the formula below, calculate every person's fitness value. Then, using each individual's fitness value, calculate it and keep track of the optimum spot $gbest$, constant of gravitation, and the forces that result from it, which are known. At each cycle, the best solution found so far should be updated. Once the accelerations have been calculated and the best solution has been updated, using the DMS PSO algorithm's global search capability, all agents' velocities may be computed using equation (20). Finally, agents' positions are revised as follows (equation (21)). The procedure comes to an end when an end condition is met. The proposed method's general phases are shown in Figure 2.

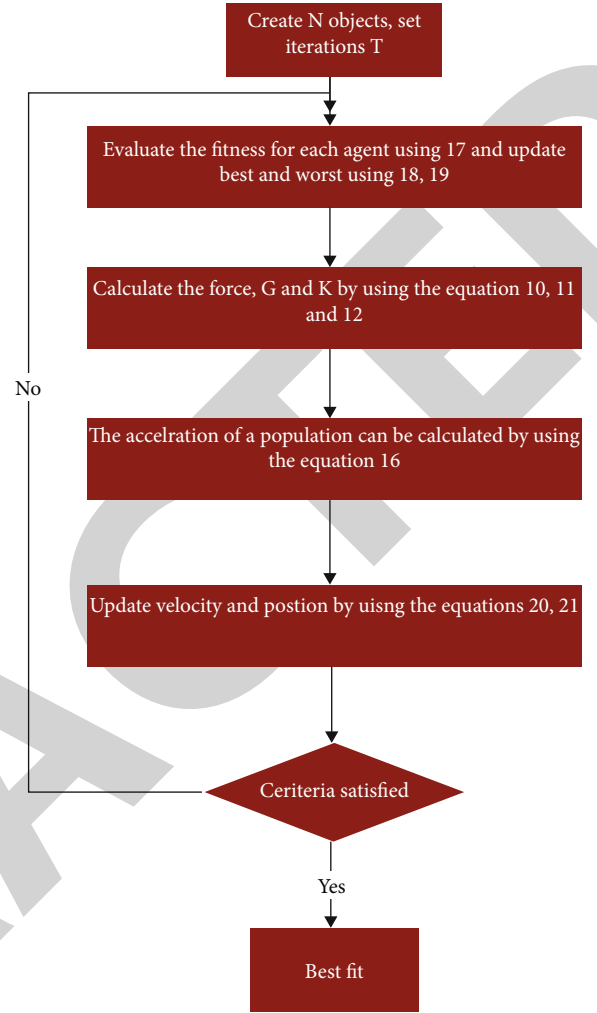


FIGURE 2: Flow chart of a GSADMSPSO.

Because of the dynamic multiswarm nature of our suggested strategy, each agent may examine the best option, and the masses are given access to a kind of local intelligence. In comparison to existing GSA versions, the proposed technique has the potential to offer better outcomes. The efficiency of the proposed methodology is examined in the next part using a variety of static, dynamic, and real-time issues.

4. GSADMSPSO for Training FNNs

The proposed approach of each search agent consists of three parts for the training of FNN: The first section discusses the biases; the second section contains the weights that connect the last component comprising the weights that link the hidden layer nodes to the output layer and the input layer nodes to the hidden layer. This section describes the proposed GSADMSPSO method for training a single layer MLP. The proposed FNNGSADMSPSO is used to reduce error and improve accuracy for correct weights and biases. Equations are used to generate output from the input in the FNN model (1–4). The weight and bias values were used in the first stage of the proposed methodology.

Equation (9) states that the error is calculated using the fitness function. Neural network learning is the process of iteratively reducing the cost function. At each iteration, the application weights and biases at FNN have been changed resulting in cost reduction. The suggested FNNGSADMSPSO method can be described as follows:

- (1) A population is randomly created. It is in charge of a collection of weights and bias values
- (2) For assessment, the MSE criteria are employed. It is chosen as the best fitness function after being calculated for each iteration on a given training dataset
- (3) To create a new solution, the best position and best global values are updated
- (4) The number of iterations during which the global solution's best fitness value was obtained remains unaltered which is tracked using a counter
- (5) During the iterations, to create a better population, the places with the worst fitness values are determined. The values of their fitness are calculated and compared to prior positions. If the opposite position has a higher fitness value, it will be introduced into the population and assigned to position 7, else it will be assigned to position 6
- (6) The proposed GSADMSPSO is used to indicate their new positions for updated positions that are not as good as their actual positions
- (7) The procedure returns to step 2 after creating a new population. The process is continued until the desired number of generations is reached
- (8) Finally, the best answer is supplied to FNN, and the test data is utilised to evaluate its performance

4.1. Fitness Function. The MLP receives the weight and bias matrices and the fitness worth of each option. The solution is calculated using the mean squared error (MSE). The fitness function of suggested algorithms is defined as MSE, which is stated in equation (9):

$$\text{MSE} = \frac{1}{N} \sum_{i=1}^n (c - o)^2, \quad (22)$$

where n is the number of training samples, o denotes the predicted values of the neural network, and c denotes the class names. The classification accuracy criteria, aside from the MSE requirement, are used to evaluate MLP's classification performance on the new dataset, which is determined as the following: Z is the sample size in the test dataset and N is the number of samples successfully classified by the classifier:

$$\text{Accuracy} = \frac{\sim Z}{Z}. \quad (23)$$

The first approach is used to apply GSA, PSOGSA, GSADMSPSO, and GG-GSA on a FNN in this study. This

TABLE 1: UCI has compiled a list of real-world datasets.

| Dataset name | # of features | # of samples |
|-------------------------|---------------|--------------|
| Glass | 9 | 214 |
| Vowel | 10 | 520 |
| Wine | 13 | 177 |
| Yeast | 8 | 1440 |
| Sonar | 60 | 200 |
| Heart | 13 | 270 |
| Wisconsin breast cancer | 9 | 680 |
| Colon cancer | 2000 | 60 |
| Shuttle | 9 | 50000 |
| Lymphoma | 4026 | 59 |
| Iris | 4 | 150 |
| Lung cancer | 56 | 32 |
| Hepatitis | 19 | 155 |
| Dermatology | 34 | 366 |
| Zoo | 16 | 101 |
| Abalone | 8 | 3842 |

TABLE 2: The parity problem with three bits (3-bit XOR).

| Input | Output |
|-------|--------|
| 0 0 0 | 0 |
| 0 0 1 | 1 |
| 0 1 0 | 1 |
| 0 1 1 | 0 |
| 1 0 0 | 1 |
| 1 0 1 | 0 |
| 1 1 0 | 0 |
| 1 1 1 | 1 |

indicates that the FNN's structure is fixed; GSA, PSOGSA, GSADMSPSO, and GG-GSA select a set of weights and biases that give the FNN the least amount of inaccuracy.

5. Results and Discussions

On 16 standard classification datasets, the proposed technique for FNN training is assessed in terms of its effectiveness using the UCI Machine Learning repository [41] which is represented in Table 1. And for three-bit parity, the suggested algorithm's skills in training FNNs are compared using benchmark problems, which are shown in Table 2. It is conceivable that every particle in this issue is randomly started in the $[0, 1]$ range. The gravitational constant (G_0) is one in FNNGSA, whereas it is set to 20. Particles' initial velocities are arbitrarily created in the range $[0, 1]$, and for each particle, at the start, the acceleration and mass parameters are both set to zero. In FNNPSOGSA, c_1 and c_2 are both set to 1, and the beginning velocities of the agents are generated at random in the range $[0, 1]$, and w declines linearly from 0.9 to 0.4. In FNNGG-GSA, the gravitational constant (G_0) is set to 1, while the value is adjusted to 20. Particles' initial velocities are

TABLE 3: In a 3-bit XOR problem, the average, best, and standard deviation of MSE for all training samples were calculated during 30 different runs.

| Hidden nodes (S) | Algorithm | Average MSE | Best MSE | Std. MSE |
|------------------|--------------|------------------|------------|----------|
| 5 | FNNGSADMSPSO | 1.178E-04 | 2.78E-11 | 3.78E-04 |
| | FNNPSOGSA | 1.31E-02 | 3.17E-10 | 2.60E-02 |
| | FNNGG-GSA | 7.34E-03 | 4.23E-08 | 5.78E-03 |
| | FNNGSA | 1.79E-01 | 4.34E-02 | 5.59E-02 |
| 6 | FNNGSADMSPSO | 2.56E-04 | 3.78E-09 | 5.43E-04 |
| | FNNPSOGSA | 4.54E-03 | 3.85E-09 | 5.63E-03 |
| | FNNGG-GSA | 3.67E-03 | 4.71E-09 | 7.56E-03 |
| | FNNGSA | 1.45E-01 | 2.96E-02 | 6.42E-02 |
| 7 | FNNGSADMSPSO | 3.67E-04 | 3.8274E-24 | 7.89E-04 |
| | FNNPSOGSA | 2.71E-03 | 1.42E-11 | 1.28E-02 |
| | FNNGG-GSA | 2.53E-05 | 4.67E-12 | 5.67E-05 |
| | FNNGSA | 1.25E-01 | 1.24E-02 | 6.53E-02 |
| 8 | FNNGSADMSPSO | 1.45E-04 | 1.13E-09 | 5.45E-05 |
| | FNNPSOGSA | 2.03E-05 | 1.25E-11 | 6.28E-05 |
| | FNNGG-GSA | 2.78E-03 | 3.35E-13 | 7.89E-03 |
| | FNNGSA | 1.14E-01 | 7.12E-03 | 7.63E-02 |
| 9 | FNNGSADMSPSO | 3.45E-08 | 3.67E-17 | 5.45E-07 |
| | FNNPSOGSA | 7.72E-06 | 5.53E-12 | 2.65E-05 |
| | FNNGG-GSA | 2.78E-04 | 3.51E-06 | 3.72E-03 |
| | FNNGSA | 9.40E-02 | 5.84E-02 | 2.11E-02 |
| 10 | FNNGSADMSPSO | 3.67E-06 | 2.89E-09 | 5.78E-06 |
| | FNNPSOGSA | 6.13E-06 | 1.55E-10 | 2.88E-05 |
| | FNNGG-GSA | 5.96E-07 | 2.34E-11 | 2.45E-06 |
| | FNNGSA | 8.04E-02 | 1.05E-02 | 5.44E-02 |
| 11 | FNNGSADMSPSO | 1.67E-06 | 5.73E-19 | 4.34E-05 |
| | FNNPSOGSA | 1.82E-05 | 4.65E-10 | 7.69E-05 |
| | FNNGG-GSA | 3.45E-04 | 4.34E-07 | 5.43E-03 |
| | FNNGSA | 7.76E-02 | 1.20E-02 | 4.31E-02 |
| 13 | FNNGSADMSPSO | 6.45E-03 | 1.87E-06 | 2.78E-02 |
| | FNNPSOGSA | 4.16E-02 | 4.62E-05 | 8.64E-02 |
| | FNNGG-GSA | 5.52E-02 | 3.45E-03 | 7.78E-02 |
| | FNNGSA | 6.57E-02 | 1.23E-02 | 2.34E-01 |
| 15 | FNNGSADMSPSO | 3.78E-02 | 5.67E-10 | 6.71E-02 |
| | FNNPSOGSA | 4.16E-03 | 4.66E-11 | 2.28E-02 |
| | FNNGG-GSA | 1.45E-04 | 3.67E-16 | 5.55E-04 |
| | FNNGSA | 6.97E-02 | 9.28E-03 | 4.12E-02 |
| 20 | FNNGSADMSPSO | 7.45E-03 | 4.78E-12 | 3.56E-02 |
| | FNNPSOGSA | 1.68E-02 | 4.12E-08 | 6.32E-02 |
| | FNNGG-GSA | 8.78E-01 | 5.67E-03 | 9.67E-01 |
| | FNNGSA | 7.50E-02 | 2.34E-02 | 3.33E-01 |
| 30 | FNNGSADMSPSO | 3.73E-05 | 2.79E-12 | 8.45E-05 |
| | FNNPSOGSA | 4.16E-03 | 4.57E-14 | 2.28E-02 |
| | FNNGG-GSA | 1.36E-04 | 4.67E-12 | 6.45E-04 |
| | FNNGSA | 6.23E-02 | 1.44E-02 | 3.91E-02 |

created arbitrarily in the range [0,1], and the initial acceleration and mass values for each particle are set to 0. When c_1 and c_2 are both set to 1, w for FNNGSADMSPSO reduces linearly from 0.9 to 0.4, and the agents' beginning velocities are produced at random in the range [0, 1].

5.1. *The XOR Issue with N Bits of Parity.* With N bits of parity, the XOR problem arises. The N bits' parity problem is a well-known nonlinear benchmark problem. The goal is to

count how many "1's" are in the input vector. The input vector's XOR result should be reimbursed. The output is "1" if the input vector has an odd number of "1's." The output is "0" if the input vector has an even number of "1's."

For three bits, Table 1 shows the problem's inputs and intended outputs: We cannot solve the XOR problem in a linear fashion without hidden layers, and we cannot solve it with a FNN either (perceptron). To solve this problem, we compare a FNN with the structure 3-S-1, where S is the

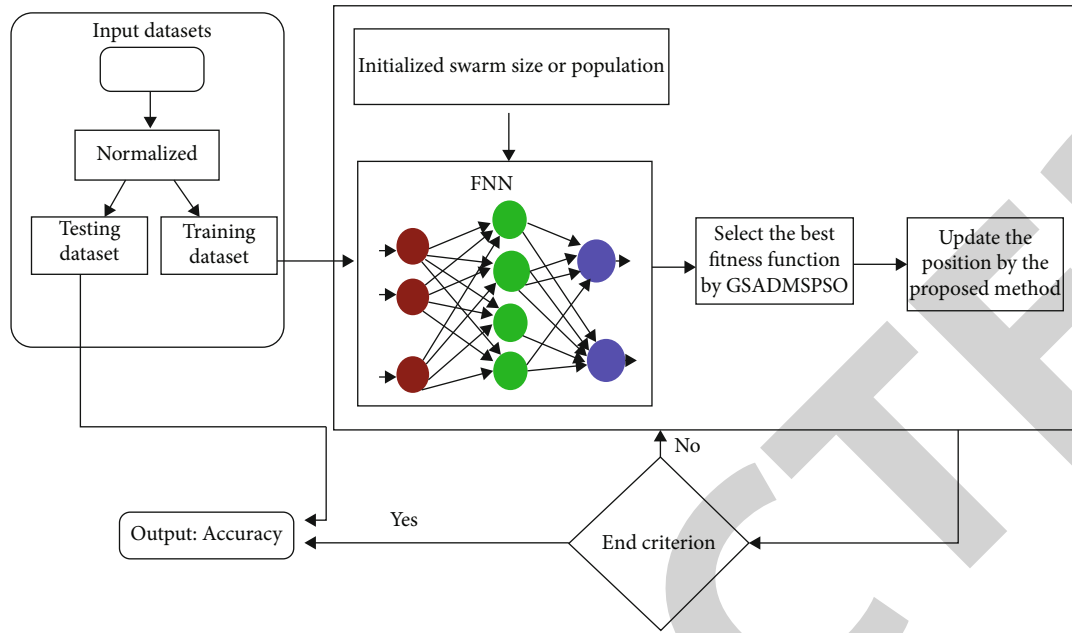


FIGURE 3: The framework of the proposed method.

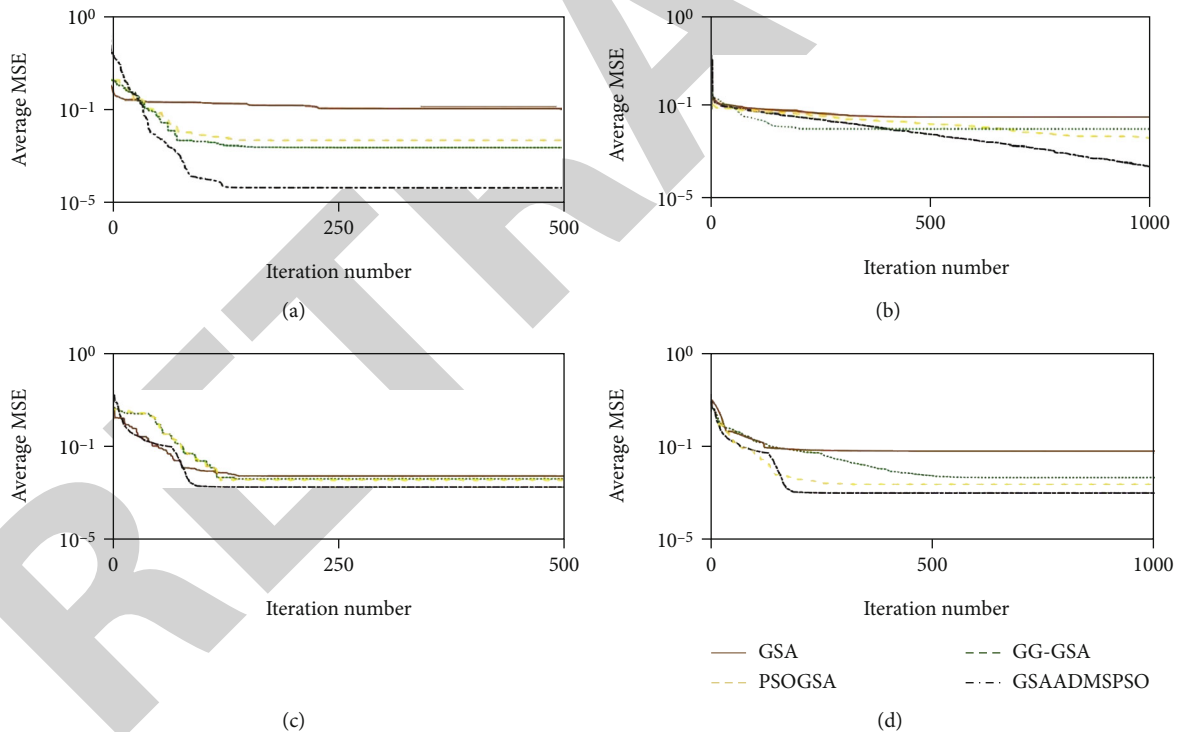


FIGURE 4: Convergence curves of different algorithms based on averages of MSE for all training samples over 30 independent runs in a 3-bit XOR problem. (a-d) Are the convergence curves for FNNs with $S = 5, 9, 13,$ and $20,$ respectively.

number of hidden nodes, to FNNs with $S = 5, 6, 7, 8, 9, 10, 11, 13, 15, 20,$ and 30 in this section.

5.2. Comparison with Other Techniques through Parity Problem with Three Bits (3-Bit XOR). On the suite of three-bit parity problem (3-bit XOR) benchmark functions, GSADMSPSO was compared to other common GSA varia-

tions to assess its performance. The suggested method was compared to GSA, PSO GSA, and GG-GSA. Variants were applied to the three-bit parity problem (3-bit XOR) mentioned in Table 2 in this section. Table 3 displays the average, best, and standard deviation of the Best Square Error (MSE) for all training samples over 30 distinct trials. According to a t -test with a significance level of 5%, the bold values

TABLE 4: Different algorithms' average performance in percent of the given features.

| Dataset | | FNNGSA | FNNGG-GSA | FNNPSOGSA | FNNGSADMSPSO |
|-------------------------|------|---------------|---------------|---------------|---------------|
| Glass | Avg. | 0.741 | 0.749 | 0.748 | 0.767 |
| | Best | 0.753 | 0.764 | 0.758 | 0.785 |
| | Std. | 0.0169 | 0.0059 | 0.0089 | 0.0086 |
| Vowel | Avg. | 0.944 | 0.965 | 0.973 | 0.981 |
| | Best | 0.953 | 0.984 | 0.989 | 0.992 |
| | Std. | 0.0045 | 0.0072 | 0.0081 | 0.0056 |
| Wine | Avg. | 0.917 | 0.961 | 0.977 | 0.961 |
| | Best | 0.933 | 0.973 | 0.983 | 0.983 |
| | Std. | 0.0127 | 0.0085 | 0.0034 | 0.0066 |
| Yeast | Avg. | 49.17 | 0.501 | 50.23 | 53.11 |
| | Best | 0.933 | 0.513 | 0.518 | 0.552 |
| | Std. | 0.0137 | 0.0114 | 0.0126 | 0.0094 |
| Sonar | Avg. | 0.922 | 0.943 | 0.932 | 0.961 |
| | Best | 0.945 | 0.958 | 0.941 | 0.973 |
| | Std. | 0.0062 | 0.0093 | 0.0095 | 0.0028 |
| Heart | Avg. | 0.748 | 0.777 | 0.753 | 0.763 |
| | Best | 0.753 | 0.789 | 0.775 | 0.771 |
| | Std. | 0.0145 | 0.0071 | 0.0038 | 0.0076 |
| Wisconsin breast cancer | Avg. | 0.959 | 0.967 | 0.971 | 0.988 |
| | Best | 0.961 | 0.971 | 0.985 | 0.992 |
| | Std. | 0.0021 | 0.0139 | 0.0048 | 0.0017 |
| Colon cancer | Avg. | 0.819 | 0.839 | 0.834 | 0.845 |
| | Best | 0.836 | 0.845 | 0.851 | 0.859 |
| | Std. | 0.0163 | 0.0062 | 0.0034 | 0.0074 |
| Shuttle | Avg. | 0.907 | 0.916 | 0.923 | 0.931 |
| | Best | 0.913 | 0.923 | 0.935 | 0.954 |
| | Std. | 0.0367 | 0.0137 | 0.0085 | 0.0073 |
| Lymphoma | Avg. | 0.799 | 0.817 | 0.827 | 0.814 |
| | Best | 0.814 | 0.825 | 0.844 | 0.826 |
| | Std. | 0.0183 | 0.0045 | 0.0067 | 0.0034 |
| Iris | Avg. | 0.921 | 0.941 | 0.957 | 0.984 |
| | Best | 0.945 | 0.963 | 0.969 | 0.994 |
| | Std. | 0.0043 | 0.0061 | 0.0092 | 0.0019 |
| Lung cancer | Avg. | 0.447 | 0.469 | 0.446 | 0.479 |
| | Best | 0.467 | 0.479 | 0.468 | 0.486 |
| | Std. | 0.0032 | 0.0056 | 0.0123 | 0.0041 |
| Hepatitis | Avg. | 0.804 | 0.815 | 0.807 | 0.823 |
| | Best | 0.828 | 0.829 | 0.821 | 0.835 |
| | Std. | 0.0149 | 0.0025 | 0.0076 | 0.0093 |
| Dermatology | Avg. | 0.944 | 0.952 | 0.947 | 0.938 |
| | Best | 0.956 | 0.967 | 0.951 | 0.946 |
| | Std. | 0.0154 | 0.0061 | 0.0152 | 0.0153 |
| Zoo | Avg. | 0.807 | 0.847 | 0.859 | 0.864 |
| | Best | 0.824 | 0.853 | 0.864 | 0.882 |
| | Std. | 0.0029 | 0.0042 | 0.0052 | 0.0073 |
| Abalone | Avg. | 0.242 | 0.248 | 0.213 | 0.249 |
| | Best | 0.246 | 0.249 | 0.236 | 0.25 |
| | Std. | 0.0578 | 0.0731 | 0.0853 | 0.0351 |

represent the best response. When compared to the other algorithms, GSADMSPSO produced the best results. The SIW-APSO-LS gives the best accuracy, according to the results. GSA, GG-GSA, PSO-GSA, and Figure 3 depict GSADMSPSO convergence curves based on MSE averages for all training samples throughout 30 different runs. The convergence curves for FNN with $S = 5, 9, 13,$ and 30 are shown in Figures 4(a)–(d). These results show that FNNPSOGSA seems to have the best FNN convergence rate.

5.3. Comparison with Other Techniques through Standard Classification Datasets. Many experiments were conducted in order to connect the results of the GSADMSPSO technique with that of the GSA, GG-GSA, and GSADMSPSO methods, and Table 4 shows the PSO-GSA feature selection techniques and outcomes in terms of averages, bests, and standard deviations. According to a t -test with a significance level of 5%, the bold values in the tables represent the best practicable solution for the difficulties.

On various datasets, Table 4 provides the average classification accuracy of the four methods. As shown in Table 4, in 12 datasets, the suggested approach achieves the highest classification accuracy. In terms of average classification accuracy, GG-GSA outperforms the other two datasets.

According to these findings, the suggested technique beats the competition in datasets with less input parameters. The suggested algorithm's improved exploration and exploitation capacity is the cause for its high performance. Figure 4 shows the convergence curves of different algorithms based on averages of MSE for all training samples over 30 independent runs in a 3-bit XOR problem.

The results show that the proposed method is very much successful in FNN training, because there is a balance between exploration and exploitation; this is the case. GSADMSPSO shows decent exploration since all search agents collaborate in updating a search agent's location. Because of the inherent social component of PSO, GSADMSPSO's exploitation is highly accurate, resulting in rapid convergence. GSADMSPSO can prevent local optima and improve search space convergence.

6. Conclusion

Many real-world issues can be solved using gravity-based search techniques. As a result, in this paper, a unique GSADMSPSO is suggested. Using GSA, PSO-GSA, GG-GSA, and GSADMSPSO, four novel training algorithms dubbed FNN-GSA, FNN-PSO-GSA, FNN-GG-GSA, and FNN-GSADMSPSO are introduced and examined in this paper. The benchmark tasks were 3-bit XOR, function, and 16 conventional categorization problems, and the results show that the suggested approach is quite successful in FNN training, because there is a decent trade-off between exploration and exploitation; this is the case. GSADMSPSO exhibits good exploration since all search agents collaborate in updating a search agent's location. Because of the inherent social component of PSO, GSADMSPSO's exploitation is highly accurate, resulting in rapid convergence. GSADMSPSO can prevent local optima and improve search space convergence.

Data Availability

Data will be provided on request.

Conflicts of Interest

The authors declare that they have no conflicts of interest.

References

- [1] F. B. Fitch, W. S. McCulloch, and P. Walter, "A logical calculus of the ideas immanent in nervous activity. Bulletin of mathematical biophysics," *Journal of Symbolic Logic* 9, vol. 5, no. 2, pp. 115–133, 1994.
- [2] G. Bebis and M. Georgiopoulos, "Feed-forward neural networks," *IEEE Potentials*, vol. 13, no. 4, pp. 27–31, 1994.
- [3] T. Kohonen, "The self-organizing map," *Proceedings of the IEEE*, vol. 78, no. 9, pp. 1464–1480, 1990.
- [4] J. Park and I. W. Sandberg, "Approximation and radial-basis-function networks," *Neural Computation*, vol. 5, no. 2, pp. 305–316, 1993.
- [5] G. Dorffner, "Neural networks for time series processing," *Neural Network World*, 1996.
- [6] S. Ghosh-Dastidar and H. Adeli, "Spiking neural networks," *International Journal of Neural Systems*, vol. 19, no. 4, pp. 295–308, 2009.
- [7] M. A. Khan, W. U. H. Abidi, M. A. Al Ghamdi et al., "Forecast the influenza pandemic using machine learning," *Computers, Materials and Continua*, vol. 66, no. 1, pp. 331–340, 2020.
- [8] W. U. H. Abidi, M. S. Daoud, B. Ihnaini et al., "Real-time skill bidding fraud detection empowered with fussed machine learning," *IEEE Access*, vol. 9, pp. 113612–113621, 2021.
- [9] R. Caruana and A. Niculescu-Mizil, "An empirical comparison of supervised learning algorithms," in *Proceedings of the 23rd international conference on Machine learning*, pp. 161–168, New York, 2006.
- [10] G. E. Hinton, T. J. Sejnowski, and T. A. Poggio, *Unsupervised Learning: Foundations of Neural Computation*, MIT Press, 1999.
- [11] B. Irie and S. Miyake, "Capabilities of Three-Layered Perceptrons," *IEEE International Conference on Neural Networks*, 1988, pp. 641–648, San Diego, CA, USA, 1988.
- [12] K. Hornik, M. Stinchcombe, and H. White, "Multilayer feed-forward networks are universal approximators," *Neural Networks*, vol. 2, no. 5, pp. 359–366, 1989.
- [13] D. R. Hush and B. G. Horne, "Progress in supervised neural networks," *IEEE Signal Processing Magazine*, vol. 10, no. 1, pp. 8–39, 1993.
- [14] H. Adeli and S. Hung, "An adaptive conjugate gradient learning algorithm for efficient training of neural networks," *Applied Mathematics and Computation*, vol. 62, no. 1, pp. 81–102, 1994.
- [15] J.-R. Zhang, J. Zhang, T.-M. Lok, and M. R. Lyu, "A hybrid particle swarm optimization-back-propagation algorithm for feedforward neural network training," *Applied Mathematics and Computation*, vol. 185, no. 2, pp. 1026–1037, 2007.
- [16] D. Shaw and W. Kinsner, "Chaotic simulated annealing in multilayer feedforward networks," in *Electrical and Computer Engineering, Canadian Conference on 1996*, pp. 265–269, Calgary, AB, Canada, 1996.

Retraction

Retracted: Therapeutic Significance of Serpina3n Subsequent Cerebral Ischemia via Cytotoxic Granzyme B Inactivation

BioMed Research International

Received 12 March 2024; Accepted 12 March 2024; Published 20 March 2024

Copyright © 2024 BioMed Research International. This is an open access article distributed under the Creative Commons Attribution License, which permits unrestricted use, distribution, and reproduction in any medium, provided the original work is properly cited.

This article has been retracted by Hindawi following an investigation undertaken by the publisher [1]. This investigation has uncovered evidence of one or more of the following indicators of systematic manipulation of the publication process:

- (1) Discrepancies in scope
- (2) Discrepancies in the description of the research reported
- (3) Discrepancies between the availability of data and the research described
- (4) Inappropriate citations
- (5) Incoherent, meaningless and/or irrelevant content included in the article
- (6) Manipulated or compromised peer review

The presence of these indicators undermines our confidence in the integrity of the article's content and we cannot, therefore, vouch for its reliability. Please note that this notice is intended solely to alert readers that the content of this article is unreliable. We have not investigated whether authors were aware of or involved in the systematic manipulation of the publication process.

Wiley and Hindawi regrets that the usual quality checks did not identify these issues before publication and have since put additional measures in place to safeguard research integrity.

We wish to credit our own Research Integrity and Research Publishing teams and anonymous and named external researchers and research integrity experts for contributing to this investigation.

The corresponding author, as the representative of all authors, has been given the opportunity to register their agreement or disagreement to this retraction. We have kept a record of any response received.

References

- [1] M. S. Aslam, M. S. Aslam, K. S. Aslam, A. Iqbal, and L. Yuan, "Therapeutic Significance of Serpina3n Subsequent Cerebral Ischemia via Cytotoxic Granzyme B Inactivation," *BioMed Research International*, vol. 2022, Article ID 1557010, 13 pages, 2022.

Research Article

Therapeutical Significance of Serpina3n Subsequent Cerebral Ischemia via Cytotoxic Granzyme B Inactivation

Mehwish Saba Aslam ¹, Mobeena Saba Aslam ², Komal Saba Aslam,³ Asia Iqbal,⁴ and Liudi Yuan ^{1,5}

¹Department of Microbiology and Immunology, Medical School of Southeast University, Nanjing, China

²Department of Pharmacology, Poonch Medical College, Rawalakot Azad Jammu & Kashmir, Pakistan

³Department of Pathology, Gandhara University, Peshawar, Pakistan

⁴Department of Wildlife and Ecology, University of Veterinary and Animal Sciences, Lahore, Pakistan

⁵Department of Biochemistry and Molecular Biology, Medical School of Southeast University, Key Laboratory for Developmental Genes and Human Disease, Ministry of Education, Institute of Life Sciences, Southeast University, Nanjing, China

Correspondence should be addressed to Mehwish Saba Aslam; mehwishesaba19@outlook.com, Mobeena Saba Aslam; mobeena2050@gmail.com, and Liudi Yuan; yid@seu.edu.cn

Received 25 February 2022; Accepted 16 April 2022; Published 29 May 2022

Academic Editor: Cai Mei Zheng

Copyright © 2022 Mehwish Saba Aslam et al. This is an open access article distributed under the Creative Commons Attribution License, which permits unrestricted use, distribution, and reproduction in any medium, provided the original work is properly cited.

Ischemic stroke is a devastating CNS insult with few clinical cures. Poor understanding of underlying mechanistic network is the primary limitation to develop novel curative therapies. Extracellular accumulation of granzyme B subsequent ischemia promotes neurodegeneration. Inhibition of granzyme B can be one of the potent strategies to mitigate neuronal damage. In present study, we investigated the effect of murine Serpina3n and human (homolog) SERPINA3 against cerebral ischemia through granzyme B inactivation. Recombinant Serpina3n/SERPINA3 were expressed by transfected 293 T cells, and eluted proteins were examined for postischemic influence both *in vitro* and *in vivo*. During *in vitro* test, Serpina3n was found effective enough to inhibit granzyme B, while SERPINA3 was ineffectual to counter cytotoxic protease. Treatment of hypoxic culture with recombinant Serpina3n/SERPINA3 significantly increased cell viability in dosage-dependent manner, recorded maximum at the highest concentration (4 mM). Infarct volume analysis confirmed that 50 mg/kg dosage of exogenous Serpina3n was adequate to reduce disease severity, while SERPINA3 lacked behind in analeptic effect. Immunohistochemical test, western blot analysis, and protease activity assay's results illustrated successful diffusion of applied protein to the ischemic lesion and reactivity with the target protease. Taken together, our findings demonstrate therapeutic potential of Serpina3n by interfering granzyme B-mediated neuronal death subsequent cerebral ischemia.

1. Introduction

Ischemic stroke is a pathological state accounting 80,000 victims/year across the globe [1] with limited effective therapeutical approaches for functional restrain [2]. Regardless of constant efforts to develop alternative drugs, tissue plasminogen activator (tPA) is the only available FDA-approved clinical treatment against ischemia [3]. Major obstacles in finding novel effective therapeutics have been intricate responses of surveillance mechanisms and their complexed interactivities. This multifaceted pathophysiol-

ogy involves stimulation of numerous immune responses that leads to neuroinflammation with heterogenous forms of neuronal death [4]. One of the factors with detrimental effect is secretion of proteases subsequent ischemia [5, 6]. Among proteases, granzyme B is a prime proapoptotic acid hydrolase released by cytotoxic T-lymphocytes at the lesion site that initiates neuronal demyelination by activating caspases and other apoptotic progenitor protein molecules [7–11]. Inhibition of granzyme B can be one of the possible approaches to reduce clinical severity and therefore serves research requisite.

Serpina3n is a ~44-55 kDa murine serine protease inhibitor which shares 61% homology with human ortholog SERPINA3 [12] and exhibits wide range of target proteases [13, 14]. Specie-specific Serpina3n/SERPINA3 performs important physiological roles during both quiescent and pathological states by inhibiting attributed proteases [15]. Reported functions of Serpina3n/SERPINA3 during various pathologies especially during CNS calamities have made them emerging aspirations for research studies [16, 17]. Upregulated expression of Serpina3n (by reactive astrocytes [18] or neurons [19]) during CNS (central nervous system) insults reduces neuronal damage by protease inhibition [17] and has been proposed as a biomarker of astrogliosis [18], while SERPINA3 still needs validation for such scenario. Serpina3n has a special affinity for granzyme B and is believed to be the only known extracellular inhibitor of granzyme B till date, while its analog SERPINA3 is unable to counter granzyme B [20]. Owing to the inhibitory and anti-inflammatory properties of Serpina3n during CNS pathologies and taking SERPINA3 as a counterpart, in the current study, we attempted to investigate the following:

- (i) Potential therapeutical function of Serpina3n subsequent ischemic stroke via granzyme B inactivation
- (ii) Postischemic effect of SERPINA3
- (iii) Brief comparison between therapeutical efficacy of Serpina3n and SERPINA3 against ischemia
- (iv) Delivery of the exogenous protein to the lesion site
- (v) Immunoreactivity of the applied proteins

2. Materials and Methods

2.1. Materials and Reagents. Lentivirus plasmids, empty backbone of pLenti CMV Blast DEST (plasmid #17451) addgene, pLenti CMV Puro DEST (plasmid #17452) addgene, psPAX2, pMD2.G, 293 T cells, N2A cells, XL 1 E. Coli, DMEM (Gibco), FBS (BioExcell), Blastidine (Invivogen company), puromycin (Invivogen company), prestained marker (Yeaseen), streptomycin/penicillin solution (Gibco), anti-rabbit granzyme B (Abcam, cat. No. ab53097), anti-goat GFAP (Abcam, cat. No. ab53554), anti-hamster Serpina3n (Merck cat. No. MABC1182), anti-chicken MAP-2 (Abcam cat. No. ab5392), Hoechst 33258 (Sigma-Aldrich cat. No. 14530), anti-mouse 6his-tag (Proteintech, cat. No. 66005-1-Ig), anti-rabbit C-Myc (Proteintech, cat. No. 10828-1-AP), glucose oxidase (Sigma, cat. No. G7141), and catalase (Sangon, cat. No. A001847). Cell culture plates (Nest Biotechnology Co., Ltd.). Human granzyme B gene sequences were stored in our laboratory (EC:3.4.21.79).

2.2. Gene Amplification and Construction of Vector. Transfer vectors were constructed by inserting gene of interest using pLenti CMV Blast plasmid backbone and packaged as previously described [21, 22]. Briefly, Serpina3n (Accession no: NM_009252.2) and SERPINA3 (Accession no: NM_001085.5) genes were amplified with listed primers under following conditions (Table 1).

Lentiviral transfer vectors carrying genes of interest, i.e., SERPINA3 and Serpina3n, with reporter peptide sequences (c-Myc, 6-histidine, and mluc2) driven by CMV promoter were constructed and multiplied by ampicillin resistant XL1 E. Coli (Table 2). Successful plasmid construction was analyzed and confirmed by double enzyme digestion and direct DNA sequencing.

2.3. Transfection of 293 T Cells. Lentiviral preparations were used to get stable expression of recombinant proteins by human embryonic kidney derived 293 T cells [23]. Briefly, 6-well plate was seeded with $\sim 0.3 \times 10^6$ 293 T cells in glucose-rich DMEM+10% FBS supplemented with penicillin and streptomycin followed by incubation at 37°C with 5% CO₂ for 18 hrs or till 60-70% confluency. Lentiviral transfection mix was prepared using PEI transfection reagent (1 mg/ml), transfection buffer (15 mM NaCl), transformed vector, and packaging system psPAX2 and pMD2.G in 1:2:1, respectively, and incubated at room temperature for 30 mins. The suspension was mixed by pipetting and gently added dropwise to 293 T cells and plate was returned to incubator. 48 hrs posttransfection, 70% confluence was confirmed through green-polarized microscopy, and cell media were replaced with fresh complete growth media supplemented with Blastidine (selection marker 1:1000) followed by incubation at 37°C and 5% CO₂.

2.4. Selection and Propagation of Recombinant Clone. To get consistent expression of recombinant proteins and to rule out any ambiguity in future experiments, single stable clone for each recombinant protein, i.e., Serpina3n/SERPINA3, was selected. After 4 days, transfected cells were trypsinized (0.05% trypsin-EDTA) and diluted in Blastidine-supplemented growth media to inoculate ~ 50 cells/well in 96-well plate. Plates were incubated at 37°C with 5% CO₂ till the survived cells colonized large enough. Transformants were stored in liquid nitrogen as master stocks.

2.5. Protein Purification. For large-scale protein expression, selected clones of Serpina3n and SERPINA3 were propagated by inoculating about 2.2×10^6 cells in complete growth media plus Blastidine (1:1000) per 100 mm plate at 37°C and 5% CO₂. Collected supernatants were dialyzed through cellulose dialysis tube at 4°C with two exchanges of 1XPBS after 8-10 hrs. Later, expressed proteins were purified in two steps.

- (i) Purification: 400 ml of dialyzed supernatants was centrifuged at 12000 rpm, 4°C for 15 mins to remove traces of cellular debris, and loaded onto preequilibrated Ni-NTA column followed by washing with 250 ml of 10 mM imidazole and eluted with 25 ml of 250 mM imidazole
- (ii) Enrichment: eluted part was ultrafiltered by centrifugation at 14000 rpm, 4°C for 30mins with exchange of imidazole to 1XPBS. Obtained protein samples were analyzed through western blots probed with 6-histidine, Serpina3n, and c-Myc primary antibodies

TABLE 1

| Specie | Common name | Primer sequences (5'-3') | Genomic amplicon size (bp) |
|--------|-------------|--|----------------------------|
| Murine | Serpina3n | Forward primer: 5'ttaaccggtgccaccatggccttcacgcagctctggg3' Reverse primer: 5'ttatagccaagatagccaacccaaagctagcgct3' | 1254 |
| Human | SERPINA3 | Forward primer: 5'ttaaccggtgccaccatggagagaatgttacctctct3' Reverse primer: 5'tgagcaaagtcaccaatccaagcaagccgctagcgct3' | 1269 |

TABLE 2

| Cycle step | Temperature | Time | Cycles |
|----------------------|-------------|--------|--------|
| Initial denaturation | 94°C | 15 sec | 1 |
| Denaturation | 94°C | 15 sec | |
| Annealing | 55°C | 60 sec | 40 |
| Extension | 70°C | 40 sec | |
| Final extension | 70°C | 30 sec | |
| Hold | 4°C | ∞ | 1 |

3. In Vitro Studies

3.1. Cell Culture and Maintenance of Cell Line. Mouse neuroblastoma cells (N2A) were defrosted, cultured, and maintained using DMEM supplemented with 10% FBS, 1% penicillin/streptomycin solution at 37°C with 5% CO₂, and 95% air. Upon confluency, the cells were trypsinized and re-plated.

3.2. In Vitro Ischemic Model. Enzymatic ischemia/reperfusion was introduced to the cultured cells as described earlier [24]. Briefly, N2A cells were seeded in 96-well plate at about 10⁴ cells/100 μl/well in normal growth media and incubated till 70-80% confluency. Hypoxic media was prepared by diluting stock solutions of glucose oxidase (50 mM sodium acetate buffer, pH = 5.1) and catalase (50 mM Tris-HCL buffer, pH = 7 – 8) in glucose free DMEM at a constant ratio of 10:1 supplemented with (5 mM) 2-deoxyglucose to get uniform 2% oxygen concentration at cell surface. Upon confluency, hypoxia was introduced to test groups by incubating cells with hypoxic media for 4 hrs at 37°C and 5% CO₂, while in negative control, media were replaced with fresh media (4 replicates/group). Reperfusion was introduced for 3 hrs by replacing hypoxic media with normal growth media supplemented with different concentrations of recombinant Serpina3n and SERPINA3 proteins, i.e., 1 mM, 2 mM, 3 mM, and 4 mM, while positive control was supplied with complete growth media only. Cell viability was measured by adding CCK8 10 μl/well, and absorbance was measured at 450 nm by microplate reader.

3.3. Generation of Granzyme B Transformants. Lentiviral transfection method was used to get stable expression of human granzyme B by 293 T cells [22, 23]. Briefly, 6-well plate was inoculated with ~0.3 × 10⁶ cells in glucose-rich media and placed in incubator for 18 hrs. Lentiviral transfection mix containing PEI (1 mg/ml), transfection buffer (15 mM NaCl), transformed vector (pLenti CMV puro DEST), and packaging system psPAX2 and pMD2.G were

mixed in 1:2:1 proportion and left at room temperature for half an hour. The suspension was thoroughly mixed and used to transfect 293 T cells. After 48 hrs, transfection efficiency was confirmed by RFP (red fluorescent protein), and media were replaced with fresh complete media supplemented with puromycin (selection marker 1:5000) to screen transformed cells. The expression of the screened clone was confirmed by immunoblot probed with reporter 6-histidine and granzyme B primary antibodies. Transformants were stored in liquid nitrogen as master stocks.

3.4. Fluorometric Granzyme B Activity Assay. For the protease activity assay, 96-well plate was seeded with granzyme B transformants ~10⁴ cells/well [25]. Upon 80-90% confluency, the media were decanted and cells were incubated with reaction mix containing two different concentrations, either 1 mM or 2 mM of Serpina3n and SERPINA3 in a reaction buffer (50 mM HEPES, 10% sucrose, 0.1% CHAPS, and 5 mM DTT) to the total volume of 50 μl/well for 1 hr at 37°C. To assess inhibition of granzyme B, colorimetric substrate acetyl (Ac)-IEPD-p-nitroaniline (pNA) (Sigma) 200 μM final concentration in a reaction buffer 20 μl/well was incubated with test groups for 30 mins. The substrate cleavage was measured at 405 nm.

4. In Vivo Studies

4.1. Animals. All animal experiments were performed according to the guidelines issued by the Institutional Ethics Committee of Southeast University, Nanjing, China, and National Institutes of Health Guide for the Care and Use of Laboratory Animals (NIH Publications No. 8023, revised 1978). Animals were housed in cages at constant room temperature of 25°C-26°C with free access to food and water.

4.2. Photothrombotic Stroke Model. Photothrombotic stroke model was produced by the photoillumination of preinjected photosensitive dye Rose Bengal [26]. Briefly, C57BL/6 mice weighing 20-25 g were anesthetized with 1% pentobarbital intraperitoneal injection (75 mg/kg) and placed on stereotaxic frame supplied with DC temperature control module to maintain body's temperature at 37°C throughout the experiment. Toes were gently pinched to ensure deep anesthesia. The skull hair was removed with hair removal cream and area was sterilized with 70% ethanol. A small cranial window of about 2-3 mm was made by incising skin along midline of the skull, and skin retractors were used to keep the scalp exposed. Eye gel was applied and 1% Rose Bengal was injected subcutaneously at the scruff of the neck

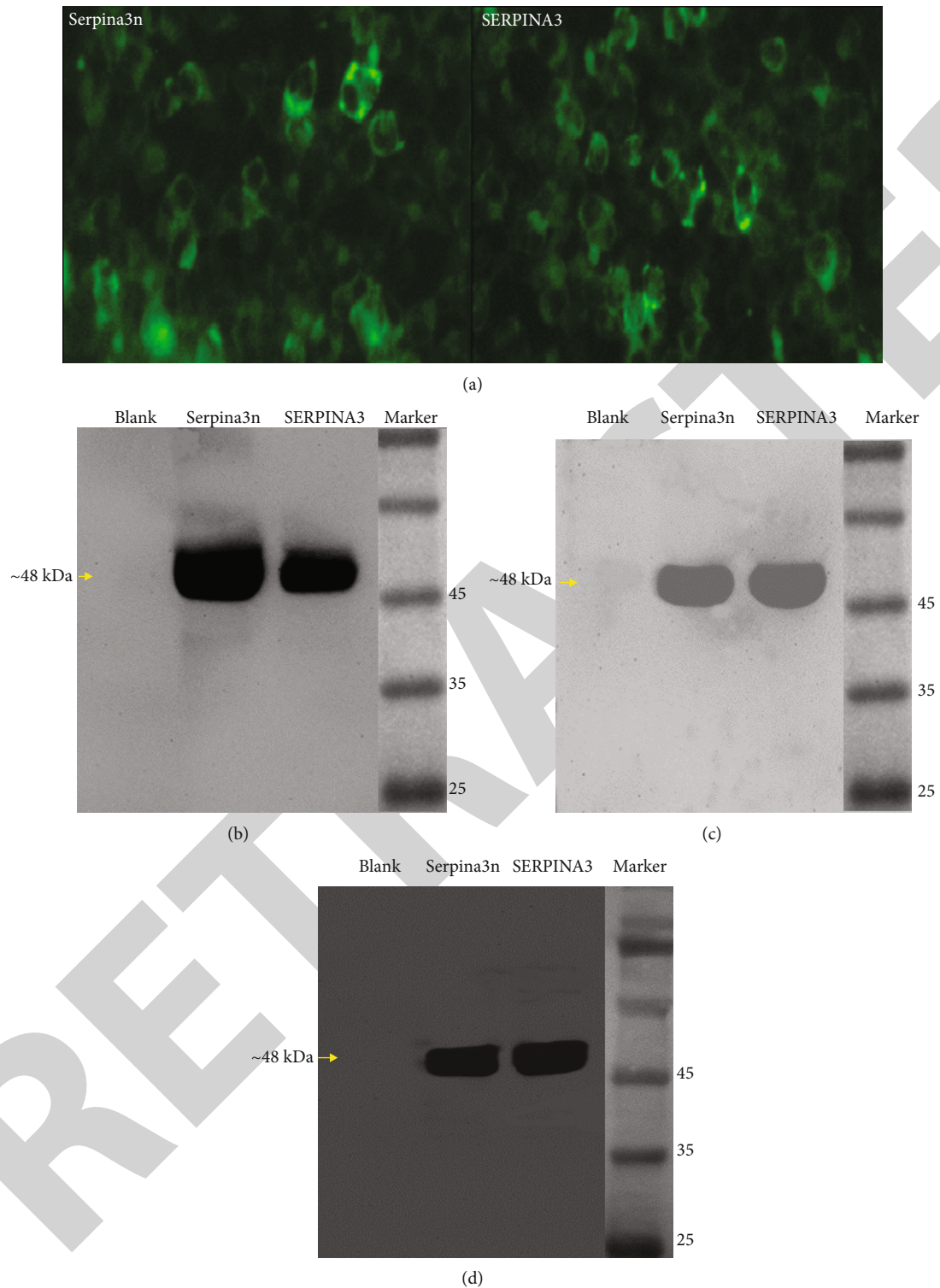


FIGURE 1: Expression of Serpina3n and SERPINA3 confirmed through (a) green fluorescence by 293 T cells. (b) Immunoblot probed with reporter 6-histidine displaying band ~48 kDa. (c) Reprobed with Serpina3n antibody representing similar band weight ~48 kDa. (d) Reporter c-Myc marked similar band size ~48 kDa.

followed by right parietal cortex exposure to 532 nm laser beam (50 mW) for 20-30 mins to induce focal ischemia. Ischemia induction procedure remained the same for all animal experiments except *in vivo* treatment test.

4.3. *Triple Immunofluorescence*. In order to investigate post-ischemic endogenous upregulated expression of Serpina3n specifically at focal region and its probable secretory source, photothrombotic stroke models were randomly assigned to

3 groups ($n = 3/\text{group}$) tagged with postischemic euthanasia time points, i.e., 24 hrs, 48 hrs, and 72 hrs [27]. Ischemic mice were sacrificed at 3 different time points 24 hrs, 48 hrs, and 72 hrs. 25 μm thick brain coronal sections derived from each cohort were stained with cocktail of primary antibodies, i.e., anti-chicken MAP-2 (1:250), anti-goat GFAP (1:1000), anti-hamster Serpina3n (1:500), and Hoechst (1:1000). Images were photographed through confocal microscope and processed by ImageJ software.

4.4. In Vivo Serpinas Treatments. Reversible MCA occlusion surgery was performed as previously described [28]. Briefly, mice were anesthetized with 4% isoflurane and maintained at 2%. Body temperature was maintained at $37^\circ\text{C} \pm 0.5^\circ\text{C}$ by employing heating pad throughout the surgery. Through midline incision on the neck, right common carotid artery (CCA), right external carotid artery (ECA), and right internal carotid artery (ICA) were exposed. A 3-0 silicon coated suture was advanced into the ICA till it hit the opening of MCA. After 60 mins of occlusion, monofilament was withdrawn. Incisions were closed and mice were maintained at 37°C . Ischemic mice were randomly assigned to 3 treatment groups, designated as ischemic-untreated group, Serpina3n-treated group, and SERPINA3-treated group ($n = 6/\text{group}$). Healthy mice were included as control group. After 2 hrs of stroke induction, testing cohorts were administered with either 50 mg/kg of Serpina3n or 50 mg/kg of SERPINA3 via tail vein. Ischemic-untreated group was given purified supernatants of nontransfected 293 T cells. After treatment, animals were caged with sufficient food and water for recovery.

4.5. Neurobehavioral Deficits. 24 hrs posttreatment, neurological scores were assigned on a scale of 0 to 5 [29]: normal (0), difficulty in extending forelimb (1), unable to extend forelimb (2), mild circling (3), severe circling (4), and falling on contralateral side (5).

For motor function examination, rotarod test was performed after 2-5 mins of neurodeficit scoring. Before surgery, mice were trained for 3 consecutive days. Treatment cohorts ($n = 6/\text{group}$) were placed on the rotarod with gradual increase of speed from 10 to 30 revolutions per minute (rpm) over 120 sec and latency to fall was recorded. The mean duration (in seconds) was recorded from 3 rotarod measurements and analyzed by comparison.

4.6. Brain Infarct Analysis. After neurobehavioral testing, brains were harvested and sliced into 2 mm thick sections. The sections were stained with 2% TTC at 37°C for 30 mins. Viable brain tissue appeared brick red, whereas infarct portion remained unstained and appeared as white. ImageJ software was used by blind observer to calculate the infarction volume by processing the images of stained sections.

4.7. Immunoreactivity and Histochemical Detection of Recombinant Protein. After *in vivo* treatment, it was necessary to confirm delivery and immunoreactivity of applied protein specifically at focal area [30]. To assess *in vivo* reactivity 24 hrs posttreatment, brains from Serpina3n-treated and ischemic-untreated groups ($n = 3/\text{group}$) were harvested on ice and washed with chilled 1XPBS followed by dissection

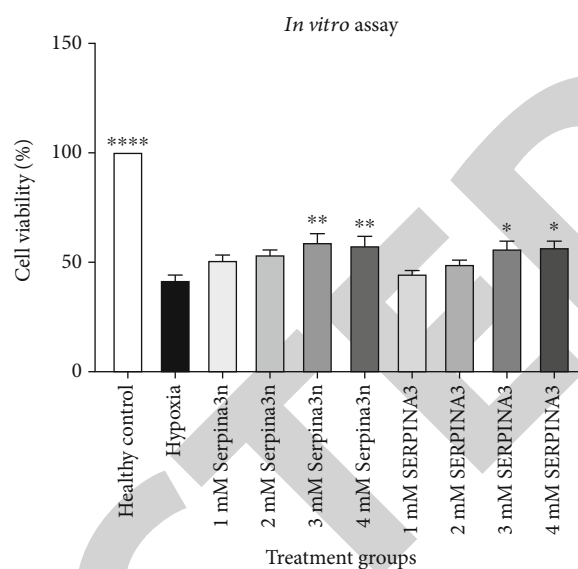


FIGURE 2: Effect of Serpina3n and SERPINA3 on viability of N2A cells. The data is expressed as percentage and analyzed for statistical significance using one-way ANOVA with Bonferroni post hoc test with $P < 0.05$ as significant value (* $P < 0.05$, ** $P < 0.01$, *** $P < 0.001$, and **** $P < 0.0001$ vs. hypoxic group).

into six equal parts. Each tissue chunk was aliquoted in 500 μl of lysis buffer (0.1 M EDTA, 0.5% (w/v) SDS, and 10 mM Tris-Cl (pH 8.0)) containing protease inhibitors and lysed mechanically with tissue homogenizer on ice. The lysates were centrifuged at 12000 rpm, 4°C for 20 mins. The supernatants were collected and analyzed by western blot probed with reporter c-Myc and granzyme B primary antibodies. In order to investigate inhibition of granzyme B in lysates, 50 μl aliquots of lysed supernatants from Serpina3n-treated and ischemic-untreated group were incubated with 200 μM final concentration of granzyme B fluorometric substrate acetyl (Ac)-IEPD-p-nitroaniline for 0.5 hr at 37°C . The substrate cleavage was measured at 405 nm. Moreover, for the detection of exogenous protein at lesion, 20 μm thick cryosections (~ 10 sections/animal) derived from Serpina3n-treated, ischemic-untreated, and healthy cohorts were stained with mix of anti-rabbit c-Myc (1:800) and anti-hamster Serpina3n (1:500) at 4°C . Fluorescent images were obtained using confocal microscope and processed by ImageJ.

5. Statistical Analysis

Statistical data is presented as mean \pm SEM. Two-way ANOVA analysis followed by Bonferroni post hoc test or Tukey's multiple comparisons test was performed for statistical differences among groups. $P < 0.05$ was set as significant difference in all cases.

6. Results

6.1. Recombinant Serpina3n and SERPINA3 Protein Expression and Purification. Cell supernatants containing Serpina3n and SERPINA3 were collected and purified. The

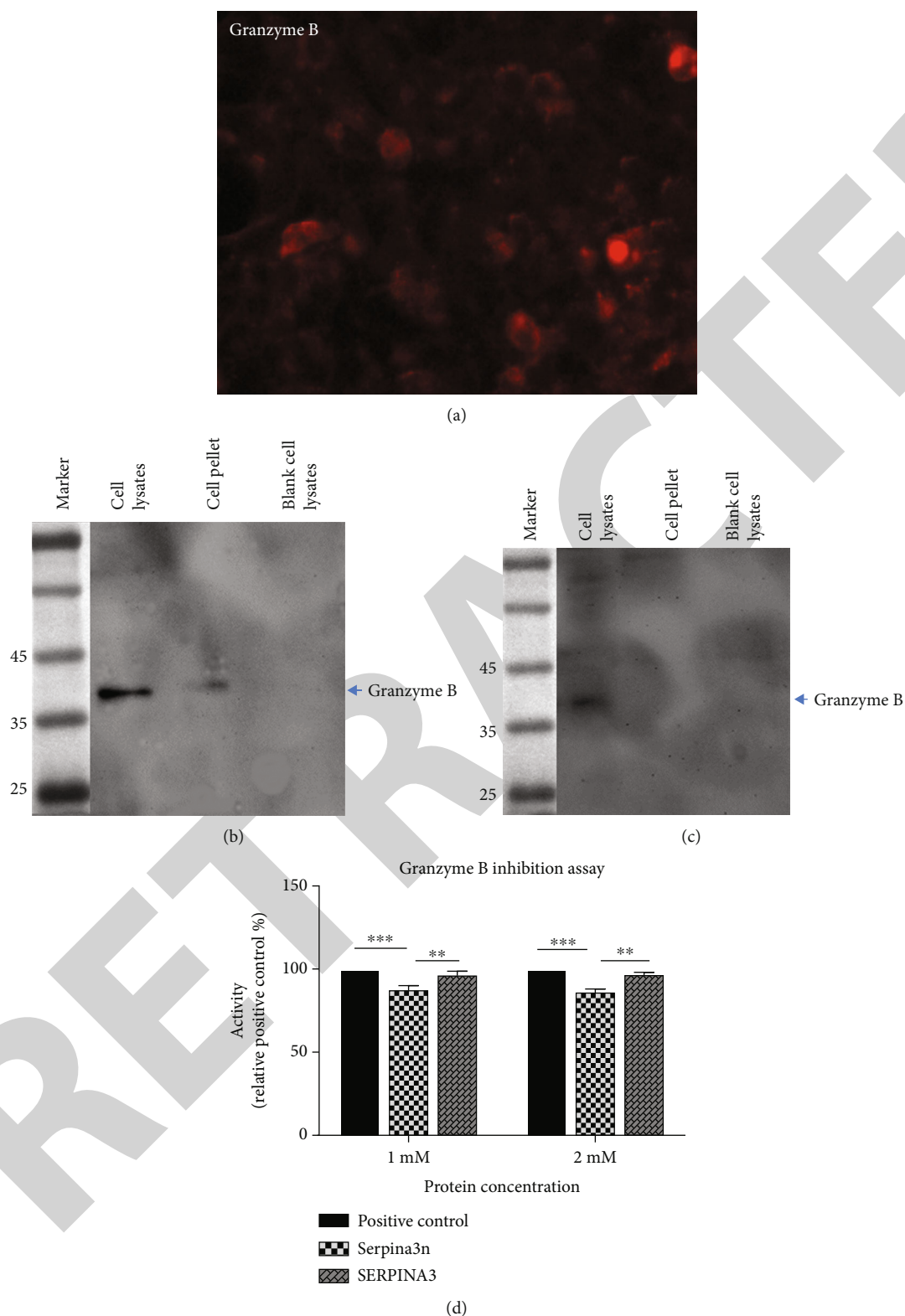


FIGURE 3: Expression of granzyme B was confirmed through (a) RFP by 293 T cells. (b) Immunoblot of cell lysates probed with granzyme B ~37 kDa. (c) Reprobed with 6-histidine reporter peptide representing same band weight ~37 kDa. (d) Fluorometric assay of granzyme B indicating significant inhibitory effect of Serpina3n *in vitro* at different concentrations. The data is expressed as mean \pm SEM and analyzed for statistical significance using two-way ANOVA with Bonferroni post hoc test taking $P < 0.05$ as significant value (* $P < 0.05$, ** $P < 0.01$, *** $P < 0.001$, and **** $P < 0.0001$ vs. positive control).

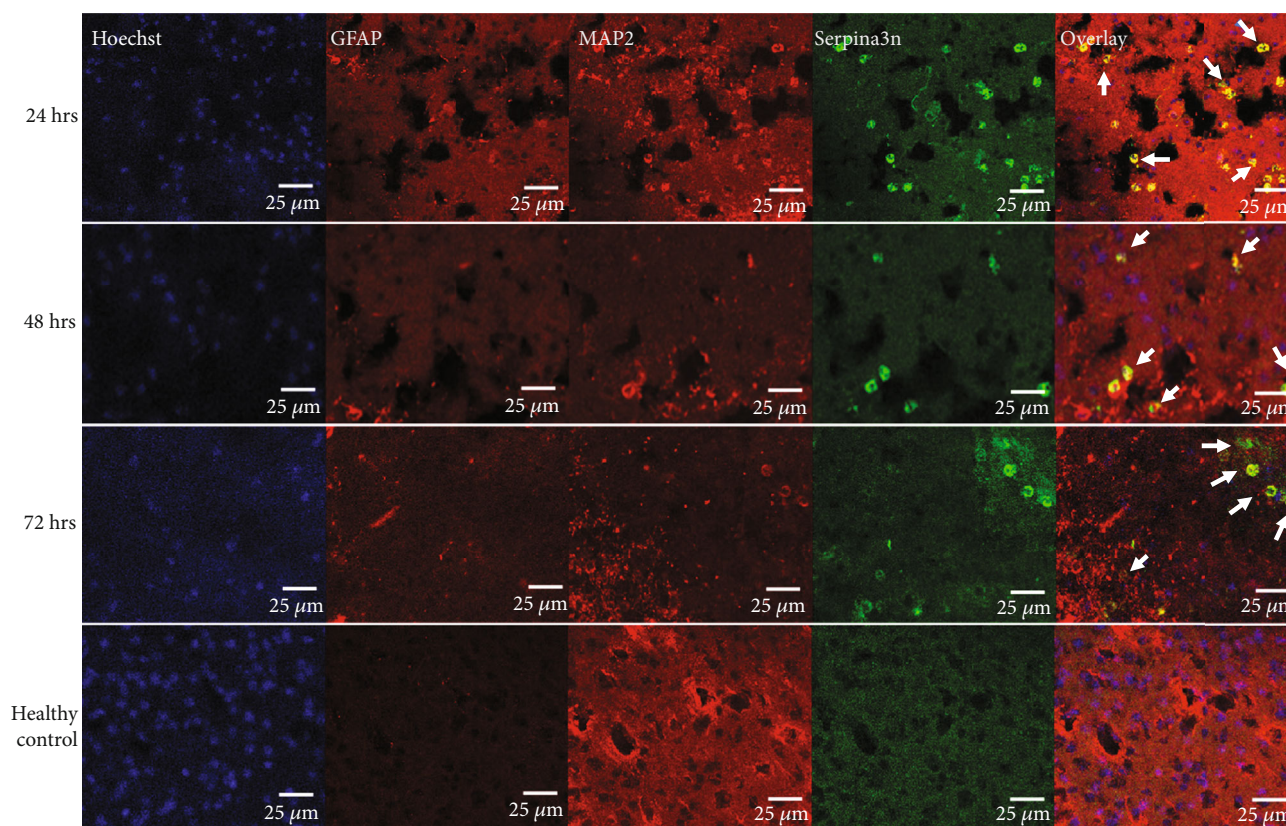


FIGURE 4: Triple immunohistochemical staining of postischemic brain sections collected at 3 time points 24 hrs, 48 hrs, and 72 hrs to observe the endogenous over expression of Serpina3n. Confocal images processed by ImageJ showing overlaid fluorescence of MAP-2 and Serpina3n reflecting neurons as the probable source of Serpina3n.

protein's expression was confirmed by immunoblot probed with 6-histidine, Serpina3n, and c-Myc primary antibodies, all displayed ~48 kDa band (Figure 1). Purified proteins were further used in *in vitro* and *in vivo* experiments to assess proposed therapeutical efficacy during cerebral infarction.

6.2. Reduction in Neuronal Death In Vitro. Ischemia is associated with oxygen and glucose deprivation that destroys physiological balance between crucial cellular mechanics triggering apoptotic phenotypes, so we asked whether Serpina3n/SERPINA3 can improve cell survival against it. Post-hypoxia significant difference was observed in cell viability between the treated and untreated groups. The survived cells were significantly higher in wells containing higher concentrations of Serpina3n or SERPINA3 as compared to the positive control indicating therapeutical effect of recombinant proteins in pseudo stroke model. However, different concentrations of SERPINA3 did not show as much increase in cell viability as observed in the groups treated with Serpina3n (Figure 2).

6.3. Inhibition of Granzyme B by Recombinant Proteins. Expression of granzyme B by selected clone was confirmed by RFP and western blot probed with granzyme B and 6-histidine primary antibodies that displayed ~37 kDa band (Figure 3). In order to confirm Serpina3n-granzyme B reactivity, monolayer culture was used to analyze inhibition of

protease in extracellular microenvironment. Preincubation of transformed cells with exogenous Serpina3n effectively inhibited cleavage of colorimetric substrate, while SERPINA3 was not observed with any inhibitory effect against the protease (Figure 3).

6.4. Endogenous Overexpression of Murine Serpina3n and Triple Immunostaining. Postischemic upregulated expression of endogenous Serpina3n was confirmed by harvesting brains from photothrombotic mice at 3 different time points, i.e., 24 hrs, 48 hrs, and 72 hrs. Coronal sections were immunostained with cocktail of antibodies, GFAP, MAP-2, Serpina3n, and Hoechst. Serpina3n fluorescence was distinctly prominent at focal region of ischemic brain as compared to healthy brain (Figure 4). Our data showed colocalized fluorescence of Serpina3n and MAP-2 indicating that neurons secrete Serpina3n and contribute to Serpina3n concentration during traumatic injury under our experimental conditions.

6.5. Neurological Functions of Treated Mice. After 24 hrs of treatment, neurological scores and motor deficit readings were recorded and analyzed. Mice from ischemic-untreated batch demonstrated higher scores by exhibiting serious neurological impairments as compared to healthy and other treatment groups. Significant improvement in neurological functions was observed in the group administrated with Serpina3n.

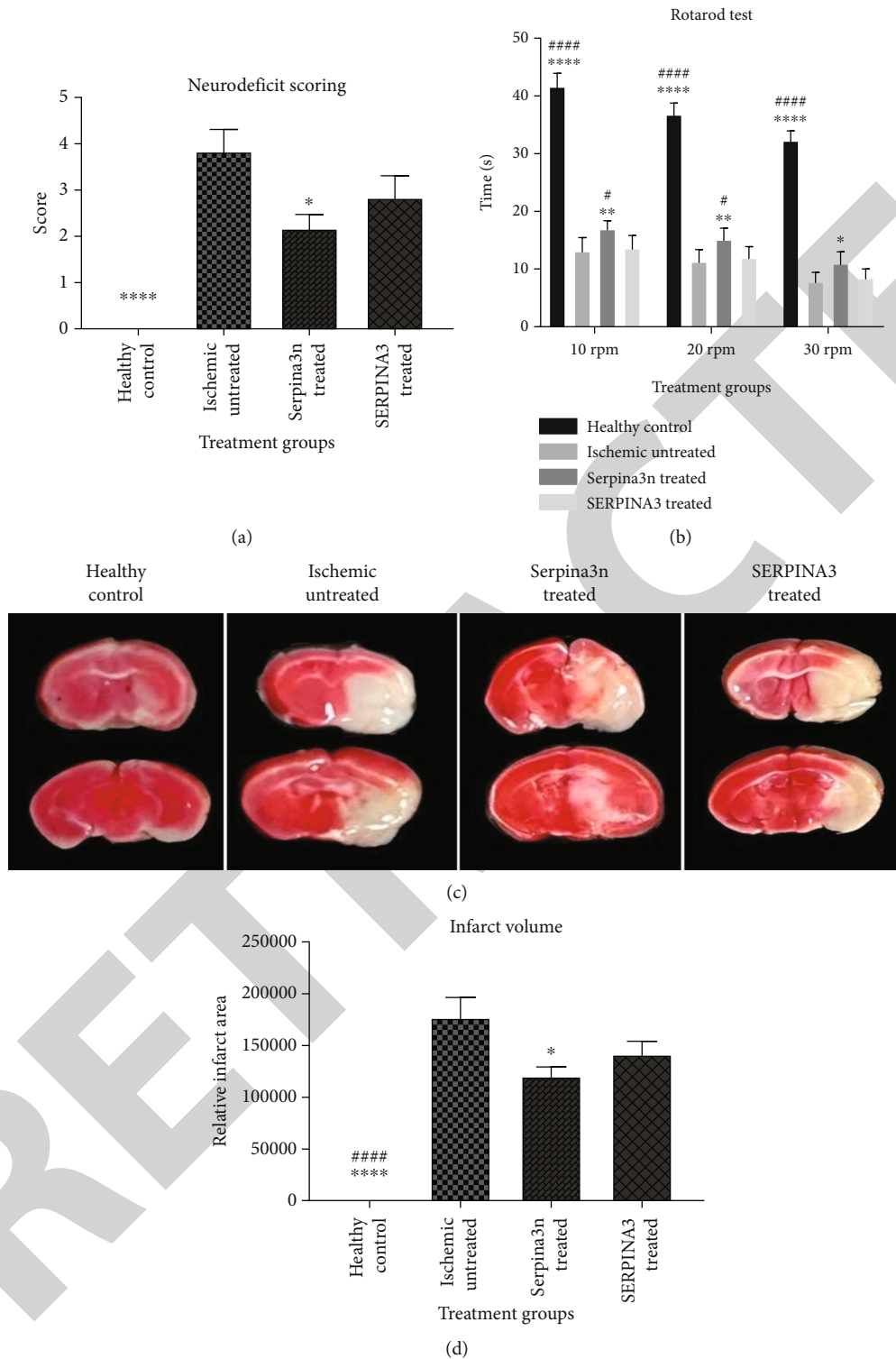
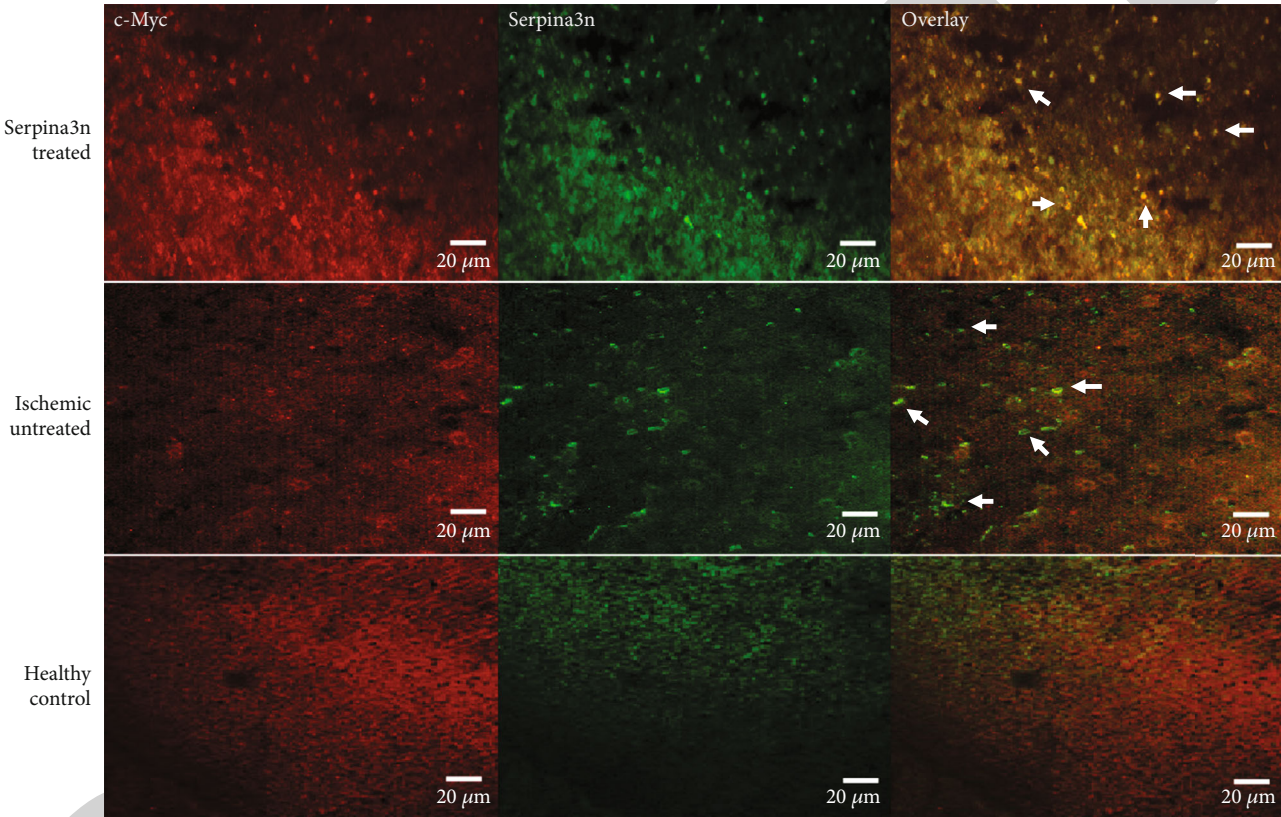
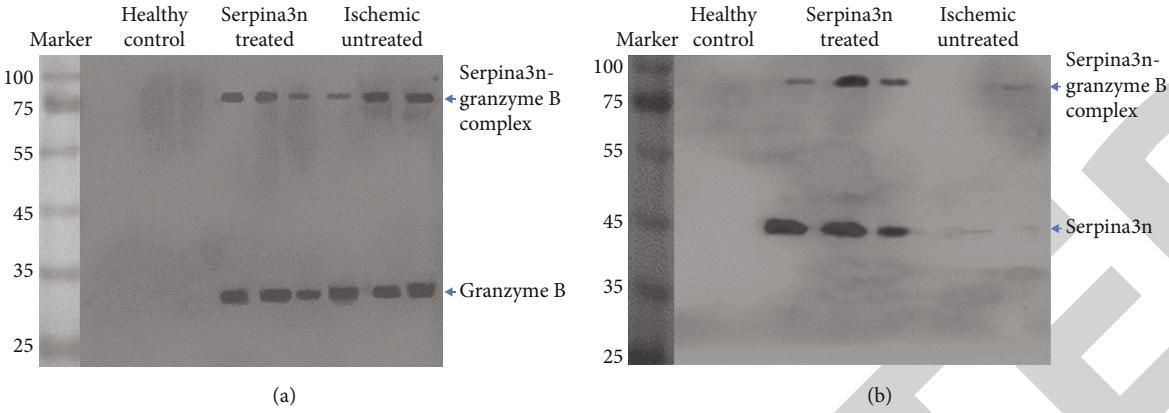


FIGURE 5: (a) Graph representing neurodeficit score between treatment groups. The data is expressed as mean \pm SEM and analyzed for statistical significance using two-way ANOVA with Bonferroni post hoc test (* $P < 0.05$, ** $P < 0.01$, *** $P < 0.001$, and **** $P < 0.0001$ vs. ischemic-untreated group). (b) Representative graph for time on rotarod by different treatment cohorts. Values expressed as mean \pm SEM analyzed by two-way ANOVA with Tukey's test for significant difference (* $P < 0.05$, ** $P < 0.01$, *** $P < 0.001$, and **** $P < 0.0001$ vs. ischemic-untreated group; # $P < 0.05$, ## $P < 0.01$, ### $P < 0.001$, and **** $P < 0.0001$ vs. SERPINA3-treated group). (c) TTC-stained coronal brain sections from different treatment groups showing infarction volume. (d) Graph representing comparative infarction area between different treatment cohorts. The data is expressed as mean \pm SEM and analyzed for statistical significance using one-way ANOVA with Tukey's multiple comparisons test (* $P < 0.05$, ** $P < 0.01$, *** $P < 0.001$, and **** $P < 0.0001$ vs. ischemic-untreated group; # $P < 0.05$, ## $P < 0.01$, ### $P < 0.001$, and **** $P < 0.0001$ vs. SERPINA3-treated group).



(c)
FIGURE 6: Continued.

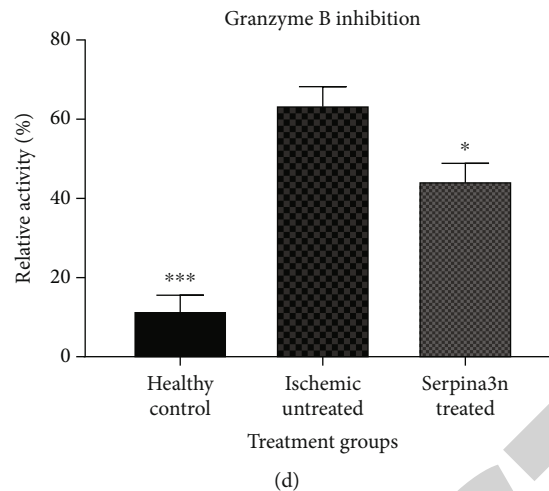


FIGURE 6: (a) Immunoblot of brain lysates probed with granzyme B marked bands at ~32 kDa and ~80 kDa representing endogenous granzyme B and Serpina3n-granzyme B complex, respectively. (b) Immunoblot probed with c-Myc exhibited bands at ~48 kDa and ~80 kDa representing recombinant Serpina3n and Serpina3n-granzyme B complex, respectively. (c) Delivery of exogenous proteins to the focal region was confirmed by extensive overlaid fluorescence of Serpina3n and reporter c-Myc among treatment group, while no such overlaid staining appeared in ischemic-untreated group. (d) Fluorometric assay of granzyme B with brain lysates derived from different treatment groups demonstrating significant inhibitory effect of Serpina3n *in vivo*. The data is expressed as mean \pm SEM and analyzed for statistical significance using two-way ANOVA with Bonferroni post hoc test taking $P < 0.05$ as significant value (* $P < 0.05$, ** $P < 0.01$, *** $P < 0.001$, and **** $P < 0.0001$ vs. ischemic untreated).

However, SERPINA3-treated mice did not show impressive improvement in comparison to ischemic-untreated animals.

During rotarod test, healthy and Serpina3n groups showed significantly longer retention time on rod as compared to ischemic-untreated and SERPINA3-treated mice. No significant difference in neurodeficit scores and retention time on rod was observed between Serpina3n- and SERPINA3-treated groups (Figure 5).

6.6. Brain Infarct Volume Analysis. After witnessing neuroprotective effect of recombinant proteins *in vitro*, we attempted to assess their therapeutical efficacy *in vivo*. TTC-stained brain sections derived from Serpina3n group showed significantly reduced infarct as compared to ischemic-untreated group. No significant difference was observed in infarct volume between Serpina3n- and SERPINA3-treated groups. (Figure 5).

6.7. Blood-Brain Barrier and Serpina3n-Granzyme B Reactivity. The immunoblot probed with c-Myc antibody contained bands of ~48 kDa (reflecting exogenous Serpina3n) and ~80 kDa (reflecting Serpina3n-granzyme B complex as calculated), while no such bands were observed for ischemic-untreated and healthy control. Second blot probed with granzyme B antibody exhibited bands at ~32 kDa (representing endogenous granzyme B) and ~80 kDa (representing Serpina3n-granzyme B complex) for both ischemic-untreated and Serpina3n-treated mice but not in healthy control as expected, demonstrating successful infiltration and reactivity of Serpina3n at lesion. Immunohistochemical analyses revealed colocalized staining of reporter c-Myc and Serpina3n among treated mice indicating successful diffusion of exogenous Serpina3n into focal region. Dense fluorescence of Serpina3n in treated group reflected the

presence of both applied and endogenous Serpina3n in treated mice. Fluorescence exhibited by ischemic untreated reflected postischemic innate response. Serpina3n and granzyme B reactivity was further confirmed by significantly reduced cleavage of colorimetric granzyme B substrate in lysates derived from Serpina3n-treated cohort as compared to ischemic-untreated group (Figure 6). This data suggested successful *in vivo* delivery and immunoreactivity of applied Serpina3n subsequent ischemia.

7. Discussion

In current times, keen efforts are devoted for developing new therapeutical strategies against ischemic stroke through mechanistic scrutiny of perplexed contributors [31]. Post-trauma protease-mediated neuronal apoptosis is one of the intrinsic contributing mechanisms [5, 11] which needs effective intervention to prevent disease advancement. Serpina3n and SERPINA3 are specie-specific serine protease inhibitors with a range of potent and practicing medical implications [32]. Serpina3n is an emerging protease inhibitor with an extensive literature reporting its potentialities during different pathologies [32] as compared to SERPINA3 that exhibits slightly limited functional exploration [33]. In present study, we attempted to investigate potential therapeutical efficacy of recombinant murine Serpina3n and its human isomer SERPINA3 against CNS stroke by specifically targeting a proapoptotic protease granzyme B, which is distinguishing target between the two [20] and also involved in neuronal demyelination during CNS insults [17].

Histochemical test was performed to confirm the endogenous upregulated expression of Serpina3n and to investigate the probable source of expression after traumatic injury.

Immunofluorescence findings confirmed postischemic-inflated expression of endogenous Serpina3n as reported earlier by Zamanian et al. [18]. Our data illustrated overlaid fluorescence of Serpina3n with MAP-2 instead of GFAP which is in coherence with the recent study reporting 79% neurons positive for Serpina3n after hippocampal injury [19]. Presumably in addition to neurons, astrocytes and oligodendrocytes might also contribute to the density of Serpina3n at lesion site. However, it needs further investigation and experimental proofs to validate the conflicting astrocytic or neuronal upregulated expression of Serpina3n.

In vitro enzymatic ischemia/reperfusion model was generated to study the effect of Serpina3n/SERPINA3 in monolayer culture. Findings demonstrated neuroprotective effect of Serpina3n and SERPINA3 on hypoxic cells with significantly pronounced cell viability at the highest concentration (4 mM). The key mechanism behind the neurorestorative behavior of Serpina3n in hypoxic culture might be due to an effective obstruction of apoptotic cascades followed by MMP-2 [19] and MMP-9 [34]. Serpina3n effectively impedes MMP-2 and MMP-9 to restore neuronal integrity. Neuroprotection induced by SERPINA3 was limited in comparison to Serpina3n, yet there was promising cell survival against positive control which opens a new door to investigate the probable mechanism.

Granzyme B retains 70% of its activities in plasma [35]. For that reason, upregulated protease levels subsequent ischemic injury become more pernicious [36]. Serpina3n is the only known secretory protease inhibitor that inactivates granzyme B by forming irreversible complex [37] and prevents proteolytic disruption. In order to investigate, whether Serpina3n/SERPINA3 inhibit cytotoxic protease granzyme B, purified proteins were incubated with granzyme B transformants. Results revealed that Serpina3n successfully inhibited granzyme B *in vitro* as indicated by the reduced cleavage of (Ac)-IEPD-p-nitroaniline, while SERPINA3 was unable to bind to granzyme B due to lack of substrate specificity. Resulting data was consistent with the previous reports signifying the critical role of RCL (reactive central loop) for proteolytic inactivation [20]. The inability of SERPINA3 to inhibit granzyme B might be due to amino acids present at P1, P3', and P4' positions of RCL, which have been identified as the most crucial loci to specify the target protease [15]. Additionally, difference in innate meta stable stressed state, cofactors, and glycosylation pattern might also be the contributing factors.

In order to address the postischemic role, *in vivo* study was performed using MCAO mice that underwent different treatments. As ischemic insult is associated with dementia, behavioral, and sensory-motor impairments, our neurological recordings revealed that a single intravenous dose (50 mg/kg) of Serpina3n was adequate to reduce clinical severity in ischemic mice. Analysis of infarct volume illustrated that SERPINA3 was lacking behind in curative effect. The prime reason behind pronounced therapeutical efficacy of Serpina3n can be its aptness to inhibit a wide range of serine proteases, i.e., MMP-2, MMP-9, leukocyte elastase, and granzyme B which contribute to the neuronal damage [11, 16, 19, 38, 39]. Postischemic-elevated granzyme B levels pro-

mote neuronal death not only through activation of cellular caspases, i.e., caspase-3, PARP, lamins, HSP-70, and Bid [10, 11], but also through a noikis [11, 40, 41]. In such case, Serpina3n treatment may prevent granzyme B-mediated neuronal degeneration in more than one way to reduce the ultimate damage of ischemia. On that account, it becomes essential to appraise the neuroprotective function of Serpina3n against neuronal degeneration during cerebral stroke.

In order to protect the brain from any relapse, the blood-brain barrier performs a unique service by becoming a major check point for all circulating entities and tightly regulating the exchange of diffusible materials [35, 42]. Most of the circulating molecules, cells, and potential risky substances do not succeed to infiltrate brain across highly selective semi-permeable border [36]. After witnessing the therapeutical efficacy of exogenous Serpina3n against ischemia, we aimed to confirm the successful delivery and immunoreactivity of applied protein at the injured region. For this purpose, we have performed western blot, immunohistochemical, and granzyme B activity tests with ischemic-treated and ischemic-untreated mice. Two immunoblots probed with different antibodies displayed a similar band of ~80 kDa. This band weight signified effective inhibition of granzyme B as well as successful diffusion of applied Serpina3n into the brain. Colocalized dense fluorescence of Serpina3n and c-Myc among treated group further validated the presence of exogenous Serpina3n at lesion site. Serpina3n fluorescence seen in ischemic-untreated group reflected postischemic overexpression of endogenous Serpina3n [18]. Granzyme B activity assay has shown reduced cleavage of calorimetric substrate in Serpina3n-treated group as compared to ischemic-untreated cohort indicating effective inhibition of granzyme B *in vivo*.

8. Concluding Remarks

In conclusion, inhibition of granzyme B by Serpina3n can be considered as one of the possible approaches to mitigate postischemic damage. This hypothesis was verified and supported by our experimental data. In present study, we have analyzed and confirmed postischemic neuroprotective role of recombinant Serpina3n both *in vivo* and *in vitro* by assuming granzyme B as target protease responsible for neuronal apoptosis [17]. However, the promising restorative effect of SERPINA3 in hypoxic culture was taken as a pleasant surprise which needs further studies to investigate complex underlying mechanisms and identification of involved elements intervening postischemic inflammation and neurodegeneration.

Data Availability

All experimental and analyzed data is included in the manuscript.

Conflicts of Interest

Authors declared no conflict of interest.

Authors' Contributions

Experiments were designed, conducted, and analyzed by Mehwish Saba Aslam accompanied by apt and fruitful discussions with Miss Liudi Yuan. Cerebral ischemia was induced and analyzed by Dr. Mobeena Saba Aslam along with the provision of necessary support and expert view for the experiments. Dr. Komal Saba Aslam participated in animal experiments and performed immunohistochemical tests. Asia Iqbal helped in data analysis. The manuscript was drafted by Mehwish Saba Aslam and reviewed by Miss Liudi Yuan.

Acknowledgments

We would like to thank Mr. Sheng Zhao (Southeast University, Nanjing) for providing necessary support at the initiation of the hypothesis. This work was supported by the Open Funds of the Key Laboratory for Developmental Genes and Human Disease, Ministry of Education, China (201801).

References

- [1] O. A. Sveinsson, O. Kjartansson, and E. M. Valdimarsson, "Cerebral ischemia/infarction - epidemiology, causes and symptoms," *Læknablaðið*, vol. 100, no. 5, pp. 271–279, 2014.
- [2] O. A. Sveinsson, O. Kjartansson, and E. M. Valdimarsson, "Cerebral ischemia/infarction - diagnosis and treatment," *Læknablaðið*, vol. 100, no. 7-8, pp. 393–401, 2014.
- [3] C. Ajmone-Marsan, "National Institute of Neurological Diseases and Stroke, National Institutes of Health: clinical neurophysiology and epilepsy in the first 25 years of its intramural program," *Journal of Clinical Neurophysiology*, vol. 12, no. 1, pp. 46–56, 1995.
- [4] J. Kriz, "Inflammation in ischemic brain injury: timing is important," *Critical Reviews in Neurobiology*, vol. 18, no. 1-2, pp. 145–157, 2006.
- [5] T. Yamashima, "Implication of cysteine proteases calpain, cathepsin and caspase in ischemic neuronal death of primates," *Progress in Neurobiology*, vol. 62, no. 3, pp. 273–295, 2000.
- [6] G. V. Chaitanya and P. P. Babu, "Activation of calpain, cathepsin-b and caspase-3 during transient focal cerebral ischemia in rat model," *Neurochemical Research*, vol. 33, no. 11, pp. 2178–2186, 2008.
- [7] A. Rensing-Ehl, U. Malipiero, M. Irmeler, J. Tschopp, D. Constam, and A. Fontana, "Neurons induced to express major histocompatibility complex class I antigen are killed via the perforin and not the Fas (APO-1/CD95) pathway," *European Journal of Immunology*, vol. 26, no. 9, pp. 2271–2274, 1996.
- [8] F. Giuliani, C. G. Goodyer, J. P. Antel, and V. W. Yong, "Vulnerability of human neurons to T cell-mediated cytotoxicity," *Journal of Immunology*, vol. 171, no. 1, pp. 368–379, 2003.
- [9] R. Nitsch, E. E. Pohl, A. Smorodchenko, C. Infante-Duarte, O. Aktas, and F. Zipp, "Direct impact of T cells on neurons revealed by two-photon microscopy in living brain tissue," *The Journal of Neuroscience*, vol. 24, no. 10, pp. 2458–2464, 2004.
- [10] J. A. Trapani, "Granzymes: a family of lymphocyte granule serine proteases," *Genome Biology*, vol. 2, no. 12, pp. 1–7, 2001.
- [11] G. V. Chaitanya, M. Schwaninger, J. S. Alexander, and P. P. Babu, "Granzyme-b is involved in mediating post-ischemic neuronal death during focal cerebral ischemia in rat model," *Neuroscience*, vol. 165, no. 4, pp. 1203–1216, 2010.
- [12] S. Forsyth, A. Horvath, and P. Coughlin, "A review and comparison of the murine alpha1-antitrypsin and alpha1-antichymotrypsin multigene clusters with the human clade A serpins," *Genomics*, vol. 81, no. 3, pp. 336–345, 2003.
- [13] C. Baker, O. Belbin, N. Kalsheker, and K. Morgan, "SERPINA3 (aka alpha-1-antichymotrypsin)," *Frontiers in Bioscience*, vol. 12, no. 8-12, pp. 2821–2835, 2007.
- [14] S. F. Forsyth, P. D. French, E. Macfarlane, S. E. Gibbons, and R. F. Miller, "The use of therapeutic drug monitoring in the management of protease inhibitor-related toxicity," *International Journal of STD & AIDS*, vol. 16, no. 2, pp. 139–141, 2005.
- [15] P. G. Gettins, "Serpins structure, mechanism, and function," *Chemical Reviews*, vol. 102, no. 12, pp. 4751–4804, 2002.
- [16] L. Vicuña, D. E. Storchlic, A. Latremoliere et al., "The serine protease inhibitor SerpinA3N attenuates neuropathic pain by inhibiting T cell-derived leukocyte elastase," *Nature Medicine*, vol. 21, no. 5, pp. 518–523, 2015.
- [17] Y. Haile, K. Carmine-Simmen, C. Olechowski, B. Kerr, R. C. Blackley, and F. Giuliani, "Granzyme B-inhibitor serpin3n induces neuroprotection In Vitro and In Vivo," *Journal of Neuroinflammation*, vol. 12, no. 1, p. 157, 2015.
- [18] J. L. Zamanian, L. Xu, L. C. Foo et al., "Genomic analysis of reactive astrogliosis," *The Journal of Neuroscience*, vol. 32, no. 18, pp. 6391–6410, 2012.
- [19] Z. M. Wang, C. Liu, Y. Y. Wang et al., "SerpinA3N deficiency deteriorates impairments of learning and memory in mice following hippocampal stab injury," *Cell Death Discovery*, vol. 6, no. 1, pp. 1–11, 2020.
- [20] S. Sipione, K. C. Simmen, S. J. Lord et al., "Identification of a novel human granzyme B inhibitor secreted by cultured sertoli cells," *Journal of Immunology*, vol. 177, no. 8, pp. 5051–5058, 2006.
- [21] M. Sena-Esteves and G. Gao, "Production of high-titer retrovirus and lentivirus vectors," *Cold Spring Harbor Protocols*, vol. 2018, no. 4, article pdb.prot095687, 2018.
- [22] A. Storck, J. Ludtke, L. Kopp, and L. Juckem, "Development and optimization of a high titer recombinant lentivirus system," *BioTechniques*, vol. 63, no. 3, pp. 136–138, 2017.
- [23] Y. Tang, K. Garson, L. I. Li, and B. C. Vanderhyden, "Optimization of lentiviral vector production using polyethylenimine-mediated transfection," *Oncology Letters*, vol. 9, no. 1, pp. 55–62, 2015.
- [24] G. A. Kurian and B. Pemaih, "Standardization of in vitro cell-based model for renal ischemia and reperfusion injury," *Indian Journal of Pharmaceutical Sciences*, vol. 76, no. 4, pp. 348–353, 2014.
- [25] L. S. Ang, W. A. Boivin, S. J. Williams et al., "Serpin3n attenuates granzyme B-mediated decorin cleavage and rupture in a murine model of aortic aneurysm," *Cell Death & Disease*, vol. 2, no. 9, article e209, 2011.
- [26] F. Chen, Y. Suzuki, N. Nagai et al., "Rat cerebral ischemia induced with photochemical occlusion of proximal middle cerebral artery: a stroke model for MR imaging research," *Magma*, vol. 17, no. 3-6, pp. 103–108, 2004.

Retraction

Retracted: Acetochlor Affects Bighead Carp (*Aristichthys Nobilis*) by Producing Oxidative Stress, Lowering Tissue Proteins, and Inducing Genotoxicity

BioMed Research International

Received 12 March 2024; Accepted 12 March 2024; Published 20 March 2024

Copyright © 2024 BioMed Research International. This is an open access article distributed under the Creative Commons Attribution License, which permits unrestricted use, distribution, and reproduction in any medium, provided the original work is properly cited.

This article has been retracted by Hindawi following an investigation undertaken by the publisher [1]. This investigation has uncovered evidence of one or more of the following indicators of systematic manipulation of the publication process:

- (1) Discrepancies in scope
- (2) Discrepancies in the description of the research reported
- (3) Discrepancies between the availability of data and the research described
- (4) Inappropriate citations
- (5) Incoherent, meaningless and/or irrelevant content included in the article
- (6) Manipulated or compromised peer review

The presence of these indicators undermines our confidence in the integrity of the article's content and we cannot, therefore, vouch for its reliability. Please note that this notice is intended solely to alert readers that the content of this article is unreliable. We have not investigated whether authors were aware of or involved in the systematic manipulation of the publication process.

Wiley and Hindawi regrets that the usual quality checks did not identify these issues before publication and have since put additional measures in place to safeguard research integrity.

We wish to credit our own Research Integrity and Research Publishing teams and anonymous and named external researchers and research integrity experts for contributing to this investigation.

The corresponding author, as the representative of all authors, has been given the opportunity to register their agreement or disagreement to this retraction. We have kept a record of any response received.

References

- [1] Y. Mahmood, R. Hussain, A. Ghaffar et al., "Acetochlor Affects Bighead Carp (*Aristichthys Nobilis*) by Producing Oxidative Stress, Lowering Tissue Proteins, and Inducing Genotoxicity," *BioMed Research International*, vol. 2022, Article ID 9140060, 12 pages, 2022.

Research Article

Acetochlor Affects Bighead Carp (*Aristichthys Nobilis*) by Producing Oxidative Stress, Lowering Tissue Proteins, and Inducing Genotoxicity

Yasir Mahmood ¹, Riaz Hussain ², Abdul Ghaffar ¹, Farah Ali ³, Sadia Nawaz ⁴,
Khalid Mehmood ⁵ and Ahrar Khan ^{6,7}

¹Department of Zoology, Islamia University of Bahawalpur, 63100, Pakistan

²Department of Pathology, Faculty of Veterinary and Animal Sciences, Islamia University of Bahawalpur-63100, Pakistan

³Department of Theriogenology, Faculty of Veterinary and Animal Sciences, Islamia University of Bahawalpur-63100, Pakistan

⁴Institute of Biochemistry and Biotechnology, University of Veterinary and Animal Sciences, Lahore, Pakistan

⁵Department of Clinical Medicine and Surgery, Faculty of Veterinary and Animal Sciences, Islamia University of Bahawalpur-63100, Pakistan

⁶Faculty of Veterinary Science, University of Agriculture, Faisalabad 38040, Pakistan

⁷Shandong Vocational Animal Science and Veterinary College, Weifang 261061, China

Correspondence should be addressed to Riaz Hussain; dr.riaz.hussain@iub.edu.pk and Ahrar Khan; ahrar1122@yahoo.com

Received 31 March 2022; Accepted 9 May 2022; Published 23 May 2022

Academic Editor: Abdelmotaleb Elokil

Copyright © 2022 Yasir Mahmood et al. This is an open access article distributed under the Creative Commons Attribution License, which permits unrestricted use, distribution, and reproduction in any medium, provided the original work is properly cited.

Acetochlor is persistently used in the agroproduction sector to control broadleaf weeds. Due to frequent and continuous applications, this herbicide can reach nearby water bodies and may induce deleterious changes in aquatic life. Therefore, investigation of harmful impacts of different environmental pollutants, including herbicides, is vital to knowing the mechanisms of toxicity and devising control strategies. The current experiment included bighead carp ($n = 80$) to estimate adverse impacts. Fish were randomly placed in 4 different experimental groups (T0-T3) and were treated for 36 days with acetochlor at 0, 300, 400, and 500 $\mu\text{g/L}$. Fresh blood without any anticoagulant was obtained and processed for nuclear and morphological changes in erythrocytes. At the same time, various visceral organs, including the gills, liver, brain, and kidneys, were removed and processed on days 12, 24, and 36 to determine oxidative stress and various antioxidant biomarkers. Comet assays revealed significantly increased DNA damage in isolated cells of the liver, kidneys, brain, and gills of treated fish. We recorded increased morphological and nuclear changes ($P \leq 0.05$) in the erythrocyte of treated fish. The results on oxidative stress showed a higher quantity of oxidative biomarkers and a significantly ($P \leq 0.05$) low concentration of cellular proteins in the gills, liver, brain, and kidneys of treated fish compared to unexposed fish. Our research findings concluded that acetochlor renders oxidative stress in bighead carp.

1. Introduction

Insecticides/pesticides especially herbicides have become a severe threat in the last few years. These have become a serious hazard to health because of their uncontrolled use in the aquatic environment and agriculture [1–6]. In the marine and terrestrial ecosystem, various ailments are caused in dif-

ferent animals due to unintended exposure to insecticides/pesticides, herbicides, and fungicides [7–11]. Various earlier reports have highlighted that aquatic species are mainly and extensively susceptible to several natural and synthetic toxicants than terrestrial animals because of the entry of insecticides/pesticides from agriculture, production sites/industries into water [12–15]. The use of pesticides in agriculture



FIGURE 1: Various organs of the fish treated with acetochlor showing normal brain, congested gills, and kidneys.

results in diffusing pollution where many soils, contaminating materials, leach to groundwater and ultimately reach drinking water. Since using several pesticides is a common practice, their leaching leads to the risk up to an alarming level [5].

Several studies have recorded that disclosure to synthetic composites, including herbicides, and by-products of various antiseptics, pesticides, fluorinated substances, and insecticides [7, 9, 16] cause deleterious effects to the aquatic life. It is also observed that even exposure to residues of natural and synthetic chemical compounds via the food chain renders abnormalities in multiple tissues of animals/fish, ultimately leading to disruption of several metabolic processes [4, 11, 17–20]. Aquatic animals, particularly fish, are considered the most susceptible to insecticides/pesticides and are reliable test specimens for the evaluation of the quality of the aquatic environment [21–24].

Bighead carp (*Aristichthys nobilis*) is commonly found in Pakistan's rivers and freshwater lakes and is a cultivable fish species. There are different scientific synonyms of bighead carp, such as *Cephalus hypothalamus* (Hong Kong), *Leuciscus nobilis* (Canton), *Hypophthalmichthys mandschuricus* (Shanghai), and *Hypophthalmichthys simony*. *Hypophthalmichthys nobilis* has another name like *Aristichthys nobilis* based on the divergent form of a branchial row, pharyngeal dentition, and length of the abdominal keel. It is demonstrated that various environmental contaminants like herbicides and insecticides mainly induce toxic effects via rapid induction of oxidative stress leading to depletion of antioxidant biomarkers in exposed animals [25–29]. The evaluation of hematological and biochemical biomarkers acts as useful and reliable bioindicators of toxicity in aquatic animals [3, 9, 30]. Moreover, serum biochemistry and different biomarkers in visceral tissues, such as various enzymes and proteins, are routinely used to assess health of aquatic animals [11, 31, 32].

The toxicity of acetochlor on behavior, growth and reproduction, and oxidative stress in different organisms have been reported [24, 33]. Various studies have investigated that numerous synthetic and natural pollutants disrupt the normal physiological processes of cells by interfering with various cellular proteins (p38 mitogen-activated protein, C-reactive protein, and G protein-coupled receptors), hormonal-signaling pathways, redox-sensitive signal transduction pathways, kinase and transcription factor AP-1 leading to induction of inflammation, and alterations in the blood and necrosis of various organs in exposed organisms [34, 35]. Moreover, it is also determined that different chemicals act as endocrine-disrupting compounds and cause abnormalities in redox homeostasis mechanisms, lowering cellular proteins/antioxidant enzymes, thus, mitochondrial dysfunctions and apoptosis [36, 37]. However, insufficient information is available about producing oxidative stress, lowering tissue proteins, and inducing genotoxicity due to chlorinated herbicides such as “acetochlor” in freshwater fish, especially bighead carp.

A chlorinated herbicide like acetochlor is commonly used on soybeans, maize, sugar beets, and different cereal crops to remove broadleaf weeds [38–40]. Acetochlor can enter the body of different aquatic animals via direct contact with contaminated water, ingestion, and dermal interaction resulting in physiological changes. Acetochlor is routinely used to control weeds in China and many other countries worldwide. It inhibits the growth of weeds at the early developmental stage by affecting cell integrity [41]. In China, acetochlor has been used for many years [24]. In 2010 and 2011, a study was carried out in North Carolina and Iowa states involving 33,484 people; however, acetochlor was used on 4,026 people, and there was a high probability of cancer among exposed people. Since the registration of acetochlor in 1994, it has become an herbicide of choice in the USA [42]. The organisms present in aquatic ecosystems are very

TABLE 1: Oxidative stress parameters and levels of cellular proteins/antioxidant enzymes present in liver tissue of bighead carp exposed to different levels of acetochlor.

| Biochemical parameters/days | Groups/treatments | | | |
|--|---------------------------|---------------------------|---------------------------|---------------------------|
| | T0 (0.0 $\mu\text{g/L}$) | T1 (300 $\mu\text{g/L}$) | T2 (400 $\mu\text{g/L}$) | T3 (500 $\mu\text{g/L}$) |
| ROS (optical density) | | | | |
| 12 | 0.35 \pm 0.03 | 0.36 \pm 0.02 | 0.39 \pm 0.03 | 0.83 \pm 0.07* |
| 24 | 0.36 \pm 0.01 | 0.37 \pm 0.01 | 0.66 \pm 0.02* | 0.85 \pm 0.05* |
| 36 | 0.38 \pm 0.04 | 0.41 \pm 0.03 | 0.73 \pm 0.02* | 0.91 \pm 0.05* |
| TBARS (nmol/TBARS formed/mg protein/min) | | | | |
| 12 | 37.41 \pm 2.93 | 39.22 \pm 1.95 | 41.06 \pm 1.15 | 54.92 \pm 3.74* |
| 24 | 38.88 \pm 1.94 | 40.67 \pm 2.95 | 50.43 \pm 1.97* | 56.24 \pm 2.92* |
| 36 | 40.01 \pm 3.94 | 41.94 \pm 2.93 | 51.87 \pm 2.34* | 58.82 \pm 4.53* |
| Reduced GSH ($\mu\text{mol/g}$ tissue) | | | | |
| 12 | 8.65 \pm 1.17 | 7.64 \pm 0.06 | 6.63 \pm 0.13 | 5.62 \pm 0.15* |
| 24 | 8.37 \pm 1.12 | 7.43 \pm 1.10 | 6.04 \pm 0.02* | 5.55 \pm 0.12* |
| 36 | 8.33 \pm 1.14 | 7.37 \pm 1.05 | 5.92 \pm 1.15* | 5.47 \pm 0.14* |
| Cellular proteins/antioxidant enzymes | | | | |
| SOD (units/mg protein) | | | | |
| 12 | 11.64 \pm 0.12 | 10.96 \pm 0.12 | 10.28 \pm 0.13 | 10.26 \pm 0.11 |
| 24 | 11.65 \pm 0.15 | 10.31 \pm 0.15 | 9.45 \pm 0.15* | 7.57 \pm 0.14* |
| 36 | 10.74 \pm 0.18 | 9.67 \pm 0.18 | 7.09 \pm 0.18* | 7.03 \pm 0.17* |
| CAT (units/min) | | | | |
| 12 | 8.69 \pm 0.19 | 7.51 \pm 0.19 | 7.13 \pm 0.19 | 5.15 \pm 0.19* |
| 24 | 7.98 \pm 0.17 | 7.34 \pm 0.16 | 5.62 \pm 0.16* | 5.02 \pm 0.16* |
| 36 | 7.94 \pm 0.16 | 7.01 \pm 0.16 | 5.45 \pm 0.16* | 4.94 \pm 0.16* |
| POD (units/ μg) | | | | |
| 12 | 4.07 \pm 0.09 | 3.53 \pm 0.09 | 2.77 \pm 0.09* | 2.46 \pm 0.09* |
| 24 | 4.02 \pm 0.08 | 3.46 \pm 0.09 | 2.62 \pm 0.09* | 2.40 \pm 0.09* |
| 36 | 3.95 \pm 0.09 | 3.38 \pm 0.09 | 2.54 \pm 0.09* | 2.39 \pm 0.09* |

Mean \pm SE values with asterisks in a row vary significantly ($P \leq 0.05$) as compared to the control group.

delicate and diversified, and almost all reflect the exact physical and biochemical changes when exposed to various toxicants [24, 26, 43]. As discussed above, herbicides render various biochemical alternations, especially oxidative stress in aquatic species, and no comprehensive study was available about bighead carp; hence, we planned this research to understand the development of oxidative stress caused by acetochlor in general, but in particular how oxidative stress behaves in body tissues of the *Aristichthys nobilis* (bighead carp).

2. Materials and Methods

2.1. Chemicals. Acetochlor was procured from the local commercial market (M/S Ali Akbar Enterprises, Pakistan) district Lodhran, Pakistan. Different other experimental chemicals of analytical grade were purchased from Sigma Aldrich (USA) and Merck (Germany). To estimate serum biochemical parameters, we obtained different commercial kits from Randox Company (Pvt.) Pakistan.

2.2. Experimental Species and Management. This study was conducted on bighead carp ($n = 80$) freshwater fish (*Aristichthys nobilis*) obtained from a local commercial fish farm. All the fish had uniform size, body weight (140 - 155 g), and age. The experimental test specimens were transferred to the laboratory in plastic bags with adequate oxygen. We kept all experimental specimens in aquaria made of glass (14" L, 10" W, and 12" H) for 10 days to allow them to acclimatize. All experimental fish were fed commercial feed at 2-3% of body weight twice daily, i.e., morning and evening. All aquaria had their residual feed and fecal contents eliminated.

2.3. Experimental Groups. After acclimatizing the fish, all experimental fish ($n = 80$) were randomly divided into four equal groups (T0-T3). Each aquarium was having 100 L water carrying capacity. Group T0 served as the control group, whereas fish of groups T1, T2, and T3 were treated with acetochlor at 300, 400, and 500 $\mu\text{g/L}$ for 36 days, respectively. During the entire experiment, residual feed and fecal elements were drained and removed daily. All experimental test specimens

TABLE 2: Oxidative stress parameters and levels of cellular proteins/antioxidant enzymes in kidney tissues of bighead carp exposed to different levels of acetochlor.

| Biochemical parameters/days | Groups/treatments | | | |
|--|---------------------------|---------------------------|---------------------------|---------------------------|
| | T0 (0.0 $\mu\text{g/L}$) | T1 (300 $\mu\text{g/L}$) | T2 (400 $\mu\text{g/L}$) | T3 (500 $\mu\text{g/L}$) |
| ROS (optical density) | | | | |
| 12 | 0.49 \pm 0.01 | 0.56 \pm 0.01 | 0.62 \pm 0.01* | 0.70 \pm 0.01* |
| 24 | 0.52 \pm 0.01 | 0.58 \pm 0.01 | 0.64 \pm 0.01* | 0.73 \pm 0.01* |
| 36 | 0.55 \pm 0.01 | 0.61 \pm 0.01 | 0.69 \pm 0.01* | 0.77 \pm 0.01* |
| TBARS (nmol/TBARS formed/mg protein/min) | | | | |
| 12 | 28.50 \pm 0.5 | 32.20 \pm 0.5 | 35.91 \pm 0.5* | 39.62 \pm 0.5* |
| 24 | 29.07 \pm 0.6 | 33.07 \pm 0.6 | 37.06 \pm 0.6* | 41.05 \pm 0.6* |
| 36 | 29.71 \pm 0.7 | 33.78 \pm 0.7 | 37.78 \pm 0.7* | 41.82 \pm 0.7* |
| Reduced GSH ($\mu\text{mol/g}$ tissue) | | | | |
| 12 | 7.69 \pm 0.3 | 6.44 \pm 0.3 | 5.20 \pm 0.2* | 3.94 \pm 0.2* |
| 24 | 7.61 \pm 0.3 | 6.39 \pm 0.2 | 5.17 \pm 0.2* | 3.88 \pm 0.2* |
| 36 | 7.55 \pm 0.3 | 6.34 \pm 0.2 | 5.09 \pm 0.2* | 3.84 \pm 0.2* |
| Cellular proteins/antioxidant enzymes | | | | |
| SOD (units/mg protein) | | | | |
| 12 | 15.50 \pm 0.32 | 13.52 \pm 0.3 | 11.55 \pm 0.32* | 9.54 \pm 0.32* |
| 24 | 15.39 \pm 0.35 | 13.13 \pm 0.3 | 10.98 \pm 0.35* | 8.76 \pm 0.35* |
| 36 | 15.25 \pm 0.36 | 13.09 \pm 0.3 | 10.85 \pm 0.36* | 8.67 \pm 0.36* |
| CAT (units/min) | | | | |
| 12 | 5.11 \pm 0.1 | 4.57 \pm 0.09 | 4.03 \pm 0.09 | 3.45 \pm 0.07* |
| 24 | 5.07 \pm 0.1 | 4.55 \pm 0.09 | 3.97 \pm 0.08* | 3.42 \pm 0.07* |
| 36 | 5.03 \pm 0.1 | 4.44 \pm 0.09 | 3.91 \pm 0.08* | 3.29 \pm 0.06* |
| POD (units/ μg) | | | | |
| 12 | 5.97 \pm 0.13 | 5.32 \pm 0.13 | 4.66 \pm 0.11 | 4.03 \pm 0.10* |
| 24 | 5.91 \pm 0.13 | 5.29 \pm 0.12 | 4.62 \pm 0.11* | 3.94 \pm 0.10* |
| 36 | 5.88 \pm 0.13 | 5.26 \pm 0.12 | 4.59 \pm 0.10* | 3.88 \pm 0.10* |

Mean \pm SE values with asterisks in a row vary significantly ($P \leq 0.05$) as compared to the control group.

were carefully observed twice daily for any noticeable clinical and behavioral ailments.

2.4. Blood Analysis and Genotoxicity Assessment. Blood (2.5 mL) was drawn from the caudal vein of each fish with the help of a hypodermic needle (26 gauge) on days 12, 24, and 36 [8]. A thin blood smear was made from each fish's fresh blood without anticoagulant to examine nuclear and morphological changes in erythrocytes. Blood smears were dried right away, fixed with 100% methyl alcohol, and stained with Giemsa's stain. A light microscope with an oil immersion lens was used to examine 1500 erythrocytes from each fish, aided by a computer [8].

Under alkaline conditions, Comet assay or single-cell gel electrophoresis was used to estimate DNA damage in various tissues, i.e., the gills, brain, liver, and kidneys [1, 4]. After dissecting, these tissues were isolated and immersed separately in chilled normal saline solution, homogenized, and centrifuged (0.2g). Every tissue's supernatant with suspended single cells was isolated and subjected to single-cell gel electrophoresis or Comet assay

[1]. Briefly, agarose with normal point (1%) and low melting point (1%) was dissolved in Milli-Q water and prepared thin smears on frosted glass slides [1]. After preparation, the cells present on slides were lysed in a cold buffer solution. Then, the slides were electrophoresed in a horizontal tank with a refrigerated electrophoresis solution at 25 V for 30 minutes [9]. After electrophoresis, the slides were neutralized using an ice-cold 0.4 M tris buffer (pH 7.5). Finally, ethidium bromide-stained slides were examined under a fluorescence microscope at a magnification of 40x. A total of 500 cells/fish/slide were observed to estimate the occurrence of damaged DNA in each slide and tissue sample.

2.5. Tissues Biochemical Changes. Homogenates from tissues of gills, liver, brain, and kidneys were prepared and subjected to the determination of various biochemical parameters including ROS [44], TBARS [45], and GSH [46], similarly, from the homogenates assessed cellular proteins/antioxidant enzymes including POD [47], SOD [48], and CAT [47].

TABLE 3: Oxidative stress parameters and levels of tissue proteins/antioxidant enzyme in gill tissue of bighead carp treated with various levels of acetochlor.

| Biochemical parameters/days | Groups/treatments | | | |
|--|---------------------------|---------------------------|---------------------------|---------------------------|
| | T0 (0.0 $\mu\text{g/L}$) | T1 (300 $\mu\text{g/L}$) | T2 (400 $\mu\text{g/L}$) | T3 (500 $\mu\text{g/L}$) |
| ROS (optical density) | | | | |
| 12 | 0.32 \pm 0.01 | 0.38 \pm 0.01 | 0.46 \pm 0.02* | 0.53 \pm 0.04* |
| 24 | 0.34 \pm 0.01 | 0.41 \pm 0.02 | 0.49 \pm 0.02* | 0.56 \pm 0.04* |
| 36 | 0.36 \pm 0.01 | 0.43 \pm 0.02 | 0.51 \pm 0.03* | 0.58 \pm 0.04* |
| TBARS (nmol/TBARS formed/mg protein/min) | | | | |
| 12 | 40.66 \pm 0.60 | 44.46 \pm 0.62 | 48.26 \pm 0.61* | 52.06 \pm 0.62* |
| 24 | 41.12 \pm 0.61 | 44.87 \pm 0.61 | 48.63 \pm 0.61* | 52.38 \pm 0.63* |
| 36 | 41.19 \pm 0.61 | 45.03 \pm 0.62 | 48.81 \pm 0.62* | 52.69 \pm 0.63* |
| Reduced GSH ($\mu\text{mol/g}$ tissue) | | | | |
| 12 | 2.57 \pm 0.06 | 2.23 \pm 0.06 | 1.89 \pm 0.06* | 1.55 \pm 0.06* |
| 24 | 2.43 \pm 0.05 | 2.12 \pm 0.05 | 1.82 \pm 0.05* | 1.51 \pm 0.05* |
| 36 | 2.33 \pm 0.05 | 2.04 \pm 0.05 | 1.75 \pm 0.05* | 1.46 \pm 0.05* |
| Cellular proteins/antioxidant enzymes | | | | |
| SOD (units/mg protein) | | | | |
| 12 | 10.78 \pm 0.2 | 9.72 \pm 0.2 | 8.67 \pm 0.2 | 7.20 \pm 0.1* |
| 24 | 10.67 \pm 0.2 | 9.52 \pm 0.2 | 8.36 \pm 0.2 | 7.21 \pm 0.1* |
| 36 | 10.56 \pm 0.2 | 9.31 \pm 0.2 | 8.06 \pm 0.1 | 6.82 \pm 0.1* |
| CAT (units/min) | | | | |
| 12 | 3.02 \pm 0.04 | 2.74 \pm 0.05 | 2.47 \pm 0.05 | 2.18 \pm 0.04* |
| 24 | 2.97 \pm 0.05 | 2.68 \pm 0.05 | 2.42 \pm 0.05* | 2.14 \pm 0.05* |
| 36 | 2.94 \pm 0.05 | 2.66 \pm 0.05 | 2.38 \pm 0.05* | 2.07 \pm 0.05* |
| POD (units/ μg) | | | | |
| 12 | 0.40 \pm 0.02 | 0.36 \pm 0.02 | 0.31 \pm 0.01* | 0.25 \pm 0.01* |
| 24 | 0.39 \pm 0.02 | 0.34 \pm 0.02 | 0.29 \pm 0.01* | 0.23 \pm 0.01* |
| 36 | 0.38 \pm 0.02 | 0.33 \pm 0.02 | 0.28 \pm 0.01 | 0.21 \pm 0.01* |

Mean \pm SE values with asterisks in a row vary significantly ($P \leq 0.05$) as compared to the control group.

2.6. *Statistical Analysis.* The trial's research findings are reported as mean \pm SE. The data from our study (all experiments) were analyzed using ANOVA with SPSS statistics (version 20) software, and the group means were compared using a post hoc Tukey's test. We set a significance level at $P \leq 0.05$.

3. Results

3.1. *Physical Findings.* At necropsy, different macroscopic lesions, including hyperemic and congested gills, edematous and congested kidneys, mild to moderate congestion in brain, hyperemic muscles, and congested and moderately friable liver were examined in fish of group T3 at days 24 and 36 of the study (Figure 1).

3.2. *Reactive Oxygen Species and Cellular Proteins/Antioxidant Enzymes in the Liver.* The concentration of ROS and TBARS in the liver significantly ($P \leq 0.05$) increased in the fish of groups T2 (400 $\mu\text{g/L}$) and T3 (500 $\mu\text{g/L}$) treated with acetochlor after experimental days

12, 24, and 36. GSH, SOD, CAT, and POD concentration dropped significantly ($P \leq 0.05$) in the liver of fish of groups T2 and T3 treated with 400 $\mu\text{g/L}$ and 500 $\mu\text{g/L}$ acetochlor after days 12, 24, and 36 of the experiment, respectively (Table 1).

3.3. *Reactive Oxygen Species and Cellular Proteins/Antioxidant Enzymes in Kidneys.* The quantity of ROS and TBARS increased significantly ($P \leq 0.05$) in the kidneys of fish of groups T2 (400 $\mu\text{g/L}$) and T3 (500 $\mu\text{g/L}$) treated with acetochlor after days 12, 24, and 36 of the experiment. GSH contents dropped significantly ($P \leq 0.05$) in the fish of groups T2 and T3 treated with acetochlor after days 12, 24, and 36 in kidneys (Table 2). SOD and CAT in the kidneys decreased significantly in the fish of groups T2 and T3 after days 12, 24, and 36. POD dropped significantly ($P \leq 0.05$) in the kidneys of fish of groups T2 and T3 after days 12, 24, and 36 (Table 2).

3.4. *Reactive Oxygen Species and Cellular Proteins/Antioxidant Enzymes in Gills.* The quantity of ROS and

TABLE 4: Oxidative stress parameters and levels of cellular proteins/antioxidant enzymes in brain tissues of bighead carp exposed to different levels of acetochlor.

| Biochemical parameters/days | Groups/treatments | | | |
|--|---------------------------|---------------------------|---------------------------|---------------------------|
| | T0 (0.0 $\mu\text{g/L}$) | T1 (300 $\mu\text{g/L}$) | T2 (400 $\mu\text{g/L}$) | T3 (500 $\mu\text{g/L}$) |
| ROS (optical density) | | | | |
| 12 | 0.40 \pm 0.02 | 0.50 \pm 0.02 | 0.61 \pm 0.03* | 0.70 \pm 0.03* |
| 24 | 0.45 \pm 0.02 | 0.54 \pm 0.02 | 0.63 \pm 0.03* | 0.71 \pm 0.04* |
| 36 | 0.52 \pm 0.02 | 0.60 \pm 0.03 | 0.65 \pm 0.03* | 0.75 \pm 0.04* |
| TBARS (nmol/TBARS formed/mg protein/min) | | | | |
| 12 | 18.59 \pm 0.4 | 22.28 \pm 0.4 | 25.96 \pm 0.5* | 29.65 \pm 0.6* |
| 24 | 19.07 \pm 0.4 | 22.76 \pm 0.4 | 26.45 \pm 0.5* | 30.13 \pm 0.6* |
| 36 | 19.17 \pm 0.4 | 22.91 \pm 0.5 | 26.65 \pm 0.6* | 30.39 \pm 0.6* |
| Reduced GSH ($\mu\text{mol/g}$ tissue) | | | | |
| 12 | 2.99 \pm 0.06 | 2.59 \pm 0.06 | 2.18 \pm 0.05* | 1.78 \pm 0.04* |
| 24 | 2.95 \pm 0.06 | 2.55 \pm 0.05 | 2.15 \pm 0.04* | 1.76 \pm 0.03* |
| 36 | 2.87 \pm 0.06 | 2.49 \pm 0.05 | 2.09 \pm 0.04* | 1.72 \pm 0.03* |
| Cellular proteins/antioxidant enzymes | | | | |
| SOD (units/mg protein) | | | | |
| 12 | 13.64 \pm 0.3 | 12.08 \pm 0.3 | 10.51 \pm 0.2* | 8.95 \pm 0.2* |
| 24 | 13.55 \pm 0.3 | 11.99 \pm 0.2 | 10.42 \pm 0.2* | 8.86 \pm 0.1* |
| 36 | 13.44 \pm 0.3 | 11.87 \pm 0.2 | 10.31 \pm 0.2* | 8.74 \pm 0.1* |
| CAT (units/min) | | | | |
| 12 | 4.15 \pm 0.08 | 3.65 \pm 0.08 | 3.15 \pm 0.07* | 2.65 \pm 0.06* |
| 24 | 4.11 \pm 0.08 | 3.57 \pm 0.08 | 3.03 \pm 0.07* | 2.49 \pm 0.06* |
| 36 | 4.06 \pm 0.08 | 3.51 \pm 0.07 | 2.97 \pm 0.07* | 2.42 \pm 0.06* |
| POD (units/ μg) | | | | |
| 12 | 3.13 \pm 0.06 | 2.78 \pm 0.06 | 2.43 \pm 0.05* | 2.08 \pm 0.04* |
| 24 | 3.10 \pm 0.06 | 2.72 \pm 0.05 | 2.34 \pm 0.05* | 1.97 \pm 0.04* |
| 36 | 3.03 \pm 0.06 | 2.66 \pm 0.05 | 2.30 \pm 0.05* | 1.93 \pm 0.04* |

Mean \pm SE values with asterisks in a row vary significantly ($P \leq 0.05$) as compared to the control group.

TBARS increased significantly ($P \leq 0.05$) in the fish of groups T2 and T3 treated with 400 $\mu\text{g/L}$ 500 $\mu\text{g/L}$ acetochlor, respectively, after days 12, 24, and 36 of the experiment. GSH, SOD, CAT, and POD concentration dropped significantly ($P \leq 0.05$) in the fish of groups T2 and T3 treated with 400 $\mu\text{g/L}$ and 500 $\mu\text{g/L}$ acetochlor after days 12, 24, and 36 of the experiment, respectively (Table 3).

3.5. Reactive Oxygen Species and Cellular Proteins/Antioxidant Enzymes in the Brain. The quantity of ROS and TBARS in the brain increased significantly ($P \leq 0.05$) in the fish of groups T2 and T3 treated with 400 $\mu\text{g/L}$ acetochlor after days 12, 24, and 36 of the experiment. GSH contents, SOD, CAT, and POD decreased significantly ($P \leq 0.05$) in the brain of fish of groups T2 (400 $\mu\text{g/L}$) and T3 (500 $\mu\text{g/L}$) treated with acetochlor after days 12, 24, and 36 of the experiment (Table 4).

3.6. Genotoxicity. The results of nuclear and morphological changes in erythrocytes of treated fish showed significantly ($P \leq 0.05$) higher values of micronuclei, condensed nuclei,

lobed nuclei, red blood cells with a pear shape, and pear shape erythrocytes (Figure 2). A significantly ($P \leq 0.05$) increased frequency of DNA damage (Table 5) was recorded in isolated cells of the liver, kidneys, gills, and brain at different intervals of the experiment when compared with that of normal fish (Figure 3).

4. Discussion

In the present study, various oxidative stress parameters increased significantly in acetochlor-treated freshwater fish. Acetochlor is a toxic herbicide [49]. Increased oxidative stress could be caused by the toxic effect of acetochlor on different biological processes such as metabolism [50–52]. Many intrinsic and extrinsic factors are found to induce oxidative stress in different animals. Oxidative stress may be caused by an imbalance between ROS production and antioxidant defenses [51, 53]. Another possibility could be due to the reaction of toxicants with water to produce superoxide, which resultantly increased oxidative stress in freshwater fish [9, 50].

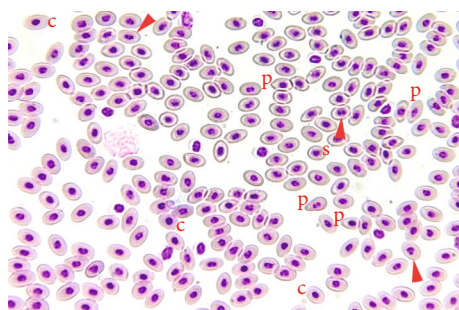


FIGURE 2: Blood smear of fish treated with acetochlor (500 µg/L) stained with Giemsa stain showing pear-shaped erythrocytes (p), spherocytes (s), condensed nuclei (c), and micronucleus (arrowheads). 1000x.

TABLE 5: Frequency of DNA damage (%) in isolated cells of different tissues of bighead carp exposed to different levels of acetochlor.

| Parameters/days | Groups/treatments | | | |
|-------------------------|-------------------|---------------|---------------|---------------|
| | T0 (0.0 µg/L) | T1 (300 µg/L) | T2 (400 µg/L) | T3 (500 µg/L) |
| Hepatocyte (%) | | | | |
| 12 | 2.35 ± 0.04 | 2.37 ± 0.05 | 2.39 ± 0.03 | 4.42 ± 0.34* |
| 24 | 2.37 ± 0.09 | 2.42 ± 0.06 | 3.47 ± 0.16* | 4.52 ± 0.29* |
| 36 | 2.43 ± 0.02 | 2.56 ± 0.02 | 3.70 ± 0.27* | 5.84 ± 0.22* |
| Kidney cells (%) | | | | |
| 12 | 2.15 ± 0.14 | 2.25 ± 0.11 | 2.31 ± 0.14 | 3.21 ± 0.19* |
| 24 | 2.17 ± 0.13 | 2.23 ± 0.16 | 3.75 ± 0.19* | 3.59 ± 0.28* |
| 36 | 2.22 ± 0.11 | 2.56 ± 0.18 | 3.87 ± 0.25* | 4.81 ± 0.31* |
| Gills cells (%) | | | | |
| 12 | 1.15 ± 0.09 | 1.18 ± 0.04 | 1.39 ± 0.05 | 2.03 ± 0.14* |
| 24 | 1.17 ± 0.07 | 1.23 ± 0.05 | 2.32 ± 0.02* | 2.45 ± 0.19* |
| 36 | 1.13 ± 0.08 | 1.16 ± 0.22 | 2.70 ± 0.04* | 2.89 ± 0.12* |
| Brain cells (%) | | | | |
| 12 | 1.31 ± 0.11 | 1.33 ± 0.02 | 1.39 ± 0.11 | 1.41 ± 0.01 |
| 24 | 1.27 ± 0.12 | 1.31 ± 0.08 | 1.41 ± 0.03 | 2.33 ± 0.18* |
| 36 | 1.29 ± 0.09 | 1.37 ± 0.008 | 3.11 ± 0.16* | 2.67 ± 0.13* |

Mean ± SE values with asterisks in a row vary significantly ($P \leq 0.05$) as compared to the control group.

ROS are naturally formed in an aerobic environment and, at physiological levels, are suggestive of oxidative eustress, or low-level oxidative stress [54]; however, ROS formed under pathological conditions and resulting in increased ROS indicates oxidative distress [55]. Enzymatic and nonenzymatic antioxidants are important for maintaining the oxidative eustress balance and redox status and provide a defense against ROS formation [54, 56]. Pesticides/herbicides are known to induce ROS and lead to oxidative stress in fish [57–60]. The antioxidant enzymes (CAT, SOD, GST, and GPx) inhibit oxidative stress, and the actions of these enzymes are usually used to monitor the risk of pesticides/herbicides [61]. Glutathione reductase is also a suitable biomarker for assessing the effect of pesticides/herbicides on aquatic organisms [60, 62].

Increased oxidative stress found in the present study could have resulted from the negative impact of contaminants linked with the generation of oxidative stress. An

increase in ROS may result from stress caused by the contaminant on intracellular constituents' modification, defense system activity, and ROS-based signaling [3, 63]. ROS production is a natural cellular activity that is involved in varied aspects of cellular signaling, as well as in the defense mechanism of the immune system. In the present study, excessive ROS production could have resulted from acetochlor treatment that could have rendered severe damage to cellular macromolecules, such as proteins, lipids, and DNA, resulting in detrimental effects on cells [24, 33, 41, 64]. In the cells, altered nuclear processes reduce metabolic activity, induce cell membrane leakage or blockage, and decrease cell proliferation and viability; thus, oxidative stress is an important factor contributing to cell and tissue damage [49, 52].

Significantly ($P \leq 0.05$) increased oxidative stress parameters were observed in the liver and the brain of fish treated with acetochlor, in the present study. Increased oxidative stress in the brain may be the effect of the induction of

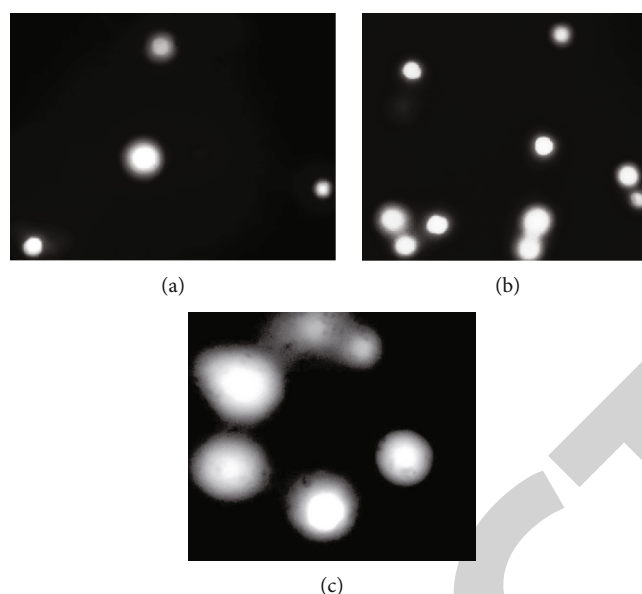


FIGURE 3: Comet assay showing DNA damage in isolated cells of the liver, kidneys, gills, and brain of fish treated with acetochlor at 300 $\mu\text{g/L}$ (a), 400 $\mu\text{g/L}$ (b), and 400 $\mu\text{g/L}$ (c). Note the frequency and intensity is increasing with the dose of acetochlor is increasing.

neurotransmitters and stress hormones released in the brain due to acetochlor treatment [65, 66]. In the current study, total protein and GSH contents in various tissues of bighead carp could be attributed to reduced tissue activities, higher usage of energy/body proteins to counteract oxidative stress, and lower protein levels in the body and tissues. It has been reported that various poisonous substances are liable for the diminution of body proteins, as well as distinct tissues of fish (*Oreochromis spilurus*, *Mystus vittatus*, *Channa punctatus*, and *Labeo rohita*), such as the liver, brain, kidneys, and gills [3, 9, 63].

Other possibility of raised oxidative stress in the present study could be the formation of free radicals as a result of toxicity induced by the acetochlor [67, 68]. The toxicant-mediated pathways can greatly increase ROS formation and excessive levels of free radicals, which might affect the metabolism [69–71]. The oxidative stress in the liver that might be the source of free radical's formation, those could interfere with intracellular signal transmission and regulation of genes, resulting in inflammation in the liver [72]. Disturbance in tissue proteins/antioxidant enzymes and production of ROS could lead to liver inflammation [70, 73, 74]. Various studies have reported different synthetic chemicals/pesticides that cause increased release of free radicals like ROS, resulting in increased induction of oxidative stress in various tissues [75], ultimately leading to activation and depletion of the body's defense responses (GSH, glutathione-S-transferase, SOD, and CAT) in exposed organisms [24, 63, 65]. Previously, it was recorded that acetochlor reduced the concentrations of different tissue proteins/antioxidant parameters like SOD and GSH at very low doses.

Moreover, acetochlor altered and damaged HepG2 cells via triggering apoptosis signals and increased deposition of calcium in cells, reduced mitochondrial transmembrane potential, and a lower quantity of ATP [24]. ROS can cause damage to biomolecules leading to cell and tissue injury

[76]. Moreover, it is recorded that acetochlor/herbicides mainly induce an increased lipid peroxidation and ROS production process, leading to damage to DNA, proteins, lipids, and carbohydrates that consequently affect the immune functions [77–82].

The nuclear and morphological alterations in RBCs of bighead carp like condensed nuclei, micronuclei, pear shape erythrocyte, and spherocyte could be due to the toxic effects of herbicides on hematopoietic tissues. Previous studies have recorded the occurrence of nuclear and morphological alterations in erythrocytes of humans [83, 84], birds [7, 9], and fish [21, 24, 25, 63, 85] might be related to mitochondrial damage.

5. Conclusions

This study concluded that acetochlor leads to significantly ($P < 0.05$) higher morphological and nuclear abnormalities in erythrocytes in treated fish. There was significantly increased DNA damage in isolated cells of treated fish's gills, liver, brain, and kidneys. The results on oxidative stress showed a higher quantity of different oxidative biomarkers and a significantly ($P < 0.05$) lower concentration of various cellular proteins/antioxidant enzymes in the liver, gills, kidneys, and brain of treated bighead carp compared to unexposed fish. Our research findings concluded that acetochlor causes harmful pathobiochemical changes in different tissues of the bighead carp.

6. Limitations of the Study

As this is a laboratory study and carried out within limited sources, this type of study is carried out under field conditions involving various other carp species to carry out a broad conclusion. Moreover, remedial measures are searched out for the amelioration of acetochlor and other insecticides/pesticides/herbicides so that farmers could get more profit from fish farming.

Abbreviations

| | |
|--------|---|
| ANOVA: | Analysis of variance |
| CAT: | Catalase |
| GSH: | Reduced glutathione |
| POD: | Peroxidase |
| ROS: | Reactive oxygen species |
| SE: | Standard error |
| SOD: | Superoxide dismutase |
| TBARS: | Thiobarbituric acid reactive substance. |

Data Availability

The data that support the findings of this study are available from the corresponding author upon reasonable request.

Conflicts of Interest

The authors declare that there is no conflict of interest regarding the publication of this paper.

Authors' Contributions

Abdul Ghaffar and Riaz Hussain planned and designed the research work. Riaz Hussain and Yasir Mahmood executed the study and obtained the data. Riaz Hussain and Ahrar Khan analyzed the collected data. Riaz Hussain, Ahrar Khan, and Khalid Mehmood interpreted the data. Riaz Hussain, Ahrar Khan, Sadia Nawaz, and Yasir Mahmood prepared the manuscript paper. All authors read and approved the final version of the manuscript.

References

- [1] R. Hussain, F. Mahmood, M. Z. Khan, A. Khan, and F. Muhammad, "Pathological and genotoxic effects of atrazine in male Japanese quail (*Coturnix japonica*)," *Ecotoxicology*, vol. 20, no. 1, pp. 1–8, 2011.
- [2] Q. Mujahid, A. Khan, M. F. Qadir et al., "Allethrin induced toxicopathological alterations in adult male albino rats," *Agrobiological Records*, vol. 5, pp. 8–14, 2021.
- [3] A. Ghaffar, R. Hussain, N. Ahmad et al., "Evaluation of hematobiochemical, antioxidant enzymes as biochemical biomarkers and genotoxic potential of glyphosate in freshwater fish (*Labeo rohita*)," *Chemistry and Ecology*, vol. 37, no. 7, pp. 646–667, 2021.
- [4] R. Hussain, F. Ali, A. Rafique et al., "Exposure to sub-acute concentrations of glyphosate induce clinico-hematological, serum biochemical and genotoxic damage in adult cockerels," *Pakistan Veterinary Journal*, vol. 39, no. 2, pp. 181–186, 2019.
- [5] L. Ahmad, S. T. Gul, M. K. Saleemi et al., "The effect of different repeated doses of cypermethrin on the behavioral and histological alterations in the brain of rabbits (*Oryctolagus cuniculi*)," *International Journal of Veterinary Science*, vol. 10, no. 4, pp. 347–354, 2021.
- [6] R. Tahir, A. Ghaffar, G. Abbas et al., "Pesticide induced hematological, biochemical and genotoxic changes in fish: a review," *Agrobiological Records*, vol. 3, pp. 41–57, 2021.
- [7] R. Hussain, F. Mahmood, A. Khan, M. T. Javed, S. Rehan, and T. Mehdi, "Cellular and biochemical effects induced by atrazine on blood of male Japanese quail (*Coturnix japonica*)," *Pesticide Biochemistry and Physiology*, vol. 103, no. 1, pp. 38–42, 2012.
- [8] A. Ghaffar, R. Hussain, A. Abbas et al., "Assessment of genotoxic and pathological potentials of fipronil insecticide in *Labeo rohita* (Hamilton, 1822)," *Toxin Reviews*, vol. 40, no. 4, pp. 1289–1300, 2021.
- [9] R. Akram, A. Ghaffar, R. Hussain et al., "Hematological, serum biochemistry, histopathological and mutagenic impacts of triclosan on fish (bighead carp)," *Agrobiological Records*, vol. 7, pp. 18–28, 2022.
- [10] M. L. Namratha, M. Lakshman, M. Jeevanalatha, and B. A. Kumar, "Hematological alterations induced by glyphosate and ameliorative effect of ascorbic acid in Wistar rats," *Continental Veterinary Journal*, vol. 1, no. 1, pp. 32–36, 2020.
- [11] A. Ghaffar, R. Hussain, S. Noreen et al., "Dose and time-related pathological and genotoxic studies on thiamethoxam in fresh water fish (*Labeo rohita*) in Pakistan," *Pakistan Veterinary Journal*, vol. 40, no. 2, pp. 151–156, 2020.
- [12] P. Sivashanmugam, V. Mullainadhan, and B. Karundevi, "Dose-dependent effect of bisphenol-A on insulin signaling molecules in cardiac muscle of adult male rat," *Chemico-Biological Interactions*, vol. 266, pp. 10–16, 2017.
- [13] K. Baralic, A. Buha Djordjevic, K. Živančević et al., "Toxic effects of the mixture of phthalates and bisphenol A—subacute oral toxicity study in Wistar rats," *International Journal of Environmental Research and Public Health*, vol. 17, article 746, 2020.
- [14] A. A. Warra and M. N. V. Prasad, "Chapter 16 - African perspective of chemical usage in agriculture and horticulture—their impact on human health and environment," in *Agrochemicals Detection, Treatment and Remediation Pesticides and Chemical Fertilizers*, M. N. V. Prasad, Ed., pp. 401–436, Butterworth-Heinemann Publishers, 2020.
- [15] A. H. Mahmoud, M. N. Darwish, Y. O. Kim et al., "Fenvalerate induced toxicity in zebra fish, *Danio rerio* and analysis of biochemical changes and insights of digestive enzymes as important markers in risk assessment," *Journal of King Saud University - Science*, vol. 32, pp. 1569–1580, 2020.
- [16] R. Hussain, A. Khan, F. Mahmood, S. Rehan, and F. Ali, "Clinico-hematological and tissue changes induced by butachlor in male Japanese quail (*Coturnix japonica*)," *Pesticide Biochemistry and Physiology*, vol. 109, pp. 58–63, 2014.
- [17] S. A. Gaston, L. S. Birnbaum, and L. C. Jackson, "Synthetic chemicals and cardiometabolic health across the life course among vulnerable populations: A Review of the Literature from 2018 to 2019," *Current Environmental Health Reports*, vol. 7, pp. 30–47, 2020.
- [18] I. M. Merdana, N. L. Watiniasih, I. W. Sudira et al., "The effect of ethanolic extract of *Myrmecodia pendans* on gentamicin induced nephrotoxicity in Wistar rats," *International Journal of Veterinary Science*, vol. 10, no. 2, pp. 96–101, 2021.
- [19] W. R. Scarano, A. Bedrat, L. G. Alonso-Costa et al., "Exposure to an environmentally relevant phthalate mixture during prostate development induces microRNA upregulation and transcriptome modulation in rats," *Toxicology Science*, vol. 171, no. 1, pp. 84–97, 2019.
- [20] L. Zhou, H. Chen, Q. Xu et al., "The effect of di-2-ethylhexyl phthalate on inflammation and lipid metabolic disorder in rats," *Ecotoxicology and Environment Safety*, vol. 170, pp. 391–398, 2019.

- [21] A. Ghaffar, R. Hussain, M. Aslam, G. Abbas, and A. Khan, "Arsenic and urea in combination alters the hematology, biochemistry and protoplasm in exposed Rahu fish (*Labeo rohita*) (Hamilton, 1822)," *Turkish Journal of Fisheries and Aquatic Science*, vol. 16, no. 2, pp. 289–296, 2016.
- [22] R. M. Sjerps, P. J. Kooij, A. van Loon, and A. P. Van Wezel, "Occurrence of pesticides in Dutch drinking water sources," *Chemosphere*, vol. 235, pp. 510–518, 2019.
- [23] R. Hussain, A. Ghaffar, H. M. Ali et al., "Analysis of different toxic impacts of Fipronil on growth, hemato-biochemistry, protoplasm and reproduction in adult cockerels," *Toxin Reviews*, vol. 37, no. 4, pp. 294–303, 2018.
- [24] T. Huang, S. Wang, C. L. Souders II et al., "Exposure to acetochlor impairs swim bladder formation, induces heat shock protein expression, and promotes locomotor activity in zebrafish (*Danio rerio*) larvae," *Ecotoxicology and Environment Safety*, vol. 228, article 112978, 2021.
- [25] A. Ghaffar, R. Hussain, G. Abbas et al., "Arsenic and copper sulfate in combination causes testicular and serum biochemical changes in white leghorn cockerels," *Pakistan Veterinary Journal*, vol. 37, pp. 375–380, 2018.
- [26] A. Ghaffar, R. Hussain, G. Abbas et al., "Sodium arsenate and/or urea differently affect clinical attributes, hemato-biochemistry and DNA damage in intoxicated commercial layer birds," *Toxin Reviews*, vol. 37, no. 3, pp. 206–215, 2018.
- [27] H. H. Ahmed, N. E. S. El-Toukhey, S. S. Abd El-Rahman, and A. K. Hendawy, "Efficacy of melatonin against oxidative stress, DNA damage and histopathological changes induced by nicotine in liver and kidneys of male rats," *Journal of Veterinary Science*, vol. 10, no. 1, pp. 31–36, 2021.
- [28] A. Ghaffar, K. Rani, R. Hussain, M. Mehreen, T. Rubi, and S. Yasin, "Histopathological and serum biochemical 418 changes induced by sub-chronic doses of triazophos in quail," *Pakistan Veterinary Journal*, vol. 35, pp. 13–14, 2015.
- [29] A. Ghaffar, R. Hussain, G. Abbas et al., "Fipronil (Phenylpyrazole) induces hemato-biochemical, histological and genetic damage at low doses in common carp, *Cyprinus carpio* (Linnaeus, 1758)," *Ecotoxicology*, vol. 27, no. 9, pp. 1261–1271, 2018.
- [30] M. Aranha, M. S. Garcia, D. C. Cavalcante et al., "Biochemical and histopathological responses in peripubertal male rats exposed to agrochemicals isolated or in combination: a multivariate data analysis study," *Toxicology*, vol. 447, article 152636, 2021.
- [31] T. Rehman, S. Naz, R. Hussain et al., "Exposure to heavy metals causes histopathological changes and alters antioxidant enzymes in fresh water fish (*Oreochromis niloticus*)," *Asian Journal of Agriculture and Biology*, vol. 2021, no. 1, 2021.
- [32] S. Naz, R. Hussain, Q. Ullah, A. M. M. Chatha, A. Shaheen, and R. U. Khan, "Toxic effect of some heavy metals on hematology and histopathology of major carp (*Catla catla*)," *Environmental Science and Pollution Research*, vol. 28, no. 6, pp. 6533–6539, 2021.
- [33] J. Zhang, S. Jiang, M. Zhang, and X. Wu, "Monitoring the Acute and Subacute Toxicity Effects of Herbicide Acetochlor by Bacterivorous Nematode," in *International Conference on New Technology of Agricultural*, pp. 669–672, Zibo, China, 2011.
- [34] N. D. Vaziri and B. Rodriguez-Iturbe, "Mechanisms of disease: oxidative stress and inflammation in the pathogenesis of hypertension," *Nature Clinical Practice Nephrology*, vol. 2, no. 10, pp. 582–593, 2006.
- [35] M. Rosaria, A. Monnolo, C. Annunziata, C. Pirozzi, and M. C. Ferrante, "Oxidative stress and BPA toxicity: an antioxidant approach for male and female reproductive dysfunction," *Antioxidants*, vol. 9, no. 5, p. 405, 2020.
- [36] G. Lenaz, "Mitochondria and reactive oxygen species. Which role in physiology and pathology?," in *Advances in Mitochondrial Medicine, Advances in Experimental Medicine and Biology*, R. Scatena, P. Bottoni, and B. Giardina, Eds., vol. 942, Springer, Dordrecht, 2012.
- [37] A. L. F. Destro, S. B. Silva, K. P. Gregorio et al., "Effects of sub-chronic exposure to environmentally relevant concentrations of the herbicide atrazine in the Neotropical fish *Astyanax altiparanae*," *Ecotoxicology and Environmental Safety*, vol. 208, article 111601, 2021.
- [38] L. P. Gianessi and N. P. Reigner, "The value of herbicides in U.S. crop production," *Weed Technology*, vol. 21, no. 2, pp. 559–566, 2007.
- [39] Z. Q. Jia, Y. C. Zhang, Q. T. Huang, A. K. Jones, Z. J. Han, and C. Q. Zhao, "Acute toxicity, bioconcentration, elimination, action mode and detoxification metabolism of broflanilide in zebrafish, *Danio rerio*," *Journal of Hazardous Materials*, vol. 394, article 122521, 2020.
- [40] M. G. Taha, S. M. A. El-Hamamsy, N. S. Ahmed, and M. M. Ali, "Amelioration effect of *Carica papaya* fruit extracts on doxorubicin – induced cardiotoxicity in rats," *International Journal of Veterinary Science*, vol. 9, pp. 349–354, 2020.
- [41] Y. Mahmood, A. Ghaffar, and R. Hussain, "New insights into hemato-biochemical and histopathological effects of acetochlor in bighead carp (*Aristichthys nobilis*)," *Pakistan Veterinary Journal*, vol. 41, pp. 538–544, 2021.
- [42] C. C. Lerro, S. Koutros, G. Andreotti et al., "Use of acetochlor and cancer incidence in the agricultural health study," *International Journal of Cancer*, vol. 137, no. 5, pp. 1167–1175, 2015.
- [43] G. Jabeen, F. Manzoor, and M. Arshad, "Effect of cadmium exposure on hematological, nuclear and morphological alterations in erythrocyte of fresh water fish (*Labeo rohita*)," *Continental Veterinary Journal*, vol. 1, no. 1, pp. 20–24, 2021.
- [44] I. Hayashi, Y. Morishita, K. Imai, M. Nakamura, K. Nakachi, and T. Hayashi, "High-throughput spectrophotometric assay of reactive oxygen species in serum," *Mutation Research*, vol. 631, no. 1, pp. 55–61, 2007.
- [45] M. Iqbal, S. Sharma, H. Rezazadeh, N. Hasan, M. Abdulla, and M. Athar, "Glutathione metabolizing enzymes and oxidative stress in ferric nitrilotriacetate mediated hepatic injury," *Redox Reports*, vol. 2, no. 6, pp. 385–391, 1996.
- [46] D. J. Jollow, J. R. Mitchell, N. Zampaglione, and J. R. Gillette, "Bromobenzene-induced liver necrosis. Protective role of glutathione and evidence for 3,4-bromobenzene oxide as the hepatotoxic metabolite," *Pharmacology*, vol. 11, no. 3, pp. 151–169, 1974.
- [47] B. Chance and A. Maehly, "[136] Assay of catalases and peroxidases," *Methods in Enzymology*, vol. 2, pp. 764–775, 1955.
- [48] P. Kakkar, B. Das, and P. Viswanathan, "A modified spectrophotometric assay of superoxide dismutase," *Indian Journal of Biochemistry and Biophysics*, vol. 21, no. 2, pp. 130–132, 1984.
- [49] J. Jiang, S. Wu, X. Liu et al., "Effect of acetochlor on transcription of genes associated with oxidative stress, apoptosis, immunotoxicity and endocrine disruption in the early life stage of zebrafish," *Environmental Toxicology and Pharmacology*, vol. 40, no. 2, pp. 516–523, 2015.

- [50] H. Wang, Z. Meng, L. Zhou et al., "Effects of acetochlor on neurogenesis and behaviour in zebrafish at early developmental stages," *Chemosphere*, vol. 220, pp. 954–964, 2019.
- [51] W. Xue, Y. Zhang, and W. Wei, "Single and binary-combined toxic effects of acetochlor and Cu^{2+} on goldfish (*Carassius auratus*) larvae," *Comparative Biochemistry and Physiology C Toxicology and Pharmacology*, vol. 250, article 109165, 2021.
- [52] Y. Chang, L. Mao, L. Zhang, Y. Zhang, and H. Jiang, "Combined toxicity of imidacloprid, acetochlor, and tebuconazole to zebrafish (*Danio rerio*): acute toxicity and hepatotoxicity assessment," *Environmental Science and Pollution Research International*, vol. 27, no. 10, pp. 10286–10295, 2020.
- [53] K. Birnie-Gauvin, D. Costantini, S. J. Cooke, and W. G. Willmore, "A comparative and evolutionary approach to oxidative stress in fish: a review," *Fish and Fisheries*, vol. 18, no. 5, pp. 928–942, 2017.
- [54] V. S. de Oliveira, A. J. G. Castro, K. Marins et al., "Pyriproxyfen induces intracellular calcium overload and alters antioxidant defenses in *Danio rerio* testis that may influence ongoing spermatogenesis," *Environmental Pollution*, vol. 270, article 116055, 2021.
- [55] H. Sies and D. P. Jones, "Reactive oxygen species (ROS) as pleiotropic physiological signalling agents," *Nature Reviews Molecular Cell Biology*, vol. 21, no. 7, pp. 363–383, 2020.
- [56] B. Halliwell and J. M. C. Gutteridge, *Free Radicals in Biology and Medicine*, Oxford Univ. Press, London, 4th Ed. edition, 2007.
- [57] J. A. Adeyemi, A. da Cunha Martins-Junior, and F. Barbosa Jr., "Teratogenicity, genotoxicity and oxidative stress in zebrafish embryos (*Danio rerio*) co-exposed to arsenic and atrazine," *Comparative Biochemistry and Physiology*, vol. 172–173, pp. 7–12, 2015.
- [58] O. M. Ighodaro and O. A. Akinloye, "First line defence antioxidants-superoxide dismutase (SOD), catalase (CAT) and glutathione peroxidase (GPX): their fundamental role in the entire antioxidant defence grid," *Alexandria Journal of Medicine*, vol. 54, no. 4, pp. 287–293, 2018.
- [59] K. Maharajan, S. Muthulakshmi, B. Nataraj, M. Ramesh, and K. Kadirvelu, "Toxicity assessment of pyriproxyfen in vertebrate model zebrafish embryos (*Danio rerio*): A multi biomarker study," *Aquatic Toxicology*, vol. 196, pp. 132–145, 2018.
- [60] S. K. Veedu, G. Ayyasamy, H. Tamilselvan, and M. Ramesh, "Single and joint toxicity assessment of acetamiprid and thiamethoxam neonicotinoids pesticides on biochemical indices and antioxidant enzyme activities of a freshwater fish *Catla catla*," *Comparative Biochemistry and Physiology, Part C*, vol. 257, article 109336, 2022.
- [61] Y. Jin, X. Zhang, L. Shu et al., "Oxidative stress response and gene expression with atrazine exposure in adult female zebrafish (*Danio rerio*)," *Chemosphere*, vol. 78, no. 7, pp. 846–852, 2010.
- [62] A. Khare, N. Chhawani, and K. Kumari, "Glutathione reductase and catalase as potential biomarkers for synergistic intoxication of pesticides in fish," *Biomarkers*, vol. 24, no. 7, pp. 666–676, 2019.
- [63] G. Afzal, H. I. Ahmad, R. Hussain et al., "Bisphenol A induces histopathological, hematobiochemical alterations, oxidative stress, and genotoxicity in common carp (*Cyprinus carpio* L.)," *Oxidative Medicine and Cellular Longevity*, vol. 2022, Article ID 5450421, 14 pages, 2022.
- [64] P. Khanna, C. Ong, B. H. Bay, and G. H. Baeg, "Nanotoxicity: an interplay of oxidative stress, inflammation and cell death," *Nanomaterials*, vol. 5, no. 3, pp. 1163–1180, 2015.
- [65] P. A. Rani, L. K. Mun, G. Hande, and S. Valiyaveetil, "Cytotoxicity and genotoxicity of silver nanoparticles in human cells," *ACS Nano*, vol. 3, pp. 279–290, 2009.
- [66] J. Q. Wang, R. Hussain, A. Ghaffar et al., "Clinico-hematological, mutagenic, and oxidative stress induced by pendimethalin in freshwater fish bighead carp (*Hypophthalmichthys nobilis*)," *Oxidative Medicine and Cellular Longevity*, vol. 2022, Article ID 2093822, 15 pages, 2022.
- [67] M. Valko, H. Morris, and M. Cronin, "Metals, toxicity and oxidative stress," *Current Medicinal Chemistry*, vol. 12, no. 10, pp. 1161–1208, 2005.
- [68] R. Hussain, A. Ghaffar, G. Abbas et al., "Thiamethoxam at sublethal concentrations induces histopathological, serum biochemical alterations and DNA damage in fish (*Labeo rohita*)," *Toxin Reviews*, vol. 41, no. 1, pp. 154–164, 2022.
- [69] F. Regoli and M. E. Giuliani, "Oxidative pathways of chemical toxicity and oxidative stress biomarkers in marine organisms," *Marine Environmental Research*, vol. 93, pp. 106–117, 2014.
- [70] Y. Liu, K. Fang, X. Zhang, T. Liu, and X. Wang, "Enantioselective toxicity and oxidative stress effects of acetochlor on earthworms (*Eisenia fetida*) by mediating the signaling pathway," *Science of Total Environment*, vol. 766, article 142630, 2021.
- [71] A. Ghaffar, S. Ashraf, R. Hussain et al., "Clinico-hematological disparities induced by triazophos (organophosphate) in Japanese quail," *Pakistan Veterinary Journal*, vol. 34, pp. 257–259, 2014.
- [72] C. Webb and D. Twedt, "Oxidative stress and liver disease," *Veterinary Clinics of North America: Small Animal Practice*, vol. 38, no. 1, pp. 125–135, 2008.
- [73] K. Tanikawa and T. Torimura, "Studies on oxidative stress in liver diseases: important future trends in liver research," *Medical Molecular Morphology*, vol. 39, no. 1, pp. 22–27, 2006.
- [74] A. Ghaffar, R. Hussain, A. Khan, and R. Z. Abbas, "Hematobiochemical and genetic damage caused by triazophos in fresh water fish, *Labeo rohita*," *International Journal of Agriculture and Biology*, vol. 17, no. 3, pp. 637–642, 2015.
- [75] R. Lackner, "Oxidative stress," in *Fish by Environmental Pollutants Fish Ecotoxicology*, pp. 203–224, Springer, 1998.
- [76] L. J. Marnett, "Lipid peroxidation-DNA damage by malondialdehyde," *Mutation Research/Fundamental and Molecular Mechanisms of Mutagenesis*, vol. 424, no. 1-2, pp. 83–95, 1999.
- [77] R. O. Sule, L. Condon, and A. V. Gomes, "A common feature of pesticides: oxidative stress—the role of oxidative stress in pesticide-induced toxicity," *Oxidative Medicine and Cellular Longevity*, vol. 2022, Article ID 5563759, 31 pages, 2022.
- [78] L. J. Su, J. H. Zhang, H. Gomez et al., "Reactive oxygen species-induced lipid peroxidation in apoptosis, autophagy, and ferroptosis," *Oxidative Medicine and Cellular Longevity*, vol. 2019, Article ID 5080843, 13 pages, 2019.
- [79] L. J. Marnett, "Oxy radicals, lipid peroxidation and DNA damage," *Toxicology*, vol. 181–182, pp. 219–222, 2002.
- [80] Ü. Acar, B. E. İnanan, F. Z. Navruz, and S. Yılmaz, "Alterations in blood parameters, DNA damage, oxidative stress and antioxidant enzymes and immune-related genes expression in Nile tilapia (*Oreochromis niloticus*) exposed to glyphosate-based herbicide," *Comparative Biochemistry and Physiology, Part C*, vol. 249, article 109147, 2021.

Retraction

Retracted: Exploration of ACE-Inhibiting Peptides Encrypted in *Artemisia annua* Using *In Silico* Approach

BioMed Research International

Received 12 March 2024; Accepted 12 March 2024; Published 20 March 2024

Copyright © 2024 BioMed Research International. This is an open access article distributed under the Creative Commons Attribution License, which permits unrestricted use, distribution, and reproduction in any medium, provided the original work is properly cited.

This article has been retracted by Hindawi following an investigation undertaken by the publisher [1]. This investigation has uncovered evidence of one or more of the following indicators of systematic manipulation of the publication process:

- (1) Discrepancies in scope
- (2) Discrepancies in the description of the research reported
- (3) Discrepancies between the availability of data and the research described
- (4) Inappropriate citations
- (5) Incoherent, meaningless and/or irrelevant content included in the article
- (6) Manipulated or compromised peer review

The presence of these indicators undermines our confidence in the integrity of the article's content and we cannot, therefore, vouch for its reliability. Please note that this notice is intended solely to alert readers that the content of this article is unreliable. We have not investigated whether authors were aware of or involved in the systematic manipulation of the publication process.

Wiley and Hindawi regrets that the usual quality checks did not identify these issues before publication and have since put additional measures in place to safeguard research integrity.

We wish to credit our own Research Integrity and Research Publishing teams and anonymous and named external researchers and research integrity experts for contributing to this investigation.

The corresponding author, as the representative of all authors, has been given the opportunity to register their agreement or disagreement to this retraction. We have kept a record of any response received.

References

- [1] M. N. Shahid, M. Zawar, A. Jamal, B. B. Mohamed, S. Khalid, and F. S. Bahwerth, "Exploration of ACE-Inhibiting Peptides Encrypted in *Artemisia annua* Using *In Silico* Approach," *BioMed Research International*, vol. 2022, Article ID 5367125, 10 pages, 2022.

Research Article

Exploration of ACE-Inhibiting Peptides Encrypted in *Artemisia annua* Using *In Silico* Approach

Muhammad Naveed Shahid ¹, Maryam Zawar ¹, Adil Jamal ²,
Bahaeldeen Babiker Mohamed ³, Sana Khalid ⁴ and Fayez Saeed Bahwerth ⁵

¹Department of Botany, Division of Science and Technology, University of Education, Lahore, Pakistan

²Sciences and Research, College of Nursing, Umm Al Qura University, Saudi Arabia

³Institute of Environment Natural Resources, The National Centre of Research, Khartoum, Sudan

⁴Department of Botany, Lahore College for Women University, Lahore, Pakistan

⁵Central Laboratory and Blood Bank, King Faisal Hospital, Makkah-24235, Saudi Arabia

Correspondence should be addressed to Bahaeldeen Babiker Mohamed; bahaeldeen.elhag@ncr.gov.sd

Received 27 March 2022; Accepted 27 April 2022; Published 23 May 2022

Academic Editor: Abdelmoteleb Elokil

Copyright © 2022 Muhammad Naveed Shahid et al. This is an open access article distributed under the Creative Commons Attribution License, which permits unrestricted use, distribution, and reproduction in any medium, provided the original work is properly cited.

The renin-angiotensin system (RAS) is involved in body fluid regulation, but one of its enzymes, angiotensin-converting enzyme (ACE), indirectly causes hypertension by constricting blood vessels. Autoimmune illness is linked to the increased risk of hypertension and cardiovascular disease. In this study, ACE-inhibiting peptides were studied from *Artemisia annua* proteins. *In silico* hydrolysis of proteins was performed by BIOPEP-UWM using proteolytic enzymes from plant, microbial, and digestive sources. The physicochemical properties of 1160 peptides were determined using the peptide package of R studio. Di- and tripeptides were mostly released with a molecular weight of 170 to 350 Da. PeptideRanker was used to select 16 peptides from a pool of 1160 peptides based on their likelihood of being bioactive. Molecular docking was performed by DS 2020 and AutoDock Vina, which revealed that the stability of the ligand-receptor complex is due to hydrogen bonding and electrostatic and hydrophobic interactions. Their binding energies ranged from -31.81 to -20.09 kJ/mol. For drug-likeness evaluation, an online tool SwissADME was used that follows the ADME rule (absorption, distribution, metabolism, and excretion) to check the pharmacokinetics and drug-likeness of the compound. In the future, the released peptides can be used to make functional nutraceutical foods against hypertension.

1. Introduction

Most cardiovascular diseases caused by hypertension have a high death ratio, and approximately 66% of hypertension cases are found, especially in developing countries [1]. Auto-immune illnesses, such as systemic lupus erythematosus and rheumatoid arthritis, are linked to an increased risk of hypertension and cardiovascular disease [2]. A major community-based research, for example, discovered a higher prevalence of hypertension among RA patients (31%), compared to the general population (23%) [3]. A hormone system renin-angiotensin system (RAS) is involved in body fluid regulation but indirectly increases blood pressure [4]. Angiotensin-converting enzymes in the RAS system convert angiotensin

I to angiotensin *II*, which narrows the blood vessels and causes hypertension [5]. From different natural resources, many ACE-inhibiting peptides have been studied to stabilize blood pressure [6].

As the frequency of hypertension increased day by day, antihypertensive activity of most of the bioactive peptides was studied and gained much attention [7]. For the inhibition of ACE, many antihypertensive drugs have been discovered, such as captopril, lisinopril, and aliskiren. On the one hand, these drugs are beneficial, but at the same time, they cause serious side effects, such as disturbing the potassium level, loss of taste, and dizziness [8]. Therefore, antihypertensive peptides were studied from different sources, such as chia seeds, sesame seeds, and flaxseeds.

TABLE 1: List of selected proteins and their attributes.

| S. no. | Accession no. | Protein | Function | Residue length | MW (kDa) |
|--------|---------------|---|--|----------------|----------|
| 1 | Q9LLR9 | Epi-cedrol synthase | Terpenoid biosynthesis | 547 | 63.57 |
| 2 | Q9SPN0 | R-linalool synthase QH1, chloroplastic | Terpenoid biosynthesis | 567 | 65.71 |
| 3 | Q8SA63 | Beta-caryophyllene synthase | Sesquiterpene biosynthesis | 548 | 63.75 |
| 4 | Q94G53 | (-)-beta-Pinene synthase, chloroplastic | Monoterpene biosynthesis | 582 | 67.52 |
| 5 | Q1PS23 | Amorpha-4,11-diene 12-monooxygenase | Antimalarial endoperoxide artemisinin biosynthesis | 495 | 55.72 |
| 6 | Q9AR04 | Amorpha-4,11-diene synthase | Antimalarial endoperoxide artemisinin biosynthesis | 546 | 63.94 |
| 7 | Q43319 | 3-Hydroxy-3-methylglutaryl coenzyme A reductase | Isoprenoid biosynthesis | 560 | 60.34 |
| 8 | Q9SWQ3 | Hydroxymethylglutaryl-CoA reductase (NADPH) | Isoprene biosynthesis | 567 | 61.7 |
| 9 | C5H429 | Artemisinic aldehyde delta(11(13)) reductase | Antimalarial endoperoxide artemisinin biosynthesis | 388 | 42.59 |
| 10 | C5I9X1 | Aldehyde dehydrogenase 1 | Sesquiterpene biosynthesis | 499 | 53.8 |
| 11 | P49350 | Farnesyl pyrophosphate synthase | Sesquiterpene biosynthesis | 343 | 39.41 |

By hydrolysis of mung bean proteins, five ACE-inhibiting peptides (LPRL, YADLVE, LRLESF, HLNVVHEN, and PGSGCAGTDL) were released, and their effect was studied when given to hypertensive rats. The results showed that YADLVE was more effective than others [9]. Banana pulp was purified into three protein extracts as purified, partially purified, and crude. Upon hydrolysis with proteolytic enzymes, the crude extract released more ACE-inhibiting peptides (85.20%) [10].

Liang et al. [11] identified a peptide IAF from pumpkin seeds using *in silico* approaches. By molecular docking, a strong interaction was found between IAF and ACE, which shows hydrogen bonding between two residues of ACE, His513 and Glu162, with IAF. Similarly, many antihypertensive peptides are released from different plant sources, such as bitter melon seeds [12], peach seeds [13], cottonseed [14], hemp seeds [15], sesame seeds [16], and date seeds [17].

Four novel ACE-inhibiting peptides (MAF, NMF, HPF, and MCG) were identified from quinoa proteins. Hydrolysis of proteins was performed by an *in silico* method using plant proteolytic enzymes, ficin, papain, and stem bromelain [18]. *Artemisia annua* is a short-day plant containing a high protein content and several essential amino acids. Due to high antimalarial activity, the Nobel Prize was awarded to the species in 2015 [19].

In this research, antihypertensive peptides were studied from *A. annua* proteins using bioinformatics tools. A molecular docking study revealed the stability of the peptide and ACE complex. These peptides act as inhibitors of angiotensin-converting enzyme (ACE). The released peptides are then incorporated into food products to make functional foods.

2. Materials and Methods

2.1. Hydrolysis of Proteins by Proteolytic Enzymes. Proteins were selected on the basis of secondary metabolite synthesis, and for sequence retrieval, the UniProt database ([https://](https://www.uniprot.org/)

TABLE 2: The source of the enzyme, type of enzyme, and released ACE inhibitory peptides by each enzyme are listed.

| Enzyme source | Enzyme type | Total no. of ACE-inhibiting peptides |
|---------------|------------------------|--------------------------------------|
| Plant | Papain | 204 |
| | Ficin | 252 |
| | Stem bromelain | 175 |
| | Thermolysin | 141 |
| Microbial | Subtilisin | 164 |
| | Proteinase P1 | 83 |
| Digestive | Trypsin | 21 |
| | Pepsin | 51 |
| | Pancreatic elastase II | 69 |
| Total | | 1160 |

www.uniprot.org/) was used. The BIOPEP-UWM database [20] (<http://www.uwm.edu.pl/Biochemia/Index.php/En/Biopep>) was used to hydrolyze the proteins by different proteolytic enzymes. Nine types of proteases from three sources were used: plant proteases (papain, ficin, and stem bromelain), digestive enzymes (pancreatic elastase II, pepsin, and trypsin), and microbial enzymes (subtilisin, thermolysin, and proteinase P1). After hydrolysis, ACE-inhibiting peptides were selected using the BIOPEP-UWM “search for active fragment” feature.

2.2. Physicochemical Parameters of ACE Inhibitory Peptides Released by Proteolytic Enzymes. Using the “peptides” package in RStudio [21], the physicochemical properties of the released peptides were studied. The properties include molecular weight, net charge, isoelectric point, hydrophobicity, and Boman index.

2.3. Molecular Docking of Antihypertensive Peptides with ACE Receptor. From released ACE inhibitory peptides, only

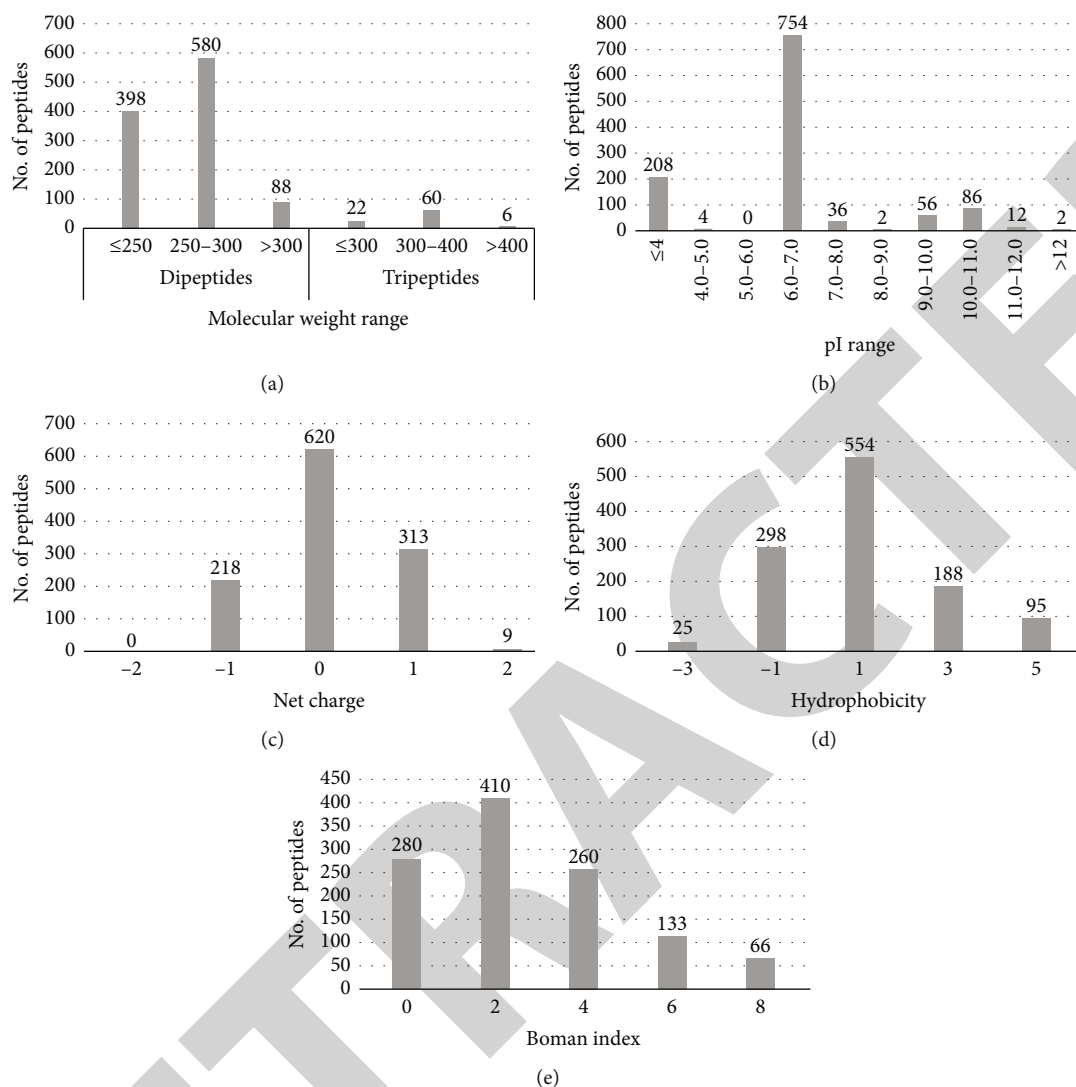


FIGURE 1: Physiochemical parameters of ACE-inhibiting peptides: (a) molecular weight, (b) isoelectric point, (c) net charge, (d) hydrophobicity, and (e) Boman index.

16 peptides were selected for molecular docking using the PeptideRanker tool (<http://distilldeep.ucd.ie/PeptideRanker/>). These 16 peptides with the inhibitory drug captopril were used as ligands, and their structures were generated using Discovery Studio 2020 (<https://discover.3ds.com/discovery-studio-visualizer-download>). Human ACE structure was used as receptor for docking. AutoDock Vina [22] was used to prepare the receptor by removing the water molecules and adding charges to the protein. For ligand binding, a site was constructed (radius 13 Å; coordinates x : 38.7154, y : 35.4135, and z : 41.6065).

For docking result visualization, Discovery Studio 2020 was used, and hydrogen bonding and electrostatic and hydrophobic interactions were studied between the ligand and receptor residues.

2.4. Evaluation of Drug-Like Properties of Peptides. The drug-like properties of peptides were evaluated *in silico*

using SwissADME (<http://www.swissadme.ch>). This tool follows the ADME rule (absorption, distribution, metabolism, and excretion) to check the pharmacokinetics and drug-likeness of compounds. ToxinPred (<http://crdd.osdd.net/raghava/toxinpred/>) was used to predict the toxicity of compounds.

3. Results

3.1. Proteolytic Enzyme Sources and Effect on Antihypertensive Peptides. A total of 11 proteins of *Artemisia annua* were selected, and their characteristics are shown in Table 1. On hydrolysis, most of the released peptides were di- and tripeptides. The number of released peptides depends on the enzyme source and type (Table 2). A total of 1160 ACE inhibitory peptides were released, from which 631, 141, and 388 were released by plant, digestive, and microbial proteases, respectively. Approximately 54.3% of

peptides were released by plants, of which 32.3%, 28%, and 40% were released by enzymes, papain, stem bromelain, and ficin, respectively. Microbial proteases release 33.4% of ACE inhibitory peptides with a high degree of hydrolysis by thermolysin (36.3%), proteinase P1 (21.3%), and subtilisin (42.2%). However, fewer peptides were released by digestive enzymes (12.2%) than by the other two types. For trypsin, pepsin, and pancreatic elastase II, the degree of hydrolysis was 14.8%, 36%, and 49%, respectively. The number of peptides revealed that plant proteases were superior to microbial and digestive enzymes.

3.2. Physicochemical Parameters of ACE Inhibitory Peptides Released by Proteolytic Enzymes. The physicochemical parameters of ACE-inhibiting peptides that have been released by hydrolysis were demonstrated (Figure 1). The molecular weight varies between 170 and 410 Da. The molecular weights of dipeptides ranged from 170 to 350 Da, and they were abundantly released from proteins. The MW of the majority of the dipeptides ranged between 250 and 300 Da. Tripeptides ranging in size from 300 to 410 Da were also found (Figure 1(a)). The isoelectric point of peptides ranged from 3.8 to 12.5, and approximately 212 peptides had a pI less than 5 with a net charge of -1, which indicates the presence of amino acids with negative charges in most of the peptides.

Approximately 790 peptides had $pI \leq 8$ with a net charge of zero, while 180 peptides had $pI \leq 11$ with a net charge of 1. These peptides mostly contain amino acids with positive charges (Figures 1(b) and 1(c)). The hydrophobicity of the 1160 peptides ranged from -3.50 to 5.00. Approximately 494, 196, and 410 peptides were neutral, hydrophilic, and hydrophobic, respectively (Figure 1(d)). The ACE inhibitory peptide Boman index ranged from -3.62 to 14.92, and most of the peptides had BI less than 2 (Figure 1(e)).

3.3. Molecular Docking of Antihypertensive Peptides with ACE Receptor. The probability of peptides' bioactivity was predicted by PeptideRanker using score values ranging from 0.021 to 0.99. The first 16 peptides with a probability value close to 1 were selected for docking. The binding energies of the ligand-receptor complex ranged from -31.81 to -20.09 (Table 3). According to the results, most of the peptides showed strong hydrogen bonding as well as electrostatic and hydrophobic interactions with ACE residues (Asn70, Val518, His513, Thr140, and Phe512), which showed the ACE-inhibiting properties of peptides (Figure 2). RF and RW interacted with ACE active site pockets as S1 and S2, respectively.

GW interacted with Asp141, Val148, and Ile73 via hydrogen bonding and hydrophobic interactions. Hydrophobic amino acids of peptides, present near the C-terminus, strongly interact with active site residues. Hydrogen bonds were displayed (Table 4) that are found in ligand-receptor complexes. His348, Glu372, and His344 coordinates interact with the zinc ion present in the ACE structure, showing the importance of Zn in ACE inhibition. As none of the peptides interacted with Zn ions, peptides showed low inhibitory activity compared to captopril (Table 3).

TABLE 3: Evaluated binding energies and Zn II coordination distances of ligand-receptor complexes.

| Ligand | Affinity energy (kJ/mol) | Zn coordination | |
|-----------|--------------------------|-----------------|-------------------------------|
| | | Distance (Å) | Atom |
| AF | -26.98 | | No zinc coordination |
| FG | -26.79 | | No zinc coordination |
| FP | -23.02 | | No zinc coordination |
| FY | -31.81 | | No zinc coordination |
| FR | -25.12 | | No zinc coordination |
| GW | -22.19 | | No zinc coordination |
| LW | -28.47 | | No zinc coordination |
| MW | -23.02 | | No zinc coordination |
| RF | -30.98 | | No zinc coordination |
| RW | -27.44 | | No zinc coordination |
| WG | -28.88 | | No zinc coordination |
| WL | -24.28 | | No zinc coordination |
| YF | -28.28 | | No zinc coordination |
| CF | -27.95 | | No zinc coordination |
| GF | -20.09 | | No zinc coordination |
| MF | -21.35 | | No zinc coordination |
| Captopril | -26.78 | 2.76 | Sulfhydryl group of captopril |

3.4. Drug-Likeness Evaluation. The peptide drug-likeness profile was demonstrated (Table 5). The results revealed numerous similarities of peptides when compared to the inhibitory drug captopril. As the number of ROTB and TPSA of RF, RW, and FP peptides were not according to the required value, they were present outside the estimated range (see the shaded region in Figure 3).

All of the other peptides had the same bioavailability as captopril (0.55). None of the peptides showed CYP3A4 inhibition except for RF, RW, and FR, and all the peptides also had a high GIA. Except for MW and WL, all other peptides acted as P-glycoprotein substrates and had high bioavailability and GIA.

4. Discussion

For the breakdown of peptide links in proteins, proteolytic enzymes (also known as proteases or proteinases) were used. Because of their critical roles in biological processes, they are vital in medicine, pharmaceuticals, biotechnology, and a variety of research applications, such as protein digestion, peptide synthesis, cell culture, and peptide sequencing [23]. The amino acid specificity at both terminals determines the type of protease used for peptide synthesis [24]. As most ACE inhibitory peptides consist of 2-12 amino acids, the binding of peptides with ACE residues becomes very easy [25].

This is due to the wide range of specificity of amino acids, such as papain, which primarily cleaves hydrophobic and basic amino acids [23]. The peptide's affinity for ACE was increased when positively charged amino acids and basic amino acids were present at the C and N termini, respectively. As a result, antihypertensive activity also increased [26].

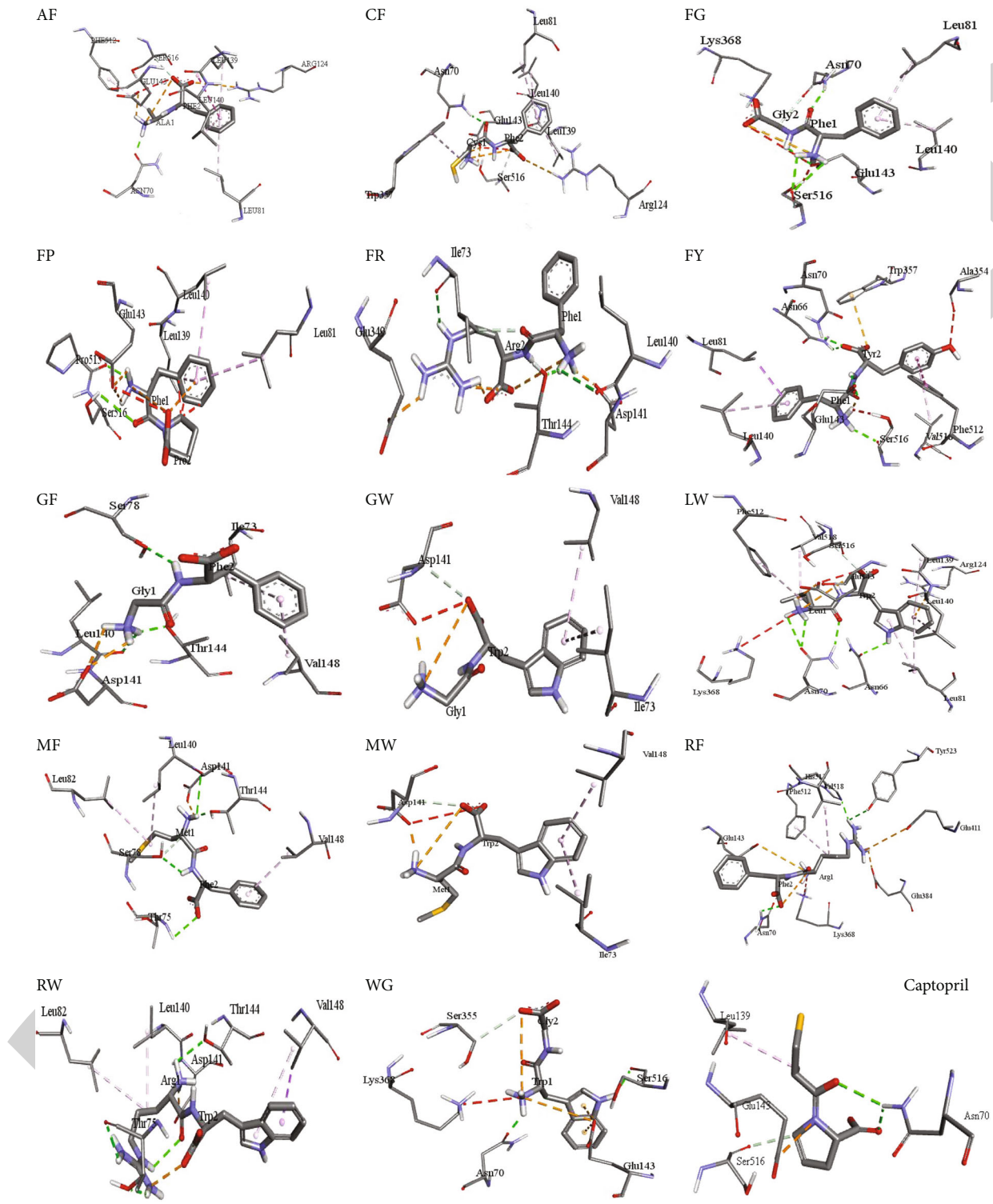


FIGURE 2: The best pose of ligand docked with receptor showing hydrogen bonding as well as hydrophobic and electrostatic interaction.

The hydrophobicity of amino acid side chains typically depends on the molecular weight of the peptides [27]. Amino acid hydrophobicity at the C-terminus influences ACE inhibition activity, as higher hydrophobicity directly increases the inhibition action [28]. Most of the dipeptides had high hydrophobicity at the C-terminus; therefore, the

inhibition action of peptides increased [29]. Hydrogen bonding plays an important role in the structure of ligand-receptor complexes [30].

Coordination with other residues, on the other hand, caused distortion of Zn ions, due to which ACE lost its inhibitory action [31]. The optimized cutoff values for

TABLE 4: In the best docking pose of the ligand-receptor complex, hydrogen bonds and their distances (Å) with ACE residues are shown.

| ACE residues in H-bonding | Number of H-bonds and their corresponding distance (Å) | | | | | | | | | | | | | | Captopril | | |
|------------------------------|--|---------|--------------|---------|--------------|---------|---------|--------------|--------------|---------|---------|---------|--------------|---------|-----------|--------------|---------|
| | FG | FP | AF | FR | FY | GW | LW | RF | RW | WG | MW | WL | YF | CF | | GF | MF |
| THR144:OG1 | | 1 (2.7) | | 1 (2.1) | | | | | 1 (2.6) | | | 1 (3.7) | 1 (1.9) | | 1 (2.0) | 1 (2.0) | |
| TYR2:O | | | | | 2 (2.1, 2.3) | | | | | | | | | | | | |
| ASN70:OD1 | 1 (3.3) | | 1 (1.9) | | | 1 (2.6) | | | | 1 (1.9) | | | | | | | 1 (2.8) |
| LEU140:O | | | | 1 (3.0) | | | | 2 (2.9, 2.5) | | | | | 1 (2.7) | | 1 (2.6) | 1 (3.0) | 1 (3.7) |
| ILE73:O | | | | 1 (2.6) | | | 1 (2.3) | | | | | 1 (2.5) | | | | | |
| SER516:O | 2 (2.7, 2.9) | | | | 1 (2.3) | | | | | 1 (2.2) | | | | 1 (2.0) | | | 1 (3.3) |
| PHE1:O | 1 (2.1) | 1 (3.0) | | 1 (3.6) | | | | 1 (2.2) | | | | | | | 1 (3.3) | 1 (2.9) | |
| TRP2:O | | | | | | | 1 (3.8) | | | 2 (3.4) | | | | | | | |
| ARG1:O | | | | | | | | 1 (2.8) | | | | | | | | | |
| PRO515:O | | 1 (2.4) | | | | | | | | | | | | | | | |
| GLU143:OE1 | 1 (2.5) | | 1 (2.1) | | 1 (2.7) | | | | | | | | | | | | 1 (3.6) |
| LEU1:O | | | | | | 1 (2.4) | | | | | | 1 (3.6) | | | | | |
| THR75:O | | | | 1 (2.6) | | | | | 2 (2.4, 2.0) | | | | | 1 (2.0) | | | |
| TYR523:OH | 1 (2.0) | | | | | | 1 (2.6) | | | | | | | 1 (2.6) | | | |
| ASN66:OD1 | | | 1 (3.2) | | | 1 (2.5) | | | | 1 (3.0) | | | | | | | 1 (2.2) |
| SER78:OG | | | | | | | | | | | | | 2 (2.3, 2.4) | 1 (2.5) | 1 (2.5) | 2 (3.6, 2.8) | |
| TRP2:OXT | | | | 1 (3.8) | | 1 (3.0) | 1 (3.0) | | 1 (2.3) | 1 (3.8) | | | | | | | |
| HIS513:NE2 | 1 (2.4) | | 2 (2.5, 3.0) | | | | 1 (2.1) | | | | | | | | | | |
| ASP141:OD1 | | | | | | | | | | | 1 (2.5) | | | 1 (2.3) | | | |
| Total | 6 | 4 | 5 | 6 | 4 | 3 | 4 | 5 | 5 | 3 | 3 | 6 | 3 | 4 | 4 | 5 | 5 |

TABLE 5: *In silico* drug-likeness assessment illustrating the antihypertensive peptide ADMET profile.

| Rule | Physicochemical properties | | | | Toxicity | | Lipophilicity | | Drug-likeness | | Pharmacokinetics | | |
|-----------|----------------------------|----------|---------|---------|------------|-----------------------|---------------|---------------------|-----------------------|----------------|------------------|--------------------------|------------------|
| | Mol. wt. (g/mol) | ROTB (n) | HBA (n) | HBD (n) | ESOL log S | ToxinPred (SVM score) | TPSA (Å) | ClogP _{ow} | Bioavailability score | Lipinski filer | GIA | P-glycoprotein substrate | CYP3A4 inhibitor |
| AF | <500 | <10 | <10 | <5 | — | — | <140 | <5 | — | — | — | — | — |
| FG | 236.27 | 6 | 4 | 3 | 0.39 (HS) | Nontoxic -0.8 | 92.42 | 0.05 | 0.55 | Yes (0) | High | No | No |
| FP | 222.24 | 6 | 4 | 3 | 0.48 (HS) | Nontoxic -0.8 | 92.42 | -0.16 | 0.55 | Yes (0) | High | No | No |
| FR | 262.3 | 5 | 4 | 3 | -0.51 (VS) | Nontoxic -0.8 | 83.63 | 0.32 | 0.55 | Yes (0) | High | No | No |
| FY | 321.37 | 11 | 5 | 6 | 0.79 (HS) | Nontoxic -0.8 | 154.32 | -0.66 | 0.55 | Yes (1) | Low | No | No |
| GW | 328.36 | 8 | 5 | 4 | -0.66 (VS) | Nontoxic -0.8 | 112.65 | 0.83 | 0.55 | Yes (0) | High | No | No |
| LW | 261.28 | 6 | 4 | 4 | 0.23 (HS) | Nontoxic -0.8 | 108.21 | -0.18 | 0.55 | Yes (0) | High | No | No |
| MW | 317.38 | 8 | 4 | 4 | -0.18 (VS) | Nontoxic -0.79 | 108.21 | 1.09 | 0.55 | Yes (0) | High | No | No |
| RF | 335.42 | 9 | 4 | 4 | -0.67 (VS) | Nontoxic -0.8 | 133.51 | 0.86 | 0.55 | Yes (0) | High | Yes | No |
| RW | 321.37 | 11 | 5 | 6 | 0.77 (HS) | Nontoxic -0.8 | 154.32 | -0.59 | 0.55 | Yes (1) | Low | No | No |
| WG | 360.41 | 11 | 5 | 7 | 0.26 (HS) | Nontoxic -0.8 | 170.11 | -0.44 | 0.55 | Yes (1) | Low | No | No |
| WL | 261.28 | 6 | 4 | 4 | -0.11 (VS) | Nontoxic -0.8 | 108.21 | 0.08 | 0.55 | Yes (0) | High | No | No |
| YF | 317.38 | 8 | 4 | 4 | -1.11 (VS) | Nontoxic -0.8 | 108.21 | 1.13 | 0.55 | Yes (0) | High | Yes | No |
| CF | 328.36 | 8 | 5 | 4 | -0.66 (VS) | Nontoxic -0.8 | 112.65 | 0.78 | 0.55 | Yes (0) | High | No | No |
| GF | 268.33 | 7 | 4 | 3 | 0.32 (HS) | Nontoxic -0.79 | 131.22 | -0.02 | 0.55 | Yes (0) | High | No | No |
| MF | 222.24 | 6 | 4 | 3 | 0.32 (HS) | Nontoxic -0.8 | 92.42 | -0.23 | 0.55 | Yes (0) | High | No | No |
| Captopril | 296.39 | 9 | 4 | 3 | -0.25 (VS) | Nontoxic -0.8 | 117.72 | 0.72 | 0.55 | Yes (0) | High | No | No |
| | 217.29 | 4 | 3 | 1 | -1.14 (VS) | | 96.41 | 0.62 | 0.56 | Yes (0) | High | No | No |



FIGURE 3: Oral bioavailability range of the ACE-inhibiting peptides and inhibitory drug (captopril). LIPO: lipophilicity ($\text{ClogP}_{o/w} < 5$); SIZE: molecular size ($\text{mol} < 500 \text{ g/mol}$); INSOLU: solubility; POLAR: polarity ($\text{TPSA} < 130 \text{ \AA}^2$); $\log S$ (ESOL) < 6 ; INSATU: insaturation (fraction $\text{Csp3} < 1$); FLEX: flexibility (number of rotatable bonds < 9). The colorful zone represents the optimum physicochemical space for oral bioavailability.

molecules being permeable have been proposed, which include $\text{PSA} < 140$, $\text{ClogP} < 5$, $\text{HBA} < 10$, $\text{HBD} < 5$, and $\text{MW} < 350$ [32]. By following these optimized values, the oral administration properties of molecules increased [33]. The flexibility and polarity of the drugs affect their oral bioavailability. The number of ROTB and TPSA represents the flexibility and polarity of a compound. The oral bioavailability of a compound becomes low and high due to the pres-

ence of more rotatable bonds and small topological surface areas, respectively [34].

ACE inhibitors are partially metabolized by CYP3A4 because they have little effect on cytochrome interactions [35, 36]. The CYP3A5 enzyme family is important in drug metabolism [37]. Interactions between drug-active compounds and any of the CYP isozymes can result in drug bioaccumulation (when a CYP isozyme is activated) or rapid

metabolism (when a CYP isozyme is inhibited) in the body. Both scenarios are undesirable because the first can result in overdosing and the second in toxicity [38].

ACE inhibitors are routinely given for the treatment of hypertension and renal dysfunction in systemic lupus erythematosus (SLE) patients, despite the fact that no randomised controlled studies have been conducted [39]. The use of ACE inhibitors during SLE is generally well tolerated and associated with a delay in the onset of renal involvement and a decrease in the risk of disease relapse in SLE patients, which is likely due to a decrease in angiotensin II as well as the immunomodulatory effect of renin-angiotensin system blockade [40]. As a result, in individuals with autoimmune illness, RAS blockage may have a dual impact in controlling the autoimmune disease and its accompanying hypertension [41].

5. Conclusion

Artemisia annua proteolytic enzymes (papain, ficin, and stem bromelain) produced more antihypertensive peptides than microbial (thermolysin, proteinase P1, and subtilisin) and digestive (trypsin, pepsin, and pancreatic elastase I) enzymes. In molecular docking, a stable interaction between ligands and receptors by hydrogen bonding was studied. In addition, *in silico* drug-likeness evaluation of the ACE-inhibiting peptides revealed that all peptides followed at least four of the five rules of Lipinski filters, but FR, RW, and RF violated one of the rules. As peptides are released from proteins of medicinal plants through proteolytic enzyme hydrolysis, therefore they are used in therapeutic settings and have the ability to improve food products by being used as nutraceuticals.

Data Availability

All data is available in the main manuscript.

Conflicts of Interest

The authors declare no conflicts of interest.

References

- [1] S. Singh, R. Shankar, and G. P. Singh, "Prevalence and associated risk factors of hypertension: a cross-sectional study in urban Varanasi," *International Journal of Hypertension*, vol. 2017, Article ID 5491838, 10 pages, 2017.
- [2] V. L. Wolf and M. J. Ryan, "Autoimmune disease-associated hypertension," *Current Hypertension Reports*, vol. 21, no. 1, pp. 1–9, 2019.
- [3] A. M. Tobin, D. J. Veale, O. Fitzgerald et al., "Cardiovascular disease and risk factors in patients with psoriasis and psoriatic arthritis," *The Journal of Rheumatology*, vol. 37, no. 7, pp. 1386–1394, 2010.
- [4] C. Guang, R. D. Phillips, B. Jiang, and F. Milani, "Proteases cles du systeme renine-angiotensine : enzyme de conversion de l'angiotensine 1 et 2 et renine," *Archives of Cardiovascular Diseases*, vol. 105, no. 6-7, pp. 373–385, 2012.
- [5] P. C. J. L. Santos, J. E. Krieger, and A. C. Pereira, "Renin-angiotensin system, hypertension, and chronic kidney disease: pharmacogenetic implications," *Journal of Pharmacological Sciences*, vol. 120, no. 2, pp. 77–88, 2012.
- [6] M. Koyama, S. Hattori, Y. Amano, M. Watanabe, and K. Nakamura, "Blood pressure-lowering peptides from neo-fermented buckwheat sprouts: a new approach to estimating ACE-inhibitory activity," *PLoS One*, vol. 9, no. 9, article e105802, 2014.
- [7] B. Hernández-Ledesma, C. M. del Mar, and I. Recio, "Antihypertensive peptides: production, bioavailability and incorporation into foods," *Advances in Colloid and Interface Science*, vol. 165, no. 1, pp. 23–35, 2011.
- [8] J. Chen, B. Ryu, Y. Zhang et al., "Comparison of an angiotensin-I-converting enzyme inhibitory peptide from tilapia (*Oreochromis niloticus*) with captopril: inhibition kinetics, in vivo effect, simulated gastrointestinal digestion and a molecular docking study," *Journal of the Science of Food and Agriculture*, vol. 100, no. 1, pp. 315–324, 2020.
- [9] C. Sonklin, M. A. Alashi, N. Laohakunjit, O. Kerdchoechuen, and R. E. Aluko, "Identification of antihypertensive peptides from mung bean protein hydrolysate and their effects in spontaneously hypertensive rats," *Journal of Functional Foods*, vol. 64, p. 103635, 2020.
- [10] J. M. Ferreras, M. C. M. Clemencia, A. Hizon-Fradejas, L. Y. Uy, and M. A. Torio, "Isolation, purification and characterization of proteins in "Señorita" banana (*Musa acuminata* (AAA)'Señorita') pulp with bioactive peptides exhibiting antihypertensive and antioxidant activities," *Applied Sciences*, vol. 11, no. 5, p. 2190, 2021.
- [11] F. Liang, J. Shi, T. Zhang, and R. Zhang, "A novel angiotensin-I-converting enzyme (ACE) inhibitory peptide IAF (Ile-Ala-Phe) from pumpkin seed proteins: in silico screening, inhibitory activity, and molecular mechanisms," *European Food Research and Technology*, vol. 247, no. 9, pp. 2227–2237, 2021.
- [12] A. D. Priyanto, R. J. Doerksen, C. I. Chang et al., "Screening, discovery, and characterization of angiotensin-I converting enzyme inhibitory peptides derived from proteolytic hydrolysate of bitter melon seed proteins," *Journal of Proteomics*, vol. 128, pp. 424–435, 2015.
- [13] R. Vásquez-Villanueva, J. M. Orellana, M. L. Marina, and M. C. García, "Isolation and characterization of angiotensin converting enzyme inhibitory peptides from peach seed hydrolysates: in vivo assessment of antihypertensive activity," *Journal of Agricultural and Food Chemistry*, vol. 67, no. 37, pp. 10313–10320, 2019.
- [14] D. Gao, F. Zhang, Z. Ma et al., "Isolation and identification of the angiotensin-I converting enzyme (ACE) inhibitory peptides derived from cottonseed protein: optimization of hydrolysis conditions," *International Journal of Food Properties*, vol. 22, no. 1, pp. 1296–1309, 2019.
- [15] S. A. Malomo, J. O. Onuh, A. T. Girgih, and R. E. Aluko, "Structural and antihypertensive properties of enzymatic hemp seed protein hydrolysates," *Nutrients*, vol. 7, no. 9, pp. 7616–7632, 2015.
- [16] R. Wang, X. Lu, Q. Sun, J. Gao, L. Ma, and J. Huang, "Novel ACE inhibitory peptides derived from simulated gastrointestinal digestion in vitro of sesame (*Sesamum indicum* L.) protein and molecular docking study," *International Journal of Molecular Sciences*, vol. 21, no. 3, p. 1059, 2020.
- [17] P. Ambigaipalan, A. S. Al-Khalifa, and F. Shahidi, "Antioxidant and angiotensin I converting enzyme (ACE) inhibitory

Retraction

Retracted: Growth Response in *Oryctolagus cuniculus* to Selenium Toxicity Exposure Ameliorated with Vitamin E

BioMed Research International

Received 12 March 2024; Accepted 12 March 2024; Published 20 March 2024

Copyright © 2024 BioMed Research International. This is an open access article distributed under the Creative Commons Attribution License, which permits unrestricted use, distribution, and reproduction in any medium, provided the original work is properly cited.

This article has been retracted by Hindawi following an investigation undertaken by the publisher [1]. This investigation has uncovered evidence of one or more of the following indicators of systematic manipulation of the publication process:

- (1) Discrepancies in scope
- (2) Discrepancies in the description of the research reported
- (3) Discrepancies between the availability of data and the research described
- (4) Inappropriate citations
- (5) Incoherent, meaningless and/or irrelevant content included in the article
- (6) Manipulated or compromised peer review

The presence of these indicators undermines our confidence in the integrity of the article's content and we cannot, therefore, vouch for its reliability. Please note that this notice is intended solely to alert readers that the content of this article is unreliable. We have not investigated whether authors were aware of or involved in the systematic manipulation of the publication process.

Wiley and Hindawi regrets that the usual quality checks did not identify these issues before publication and have since put additional measures in place to safeguard research integrity.

We wish to credit our own Research Integrity and Research Publishing teams and anonymous and named external researchers and research integrity experts for contributing to this investigation.

The corresponding author, as the representative of all authors, has been given the opportunity to register their agreement or disagreement to this retraction. We have kept a record of any response received.

References

- [1] R. Rehman, N. Sial, A. Ismail et al., "Growth Response in *Oryctolagus cuniculus* to Selenium Toxicity Exposure Ameliorated with Vitamin E," *BioMed Research International*, vol. 2022, Article ID 8216685, 9 pages, 2022.

Research Article

Growth Response in *Oryctolagus cuniculus* to Selenium Toxicity Exposure Ameliorated with Vitamin E

Rukhshanda Rehman ¹, Nuzhat Sial,¹ Amina Ismail,¹ Shabir Hussain ², Sobia Abid,¹ Maryium Javed,¹ Khansa Nadeem,¹ and Muhammad Ayoub³

¹Department of Zoology, The Islamia University, Bahawalpur, Pakistan

²School of Information Engineering, Zhengzhou University, China

³School of Computer Science and Engineering, Central South University, Changsha, China

Correspondence should be addressed to Rukhshanda Rehman; fa18s8pa006@iub.edu.pk

Received 28 January 2022; Revised 11 April 2022; Accepted 13 April 2022; Published 9 May 2022

Academic Editor: Abdelmoteleb Elokil

Copyright © 2022 Rukhshanda Rehman et al. This is an open access article distributed under the Creative Commons Attribution License, which permits unrestricted use, distribution, and reproduction in any medium, provided the original work is properly cited.

The adverse impacts of high temperature during the summer season on the rabbit industry have gained increased global attention. In this study, the comparative effects of biological (BIO) and chemical (CH) nanoselenium (nano-Se) combined with vitamin E on the growth and immune performances of rabbits were observed. A total of 200 white male rabbits of similar age (90 days) were divided into five treatment groups (T0, T1, T2, T3, and T4), 40 animals in each treatment. The rabbits in the first treatment group (T0) was fed basal diet; (T1) basal diet supplemented with 35 mg biological synthesized nanoselenium/kg diet; (T2) basal diet with 35 mg biological nanoselenium/kg diet+150 mg Vit. E/kg; (T3) basal diet+35 mg chemically synthesized nanoselenium/kg diet; and (T4) basal diet+35 mg of chemical nanoselenium/kg diet+150 mg Vit. E/kg. The duration of this experiment was 63 days. The body weight of each rabbit was recorded weekly. Results revealed a significant ($P < 0.05$) increase in live body weight (LBW), total body gain (TBG), and feed conversion ratio (FCR) of rabbits treated with BIO-Se+Vit. E (T2) compared to the other groups. Selenium concentrations in the kidneys and liver were significantly higher ($P < 0.05$) in animals fed with BIO-Se+Vit. E (T2). The concentrations of serum urea, glutamyl transferase (GGT), and triglycerides (TG) were lower in untreated (T0) and treated groups (T1, T2, T3, and T4). From the results of this study, it can be concluded that biological nano-Se gave maximum improvement for the parameters under study compared to the chemically synthesized nanoselenium by playing a role in alleviating heat stress, increasing the growth performance, and enhancing the immunity of growing white male rabbits. Further addition of Vit. E is an alternative method to maximize productivity with no adverse effects during the fattening period of growing white male rabbits.

1. Introduction

Rabbit farming has an extraordinary capability and valuable contribution in enhancing meat production, meal safety, and national economy in growing nations [1]. Rabbit farming has less economic risk and is less expensive than poultry or cattle farming. It requires less space, which is much suitable for the welfare of the rural atmosphere of any country [2]. Rabbit breeder profitability has extended due to enhancing genetic selection and reproductive control [3]. The meat obtained from rabbits contains less sodium content [4] and cholesterol [5]. Regarding the amount of fat material, its meat is marked with

decreasing fat, calories, and cholesterol amount [6, 7]. In summer, heat stress is the prominent problem rabbit producers face every year [8]. Sweat glands are not present on the skin of rabbits (except ear), due to which they are more sensitive to thermal stress [7]. With the rise of rabbit production, the need for animal supplements has become a necessary part of their daily diet [9]. Selenium in a hot summer environment is helpful in the antioxidant status and production [10]. As an important trace element for everyday physiological function in animals and human beings, selenium plays an essential function in growth, replica, antioxidative mechanism, hormone metabolism, anticarcinogenesis, and immunomodulation [11]. The

lower level of selenium in the daily diet badly affects the working of the immune system [9]. The lower level of selenium and vitamin E deficiency result in severe disease, including Kashin-Beck disease, a form of osteoarthritis [12]. Supplementing selenium can recover this abnormality with vitamin E [12].

The technology and nanotechnology are ancient and are used firstly in chemistry by the time for preparation of Roman's use of cement [13]. The concept of nanotechnology depends on decreasing particle length to change an element's physical and chemical nature [14, 15]. These days, nanoparticles are substantially considered in livestock and poultry due to chemical and physical residences [8]. Nanoparticle diameter is not more than 100 nm [15].

Vit. E is necessary for growth, better immunity, tissue cohesion, breeding, and sickness control and an antioxidant characteristic in all the body systems [1, 16]. Both Se and Vit. E are an essential and efficient antioxidant that help rabbits against lipid and protein oxidation of the outer surface membrane of different organs [17]. Combining Vit. E and Se at high value as required for nutritional requirements gives better immunity [18]. The green method proves more beneficial as compared to other chemical methods. Many types of protein pigments, multivitamins, algae carbohydrates, and lipids are present in plants. Green chemistry (plants) has been investigated successfully for metal NPs (nanoparticles) like Au, Ag, Se, MgO, CuO, and ZnO NP synthesis [19]. There are questions about using the chemical form of nano-Se [20]. The green synthesis is an environment friendly alternative to the basic chemical and physical methods as this technique removes the usage of toxic chemicals [21, 22]. Now, the synthesis of nanoparticles by the green method is a new approach that uses plants that have biomedical uses [20, 23]. To obtain the biocompatible effectiveness, this tactic is eco-friendly, safer, and easy [24]. Worldly different work has been done about the biomedical applications of selenium nanoparticles [25]. Recently, it is reported that the therapeutic margin of SeNPs has good medicinal properties and lowers the level of toxicity [26]. Researchers are studying the effects produced by BIO and CH nano-Se in growing rabbits [27]. In this study, the comparative effects of biological (BIO) and chemical (CH) nanoselenium (nano-Se) combined with Vit. E on the growth performance, serum biochemicals, and selenium metabolism (concentration of selenium in the kidneys, liver, and blood serum) of white male rabbits have been studied.

2. Materials and Methods

2.1. Nanoparticle Synthesis. Biological selenium (BIO) and green method were used for the preparation of plant extract; the garlic gloves were purchased from the local market, washed with distilled water, and dried. Make a paste of garlic gloves in pistil and mortar, and add this paste into the distilled water. The prepared mixture is heated on 70 to 80°C heat for 2 to 3 hours. After preparation of the plant extract, stop heating and cool down at room temperature and filter the mixture solution by using the filter paper and use the extract for further analysis. For the preparation of selenium nanoparticles, sodium selenite (Na_2SeO_3) was used as the

solvent throughout the experiment. The garlic extract was filtered using Whatman No. 1 filter paper. To synthesize selenium nanoparticles (SeNPs), 20 mL of the garlic extract was mixed with 100 mL of 40 mM sodium selenite solution and heated in a magnetic stirrer with 150 rpm at 60°C until the color changed to brick red after 2 to 3 days from pale yellow which designates the formation of colloidal SeNPs. After 24 h of incubation, the preparation was centrifuged at 10,000 rpm for 30 min, then washed three times with double-distilled water and ethanol [28]. Furthermore, it was dried into the oven at 60 to 70°C temperature. Released selenium nanoparticles ranged in size from a hundred to 550 nm, with an average size of 245 nm.

Chemical selenium (CH), a stock of aq. solution of ascorbic acid 50 mM, and sodium selenite 100 mM were prepared. Different ratios of ascorbic acid and sodium selenite 100 mM were combined from stock solution (1:1 to 1:6). Ascorbic acid was added to the sodium selenite solution under constant magnetic stirring at room temperature at different RPMs (200, 600, and 1000 rpm). The mixture was allowed to react in concentrated form until the colour of the solution started to change from colourless to orange. When colour was changed, the mixture was diluted by double-distilled water [24]. Analytical tools analysed the prepared particles by Raman spectroscopy UV-VIS spectroscopy.

2.2. Animals and Experimental Groups. A total of 200 male rabbits (966 ± 12 g average body weight and 90 days old) were divided into five treatment groups (T0, T1, T2, T3, and T4), 40 animals in each treatment, each with four replicates (ten rabbits each); during the whole experimental period, hygienic environment was provided to avoid any chemical and biological infections. The first group (T0) was fed ad libitum, served as untreated (control), while in the other groups, (T1) second group diet was provided basal diet+(BIO 35 mg) biological nanoselenium/kg diet; (T2) third group diet was basal diet+(BIO 35 mg) biological nanoselenium/kg diet+50 mg Vit. E/kg; (T3) basal diet+(CH 35 mg) chemical nanoselenium/kg diet; and (T4) basal diet+(CH 35 mg) chemical nanoselenium/kg diet+150 mg Vit. E/kg. An equal amount of BIO-Se and CH-Se was used to check which method gave better effect on rabbits. Basal diet's chemical analysis was done before the beginning of the experiment. The total ingredients and the chemical composition of the basal diets are shown in Tables 1 and 2. The rabbits' diet was prepared according to requirements for the growing animals as described by the National Research Council (NRC) [29]. All the experimental animals were kept hygienic to ensure good health and avoid any parasite attack. The average ambient temperatures ranged between 30.6 and 36.0°C during the summer season, and relative humidity ranged from 68.5 to 71.0%.

2.3. Data Collection and Estimated Parameters

2.3.1. Growth Performance. During the total experimental period, the measurements of growth performance traits were taken every week, which includes the live body weight of the rabbits (LBW), total body weight gain (TBWG), amount of

TABLE 1: Chemical composition of the basal experimental diet.

| Items (ingredients) | Content (%) |
|----------------------|-------------|
| Clover hay | 39.50 |
| Bone meal | 0.75 |
| Wheat bran | 30.00 |
| Calcium carbonate | 0.68 |
| Yellow corn | 12.00 |
| Sodium chloride | 0.57 |
| Soybean meal (44%) | 12.00 |
| Vitamins and mineral | 0.34 |
| Molasses | 4.00 |
| 1 DL-methionine | 0.16 |
| Total | 100 |

TABLE 2: Chemical composition of the basal experimental diet.

| Items (ingredients) | Chemical composition (%) |
|-----------------------------|--------------------------|
| Dry matter (DM) | 90.23 |
| Crude protein (CP) | 17.07 |
| G.E (kcal/kg)** | 2600 |
| Crude fibre (CF) | 15.25 |
| Ether extract (EE) | 3.03 |
| Nitrogen-free extract (NFE) | 50.51 |
| Total phosphorous (P) | 0.50 |
| Total calcium (a) | 0.90 |
| Ash | 7.45 |
| Methionine+cysteine*** | 0.66 |
| Lysine*** | 0.90 |

*Each 3 kilograms of premix contains Vit. A 12000000 IU, Vit. D 31500000 IU, Vit. E 50 g, Vit. K 32 g, Vit. B1 2 g, Vit. B2 6 g, Vit. B12 0.01 g, Chol. Chlod 1200 g, biotin 0.2 g, niacin 50 g, pantothenic acid 20 g, folic acid 5 g, magnesium 400 g, Copper 5 g, iodine 0.75 g, selenium 0.2 g, iron 75 g, manganese 30 g, and zinc 70 g. ***It was determined according to [30]. ****It was calculated according to [29].

feed taken by rabbits (FI), and also their feed conversion ratio (FCR).

2.3.2. *Economic Efficiency of the Experimental Diets.* Economic efficiency can be measured according to the feed intake and the price of one kg weight. Raya equation was used to calculate the economic efficiency [15].

$$\frac{\text{Feed consumed (g) during a certain period}}{\text{Body weight gained (g) during the same period}}, \quad (1)$$

where net revenue = selling price of weight gain (LE) – total feed cost. The selling price of weight gain = average weight gain (kg/head) * price of one kg of live body weight (LE). Total feed cost = average feed consumption (kg/head) × price of one kg of feed (LE).

2.3.3. *Chemical Analysis of Experimental Diets.* The chemical composition of the experimental basal diet was determined in the Chemical Laboratory for Foods and Feedstuffs. Chemical analysis was performed according to the procedure described by International Standard Methods (ISO) as shown in Tables 1 and 2. Crude ash was according to ISO 5984:2002; moisture content was according to ISO 6496:1999; crude fat was according to the method described in Official Journal of the European Union (EN), 2009; crude protein was according to ISO 5983-1:2002; and crude fibre was according to the Official Journal of the European Union (EN), 2009 described method.

2.3.4. *Serum Biochemical, Antioxidant, and Inflammatory Indices.* Blood was collected in the sterile test tubes. After the coagulation of the samples at room temperature, for about twenty minutes, centrifugation was done. After that, it was preserved. The spectrophotometric technique with diagnostic kits was used to check the serum content of different parameters under study. The determination of malondialdehyde (MDA) level of lipid peroxidation was evaluated [31].

2.3.5. *Sample Collection for Selenium Metabolism in Blood Serum, Kidney, Liver, and Muscles.* Rabbits were selected randomly from the experimental groups to determine selenium concentration in the blood serum, kidneys, liver, and muscles. Animals have fasted for 10–12 hours before the process. Islamic method was used for slaughtering. Animals were weighed before and after they got slaughtered. Blood samples were collected from each rabbit into clean and dry nonheparinised tubes. Blood samples were centrifuged at 3000 rpm for 15 min to obtain clear serum and stored at -20°C until the determination of selenium concentration serum. Rabbits were deskinning and dressed out, and the hot carcass was taken to determine selenium concentration in the muscles, liver, and kidneys. Samples of the liver, kidneys and muscles were collected (30 g of each). Each sample was kept separately in a polythene bag with an identification card showing the sample type. Samples were transported to the laboratory to determine Se concentration in the indicated organ tissues.

2.4. *Statistical Analysis.* Data on all the parameters were subjected to ANOVA using IBM SPSS statistics (version 20) to calculate the significant difference. Mean ± SE in all the groups were subjected to post hoc Tukey's test at $P < 0.05$.

3. Results

3.1. *UV-Visible.* The absorbance peak of nano-Se is 280 nm. In general, spherical Se NPs present peaks at around 270 nm to 300 nm linked with local surface plasmon resonance that depends on their size, morphology, and agglomeration. The UV spectrum exhibited a maximum absorption peak at 229 nm, which is attributed to the transition of the atomic C-C bonds and a shoulder peak at 300 nm is due to the n-transition of the C-O group. The absorbance peak for BIO-Se and CH-Se has been shown in Figures 1 and 2.

3.2. *Effects of Biologically and Chemically Synthesized Nanoselenium with Vit. E on Growth.* The results showed that biological and chemical nanoselenium supplementation

along vitamin E caused a significant increase in live body weight at weeks 14, 16, 18, and 20 of the experiment. In comparison, biologically synthesized selenium gave better results than CH-selenium on growth. The same results with the addition of Vit. E, rabbits of group T2 (BIO-selenium with Vit. E) showed a significant ($P < 0.05$) increase in growth than T4 (CH-selenium with Vit. E), as shown in Table 3.

The result shows that the total body weight gain (TBWG) of white male was significantly ($P < 0.05$) increased in the T2 group (BIO-Se with Vit. E supplementation) and T4 group (CH-selenium with Vit. E supplementation) in our experimental study as shown in Table 4.

Feed intake was significantly high in the T2 group (BIO-se with Vit. E supplemented), followed by the T4 group as shown in Table 5.

The feed conversion ratio was significantly ($P < 0.05$) improved in groups T2 (BIO-Se along with Vit. E) and T4 (CH-Se along with Vit. E), as shown in Table 6.

3.3. Blood Serum Metabolite. The T2 (BIO-Se with Vit. E) group has a significantly lowered ($P < 0.01$) serum urea content in comparison to the other groups (T1, T3, and T4) and T0 group. The highest values were recorded with T0 (control), while the T1 (BIO-Se), T3 (CH-selenium), and T4 (CH-Se with Vit. E) treatments gave medium values. The treatments of BIO-Se with Vit. E (T2) and CH-Se (T3) produced the reduced values of TG and GGT in the blood serum of white male rabbits. Furthermore, the highest TG and GGT were in the CH-Se with the Vit. E (T3) and control group (T0), respectively. Not any significant effect on the total bilirubin, direct and indirect bilirubin was observed in the serum of white male rabbits by any additive, as shown in Table 7.

3.4. Antioxidant Parameters. The level of SOD was significantly lowered by supplementation of nano-Se. The T1 (BIO-Se) and T2 (BIO-Se with Vit. E) groups gave decreased values for the level of SOD than the other groups. The antioxidant indicators' maximum values were in T0 (control group). The other white male rabbit (except T4) had significantly lowered for the production of nitric oxide (NO) and MDA as compared to T0 (control group). The CAT levels were improved in growing white male rabbits after supplementation with nano-Se (CH-Se, BIO-Se) as shown in Table 7.

3.5. Selenium (Se) Concentration in the Kidney, Liver, Body Muscles, and Blood Serum of Rabbits. The concentration of selenium was significantly ($P < 0.05$) increased in the group of rabbits fed BIO-Se with Vit. E (T2) and T4 (CH-Se with Vit. E). Addition of Vit. E results in a higher concentration of selenium in the kidney and liver. On the other hand, in blood serum and body muscle, selenium concentration increases significantly in group T1 (BIO-selenium) and T3 (CH-Se), as shown in Table 8.

3.6. Economic Efficiency of the Experimental Diets. The obtained results showed that BIO-Se supplementation was beneficial in achieving the highest economic efficiency and the groups having BIO-selenium with Vit. E and CH-Se with

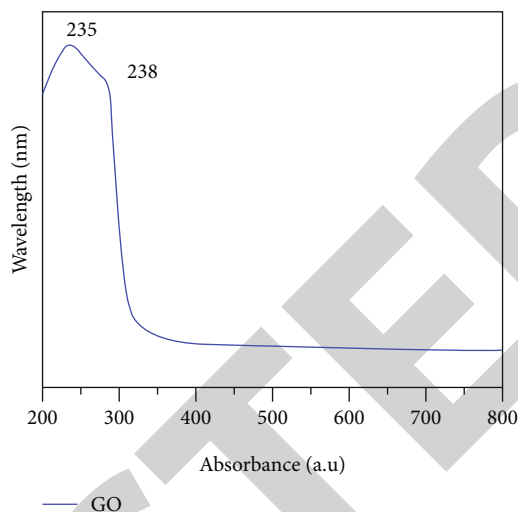


FIGURE 1: UV-visible spectrum of Se NPs (green synthesis).

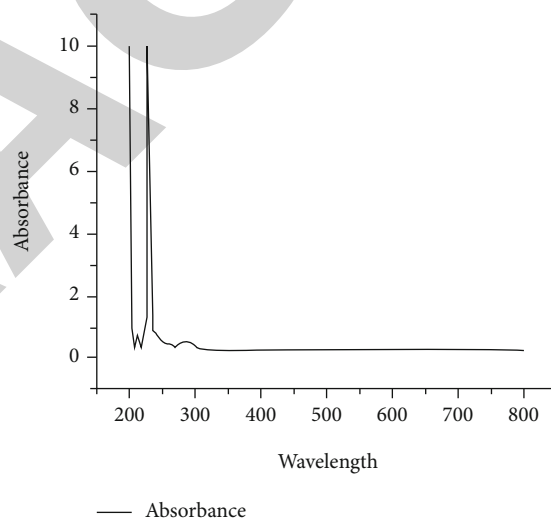


FIGURE 2: UV-visible spectrum of Se NPs (chemical synthesis).

Vit. E fed gave the lowest economic efficiency. Addition of Vit. E decreased economic efficiency as shown in Table 9.

The selling price of live body weight for rabbits = 40 LE/kg; price of the diet without additive = 4.2 LE/kg; price of the diet with Vit.E = 4.35 LE/kg; price of the diet with chemical nanoselenium = 4.23 LE/kg; price of diet with chemical nanoselenium and Vit.E = 4.55 LE/kg; price of diet with biological nanoselenium = 4.32 LE/kg; and price of the diet with biological nano – selenium&Vit.E = 4.65 LE/kg.

4. Discussion

The rabbit industry has suffered a lot due to global warming; their economic profit and productivity get disturbed [32]. Different dietary manipulations are used to overcome the negative influences of heat stress in rabbits [33]. In animals

TABLE 3: Effect of biological and chemically synthesized nanoselenium with Vit. E on live body weight (LBW; g) of the growing rabbits at different ages (mean \pm SE).

| Weeks | T0 (control) | T1 | T2 | T3 | T4 |
|-------|--------------------|--------------------|---------------------|--------------------|---------------------|
| 12 | 958.22 \pm 3.61 | 972.43 \pm 4.52 | 1002.82 \pm 4.07* | 960.01 \pm 6.17 | 996.03 \pm 2.21* |
| 14 | 1224.24 \pm 4.65 | 1236.09 \pm 5.02 | 1288.43 \pm 7.68* | 1240.32 \pm 7.16 | 1271.98 \pm 7.40* |
| 16 | 1511.09 \pm 4.63 | 1538.98 \pm 4.29 | 1594.65 \pm 5.55* | 1518.19 \pm 6.83 | 1573.03 \pm 6.78* |
| 18 | 1880.08 \pm 6.43 | 1895.01 \pm 5.37 | 1995.23 \pm 6.78* | 1904.95 \pm 4.28 | 2158.92 \pm 7.02* |
| 20 | 2106.98 \pm 6.25 | 2111.65 \pm 3.97 | 2171.04 \pm 6.00* | 2121.03 \pm 6.64 | 2142.09 \pm 6.37* |

TABLE 4: Effect of biologically and chemically synthesized nanoselenium with Vit. E on total body weight gain (TBWG; g) of the growing rabbits at different ages (mean \pm SE).

| Weeks | T0 (control) | T1 | T2 | T3 | T4 |
|-------|------------------|------------------|--------------------|-------------------|--------------------|
| 12–14 | 26.11 \pm 5.75 | 27.51 \pm 6.09 | 36.53 \pm 11.80* | 30.54 \pm 8.80 | 34.33 \pm 10.09* |
| 15–16 | 28.21 \pm 5.41 | 28.34 \pm 5.67 | 31.26 \pm 9.84* | 29.20 \pm 11.68 | 33.43 \pm 10.64* |
| 17–18 | 26.04 \pm 8.88 | 27.71 \pm 4.96 | 32.56 \pm 7.38* | 28.06 \pm 7.18 | 30.41 \pm 9.36* |
| 19–20 | 24.84 \pm 7.99 | 26.91 \pm 5.99 | 35.05 \pm 7.22* | 28.75 \pm 8.27 | 32.16 \pm 11.18* |

TABLE 5: Effect of biologically and chemically synthesized nanoselenium with Vit. E on feed intake (FI; g) of the growing rabbits at different ages (mean \pm SE).

| Weeks | T0 (control) | T1 | T2 | T3 | T4 |
|-------|------------------|------------------|--------------------|------------------|--------------------|
| 12–14 | 78.9 \pm 3.05 | 80.09 \pm 2.06 | 90.03 \pm 2.83* | 78.09 \pm 1.87 | 99.91 \pm 1.74* |
| 15–16 | 84.07 \pm 1.45 | 81.71 \pm 1.65 | 92.70 \pm 1.48* | 86.17 \pm 1.79 | 98.49 \pm 2.28* |
| 17–18 | 98.51 \pm 2.80 | 96.19 \pm 1.90 | 122.84 \pm 2.56* | 98.19 \pm 2.27 | 105.04 \pm 1.68* |
| 19–20 | 85.11 \pm 2.04 | 83.61 \pm 1.76 | 118.03 \pm 1.65* | 87.61 \pm 1.82 | 109.48 \pm 1.48* |

TABLE 6: Effect of biologically and chemically synthesized nanoselenium with Vit. E on feed conversion ratio (FCR; g feed/g gain) of the growing rabbits at different ages (mean \pm SE).

| Weeks | T0 (control) | T1 | T2 | T3 | T4 |
|-------|-----------------|------------------|------------------|-----------------|------------------|
| 12–14 | 4.1 \pm 0.17 | 3.18 \pm 0.10 | 5.15 \pm 0.16* | 3.75 \pm 0.13 | 5.81 \pm 0.15* |
| 15–16 | 4.09 \pm 0.10 | 3.11 \pm 0.09 | 5.0 \pm 0.09* | 3.9 \pm 0.24 | 5.02 \pm 0.24* |
| 17–18 | 4.09 \pm 0.11 | 3.84 \pm 0.122 | 5.41 \pm 0.12* | 3.83 \pm 0.13 | 5.05 \pm 0.13* |
| 19–20 | 4.16 \pm 0.15 | 3.58 \pm 0.11 | 5.55 \pm 0.13* | 3.58 \pm 0.12 | 5.09 \pm 0.19* |

with a lower Se level suffering from different diseases, GSH Px activity in organs and tissues decreased [12].

There are different methods for the synthesis of nano-Se. Chemically synthesized nano-Se has been widely used in animals. The conventional methods used to produce NPs are toxic, expensive, and nonenvironment friendly. To overcome these problems, researchers have found the green routes, i.e., the naturally occurring sources and their products that can be used to synthesize NPs [34].

The present research shows that feeding biological nano-Se helped to improve LBW, BWG, and FCR in heat-stressed rabbits compared to the chemical nano-Se and control. However, this study agrees with the result stated by Sheiha

et al. who reported that improved effects showed for biologically synthesized selenium as compared to the chemically synthesized and reported BIO-selenium (25 or 50 mg/kg) have better growth and LBW as compared to the CH-selenium (25 or 50 mg/kg) and control groups of growing rabbits [27].

Several studies support that addition of nano-Se separately as well as in combination with other dietary manipulations results in the enhanced growth of the rabbits. The addition of selenium to the diet of the rabbits results in enhanced FCR and reduced FI [18]. In a study, it is stated that the addition of 0.70 mg/kg selenium to the diet of the rabbits results in enhanced growth parameters [24]. The

TABLE 7: Effect of biologically and chemically synthesized nanoselenium with Vit. E on blood serum metabolites (mean \pm SE).

| Items | T0 (control) | T1 | T2 | T3 | T4 |
|----------------------------|-----------------|-------------------|-------------------|-------------------|--------------------|
| Creatinine (mg/dL) | 1.45 \pm 0.21 | 4.14 \pm 0.33* | 1.12 \pm 0.24 | 1.25 \pm 0.20 | 2.34 \pm 0.19* |
| Urea (mg/dL) | 52.8 \pm 0.06 | 51.1 \pm 0.11 | 44.84 \pm 0.12* | 49.41 \pm 0.09 | 51.33 \pm 0.14 |
| GGT (U/L) | 5.36 \pm 0.03 | 5.01 \pm 0.09 | 4.73 \pm 0.12* | 4.94 \pm 0.03 | 5.47 \pm 0.06 |
| TG (mg/dL) | 144 \pm 0.21 | 75.43 \pm 0.17* | 73.08 \pm 0.11* | 73.73 \pm 0.09* | 107.32 \pm 0.08* |
| Total protein (mg/dL) | 4.08 \pm 0.21 | 5.86 \pm 0.27* | 5.44 \pm 0.31* | 5.79 \pm 0.24* | 5.66 \pm 0.33* |
| Albumin (mg/dL) | 2.11 \pm 0.10 | 3.55 \pm 0.11* | 3.14 \pm 0.09* | 3.41 \pm 0.11* | 3.34 \pm 0.11* |
| Globulin (mg/dL) | 1.87 \pm 0.07 | 2.33 \pm 0.06* | 2.3 \pm 0.09* | 2.42 \pm 0.08* | 2.31 \pm 0.06* |
| Total bilirubin (mg/dL) | 0.87 \pm 0.11 | 0.88 \pm 0.06 | 0.810.09 | 0.83 \pm 0.06 | 0.89 \pm 0.77 |
| Direct bilirubin (mg/dL) | 0.2 \pm 0.01 | 0.19 \pm 0.04 | 0.21 \pm 0.07 | 0.21 \pm 0.08 | 0.2 \pm 0.03 |
| Indirect bilirubin (mg/dL) | 0.75 \pm 0.03 | 0.76 \pm 0.09 | 0.73 \pm 0.11 | 0.73 \pm 0.07 | 0.7 \pm 0.13 |
| NO (μ mol/L) | 0.25 \pm 0.05 | 0.19 \pm 0.07* | 0.19 \pm 0.04* | 0.21 \pm 0.04 | 0.23 \pm 0.09 |
| MDA (nmol/mL) | 0.3 \pm 0.02 | 0.25 \pm 0.11* | 0.23 \pm 0.09* | 0.21 \pm 0.07* | 0.28 \pm 0.12* |
| SOD (U/mL) | 0.28 \pm 0.03 | 0.23 \pm 0.05* | 0.21 \pm 0.08* | 0.24 \pm 0.06 | 0.26 \pm 0.04 |
| GSH (ng/mL) | 0.12 \pm 0.06 | 0.15 \pm 0.02* | 0.15 \pm 0.10* | 0.18 \pm 0.16* | 0.11 \pm 0.13 |
| CAT (ng/mL) | 0.2 \pm 0.08 | 0.15 \pm 0.06 | 0.24 \pm 0.02 | 0.28 \pm 0.01 | 0.05 \pm 0.07* |

*NO: nitric oxide; MDA: malondialdehyde; GSH: reduced glutathione; SOD: superoxide dismutase; CAT: catalase.

TABLE 8: Concentration (μ g/kg) of selenium in the liver, kidney, and blood serum of the growing rabbits at different ages (mean \pm SE).

| Items | T0 (control) | T1 | T2 | T3 | T4 |
|-------------|----------------|-----------------|-----------------|-----------------|-----------------|
| Kidneys | 3.98 \pm 1.6 | 4.64 \pm 2.1 | 8.09 \pm 2.0* | 4.61 \pm 1.5 | 7.24 \pm 0.9* |
| Liver | 3.42 \pm 0.6 | 4.41 \pm 1.5 | 7.89 \pm 1.9* | 4.9 \pm 0.24 | 6.08 \pm 1.2* |
| Muscles | 2.4 \pm 0.9 | 4.12 \pm 1.7* | 3.08 \pm 0.7 | 4.42 \pm 0.6* | 3.32 \pm 1.3 |
| Blood serum | 3.36 \pm 0.7 | 5.84 \pm 0.8* | 4.41 \pm 1.6 | 5.91 \pm 0.9* | 4.07 \pm 0.7 |

TABLE 9: Effect of biologically and chemically synthesized nanoselenium with Vit. E on economic efficiency (EE) at different ages of growing rabbits.

| Weeks | T0 | T1 | T2 | T3 | T4 |
|-------|-----|-----|-----|-----|-----|
| 12–14 | 210 | 280 | 198 | 244 | 184 |
| 15–16 | 324 | 377 | 284 | 339 | 268 |
| 17–18 | 160 | 245 | 148 | 210 | 133 |
| 19–20 | 282 | 349 | 242 | 311 | 227 |

authors in [3] reported that the combination of nanoselenium with prevalent garlic oil and much better results were obtained in the BW bodyweight of rabbits [32]. In another study, it is stated that the combination of nanozinc and nanoselenium gave better results in the growth of the rabbits as compared to the control group [9] and reported that diet with 60 mg nanozinc or 0.3 mg nanoselenium had a maximum value of growth parameters. In a study, it is reported that a combination of organic and inorganic selenium had higher live body weight (LBW) growth ($P < 0.05$), good feed conversation ratio (FCR), and total body weight gain (TBWG) [10]. Elkholy et al. studied the comparison of different forms of selenium used as a supplement in the diet

of rabbits and their overall effect on production, and they concluded that selenium in either form organic or inorganic form put beneficial effects on survival, on growth rate, and in the meat of rabbits [4]. Addition of Vit. E in this study showed a significant ($P < 0.05$) increase in growth. It is stated that the addition of Vit. E results in increased body weight [35, 36], and that agrees with the results. Dalle Zotte and Szendrő interpreted the improvement in body weight by dietary addition of Vit. E [37]. Rooke et al. and Ebeid et al. studied that Vit. E is essential for growth, immunity characteristic increase, tissue cohesion, breeding, sickness control, and having an antioxidant characteristic in all the body systems [1, 16]. Marounek et al. and Ebeid et al. reported that live body weight and total weight gain have remarkable effects by adding the Vit. E [1, 38]. Shara et al. worked on the effect of selenium plus Vit. E along with AD3E vitamins and concluded that diet supplemented with Vit. E improved BW ($P < 0.005$) and decreased ($P < 0.001$) daily water intake [39].

The administration of nano-Se (BIO-selenium with Vit. E or CH-selenium) reduced the level of blood urea as compared to the T0 group, results of GGT and TG for rabbits fed (BIO-selenium, BIO-selenium with Vit. E, or CH-selenium) were decreased than the T0 group. Concerning the liver and kidney functions, level of creatinine and total, indirect, and direct

bilirubin did not show any remarkable changes. Abdel-Wareth et al. reported that the group of rabbits fed with nanoselenium had a lower level of urea [32]. Additionally, a significant reduction was reported in the TG level as a response to nano-Se supplementation in broiler chicks [40]. Our results concluded that nano-Se improved liver and kidney functions, thus alleviating the adverse influences of a hot environment.

In conclusion, the dietary addition of nanoselenium led to increased concentrations of total protein in the blood serum of white male rabbits. This result agrees with the work of [41]. It was reported that supplementation of nanoselenium increases the amount of total protein in the blood [42]. This result disagrees with the work of Šperanda et al. They reported that there is no significant change or increase in the total protein level of blood by supplementation of nanoselenium [43].

In our study, feeding rabbits with nanoselenium improved the antioxidant activities by significantly increasing the activities of GSH and CAT in comparison to the heat stress group and also decreased the level of NO and MDA in the groups (BIO-selenium, BIO-selenium with Vit. E, or CH-selenium) as compared to the other groups. El-Deep et al. [44] reported that fed nano-Se (0.2–0.3 mg/kg) in poultry improved the reduced glutathione (GSH-P) activity in the blood serum. Zhou et al. stated that Se supplementation contributes to several immune functions, such as reducing the levels and duration of inflammatory infections, minimising glucocorticoids (which are an indicator for immunity disorder) [45] and also the arrangement of the function of T lymphocyte cells. Se is an essential trace element for combating oxidative stress, hence the cell's redox state, due to its integration as selenocysteine into GSH-Px [46].

Our results showed that biological nano-Se and Vit. E increase selenium concentration in the kidney and liver. In contrast, Se concentration in muscles and blood serum was not significantly affected by Vit. E addition to the diet. The result agrees with the previous work of Abd Allah et al. who reported that adding Vit. E to the basal diet significantly ($P < 0.05$) increased level of Se in the kidneys and liver of all rabbit groups.

The result disagreed with the previous research of Ebeid et al. and ElKholly et al., who observed that the concentration of Se (g/kg) in the hind leg significantly increased ($P < 0.05$) in rabbits fed the diet supplemented with selenium plus Vit. E compared with those fed with diet Vit. E only [1, 4].

Abdel-Wareth et al. reported that basal diet fed with selenium and garlic oil to the growing rabbits results in improved and efficient kidney and liver functions [32]. Sheiha et al. concluded that supplementation of nanoselenium improves liver and kidney functions and decreases the adverse effect of hot temperature [27].

Abdel-Wareth et al. reported that being fed with nanoselenium results in a lower level of urea in the kidneys and liver than the control [32]. Lee et al. stated that GSH-Px non-selenium-dependent forms are more present in the liver and kidney of rabbits [47]. On the other side, the lungs, heart, and blood serum have only selenium-dependent GSH-Px activity.

El-Deep et al. and Lebas et al. reported that reducing the oxidative pressure on different organs of rabbits is more relayed on Vit. E and significantly less on selenium [48].

Abd Allah et al. stated that basically, selenium moves from the blood into tissues and presents in protein in the kidney, liver, muscles, and blood serum [49].

Economic efficiency was highest in BIO-selenium supplemented groups and lowest in Vit. E supplemented groups. It is reported that the highest economic efficiency was recorded with rabbits fed supplemental nanoselenium [50]. Abd Allah et al. reported that economic efficiency was lowest for the rabbits fed Org-Se plus Vit. E compared to the other groups [49].

El-Monie et al. reported that the economic feed efficiency in their study showed that using BET, VC, or VE in the growing rabbit diets was more economical than the non-supplemented diets [41]. Ebeid et al. indicated that EE was highest for rabbits fed with the nanoselenium compared to the other group fed with organic selenium and the control group [1]. Abd Allah et al. reported that from the economic point of view to ameliorating the adverse effects of heat stress on growing rabbits during the hot summer conditions in Egypt, it is advisable to supply the basal rabbit diet with Se, either as nano-Se or Org-Se only without Vit. E diet [49].

5. Conclusion

In view of the above findings, nano-Se is an essential element that helps growing white male rabbits to cope with heat stress's adverse effects. The best results in this study were retrieved for BIO-Se compared to the CH-Se. Growth parameters increased significantly with BIO-selenium with Vit. E, T2 group. So in the light of this study, we conclude that supplementation of BIO-Se with Vit. E improves growth and antioxidant status and regulates the inflammatory cytokine responses and selenium metabolism in growing white male rabbits. Moreover, the addition of Vit. E also plays an important antioxidant role along with selenium.

Data Availability

Data is openly available for readers.

Conflicts of Interest

The authors declare that there is no conflict of interest.

References

- [1] T. Ebeid, H. S. Zeweil, M. M. Basyony, W. M. Dosoky, and H. Badry, "Fortification of rabbit diets with vitamin E or selenium affects growth performance, lipid peroxidation, oxidative status and immune response in growing rabbits," *Livestock Science*, vol. 155, no. 2-3, pp. 323–331, 2013.
- [2] M. R. Amin, M. A. Taleb, and J. Rahim, *Rabbit farming: a potential approach towards rural poverty alleviation*, Department of Public Administration, Comilla University, Comilla, Bangladesh, 2011.
- [3] I. Marai, M. Ayyat, and A. El-Monem, "Growth performance and reproductive traits at first parity of New Zealand White female rabbits as affected by heat stress and its alleviation under Egyptian conditions," *Tropical Animal Health and Production*, vol. 33, no. 6, pp. 451–462, 2001.

- [4] K. Elkholy, T. El-Deen, A. El-Latif, and A. Mekawy, "Effect of dietary addition of two selenium source on productive efficiency and selenium content in tissues in growing rabbits," *Journal of Sustainable Agricultural Sciences*, vol. 45, no. 1, pp. 27–36, 2019.
- [5] A. Okab, S. G. El-Banna, and A. Koriem, "Influence of environmental temperatures on some physiological and biochemical parameters of New-Zealand rabbit males," *Slovak Journal of Animal Science*, vol. 41, no. 1, pp. 12–19, 2008.
- [6] R. Parigi-Bini, G. Xiccato, M. Cinetto, and A. Dalle Zotte, "Energy and protein utilization and partition in rabbit does concurrently pregnant and lactating," *Animal Science*, vol. 55, no. 1, pp. 153–162, 1992.
- [7] S. Lukefahr, C. Nwosu, and D. Rao, "Cholesterol level of rabbit meat and trait relationships among growth, carcass and lean yield performances," *Journal of Animal Science*, vol. 67, no. 8, pp. 2009–2017, 1989.
- [8] G. Marappan, P. Beulah, R. D. Kumar, S. Muthuvel, and P. Govindasamy, "Role of nanoparticles in animal and poultry nutrition: modes of action and applications in formulating feed additives and food processing," *International Journal of Pharmacology*, vol. 13, no. 7, pp. 724–731, 2017.
- [9] T.-E. Din and T. Noha, "Effects of dietary nano-zinc and nano-selenium addition on productive and physiological performance of growing rabbits at fattening period," *Egyptian Journal of Nutrition and Feeds*, vol. 22, no. 1, pp. 79–89, 2019.
- [10] S. A. Amer, A. E. Omar, and M. E. Abd el-Hack, "Effects of selenium-and chromium-enriched diets on growth performance, lipid profile, and mineral concentration in different tissues of growing rabbits," *Biological Trace Element Research*, vol. 187, no. 1, pp. 92–99, 2019.
- [11] B. R. Cardoso, B. R. Roberts, A. I. Bush, and D. J. Hare, "Selenium, selenoproteins and neurodegenerative diseases," *Metalomics*, vol. 7, no. 8, pp. 1213–1228, 2015.
- [12] B. Turan, C. Balcik, and N. Akkas, "Effect of dietary selenium and vitamin E on the biomechanical properties of rabbit bones," *Clinical Rheumatology*, vol. 16, no. 5, pp. 441–449, 1997.
- [13] D. Schaming and H. Remita, "Nanotechnology: from the ancient time to nowadays," *Foundations of Chemistry*, vol. 17, no. 3, pp. 187–205, 2015.
- [14] V. Prida, P. Gorr a, G. V. Kurlyandskaya, M. L. S nchez, B. Hernando, and M. Tejedor, "Magneto-impedance effect in nanostructured soft ferromagnetic alloys," *Nanotechnology*, vol. 14, no. 2, pp. 231–238, 2003.
- [15] T. E. Raya, S. J. Fonken, R. W. Lee et al., "Hemodynamic effects of direct angiotensin II blockade compared to converting enzyme inhibition in rat model of heart failure," *American Journal of Hypertension*, vol. 4, no. 4_Part_2, pp. 334S–340S, 1991.
- [16] J. Rooke, J. Robinson, and J. Arthur, "Effects of vitamin E and selenium on the performance and immune status of ewes and lambs," *The Journal of Agricultural Science*, vol. 142, no. 3, pp. 253–262, 2004.
- [17] V. Koinarski, N. Georgieva, V. Gadjeva, and P. Petkov, "Antioxidant status of broiler chickens, infected with *Eimeria acervulina*," *Revue de Médecine Vétérinaire*, vol. 156, no. 10, p. 498, 2005.
- [18] N. Ziaei and E. E. Pour, "The effects of different levels of vitamin-E and organic selenium on performance and immune response of laying hens," *African Journal of Biotechnology*, vol. 12, no. 24, 2013.
- [19] V. Alagesan and S. Venugopal, "Green synthesis of selenium nanoparticle using leaves extract of *withania somnifera* and its biological applications and photocatalytic activities," *Bionanoscience*, vol. 9, no. 1, pp. 105–116, 2019.
- [20] B. Hosnedlova, M. Kepinska, S. Skalickova et al., "Nano-selenium and its nanomedicine applications: a critical review," *International Journal of Nanomedicine*, vol. Volume 13, pp. 2107–2128, 2018.
- [21] H. A. Salam, R. Sivaraj, and R. Venckatesh, "Green synthesis and characterization of zinc oxide nanoparticles from *Ocimum basilicum* L. var. *purpurascens* Benth.-Lamiaceae leaf extract," *Materials Letters*, vol. 131, pp. 16–18, 2014.
- [22] D. H. Samak, Y. S. el-Sayed, H. M. Shaheen et al., "Developmental toxicity of carbon nanoparticles during embryogenesis in chicken," *Environmental Science and Pollution Research*, vol. 27, no. 16, pp. 19058–19072, 2020.
- [23] S. Lampis, E. Zonaro, C. Bertolini, P. Bernardi, C. S. Butler, and G. Vallini, "Delayed formation of zero-valent selenium nanoparticles by *Bacillus mycoides* SeITE01 as a consequence of selenite reduction under aerobic conditions," *Microbial Cell Factories*, vol. 13, no. 1, p. 35, 2014.
- [24] X. Li, H. Xu, Z. S. Chen, and G. Chen, "Biosynthesis of nanoparticles by microorganisms and their applications," *Journal of Nanomaterials*, vol. 2011, 16 pages, 2011.
- [25] M. Shakibaie, H. Forootanfar, Y. Golkari, T. Mohammadi-Khorsand, and M. R. Shakibaie, "Anti-biofilm activity of biogenic selenium nanoparticles and selenium dioxide against clinical isolates of *Staphylococcus aureus*, *Pseudomonas aeruginosa*, and *Proteus mirabilis*," *Journal of Trace Elements in Medicine and Biology*, vol. 29, pp. 235–241, 2015.
- [26] C. Ferro, H. F. Florindo, and H. A. Santos, "Selenium nanoparticles for biomedical applications: from development and characterization to therapeutics," *Advanced Healthcare Materials*, vol. 10, no. 16, p. 2100598, 2021.
- [27] A. M. Sheiha, S. A. Abdelnour, M. E. Abd el-Hack et al., "Effects of dietary biological or chemical-synthesized nano-selenium supplementation on growing rabbits exposed to thermal stress," *Animals*, vol. 10, no. 3, p. 430, 2020.
- [28] V. Jay and R. Shafkat, "Synthesis of selenium nanoparticles using *Allium sativum* extract and analysis of their antimicrobial property against gram positive bacteria," *The Pharma Innovation*, vol. 7, no. 9, pp. 262–266, 2018.
- [29] D. Sauviant, J.-M. Perez, and G. Tran, *Tables of composition and nutritional value of feed materials: pigs, poultry, cattle, sheep, goats, rabbits, horses and fish*, Wageningen Academic Publishers, 2004.
- [30] R. Amin and H. El-Matarawy, "Effect of vitamin E and selenium supplementation on growth performance, digestibility, carcass traits and blood components of Bouscat rabbits," *Journal of Productivity and Development*, vol. 12, no. 1, pp. 13–24, 2007.
- [31] M. Uchiyama and M. Mihara, "Determination of malonaldehyde precursor in tissues by thiobarbituric acid test," *Analytical Biochemistry*, vol. 86, no. 1, pp. 271–278, 1978.
- [32] A. Abdel-Wareth, A. E. Ahmed, H. A. Hassan, M. S. Abd el-Sadek, A. A. Ghazalah, and J. Lohakare, "Nutritional impact of nano-selenium, garlic oil, and their combination on growth and reproductive performance of male Californian rabbits," *Animal Feed Science and Technology*, vol. 249, pp. 37–45, 2019.
- [33] A. A. Al-Sagheer, A. H. Daader, H. A. Gabr, A. El-Moniem, and A. Elham, "Palliative effects of extra virgin olive oil, gallic

Retraction

Retracted: Diversity of Rotavirus Strains among Children with Acute Diarrhea in Karachi, Pakistan

BioMed Research International

Received 12 March 2024; Accepted 12 March 2024; Published 20 March 2024

Copyright © 2024 BioMed Research International. This is an open access article distributed under the Creative Commons Attribution License, which permits unrestricted use, distribution, and reproduction in any medium, provided the original work is properly cited.

This article has been retracted by Hindawi following an investigation undertaken by the publisher [1]. This investigation has uncovered evidence of one or more of the following indicators of systematic manipulation of the publication process:

- (1) Discrepancies in scope
- (2) Discrepancies in the description of the research reported
- (3) Discrepancies between the availability of data and the research described
- (4) Inappropriate citations
- (5) Incoherent, meaningless and/or irrelevant content included in the article
- (6) Manipulated or compromised peer review

The presence of these indicators undermines our confidence in the integrity of the article's content and we cannot, therefore, vouch for its reliability. Please note that this notice is intended solely to alert readers that the content of this article is unreliable. We have not investigated whether authors were aware of or involved in the systematic manipulation of the publication process.

Wiley and Hindawi regrets that the usual quality checks did not identify these issues before publication and have since put additional measures in place to safeguard research integrity.

We wish to credit our own Research Integrity and Research Publishing teams and anonymous and named external researchers and research integrity experts for contributing to this investigation.


The corresponding author, as the representative of all authors, has been given the opportunity to register their agreement or disagreement to this retraction. We have kept a record of any response received.

References

- [1] N. T. Bukhari, G. Parveen, P. A. Ali et al., "Diversity of Rotavirus Strains among Children with Acute Diarrhea in Karachi, Pakistan," *BioMed Research International*, vol. 2022, Article ID 5231910, 6 pages, 2022.

Research Article

Diversity of Rotavirus Strains among Children with Acute Diarrhea in Karachi, Pakistan

Nain Tarra Bukhari,¹ Gulnaz Parveen ,² Pir Asmat Ali,³ Amtul Sami,⁴ Yasmeen Lashari,⁵ Naila Mukhtar,⁶ Raisa Bano,⁷ Nargis Haider,⁸ Atiya Hussain Khowaja,⁹ and Shahana Urooj Kazmi⁴

¹Clinical Laboratory Sciences, Women University, Swabi, Pakistan

²Department of Botany, Women University, Swabi, Pakistan

³Department of Zoology, Women University, Swabi, Pakistan

⁴Department of Microbiology and Molecular Biotechnology, Women University, Swabi, Pakistan

⁵Department of Pathology, Bolan Medical College, Quetta, Pakistan

⁶Department of Botany, University of Okara, Pakistan

⁷Department of Public Health & Bioinformatics, Women University, Swabi, Pakistan

⁸Department of Physiology, Bolan Medical College, Quetta, Pakistan

⁹Agha Khan Medical University and Hospital, Karachi, Pakistan

Correspondence should be addressed to Gulnaz Parveen; gulnaz.malik3@gmail.com

Received 19 February 2022; Revised 17 March 2022; Accepted 29 March 2022; Published 23 April 2022

Academic Editor: Hafiz Ishfaq Ahmad

Copyright © 2022 Nain Tarra Bukhari et al. This is an open access article distributed under the Creative Commons Attribution License, which permits unrestricted use, distribution, and reproduction in any medium, provided the original work is properly cited.

One of the common viral pathogens in infectious diarrhea is *Rotavirus*; in developing countries, it is a primary cause of deaths in children less than five years of age. This study was planned to find out the etiologic agents of acute watery diarrhea. In this study, 1465 stool samples were analyzed with the symptoms of acute diarrhea. Demographic data analysis showed no. of episodes of diarrhea, vomiting, and fever. All samples were checked by ELISA technique for the presence of *Rotavirus* circulating strains. More than 6% patients were found to be positive with Rotavirus. Common *Rotavirus* genotypes, including G2P4, G2P6, G3P4, G8P4, G8P6, G9P4, and G10P4, were detected in patients through RT-PCR. This study concluded that detection of rotavirus strain diversity and management of diarrheal patients may identify assortment of emerging strains and reduce emergence of antimicrobial resistance and repeated episodes of diarrhea, which may also help to avoid and manage the essential nutrients lost leading to malnutrition and stunted growth, as well as to reduce high mortality rate in young children less than five years.

1. Introduction

Rotavirus is considered the major cause of severe gastroenteritis ranges from asymptomatic self-limiting watery diarrhea to life threatening infection in children worldwide. Malnutrition and stunted growth can occur if mismanaged in symptomatic cases ([1] [2]). Among these reported cases, 30% etiological agent are bacterial, viral, or parasitic [3]. Recently, 40-50% severe cases of infantile watery diarrhea are attributed to *Rotavirus* worldwide causing 600,000 deaths per year in African and Asian countries [4]. In a

WHO 2015 report, 1.7 billion reported cases accounts 9% cumulative infantile deaths resulting in elevated health budget. According to earlier studies, 5.2 million bacterial, etiological agents along with 2.5 million parasitic and 30.9 million viruses cause diarrheal episodes [5]. In Pakistan due to multiple and recurrent diarrheal episodes > 150,000, deaths occur annually, leading infants towards malnutrition and retarded growth [6]. Almost 35%-50% of infected infants were between 1 and 2 years of age bracket [7]. Similarly, 2.5% cases were moderate in severity which progressed to life-threatening situation and were from low-socioeconomic

TABLE 1: *Rotavirus* VP7 primer list.

| Primer | Human sequence (5'-3') | Position (nt) | Strain (genotype) | References |
|--------|---------------------------|---------------|---------------------|------------|
| aAT8 | GTCACACCATTGTGAAATTTCG | 178-198 | 69 M (G8) 885 bp | [21] |
| aBT1 | CAAGTACTCAAATCAATGATGG | 314-335 | Wa (G1) 749 bp | [21] |
| aCT2 | CAATGATATTAACACATTTTCTGTG | 411-435 | DS-1 (G2) 652 bp | |
| aDT4 | CGTTTCTGGTGAGGAGTTG | 480-498 | ST-3 (G4) 583 bp | |
| aET3 | CGTTTGAAGAAGTTGCAACAG | 689-709 | P 374 bp (G3) | [22] |
| mG3 | ACGAACTCAACACGAGAGG | 250-269 | 682 bp | |
| aFT9 | CTAGATGTAAC TACA ACTAC | 757-776 | W161 (G9) 306 bp | [22] |
| mG9 | CTTGATGTGACTAYAAATAC | 757-776 | 179 bp | |

settings, and the numbers of rotavirus cases were high where no health care facility was available [8]. The seasonal variation marker indicated that infection persists throughout the year having no correlation with rainy season while rise in no. of cases was reported in dry season. *Rotaviruses* in Pakistan are highlighted recently as an important nonbacterial etiological agent in young children [9]. Electron microscopy was only a tool to detect the virus, but recently, more advance techniques like enzyme-linked immunosorbent assay (ELISA) or latex agglutination rapid system and PCR method are in routine use to avoid blind therapy and emergence of MDR pathogens [10].

The study was designed based on reports that in Pakistan after every minute a child dies due to diarrhea [11]. It is reported that 140,000 young population under five got *Rotavirus* infection, resulting, so leading them to malnutrition and stunted growth. This serious issue of high morbidity and mortality warrants investigation [12]. The aims and objectives of this present study are molecular identification of prevalent pathogenic strains of viral etiological agent, i.e., *Rotavirus* VP4, P8, P4, P6, P9, P10, and P11 and *Rotavirus* VP7, G8, G1, G2, G4, G3, and G9 by a PCR method using specific primer sets.

2. Material and Method

In this study, 1465 stool samples of acute watery diarrhea in premarked containers in duplicate in cold storage were collected from NICH and Civil Hospital Karachi and transported within 24 hours to central lab. Patients with complaint of acute watery diarrhea were included in the age bracket of 4 weeks to <5 years while those having other morbid conditions or bloody diarrhea were excluded and informed consent was taken. The questionnaire was designed to focus the parameters like No. of episode of diarrhea, fever, and vomiting.

2.1. Detection of Rotavirus by Sandwich ELISA. To detect the group-specific antigen, polyclonal antibody attached to wells in a sandwich enzyme immunoassay was used. The presence

of rotavirus antigen was compared to color intensity above the cutoff value in the sample by adding 1-gram sample in 1 : 100 dilutions.

2.2. Procedure of ELISA. *Rotavirus* antigen was detected by an ELISA kit method. Diluent buffer was added in 1 : 11 ratio whereas wash buffer and distilled water in 1 : 10 were made in test tubes. 100 μ l of diluted stool sample was taken. 100 μ l conjugate was added in assigned wells along with positive and negative controls. 60 minutes incubation at room temperature. Washing with diluted buffer 300 μ l. 15 minutes' incubation in dark chamber after addition of 100 μ l of substrate finally added 50 μ l of stop solution, ELISA plate reader at 450 nm for results.

2.3. Genotyping of Rota Isolates. *Rotavirus* genotyping was carried out using primer sets against capsid protein VP4 and VP7 coding genes from *Rotavirus* genomic RNAs (Tables 1 and 2). PCR mix contains a total volume of 50 μ l by adding 50 μ l of PCR mix, Invitrogen kit. Add 5 μ l of cDNA. Briefly spin before transfer to the thermocycler. First, cycle for 94°C for 2 min followed by 94°C, 50°C, and 72°C for 1 min in 35 cycles then for 7 minutes in 72 cycles followed by 15°C on hold. Second round PCR mix consists of 5 μ l of the abovementioned amplified products in 50 μ l of master mix in microcentrifuge tubes, before transfer to the thermocycler.

At 100 mA *Rotavirus* genomic RNAs polyacrylamide gel by electrophoresis was detected in tank with buffer for 30 min. The migration of individual RNA genome segments was studied and compared with marker genome segments.

2.4. RT-PCR. Reverse transcriptase PCR was performed by taking genomic RNA 1 μ g in 25 μ l of RNase inhibitor (20 U of RNase out and DNA polymerase containing distilled water). At 50°C for 60 min, the process for reverse transcription was performed in a heating chamber. The termination of reaction was at 85°C for 5 min. Cooling of mix, 2 U of RNase H in 1 μ l followed by incubation 20 min at 37°C. 50- μ l processed for PCR containing 2.0 μ l of the RT-PCR

TABLE 2: Rotavirus VP4 primer list.

| Primer | Human sequence (5' -3') | Position (nt) | Strain genotype | References |
|-------------------|-------------------------|---------------|---------------------|------------|
| 1T-1 1T-1D dP [9] | ACTTGATAACGTGC | 339-356 | KU P8 | [21] |
| | TCTACTGGRITTRACNTGC | 339-356 | P8 | |
| 2T-1 | CTATTGTTAGAGGTTAGAGTC | 474-494 | RV5 P4 | |
| 3T-1 | TGTTGATTAGTTGGATTCAA | 259-278 | 1076 P6 | [22] |
| 4T-1 | TGAGACATGCAATTGGAC | 385-402 | K8 P9 | [21] |
| 5T-1 | ATCATAGTTAGTAGTCGG | 575-594 | 69M P10 | [21] |
| mP11 | GTAAACATCCAGAATGTG | 305-323 | MC435 P11 312 bp | [21] |

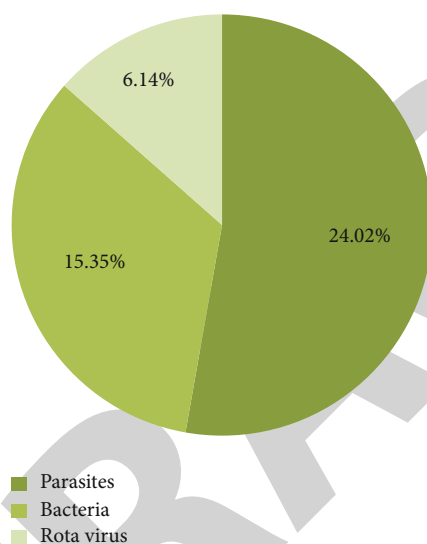


FIGURE 1: Overall pathogen distribution.

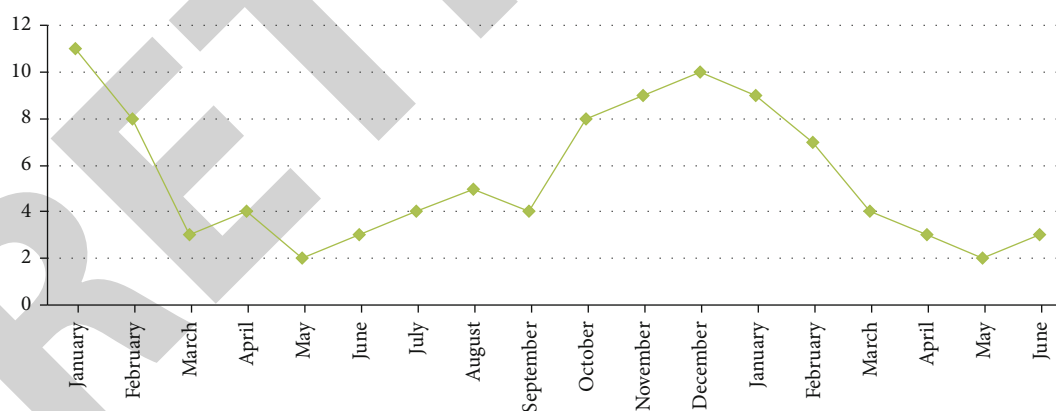


FIGURE 2: Seasonal variation of rotavirus.

products. Amplification buffer 5 μ l, 1.5 μ l of forward and reverse primer each adding, 2.5 U DNA polymerase. Denaturation of Template (94°C, 2 min), 30 cycles of PCR were set. PCR cycle set for denaturation step (94°C for 30 s), annealing (55°C for 30 s), and extension (68°C for 3 min for gene 4 and for 2 min for gene 6). Additional incubation (72°C, 7 min) followed by PCR. PCR purification kit (Qia-gen) to collect purified DNA. By using RT-PCR as templates, VP4 and VP6 gene sequences were determined.

TABLE 3: Vaccination status.

| Vaccinated | No. of children (n) | % |
|------------|---------------------|-------|
| Yes | 139 | 9.5 |
| No | 1326 | 90.5 |
| Total | 1465 | 100.0 |

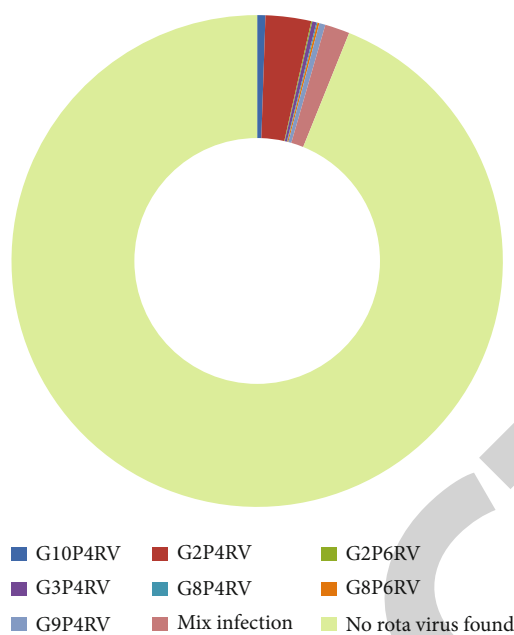


FIGURE 3: Rotavirus subtypes.

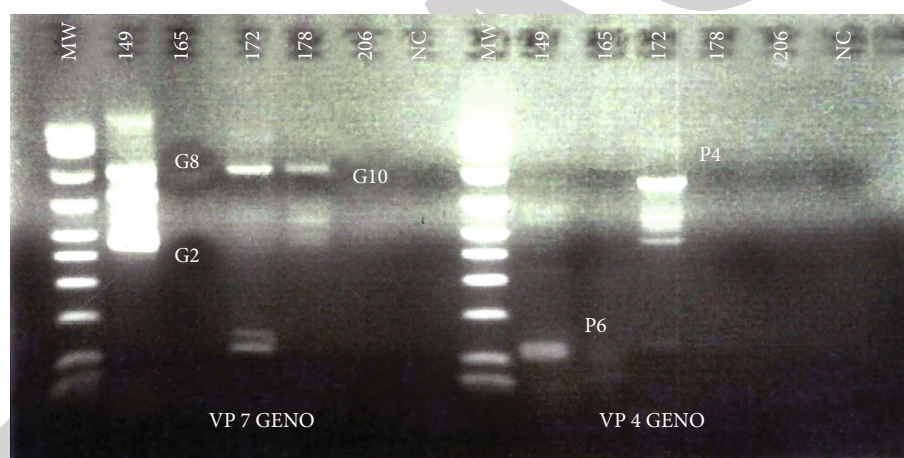


FIGURE 4: Rotavirus genotypes showing gene expression of VP-7 and VP-4 capsid protein coding genes.

3. Result and Discussion

The current study found that many diversified strains of human *Rotavirus* are circulating in the community of Karachi as population belongs to nearby rural areas, where human interaction with animals makes it possible for the assortment for human and animal strains and emergence of new strains.

In the present study, a prevalence of 6% (Figure 1) RVA in diarrheal cases from Pakistan was not too high as compared to those of other reported studies, but it is in correlation with reports that say *Rotavirus* infection prevalence rate in Eastern countries reported 40.5%-60.5% [13]. Similarly, 30%-56% prevalence was reported in Far East countries. A report from Karachi, Pakistan, a prevalence of RVA infections a little higher at 17% was noted which is probably due to the fact that we included patients with acute illness

rather than advanced stage [14]. In Karachi, during the years from 2005 to 2007, different strains of *Rotavirus* in stool samples of children under five years of age—i.e., G9P8, G1P8, and G1P4, were of prime importance in addition to G2P4 (6%), G4P6, G9P6, and G9P4, whereas 2.4% mixed infection caused by more than one strain was also identified [13, 15].

In another study from Pakistan, G1P8, G2P4, G1P6, G9P8, G9P6, G12P6, G6P1, and mix infection with other pathogens were reported as causative etiological agents. These findings are indicative that RV genotype prevalence can be in various combinations and seasonal variation does not affect the prevalence of infection (Figure 2). Rotavirus genotypes G1P4, G1P6, G4P6, G9P4, G12P6, and G6P4 isolated from animals can have recurrent episodes of appearance or disappearance periodically. Our current study also highlighted that RT-PCR sometime does not detect false

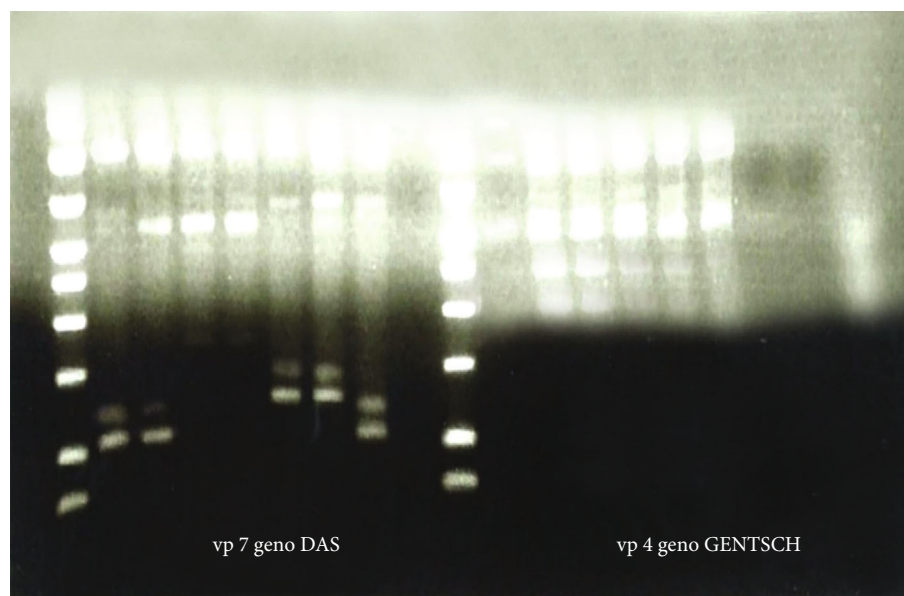


FIGURE 5: Rotavirus genotypes VP-7 and VP-4 and primers for nonspecific protein expression genes.

ELISA positive RV strains (due to multiple reasons like mutations in the genome, diminished viral load, or loss of viral antigenic sites during preservation) or there could be false positive ELISA results [15]. In present study, the data analysis of sick children showed that only 9.5% patients were found vaccinated and 90.5% children did not get vaccine against common diseases (Table 3). Similar results were obtained from.

In *Rotavirus* infection due to assortment of genes, several G types (G2, G3, G8, G9, and G10) and circulating P-types are a cause of mix infection in a single patient in multiple cases [16]. It is also reported in this study that 1.63% mixed VP7 infections: G1G2P4, G2G9P4, G2G9P6, and G2G9P8, were recorded in positive cases (Figure 3). A similar finding with 2.4% prevalence rate in Pakistan was also reported by Ali et al., [17]. Similarly, in South Korea, prevalence was reported mixed infections of 10% and 15% with interspecies transmission [18]. By using primer set against outer G and P antigen, molecular identification was done by visualizing bands of specific Bp on gel images which indicated the *Rotavirus* subtypes G2P4, G10P4, G9P4, and G3P4 (Figures 4 and 5).

Pathogenesis might be the result of several assortments of human and animal strain resulting in origin of G11; however, from Pakistan, most of the focus was on VP7 and VP4 genotyping studies from different cities [19, 20]. It is reported that presence of animal origin RV strain among Pakistani patient is a result of interaction between humans and their livestock and reassortment of genes resulting new strains [19, 20]

In this study, it is noted that the presence of new mix strains of *Rotavirus* was detected in our population beside common circulating strains around the Globe. *Rotavirus* genotypes which were detected in our patients were G10P4, G2P4, G2P6, G3P4, G8P4, G8P6, and G9P4.

4. Conclusions

Spectrum of etiological agents is involved in diarrhea which is a huge health burden worldwide as well in Pakistan. The data of the current study indicate that by conducting prevalence studies and identifying risk factors disease can be timely prevented or managed. Thus, morbidity and high mortality in infants can be reduced. This issue warrants broad-spectrum investigation.

Data Availability

Data can be provided on demand.

Conflicts of Interest

The authors declare that they have no conflicts of interest.

References

- [1] V. Banga-Mingo, D. Waku-Kouomou, J. C. Gody et al., "Molecular surveillance of rotavirus infection in Bangui, Central African Republic, October 2011-September 2013," *Infection, Genetics and Evolution*, vol. 28, pp. 476-479, 2014.
- [2] D. Ouermi, D. Soubeiga, W. M. C. Nadembega et al., "Molecular epidemiology of rotavirus in children under five in Africa (2006-2016): a systematic review," *Pakistan journal of biological sciences: PJBs*, vol. 20, no. 2, pp. 59-69, 2017.
- [3] C. Troeger, M. Forouzanfar, P. C. Rao et al., "Estimates of global, regional, and national morbidity, mortality, and aetiologies of diarrhoeal diseases: a systematic analysis for the Global Burden of Disease Study 2015," *The Lancet Infectious Diseases*, vol. 17, no. 9, pp. 909-948, 2017.
- [4] H. Wang, M. Naghavi, C. Allen et al., "Global, regional, and national life expectancy, all-cause mortality, and cause-specific mortality for 249 causes of death, 1980-2015: a

Retraction

Retracted: CRISPR-Cas System: An Adaptive Immune System's Association with Antibiotic Resistance in Salmonella enterica Serovar Enteritidis

BioMed Research International

Received 12 March 2024; Accepted 12 March 2024; Published 20 March 2024

Copyright © 2024 BioMed Research International. This is an open access article distributed under the Creative Commons Attribution License, which permits unrestricted use, distribution, and reproduction in any medium, provided the original work is properly cited.

This article has been retracted by Hindawi following an investigation undertaken by the publisher [1]. This investigation has uncovered evidence of one or more of the following indicators of systematic manipulation of the publication process:

- (1) Discrepancies in scope
- (2) Discrepancies in the description of the research reported
- (3) Discrepancies between the availability of data and the research described
- (4) Inappropriate citations
- (5) Incoherent, meaningless and/or irrelevant content included in the article
- (6) Manipulated or compromised peer review

The presence of these indicators undermines our confidence in the integrity of the article's content and we cannot, therefore, vouch for its reliability. Please note that this notice is intended solely to alert readers that the content of this article is unreliable. We have not investigated whether authors were aware of or involved in the systematic manipulation of the publication process.

Wiley and Hindawi regrets that the usual quality checks did not identify these issues before publication and have since put additional measures in place to safeguard research integrity.

We wish to credit our own Research Integrity and Research Publishing teams and anonymous and named external researchers and research integrity experts for contributing to this investigation.


The corresponding author, as the representative of all authors, has been given the opportunity to register their agreement or disagreement to this retraction. We have kept a record of any response received.

References

- [1] M. Z. Haider, M. A. B. Shabbir, T. Yaqub et al., "CRISPR-Cas System: An Adaptive Immune System's Association with Antibiotic Resistance in Salmonella enterica Serovar Enteritidis," *BioMed Research International*, vol. 2022, Article ID 9080396, 7 pages, 2022.

Research Article

CRISPR-Cas System: An Adaptive Immune System's Association with Antibiotic Resistance in *Salmonella enterica* Serovar Enteritidis

Muhammad Zulqarnain Haider,¹ Muhammad Abu Bakr Shabbir ,¹ Tahir Yaqub,¹ Adeel Sattar,² Muhammad Kashif Maan,³ Sammina Mahmood,⁴ Tahir Mehmood,⁵ and Hassaan Bin Aslam¹

¹Institute of Microbiology, Faculty of Veterinary Sciences, University of Veterinary & Animal Sciences, Lahore, Pakistan

²Department of Pharmacology and Toxicology, Faculty of Biosciences, University of Veterinary and Animal Sciences, Lahore, Pakistan

³Department of Veterinary Surgery and Pet Centre, Faculty of Veterinary Sciences, University of Veterinary and Animal Sciences, Lahore, Pakistan

⁴Department of Botany, Division of Science and Technology, Bank Road Campus, University of Education, Lahore, Pakistan

⁵Centre for Applied Molecular Biology (CAMB), University of the Punjab, Lahore 53700, Pakistan

Correspondence should be addressed to Muhammad Abu Bakr Shabbir; abubakr.shabbir@uvas.edu.pk

Received 11 February 2022; Accepted 15 March 2022; Published 28 March 2022

Academic Editor: Abdelmotalieb Elokil

Copyright © 2022 Muhammad Zulqarnain Haider et al. This is an open access article distributed under the Creative Commons Attribution License, which permits unrestricted use, distribution, and reproduction in any medium, provided the original work is properly cited.

Several factors are involved in the emergence of antibiotic-resistant bacteria and pose a serious threat to public health safety. Among them, clustered regularly interspaced short palindromic repeat- (CRISPR-) Cas system, an adaptive immune system, is thought to be involved in the development of antibiotic resistance in bacteria. The current study was aimed at determining not only the presence of antibiotic resistance and CRISPR-Cas system but also their association with each other in *Salmonella enteritidis* isolated from the commercial poultry. A total of 139 samples were collected from poultry birds sold at the live bird markets of Lahore City, and both phenotypic and genotypic methods were used to determine antimicrobial resistance. The presence of the CRISPR-Cas system was determined by PCR, followed by sequencing. All isolates of *S. enteritidis* (100%) were resistant to nalidixic acid, whereas 95% of isolates were resistant to ampicillin. Five multidrug-resistant isolates (MDR) such as *S. enteritidis* isolate (S. E1, S. E2, S. E4, S. E5, and S. E8) were found in the present study. The CRISPR-Cas system was detected in all of these MDR isolates, and eight spacers were detected within the CRISPR array. In addition, an increased expression of CRISPR-related genes was observed in the standard strain and MDR *S. enteritidis* isolates. The association of the CRISPR-Cas system with multiple drug resistance highlights the exogenous acquisition of genes by horizontal transfer. The information could be used further to combat antibiotic resistance in pathogens like *Salmonella*.

1. Introduction

Antibiotic resistance is a natural phenomenon, and the emergence of antibiotic-resistant bacteria necessitates updating treatment regimens [1]. Globally, deaths with antibiotic-resistant pathogens are expected to increase from 700,000 fatalities per year in 2014 to 10 million by 2050, which could

result in a total cost of \$100 trillion [2]. *S. enteritidis* is one of the most common *Salmonella* serovars causing foodborne infections and has veterinary and public health concerns [3]. The resistance of *S. enteritidis* to penicillin, aminoglycosides, β -lactams, and fluoroquinolones has been reported worldwide, including Pakistan [4, 5]. It has conclusively been shown that *Salmonella* can acquire these resistance genes

via mobile genetic elements (MGEs) like plasmids, which allow host bacteria more flexibility to disseminate these genes across varied bacterial populations [6].

The CRISPR-Cas system is an acquired immune system that protects bacteria from MGEs, including viruses, plasmids, and transposons [7]. The genome architecture of a CRISPR-Cas locus typically has three parts: sequence of CRISPR arrays, a cas gene locus, and AT-rich leader region [8]. The CRISPR arrays consist of direct repeat sequences of 21-48 base pairs (bp) separated by 26-72 bp long spacer sequences. The spacers are 4-10 highly conserved short nucleic acid sequences obtained from previous encounters with MGEs [9]. The mechanism of action of the CRISPR-Cas system is generally divided into three stages: acquisition of new spacers (the adaptation stage), crRNA biogenesis (the CRISPR transcripts), and interference against foreign invaders directed by crRNAs [10].

Overall, the CRISPR-Cas system is divided into three types: types I, II, and III [11]. *S. enteritidis* have a type I-E CRISPR system and consists of a cas operon and two CRISPR arrays, CRISPR1 and CRISPR2, separated by 16 bp [12]. The cas operon is located next to the CRISPR1 array [7] and consists of a cluster of cas3, cas2, cas1, cas6e, cas7, cse2, and cse1 and cas5 genes [13]. Apart from defending bacteria against invaders, the CRISPR-Cas system has been suggested to increase bacterial virulence, but its role in antibiotic resistance is still under debate [11].

The literature is scarce regarding the CRISPR-Cas system's role in the development of antibiotic resistance; hence, the present study is designed to determine the association of the CRISPR-Cas system with antibiotic resistance in MDR *S. enteritidis* isolated from the commercial poultry. Later, the CRISPR-Cas system identified from these isolates was analyzed to identify spacer sequences. At last, an association of the CRISPR-Cas system was determined through qRT-PCR.

2. Materials and Methods

2.1. Bacterial Isolation and Growth Conditions. A total of 139 samples, including sixty-nine freshly passed poultry droppings and seventy cloacal swab samples, were collected from major commercial poultry markets (Tollinton and Sheranwala) of Lahore. Samples were kept in peptone broth, transported to the bacteriology laboratory, and stored at 4°C. Samples were enriched in selenite broth and subcultured on Salmonella Shigella Agar and then incubated at 37°C for 24-28 hours. Black-centered colonies were subcultured for purification after incubation [14].

2.2. Identification of Salmonella. The DNA of all biochemically confirmed isolates was extracted by a commercially available GF-1 nucleic acid extraction kit from Vivantis (Vivantis, Malaysia). Molecular identification of the genus and species was performed by PCR using previously used specific primers [15, 16]. For reaction mixture, 6.5 µL of nuclease-free water, 12.5 µL of 2x PCR Taq Plus MasterMix (abm, Canada), 2 µL each of forward and reverse primers, and 2 µL of DNA template were used and amplified in a C1000™ thermal cycler (Bio-Rad, Singapore). The cyclic

conditions used for the PCR were the following: primary denaturation for 2 minutes at 94°C, denaturation for 40 seconds at 94°C, annealing for 50 seconds at the ideal temperature of different primers given in Table 1, and extension for 50 seconds at 72°C. The amplicons were electrophoresed using 1.5% agarose gel for 30 minutes at 100 volts and later on visualized using a gel documentation system (Omega Fluor Plus Systems, Aplegen Inc., California, USA) and GeneRuler™ 100 bp plus DNA ladder.

2.3. Antibiotic Resistance Profiling. The PCR-confirmed *S. enteritidis* isolates were tested for antibiotic susceptibility using the Kirby-Bauer disc diffusion method [17]. The optical density of *S. enteritidis* culture was set at 0.5 McFarland units and seeded on a plate (150 mm) containing Mueller-Hinton (MH) agar. Antibiotic discs with a single concentration of nalidixic acid (30 µg), ampicillin (10 µg), gentamicin (10 µg), chloramphenicol (30 µg), tetracycline (30 µg), and sulfamethoxazole (25 µg) were placed on the agar surface. After 24 hours of incubation at 37°C, the diameter of the zone of inhibition was determined. Isolates were classified as resistant, intermediate, or sensitive using the Clinical Laboratory Standards Institute's (CLSI) guidelines [18].

2.4. Detection of Antibiotic Resistance Genes. Antibiotic-resistant genes such as *gyrA*, *bla*_{TEM-1}, and *tetB* were screened by PCR as described previously [19–21]. Nuclease-free water (6.5 µL), 2x PCR Taq plus MasterMix (12.5) (abm, Canada), forward and reverse primers (2 µL) each, and DNA template (2 µL) were used to make a PCR mixture (25 µL). After that, PCR products were electrophoresed for 30 minutes using 1.5% gel.

2.5. CRISPR-Cas System Detection. The specific primers (*cas3*, *cas2*, and *cas1*) were designed online using the tool Primer 3 (<http://primer3.ut.ee/>) and are mentioned in Table 1. The amplified PCR products were electrophoresed on a 1.5 percent gel and analyzed using a gel documentation system (Omega Fluor Plus Systems, Aplegen Inc., California, USA). Afterwards, the amplified MDR and *cas3* genes were subjected to DNA sequencing by a commercial facility (Advance Bioscience International, Lahore, Pakistan).

2.6. Detection of CRISPR Spacers. The online bioinformatics tool CRISPR-Finder (<https://crispr.i2bc.paris-saclay.fr/Server/>) was used to identify CRISPR spacer sequences [22]. Spacers were retrieved from CRISPR-Finder output using a nucleotide BLAST search (<https://blast.ncbi.nlm.nih.gov/>) and analyzed for their identity on GenBank. Because of the small spacer length (50 nt) and relatively large database (more than 10¹⁰ nt), the significance of alignment was calculated using an *E* value of 0.02 [23]. Alignment with an *E* value less than the cutoff value and greater than 80% similarity was chosen from all isolates.

2.7. Identification of CRISPR Gene Expression after Exposure to Antimicrobials by qRT-PCR. One MDR *S. enteritidis* isolate and its standard strain were exposed (1/2 MPC) to six antibiotics. The QIAamp Viral RNA Mini Kit (QIAGEN, Hilden, Germany) was used to extract RNA from each

TABLE 1: Primers used for the identification of genus and species antibiotic-resistant genes and CRISPR-Cas genes of *Salmonella enteritidis* isolated from poultry.

| Target gene | Amplicon (bp) | Primers (5'-3') | T _m | Reference |
|-------------|---------------|--|----------------|------------|
| InvA | 423 | F: TCGTGACTCGCGTAAATGGCGAA R: GCAGGCGCACGCCATAATCAATA | 63°C | [15] |
| IE | 316 | F: AGTGCCATACTTTTAATGAC R: ACTATGTCGATACGGTGGG | 55°C | [16] |
| gyrA | 610 | F: CGAGAGAAATTACACCGGTCA R: AGCCCTTCAATGCTGATGTC | 55°C | [19] |
| blaTEM-1 | 643 | F: CAGCGGTAAGATCCT TGAGA R: ACTCGCCGTCGTGTAGATAA | 54°C | [20] |
| tetB | 659 | F: TTGGTTAGGGGCAAGTTTTG R: GTAATGGGCCAATAACACCG | 57°C | [21] |
| Cas1 | 892 | F: CCAGTGATTCAAGTTCCGGT R: GTGACGTTCTGACCGCTCAA | 55°C | This study |
| Cas2 | 262 | F: AACCAAACGCAGTCCATCCA R: TATGGTGGTTGTGGTCACGG | 55°C | This study |
| Cas3 | 692 | F: GCAAAGTCCGTCACCACAAT R: GATTTAGCGCCGGTGGATTT | 55°C | This study |
| Cas3* | 201 | F: GGGATAGACATAGGCGCTGT R: GATTTAGCGCCGGTGGATTT | 55°C | This study |

sample. A Revert Aid First-Strand cDNA Kit (Thermo Scientific, USA) was used to make cDNA.

The CFX96 real-time PCR thermocycler (Bio-Rad, Singapore) was used for amplification. Preincubation at 95°C for 3 minutes was followed by 45 cycles of 10 seconds at 95°C and 40 seconds at 52°C in the cycling conditions for amplification. The specific primers used were cas3*F (GGGATAGACATAGGCGCTGT) and cas3*R (GATTTAGCGCCGGTGGATTT) (Table 1). A housekeeping gene (16S rRNA) was used as an internal control for normalization. The experiment was repeated three times to calculate the mean fold change.

3. Results

3.1. Confirmed Bacterial Isolates. The collected samples were cultured and processed through conventional bacteriological methods; 45% (62/139) isolates were confirmed as *Salmonella*. From these 62 isolates, 32% (20/62) isolates were confirmed as *S. enteritidis* through PCR (Figure 1).

3.2. Antibiotic-Resistant Profiling of Poultry Isolates of *S. Enteritidis*. The susceptibility of 20 confirmed *S. enteritidis* isolates to six antibiotics was determined. All *S. enteritidis* isolates were resistant (100%) to nalidixic acid, and 95% were found resistant to ampicillin. The intermediate levels of resistance to tetracycline (60%), gentamicin (50%), and chloramphenicol (45%) and low levels of resistance to sulfamethoxazole (30%) were found in the present study (Table 2).

3.3. Detection of Antibiotic Resistance Genes. Antibiotic resistance-associated genes (*gyrA*, *tetB*, and *blaTEM-1*) in all confirmed *S. enteritidis* isolates were detected by PCR as shown in Figure 2. Out of 20 isolates, 5 were MDR (only

one or two antibiotic classes remain sensitive to bacterial isolates) and contained all 3 antibiotic-resistant genes. At the same time, 1 or 2 of these antibiotic-resistant genes were present in non-MDR isolate.

3.4. CRISPR-Cas System Detection. A conventional PCR was performed to detect the presence of the CRISPR-Cas system in these confirmed 20 *S. enteritidis* isolates. The CRISPR-Cas genes such as cas1, cas2, and cas3 amplified through PCR are shown in Figure 3.

3.5. Spacer's Identification and Analysis of Poultry Isolates of *S. Enteritidis*. CRISPR-Finder analysis revealed that the CRISPR array has a direct repeat sequence of 29 bp: 5'-GTGTTCCCCGCGCCAAGCGGGGATAAACCG-3' separated by spacer sequences of 32-40 bp. The 8 spacer sequences were present in all four isolates. All spacers revealed homology with the CRISPR and chromosome regions of different *S. enteritidis* strains, as shown in Table 3. Based on bioinformatics analysis, it is safer to say that antibiotic resistance genes are also carried by CRISPR-Cas system-carrying isolates, which may have an association with antibiotic resistance.

3.6. CRISPR-Cas Gene Expression in the Standard Strain and MDR Isolate. The qRT-PCR was used to determine the association between the CRISPR-Cas system and antibiotic resistance. Increased cas3 gene expression was found in the *Salmonella* ATCC 13076 strain and MDR *S. enteritidis* isolate, as shown in Figure 4. This high expression might be because the CRISPR-Cas system regulates several genes that play a role in maintaining the membrane integrity and overcoming different stress such as antibiotic resistance [24].

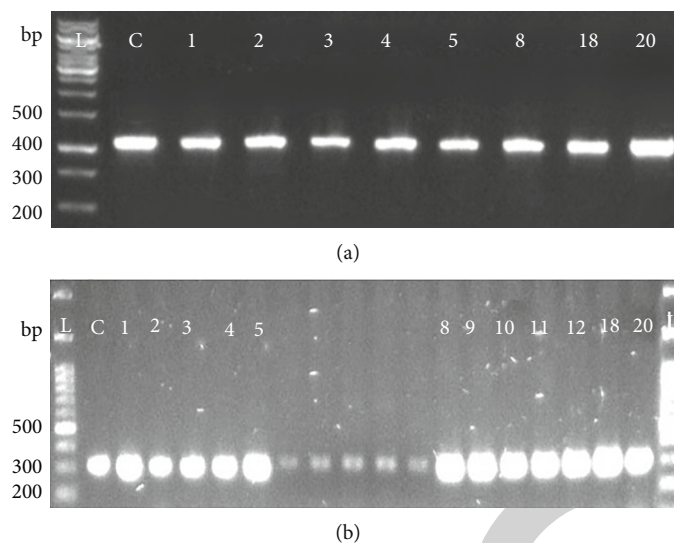


FIGURE 1: Identification of *Salmonella* isolates: presence of the (a) *invA* gene and (b) *IE* gene by PCR to identify the *Salmonella* genus and *S. enteritidis* species. L indicates the 100-base pair (bp) ladder. The numeric characters represent the sequential number of *S. enteritidis* of isolates.

TABLE 2: Antibiotic susceptibility patterns (Kirby-Bauer) of *S. enteritidis* against different antibiotics.

| Antibiotics | Disk (μg) | Antibiotic resistance profile <i>S. enteritidis</i> ($n = 20$) | | |
|-------------|------------------------|---|------------------|---------------|
| | | Sensitive (%) | Intermediate (%) | Resistant (%) |
| AMP | 10 | 0 | 5 | 95 |
| CHL | 30 | 40 | 15 | 45 |
| CN | 10 | 35 | 15 | 15 |
| TE | 30 | 35 | 5 | 60 |
| NA | 30 | 0 | 0 | 100 |
| SXT | 25 | 45 | 25 | 30 |

AMP: ampicillin; CHL: chloramphenicol; CN: gentamicin; TE: tetracycline; NAL: nalidixic acid; SXT: sulfamethoxazole.

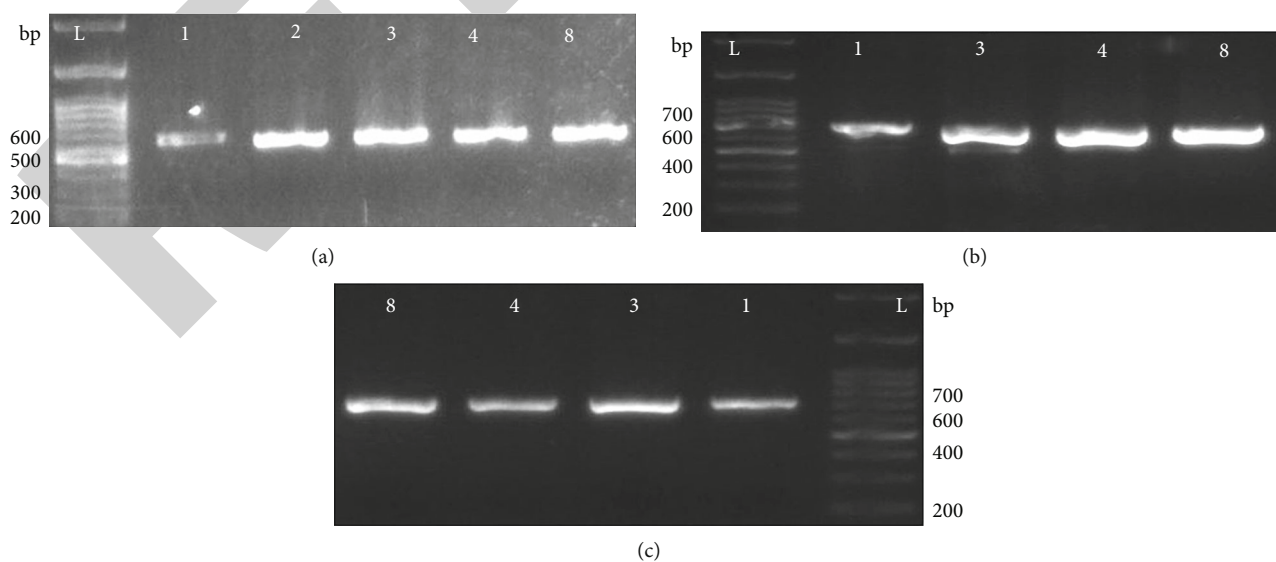


FIGURE 2: Detection of antibiotic resistance genes: presence of the (a) *gyrA* gene, (b) *tetB* gene, and (c) *bla*_{TEM-1} gene by PCR for the detection of drug resistance in *S. enteritidis* species. L indicates the 100-base pair (bp) ladder. The numeric characters represent the sequential number of *S. enteritidis* of isolates.

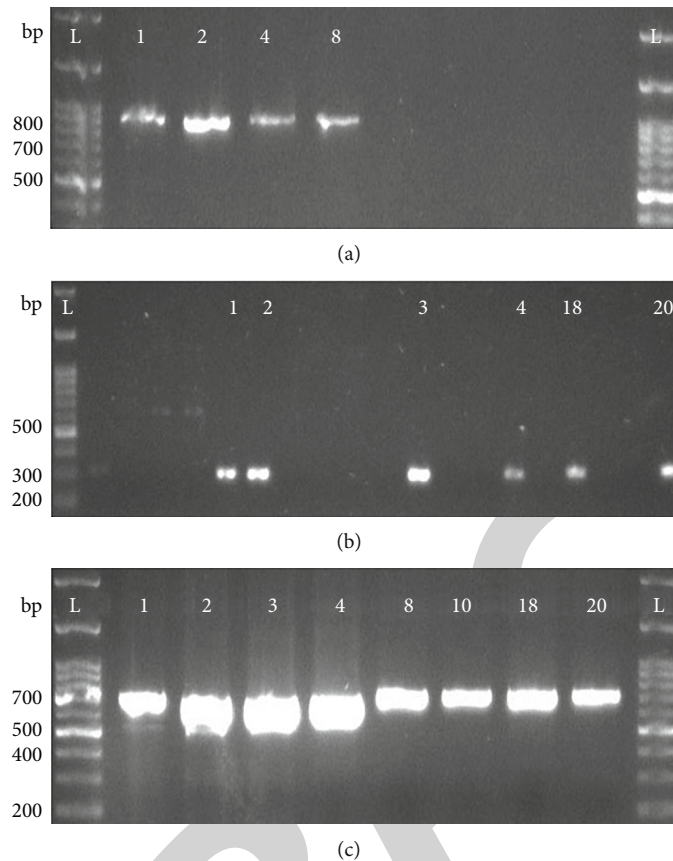


FIGURE 3: Detection of the CRISPR-Cas system: presence of the (a) cas1 gene, (b) cas2 gene, and (c) cas3 gene by PCR for the detection of the CRISPR-Cas system in *S. enteritidis* species. L indicates the 100-base pair (bp) ladder. The numeric characters represent the sequential number of *S. enteritidis* of isolates.

TABLE 3: Spacer sequence homology of poultry isolates of *S. enteritidis* to other strains.

| Homology to other strains | | | | | | | | |
|---------------------------|-----------|---------------------------------|----------------------------------|-----------------------------------|---|-------------------------------------|----------------------------------|--|
| Poultry isolates | +SE95 (%) | + <i>S. enteritidis</i> SEO (%) | + <i>S. enteritidis</i> SE81 (%) | + <i>S. enteritidis</i> SE104 (%) | + <i>S. enteritidis</i> SAP18-H9654 (%) | + <i>S. enteritidis</i> 95-0621 (%) | + <i>S. enteritidis</i> SE74 (%) | |
| S.E1 | 99.13 | – | 98.98 | 99.13 | – | – | 99.13 | |
| S.E4 | 99.12 | – | 99.12 | 99.12 | – | – | 99.12 | |
| S.E5 | – | 99.41 | – | – | 99.41 | 99.41 | – | |
| S.E8 | – | 99.70 | – | – | 99.70 | 99.70 | – | |

“+” indicates homology to the clustered regularly interspaced short palindromic repeat region of the strain. “–” means not significant.

4. Discussion

The CRISPR-Cas system, known as bacteria’s adaptive immune system, has some additional functions, increasing bacterial virulence [11]. However, its role in antibiotic resistance has not been thoroughly considered. Therefore, the involvement of the said system in antibiotic resistance of *S. enteritidis* is assessed in this study through phenotypic and genotypic methods and bioinformatic analysis. The findings highlight that the CRISPR-Cas system is involved in antibiotic resistance, and the result is in the lines of earlier literature [24].

The present study employed genus-specific and species-specific PCR to detect *S. enteritidis*; such an approach has also been used in the previously described studies [15, 16].

The sample prevalence of *Salmonella* was 45% (62/139). The current study’s findings are consistent with a previous study describing *S. enteritidis* as the most prevalent serovar [25] prevailing in poultry.

Antibiotics are reported to be irrationally used in chicken production as growth promoters, for prophylaxis, and to treat *Salmonellae* and other bacterial infections. This irrational use of antibiotics in feed and drinking water could result in antibiotic resistance. Transfer of such antibiotic-resistant *Salmonellae* to humans could occur *via* a contaminated food chain that could have strong public health concerns [26]. It is apparent from this study that most of the isolates of *S. enteritidis* were resistant to nalidixic acid (quinolones) and ampicillin (95%). These findings are in

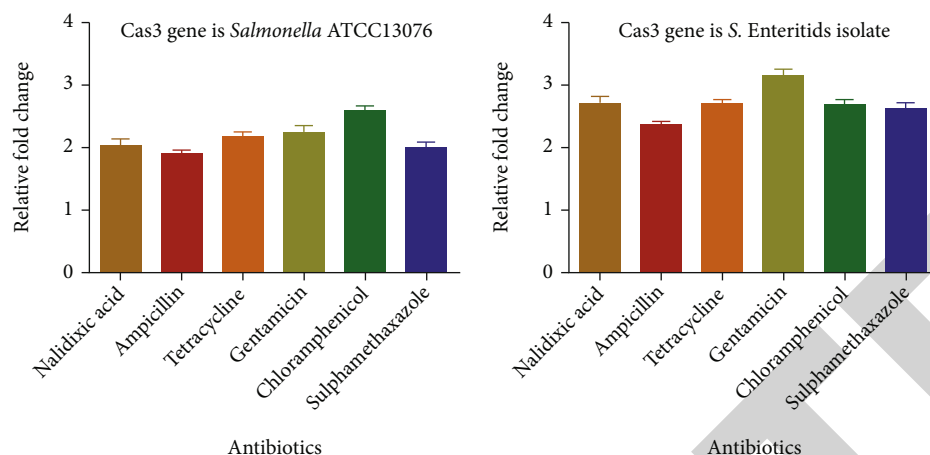


FIGURE 4: Clustered regularly interspaced short palindromic repeat- (CRISPR-) Cas gene (cas3) expression in *S. enteritidis* and *Salmonella* ATCC13076 under the exposure of different antibiotics.

good agreement with the results of previous studies where the highest resistance to quinolones and ampicillin was found when compared to other antibiotics [26, 27]. Interestingly, the intermediate resistance levels estimated against gentamycin, chloramphenicol, and tetracycline are also consistent with the previous literature [27, 28].

The CRISPR-Cas system in *S. enteritidis* isolated from poultry was confirmed by PCR using CRISPR-Cas gene-specific primers. The CRISPR-Cas system was found in all *S. enteritidis* with antibiotic resistance confirmed. Likewise, recently, a study reported similar findings, which are in accordance with the results of our study [29].

With the help of cas proteins, the CRISPR-Cas system can integrate spacers derived from the invader's mobile genetic elements [30]. Upon bioinformatic analysis, spacers were found in four of the MDR *S. enteritidis* poultry isolates. Several *S. enteritidis* strains exhibit similarities with these spacer sequences. Homology was found with the CRISPR region and chromosomes of *S. enteritidis* strain SE 95 and *S. enteritidis* strain SEO in some cases. The present finding is also supported by the findings of the previous study [24] where they also found spacer homology in the genetic elements of *C. jejuni* strains with their closely related spacer-carrying strains.

In the current study, the authors used qRT-PCR to determine the association between the CRISPR-Cas system and antibiotic resistance. The CRISPR gene expression was increased in the MDR poultry isolate of *S. enteritidis* than its standard strain suggesting the association of the said system with antibiotic resistance. As mentioned earlier, this increased expression of CRISPR genes might be because the said system regulates several genes that play roles in membrane integrity and provide resistance against different membrane stressors such as antibiotics, as also reported by Samson and colleagues in 2015 [31]. Although the present study provides baseline information regarding the association of the CRISPR system with antibiotic resistance, there is still a need to look deeper to understand whether this system promotes antibiotic resistance alone or by regulating several other genes.

5. Conclusion

The CRISPR-Cas system did have an association or role in antibiotic resistance because high antibiotic resistance in poultry isolates and similarity of spacers with other *S. enteritidis* strains suggest that this system is involved in antibiotic resistance.

Data Availability

All data are available.

Conflicts of Interest

The authors declare no conflict of interest.

References

- [1] S. Dhingra, N. A. A. Rahman, E. Peile et al., "Microbial resistance movements: an overview of global public health threats posed by antimicrobial resistance, and how best to counter," *Frontiers in Public Health*, vol. 8, p. 531, 2020.
- [2] Y. He, Q. Yuan, J. Mathieu et al., "Antibiotic resistance genes from livestock waste: occurrence, dissemination, and treatment," *NPJ Clean Water.*, vol. 3, no. 1, pp. 1–11, 2020.
- [3] M. Pandey and E. S. K. Goud, *Non-Typhoidal Salmonellosis: A Major Concern for Poultry Industry*, IntechOpen, 2021.
- [4] M. Asif, H. Rahman, M. Qasim, T. A. Khan, W. Ullah, and Y. Jie, "Molecular detection and antimicrobial resistance profile of zoonotic *Salmonella enteritidis* isolated from broiler chickens in Kohat, Pakistan," *Journal of the Chinese Medical Association*, vol. 80, no. 5, pp. 303–306, 2017.
- [5] S. Yasmin, M. Nawaz, A. A. Anjum et al., "Antibiotic susceptibility pattern of *Salmonellae* isolated from poultry from different districts of Punjab, Pakistan," *Pakistan Veterinary Journal*, vol. 40, pp. 98–102, 2019.
- [6] H. El-Sharkawy, A. Tahoun, A. E.-G. A. El-Gohary et al., "Epidemiological, molecular characterization and antibiotic resistance of *Salmonella enterica* serovars isolated from chicken farms in Egypt," *Gut Pathogens*, vol. 9, no. 1, pp. 1–12, 2017.

Retraction

Retracted: Deleterious Effects of Amoxicillin on Immune System and Haematobiochemical Parameters of a Rabbit

BioMed Research International

Received 12 March 2024; Accepted 12 March 2024; Published 20 March 2024

Copyright © 2024 BioMed Research International. This is an open access article distributed under the Creative Commons Attribution License, which permits unrestricted use, distribution, and reproduction in any medium, provided the original work is properly cited.

This article has been retracted by Hindawi following an investigation undertaken by the publisher [1]. This investigation has uncovered evidence of one or more of the following indicators of systematic manipulation of the publication process:

- (1) Discrepancies in scope
- (2) Discrepancies in the description of the research reported
- (3) Discrepancies between the availability of data and the research described
- (4) Inappropriate citations
- (5) Incoherent, meaningless and/or irrelevant content included in the article
- (6) Manipulated or compromised peer review

The presence of these indicators undermines our confidence in the integrity of the article's content and we cannot, therefore, vouch for its reliability. Please note that this notice is intended solely to alert readers that the content of this article is unreliable. We have not investigated whether authors were aware of or involved in the systematic manipulation of the publication process.

Wiley and Hindawi regrets that the usual quality checks did not identify these issues before publication and have since put additional measures in place to safeguard research integrity.

We wish to credit our own Research Integrity and Research Publishing teams and anonymous and named external researchers and research integrity experts for contributing to this investigation.

The corresponding author, as the representative of all authors, has been given the opportunity to register their agreement or disagreement to this retraction. We have kept a record of any response received.

References

- [1] K. Hussain, M. H. Lashari, U. Farooq, and T. Mehmood, "Deleterious Effects of Amoxicillin on Immune System and Haematobiochemical Parameters of a Rabbit," *BioMed Research International*, vol. 2022, Article ID 8691261, 8 pages, 2022.

Research Article

Deleterious Effects of Amoxicillin on Immune System and Haematobiochemical Parameters of a Rabbit

Khalid Hussain,¹ Mushtaq Hussain Lashari ¹, Umer Farooq ², and Tahir Mehmood³

¹Department of Zoology, The Islamia University of Bahawalpur, Bahawalpur, Pakistan

²Department of Physiology, Faculty of Veterinary and Animal Sciences, The Islamia University of Bahawalpur, Pakistan

³Centre for Applied Molecular Biology (CAMB), University of the Punjab, Lahore, 53700 Punjab, Pakistan

Correspondence should be addressed to Mushtaq Hussain Lashari; mushtaq.hussain@iub.edu.pk

Received 13 February 2022; Revised 2 March 2022; Accepted 8 March 2022; Published 23 March 2022

Academic Editor: Abdelmoteleb Elokil

Copyright © 2022 Khalid Hussain et al. This is an open access article distributed under the Creative Commons Attribution License, which permits unrestricted use, distribution, and reproduction in any medium, provided the original work is properly cited.

The present study is aimed at evaluating the haematobiochemical and immune system alterations in rabbit's exposure to amoxicillin. Thirty-two healthy rabbits were randomly divided into four ($n = 8$) groups comprising of three experimental groups and one control group. After 7 days of the acclimatization period, the study animals were given different doses of amoxicillin orally (100, 150, and 200 mg/kg body weight) for 21 days. The hematological results revealed that red blood cells, hemoglobin, mean corpuscular hemoglobin, and mean corpuscular hemoglobin concentration decreased significantly ($P < 0.05$) whereas white blood cells, neutrophils, and granulocyte exhibited a significantly increasing trend. Serum biochemical analysis showed a significantly increased concentration of HDL, LDL, serum globulin cholesterol, triglyceride, urea, uric acid, creatine, and calcium while plasma fibrinogen, blood sugar, albumin, and total protein were decreased significantly. Furthermore, liver function enzymes such as alanine transaminase (ALT), aspartate transaminase (AST), alkaline phosphatase (ALP), lactate dehydrogenase (LDH), and bilirubin significantly increased. Antioxidant enzymes and oxidative stress parameters such as malondialdehyde concentrations (MDA) increased significantly while catalase, superoxide dismutase, reduced glutathione, and peroxidase reduced significantly in antibiotic amoxicillin-treated groups as compared to the untreated control group ($P < 0.05$). Microscopic histopathological examination showed negative structural changes in liver, kidney, and heart tissues due to karyorrhexis; a disorganized hepatic cord in the liver; increased Bowman's space, necrotic renal tubules, and degenerative glomerulus in the kidney; and necrotic cardiac cells and cytoplasmic vacuolization in the heart, in antibiotic amoxicillin-treated rabbit groups as compared to the control group. In conclusion, amoxicillin induced stress and physiological and immunological impairments due to the adverse effects on haematobiochemical parameters and histopathological and tissue protein changes in target animals.

1. Introduction

Development in technology, industrial expansion, and extensive use of synthetic chemicals to enhance the production potential of crops and livestock animals and to control various diseases have become huge threats to both the environment and public health [1, 2]. Exposure to various environmental pollutants, industrial wastes, insecticide, pesticide, and heavy metals and the use of antibiotics in different animals and human not only induce death but also affect the life expectancy of various organisms [3]. Numerous studies highlighted that different synthetic compounds including antibiotics from

multiple resources directly enter into public health ultimately leading to adverse effects [4]. Exposure to such type of antibiotics induces disturbance in normal physiological functions and reproductive dysfunction in target and nontarget animals [5]. Feeding to increasing human population is a global problem with thorough rethinking to increase food production especially from livestock to meet the global demand that can be mainly achieved through the prevention and treatment of stock from bacterial infections [6]. Antibiotics play a vital role in controlling pathogenic infections for a long time [7]. Tetracyclines, oxytetracyclines, sulfamethazine, penicillin G, and lincomycin are extensively used in veterinary practice to treat

bacterial infections [8], although antibiotics are generally considered safe and well tolerated but still associated with a wide range of adverse effects. Multiple ranges of the pharmacodynamic effects of different antibiotics on blood constituents, serum enzymes, and electrolytes of the laboratory and domesticated animals are observed [9], including mutagenicity, nephropathy (gentamicin), hepatotoxicity, bone marrow toxicity, reproductive dysfunction (chloramphenicol), and carcinogenicity (oxytetracycline). The long-term antibiotic abuse leads to increase of drug-resistant bacteria for humans and animals. Amoxicillin is extensively used in the treatment of a wide range of diseases in veterinary and human. Amoxicillin is a bactericidal aminopenicillin, which eliminates principally by tubular secretion and glomerular filtration. Due to its broad spectrum activity, cheapness, favorable pharmacokinetics, and antimicrobial efficacy, amoxicillin is widely used in the poultry industry [10] and for preoperative antibiotic prophylaxis in veterinary medicine [11]. Since antibiotics are associated with adverse effects, the European Union introduced a general prohibition for the use of antibiotics as growth promoters [12]. Besides that, mostly, livestock producers use variable doses of various antibiotics to treat various kinds of infections in livestock. It is also a common practice to treat the entire stock, regardless of the affected ones [13]. Furthermore, antibiotics are also being recommended improperly for viral infections. These practices eventually lead to antibiotic remains entering the human food chain through an animal-derived food source such as meat, milk, and eggs and also become the reason of several health concerns in human beings along with livestock. But the mechanism of work about these antibiotics is still not clearly understood, and a lot of debates have been going on among scientists and researchers to conclude their adverse side effects. Therefore, the present study is designed to investigate the possible haematobiochemical and histopathological changes in a healthy local breed of rabbit after administration of variable doses of amoxicillin.

2. Materials and Methods

Apparently, 32 healthy adult rabbits (*Oryctolagus cuniculus*), about 1 year old (weight 1.5 kg), were collected from local market in Bahawalpur, Punjab. The study was approved in full by the “ethical review committee for the use of animals” which comes under the administrative control of the office of research, innovation and commercialization of the Islamia University of Bahawalpur, Pakistan. The rabbits were then transferred to a laboratory of animal toxicology in the department of zoology, the Islamia University of Bahawalpur, Pakistan. After that, rabbits were kept under similar management and environmental conditions, for example, the laboratory temperature was maintained at 25–27°C throughout the study. After shifting, rabbits were given the adjustment period to the research laboratory conditions for 7 days. During the adjustment period, drinking water was changed on a daily basis ad libitum and fed twice daily seasonal fodder *Trifolium alexandrinum* in the morning and evening. Rabbits were divided into 4 groups composed of 3 experimental and 1 control with 8 rabbits each group. Amoxicillin of GlaxoSmithKline was bought from a registered pharmaceutical shop in Bahawalpur.

Variable doses of amoxicillin 100 mg/kg, 150 mg/kg, and 200 mg/kg body weight were fed orally to the animals of experimental groups A, B, and C, respectively, on a daily basis for 21 days, to investigate its effects on hematology and serum biochemistry.

2.1. Blood and Serum Analysis. Three mL of blood was collected from the marginal ear vein for hematological and biochemical analysis. Hematological parameters such as red blood cell count, hemoglobin, hematocrit, and total and differential white blood cell count were evaluated by using a hematological analyzer. The serum was used to estimate different liver function tests such as ALT and ALP which were determined according to earlier protocol plasma glucose concentrations, plasma urea concentrations, plasma creatinine, serum calcium, plasma albumin, total protein, cholesterol, and triglycerides, and uric acid was determined by using a Chem Analyzer model, BTS BioSystem, Spain, and diagnostic kits manufactured by BioMed Diagnostics, GmbH, Germany, following the user’s manual.

2.2. Statistical Analysis. The data from all study groups were statistically analyzed by using Statistical Package for Social Sciences (SPSS) and was expressed as mean \pm SD. One-way ANOVA with Tukey’s as a post hoc test was applied with a significance level set at $P < 0.05$.

3. Results

3.1. Clinical Signs. Clinical signs such as diarrhea, loss of body weight, tremors, skin coloration, lacrimation, gasping, dilation of pupil, and faintness were observed from mild to very severe in antibiotic amoxicillin-treated groups when compared with control groups (Table 1).

3.2. Relative Body and Organ Weight of Rabbits. Body weight of treated rabbits (groups) reduced significantly which were exposed to variable doses of amoxicillin as compared to that of the untreated control group. The relative weight of organs like the liver, kidney, heart, brain, and ovary decreased significantly whereas the relative weight of organs like the lungs, spleen, and testis increased significantly in the antibiotic amoxicillin-treated group as compared to the control group (Table 2).

3.3. Hematological Studies. The analysis of hematological parameters of control and experimental groups showed that total white blood cells (total WBC), granulocytes, neutrophils, and platelets significantly increased while red blood cells, hemoglobin, hematocrit, mean corpuscular volume (MCH), mean corpuscular hemoglobin concentration (MCHC), lymphocyte, and monocyte significantly decreased as compared to the control group. The values of the mean corpuscular volume (MCV) showed nonsignificant difference in antibiotic-treated groups as compared to the controlled group ($P < 0.05$) (Table 3).

3.4. Biochemical Parameter. The analysis of serum biochemical parameters of control and experimental groups showed that concentrations of HD lipoproteins, LD lipoproteins,

TABLE 1: Severity of different clinical signs in rabbits exposed to variable doses of amoxicillin.

| Clinical ailments | Groups/treatments | | | |
|---------------------|---------------------|---------------|---------------|---------------|
| | Control (0.0 mg/kg) | A (100 mg/kg) | B (150 mg/kg) | C (200 mg/kg) |
| Diarrhea | – | + | ++ | ++++ |
| Loss of body weight | – | + | + | +++ |
| Tremors | – | + | ++ | +++ |
| Gasping | – | ++ | +++ | ++++ |
| Skin coloration | – | – | +++ | +++ |
| Lacrimation | – | + | + | ++ |
| Faintness | – | – | +++ | ++++ |
| Dilation of pupil | – | – | + | ++ |

Normal: –; mild: +; moderate: ++; severe: +++; very severe: ++++.

cholesterol, triglyceride, urea, uric acid, creatine, calcium, and serum globulin significantly increased while blood sugar, albumin, total protein, and plasma fibrinogen significantly decreased in antibiotic-treated groups when compared to the controlled group ($P < 0.05$) (Table 4).

3.5. Antioxidant Enzymes. Analyses from the results of antioxidant enzymes and oxidative stress biomarker showed that values of malondialdehyde concentrations (MDA) increased significantly while catalase, superoxide dismutase, reduced glutathione, and peroxidase reduced significantly in antibiotic amoxicillin-treated groups as compared to the untreated control group ($P < 0.05$) (Table 5).

3.6. Liver Function Enzymes. Liver function tests showed that ALT, AST, ALP, LDH, and bilirubin of antibiotic-treated rabbits groups significantly increased as compared to those of the control group ($P < 0.05$) (Table 6).

3.7. Gross and Histopathological Studies. Histopathological examination of the liver showed karyorrhexis, cytoplasmic vacuolation, disorganized hepatic cord, bile duct hyperplasia, necrosis, and hydropic changes in hepatocytes. In the kidney, different pathological ailments like increased Bowman's space, congestion, necrosis of renal tubular epithelial cell, nuclear hypertrophy, necrosis of renal tubules, degeneration of the renal tubule, degenerative changes in kidney glomerulus, widening of the urinary space, hemorrhage b/w tubule, and cell infiltration with pyknotic nuclei were observed, while in heart necrosis of cardiac cells, cytoplasmic vacuolization, congestion, neutrophilic myocarditis, myofibrilolysis, and pyknotic nuclei in amoxicillin-treated rabbits were seen after 21 days of exposure to a higher dose (200 mg/kg body weight) of antibiotic amoxicillin-treated rabbit groups as compared to the control group (Table 7 and Figure 1).

4. Discussion

The results on the hematological profile exhibited an increased population of the total leukocytic count. The increased population of these cells in treated rabbits can be related to different tissue damages by amoxicillin. Different previous studies have also reported similar results in amoxicillin-treated sheep [11]. The present study showed that granulocytes significantly

increased. This shows that amoxicillin treatment induced severe damage to the vital organ of rabbits; as a result, granulocytes increased to counter that damage. In present study, neutrophils significantly increased in experimental groups when compared with control ones and the increased number of neutrophils also shows that the damage is caused to blood-forming tissues in bone marrow along with other vital organs of the rabbits. In present study, lymphocyte significantly decreased in experimental groups as compared to the control group. Lymphocytopenia could be due to its decreased production of from bone marrow or its destruction in the body. In this study, monocyte significantly decreased in experimental groups as compared to the control group. Monocytopenia might be due to its decreased production of from bone marrow or its destruction in the body.

Similar findings were reported by Olaniyan Added in list & Oladega, 2019, as increased blood platelets. This significant increase in platelet number shows that amoxicillin induced bleeding with organ and tissue damage; as a result, platelets increase to control bleeding or injury that occurs in the rabbit body. But a contrary result reported in platelets with a significantly decreasing trend was observed when the rabbits were given subcutaneous injection of amoxicillin supplemented with raw cucumber fruit juice (Olaniyan & Oladega, 2019).

In present study, red blood cells (RBC) significantly decreased in experimental groups as compared to the control group. Similar findings were observed by Added in list & Oladega, (2019). Contrary to our result of a significant decrease, a significantly increasing pattern was observed in RBC count when rabbits were supplemented with raw cucumber fruit juice (Olaniyan & Oladega, 2019).

In present study, hemoglobin (HB) significantly decreased in the experimental groups as compared to the control group. Similar results to those of ours were observed when the rabbits were given subcutaneous injection of amoxicillin supplemented with raw cucumber fruit juice. This could be as a result of the destruction of red blood cells or reduced production from haemopoietic tissues of the rabbit (Added in list & Oladega, 2019). As a result, a decreased concentration of hemoglobin is reported because hemoglobin is a constituent of RBC. Contrary to our result of a significant decrease, a significantly increasing trend was observed in hemoglobin concentration when rabbits

TABLE 2: Relative body and organ weight in rabbits injected with variable doses of amoxicillin.

| Body and organ weight | Groups/treatments | | | |
|-------------------------------|---------------------|-----------------|-----------------|-----------------|
| | Control (0.0 mg/kg) | A (100 mg/kg) | B (150 mg/kg) | C (200 mg/kg) |
| Body weight (g) | 1289.3 ± 21.2 | 1223.5 ± 17.1* | 1170.1 ± 10.4* | 1125.4 ± 5.3* |
| Liver (×10 ³ ppm) | 33.95 ± 0.31 | 31.40 ± 1.54* | 29.50 ± 0.51* | 27.70 ± 1.30* |
| Kidney (×10 ³ ppm) | 4.78 ± 0.36 | 3.33 ± 0.60* | 3.19 ± 0.18* | 2.97 ± 0.13* |
| Lungs (×10 ³ ppm) | 5.62 ± 0.13 | 7.18 ± 5.63* | 7.71 ± 0.44* | 8.66 ± 0.69* |
| Heart (×10 ³ ppm) | 3.90 ± 0.20 | 2.79 ± 0.34* | 2.47 ± 0.04* | 2.22 ± 0.13* |
| Brain (×10 ³ ppm) | 6.91 ± 0.29 | 5.73 ± 1.10* | 4.8 ± 0.21* | 4.22 ± 0.43* |
| Spleen (×10 ³ ppm) | 281.00 ± 52.70 | 298.00 ± 27.10* | 364.00 ± 28.30* | 398.00 ± 10.18* |
| Testis (×10 ³ ppm) | 828 ± 49.21 | 916 ± 24.51* | 952 ± 28.51* | 1080 ± 20.2* |
| Ovary (×10 ³ ppm) | 163.57 ± 6.51 | 161.23 ± 5.43* | 157.13 ± 2.66* | 146.23 ± 2.37* |

The data are represented as mean ± SD. Values bearing an asterisk in each row show significant difference as compared to that control group ($P < 0.05$).

TABLE 3: Hematological parameters of rabbits exposed to variable doses of amoxicillin.

| Parameters | Groups/treatments | | | |
|--|---------------------|-----------------|-----------------|-----------------|
| | Control (0.0 mg/kg) | A (100 mg/kg) | B (150 mg/kg) | C (200 mg/kg) |
| Total white blood cells (10 ³ /μL) | 4.96 ± 0.73 | 5.03 ± 0.63 | 6.46 ± 1.36* | 7.71 ± 1.26* |
| Lymphocytes (10 ³ /μL) | 3.77 ± 0.82 | 2.91 ± 0.58 | 2.53 ± 0.47* | 1.51 ± 0.28* |
| Neutrophils (10 ³ /μL) | 1.84 ± 0.88 | 2.18 ± 0.66 | 2.56 ± 0.48* | 3.82 ± 2.96* |
| Monocytes (10 ³ /μL) | 0.48 ± 0.12 | 0.40 ± 0.15 | 0.32 ± 0.13 | 0.21 ± 0.09* |
| Granulocytes (10 ³ /μL) | 2.21 ± 0.55 | 3.03 ± 0.45 | 3.23 ± 1.03* | 3.61 ± 0.73* |
| Red blood cells (10 ⁶ /μL) | 5.53 ± 0.90 | 5.52 ± 0.42 | 5.48 ± 0.50 | 4.36 ± 0.62* |
| Hemoglobin (g/dL) | 11.46 ± 0.79 | 11.43 ± 1.91 | 10.93 ± 0.99 | 10.18 ± 1.47* |
| Hematocrit (%) | 38.05 ± 3.88 | 34.53 ± 5.73* | 34.26 ± 2.63* | 27.41 ± 3.80* |
| Mean corpuscular volume (fL) | 62.90 ± 1.88 | 68.87 ± 3.48* | 62.55 ± 2.59 | 62.35 ± 1.49 |
| Mean corpuscular hemoglobin (pg) | 23.36 ± 1.11 | 19.80 ± 0.74* | 20.93 ± 0.93* | 20.61 ± 0.74* |
| Mean corpuscular hemoglobin concentration (g/dL) | 37.13 ± 1.02 | 28.77 ± 0.63* | 33.46 ± 0.69* | 33.11 ± 0.51* |
| Platelets (10 ³ /μL) | 248.87 ± 38.65 | 291.50 ± 75.72* | 355.12 ± 87.64* | 430.12 ± 40.24* |

The data are represented as mean ± SD. Values bearing an asterisk in each row show significant difference as compared to the control group ($P < 0.05$).

were supplemented with raw cucumber fruit juice (Olaniyan & Oladega, 2019) (Table 3). This present study showed that hematocrit (HCT) significantly decreased in experimental groups as compared to the control group that is due to hemolysis of RBC; as a result, the number and size of RBC reduced that resulted in the reduction of hematocrit values.

The mean corpuscular volume (MCH) significantly decreased in experimental groups as compared to control. Destruction of RBC results in degradation of hemoglobin that results in a decreased average quantity of MCH in RBCs of rabbits. In present study, the mean corpuscular hemoglobin concentration (MCHC) significantly decreased in experimental groups as compared to the control group. Due to the adverse side effects of amoxicillin treatment, destruction of RBC occurred that results in degradation of hemoglobin as well as the decreased average quantity of MCHC blood of rabbits, while in our study, the mean corpuscular volume (MCV)

means that the average size of red blood cells showed a nonsignificant difference in experimentally labelled groups.

During the current study, we observed a significantly increased trend of cholesterol in treated groups. Similar to the present result, a significant increase in cholesterol is also reported in sheep by Elmajdoub et al. In our study, we observed a significantly increasing trend in the triglyceride level of experimentally labeled groups.

The recent study showed a significantly increased urea level in experimental groups. Similar Added in list are reported in previous studies when subcutaneous injection of amoxicillin were given to rabbits (Olaniyan & Fowowe, 2020). This indicated nephrotoxicity as a result of overdose of amoxicillin which affects the kidneys, possibly causing poor kidney function (Olaniyan & Fowowe, 2020). In contrast to our results, a significant decrease in plasma urea was observed in rabbits following the administration of

TABLE 4: The biochemical parameters of rabbits exposed to variable doses of amoxicillin.

| Parameters | Groups/treatments | | | |
|------------------------|---------------------|----------------|----------------|----------------|
| | Control (0.0 mg/kg) | A (100 mg/kg) | B (150 mg/kg) | C (200 mg/kg) |
| Blood sugar | 111.37 ± 2.66 | 106.00 ± 3.02* | 105.25 ± 2.49* | 104.37 ± 1.68* |
| Cholesterol | 120.62 ± 3.88 | 124.25 ± 2.81* | 132.00 ± 4.34* | 137.00 ± 1.85* |
| Triglyceride | 144.62 ± 10.33 | 147.87 ± 3.90* | 158.25 ± 5.62* | 165.75 ± 7.42* |
| Uric acid | 1.93 ± 0.29 | 1.96 ± 0.25 | 2.20 ± 0.25* | 2.35 ± 0.20* |
| Urea | 36.25 ± 2.12 | 37.00 ± 2.13 | 38.12 ± 2.03* | 39.75 ± 2.05 |
| Creatine | 0.75 ± 0.14 | 0.80 ± 0.13 | 1.10 ± 0.20* | 1.27 ± 0.12* |
| Calcium | 10.71 ± 0.40 | 11.63 ± 0.44 | 11.72 ± 0.94* | 11.93 ± 0.77* |
| Albumin | 4.78 ± 0.18 | 4.37 ± 0.14 | 4.10 ± 0.13* | 3.85 ± 0.19* |
| Total protein | 6.66 ± 0.43 | 6.53 ± 0.21 | 6.01 ± 0.20* | 5.71 ± 0.29* |
| HD lipoprotein (mg/dl) | 41.33 ± 1.76 | 47.10 ± 2.90* | 57.03 ± 3.14* | 74.10 ± 4.10* |
| LD lipoprotein (mg/dl) | 14.10 ± 1.12 | 17.12 ± 1.77 | 26.80 ± 1.51* | 33.14 ± 1.65* |
| Plasma fibrinogen | 610.1 ± 303.7 | 464.7 ± 235.7* | 363.2 ± 65.2* | 290.0 ± 157.2* |
| Serum globulins | 2.31 ± 0.13 | 2.6 ± 0.11* | 2.80 ± 0.36* | 2.98 ± 0.23* |

The data are represented as mean ± SD. Values bearing an asterisk in each row show significant difference as compared to the control group ($P < 0.05$).

TABLE 5: Comparison of antioxidant enzymes of rabbits exposed to variable doses of amoxicillin.

| Parameters | Groups/treatments | | | |
|--------------------------------|---------------------|---------------|---------------|---------------|
| | Control (0.0 mg/kg) | A (100 mg/kg) | B (150 mg/kg) | C (200 mg/kg) |
| Malondialdehyde concentrations | 27.19 ± 1.12 | 28.15 ± 1.31 | 37.13 ± 3.23* | 52.67 ± 2.43* |
| Catalase (U/mg p) | 26.32 ± 3.50 | 23.32 ± 2.90* | 17.13 ± 1.10* | 13.12 ± 1.70* |
| Superoxide dismutase (U/mg p) | 32.16 ± 1.13 | 28.62 ± 1.80* | 22.80 ± 1.15* | 14.11 ± 1.13* |
| Reduced glutathione (U/mg p) | 31.70 ± 3.14 | 28.63 ± 2.19* | 22.92 ± 4.19* | 17.24 ± 2.13* |
| Peroxidase (U/mg p) | 2.51 ± 0.32 | 2.30 ± 0.21 | 1.62 ± 0.65* | 1.12 ± 0.11* |

The data are represented as mean ± SD. Values bearing an asterisk in each row show significant difference as compared to the control group ($P < 0.05$).

TABLE 6: Effect of variable doses of amoxicillin on liver function enzymes in rabbits.

| Parameters | Groups | | | |
|-------------------------------|---------------------|------------------|------------------|------------------|
| | Control (0.0 mg/kg) | A (100 mg/kg) | B (150 mg/kg) | C (200 mg/kg) |
| Alanine aminotransferase (IU) | 123.75 ± 4.80 | 132.37 ± 4.13* | 136.00 ± 3.02* | 140.25 ± 3.61* |
| Alkaline phosphatase (IU) | 227.75 ± 8.82 | 241.75 ± 6.75* | 249.12 ± 9.43* | 264.12 ± 4.79* |
| Bilirubin (mg/dL) | 0.52 ± 0.03 | 0.57 ± 0.01* | 0.61 ± 0.01* | 0.67 ± 0.02* |
| Aspartate transaminase (IU) | 106.00 ± 11.30 | 137.00 ± 28.30* | 159.50 ± 20.50* | 197.50 ± 21.90* |
| Lactate dehydrogenase (IU) | 445.70 ± 30.50 | 515.70 ± 218.50* | 664.70 ± 383.50* | 786.30 ± 364.90* |

The data are represented as mean ± SD. Values bearing an asterisk in each row show significant difference as compared to the control group ($P < 0.05$).

raw cucumber fruit juice supplementation (Olaniyan & Fowowe, 2020). In our study, the uric acid level significantly increased in antibiotic-treated groups because of kidney failure as a result of nephrotoxicity due to adverse side effects because of overdose treatment of amoxicillin to rabbits. In the present study, the creatine level significantly increased in treated groups due to renal failure that could be due to adverse side effects of amoxicillin on rabbits. Contrary to

our result, a significant decrease in the creatinine level was revealed in the LZM-treated rabbit groups [14] (Table 4).

In the recent biochemical examination, we observed significantly increased concentrations of HD lipoproteins, LD lipoproteins, serum globulin, and calcium levels in antibiotic amoxicillin-treated groups with respect to the untreated control group. Similar to our results, increased concentrations of serum globulin are similar to LZM-fed rabbits

TABLE 7: Severity of different histopathological changes in organs of rabbits exposed to variable doses of amoxicillin.

| Histopathological lesions | Groups/treatments | | |
|--|-------------------|---------------|---------------|
| | A (100 mg/kg) | B (150 mg/kg) | C (200 mg/kg) |
| Liver | | | |
| Karyorrhexis | + | ++ | ++++ |
| Congestion of central vein | - | - | +++ |
| Cytoplasmic vacuolation | ++ | +++ | ++++ |
| Disorganized hepatic cord | - | ++ | +++ |
| Bile duct hyperplasia | + | + | +++ |
| Necrosis and hydropic changes in hepatocytes | + | +++ | +++ |
| Pyknosis | + | ++ | ++++ |
| Vacuolar degeneration | ++ | ++++ | ++++ |
| Hemorrhages | + | ++ | +++ |
| Ceroid formation | ++ | ++ | +++ |
| Nuclear hypertrophy | ++ | ++ | ++++ |
| Congestion | ++ | +++ | +++ |
| Degeneration of hepatocyte | ++ | +++ | ++++ |
| Kidney | | | |
| Increased Bowman's space | + | ++ | ++++ |
| Congestion | + | ++ | +++ |
| Necrosis of renal tubular epithelial cell | + | ++++ | ++++ |
| Nuclear hypertrophy | + | +++ | ++++ |
| Necrosis of renal tubules | + | +++ | +++ |
| Degeneration of renal tubule | + | +++ | +++ |
| Degenerative changes in kidney glomerulus | + | ++ | +++ |
| Widening urinary space | + | +++ | +++ |
| Hemorrhage b/w tubule | + | + | ++ |
| Cell infiltration with pyknotic nuclei | + | ++ | +++ |
| Heart | | | |
| Necrosis of cardiac cells | + | +++ | ++++ |
| Cytoplasmic vacuolization | ++ | +++ | ++++ |
| Congestion | + | +++ | ++++ |
| Neutrophilic myocarditis | + | +++ | ++++ |
| Myofibrillolysis | + | +++ | ++++ |
| Pyknotic nuclei | + | ++ | +++ |

Normal: -; mild: +; moderate: ++; severe: +++; very severe: ++++.

[14]. In the present study, an increased concentration of high density lipoprotein is similar to another work in which *Nigella sativa* seed was fed to rabbits (16) A contrary to our result is reported by El-Deep et al. when they fed LZM to rabbits and found no significant difference. A contrary to our results of increased concentration of low-density lipoprotein is reported by El-Deep et al. when they fed LZM to rabbits and found no significant difference and also by El-Gindy et al. when they fed *Nigella sativa* seed as a diet to rabbits.

The present study showed that total protein, plasma fibrinogen, blood sugar, and albumin concentration significantly decreased in antibiotic-treated groups. Previously, in published literature, similar results of significantly decreased

plasma albumin have also been reported in rabbits injected with amoxicillin supplemented with raw cucumber fruit juice. Hypoalbuminemia could be due to liver damage, hepatitis, and hepatotoxicity induced by amoxicillin because liver synthesizes albumin [16]. In contrast to our results, significantly increased plasma albumin is reported in rabbits supplemented with raw cucumber fruit juice [16].

The present results showed that malondialdehyde concentrations (MDA) increased significantly while reduced glutathione, catalase, superoxide dismutase, and peroxidase decreased significantly in antibiotic amoxicillin-treated groups as compared to the untreated control group. Our recent results of increased malondialdehyde concentration are contrary to those of El-Gindy et al. when they fed *Nigella sativa* seed to

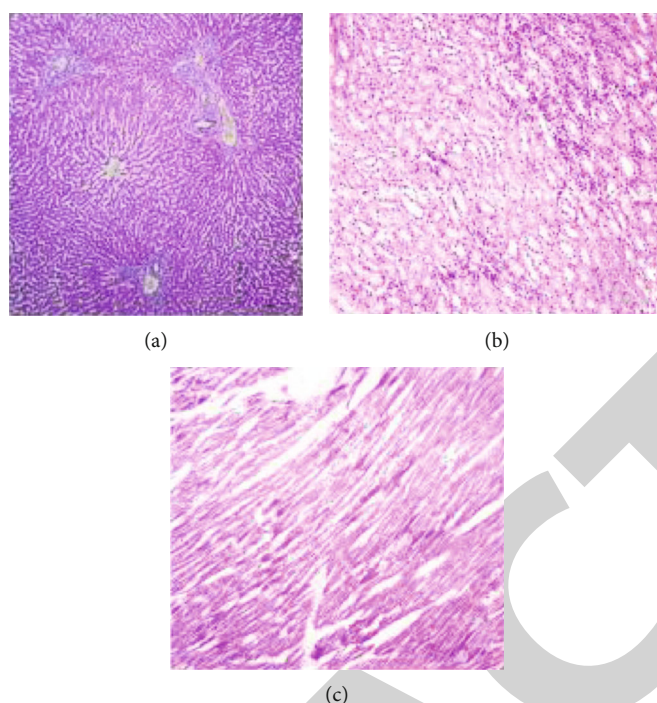


FIGURE 1: Photomicrograph of the liver (a); kidney (b), and heart (c) of treated rabbits (200 mg/kg body weight) showing different histopathological changes (400x, H&E stain).

rabbits as compared to the basal diet-fed control group. Present results are also in contrary to those of Zweil et al. when they fed peppermint and basil essential oil as supplementation to evaluate productive performance of rabbits. A contrary to our result of MDA is reported by Imbabi et al. when they used fennel essential oil as an alternative for antibiotic. In the present study, we observed decreased catalase, reduced glutathione, superoxide dismutase, and peroxidase parameters and these results are in contrary with those of Singh et al. when they fed melon seed oil as dietary supplementation to rabbits and found a significant difference and no negative effect upon 0.6% on the antioxidant parameters such as superoxide dismutase (SOD), reduced glutathione (GSH), and malondialdehyde.

The serum ALT level and AST are commonly measured to determine hepatitis and hepatocellular injury possibly due to toxic substances such as drug and infectious agents as well as to estimate liver health (Olaniyan & Adepoju, 2019; [16]). In the current study, we found significantly increased levels of ALT, ALP, AST, LDH, and bilirubin in treated groups as compared to the untreated control group (Table 6). Previously, in published literature, similar results of a significant increase in ALT and AST values have also been reported in rabbits treated with amoxicillin supplemented with raw cucumber fruit juice. Increased plasma levels of ALT and AST can be caused by liver damage, hepatitis, and hepatotoxicity induced by amoxicillin. In contrast to our results, a significant decrease in plasma ALT and AST was observed in rabbits supplemented with raw cucumber fruit juice (Olaniyan & Adepoju, 2019). Furthermore, a significant decrease in the levels of ALT and AST was revealed by El-

Deep et al. in LZM-treated rabbits. In our study, we investigated a significantly increased level of ALP in experimental-treated groups. Similar to our result, a significant increase in ALP is also reported in sheep by Elmajdoub et al. In our study, we observed that lactate dehydrogenase and bilirubin significantly increased in antibiotic-treated groups when compared with the control group.

Karyorrhexis, congestion of central vein, cytoplasmic vacuolation, disorganized hepatic cord, bile duct hyperplasia, necrosis and hydropic changes in hepatocytes, yknosis, vacuolar degeneration, hemorrhages, ceroid formation, nuclear hypertrophy, congestion, and degeneration of hepatocytes in liver were few indications of the present study, while previous studies reported that the amoxicillin-treated foetal liver showed vacuolar, fatty degenerations in the cytoplasm of the hepatocytes, devastations of mitochondria, and fragmentation of rough endoplasmic reticulum [17]. Previous studies also reported drug-induced liver injury, destruction of the biliary epithelium, lesions on the epithelium of interlobular ducts, and primary biliary cholangitis, such as inflammation and necrosis at the expense of cholangiocytes, bile duct loss, and biliary cirrhosis. Amoxicillin/clavulanic acid is associated with drug-induced liver injury and bile duct loss reported by the US Drug-Induced Liver Injury Network [18] [19] (Table 7). In our latest microscopic examination, we observed increased Bowman's space, congestion, necrosis of renal tubular epithelial cell, nuclear hypertrophy, necrosis of renal tubules, degeneration of renal tubule, degenerative changes in kidney glomerulus, widening of the urinary space, hemorrhage b/w tubule, and cell